UNIVERSITY OF SOUTHAMPTON

FACULTY OF NATURAL AND ENVIRONMENTAL SCIENCES

Ocean and Earth Science, National Oceanography Centre Southampton

The impact of future sea-level rise on the tides

by

Mark Derek Pickering

Thesis for the degree of Doctor of Philosophy

March 2014

UNIVERSITY OF SOUTHAMPTON

ABSTRACT

FACULTY OF NATURAL AND ENVIRONMENTAL SCIENCES

OCEAN AND EARTH SCIENCE

Doctor of Philosophy

The impact of future sea-level rise on the tides

by Mark Derek Pickering

Tides (along with mean sea-level and surges) are a key component in coastal extreme water levels. This investigation begins by assessing the effect of future sea-level rise (SLR) on the tides of the northwest European Continental Shelf. Tides here are dominated by semidiurnal constituents; therefore the focus is on changes in the M_2 constituent and the spring and neap tides. The validated operational Dutch Continental Shelf Model is run for the present day sea-level as well as uniform 2 and 10m SLR scenarios. M_2 tidal amplitude responds to SLR in a spatially non-uniform manner, with substantial amplitude increases and decreases in both scenarios. The North Sea M_2 tidal response is not proportional to SLR between 2 and 10m. In the 2m SLR scenario the M_2 constituent is particularly responsive in the resonant areas. Changes in the spring tide are generally larger (-49cm St. Malo to +35cm Cuxhaven) than those in the M_2, neap or shallow water tides. With SLR the depth, wave speed and wave length are increased causing changes in near resonant areas. In expansive shallow areas SLR also causes reduced energy dissipation by bottom friction. These mechanisms result in the migration of tidal amphidromes and complex patterns of non-proportional change in the tide with SLR. These substantial alterations to the tides are contrary to some previous studies.

These results motivate a subsequent investigation into the effect of future SLR on the global tides. We use a fully global forward tidal model, OTISmpi, to simulate the response of the four primary tidal constituents (M_2, S_2, K_1, O_1) as well as mean high water (MHW) and maximum range to various SLR scenarios. Attention is paid to changes at the 136 largest coastal cities (populations >1 million), where changes would have the greatest significance. A refined model setup is shown to have good skill at representing the present day tides. Uniform SLR scenarios 0.5-10m with fixed coastlines show the tidal amplitudes in shelf seas globally to respond strongly (increases and decreases) and non-proportionally to SLR. The changes in K_1 and O_1 tides are confined to Asian shelves. With 0.5m, 1m and 2m SLR MHW changes exceed ±10% of the SLR at 13, 13 and 10 of the 136 cities, respectively. Uniform SLR scenarios including coastal recession show a stronger and increasingly negative MHW response. The regularly opposing signs of change between the fixed and recession cases are explained through the opposing effect of the perturbations on the natural period of oscillation of the basin. These results suggest it may be possible to influence the sign of the tidal amplitude change through coastal management strategies. Non-uniform SLR, due to ice melt, causes the largest difference from the uniform SLR tidal response at high latitudes, in the near field (diminished response) and far field (amplified response) of the mass loss.

Changes in the tide will influence: coastal flooding, renewable and nuclear power generation, water reliant industry, sediment transport, dredging, shipping, tidal mixing fronts and intertidal habitats.

Contents

List of tables

List of figures

List of accompanying materials

The accompanying CD with this thesis includes animations of the tidal simulations presented in Chapters 2 and 3. Descriptions of the animations can be found in section 2.7 and 3.7.1 respectively. The CD also includes a pdf version of the thesis with fully hyperlinked cross referencing.

DECLARATION OF AUTHORSHIP

I, Mark Derek Pickering

declare that the thesis entitled

"The impact of future sea-level rise on the tides"

and the work presented in the thesis are both my own, and have been generated by me as the result of my own original research. I confirm that:

- this work was done wholly or mainly while in candidature for a research degree at this University;
- where any part of this thesis has previously been submitted for a degree or any other qualification at this University or any other institution, this has been clearly stated;
- where I have consulted the published work of others, this is always clearly attributed;
- where I have quoted from the work of others, the source is always given. With the exception of such quotations, this thesis is entirely my own work;
- I have acknowledged all main sources of help;
- where the thesis is based on work done by myself jointly with others, I have made clear exactly what was done by others and what I have contributed myself;
- parts of this work have been published as:

  Pickering, M.D., Wells, N.C., Horsburgh, K.J., Green, J.A.M., 2012. The impact of future sea-level rise on the European Shelf tides. Continental Shelf Research, 35, 1-15.

  and submitted for publication as:

  Pickering, M.D., Horsburgh, K.J., Blundell, J.R., Hirschi, J.J-M., Nicholls, R.J., Verlaan, M., Wells, N.C., submitted to Progress in Oceanography (Jan. 2014). The impact of future sea-level rise on the global tides.

Signed: ……

Date:……

Acknowledgements

This thesis represents the culmination of my work into a topic which has been of interest to me for some 6 years. During this period I have had the privilege of being supported by some very talented people who I pay my sincerest thanks to here. My apologies to anyone who should have been included.

Firstly thanks to my substantial PhD supervisory panel for their diverse contributions towards this research. To: Dr Kevin Horsburgh (National Oceanography Centre, Liverpool) for his excellent scientific guidance, attention to detail, editorial assistance as well as organisational and time management skills through which he always made time to feedback and meet during an often packed schedule; Dr Neil Wells (University of Southampton) for his advice and support all the way from my undergraduate thesis to completion of this PhD; Jeff Blundell (University of Southampton) for his incredibly practical and logical approach to teaching and guiding me on the daily coding, numerical modelling and high performance computing challenges of this PhD as well as for his ability to see the light hearted side of things; Dr Joel Hirschi (National Oceanography Centre, Southampton) for his diligent support of and involvement in a PhD topic outside of his usual area of expertise as well as for his caring attitude and level headed advice; Dr Martin Verlaan (Deltares and TU Delft) for his regular journeys to the UK for meetings, insightful feedback and attention to the project despite his geographical remoteness and to Professor Robert Nicholls (University of Southampton) for his practical engineering perspective and insight on the research. I would also like to thank my panel chair Professor Harry Bryden (University of Southampton) for his belief in and support of my PhD from the interview to the panel meetings themselves.

Additionally thanks to those who contributed to making the PhD possible financially. Thanks for the funding from Deltares (organised by Karel Heynert), from NERC (organised by Professor Adrian New and Dr Kevin Horsburgh) and for the fees scholarship from the school (organised by Professor Harry Bryden).

The science presented here benefited from discussions and assistance from researchers from numerous organisations including the National Oceanography Centre (NOC), University of Southampton and Deltares. Some individuals who had particular contributions were: (from NOC) Dr Andrew Coward, Dr Mark Tamisiea, Professor Alex Souza, Dr David Webb, Professor

Phil Woodworth, Dr Judith Wolf, Professor Chris Hughes, Dr Chris Wilson, Dr Paul Bell, (from University of Southampton) Dr Ivan Haigh, Professor Carl Amos, Dr Luke Blunden, (from Deltares) Dr Douwe Dillingh, Dr Bert Jagers, Firmijn Zijl, Dr John de Ronde, Dr Jan van Dalfsen, Dr Herman Gerritsen, Dr Arnout Bijlsma and Dick Verploegh.

This PhD project would not have been possible without the usage of a number of models and datasets many of which, as is increasingly the trend, are thankfully available open source. I would like to thank Deltares, Rijkswaterstaat and the KNMI for usage of the Dutch Continental Shelf Model as well as the Delft3D modelling framework. Thanks to Professor Gary Egbert and Dr Lana Erofeeva at Oregon State University for providing OTISmpi and generous advice on its usage. Thanks also to Dr Mark Tamisiea for provision of IER sea-level fingerprints and related advice, as well as Professor Alex Souza for creating the Stokes Number plots. I also appreciate the free availability of the GEBCO bathymetric dataset, FES2004 tidal atlas, University of Hawaii Sea Level Center tide gauge datasets, United Nations World Urbanization Prospects dataset and the Nicholls et al. (2008) coastal city exposure dataset. Additionally I would like to thank NOC for allowing extensive usage of the NOC Southampton Nautilus Compute Cluster as well as the IT group for keeping it running. Finally thanks to the National Oceanographic Library for permission to reproduce the cotidal chart (Figure 2.2a).

Completing this PhD required a substantial personal commitment and tenacious mindset. For this to be possible I needed a vast amount of moral support from officemates, friends and family. First of all I must thank my parents for their unwavering encouragement of this endeavour. My mum for her patience, advice and interest in some of the less exciting moments of the project and my Dad for his ability to help me take a step back and gain perspective (particularly through an endless flow of dolphins, polar bears and meerkats to remind me of the David Attenborough documentaries which originally sparked my interest in Oceanography). Also thanks to my cousins (who are somewhat surprised that I am doing a PhD at all), my aunt and my uncle who has a particular skill in finding humour where previously I only saw routine scientific terminology. Thanks also to my great friends too numerous to name. I would like to dedicate this thesis to my granddad, Peter Bishop, whom I am very pleased will be able to see the completion of this PhD.

xxx

Abbreviations

ARCoES	Adaptation and Resilience of Coastal Energy Supply
CBA	Cost Benefit Analysis
CFD	Cumulative Frequency Distribution
DCSMv5 (/DCSM98a)	Dutch Continental Shelf Model version 5
DIVA	Dynamic Interactive Vulnerability Assessment tool
ESLs	Extreme Sea-Levels
GENO	Gehele Noordzee (translates as Complete North Sea)
GIA	Glacio-Isostatic Adjustment
HW	High Water
IER	Initial Elastic Response
IPCC	Intergovernmental Panel on Climate Change
KNMI	Royal Netherlands Meteorological Institute
LGM	Last Glacial Maximum
LW	Low Water
MHW	Mean High Water
MPI	Message Passing Interface
MSL	Mean Sea-Level
MSLR	Mean Sea-Level Rise
MTR	Mean Tidal Range
NAG	Numerical Algorithms Group
NOC	National Oceanography Centre
NPG	North Pole in Greenland

OSU	Oregon State University
PDF	Probability Distribution Function
RCP	Representative Concentration Pathway
RMSE	Root Mean Square Error
ROFI	Region Of Freshwater Influence
SAL	Self-Attraction and Loading
SD	Standard Deviation
SL	Sea-Level
SLF	Sea-Level Fall
SLR	Sea-Level Rise
SSC	Suspended Sediment Concentration
SSH	Sea Surface Height
SSJPM	Skew Surge Joint Probability Method
TE2100	Thames Estuary 2100 project
UHSLC	University of Hawaii Sea-Level Center
UKCP09	United Kingdom Climate Projections 2009
VD	Vector Difference

1. Introduction

Coastal flooding represents one of the major challenges of global climate change for humanity; with mean sea-level (MSL) certain to rise over the coming centuries as well as the potential for alterations to the intensity of storm surges, wave climate and fluvial discharge. It is estimated that in 2005 in the largest 136 coastal cities alone there were 40 million people and $3,000 billion of assets exposed to independent 1 in 100 year flood events, assuming no flood defences. The probability of a 1 in 100 year event occurring in at least one of these cities is 74% every year and 99.9% every five years. The exposure is set to rise to approximately 150 million people and $35,000 billion of assets in 2070 (Nicholls et al., 2008; Hanson et al., 2011). The exact values are subject to substantial uncertainty due to the assumed warming pathway and associated sea-level rise (SLR), socio-economic development, land subsidence and adaption measures. The most high profile and high impact examples of coastal flooding occur when large storm events coincide with tidal high water (HW) and periods of large tidal ranges due to the natural astronomical variability in the tides (spring or tropic tides). Examples of this include the surges that resulted from the 1953 North Sea Storm during a spring HW (Flather, 1984; Gerritsen, 2005), the 1962 Ash Wednesday Storm over multiple perigean spring HWs (Bretschneider, 1964; Dolan, 1987), the 2010 Winter Storm Xynthia during a spring HW (Bertin et al., 2012), the 2011 Hurricane Irene near HW (Orton et al., 2012), the 2012 Hurricane Sandy during spring HW (Buxton et al.,2013) and the 2013 North Sea Storm during spring HW (Environment Agency, 2013). Often surge events occur with no impact as they coincide with tidal low water (LW) or the neap and equatorial phases of the tidal cycle (Pugh, 1987). The tides are therefore shown to be a key component in extreme water levels (Flather and Williams, 2000), with the potential to moderate or exacerbate the impact of a surge event. For this reason this thesis argues that any factor which alters the tidal characteristics, particularly the amplitude of the tide, should be considered in comparable detail to the aforementioned, well recognised, drivers of coastal flood risk.

Coastal flooding is not the only potential impact; tidal changes may also influence a wide range of factors including: renewable energy generation, nuclear and fossil fuelled energy generation, other water reliant industry,

sediment transport, dredging and shipping, tidal mixing fronts and intertidal ecology.

It is known that tidal amplitudes vary on a variety of timescales associated with the astronomical forcing from fortnightly, 6 monthly, 4.4 yearly, 8.85 yearly, to 18.6 yearly cycles (Pugh, 1987). When these cycles cause tidal amplitudes close to the highest astronomical tide through constructive interference the risk of coastal flooding, even by a moderate storm surge, is augmented. For centuries the tides have largely been considered a stationary phenomenon, subject to fairly minor secular changes from year to year (Pugh, 1987). However in the last decade there has been an increasing body of observational evidence from tide gauge data across the world that more significant and widespread secular trends in the tidal amplitudes (both positive and negative) are occurring (Woodworth et al., 1991; Flick et al., 2003; Hollebrandse, 2005; Dillingh, 2006; Pouvreau et al., 2006; Ray, 2006; Jay, 2009; Ray, 2009; Haigh et al., 2010a; Woodworth, 2010; Mueller, 2011; Mueller et al 2011). A number of these studies link the observed tidal alterations to increases in MSL. Understanding observed changes in tidal characteristics is a complex matter since tides are affected locally by numerous factors such as morphological changes, dredging, harbour creation and land reclamation. For this reason, to assess the relationship between future SLR and tidal characteristics a modelling approach is adopted where we deliberately isolate the driver of the tidal change as the SLR perturbation alone.

Numerical tidal models without data assimilation now have sufficient skill to represent the present day tides well (Egbert et al., 2004) and also allow us to make projections of the potential future alterations to the tides due to SLR. Initially a regional model for the northwest European continental shelf is adopted to assess the effect of uniform SLR on the tides. Contrary to a number of prior studies which briefly investigated the effect of SLR on European Shelf tides (Kauker, 1998; Kauker and Langenberg, 2000; Lowe et al, 2001; Lowe and Gregory, 2005; Sterl et al., 2009) our model shows that SLR could substantially alter tidal characteristics. The substantial sensitivity of European tides to SLR motivated us to extend this study to the first investigation of the global tides and future SLR. On regional and global scales this allows us to address questions such as:

i) How substantial are the alterations to tidal amplitudes caused by SLR?

ii) Where do the largest tidal alterations occur? Are they in close proximity to major coastal cities where impacts will be largest?

iii) Are changes spatially uniform or are there both increases and decreases?

iv) Are the changes proportional (or linear with respect) to the SLR imposed?

v) Is assuming constant tidal open boundary forcing with SLR to regional models a fair assumption?

vi) What are the changes when considered in terms of the individual tidal constituents, spring and neap amplitudes, mean high water (MHW), maximum tidal range and percentages?

vii) How important is the treatment of the coastline when including the SLR in the simulations (i.e. allowing for coastal recession)?

viii) How much do non-uniform SLR scenarios associated with future ice mass loss and solid Earth response influence the tidal response?

The initial assessment of the changes in the European Shelf tides is made using the operational Dutch Continental Shelf Model version 5 (Verboom et al., 1992; Gerritsen et al. 1995) and presented in Chapter 2. The global tides investigation employs the global OTISmpi model (Egbert et al., 2004) and is presented in Chapter 3. After this thorough examination and quantification of the tidal alterations, Chapter 4 extends the discussion of the aforementioned wide spectrum of potential implications of tidal alterations.

When this study was initiated there were a limited number of studies into future SLR and tidal changes. However during the project a number of additional regional studies have emerged for the European Shelf (Ward et al., 2012; Pelling et al., 2013b), the Bay of Fundy (Greenberg et al., 2012; Pelling and Green, 2013), the Bohai Sea (Pelling et al, 2013a), the San Francisco Bay (Holleman and Stacey, 2014) and the Chinese coast (Feng and Tsimplis, 2014; Feng and Tsimplis, in prep.). As well as presenting the first major comprehensive study of global tides and future SLR, efforts have been made to enable direct comparison of our global model results with those of these more recent regional studies (see Appendix 3.5).

2. The impact of future sea-level rise on the European Shelf tides

This Chapter is adapted from a publication in Continental Shelf Research:

Pickering, M.D., Wells, N.C., Horsburgh, K.J., Green, J.A.M., 2012. The impact of future sea-level rise on the European Shelf tides. Continental Shelf Research, 35, 1-15.

2.1 Abstract

This Chapter investigates the effect of future SLR on the tides of the northwest European Continental Shelf. The European shelf tide is dominated by semidiurnal constituents. This study therefore focuses primarily on the changes in the M_2 tidal constituent and the spring and neap tidal conditions. The validated operational Dutch Continental Shelf Model is run for the present day sea-level (SL) as well as 2 and 10 m SLR scenarios.

The M_2 tidal amplitude responds to SLR in a spatially non-uniform manner, with substantial amplitude increases and decreases in both scenarios. The M_2 tidal response is non-linear between 2 and 10 m with respect to SLR, particularly in the North Sea. Under the 2 m SLR scenario the M_2 constituent is particularly responsive in the resonant areas of the Bristol Channel and Gulf of St. Malo (with large amplitude decreases) and in the southeastern German Bight and Dutch Wadden Sea (with large amplitude increases). Changes in the spring tide are generally greater still than those in the M_2 or neap tides. With 2 m SLR the spring tidal amplitude increases up to 35 cm at Cuxhaven and decreases up to -49cm at St. Malo. Additionally the changes in the shallow water tides are larger than expected. With SLR the depth, wave speed and wave length (tidal resonance characteristics) are increased causing changes in near resonant areas. In expansive shallow areas SLR causes reduced energy dissipation by bottom friction. Combined these mechanisms result in the migration of the amphidromes and complex patterns of non-linear change in the tide with SLR.

Despite the significant uncertainty associated with the rate of SLR over the next century, substantial alterations to tidal characteristics can be expected under a high end SLR scenario. Contrary to existing studies this Chapter highlights the

importance of considering the modification of the tides by future SLR. These substantial future changes in the tides could have wide reaching implications; including for example, correctly calculating design level requirements for flood defences, the availability of tidal renewable energy and dredging requirements.

2.2 Introduction

Over the last century, the average global rate of SLR was 1.7 mm yr^{-1} (Church and White, 2006). In the last decade an accelerated rate of 3.1mm yr^{-1} was observed (Cazenave and Nerem, 2004); although greater than the 20th century average this is not significantly larger than other decadal rates observed during the last century (Holgate, 2007; Haigh et al., 2010a). Current IPCC estimates of SLR over the 21st century infer average rates of 1.8–5.9 mm yr^{-1} (Meehl et al., 2007). Other research increases uncertainty in future estimates suggesting that during previous natural de-glaciations higher rates of 16 mm yr^{-1} have occurred (Rohling et al., 2008) and for the next century 15–20 mm yr^{-1} cannot be ruled out (Rahmstorf, 2007; Pfeffer et al., 2008; Convey et al., 2009).

Since the Last Glacial Maximum (LGM) some 18,000–22,000 years ago SL has risen by around 125 m with significant alterations to the global bathymetry by glacio-isostatic adjustment (GIA) (Peltier, 2004). Global tidal modelling studies show this SLR has profoundly affected the amplitude of the open ocean tides due to changing ocean basin geometry (Egbert et al., 2004; Green, 2010). These rapid changes in the tidal amplitude are supported by paleo-oceanographic evidence on continental shelves around the Atlantic Ocean; such as the Bay of Fundy (Shaw et al., 2010). European Shelf modelling studies also consider LGM to present day SLR finding significant changes in tidal characteristics (Austin, 1991; Shennan et al., 2000; Uehara et al., 2006) and sediment transport regimes (Gerritsen and Berentsen, 1998). Greenberg et al. (2012) consider the effect of future SLR and GIA on tidal range around the Bay of Fundy concluding that the resulting substantial increases in tidal range will increase the risk of coastal flooding.

On shorter timescales, tide gauge data suggests that during the last century tidal characteristics have been changing globally (Woodworth, 2010). This has been shown for primary tidal constituents in the Gulf of Maine (Ray, 2006), the North Atlantic (Ray, 2009; Müller, 2011), eastern Pacific Ocean (Jay, 2009), the

coasts of North America (Flick et al., 2003) and coastlines around the European Shelf (Woodworth et al., 1991). Various hypothesises have been put forward for the cause of these observed changes, including SLR, localised effects of dredging (Bolle et al., 2010), building of ports, long timescale meteorological effects including gyre spin up (Woodworth, 2010), alterations to the internal tide (Colosi and Munk, 2006) and alterations to the resonant interaction of the ocean and shelf tide (Arbic and Garrett, 2010).

Previous European Shelf studies on the effect of climate change on coastal extreme water levels consider the effect of future SLR on the tide and storm surge. These studies suggest the effects are negligible when considering mid (0.5 m) to high end (2.0 m) SLR scenarios for 2100 (Flather et al., 2001; Lowe et al., 2001; Sterl et al., 2009). The few studies which have identified any substantial changes to the European tides with SLR used high resolution models (von Storch and Woth, 2008). Egbert et al. (2004) highlight the dependence of accurate tidal solutions on bottom topography, suggesting that a model grid with a resolution higher than ¼° is required. Fully evaluating this effect of SLR is important as changes in tidal amplitude have implications for regional extreme water levels both directly by increases or decreases in tidal amplitude and indirectly by altering storm surge elevations through the tide-surge interaction (e.g. Prandle and Wolf, 1978; Horsburgh and Wilson, 2007). Changes in these extreme water levels in turn change the appropriate design levels for coastal flood defences.

The overall aim of this Chapter is to assess the potential impact of future SLR on the European Shelf tides. The first objective is to assess the effect of SLR on the dominant semi-diurnal M_2 tidal constituent; as well as assess the linearity of any response. The second objective is to assess the effect of 2 m SLR on the complete shelf tide, focusing on comparing spring and neap tidal conditions. To address these objectives the high resolution Delft3D Dutch Continental Shelf Model is used (see Verboom et al., 1992; Gerritsen et al., 1995) introducing uniform SLR to the present day bathymetry. The simulations use the 2 m SLR value (20 mm yr^{-1}) which, although very low probability (Nicholls et al., 2011), is taken as the upper limit for SLR during the next century (Pfeffer et al., 2008) or a low to middle scenario for 2200 SLR (Vellinga et al., 2009). A hypothetical 10 m SLR value is used to assess the sensitivity and linearity of the modelled tidal response with respect to SLR. The latter value is extreme but

justifiable in the context of long time scale mean sea-level rise (MSLR). It lies between 6.5 m assuming total loss of the Greenland ice sheet (Chen et al., 2006) and 70 m assuming total loss of the Greenland and Antarctic ice sheets (Huybrechts et al., 2004). The probability and timescale of such an occurrence is very uncertain. Paleo-oceanographic evidence suggests that a disequilibrium exists between present day CO_2 concentrations and SL. Assuming no further emissions equilibration would require 25 m (±5m) of SLR and this would likely take place on multi-centennial to millennial timescales (Rohling et al., 2009).

The outline of the Chapter is as follows. In the next section we describe the model, its validation, setup and assumptions. Section 2.4 contains the results. A discussion of the key findings, the mechanisms and previous studies is given in Section 2.5. Section 2.6 outlines the conclusions.

2.3 Methods

2.3.1 The model and validation

In this investigation we use the Dutch Continental Shelf Model version 5 (DCSMv5, also known as DCSM98a) which is based on the non-linear shallow water equations (Heaps, 1978; Stelling, 1984) and solved with an Alternating Direction Implicit finite difference scheme on a C-grid (Mesinger and Arakawa, 1976; Deltares, 2009a). A spherical coordinate system is chosen due to the spatial extent of the modelled domain. The model has been developed jointly by Delft Hydraulics, Rijkswaterstaat and the Royal Netherlands Meteorological Institute (KNMI) since the late 1980s and is presently employed for operational storm surge forecasting by KNMI (Verlaan et al., 2005).

The model encompasses most of the European Shelf (Figure 2.1) and has a latitudinal and longitude grid size of 1/12˚ and 1/8˚ (~8 x 8 km), respectively. Bathymetric data for the model was obtained from a combination of the GENO (Gehele Noordzee, translates as Complete North Sea) model (Voogt, 1984) and nautical charts outside this area. The Chezy parameterisation is used for bottom friction. The model has one continuous open boundary along which the phase and amplitude of elevation of the astronomical tidal constituents is

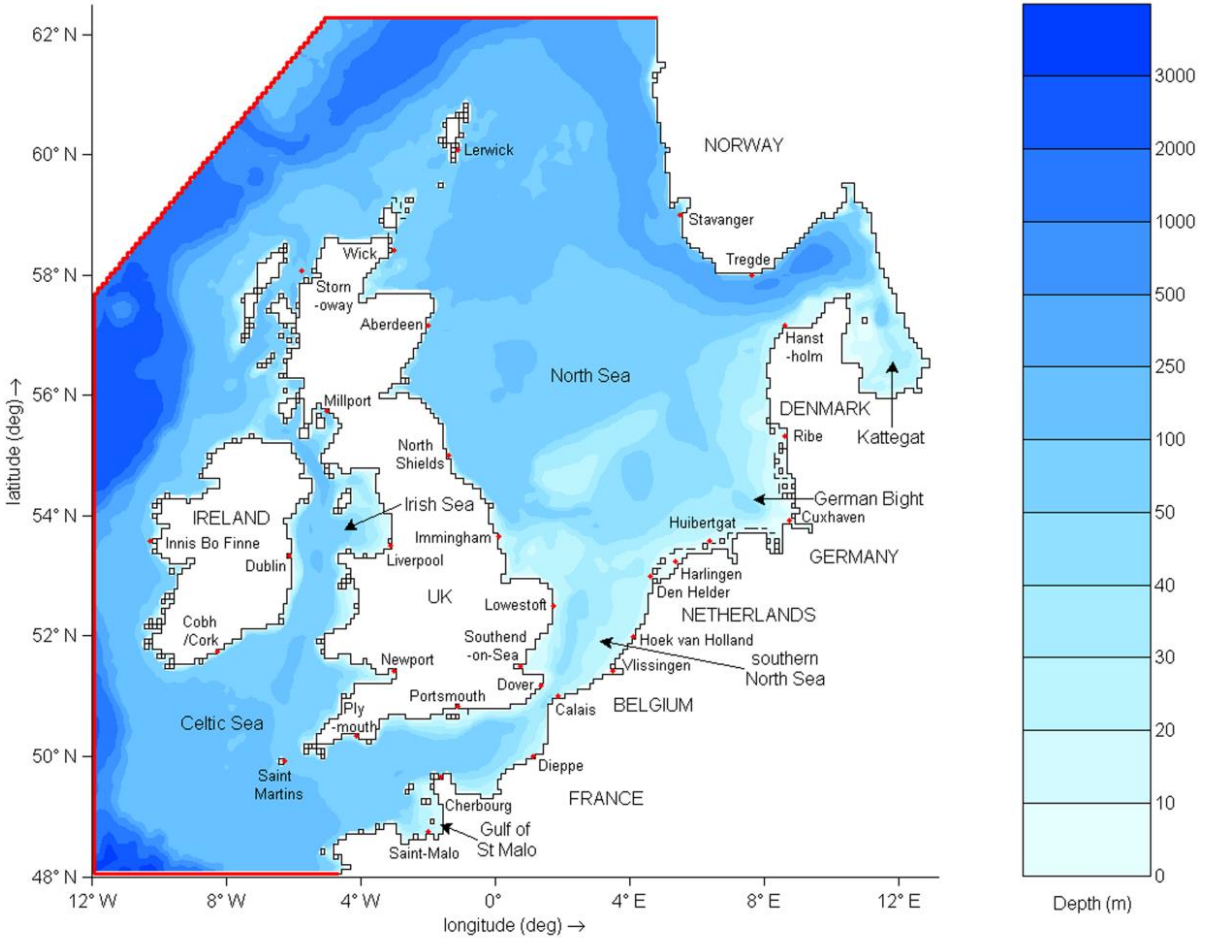

Figure 2.1. Domain of the DCSMv5 showing the 32 Sampled Ports (red dots), the bathymetry (blue shades in colour bar), the deep water open boundary (thick red line) and the closed boundaries at the land-sea margin (black lines).

prescribed. Prescribing the open boundary in deep water optimises the tidal solution on the shelf. Shallow water tides such as M_4, MS_4, $2MS_2$ and MU_2 are able to develop within the domain due to non-linear terms in the equations of motion. The direct effect of the tide generating force is not included as the European Shelf is too small and too shallow to respond significantly to the tidal potential (Gerritsen et al., 1995). The model uses an implicit numerical scheme and a timestep of 10 min has previously been found to give acceptable accuracy (Verboom et al., 1992). For drying and flooding of grid cells a threshold depth of 0.1 m is used.

The DCSMv5 has been continuously redeveloped, calibrated and validated allowing confidence in the model (see Verboom et al., 1992; Gerritsen et al., 1995; Philippart et al., 1998; Gebraad and Philippart, 1998). Since the calibration exercise undertaken in 1998, no significant alterations to the model have been made as further development was unlikely to yield significant improvements in accuracy. Importantly, the tidal calibration used tide gauge records and altimetric data from across the full model domain (Figure 2.1). The mean standard deviation (SD) of tidal water levels using 28 shelf wide tide gauges and the model is 15.4 cm (Gebraad and Philippart, 1998).

In addition to the comprehensive validations referenced above, a basic validation was performed to ensure the model was correctly reproducing the observed tide. Comparing observed M_2 cotidal charts, based solely on observations from bottom pressure sensors and tide gauges (Figure 2.2a), with our modelled M_2 cotidal charts, calculated using a Fourier transform (Figure 2.2b), allowed qualitative validation. The progression of the M_2 tide around the shelf is very well represented by the model as can be seen by the good agreement between the amphidromic systems on the two plots. The noticeable but minor discrepancy is that the model's amphidrome on the Norwegian coast is rotary and lies further to the southwest (Figure 2.2b) when compared to the observed degenerate amphidrome (Figure 2.2a). It is, however, noted by Howarth and Pugh (1983) that due to the particularly low density of bottom pressure gauges near the Norwegian coast there is reduced certainty in the exact position of these cotidal lines. Animations of the present day M_2 tidal propagation can be found on the accompanying CD ROM

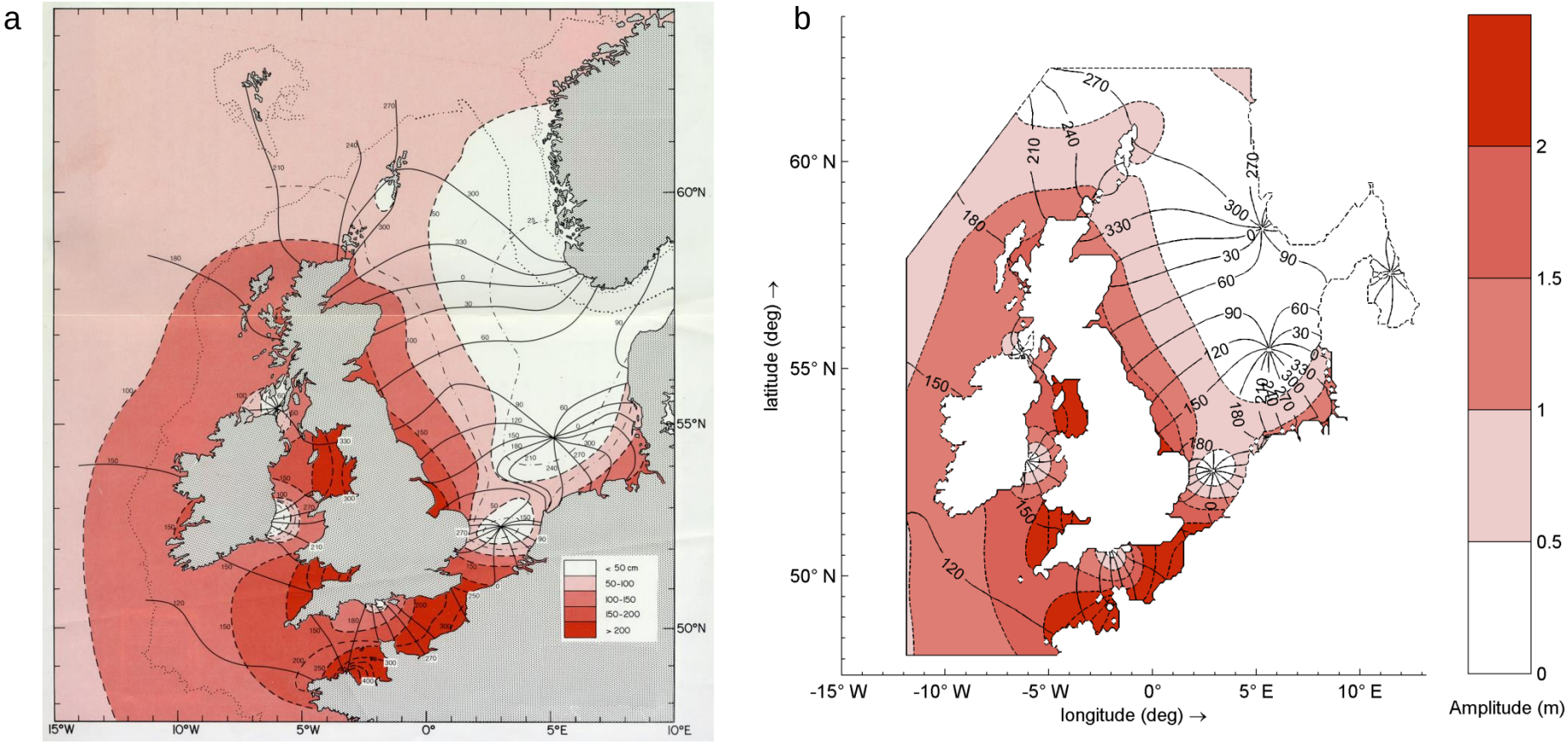

Figure 2.2 (a). Cotidal chart for the M_2 tidal constituent based solely on observational data from tide gauges and bottom pressure sensors. The dashed lines with values are lines of constant amplitude (m), solid lines with values indicate lines of constant phase (with permission: Howarth, 1990). (b) Cotidal chart for the M_2 tidal constituent based on the DCSMv5 simulation with present day sea-level (M00). Coloured contour patches give amplitude (m), solid lines with values indicate phase (intervals as in Fig. 2.2a).

Examination of individual tidal curves showed good representation of other observed tidal features, including diurnal inequality, the inequality between successive neap tides associated with the moon's orbit and double HWs and LWs at locations strongly influenced by shallow water terms.

2.3.2 Simulation set-up and assumptions

The simulations were set up to enable intercomparison and therefore all parameters were kept constant with the exception of the SL and the tidal constituents used to force the model (Table 2.1). The runs indexed with the prefix M were forced at the open boundary with only the M_2 constituent (henceforth M_2 Run) and those with the prefix A were forced with 10 semidiurnal and diurnal constituents (henceforth Full Run). The purpose of the M_2 Runs was to address objective 1 (Section 2.2). The initial focus on M_2 is due to it being the dominant tidal constituent on the European Shelf and having a fast model spin-up time. The M_2 Runs may include internally generated M_2 overtides such as M4, M6 and M8. The purpose of the Full Runs was to address objective 2 (Section 2.2). The tidal constituents in these runs represent 98% of the observed tidal range and include compound tides such as MS_2. Runs with suffixes of 00, 02 and 10 use 0 m SL, 2 m SLR and 10 m SLR (see Section 2.2 for context) for the initial conditions across the domain at the first timestep as well as for the MSL at the open boundary. All the simulations use the same start date of the 10th of January 2008, to ensure consistent astronomic forcing. This date was chosen because of the quality of the validation data available for this period.

Table 2.1. Setups of the simulations presented in this Chapter. Note that the M_2 Fourier Analysis was run for the final 5 days of the M_2 Runs (~9 M_2 periods) and harmonic analysis was conducted for all 5 simulations (see Section 2.3.2).

Run ID.	Initial Water Level (m)	Run Length (days)	Forcing Consituents	M2 Fourier Analysis
M00	0	10	M2	Yes
M02	+2	10	M2	Yes
M10	+10	10	M2	Yes
A00	0	30	M2, S2, N2, K2, NU2, L2, K1, O1, P1, Q1	No
A02	+2	30	M2, S2, N2, K2, NU2, L2, K1, O1, P1, Q1	No

The model was spun up over a 5 day period and this period was discarded from the Fourier and harmonic analyses. The cotidal charts produced were used both for validation (Section 2.3.1) and to evaluate the change in M_2 tidal

amplitude by plotting the difference between the two coamplitude fields (SLR scenario- present day control). Comparing scaled M_2 amplitude change plots for 2 m and 10 m SLR allows qualitative assessment of the linearity of the M_2 response. Harmonic analysis of the model results (Delft3D TRIANA (see Deltares, 2009b) calculates the amplitude and phase of tidal constituents at 32 selected case study ports (Figure 2.1) and allows calculation of any changes with SLR. The analysis of the M_2 Runs for the M_2 tidal constants is based on the last 5 days of the 10 day runs and these data enable quantitative assessment of the linearity of the M_2 response. The analysis of the Full Runs for the tidal constants of 34 constituents is based on the last 25 days of the 30 day runs. Only the M_2 and S_2 tidal constituents are used to present changes in the spring (M_2+S_2) and neap tides (M_2-S_2) at all ports. The other tidal constituents are only used to provide estimates of changes in other tidal species at some ports.

To aid in the interpretation of results, Figure 2.3 shows the depth change introduced to the model in each of the two SLR scenarios as a percentage of the original model depth. Viewed in conjunction with Figure 2.1, which shows the absolute depth values, one can locate shallow areas where significant alterations to the tide might be expected. This expectation only holds if large tidal alterations occur in those regions where relative depth change is also large.

Whilst it is important that the model represents the observed tide with a good degree of realism and accuracy (as has been demonstrated) it should be noted that this Chapter is concerned with the relative change between two simulations (SLR- Control). In this Chapter, due to the grid scale and time-step, we consider a significant change to be wherever there is > ±5 cm tidal amplitude change and > ±5° (~10 min) M_2 phase change.

The 32 locations for detailed tidal change analysis were chosen to provide a spatially representative sample as well as include locations of particular societal importance. For example, 6 key port cities with populations in excess of 1 million, including Dublin, Glasgow, London, Rotterdam, Amsterdam and Hamburg (Nicholls et al., 2008). Only Dublin lies directly on the coast. For the other 5 ports a nearby coastal location has been chosen, Millport, Southend-on-Sea, Hook van Holland, Harlingen and Cuxhaven (Figure 2.1). It is noted that

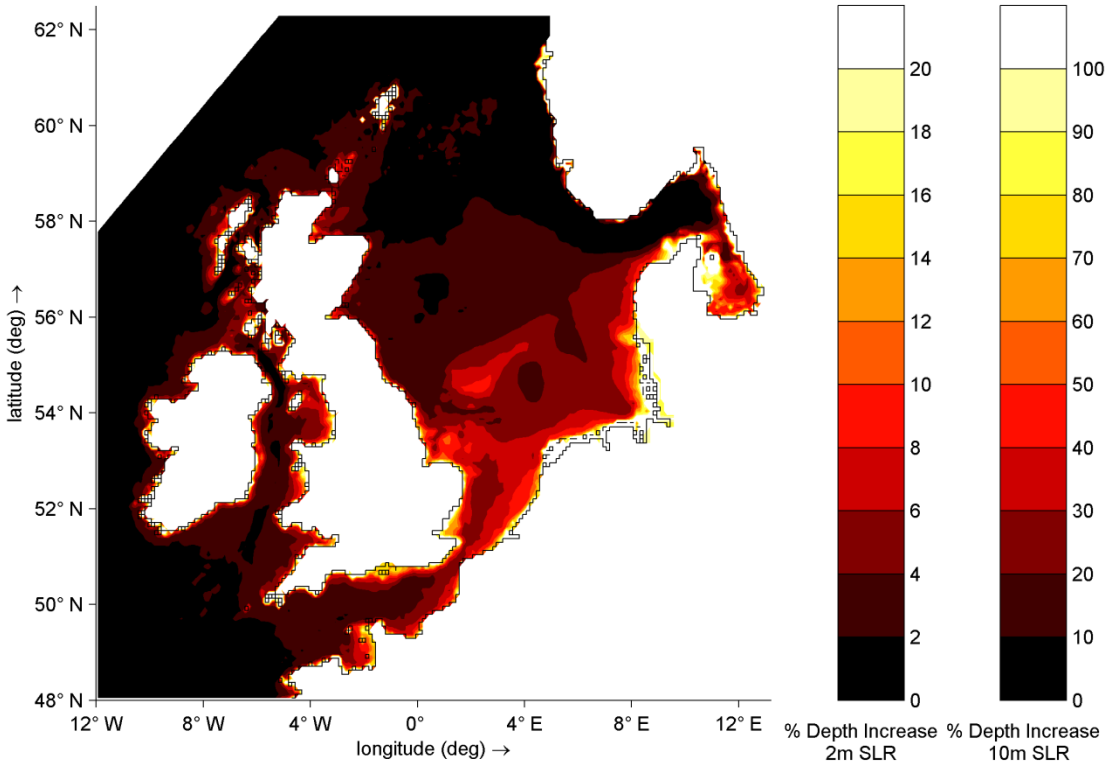

Figure 2.3. Percentage depth increases with 2m and 10m SLR with respect to present day sea-level model depth values (each colour bar represents a SLR scenario). Black and white areas indicate very small and very large percentage depth increases respectively.

London and Rotterdam have closable barriers, Amsterdam is closed off from the tide and Glasgow and Hamburg tides are modified by estuarine effects. Delfzijl is another key port; however, model resolution landward of the Frisian Island chain limits accuracy; because of this Huibertgat on the seaward side was selected.

The assumptions inherent in these model setups are now discussed. As in Gerritsen and Berentsen (1998), Flather and Williams (2000) and Sterl et al. (2009) the assumption is made that the tidal forcing at the open boundary of our model is not changed significantly due to SLR. This is justifiable as the relative depth change with SLR at the model's deep water open boundary (>200 m) is small (Figure 2.3). Additionally the boundary is far enough away from the shelf that the local tide is largely determined by the incoming Atlantic tide and to a much lesser extent by the response of the North Sea basin (Gerritsen and Berentsen, 1998; Arbic and Garrett, 2010). The assumption

therefore depends mostly on whether the Atlantic tide changes with SLR. Results from two non-data assimilative global tidal models, the Oregon State Tidal Inversion Software (OTISmpi) (Green, pers. comm.; Chapter 3) and a model under development Barotropic-OCCAM (BT-OCCAM) (Pickering, 2010), suggest that changes in M_2 amplitude in the location of the open boundary are small (< ±5 cm with 2 m SLR and < ±10 cm with 10 m SLR). Global tidal models may also have insufficiently high resolution or bathymetric accuracy to represent narrow straits (e.g. Dover), artificially amplifying the apparent tidal change due to SLR at the boundary. The open boundary assumption also implies that there is no change in the domain averaged energy dissipation, estimated to be ~200 GW (Egbert and Ray, 2001).

As MSLRs some recession will occur at the coastline. The current modelling approach assumes a vertical wall is maintained along the entirety of the present day land–sea margin or more formally that coastal recession with SLR never exceeds the area of half a grid cell (~32 km^2). This assumption is justifiable along some European coastlines, such as the Netherlands, where prolonged hard engineering schemes are in place. For other European coastlines, however, the flood defence strategies which will be adopted by 2100 are subject to substantial uncertainty. In addition, to our knowledge, a shelf scale inundation model able to simulate coastal recessions and the tides does not exist. Other modelling efforts considering SLR also use this assumption, justifying it in terms of the insignificant amount of tidal energy in the relatively small volume of water being omitted from the model (e.g. Howard et al., 2010).

In the southern Kattegat an artificial closed boundary is imposed where in reality the Kattegat is connected to the Baltic Sea by the Danish Straits. Results in the Kattegat may be influenced by the model's artificial closed boundary. Tidal flows at the semidiurnal frequency from the micro-tidal Kattegat through the narrow Danish Straits (36 and 7 km widths) are small due to tidal choking which filters out these short period oscillations (e.g. M_2). The assumption is therefore reasonable.

Our modelling approach also assumes that the SLR will occur uniformly across the European Shelf. This is sufficient for investigating the first order effects of SLR on the tide but it does not take into consideration spatially varying SLR

(see Shennan and Woodworth, 1992; Gregory and Lowe, 2000; Woodworth et al., 2009), relative SLR from localised land subsidence and uplift caused by GIA (see Shennan et al., 2009) or anthropogenic effects such as ground water removal. Including non-uniform future SLR to account for these processes may not currently improve the accuracy of the scenario, given the very large uncertainty associated with future spatial characteristics of SLR (Gregory et al., 2001), particularly on this relatively small spatial scale.

In these simulations no morphological adjustment in the seabed is permitted. SLR may cause accretion in bays and estuaries as the system attempts to maintain the original depth, offsetting the depth increase caused by SLR (Allen, 1990). Also the effect of altered tidal currents on the bed morphology, and in turn the feedback effect of this altered bathymetry on the tide has not been included in these simulations. How much of a compensatory effect this would have on the depth increase with SLR is dependent on whether the rate of SLR exceeds the rate at which the system can import sediment (Tomasin, 1974) which is in turn dependent on varying sediment availability across the shelf (Di Silvio, 1989).

All the assumptions discussed above are more valid for 2 m SLR than for 10 m SLR, and of course the lower SLR scenario is more relevant to the timescales used in the majority of coastal planning.

2.4 Results

2.4.1 Change in M_2 tide with SLR (M_2 Runs)

Results from the simulations using M_2 only tidal forcing are considered first under the 2 m SLR scenario. Figure 2.4 shows the changes in the tidal amplitudes across the shelf as well as the migration of the present day amphidromes ('0 m' in Figure 2.4). It is to be expected that changes in amphidrome position will lead to a coherent spatial pattern of amplitude change, as observed. The regions of particular increase in M_2 amplitude are shown to be the Wadden Sea in the north of the Netherlands, the northwest coast of Germany in the southeastern German Bight as well as to a lesser extent the western Irish Sea, southern North Sea, Skagerrak and southern Kattegat (noting Kattegat artificial closed boundary caveat, see Section 2.3.2).

The regions of particular decrease in M_2 amplitude are the Bristol Channel and southernmost Irish Sea, the Gulf of St. Malo and the western half of the English Channel and to a lesser extent the east coast of England between Immingham and Lowestoft. The northernmost amphidrome in the North Sea migrates northwest resulting in the increased amplitude in the Skagerrak and southeast German Bight. There is a slight northeastward migration of the southern North Sea amphidrome and the English Channel amphidrome remains degenerate.

The values given in Table 2.2 provide more detail on the magnitude of the changes in the M_2 tide with 2 m SLR. The largest absolute amplitude alterations lie beyond the colour bar limits of Figure 2.4, ranging between -39 cm at Newport and 29 cm at Cuxhaven. The three largest absolute amplitude decreases occur at Newport, Saint-Malo and Cherbourg and the largest amplitude increases occur at Cuxhaven, Harlingen and Hanstholm. To examine whether the size of the amplitude changes are simply proportional to the amplitude in the control scenario one should consider the percentage amplitude change. Table 2.2 shows the altered M_2 amplitude as a percentage of the control amplitude. The decreased amplitude at Newport in the mouth of the Severn is equivalent to 91% of the original amplitude and the increased amplitude at Cuxhaven equivalent to 121%. In percentage terms the largest M_2 changes occur at Tregde and Stavanger, 152% and 73%, respectively. These locations are micro-tidal and near an amphidrome in the control run so percentage change is very sensitive to small absolute amplitude changes. Considering non micro-tidal locations the next largest percentage changes are the 131% of original amplitude at Harlingen and the 96% at Cherbourg and Plymouth.

The changes in the phase of the M_2 tide with 2 m SLR are shown in Table 2.2. The ports are listed in an order consistent with the local progression of the M_2 tide, making cumulative phase shifts more readily identifiable. The timing of the arrival of the M_2 tidal constituent's peak amplitude is also shown to be altered in a spatially variable manner. In the English Channel most of the changes in phase are negative. The phase changes are no greater than -5˚ under the 2 m scenario where the alteration of the amphidromic system is more subtle than under the 10 m scenario. The three largest positive phase changes, indicating a later arrival of the tide, are in the vicinity of Lerwick, Wick

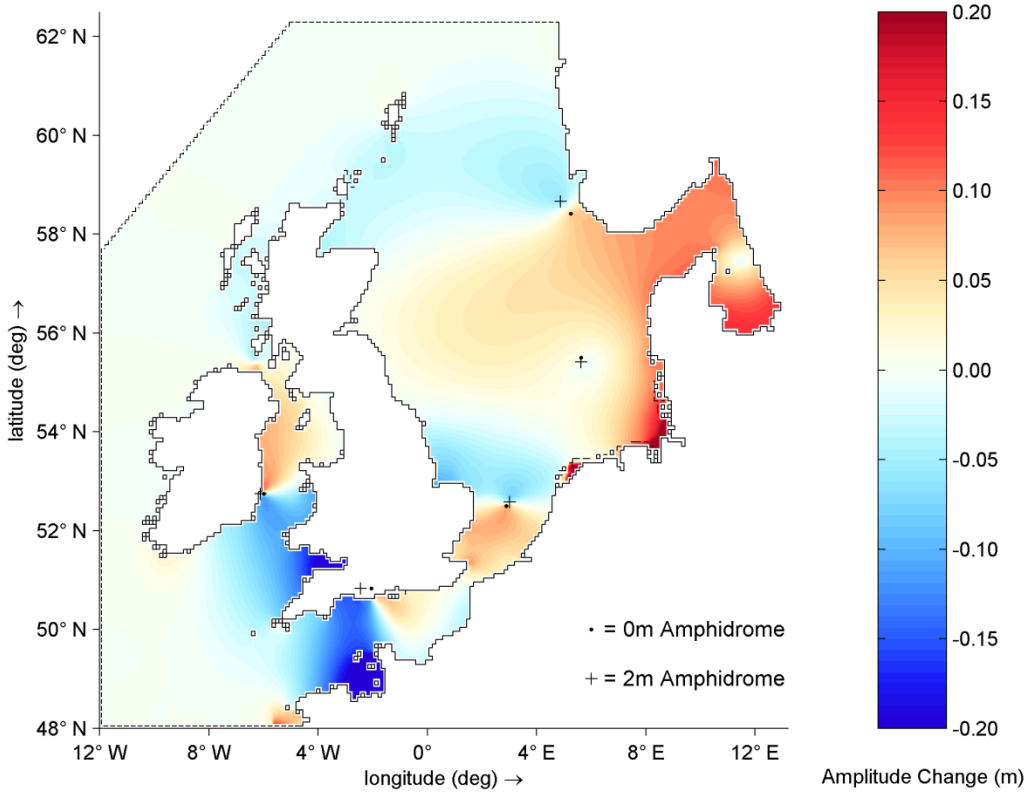

Figure 2.4. Plot shows the increases (red) and decreases (blue) of the M_2 amplitude with 2m of SLR (M02 - M00). Note that the limits of the colour bar (-0.2m to +0.2m) are different to Figure 2.5; this allows the degree of the linearity of the tidal response to be directly compared between the figures (if linear the plots would be identical). Degenerate amphidromes (Dorset, UK) are only representative estimates.

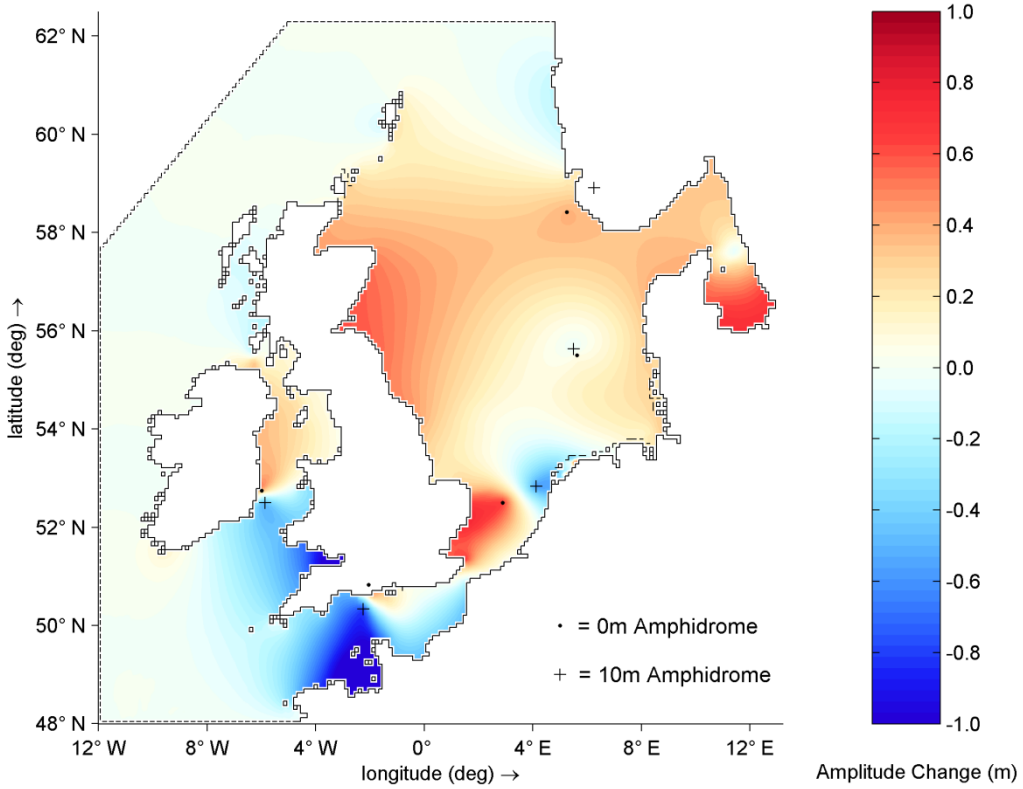

Figure 2.5. Plot shows the increases (red) and decreases (blue) of the M_2 amplitude with 10m of SLR (M10 - M00). Note that the limits of the colour bar (-1.0m to +1.0m) are different to Figure 2.4; this allows the degree of the linearity of the tidal response to be directly compared between the figures (if linear the plots would be identical). Degenerate amphidromes (Dorset, UK and Norway) are only representative estimates.

Table 2.2. Port by port results from the M_2 Run harmonic analysis showing: control amplitude and amplitude changes with SLR; amplitudes with SLR as a percentage of the control amplitude and control phase and phase changes with SLR. Control refers to present day sea-level values (M00), +2m SLR and +10m SLR to the difference between SLR and control simulations (M02 - M00 and M10– M00). A 100% value would indicate no change in amplitude with SLR. Negative (positive) changes in phase indicate earlier (later) arrival of peak amplitude (M_2 **angular velocity is 28.98°/hr). Values followed by ↑ (↓) highlight the ports with** the three largest increases (decreases). Non-linear change values are indicated by * (defined in Section 2.4.1). Ports are listed in order of phase of the nearest amphidromic system in the control simulation (Figure 2.2b). A significant change in amplitude is considered to be > ±5 cm and in phase is > ± 5° (~10 min).

	M2 Amplitude (cm)				% of Control Amplitude		M2 Phase (°/hr)			
Location	Control	+2m SLR	+10m SLR		+2m SLR	+10m SLR	Control	+2m SLR	+10m SLR	
Saint Martins	182	-3	-16	*	99	91	130	-2	-9	*
Plymouth	173	-7	-32		96	82	142	-4	-27	*
Saint-Malo	381	-33 ↓	-175 ↓		91 ↓	54 ↓	170	-2	-13	*
Cherbourg	191	-9 ↓	-72 ↓	*	96	62 ↓	230	1	10 ↑	*
Dieppe	326	-3	-43	*	99	87	309	-3	-12	*
Portsmouth	160	4	14	*	102	109	325	-3	-3	*
Dover	242	3	27	*	101	111	332	-5	-32	*
Calais	255	2	0	*	101	100	340	-5	-36	*
Innis Bo Finne	124	0	-1	*	100	99	144	0	0	
Cobh/Cork	150	-1	-6		99	96	145	-4	-17	
Newport	450	-39 ↓	-147 ↓	*	91 ↓	67	170	-7	-20	*
Liverpool	303	-1	4	*	100	101	314	-3	-11	*
Dublin	127	8	39		107	130	330	-2	-9	
Millport	156	1	9	*	101	106	342	-5	-22	*
Stornoway	154	-1	-3	*	99	98	199	0	1	*
Lerwick	51	-3	21	*	95	142	312	4 ↑	14 ↑	*
Wick	109	-3	35	*	97	132	322	2 ↑	6	*
Aberdeen	128	0	54 ↑	*	100	142	27	2 ↑	-4	*
North Shields	159	1	51	*	101	132	89	0	-13	*
Immingham	197	-6	28	*	97	114	141	-1	-13	*
Lowestoft	73	2	66 ↑	*	103	190	255	0	-20	*
Southend-on-Sea	204	3	54 ↑	*	101	126	344	-10	-53	
Vlissingen	190	7	4	*	104	102	30	-14	-71	
Hoek van Holland	94	5	2	*	105	102	58	-12	-86	*
Den Helder	81	-3	-52	*	96	36 ↓	152	-11	-41	*
Harlingen	83	26 ↑	-6	*	131 ↑	92	246	-30 ↓	-88 ↓	*
Huibertgat	108	2	-3	*	102	97	249	-10	-60	*
Cuxhaven	142	29 ↑	35	*	121	125	342	-19 ↓	-106 ↓	*
Ribe	87	10	26	*	111	130	8	-15	-92 ↓	*
Hanstholm	20	11 ↑	40	*	152 ↑	295 ↑	94	-5	-74	*
Tregde	17	9	34	*	152 ↑	298 ↑	100	-5	-77	*
Stavanger	11	-3	20	*	73 ↓	290 ↑	249	-35 ↓	133 ↑	*

and Aberdeen but values are only between 2˚ and 4˚. From Aberdeen to Immingham the M_2 tide then accelerates slightly relative to the control scenario. There are more substantial negative phase changes, around -10˚, at Southend-on-Sea and at the ports along the coast of the Netherlands. The three largest negative phase changes are seen at Stavanger, Harlingen and Cuxhaven with changes as large as -35˚ at Stavanger. The -19˚ phase change (~40 min earlier) at Cuxhaven is noteworthy as it is not near an amphidrome (Stavanger)

or in a semi-enclosed Sea (Harlingen). The largest change in phase outside of the North Sea is the -7˚ alteration at Newport.

We now consider the 10 m SLR scenario. In Figure 2.5 the regions of M_2 amplitude change are shown to have strong spatial variation, as was the case in the 2 m SLR scenario. It should be noted that the limits of the colour bar on Figure 2.5 are increased to ±100 cm, a factor 5 increase in proportion with the additional SLR introduced. Regions of particularly significant amplitude increase are shown to be the northeast coast of the United Kingdom between Aberdeen and North Shields, the western half of the southern North Sea and the southern Kattegat. Regions of particularly significant amplitude decreases occur on the northern half of the coast of the Netherlands, the western half of the English Channel and in the Bristol Channel. Figure 2.5 shows the north-eastward movement of the northern and southernmost North Sea amphidromes to result in two regions of amplitude increase on the UK's North Sea coast. Similarly the southward movement of the amphidrome in the English Channel is in line with amplitude increases near the Isle of Wight.

The details of the alterations in the M_2 amplitude with 10 m SLR are shown in Table 2.2. The M_2 amplitude alterations range between a decrease of -175 cm at Saint-Malo and an increase of 66 cm at Lowestoft, consistent with Figure 2.5. In absolute terms the three largest decreases again occur at Saint-Malo, Newport and Cherbourg and the largest increases at Lowestoft, Aberdeen and Southend-on-Sea. The decrease in M_2 amplitude at Saint-Malo causes a resultant amplitude 54% of the control. In a similar way the increase at Lowestoft translates to an amplitude 190% of the control. The largest changes in percentage terms occur at Den Helder and Tregde, 36% and 298% of the original amplitude, respectively.

The phase of the M_2 constituent is also altered under the 10 m SLR scenario. Generally the changes in the phase are negative indicating earlier arrival of the M_2 wave as depth is increased, consistent with the increased wave speed. The patterns of the phase shifts in the English Channel are made more complex by the southward migration of the amphidrome causing a transition from degenerate to rotary. Once the wave has progressed into the North Sea the negative phase changes are more consistent and cumulative. The wave arrives at Cuxhaven ~3 h and 40 min earlier than in the control scenario. The positive

phase change at Stavanger seems anomalous until it is considered that the nearby amphidrome (Figure 2.5) has migrated from rotary to degenerate, located inland of Stavanger, which does not occur in the 2 m SLR scenario. [The M_2 changes described in this section are also visible in the 32 port by port tidal curves included in Appendix 1.1.]

The ports with the largest changes are presented in Figure 2.6a–h and some interesting features are revealed. At Newport (Figure 2.6a) under the 10 m SLR scenario the substantial reduction in amplitude given in Table 2 seems to be augmented by a higher harmonic which causes a double LW. Higher harmonics can also be seen to affect the shape of the tidal curve under 10 m SLR at Vlissingen (Figure 2.6c). At Harlingen (Figure 2.6h) there is an increase in amplitude with 2 m SLR and a decrease with 10 m SLR where a higher harmonic causes a lower double HW. Complex phase changes in the English Channel are shown by the later arrival of HW with SLR at Cherbourg (Figure 2.6e) but an earlier arrival at Plymouth (Figure 2.6f).

We assess the linearity of M_2 amplitude change with SLR by comparing Figure 2.4 and 2.5. The limits of the colour bar are scaled in proportion with the SLR scenario so that if the changes were linear the plots would appear identical. Comparing the English Channel, Irish and Celtic Seas, the two plots show similar distribution of changes, suggesting fairly linear change. In the English Channel subtle differences can still be observed, for instance, the amplitude decreases in the west of the Channel. These occur in a north–south band in the 2 m scenario; however, under the 10 m scenario the area of decrease extends further west along the coast of France. In contrast, in the North Sea, linearity in the M_2 amplitude changes is much harder to identify. Under the 2 m scenario most of the changes decrease with distance from the east coast of the basin, whereas under the 10 m scenario most become smaller with distance from the west coast. In the North Sea under the 10 m scenario amplitude increases are prevalent, under the 2 m scenario there is a greater balance of amplitude increases and decreases. In four out of the five amphidromes located in Figure 2.4 and 2.5 the distance of the migration is larger under the 10 m scenario. Based on these SLR scenarios, however, no argument can be put forward for linear migration of the amphidromes as the direction of the movement is not consistent between the scenarios.

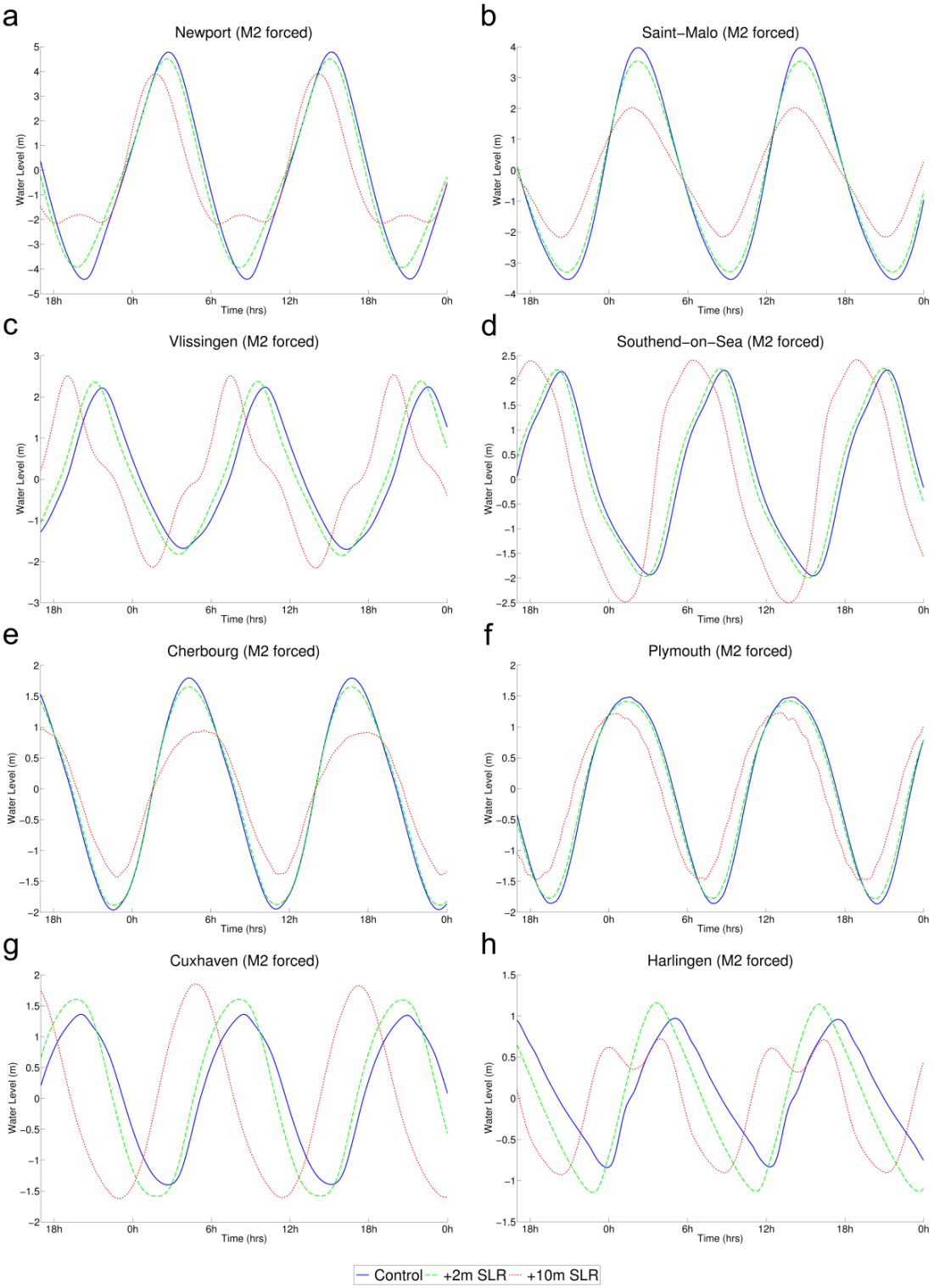

Figure 2.6a-g. Tidal curves from M_2 Runs at 8 ports where key changes occur. The three sea-level scenarios are shown 0m (blue line), 2m SLR (green line) and 10m SLR (red line). Note that the limits of the y-axis are not normalised and that ports are listed in order of decreasing amplitudes.

An additional way of assessing the differences in tidal response with respect to the imposed SLR is to compare the changes in phase and amplitude resulting from 2 and 10 m of SLR and assume an approximate factor of 5 indicates a linear change. Here we assume that any values outside the range 4.5–5.5 denote non-linear response to the SLR. In terms of the amplitude changes, the tide at 28 out of 32 ports is affected in a non-linear way by the imposed SLR. A similar non-linear effect of SLR on tidal phase is shown at 27 out of 32 ports. [Animations of the sea surface height elevations showing the M_2 tidal wave propagation at present day SL, 2 m SLR and 10 m SLR can be found in the Supplementary material.]

2.4.2 Change in spring, neap and other tides with SLR (Full Runs)

A harmonic analysis is used to assess the changes in 34 tidal constituents with 2 m SLR. Here we focus on the M_2 and S_2 constituents which are used to calculate neap (out of phase, M_2-S_2) and spring (in phase, M_2+S_2) tides (Pugh, 1987). The analysis based on 25 days of data, from simulations forced with 10 major diurnal and semidiurnal constituents (Table 2.1). The control amplitude, the absolute amplitude change and the percentage amplitude change for the M_2 and S_2 constituents, the neap and the spring tides, are summarised in Table 2.3. The change in the full spring and neap tidal curves with SLR is shown in Appendix 1.2.

Due to the different duration of data and constituents sought from the M_2 Run and Full Run with the harmonic analysis, slight variation between the control M_2 amplitudes occurs (Table 2.2 and 2.3). The root mean square error (RMSE) between the control M_2 amplitudes for simulation M00 and A00 is 5 cm; the absolute mean of the differences is 3 cm. The signs of the M_2 amplitude changes are consistent in both simulations. The RMSE between the M_2 amplitude changes is 2 cm and most of the differences between the amplitude changes are ≤ 3 cm. The two exceptions to this are a -4 cm larger decrease in M_2 amplitude at Saint-Malo and a 6 cm smaller decrease at Newport. Significant M_2 amplitude change (> ±5 cm) occurs in 12 of 32 ports in the M_2 Run and in 13 of 32 ports in the Full Run. The two forcing and analysis setups give similar amplitude change results; this increases confidence in the results of the more basic M_2 Run setup (Section 2.4.1).

Table 2.3. Port by port results from the Full Run harmonic analysis showing: for the M_2, S_2, Neap and Spring tides the control amplitude, amplitude change with 2m SLR and amplitudes with SLR as a percentage of the control amplitudes. Control refers to present day sea-level values (A00) and Change +2m SLR to the difference between the SLR and the control simulations (A02-A00). A 100.0% **value indicates no change in tidal amplitude with SLR. Values followed by ↑ (↓) highlight ports with the** 3 largest increases (decreases). Ports are listed in order of phase of the nearest amphidromic system in the control (Figure 2.2b). A significant change in amplitude is considered to be > ±5 cm. The M_2 and S_2 columns show rounded values and will not always equate with the Spring/Neap columns.

	M2			S2			M2-S2 (Neap)			M2+S2 (Spring)		
	Control Amplitude	Change +2m SLR		Control Amplitude	Change +2m SLR		Control Amplitude	Change +2m SLR		Control Amplitude	Change +2m SLR	
Location	(cm)	(cm)	(%)	(cm)	(cm)	(%)	(cm)	(cm)	(%)	(cm)	(cm)	(%)
Saint Martins	183	-3	98	64	0	100	120	-4	97	247	-3	99
Plymouth	174	-9	95	64	-2	97	110	-7	94	238	-11	95
Saint-Malo	392	-37 ↓	91 ↓	160	-13 ↓	92 ↓	232	-24 ↓	90 ↓	552	-49 ↓	91 ↓
Cherbourg	199	-11 ↓	95	77	-3 ↓	96	122	-8 ↓	94	276	-14 ↓	95
Dieppe	326	-6	98	110	0	100	216	-6	97	436	-5	99
Portsmouth	162	1	101	51	2	104	111	-1	99	212	3	102
Dover	238	2	101	77	1	101	161	1	100	315	3	101
Calais	248	2	101	79	1	102	170	0	100	327	3	101
Innis Bo Finne	126	0	100	48	0	100	78	0	100	173	0	100
Cobh/Cork	147	0	100	47	2	104	99	-2	98	194	2	101
Newport	446	-33 ↓	93 ↓	176	-10 ↓	95 ↓	270	-24 ↓	91 ↓	622	-43 ↓	93 ↓
Liverpool	299	0	100	100	1	101	199	-1	99	399	1	100
Dublin	125	9	107	37	4	110	88	5	106	162	12	108
Millport	151	2	101	44	2	105	107	0	100	196	4	102
Stornoway	157	-1	99	61	-1	99	96	-1	99	217	-2	99
Lerwick	53	-3	95	21	-1	96	32	-2	95	73	-4	95
Wick	110	-3	97	39	-1	97	70	-2	97	149	-4	97
Aberdeen	129	1	100	46	-1	98	83	1	102	174	0	100
North Shields	159	1	101	56	-1	99	103	2	102	215	0	100
Immingham	197	-5	98	70	-2	97	127	-3	98	266	-7	97
Lowestoft	72	2	103	24	-1	98	48	3	105	95	2	102
Southend-on-Sea	194	5	103	58	1	102	136	4	103	252	6	102
Vlissingen	180	10	105	50	5 ↑	110	130	5	104	230	14 ↑	106
Hoek van Holland	87	6	106	21	2	111	67	3	105	108	8	107
Den Helder	79	-4	95	23	-1	98	55	-3	94	102	-4	96
Harlingen	80	25 ↑	131 ↑	21	10 ↑	148 ↑	59	15 ↑	125 ↑	100	34 ↑	134 ↑
Huibertgat	104	2	102	28	1	104	76	1	101	131	3	102
Cuxhaven	136	27 ↑	120	33	8 ↑	123 ↑	103	20 ↑	119	169	35 ↑	121
Ribe	84	10	111	21	2	110	63	7	112	105	12	111
Hanstholm	19	10 ↑	154 ↑	3	1	125 ↑	16	10 ↑	160 ↑	22	11	150 ↑
Tregde	16	9	154 ↑	3	1	116	13	8	162 ↑	19	9	148 ↑
Stavanger	11	-4	68 ↓	6	-1	88 ↓	5	-3	46 ↓	17	-4	75 ↓

At most of the 32 ports, the change in neap tidal amplitude is smaller than the M_2 amplitude change. Our results show that changes in amplitude to the M_2 and S_2 constituents are positively correlated, with greater changes therefore occurring for spring tides and for the M_2 constituent than for neap tides (Table 2.3). There are only 5 ports of the 32 where the change in the tidal amplitude is larger on the neaps than on the springs: Saint Martins, Dieppe, Aberdeen, North Shields and Lowestoft. This occurs at stations where the M_2 amplitude change is small. Of these locations the largest change is at Dieppe where a -6 cm decrease in amplitude is experienced on the neap tide.

The change in the tidal amplitude with 2 m SLR on the spring tide (Table 2.3) indicates that 24 of the 32 ports experience larger changes in amplitude on the spring than the neap tide. At these ports the M_2 and S_2 constituents have changes of the same sign resulting in large alterations to the tidal amplitude with 2 m SLR. On the spring tide decreases in amplitude at Saint-Malo and Newport are -49 and -43 cm, respectively. These changes in amplitude represent 20–25% of the 2m SLR. The third largest reduction in amplitude of -14 cm occurs at Cherbourg. The two largest amplitude increases remain at Cuxhaven and Harlingen, 35 cm and 34 cm, respectively. This equates to ~17% of the 2 m SLR scenario. The third largest spring tide amplitude increase, 14 cm, was at Vlissingen; whereas for the M_2 and neap tides the third largest increase was at Hanstholm. Although many large S_2 changes occur in the same location as large M_2 changes (Saint-Malo, Newport, Cuxhaven, Harlingen), S_2 changes of 5 and 4 cm also occur at Vlissingen and Dublin, respectively.

Wherever significant (±5 cm) changes in amplitude occur, those changes have the same sign on both spring and neap tides, reflecting the fact that M_2 changes are larger than S_2 changes (see Table 2.3). Not surprisingly the largest changes of amplitude in response to the imposed SLR occur on the spring tide, with the exception of Dieppe. It should also be noted that the percentage amplitude changes > 10% often occur in micro-tidal regions where original tidal amplitude is small. This result is consistent with large-scale adjustment of the tidal amphidrome system, as discussed further in later sections. Our analysis provided insight into the changes in other tidal constituents beside M_2 and S_2. Harlingen, Vlissingen, Saint-Malo and Plymouth show particularly large contributions from the other semidiurnal, diurnal and higher harmonic constituents (e.g. at Harlingen there is a 15cm increase in amplitude of the

quarter-diurnals and a 9cm increase in other semi-diurnals, N2, MU2, etc.). Our results suggest that in addition to changes in the focal M_2 constituent and spring/ neap tides, changes in other tidal constituents will occur (through adjustment of their amphidromic systems). For an accurate harmonic analysis of all significant constituents a longer model run (1 year) would be required.

Animations of the Full Runs are available in the Supplementary material.

2.5 Discussion

2.5.1 M_2 and Full Runs

Comparison of the changes in M_2 amplitude in response to the imposed 2 and 10 m SLR scenarios shows that the effects scale non-linearly with SLR, particularly in the North Sea. This nonlinear dependence of tidal amplitude (and phase) on the SLR scenario means that flood risk assessments for various climate change scenarios should not be interpolated or extrapolated based on limited SLR model runs. Our work also implies that the tide and storm surge should not be simulated independently and then the SLR superimposed after, as some climate impacts studies have done (see Section 2.5.3). At some locations, phase change with SLR alters the length of double HW which also has implications for flood risk (see tidal curves in Appendix 1.1 and 1.2). Any extension of the period of HW increases the likelihood of joint probability occurrences, such as HW, surge and peak river discharge. In the 2 m SLR scenario, large M_2 amplitude increase is shown in the Dutch Wadden Sea (Figure 2.4) which could have significant implications. This is plausible given that the Wadden Sea is very shallow so 2 m SLR causes a very large relative depth change (Figure 2.3). The Wadden Sea M_2 amplitude increase should be treated with some caution due to the model resolution, although the Gebraad and Philippart (1998) validation shows the tide at Harlingen is modelled with better than mean accuracy (SD=11.4 cm).

At 24 of the 32 ports analysed, the change in tidal amplitude on spring tides is greater than the change on neap tides. Significant amplitude changes (> ±5 cm) occur at 15 of the 32 ports. Our results show significant amplitude decreases in the English Channel and Bristol Channel and significant amplitude increases in the North Sea and western Irish Sea. The largest changes in

absolute terms are in locations where the present day tidal amplitude is large, so are likely to have the most significant flooding implications. Our results also suggest that at certain locations (see Table 2.3) the S_2 tidal constituent has a particularly strong influence on the amplitude change.

2.5.2 Mechanism for the changes

An adjustment to the amphidromic system under SLR is consistent with changes to the wavelength of the co-oscillating shelf tide (see Arbic et al., 2004). Since the tide is a shallow water wave with speed $c=\sqrt{gh}$, as depth (h) is increased in the SLR simulations the tidal wave propagates more quickly in the domain. Because the wave frequency (f) remains constant, the wavelength (l) will increase with depth increase so l is proportional to $\sqrt{h}$ (e.g. Pond and Pickard, 1983). In a closed rectangular basin the first amphidrome will occur at l/4 from the solid boundary (see, for instance, Pugh, 1987), and even small changes in amphidrome position can cause significant changes to the tidal amplitude as reported here. Changes to wave phase speed also accounts for the negative phase changes in Table 2.2.

Small increases in the wavelength (caused by depth increases) may also affect the tidal characteristics of near-resonant estuaries or embayments (Flather and Williams, 2000). Many estuaries and gulfs are especially close to resonance when their length (L) is approximately a quarter of the wavelength of the tide. As wave speed increases with SLR and the gulf length remains approximately unchanged, the period of oscillation may move closer to the period of the forcing causing resonance. SLR could equally cause the natural period of oscillation to move away from resonance in which case tidal amplitude would decrease.

The Bristol Channel has the second largest tidal range in the world. Our results suggest that 2 m of SLR alters the natural oscillatory period of the channel and moves it away from resonance causing the substantial amplitude decreases shown in this area. Flather and Williams (2000) suggest that areas such as the Bristol Channel, the eastern Irish Sea and Gulf of St. Malo with large initial M_2 amplitudes experience substantial change due to these resonant mechanisms. The largest M_2 changes presented here also occur in these resonant areas and so support this hypothesis.

Results in other non-resonant areas of the domain also exhibit substantial amplitude changes. This is particularly the case in the southeastern German Bight, Skagerrak, Kattegat and Wadden Sea under 2 m SLR (Figure 2.4). The tidal energy dissipation resulting from depth-dependent bottom friction will also influence tidal dynamics, particularly in shallow water areas. Comparison of the M_2 amplitude change plots (Figure 2.4 and 2.5) with the relative depth change plot (Figure 2.3) shows that large increases in M_2 amplitude occur at or near shallow locations where relative depth change with SLR is large.

Since a Kelvin wave decays exponentially away from the coast with a length scale according to the barotropic Rossby radius ($\sqrt{gh}/f_c$ where f_c is the Coriolis parameter), then changes to depth will alter the position of the amphidromes normal to the wave propagation, as determined by the relative strength of the incoming and reflected waves (see Fig. A4.3 of Pugh (1987)). In a closed basin like the North Sea, our results have shown how changes to the tidal wavelengths (due to imposed SLR) will affect the north-south position of amphidromes whilst changes to the barotropic Rossby radius will affect the east-west position. Five of the key European shelf amphidromes can be seen in Figure 2.4 and 2.5 and the migration of all 5 amphidromes under the 10 m SLR scenario is clearly consistent with these arguments. Although less obvious, this is also the case under the 2 m SLR scenario.

2.5.3 Comparison to previous studies

Our results show changes in the tide to be greater in magnitude, and more spatially variable, than previous published studies concerned with the effect of SLR on European shelf sea tides. A summary of relevant previous studies is given in Table 2.4.

A number of modelling studies suggest that changes in the tide, or tide and surge, with SLR are negligible and therefore often do not present full results, making comparison difficult. Many of the published studies suggest that changes in the tide which do occur are linear, and many imply spatial uniformity. Some other modelling studies do give changes in tidal range comparable to those in this study (de Ronde, 1986; Flather and Williams, 2000).

Table 2.4. Summary of previous studies showing: their main results, their method as well as other papers with which they cite agreement and any agreement of their results with those of this Chapter. Abbreviations: S.- Southern; E.- **Eastern; (↑ & ↓)**- the study found both increases and decreases in range or amplitude; HW- high water; SLR- sea-level rise; (model acronyms are expanded in each reference). Note **that with no direct access to Kauker (1998) or Plüβ (2004) other published reviews have been quoted.**

Study	Main Results	Method and Cited Agreements	Accordance with this study (✔ / **x**)
de Ronde (1986)	S.North Sea: non-uniform Range Change (↑ & ↓); HW ~1hr earlier; average +15% range (-14% Den Helder, +20% near Huibergat)	5m SLR; earlier DCSM; North Sea focus; 1/8°	✔ (similar spatial distribution)
Kauker (1998)	"few cm change in tidal maxima" (Lowe et al. 2001)	"3D regional ocean model; North Sea; insufficient resolution for surges" (Lowe et al., 2001)	**x**
Kauker and Langenberg (2000)	North Sea: negligible non-linear interactions of thermal expansion and extreme water levels up to ~0.3m SLR	0.1m SLR; OPYC, 3D; North Sea; 1/2° to 1/10°; 3hr timestep	**x**
Flather and Williams (2000)	European Shelf: non-uniform Range Change (↑ & ↓); ↑ range: E. German -Bight, S. Kattagat, Bristol Channel, E. Irish Sea; ↓ range: Gulf of St. Malo	0.5m SLR; earlier POLCS3; European Shelf; 1/6°	✔ (smaller but comparable)
Flather et al. (2001)	*(as in Flather and Williams (2000))*	*(as in Flather and Williams (2000))*	*(as in Flather and Williams (2000))*
Lowe et al. (2001)	European Shelf: no significant difference in surge propagation with SLR; non -linear effect of SLR on surge propagation small and relatively unimportant	0.5m SLR; POLCSX; European Shelf- Immingham focus; 1/3°; cites agreement with Kauker (1998) results	**x**
Plüβ (2004)	"in shallow coastal areas especially SLR results in significant modulation of tidal dynamics" (von Storch and Woth,2008)	"highly increased local spatial resolutions" (von Storch and Woth 2008)	**?** (results unseen)
Lowe and Gregory (2005)	European Shelf: include effect of SLR on tide and surge but no specific results are given; states the effect was previously found to be small	0.25m & 0.33m SLR; POLCSX; European Shelf-Immingham focus; 1/3°; cites agreement with Lowe et al. (2001), Flather et al. (2001)	**x**
Sterl et al. (2009)	S. North Sea: combined tide and surge water levels and skew surge not effected by SLR; slightly faster propagation of tide and surge	2m SLR; WAQUA/DCSM98; southern North Sea- Hoek van Holland focus; 1/8°; cites agreement with Lowe et al. (2001)	**x**
Vellinga et al. (2009)	S. North Sea: 1st order approx. SLR can be added to surge heights; non -linear effects of SLR in the order of 10% of the SLR scenario	*(as in Sterl et al. (2009));* also cites agreement with Kauker and Langenberg (2000) and Lowe and Gregory (2005)	**x**
Lowe et al. (2009)	UK coast: 1st order approx. SLR can be added linearly to surge simulations; Thames: water level change <5cm, primary change in the phase for 3m SLR	3m SLR; POLCS3; UK- Thames focus; 1/8°; cites Lowe et al. (2001) when justifying addition of up to 1.9m SLR to UK Surges	**x** (except for Thames results)
Howard et al. (2010)	Thames: linear Phase & Amp. Changes (SLRs 0m- 5m); for 5m SLR total water level change <10cm, HW and Surge ~1hr earlier	multiple SLR scenarios up to 5m; POLCS3; Europe- focus Thames (Southend); 1/8°	✔ (except for linear Amp. Change)
This Paper	European Shelf: non-uniform Range Change (↑ & ↓); non-linear Phase & Amp. Changes (SLRs 2m-10m); for 2m SLR spring range change >+/-5cm at 15 ports	2m & 10m SLR; DCSMv5; European Shelf- focus 32 ports; 1/8°; cites agreement with de Ronde (1986), Flather and Williams (2000)	*N.A.*

The M_2 amplitude change plots presented in this Chapter (Figure 2.4 and 2.5) can be compared with the cotidal plots of the southern North Sea for present day SL and for a 5 m SLR scenario computed by de Ronde (1986) using an earlier version of the model used in this Chapter. Direct comparison of absolute values of amplitude change is not possible since we did not impose a 5 m SLR. de Ronde (1986) showed a northeastwardly migration of the amphidrome in the southern North Sea with SLR which is consistent with our 2 and 10 m SLR scenarios. The associated amplitude changes of de Ronde (1986) show amplitude increases in the southern North Sea, decreases further north around Den Helder and then increases again at Huibertgat. These results have similar spatial distribution to the amplitude changes presented here in Figure 2.4.

Flather and Williams (2000) present changes in mean tidal range (MTR) under a 0.5 m SLR scenario derived from the then operational UK tide-surge model. Although smaller in magnitude, comparable sign changes are presented in their results, also showing substantial increases in MTR in the German Bight, Skagerrak and Kattegat and decreases in tidal range in the Gulf of St. Malo. More modest increases in the eastern English Channel and decreases in the St Georges Channel and central North Sea are also in good agreement. However, Flather and Williams (2000) identify an increase in tidal range primarily in the eastern Irish Sea whereas Figure 2.4 shows the increase in the western Irish Sea. The second inconsistency with the Flather and Williams results is they show tidal range to increase in the Bristol Channel, although it is possible that at resonant locations tidal range may increase with certain SLRs and then decrease above some threshold.

de Ronde (1986) assumed that the changes in tidal range obtained for the English and Dutch coasts under a 5 m SLR scenario can be scaled down to give the changes with 0.2 m SLR. This approach assumes a linear response of tidal amplitude change to SLR which the results of this Chapter show to be questionable, particularly in the North Sea.

Our results for tidal amplitude changes also question previous assumptions made for storm surge changes with climate in this region. von Storch and Woth (2008) highlighted that the Kauker (1998) and Lowe et al. (2001) studies on surge propagation using coarse resolution models (1/3°) found no significant

difference between surge propagation with or without SLR. A later study by Lowe and Gregory (2005) also found that surge elevation is not significantly affected by SLR; however, this study once again used a low resolution (1/3°) model, an Immingham focus and more conservative SLR scenarios. In contrast to the results of Lowe et al. (2001) and Lowe and Gregory (2005), this Chapter finds that SLR has a significant effect on tidal water levels, and therefore is likely to affect surge generation and propagation. The present model and simulation setup play a key role in this; our model is high resolution, the SLR scenarios are larger and the tidal response across the whole shelf is considered rather than one case study location.

The Dutch Delta Committee report (Vellinga et al., 2009, Chapter II) states the effect of SLR on the surge elevations is around 10% of the SLR; referring to the work by Kauker and Langenberg (2000) and Lowe and Gregory (2005). Presently the Netherlands make a uniform 5 cm allowance in flood design levels for the effect of SLR on the surge; however, this is also intended to account for other factors such as dredging and port alterations. Contributing modelling to the Delta Committee report by Sterl et al. (2009) using the WAQUA/DCSM98 and focusing on the changes at Hoek van Holland also found that SLR did not impact the height of the storm surges. The UK Climate Projections (UKCP09, see Lowe et al. (2009)) adds SLR linearly to the surge constituent around the entire UK coastline for all SLR scenarios considered (up to 1.9m). The justification for this method is based on the Flather et al. (2001) paper which suggests this is reasonable up to 0.5 m SLR and the Howard et al. (2010) sensitivity study.

Howard et al. (2010) investigated the effect of high SLR values up to 5m on the tide and surge at the Thames Estuary grid box (Southend) using the UK operational model. The primary effect was the timing of the tide, with earlier arrival of HW by around 1 h and effect on elevation of less than 10 cm, and the authors concluded that neglecting the indirect effect of SLR is valid for SLR in excess of 2m. Their result is consistent with the results presented in this Chapter as well as those of de Ronde (1986). However, the shelf wide comparison of tidal changes in this Chapter shows that Southend (Figure 2.6d), as for Immingham and Hoek van Holland, is a location where the tidal amplitude is not particularly sensitive to SLR. The substantial alterations to

tidal amplitude with 2m SLR presented in this Chapter calls into question the validity of simply adding the SLR to the simulated UK surge elevations.

Considering that SLR has occurred throughout the 19th and 20th centuries, some evidence of changes in tidal range with SLR may be expected in the observational record. Of course the observational tide is subject to many more variables than exist in the model simulations. These include meteorological effects, land subsidence, SLR, natural morphological changes, dredging, tide gauge relocation and replacement, instrument error, datum errors and short records (Woodworth, 2010). A number of studies do manage to identify secular trends in the tidal range after natural variability (e.g. the 18.6 year nodal cycle) and sources of error have been corrected for.

Woodworth et al. (1991) provides a good European synthesis of a number of previous national studies of changes in tidal range (Cartwright, 1972; Pugh, 1982; Simon, 1982; de Ronde, 1983; Führböter and Jensen, 1985; Jensen et al., 1988; de Ronde, 1989; Führböter et al., 1990) and add their own study based on British Oceanographic Data Centre tide gauge data. Notably Woodworth et al. (1991) attempt to group changes in the tidal regimes into geographically similar areas; tidal changes within these areas are substantiated by the model results presented here. In many cases, the percentage M_2 amplitude changes with historical SLR agree (in sign) with the results of this study in the large decreases at Lerwick, St. Malo, moderate decreases at Cherbourg, large increases at Southend, Dublin, Harlingen, Delfzijl, Vlissingen, Hoek van Holland and across the German Bight. A further consistency of Woodworth (2010) with our results was that locations in the southern North Sea with tidal amplitude increase also exhibited negative changes in phase. The important agreements between the observed and our modelled changes relate to the Gulf of St. Malo being prone to large amplitude decreases, the southeast German Bight to large amplitude increases and the Dutch Wadden Sea exhibiting increases 2–3 times larger than those of the UK, Belgium or France (Woodworth et al., 1991). Several other regional studies (Hollebrandse, 2005; Dillingh, 2006; Pouvreau et al., 2006; Araújo and Pugh, 2008; Haigh et al., 2010) confirm similar tidal trends to those identified in Woodworth et al. (1991).

2.6 Conclusions

A well established and thoroughly validated regional tidal model for the European Shelf has been shown to reproduce the present day tides with a good degree of accuracy, allowing confidence in the estimates of future tidal conditions. The changes in the tide with 2m SLR are, in many cases, more substantial than suggested by previous studies. The results also show that the changes in the M_2 tidal amplitude and phase between different SLR scenarios (2 and 10 m SLR) do not scale in a linear way with respect to the imposed SLR. Changes in the S_2 amplitude are also important and influence the spring and neap tides; also other constituents including the shallow water tides exhibit change with SLR. Comparisons with the results and methods of previous studies provide new insights into the characteristics and mechanisms of the tidal regime change with SL, and those regions of the continental shelf where tides are particularly sensitive to SLR. The largest decreases of the tidal amplitude occur in the western English Channel and Bristol Channel. The largest increases occur in the North Sea and western Irish Sea. The changes in tidal amplitude are due to increases in the phase speed of the tidal wave with SLR, as well as reduced tidal energy in shallow areas where relative depth changes are large. There are consequences for both amphidromic systems and resonant gulfs.

Our results differ from previous studies which suggest that the effect of SLR on the tide and surge propagation is negligible. We propose that earlier conclusions were drawn largely from models with insufficient resolution to represent the full tidal dynamics, which used conservative SLR scenarios or based their assessment on locations unrepresentative of the entire continental shelf. Despite the importance of correctly understanding the impact of SLR on shelf tides, and the subsequent effect on storm surges, the single largest contributor to risk of coastal flooding remains the SLR itself (Lowe et al., 2009).

Tidal changes hold wide ranging implications beyond the direct physical impacts, influencing many biological, chemical and sedimentary processes. Research into future conditions involving any of these processes needs to be aware of the potential for alterations to tidal dynamics with SLR. The environmental, societal and economic implications of these results are wide

ranging; including coastal flooding, tidal renewable energy generation, sediment transport, shipping, location of tidal mixing fronts and intertidal habitats.

The design recommendations for coastal flood defences are made based on a number of factors including the amplitude of the predicted tide. It is necessary that any alteration of the astronomic tide, often considered as a constant, should be factored into the calculation of extreme water levels and hence the design specification. The recognition of this is now important as larger SLR scenarios are being considered increasingly plausible (e.g. Rahmstorf, 2007; Pfeffer et al., 2008; Convey et al., 2009). Substantial alterations to tidal amplitude and hence velocities with future SLR will alter the availability of tidal energy. This means that present day assessments of tidal energy may not be valid under future altered tidal regimes (e.g. European Commission, 1996; ABPmer et al., 2004). Changes in the tidal velocities will also have implications for the position of tidal mixing fronts which play an important role in determining primary productivity. Alterations to the position and area of the intertidal zone will have implications for those species which depend on this habitat such as the Wadden Sea home to over 10,000 species of flora and fauna (The Common Wadden Sea Secretariat, 2010).

The characteristics of future SLR will be important in determining the tidal response. Key factors will be the temporal and spatial changes in SLR. This will dictate the rapidity of the tidal changes and hence how much time is available for adaptation to mitigate the impacts. The findings of this Chapter add weight to the existing arguments for rapid mitigation of climate change in order to avoid the known impacts of SLR, such as flooding, erosion of salt marsh, saltwater intrusion, etc. (Pachauri and Reisinger, 2007). Further research into and recognition of the effect of SLR on the tide, in addition to the potential implications, is strongly recommended.

2.7 Supporting Animations

The following animations associated with this Chapter can be found on the Accompanying Materials CD or with the online version of the paper at doi:10.1016/j.csr.2011.11.011.

Animation 1. Run ID M00, 24 hours of half hourly water level maps for days 9-10 of the M_2 forced simulations with 0 m SL.

Animation 2. Run ID M02, 24 hours of half hourly water level maps for days 9-10 of the M_2 forced simulations with 2 m SLR.

Animation 3. Run ID M10, 24 hours of half hourly water level maps for days 9-10 of the M_2 forced simulations with 10 m SLR.

Animation 4. Run ID A00, 24 hours of half hourly water level maps for days 9-10 of the Fully forced simulations with 0 m SL.

Animation 5. Run ID A00, 24 hours of half hourly water level maps for days 29-30 of the Fully forced simulations with 0 m SL.

Animation 6. Run ID A02, 24 hours of half hourly water level maps for days 29-30 of the Fully forced simulations with 2 m SLR.

2.8 Supporting Figures

Tidal curves for all 32 ports in the analysis can be found Appendix 1.1 for the M_2 Runs for 0m, 2m and 10m SL scenarios and Appendix 1.2 for the Full Runs (spring and neap tides) for 0m and 2m SL scenarios (allowing comparison with tidal curves presented in other studies). A Figure with the spring and neap tidal curves for the ports in Figure 2.6 can also be found in Appendix 1.2.

3. The impact of future sea-level rise on the global tides

This Chapter has been adapted from a paper submitted for publication in Progress in Oceanography:

Pickering, M.D., Horsburgh, K.J., Blundell, J.R., Hirschi, J.J-M., Nicholls, R.J., Verlaan, M., Wells, N.C., submitted to Progress in Oceanography (Jan. 2014). The impact of future sea-level rise on the global tides.

3.1 Abstract

Tides (along with mean sea-level and surges) are a key component in coastal extreme water levels. Changes in the tides caused by SLR are therefore of importance for many applications including the analysis of coastal flooding. Motivated by a previous European Shelf study which found larger than expected non-uniform tidal changes, we investigate the effect of future SLR on the tides globally.

We address this problem using a fully global forward tidal model, OTISmpi, simulating the response of the four primary tidal constituents (M_2, S_2, K_1, O_1) to various SLR scenarios. Statistical comparisons of the modelled and observed tidal solutions show the skill of the model at representing the present day tides. The skill is improved by including model setup refinements such as a self-consistent iterative scheme for self-attraction and loading (SAL) and an internal wave drag parameterisation. The refined setup, with both good skill at representing the present day tides and a lack of any reliance on data assimilation, provides us with confidence in our future predictions. Changes in the tidal properties are assessed on a constituent basis, as well as looking at MHW and maximum range. Particular attention is paid to the changes at the 136 coastal cities with populations >1 million, where changes in water level would have the greatest significance.

Uniform SLR scenarios 0.5-10m with fixed coastlines show the tidal amplitudes in shelf seas globally to respond strongly to SLR with spatially coherent areas of increase and decrease. Changes in M_2 and S_2 occur globally in most shelf seas, whereas changes in K_1 and O_1 are confined to Asian shelves. These

scenarios show the tidal changes to be increasingly non-proportional to the SLR imposed and larger portions of the MHW changes being above proportional with higher SLR. In the 0.5m, 1m and 2m SLR scenarios changes in MHW exceed ±10% of the SLR imposed at 13, 13 and 10 of the 136 cities, respectively. Uniform SLR scenarios including coastal recession show a stronger and increasingly negative MHW response; illustrated by 14 of the 18 changes exceeding ±10% of the 2m SLR being negative. The regularly opposing signs of change between the fixed and recession cases are explained through the effect of the perturbation on the natural period of oscillation of the basin (T): SLR decreases T whereas SLR and recession increases T. These results suggest it should be possible to influence the sign of the tidal amplitude change through our coastal management strategies. The effect of non-uniform SLR, in this case fingerprints of the initial elastic response (IER) to ice mass loss, causes a modest alteration to the tidal response. The largest alterations are at high latitudes, in the near field (diminished response) and far field (amplified response) of the ice mass loss. Interestingly owing to the pattern of SLR in the fingerprints the tidal response in Asia is unchanged or amplified in all IER scenarios.

3.2 Introduction

SLR has been observed from tide gauges over the 20th century at an average rate of 1.7mm/yr (Church and White, 2011) and by altimetry over the period from 1993-2013 at average rate of 3.2mm/yr (Nerem et al., 2010). The most recent IPCC AR5 projections for 2100 SLR range from the lower end (5%) of the likely (66-100%) range for RCP2.6[1] at 0.28m to the higher end (95%) of the likely range for RCP8.5 at 0.98m (Church et al., 2014). In addition to these, medium confidence, process based model projections there are also low confidence semi-empirical models which give projections for SLR by 2081-2100 with median values from 0.4m for RCP2.6 (Jevrejeva et al. 2012) to 1.2m for RCP8.5 (Grinsted et al. 2010; Jevrejeva et al. 2012). Other methodologies suggest upper limits of 2100 SLR from 1.15m (Katsman et al., 2011) to 2.25m

[1] The IPCC AR5 uses Representative Concentration Pathways (RCPs) to explore the potential range of future emissions of important gases and aerosols. The value following RCP indicates the peak or stabilization radiative forcing in (W/m^2) for the year 2100; from the lowest RCP 2.6 to the highest RCP 8.5.

(Sriver et al., 2012). AR5 states it is virtually certain (99-100%) that SLR will continue beyond 2100 and with a low confidence estimate that SLR of 1-3m for each degree Celsius of warming will occur assuming the warming is sustained for several millennia (Church et al., 2014).

These values are global means and convey nothing about the strong spatial variability in the rates of the SLR, both observed by altimetry (Church et al., 2008) and projected (Slangen et al., submitted). Over the period 1993-2003, for example, a large portion of the spatial characteristics of the SL variability can be explained by the thermal expansion component (Church et al., 2008). SLR patterns are often found to be correlated with large scale interannual and decadal climatic variability captured by indices such as the El Nino-Southern Oscillation and the Pacific Decadal Oscillation. Therefore distinguishing the SL trend associated with climate change from the natural variability is challenging (Zhang and Church, 2012). Despite future SLR being very likely to also exhibit spatial variability (Milne et al., 2009) there are substantial uncertainties in the projected spatial characteristics (Milne et al., 2009; Slangen et al., submitted). In this Chapter, we consider the effect of future SLR on a component of extreme water levels which has received less attention- the global tides. Given the uncertainties in the future SLR patterns and the fact that ~70% of global coastlines are projected to experience a SL change within 20% of the global mean (Church et al., 2014), we initially investigate the response of tides to idealised uniform global SLR scenarios. Regional SL variability will be driven by a range of processes, including thermosteric, halosteric and ocean circulation changes, gravitational changes with ice mass loss and groundwater depletion, GIA and atmospheric loading (Church et al., 2010; Slangen et al., submitted). Future loss of ice mass will result in a response of the earth, from the IER to the longer-term viscous flow in the mantle, as well as the ocean loading. These processes, unlike aforementioned SL processes, are not subject to the uncertainties in the CMIP5 model ensemble; however the rate of future ice mass loss from Greenland and Western Antarctica is still uncertain (Rignot et al., 2011). Here we explore two predicted geometries of non-uniform SL change due to continuing ice mass variations of Greenland or Antarctica, as well as a combination of the two, using fingerprints from Mitrovica et al. (2001). These fingerprints include the static IER to present day ice mass loss and the gravitational effects but not the longer-term viscous flow effect or the

continuing GIA response to melting of late Pleistocene ice. We aim to provide justifiable scenarios for future SLR without attributing specific timescales.

Secular trends in tidal characteristics (e.g. constituent phase and amplitude) are observed in many tide gauge records (Woodworth et al., 1991; Flick et al., 2003; Hollebrandse, 2005; Dillingh, 2006; Pouvreau et al., 2006; Ray, 2006; Jay, 2009; Ray, 2009; Haigh et al., 2010a; Woodworth, 2010; Mueller, 2011). Efforts have been made to relate these observed trends in the tides to modelled changes associated with observed SLR in global tidal models (Mueller et al, 2011). Difficulties can occur as observed tides will vary due to morphological changes, dredging, harbour creation, land reclamation and tectonic effects as well as SL variability. Compounding this, the distribution of tide gauges is bias towards port locations where anthropogenic factors are most influential. Other modelling studies have tended to focus on changes in the tides associated with the large (~125m) LGM to present or Holocene (~35m) SLR (Austin, 1991; Gerritsen and Berentsen, 1998; Egbert et al. 2004; Uehara et al., 2006; Green, 2010). A selection of the methodologies and results of previous studies of future SLR and European shelf tides are reviewed in Table 2.4. Chapter 2 found substantially larger changes in the dominant semidiurnal tidal constituents of the European Shelf than previous studies (e.g. Lowe et al., 2001) with amplitudes responding non-uniformly with both increases and decreases across the shelf. Comparison with previous studies highlighted the importance of a high resolution model, a complete spatial rather than single point analysis, and a relatively large SLR scenario when identifying tidal changes with future SLR. Subsequent regional studies have also shown changes in tides with SLR in other areas such as the Bay of Fundy, USA (Greenberg et al. 2012; Pelling and Green, 2013) and the Bohai Sea, China (Pelling et al., 2013a). Regional modelling studies of changing tides are subject to issues of model intercomparability and assumptions regarding tidal characteristics around the model's open boundary. The results of Chapter 2 motivated us to investigate the effect of future SLR on the global tides using a single, global domain.

We selected the Oregon State University (OSU) OTISmpi model owing to its thorough and published validation (Egbert et al., 2004), global domain with no open boundaries, inclusion of an internal wave dissipation parameterisation (Zaron and Egbert, 2006), self-consistent iterative scheme for SAL, and lack of

requirement for any data assimilation. Global tidal models have progressed a long way since the early work of Schwiderski (1980). This has been made possible by improved observations of the global tides from satellite altimetry which complimented those from the existing tide gauge network (Provost, 2001), as well as enabling estimates of global tidal dissipation through friction at the bed and internal wave drag (Egbert and Ray, 2001).

The changes to tidal characteristics caused by future SLR presented in this Chapter have important long-term global implications. Examples include coastal flood risk and management, tidal renewable energy, sediment transport and dredging, tidal mixing fronts and intertidal ecology. By understanding the potential changes to tides, we can begin to consider where changes in tidal range will be important and how we might address this issue in these areas.

The objectives of this Chapter are: (1) to assess the effect of uniform future SLR on the four primary semidiurnal and diurnal tidal constituents; (2) to assess the importance of allowing coastal recession with SLR (i.e. changing the number of wet cells in the model domain) rather than assuming a fixed coastline; (3) to evaluate the proportionality of the tidal changes to the SLR imposed; and (4) to assess the effect on tidal changes of including non-uniform SLR associated with IER scenarios. We present global results, but also focus on regional enlargements and perform individual analysis of the 136 coastal cities with populations over 1 million in order to draw attention to localised impacts (Nicholls et al., 2008). The MHW metric is used throughout as it incorporates the combined effect of changes in all four tidal constituents; also it is regularly used in calculation of extreme water level return periods used in coastal flood defence design and by coastal engineers (Pugh and Vassie, 1980; Caires et al., 2007). Maximum tidal range is also evaluated as it is a relevant metric for renewable energy extraction.

The Chapter is structured as follows: section 3.3 gives specifics of the model setup and additional validation, the data analysis and inherent assumptions; section 3.4 presents the results of the study relating to the objectives above; before section 3.5 discusses the significance of the results and their implications, ending with the conclusions.

3.3 Method

3.3.1 Refinement of model setup and additional validation

OTISmpi solves the non-linear shallow water equations on a C-grid using a finite differences time stepping method. Details of the model and its validation can be found in Egbert et al. (2004) and references therein. Specific choices regarding model setup are detailed in this section. Egbert et al. (2004) present results for a nearly global tidal model with an open boundary in the high Arctic; here we employ the newer fully global North Pole in Greenland (NPG) version which gives similar results (Egbert et al., 2004). The lack of an open boundary condition or data assimilation in this prognostic model allows the model to evolve to a future tidal equilibrium (due to the SLR perturbation).

In advance of any adjustments to the model setup, the code was ported to the local cluster and verified using benchmark 1/8th degree, 2 constituent OTISmpi NPG solutions provided by OSU. The M_2 and K_1 tidal amplitudes were accurately replicated with a maximum grid point amplitude difference of 0.18mm - at least two orders of magnitude smaller than the tidal amplitudes of interest.

To validate the model for present day tidal solutions we make statistical comparison with the FES2004 tidal atlas solutions (Lyard et al., 2006). The FES2004 solutions are regarded as the best estimates of the global tides available, and are generated using a hydrodynamic model assimilating large datasets of tide gauge and altimetric observations (Lyard et al., 2006). We use the RMSE

$$RMSE = \sqrt{\frac{\sum_{i=1}^{n}\left[\left(Hm_i - Ho_i\right)^2\right]a_i}{\sum_{i=1}^{n} a_i}} \qquad (1)$$

where Hmi and Hoi are tidal constituent amplitudes at grid point i for the OTISmpi model solution and FES2004 observation respectively and ai is the surface area of the grid cell at point i and the Vector Difference (VD)

$$VD = \sqrt{\frac{\sum_{i=1}^{n}\left[\left(Rm_i - Ro_i\right)^2 + \left(Im_i - Io_i\right)^2\right]a_i}{\sum_{i=1}^{n} a_i}} \qquad (2)$$

where Rmi and Roi are the real parts at grid point i modelled and observed respectively; Imi and Ioi are the imaginary parts at grid point i, modelled and observed respectively. The real and imaginary parts are defined as:

$$Rm_i = Hm_i \cos(Gm_i) \quad \text{or} \quad Ro_i = Ho_i \cos(Go_i) \quad \text{and}$$

$$Im_i = Hm_i \sin(Gm_i) \quad \text{or} \quad Io_i = Ho_i \sin(Go_i)$$

where Gmi and Goi are modelled and observed phases respectively. The RMSE gives an indication of the model skill at calculating tidal amplitudes whereas the VD is a simultaneous measure of both phase and amplitude error. Global values for these statistics are given as well as the values for shelf and deep water parts; the shelf edge is defined as 200m depth. These statistics provide a quantitative means of assessing whether changes to the model setup have improved its skill at calculating present day tides.

The Default model setup in Table 3.1 includes some adjustments from the benchmarking model runs for OTISmpi mentioned above. Firstly we use version 2 (2008) of the GEBCO One Minute Grid topography (http://www.gebco.net) rather than earlier version 1. The version 2 contains a number of improvements (see documentation accompanying version 2 for details) which are reflected by small improvements (Global 0.1cm; Shelf 0.4cm; Deep water 0.1cm) in the RMSE values for M_2. Secondly the 10.4 day run length with a harmonic analysis on the last 3.5 days was extended to a 50 day run with a 10 day harmonic analysis. To ensure the model was fully spun up, run lengths up to 60 days were explored and all validation statistics converged to the Default values presented in Table 3.1 (to the nearest 0.1cm) after 50 days. This study uses a model resolution of 1/8 x 1/8 degree (~14 x 14km at its coarsest equatorial resolution). Egbert et al. (2004) showed that the M_2 elevation RMSE between OTISmpi and TOPEX/Poseidon (TPXO.5) observations largely converged by 1/8 degree with only very slight changes with a 1/12 degree.

The substantially larger computational requirement of using 1/12 degree resolution did not justify the marginal accuracy improvements.

Table 3.1. Root Mean Square Error (RMSE) and Vector Difference (VD) statistical validation (see Eq. 1 and 2 for formulations) against the FES2004 tidal atlas solutions for different physical model setups and constituents. Global statistics are also separated into Shelf (<200m) and Deep Water (>200m) parts. Details of differences between Default and Refined model setups can be found in Section 3.3.1. Statistics for the Control (also referred to as present day) setup are listed as Refined (SAL it.4).

		RMSE (cm)			VD (cm)		
Model Setup	Constituent	Global	Shelf	Deep Water	Global	Shelf	Deep Water
Default (SAL it.0)	M2	12.6	28.8	10.7	21.6	45.9	18.9
Refined (SAL it.0)	M2	15.7	28.8	14.4	20.5	43.5	17.9
Refined (SAL it.4)	M2	10.1	21.2	8.9	13.9	30.4	12.0
Refined (SAL it.4)	S2	5.0	10.8	4.3	7.1	14.8	6.3
Refined (SAL it.4)	K1	2.7	7.1	2.2	4.2	12.2	2.9
Refined (SAL it.4)	O1	2.7	5.8	2.4	3.4	8.4	2.8

With the Default model setup established (using just the M_2 and K_1 constituents), the setup was refined to improve the representation of the present day tide and to ensure the setup was appropriate for the SLR perturbation experiments. The Refined model runs were forced with, and harmonically analysed for, the dominant M_2, S_2, K_1 and O_1 constituents. These constituents have relative coefficients of 1.0 (M_2), 0.584 (K_1), 0.465 (S_2) and 0.415 (O_1); the next largest component, P_1, has a relative coefficient of only 0.193 (Pugh, 1987) therefore the cut-off for the inclusion of further tidal constituents was set at O_1. Improvements to the M_2 RMSE statistics were obtained when S_2 and O_1 were included (Global 0.3cm; Shelf 1.6cm; Deep water 0.1cm); this is most likely due to the improved levels of friction at the bed in the model with the additional constituents. The runtime increases approximately linearly with the number of components included, so despite the model's excellent parallelisation and scaling on up to (and possibly beyond) 256 compute cores, the inclusion of additional constituents with diminishing returns was deemed computationally unaffordable on the available cluster. Furthermore to satisfy the Rayleigh Criterion for the Refined set of constituents (14.77days for M_2-S_2 and 13.66days for O_1- K_1) a longer harmonic analysis window of 20days was selected.

The Refined model setup also included the internal tidal drag parameterisation described in Zaron and Egbert (2006). This yielded a substantial improvement in the M_2 RMSE (Global 5.37cm; Shelf 8.29cm; Deep water 5.34cm). This improvement is not surprising given that approximately a third of tidal energy is dissipated through internal wave drag (Egbert and Ray, 2000; Lyard et al., 2006) therefore omission of this process would lead to a substantial underestimate of the amount of energy being dissipated in the simulations. As discussed in Egbert et al. (2004) a scaling factor can be applied to the internal drag parameterisation. This was explored and although factors greater than 1 gave some improvements in the global validation statistics, the increased energy dissipation was leading to consistent under prediction of shelf tidal amplitudes therefore no scaling factor was used.

The model used the modified iterative SAL scheme described in (Egbert et al., 2004). In the Default model setup the M_2 RMSE for the tidal solution of SAL iteration 0 benefited substantially (Global 8.8cm; Shelf 10.11cm; Deep water 9.18cm) from the SAL being initialised with TPXO.5 based tidal solutions, when compared with the Refined model setup initialised with a uniform 10% reduction of the horizontal pressure gradient. The Refined model setup initialised the SAL scheme with the simple 10% correction for two reasons: (1) it was important that the model setup does not rely on any present day observational data, even if indirectly, so that the tidal regime can reach its altered future state with the SLR perturbation; (2) after four iterations of the SAL scheme the validation statistics were almost identical (<0.1cm difference) regardless of the initialisation approach. For each scenario the model was run five times with four iterations of SAL by which point the M_2 RMSE statistics were shown to have almost entirely converged (<0.07cm difference); only the tidal solutions from the 5th model run were used for analysis. The improvement of the M_2 RMSE and VD through SAL iterations with the Refined model can be seen in Table 3.1.

The bed drag coefficient (Cd) was kept at its default value of 0.003. The model also includes a drying-rewetting scheme; this yielded only slight improvements to the validation statistics and given the one third increase in computational requirement it was not included in the Refined setup.

The final RMSE and VD values for each of the four constituents including all the aforementioned model setup choices are given in Table 3.1. The satisfactorily small differences between the Refined OTISmpi and FES2004 tidal solutions, in addition to the Egbert et al. (2004) validation, give a high degree of confidence in the model's ability to represent the present day tides. The quality of the shelf validation statistics is comparable to operational regional tide-surge models (e.g. Gebraad and Philippart, 1998). Any residual model errors will exist in both the control and SLR perturbation simulations, and these will cancel out when assessing tidal changes between two model runs. In this investigation we consider amplitude changes ≥5cm or ≤-5cm to be significant.

3.3.2 Inclusion of sea-level rise (SLR)

The selection of SLR scenarios explored are given in Table 3.2, the coded abbreviations therein are used throughout this Chapter. This section discusses the subtleties of introducing SLR to the model bathymetry in different ways.

Table 3.2. Scope of SL scenarios simulated for this investigation giving the abbreviations used in the text. Advance (A) refers to the allowance for the coastline to advance in -2UA scenario. IER refers to initial elastic response (also referred to as non-uniform, NU) SLR scenarios; the ratios refer to the proportions of the average SLR coming from Greenland (G), Western Antarctic (WA) or Both (B) ice sheet melt. In addition to these scenarios a present day sea-level or Control scenario was performed for comparison.

	SLR (m)					SLF (m)
Scenario	+0.5	+1	+2	+5	+10	-2
Uniform Fixed (/Advance)	+0.5UF	+1UF	+2UF	+5UF	+10UF	-2UA
Uniform Recession	+0.5UR	+1UR	+2UR	+5UR	+10UR	
IER 2:0 Fixed			+2NUGF			
IER 0:2 Fixed			+2NUWAF			
IER 1:1 Fixed			+2NUBF			
IER 1:1 Recession			+2NUBR			

The present day bathymetry and land topography from the GEBCO version 2 dataset (2008) is 1/60th degree resolution. The OTISmpi grid generation routine averages up to 56 GEBCO depth values below MSL to give the depth of each model grid cell (1/8th degree resolution). Following practice with this model, where some of the GEBCO values are land heights, the model cell is defined as wet when >40% of the values are below MSL and the average of the wet values only is taken. This allows definition of a coastline and an ocean

mask after which all land topography is removed. The averaging of points below MSL onto a 1/8th degree grid and the 40% threshold has limitations along the Dutch coastline where in reality high narrow dykes prevent land areas below MSL from flooding. The model with no knowledge of these defended areas below MSL determines them to be wet; as a result the Dutch coastline is positioned further inland in the model than in reality. There are very few countries with extensive land areas below MSL near the coast so this is an isolated problem.

In addition to exploring the effect of multiple SLR scenarios on the tide this investigation also assesses the effect of assuming a fixed present day coastline (unrealistic, but a frequent model assumption also sometimes referred to as a vertical wall assumption) compared to allowing coastal recession with SLR. It has been suggested that the coastline SLR assumption has an important effect on the tidal response obtained (Pelling et al., 2013b).

In the fixed coastline uniform SLR scenarios from 0.5m to 10m the domain remains the same as in the present day simulation (Table 3.3- Control) and the SLR at all grid points is exactly in line with the intended perturbation. We firstly present the simpler fixed coastline SLR scenarios as a baseline against which further factors such as coastal recession can be compared. The most likely future coastline will be some combination of the two conditions, with hard engineering maintaining an approximation to the present coastline in some locations, such as the 136 cities considered in this Chapter, and coastal recession being allowed in others. In the recession scenarios, owing to the 1m vertical resolution of the GEBCO dataset only SLR scenarios >1m give any change to the wet area of the model. For this reason the 0.5m and 1m SLR recession scenarios are largely omitted from the results presented here as the results are almost identical to the 0.5m and 1.0m fixed coastline scenarios. The changes to the model domain in the recession cases for the 2m, 5m and 10m SLR are given in Table 3.3. Considering the proportions of SLR imposed the largest newly wetted area occurs with 2m SLR, with only ~1.7x and ~2.6x this area newly wetted in the 5m and 10m SLR scenarios respectively. The uniform SLR recession scenarios also include a limited number of newly dried cells; these are caused by the small lakes masking routine being invoked due to changing coastal geometry. In some coastal cells of the recession scenarios the actual SLR imposed is not in line with the intended SLR perturbation. Often

Table 3.3. The total number of wet cells in the model domain and their area for the SL scenarios in this investigation. Net changes in wet cell number and area are given and broken down into the newly wetted and newly dried cells. SLR scenarios less than 2m are not shown as the SLR must be >1m to cause any changes to the model domain due to the vertical resolution of the GEBCO topography. The limited number of newly dried cells in the SLR recession scenarios are due to specifics of the masking of small lakes routine as described in Section 3.3.2.

		Wet Cell Number		Ocean Area (km^2)		Newly Wetted		Newly Dried	
Scenario	Abbreviation	Total	Net Change	Total	Net Change	Cells	Area (km^2)	Cells	Area (km^2)
Control	Control	2736397	N.A.	361614954	N.A.	N.A.	N.A.	N.A.	N.A.
2m SLR Rec.	+2UR	2745671	9274	362879806	1264852	9283	1265590	9	739
5m SLR Rec.	+5UR	2752614	16217	363770632	2155678	16231	2156943	14	1265
10m SLR Rec.	+10UR	2761908	25511	364957948	3342993	25521	3343873	10	880
2m SLR Fixed IER Green	+2NUGF	2735990	-407	361589965	-24990	0	0	407	24990
2m SLR Fixed IER W.A.	+2NUWAF	2735845	-552	361584571	-30383	0	0	552	30383
2m SLR Fixed IER Both	+2NUBF	2736144	-253	361600678	-14277	0	0	253	14277
2m SLR Rec. IER Both	+2NUBR	2744586	8189	362902024	1287070	8644	1313422	455	26352
2m SLF Advance.	-2UA	2732440	-3957	361049329	-565625	0	0	3957	565625

Table 3.4. Due to complexities of the different coastline setups (recession and advancement) as explained in Section 3.3.2 and the non-uniform SLR scenarios, the SLR actually imposed at a particular point is not always the global SLR value. For the cities shown in Table 3.5, 3.7 and 3.13 the local SLR imposed is given for 2, 5 and 10m uniform SLR recession scenarios (UR) as well as for non-uniform SLR scenarios with a fixed coastline (+2NU_F) and with recession (+2NU_R). Although not entirely the same city list as in Table 3.12 some SLF values are also given (locations with SLF of NaN are where the model grid cell is dry with 2m SLF).

	Present Day Exposure Ranking		Local SLR (cm)			Local SLR (cm)				Local SLF (cm)
COUNTRY, City/Agglomeration	Population	Asset	+2UR	+5UR	+10UR	+2NUGF	+2NUWAF	+2NUBF	+2NUBR	-2UA
ARGENTINA, Buenos Aires	64	52	75	375	875	247	148	197	72	NaN
AUSTRALIA, Adelaide	123	103	126	249	470	194	214	204	19	-200
BANGLADESH, Chittagong	39	72	129	298	714	213	197	205	100	-200
BANGLADESH, Dhaka	14	43	12	254	754	212	196	204	-42	-200
BANGLADESH, Khulna	23	54	-111	189	689	214	198	206	-105	-200
BRAZIL, Belém	72	79	59	359	859	204	213	208	68	NaN
BRAZIL, Porto Alegre	78	83	109	397	887	245	166	205	102	-31
CAMEROON, Douala	110	128	138	438	938	195	209	202	140	-198
CANADA, Montréal	84	55	200	500	1000	21	238	130	130	-200
CHINA, Dalian	55	63	180	459	959	223	200	212	171	-200
CHINA, Fuzhou Fujian	42	48	200	489	989	232	209	220	209	-200
CHINA, Guangzhou Guangdong	2	11	186	486	942	227	205	216	202	NaN
CHINA, Shenzen	18	31	173	461	893	227	206	217	190	NaN
CHINA, Hangzhou	92	108	200	470	924	230	205	218	203	-200
CHINA, Ningbo	34	40	182	482	822	233	208	220	201	-200
CHINA, Shanghai	3	13	162	372	621	232	207	220	181	-200
CHINA, Taipei	49	59	-38	-158	143	236	212	224	-233	-200
CHINA, Tianjin	12	25	188	440	792	217	195	206	180	-190
CHINA, Xiamen	36	44	165	452	870	232	209	220	172	-190
CHINA, Zhanjiang	40	45	117	242	663	226	206	216	58	-200
NORTH KOREA, Namp'o	87	121	23	227	552	225	202	214	-25	-200
DENMARK, Copenhagen	82	53	118	279	696	29	206	117	35	-200
ECUADOR, Guayaquil	26	41	65	291	791	212	211	212	3	-200
GERMANY, Hamburg	37	18	94	388	888	31	207	119	13	NaN
GUINEA, Conakry	70	113	100	383	794	188	220	204	105	NaN
INDIA, Calcutta	6	22	173	473	973	213	198	205	178	-81
INDIA, Surat	24	46	80	346	763	205	197	201	60	NaN
INDONESIA, Palembang	48	73	87	387	887	221	230	225	112	-95
INDONESIA, Surabaya	68	88	150	369	774	220	235	227	177	-200
IRELAND, Dublin	95	62	68	354	782	-9	221	106	-27	-200
JAPAN, Hiroshima	44	24	136	303	662	237	213	225	161	-200
MALAYSIA, Kuala Lumpur	35	33	112	406	906	221	223	222	128	-71
MYANMAR, Rangoon	22	60	38	313	778	220	207	213	35	NaN
NETHERLANDS, Amsterdam	15	6	200	500	1000	32	211	122	122	-98
NETHERLANDS, Rotterdam	17	7	200	500	1000	34	210	122	122	-200
SOUTH KOREA, Inchon	43	30	128	363	793	229	205	217	130	-200
UNITED KINGDOM, Glasgow	91	68	-44	223	638	-31	220	94	94	-200
USA, Houston	67	36	100	393	893	160	239	199	99	NaN
USA, New Orleans	10	3	60	295	795	154	240	197	57	NaN
VIETNAM, Ho Chi Minh City	5	27	200	500	1000	226	218	222	221	-104

the coastal SLR imposed is less than the scenario value and in exceptional cases the perturbation causes a sea-level fall (SLF). Examples of this at particular coastal city locations can be seen in the recession columns of Table 3.4 and the cause is explained in Section 3.7.2. Over the vast majority of the domain the SLR imposed is as intended.

Early experiments allowing coastal recession with SLR led to extensive ice areas of Antarctica being erroneously flooded. These experiments called into question the accuracy of the GEBCO land/ice topography data in Antarctica. Additionally the portions of the ice anchored to land which would inundate with SLR and floating which would rise with SLR are not given in the dataset. Furthermore for the SL to rise some of the Antarctic ice would be melting. To properly include recession around the Antarctic coastline is therefore not possible with the present dataset; for this reason no recession is permitted around the Antarctic coastline by uniformly raising the land/ice topography by 15m (beyond the highest SLR scenario of 10m). This approach is further justifiable as the resonances of the shelf seas of interest, globally, are determined by their own regional geometry and bathymetry and therefore not strongly coupled to the tidal response of the Southern Ocean.

Our SLR scenarios also explore a range of non-uniform IER scenarios (Table 3.2), incorporating the SL pattern resulting from crustal rebound and alterations to the gravitational fields as determined with an elastic rebound model (Mitrovica et al., 2001). The IER scenarios presented in this Chapter all have a global average MSLR of 2m with varying proportions of this SLR (2:0, 1:1, 0:2) coming from melt of the two major ice sheets Greenland and Antarctica respectively. The patterns of non-uniform SLR used as perturbations to the bathymetry can be seen in Figure 3.36, 3.37 and 3.38. SLR values at some of the major cities in each of the IER scenarios are given in Table 3.4. In the near field of the region of mass loss SLR is small and in close proximity SLFs result, in the far field however SLR values greater than the average occur. It is noteworthy that with the mass losses occurring near the poles some tropical regions, such as Asia, experience substantial SLR under all three melt scenarios. Table 3.3 gives the domain changes in each of the four IER scenarios. When a fixed coastline assumption is made only newly dried areas occur due to SLFs in close proximity to the mass loss, around the Greenland and Western Antarctic coastlines. In the IER recession scenario where 1m

comes from each of the ice sheets, and recession is now also permitted, the net effect on the domain is overwhelmingly an increase, with somewhat more newly wetted land area than in the uniform 2m SLR recession case.

A uniform 2m SLF scenario is also tested to assess the symmetry of the tidal changes about the present day SL. The domain change under this scenario (Table 3.3) shows a substantial newly dried area. In this scenario and the IER scenarios where drying of coastal city grid cells occurs it is impossible to present tidal or SL change values, this is the cause of any null values in the tables.

3.3.3 Tidal analysis methods

Changes in tidal amplitudes are analysed at the group of 136 global port cities with populations greater than 1 million in 2005 identified in Nicholls et al. (2008) and Hanson et al. (2011). Tidal amplitude changes at these locations will be of particular importance for future coastal flood risk. Some of these cities are located up estuaries too narrow to be represented on the 1/8th degree model grid. For these locations the nearest representative wet point on the model grid was located by following the estuary downstream to the point where it meets a larger embayment included in the model domain. To accurately estimate tidal changes within the estuary a higher resolution model would be required. However, the results for representative model points can be considered as boundary conditions for the mouth of an estuarine model. It is also noted that when including coastal recession with SLR the representative model location may no longer be adjacent to the coastline, instead lying slightly offshore. For consistent analysis the tide at the same (newly offshore) point is compared however it is recognised that realistically the city location will shift inland in line with the coastal recession. In order to present manageable tables a sample of 40 of the 136 cities analysed is taken based on different selection criteria explained in the table captions (the full versions of Table 3.5, 3.6, 3.7 and 3.13 with results for all cities are available in Appendix 3.1). All city tidal change tables provide the present day population and asset exposure ranking (out of 136, with 1 being the highest) based on the Nicholls et al. (2008) assessment. When viewing the tables this provides some insight into the relative present day exposure of the cities to give context to the potential future tidal changes. Future exposure rankings will depend on future

SLR and storminess, land subsidence, population growth, economic growth, urbanisation and flood defences as well as the potential tidal changes; see Nicholls et al. (2008) and Hallegate et al. (2013) for details.

In addition to changes in the individual tidal constituents, we also present changes in the MHW. This is a useful metric for illustrating the combined effects of the constituent changes as well as for the design of coastal flood defences. Conceptually the mean of the HW values over a 15 day sea surface height (SSH) reconstruction based on four tidal constituents (Eq. 3) seems straightforward.

$$SSH_i(t) = \sum_c Hm_{ci} \cos(\omega_c t - Gm_{ci}) \quad (3)$$

where SSH at grid point i and time t (in 600s intervals up to 15 tidal days) is the sum of the four tidal constituents c (M_2, S_2, K_1, O_1) with angular frequencies ω_c in radians/s. However when you consider the variation in shape of the tidal signal at all points globally the various peaks that should be included as HWs become ambiguous. A substantial methodological development was required in order to obtain a smooth physically plausible MHW field (Figure 3.47). For an explanation of this see Section 3.7.3, and for further discussion see Haigh et al. (in prep.). As well as the absolute change in MHW with SLR the percentage change in MHW with respect to the original MHW was also assessed. The difference between MHW and mean low water, based on this method, gave the MTR. To complement these mean values the maximum tidal range for the 15 day period was also analysed. Maximum range is a useful metric for the global domain where maximum range occurs due to both spring tides (semidiurnal regions) and tropical tides (diurnal regions) (Pugh, 2004). Maximum range is an important part of the tidal cycle for both coastal flooding and renewable energy generation. The changes to the maximum HW, particularly important for coastal flooding, can be found by simply halving the maximum range change values presented. In Section 3.4.5, changes in maximum range are analysed for points deemed viable for present day tidal renewable energy. The criteria for viable renewable energy points is for tidal barrages a MTR>5m, and for tidal stream a water depth 25-100m with peak current velocities >2m/s. 15 day reconstructions of absolute current velocity times series (U) based on the

four constituents (Eq. 4) also facilitated calculations of the bed energy dissipation (ϵ) in the various SLR scenarios (Eq. 5).

$$U_i(t) = \sqrt{\left[\sum_c Hum_{ci}\, cos\left(\omega_c t - Gum_{ci}\right)\right]^2 + \left[\sum_c Hvm_{ci}\, cos\left(\omega_c t - Gvm_{ci}\right)\right]^2} \quad (4)$$

where U (m/s) at grid point i and time t (in 600s intervals up to 15 tidal days) is the sum of the four tidal constituents c (M_2, S_2, K_1, O_1) for the u component (amplitude (Hum) and phase (Gum)) and the v component (amplitude (Hvm) and phase (Gvm)) of velocity.

$$\varepsilon_i = \rho C d \overline{U_i^3} \quad (5)$$

where ϵ at grid point i is water density (ρ=1028kg/m^3) multiplied by the bed drag coefficient (Cd=0.003) and U cubed averaged over the 15 tidal day reconstruction.

Whether the tidal changes are proportional to the SLR imposed is of interest to stakeholders who may wish to interpolate between or extrapolate from the tidal changes for particular SLR scenario(s). Using the range of uniform SLR scenarios in the Chapter (Table 3.2) we assess proportionality using the normalised ratio (with respect to the SLR scenarios) of the change for any tidal property (M_2, S_2, K_1, O_1, MHW, Maximum Range) for the SLR scenario to the change in that property with 0.5m SLR. Allowing a 10% range about a ratio of unity we define a proportional response as, for example, a MHW change 9-11cm with a 1m SLR if the change with 0.5m SLR was 5cm. Ratios >1.1 (<0.9) indicate that the response is above (below) proportional and a ratio <0 indicates that the response has changed sign between the SLR scenarios and is also therefore non-proportional. This definition of proportionality is used for the stars in Table 3.5-3.7, 3.8, 3.9, 3.10 and 3.11 and Figure 3.23-3.34. These proportionality assessments are only valid for a particular model point and say nothing of the proportionality at surrounding points. Two adjacent points could both be classed as proportional but have totally different rates or signs of change; the tidal change with SLR at one point cannot therefore be scaled with respect to the SLR to represent the tidal change at another point.

3.4 Results

The results for tidal changes assuming uniform SLR and a fixed coastline are presented first (Section 3.4.1) before exploring the effect of including coastal recession (Section 3.4.2) and considering the changes in terms of their percentages and proportionality (Section 3.4.3). Tidal changes with non-uniform SLR due to IER are presented next (Section 0). Finally the results showing implications for marine renewable energy (Section 3.4.5) and comparisons with previous studies are made (Section 3.4.6).

3.4.1 Effect of uniform SLR with a fixed coastline on the tides

This section presents results for the effect of uniform SLR on the tide assuming a fixed present day coastline (UF scenarios- definitions of scenario abbreviations are given in Table 3.2). The response of the four primary tidal constituents, M_2, S_2, K_1 and O_1, to a 2m SLR is shown in Figure 3.2-3.8. The Figure 3.2-3.8 colour scales have limits scaled in proportion to the constituents' equilibrium tidal amplitudes in order to show more clearly the changes in the smaller amplitude constituents. The present day amplitude of each tidal constituent is given in Figure 3.1-3.7 allowing qualitative assessment of whether large tidal changes occur where present day amplitudes are already large; further analysis of relative tidal changes is given in Section 3.4.3. Figure 3.2 shows the M_2 response to be widespread globally with spatially coherent non-uniform amplitude changes of both signs in many shelf seas. Response in the deep ocean, where the relative depth change with SLR is small, is generally of a much smaller magnitude but with a much greater horizontal length scale. Shelf seas showing particularly strong M_2 response include the NW European Shelf, Persian Gulf, Andaman Sea (Burma), Gulf of Thailand, South China Sea, East China Sea, Sea of Okhotsk (Russia), Java Sea, Timor Sea, Arafura Sea (Australia), Bass Strait (Tasmania), Barents Sea (Svalbard), Laptev Sea (Russia), Bering Sea (Alaska), Northwest Passages (Canada), Hudson Bay (Canada), Hudson Strait (Canada), Gulf of St Lawrence (Canada) and the Patagonian Shelf. Additionally significant but localised changes at the coast may occur but not be easily identifiable in the global plots: regional figures and city tables illustrate these changes. Changes at large coastal city locations can be seen in the M_2 +2UF column of Table 3.5 (full table Appendix 3.1). At 14 locations amplitude changes of ≥20cm or ≤-20cm (≥10% of the SLR imposed) occur, with the largest

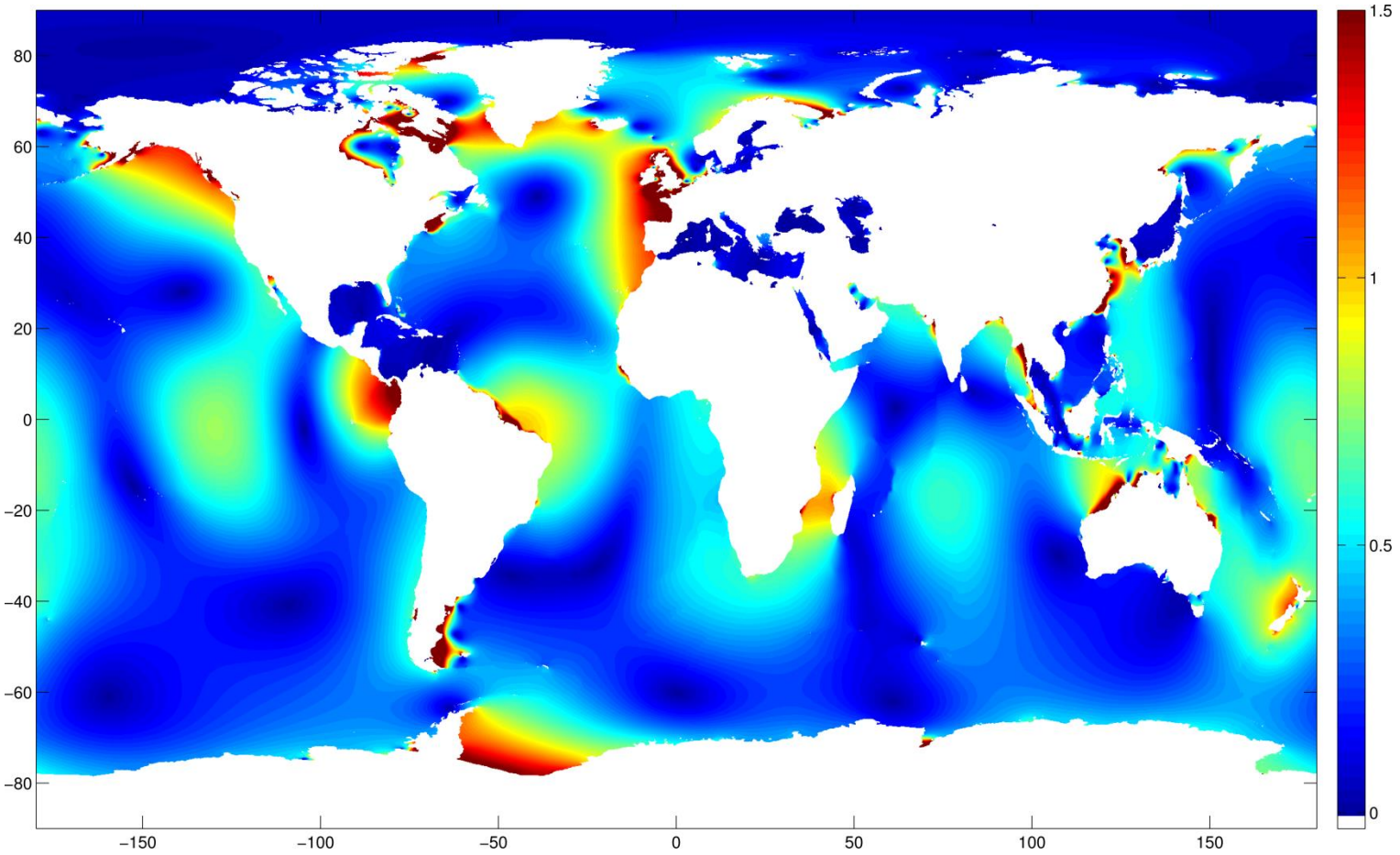

Figure 3.1. M_2 tidal amplitude (m) with present day sea-level (Control). M_2 amplitude changes presented in Figure 3.2 are relative to these values.

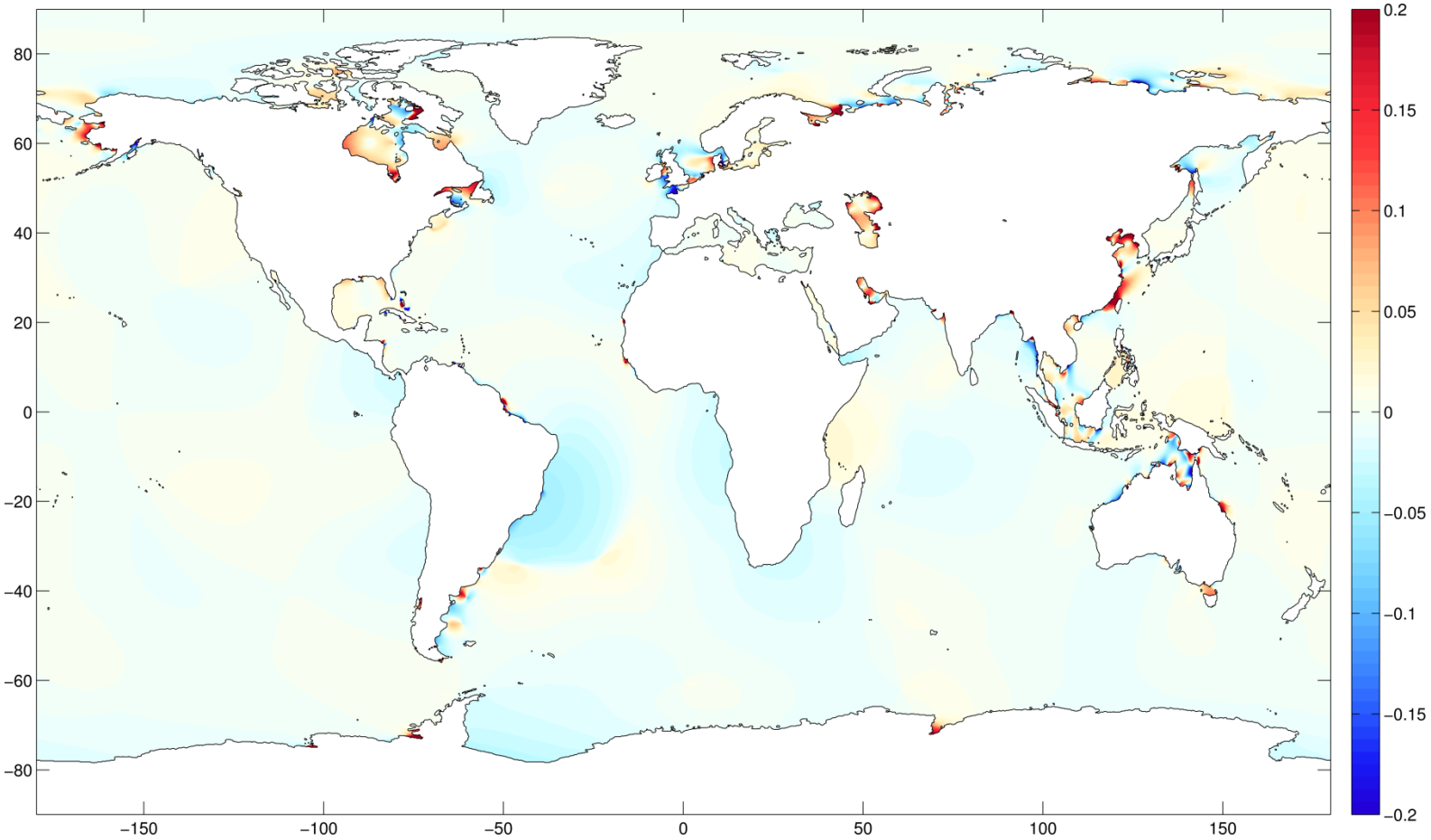

Figure 3.2. Change in M_2 amplitude (m) with 2m of uniform SLR assuming a fixed present day coastline (+2UF) (increases - red, decreases - blue). Colour scale limits between constituents scaled in proportion to equilibrium tidal amplitudes. For coastal city changes see Table 3.5.

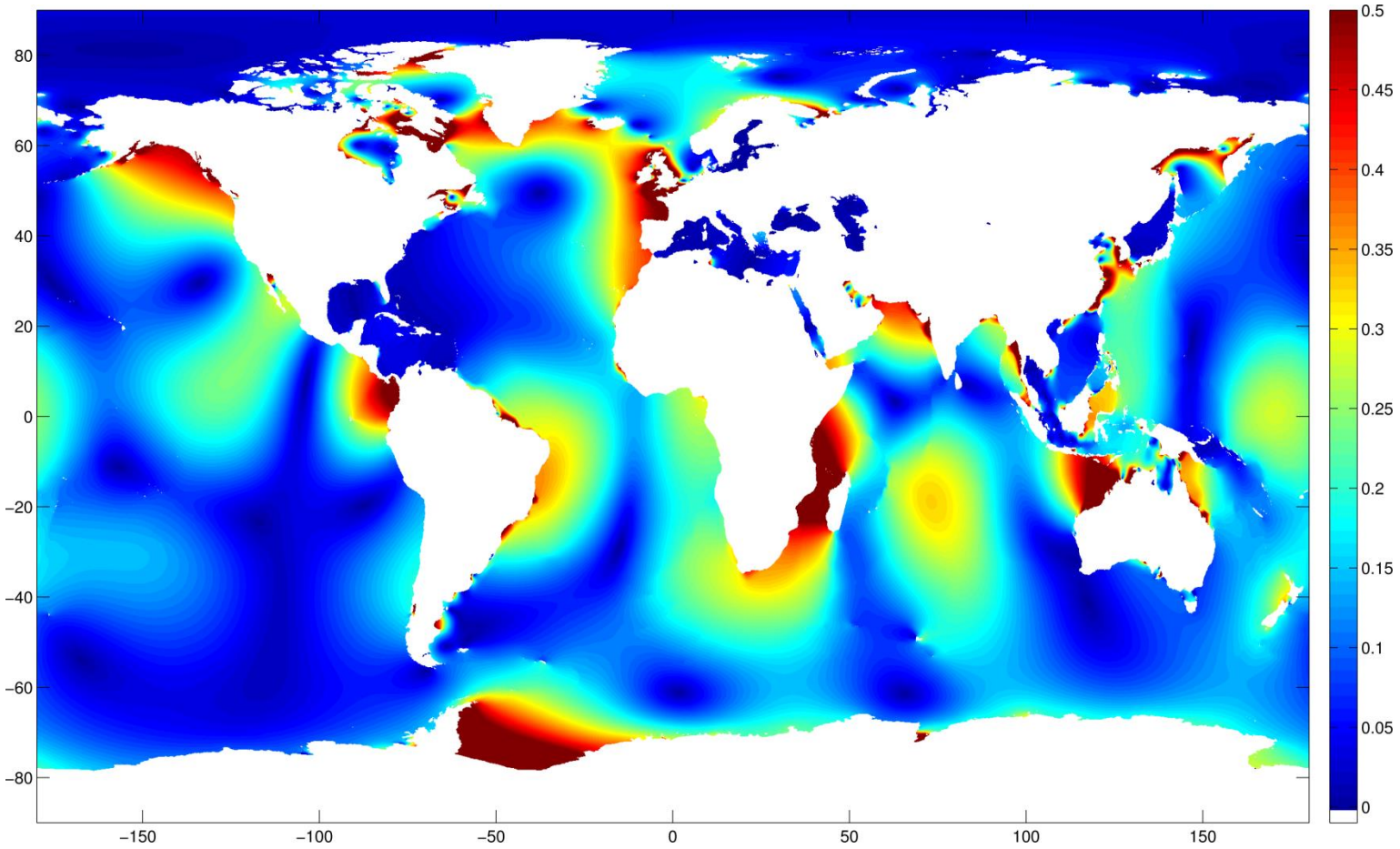

Figure 3.3. S_2 tidal amplitude (m) with present day sea-level (Control). S_2 amplitude changes presented in Figure 3.4 are relative to these values.

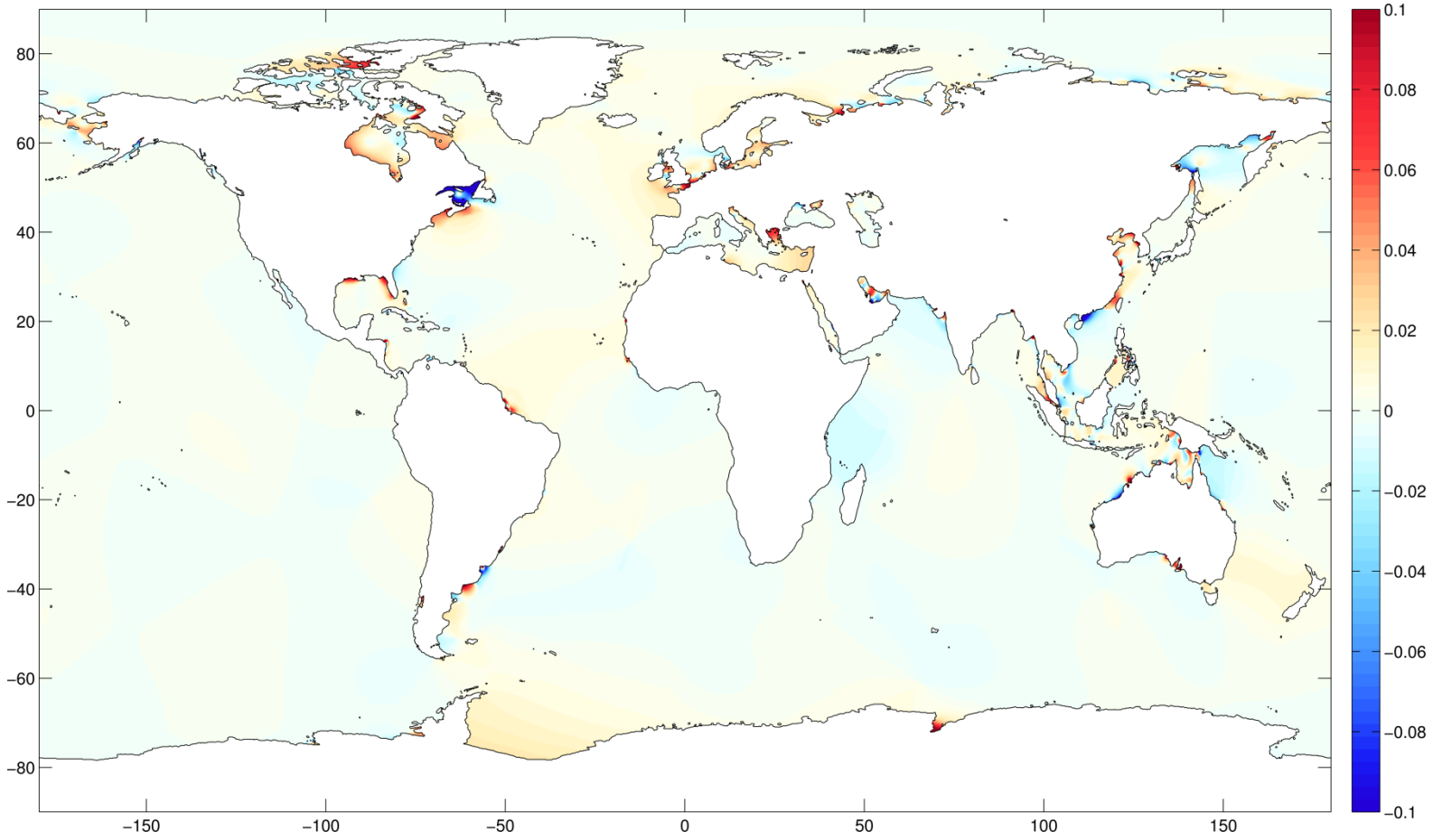

Figure 3.4. Change in S_2 amplitude (m) with 2m of uniform SLR assuming a fixed present day coastline (+2UF) (increases - red, decreases - blue). Colour scale limits between constituents scaled in proportion to equilibrium tidal amplitudes. For coastal city changes see Table 3.5.

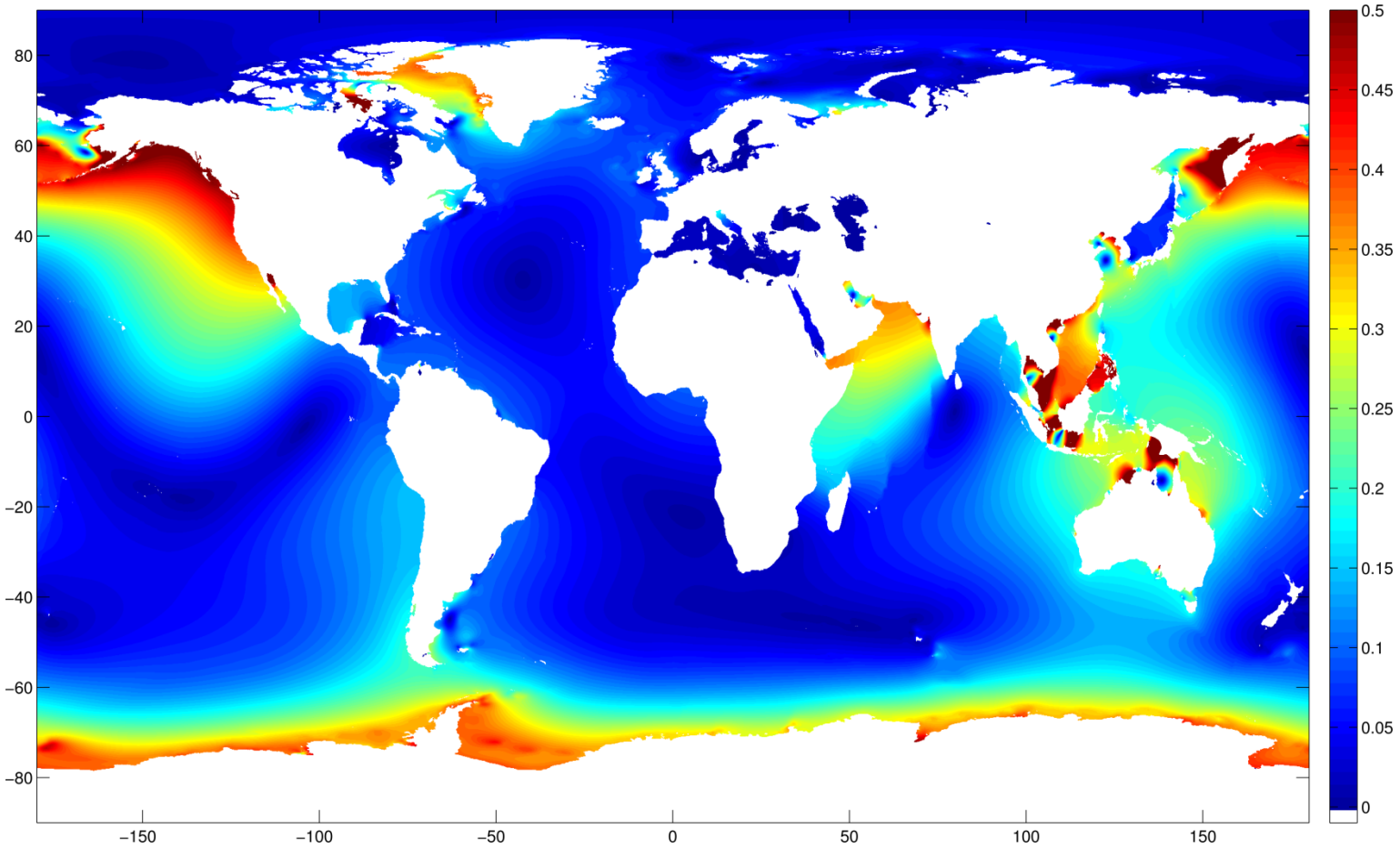

Figure 3.5. K_1 tidal amplitude (m) with present day sea-level (Control). K_1 amplitude changes presented in Figure 3.6 are relative to these values.

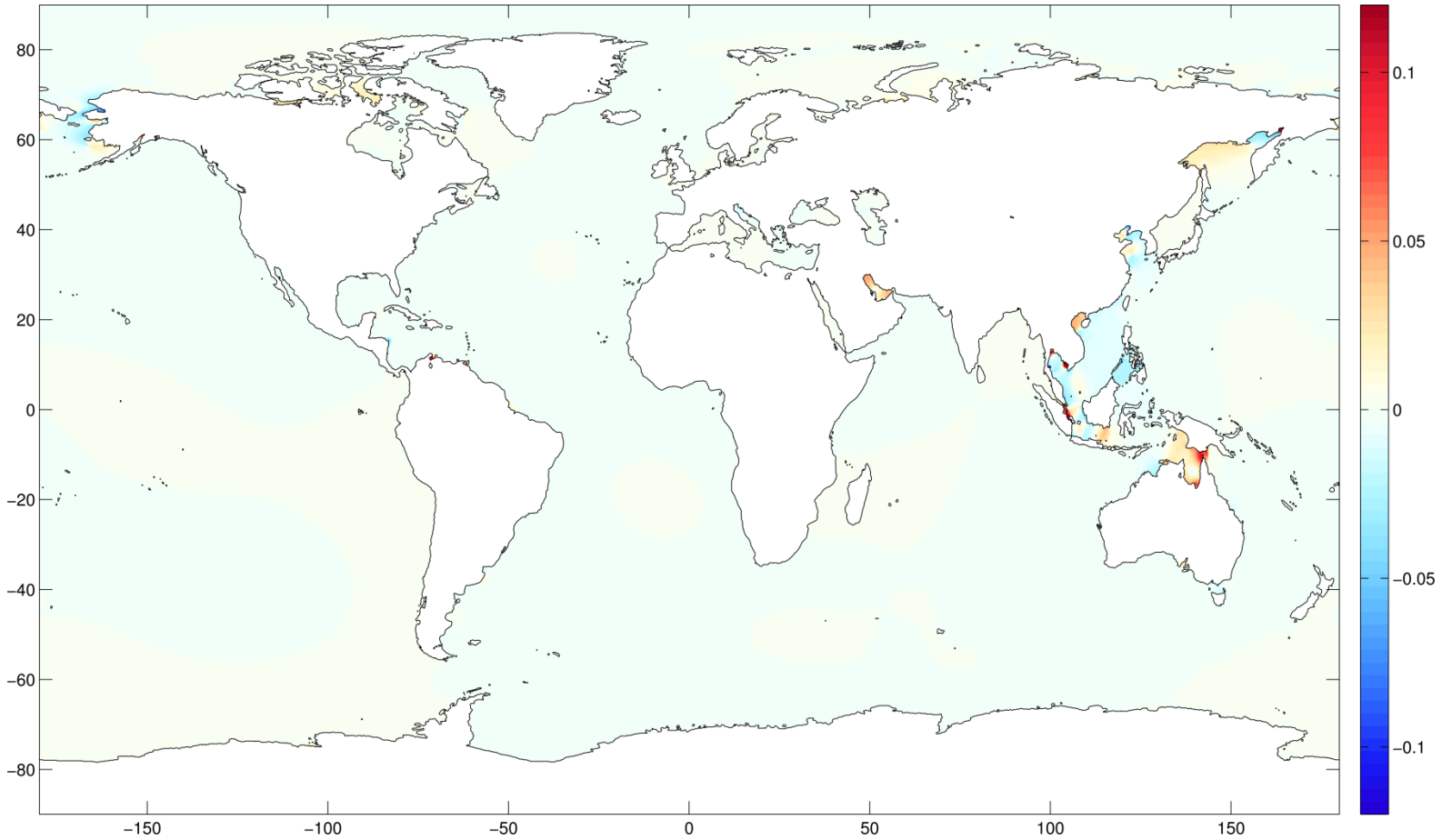

Figure 3.6. Change in K_1 amplitude (m) with 2m of uniform SLR assuming a fixed present day coastline (+2UF) (increases - red, decreases - blue). Colour scale limits between constituents scaled in proportion to equilibrium tidal amplitudes. For coastal city changes see Table 3.5.

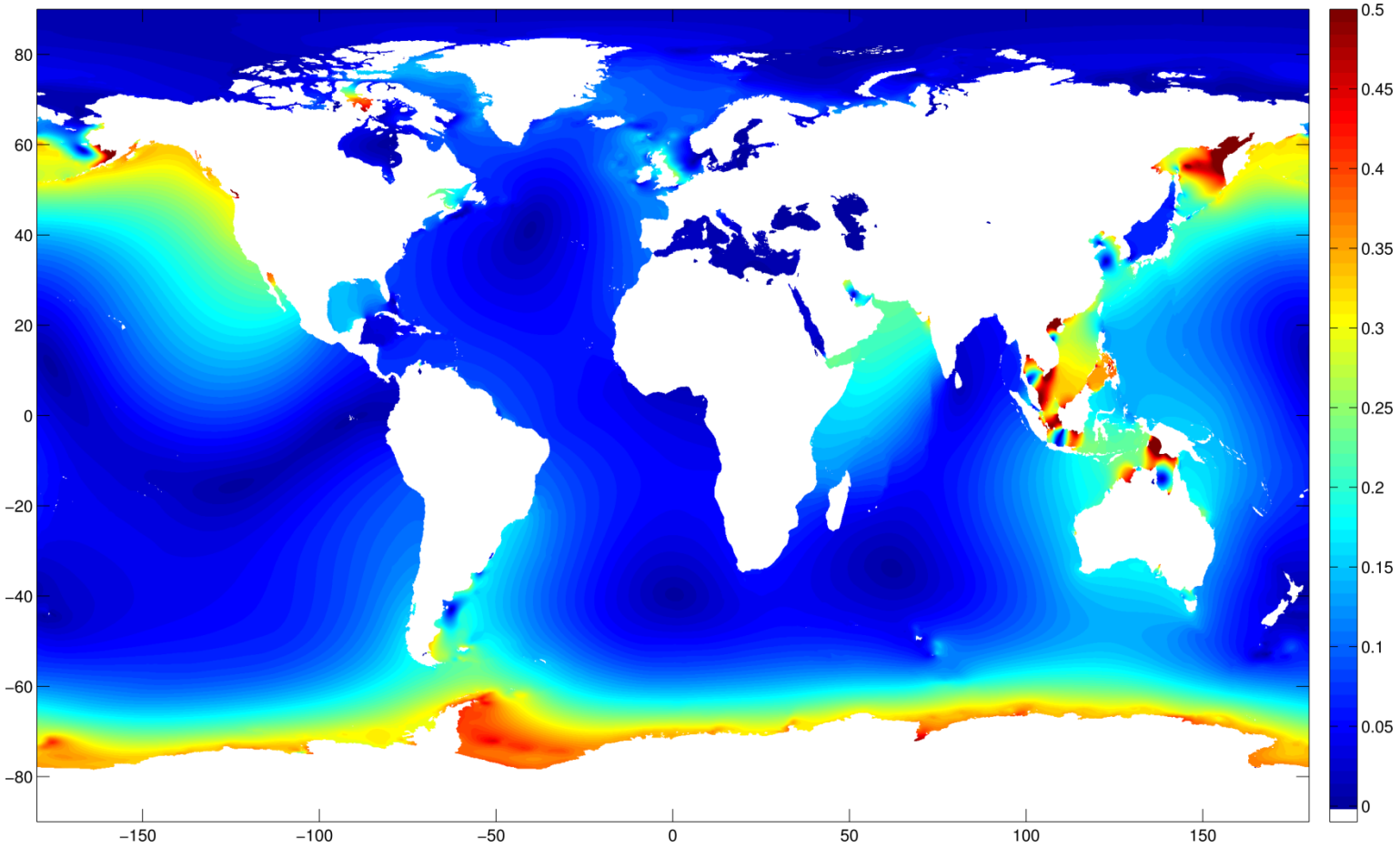

Figure 3.7. O_1 tidal amplitude (m) with present day sea-level (Control). O_1 amplitude changes presented in Figure 3.8 are relative to these values.

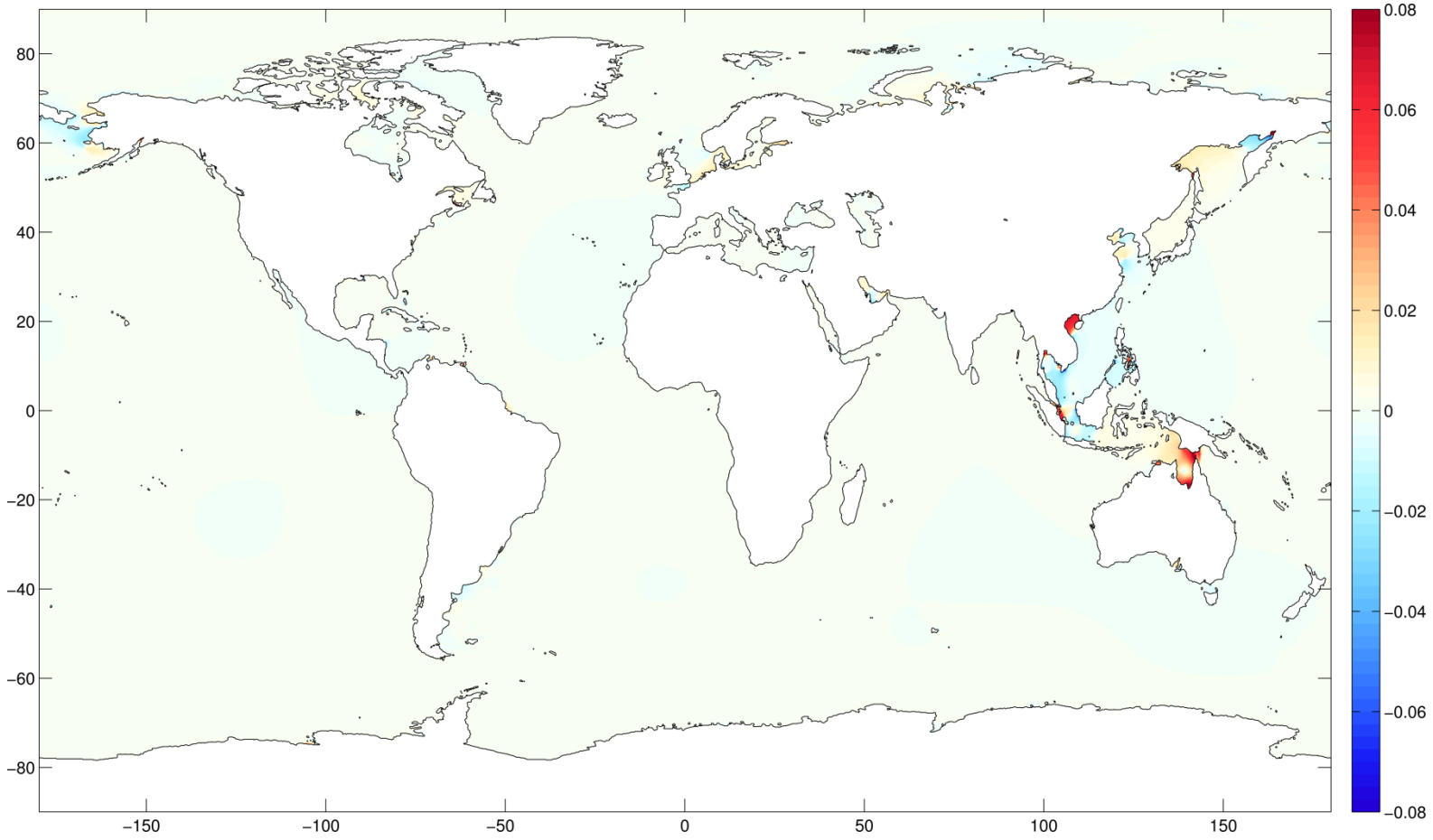

Figure 3.8. Change in O_1 amplitude (m) with 2m of uniform SLR assuming a fixed present day coastline (+2UF) (increases - red, decreases - blue). Colour scale limits between constituents scaled in proportion to equilibrium tidal amplitudes. For coastal city changes see Table 3.5.

Table 3.5. Changes in the four tidal constituents M_2, S_2, K_1, O_1, the MHW and the Maximum Range over a 15 day period with 2m of Uniform SLR both assuming a fixed present day coastline (+2UF) and permitting the coastline to recede (+2UR). This subset of 40 of the 136 coastal cities with populations >1 million is based on the locations with the 20 largest changes in MHW with a fixed coastline and with coastal recession (where MHW changes are top 20 for both coastal setups the next largest change is taken). Stars after the change value indicate a non-proportional response (outside ± 10%) with respect to the 0.5m SLR change scaled according to the SLR.

	Present Day Exposure Ranking		M2 (cm)			S2 (cm)			K1 (cm)			O1 (cm)			MHW (cm)			Max Range (cm)		
COUNTRY, City/Agglomeration	Population	Asset	Control	+2UF	+2UR	Control	+2UF	+2UR	Control	+2UF	+2UR	Control	+2UF	+2UR	Control	+2UF	+2UR	Control	+2UF	+2UR
ARGENTINA, Buenos Aires	64	52	78	-4 *	-51 *	68	-20 *	-47 *	13	-2 *	-3 *	22	0 *	-6 *	98	-15 *	-64 *	312	-46 *	-195 *
AUSTRALIA, Adelaide	123	103	54	-13 *	-31 *	73	13 *	38 *	23	-1 *	-1 *	21	0 *	-1 *	86	0 *	17 *	318	-4 *	11 *
BANGLADESH, Chittagong	39	72	153	16 *	-13 *	49	5 *	-6 *	20	0 *	-1 *	8	0 *	0 *	147	16 *	-13 *	433	43 *	-37 *
BANGLADESH, Dhaka	14	43	140	26	-1 *	41	9	0 *	20	0	0 *	8	0 *	0 *	134	25	-1 *	393	71	-1 *
BANGLADESH, Khulna	23	54	88	-4 *	19 *	34	-1 *	6 *	16	0	1 *	5	0	0 *	87	-4 *	19 *	266	-9 *	51 *
BRAZIL, Belém	72	79	251	28 *	-142 *	44	11	-23 *	9	1 *	-4 *	10	2 *	-4 *	233	28 *	-131 *	614	83 *	-340 *
BRAZIL, Porto Alegre	78	83	6	1 *	3 *	10	9	12 *	5	0 *	8 *	9	1 *	14 *	14	7	18 *	50	18 *	65 *
CAMEROON, Douala	110	128	65	-3 *	-15 *	33	-1 *	-8 *	9	0 *	0 *	2	0	0 *	70	-3 *	-16 *	204	-8 *	-46 *
CANADA, Montréal	84	55	109	23 *	154 *	160	-35 *	-92 *	24	0 *	-2 *	25	1 *	-2 *	182	-8 *	66 *	571	2 *	150 *
CHINA, Dalian	55	63	49	22	-1 *	15	4 *	-1 *	32	-2 *	-2	22	-1 *	-1 *	67	12	-3 *	197	47 *	-9 *
CHINA, Fuzhou Fujian	42	48	238	23 *	7 *	77	5 *	2 *	34	-1	-1 *	27	0	0 *	234	22	6 *	704	54	14 *
CHINA, Guangzhou Guangdong	2	11	116	-29 *	-29 *	60	-27 *	-13 *	48	-3 *	-4 *	38	-2 *	-3	121	-23 *	-19 *	480	-120	-94 *
CHINA, Shenzen	18	31	92	-17 *	-17	46	-18 *	-6 *	45	-2 *	-3 *	35	-1 *	-2 *	100	-11 *	-8 *	395	-74 *	-54
CHINA, Hangzhou	92	108	173	15	24 *	49	8	12 *	30	-1	1 *	24	-1 *	1 *	166	16	25 *	520	42	72 *
CHINA, Ningbo	34	40	64	35	21 *	19	10	6 *	26	1 *	2 *	20	0 *	1 *	68	28	20 *	232	88	60 *
CHINA, Shanghai	3	13	203	-22 *	-24	79	-5 *	-4 *	26	-1 *	-1 *	18	-2 *	-1 *	205	-21 *	-22	623	-59	-61
CHINA, Taipei	49	59	86	17	9 *	24	4 *	2 *	24	0	-1 *	19	0	0 *	85	16	8 *	276	42	21 *
CHINA, Tianjin	12	25	59	25 *	8 *	14	5 *	2 *	29	1 *	1	23	0 *	2 *	67	12 *	1 *	225	60 *	24 *
CHINA, Xiamen	36	44	217	17 *	2 *	64	4 *	1 *	38	-2	-2 *	30	-1 *	-1 *	212	15	2 *	640	36	0 *
CHINA, Zhanjiang	40	45	101	-13 *	-10 *	54	-21	-4 *	47	-2	-2 *	37	0 *	-1 *	112	-12 *	-7 *	435	-69 *	-34 *
NORTH KOREA, Namp'o	87	121	171	18	-7 *	53	3	0 *	46	-3 *	-2 *	31	-1 *	0 *	167	12 *	-6 *	548	37	-18 *
DENMARK, Copenhagen	82	53	29	9 *	16 *	4	4 *	1 *	1	0 *	0 *	1	0 *	0 *	27	9 *	15 *	67	29 *	36 *
ECUADOR, Guayaquil	26	41	157	5 *	-75 *	49	7 *	-19 *	11	0 *	-2 *	3	0 *	-1 *	152	7 *	-71 *	428	23 *	-193 *
GERMANY, Hamburg	37	18	167	-2 *	-104 *	35	4	-18 *	4	0 *	-1 *	11	2	-2 *	156	-1 *	-96 *	425	7 *	-247 *
GUINEA, Conakry	70	113	159	-21 *	-15 *	54	-8 *	-5 *	8	0 *	0	4	0 *	0 *	156	-21 *	-15 *	435	-57 *	-41 *
INDIA, Calcutta	6	22	125	-12 *	-40 *	50	-4 *	-21 *	17	0 *	0 *	5	0 *	0 *	127	-12 *	-43 *	373	-31 *	-119 *
INDIA, Surat	24	46	200	11 *	39 *	123	4 *	-8 *	50	0 *	-1 *	35	0 *	-2 *	228	9 *	26 *	759	32	55 *
INDONESIA, Palembang	48	73	16	1 *	-10 *	5	2 *	-3 *	50	15 *	-3 *	43	7 *	-3 *	76	18 *	-10 *	192	43 *	-18 *
INDONESIA, Surabaya	68	88	190	-22 *	-46 *	78	-14 *	-28 *	45	1	6 *	36	-1	4 *	194	-25	-50 *	651	-69	-136 *
IRELAND, Dublin	95	62	133	12	-24 *	36	5	-6 *	9	0 *	0	16	0 *	0 *	129	12	-22 *	363	34	-60 *
JAPAN, Hiroshima	44	24	163	-9 *	-50 *	79	-4 *	-32 *	29	0	1 *	22	0 *	2 *	175	-10 *	-58 *	539	-28 *	-146 *
MALAYSIA, Kuala Lumpur	35	33	128	4 *	-16 *	42	6 *	-3 *	30	0 *	-1 *	15	0 *	-1 *	127	6 *	-15 *	396	22 *	-42 *
MYANMAR, Rangoon	22	60	162	32	-8 *	54	13	1 *	20	1 *	0 *	9	1 *	0 *	158	33	-6 *	471	92	-13 *
NETHERLANDS, Amsterdam	15	6	84	7 *	-38 *	18	5 *	-7 *	6	0	-1 *	16	2	-4 *	76	7 *	-33 *	228	24 *	-94 *
NETHERLANDS, Rotterdam	17	7	144	-9 *	-75 *	29	2 *	-14 *	7	0 *	-2 *	20	1 *	-5 *	131	-8 *	-69 *	376	-17 *	-185 *
SOUTH KOREA, Inchon	43	30	364	12 *	-13 *	109	8 *	3 *	42	-2 *	-1 *	31	-1 *	0 *	353	13	-10 *	1045	37 *	-22 *
UNITED KINGDOM, Glasgow	91	68	138	5 *	-30 *	37	3 *	-10 *	8	0 *	0 *	15	0 *	0 *	133	5 *	-29 *	376	17 *	-79 *
USA, Houston	67	36	66	-25 *	-33 *	16	13 *	-3 *	18	-2 *	-2 *	18	-1 *	-2 *	65	-15 *	-30 *	213	-31 *	-84 *
USA, New Orleans	10	3	1	6 *	3 *	0	2	1 *	11	7 *	12 *	12	10	8 *	16	14 *	16 *	46	41 *	42 *
VIETNAM, Ho Chi Minh City	5	27	111	-31 *	-40 *	56	-14 *	-31 *	67	-2 *	-15 *	54	-3	-10 *	128	-27 *	-46 *	480	-95 *	-171 *

increase (35cm) at Ningbo and the largest decrease (-31cm) at Ho Chi Minh City. The largest M_2 increase and decrease at locations with top 20 population exposure are 26cm at Dhaka and -31cm at Ho Chi Minh City. The largest increase and decrease at locations with top 20 asset exposure are 7cm at Amsterdam and -29cm at Guangzhou Guangdong.

The S_2 constituent (Figure 3.4) also shows a global response of non-uniform coherent changes of both signs in many shelf seas with a slightly reduced overall magnitude compared with M_2. Shelf seas where the S_2 constituent responds to SLR less strongly than M_2 include the Andaman Sea, Java Sea and Bass Strait. Shelf seas that show a greater response for S_2 than for M_2 include the Aegean Sea, Gulf of Maine (USA) and Gulf of Mexico. In some locations M_2 and S_2 changes are of the same sign (e.g. Taiwan Strait and East China Sea), whereas in others the changes are of opposing sign (e.g. the western English Channel and northern Gulf of St Lawrence). Changes at large coastal city locations can be seen in the S_2 +2UF column of Table 3.5. At 12 locations amplitude changes of ≥10cm or ≤-10cm (≥5% of the SLR imposed) occur, with the largest increase (13cm) at Adelaide and the largest decrease (-35cm) at Montreal. The largest increase and decrease at locations with top 20 population exposure are 9cm again at Dhaka and -27cm at Guangzhou Guangdong. The largest increase and decrease at locations with top 20 asset exposure are 5cm again at Amsterdam and -27cm again at Guangzhou Guangdong. Significant (≥5cm or ≤-5cm) M_2 and S_2 changes of opposing sign are also apparent at Adelaide, Montreal and Houston.

The K_1 response to SLR (Figure 3.6) also shows non-uniform spatially coherent changes of both signs but with a more limited geographic spread. Changes to K_1 are apparent in the Persian Gulf, Gulf of Thailand, South China Sea, Sulu Sea (Philippines), East China Sea, Sea of Okhotsk, Java Sea, Arafura Sea, Timor Sea and Bering Sea. These are largely areas where the present day K_1 amplitudes are at their largest. Few coastal cities show significant (≥5cm or ≤-5cm) change in K_1 amplitude; Palembang and New Orleans show changes of 15cm and 7cm respectively. Significant K_1 changes not shown in Table 3.5 are 5cm at Kuwait City and 9cm at Maracaibo.

The effect of SLR on the O_1 constituent (Figure 3.8) shows similar spatial characteristics to that of K_1, but with a reduced response in the Persian Gulf

and the Timor Sea and a change in the sign of the response in the Java Sea. Again, the only coastal cities experiencing a significant response are Palembang and New Orleans (7cm and 10cm respectively). Significant O_1 changes not shown in Table 3.5 are -5cm at Maracaibo and 6cm at Hai Phong.

The MHW change shows the combined effect of the changes to the tidal constituents averaged over a 15 day period. Figure 3.9 shows the MHW change to behave in a spatially similar way to changes in the tidal constituents, with areas of both increase and decrease, largely in the shelf seas. The horizontal length scale of the change is again much larger in the deep ocean than on the shelf. Comparison of the MHW change plots for 0.5m and 1m (not shown) with 2m SLR showed almost identical spatial characteristics. The regional 2m SLR MHW changes (Figure 3.11-3.16) can therefore also be used as an indication of the nature of the change with 0.5m and 1m SLR, although the magnitude of the change is smaller and may not fit the fairly rigorous definition of proportionality (see Section 3.3.3). There are limited exceptions to this: for example, the spatial patterns of MHW change in the North Sea with 0.5m and 1m SLR differ with those with 2m SLR, and in the Baltic Sea (Sweden) changes are larger with 1m than with 2m SLR. Furthermore, although the magnitudes were larger (Figure 3.17) the spatial characteristics and signs of the 2m SLR regional maximum range change plots (not shown) were also almost identical to the MHW change plots, with the exception of small differences south of Papua, the Gulf of Carpentaria (Australia), Gulf of St. Lawrence and Bay of Fundy. The descriptions given of the regional MHW changes therefore largely also apply to the 0.5m and 1m SLR MHW changes and 2m SLR maximum range changes.

Figure 3.11 shows a significant MHW response for Europe. There are substantial MHW increases in the western Irish Sea, eastern English Channel, southern and eastern North Sea and southwest Baltic Sea and substantial decreases in the western English Channel, Celtic Sea, Bristol and St. George's Channel, North Sea, Skagerrak (Norway) and Kattegat (Denmark). Figure 3.12 shows localised MHW responses around Atlantic African and Indian Ocean coasts where substantial MHW increases occur on the northern coast of Mauritania, the coast of Guinea-Bissau and in the Persian Gulf; substantial decreases occur on the coast of Guinea, Sierra Leone, southwest coast of Saudi Arabia and east coast of Pakistan. Also noteworthy, because of their extent, are

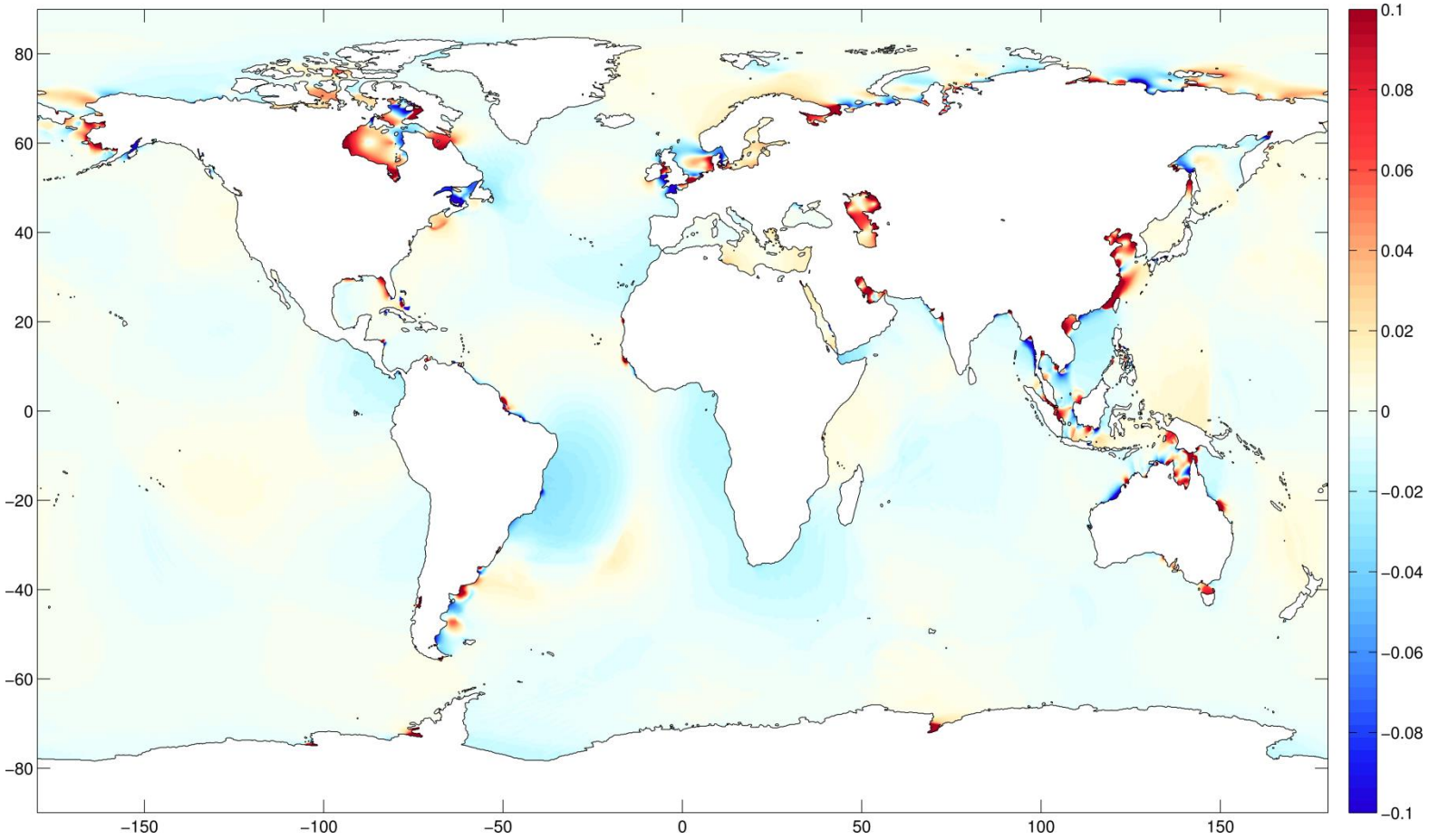

Figure 3.9. Change in MHW (m) with 2m of uniform SLR assuming a fixed present day coastline (+2UF) (increases - red, decreases - blue). For coastal city changes see Table 3.5 and 3.6.

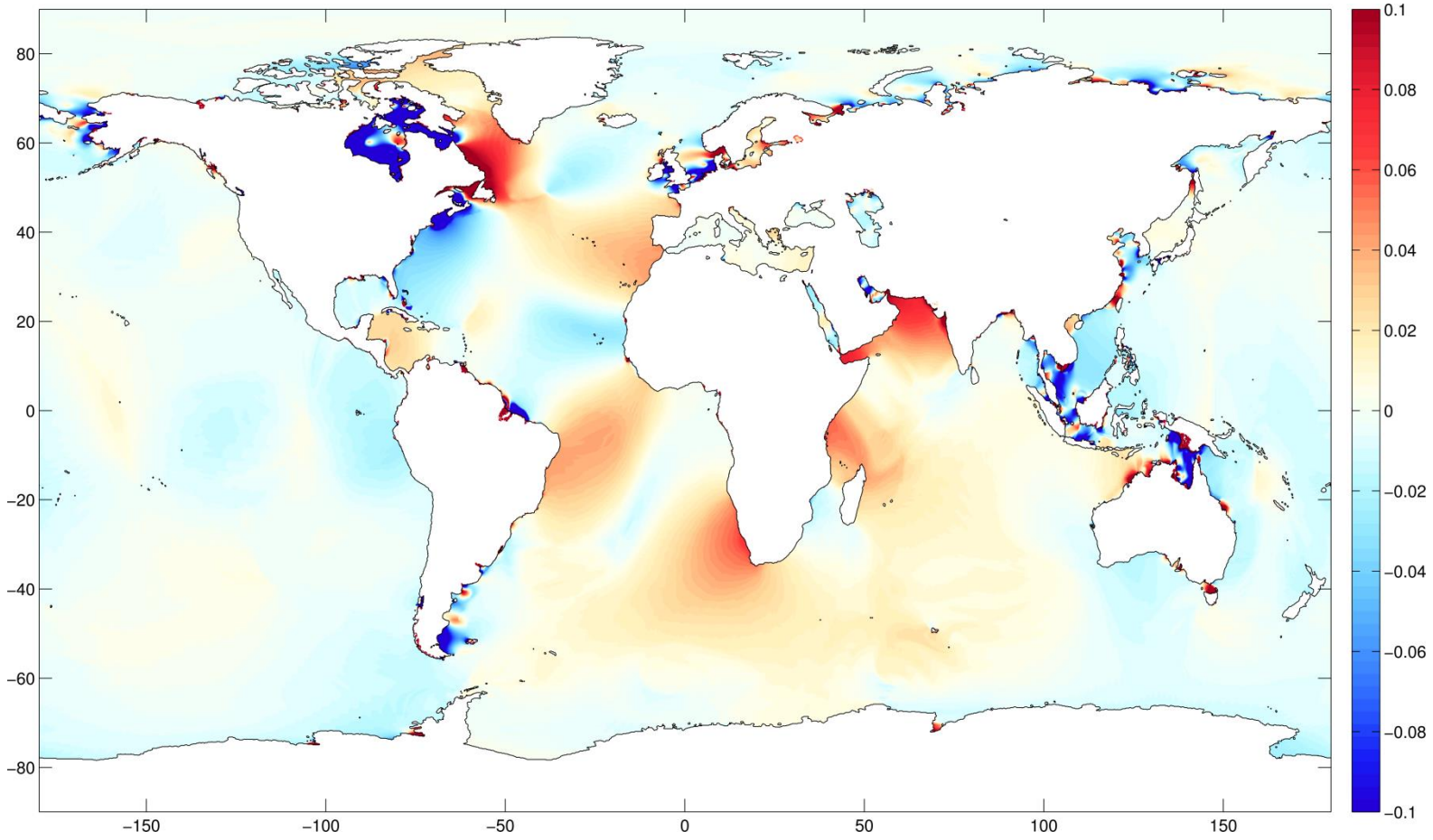

Figure 3.10. Change in MHW (m) with 2m of uniform SLR permitting coastal recession (+2UR), except around Antarctica (increases - red, decreases - blue). For coastal city changes see Table 3.5. For newly wet areas in the SLR scenario the now calculable MHW values are plotted on the positive part of the colour scale.

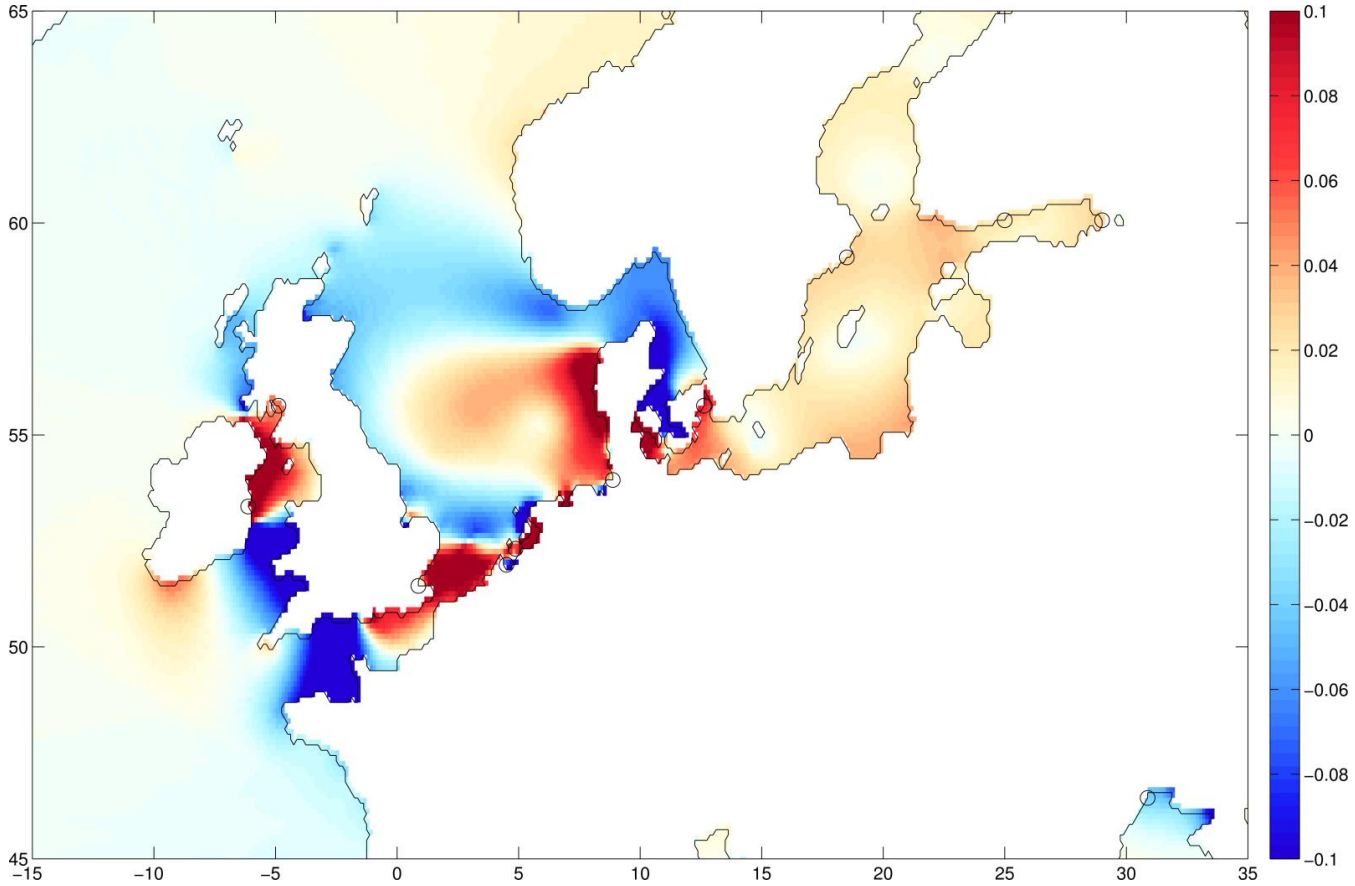

Figure 3.11. European change in MHW (m) with 2m of uniform SLR assuming a fixed present day coastline (+2UF) (increases - red, decreases - blue). For coastal city changes, marked by the black circles, see Table 3.5 and 3.6. (Regional zoom of Figure 3.9)

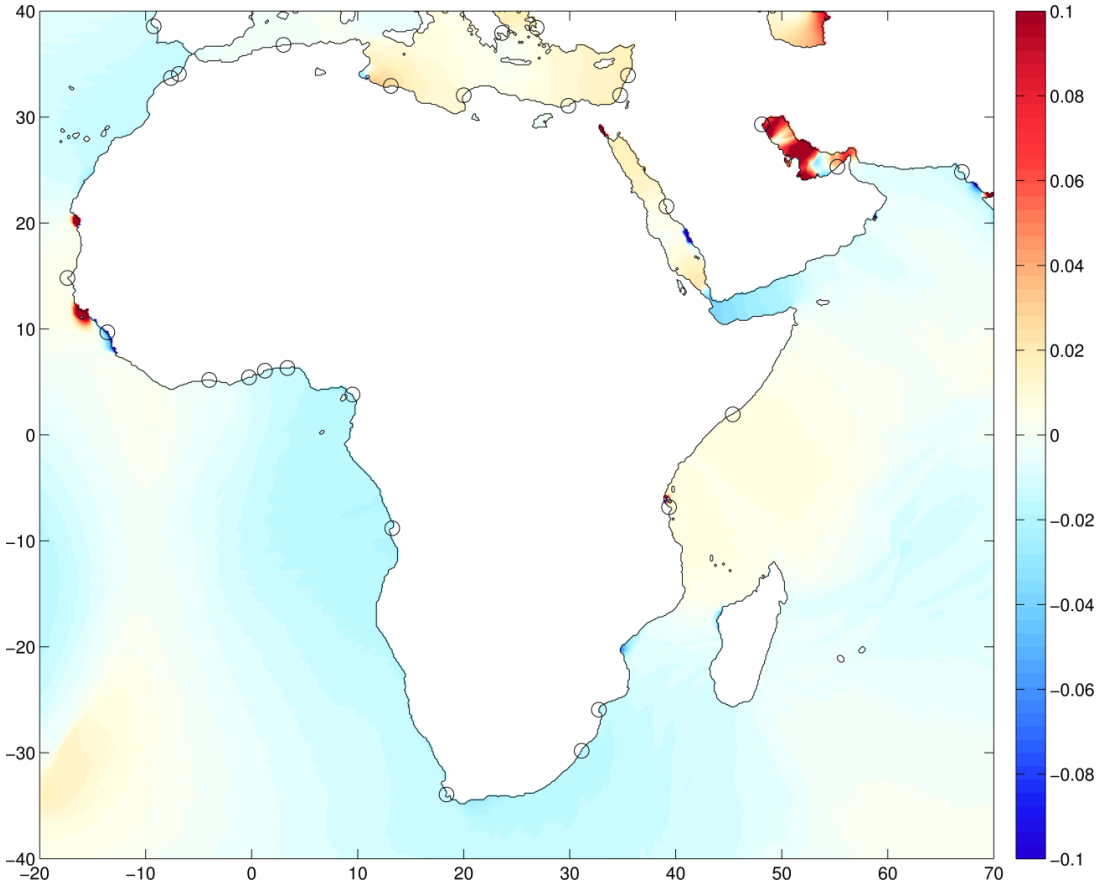

Figure 3.12. African change in MHW (m) with 2m of uniform SLR assuming a fixed present day coastline (+2UF) (increases - red, decreases - blue). For coastal city changes, marked by the black circles, see Table 3.5 and 3.6. (Regional zoom of Figure 3.9)

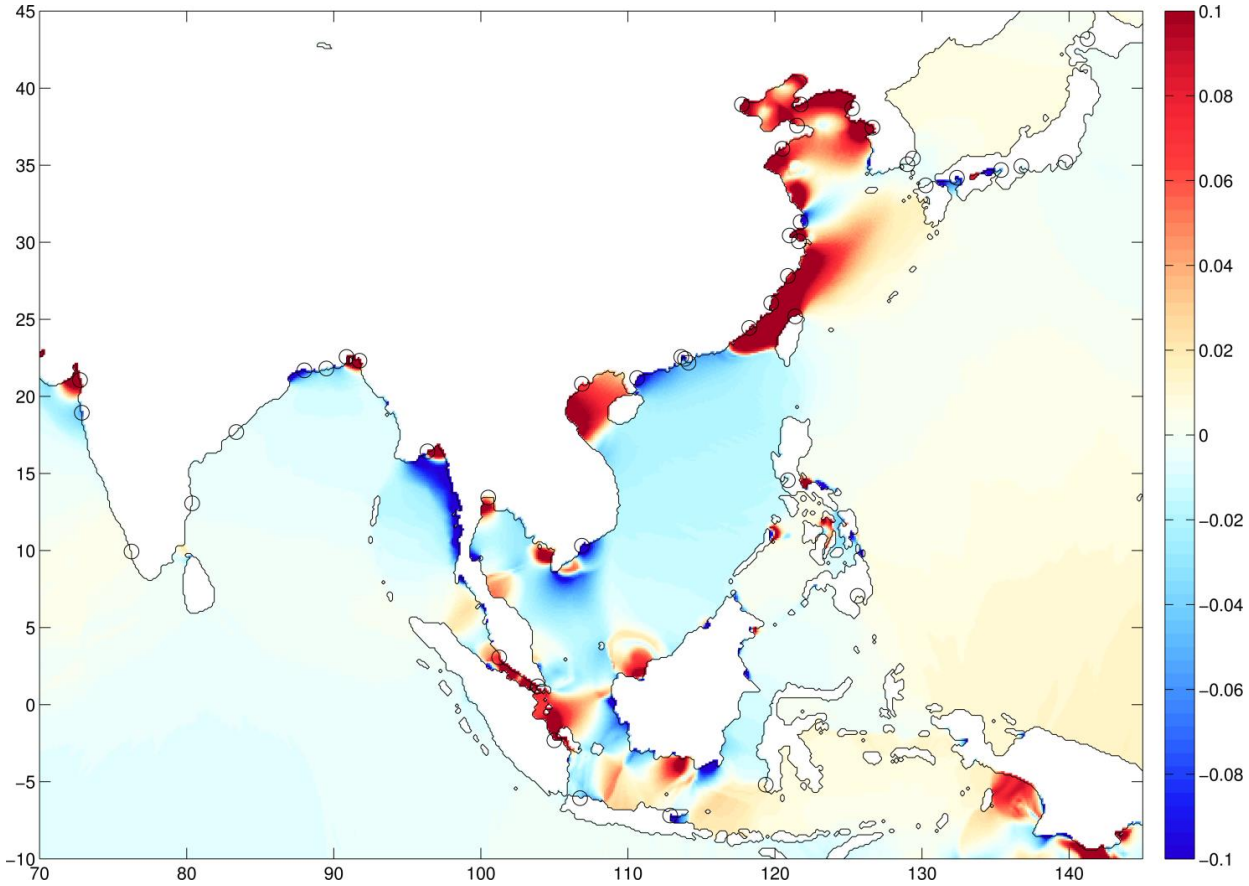

Figure 3.13. Asian change in MHW (m) with 2m of uniform SLR assuming a fixed present day coastline (+2UF) (increases - red, decreases - blue). For coastal city changes, marked by the black circles, see Table 3.5 and 3.6. (Regional zoom of Figure 3.9)

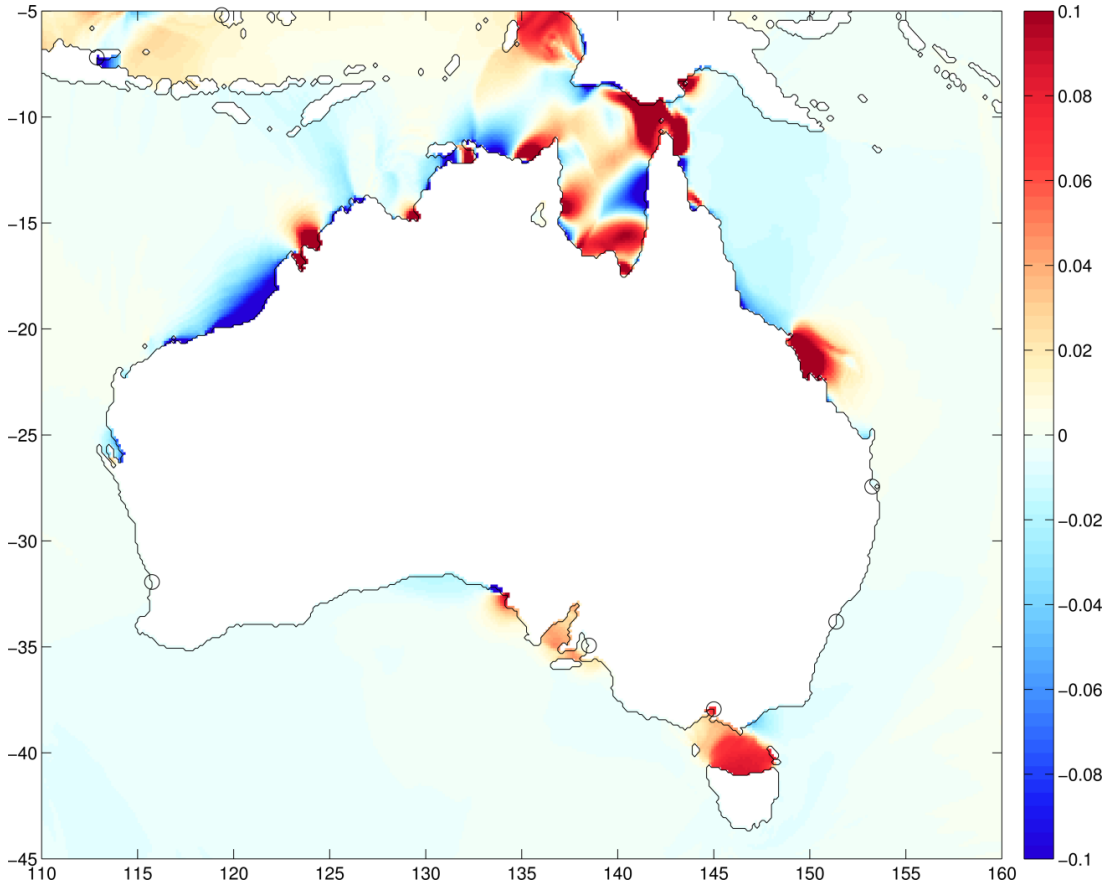

Figure 3.14. Australian change in MHW (m) with 2m of uniform SLR assuming a fixed present day coastline (+2UF) (increases - red, decreases - blue). For coastal city changes, marked by the black circles, see Table 3.5 and 3.6. (Regional zoom of Figure 3.9)

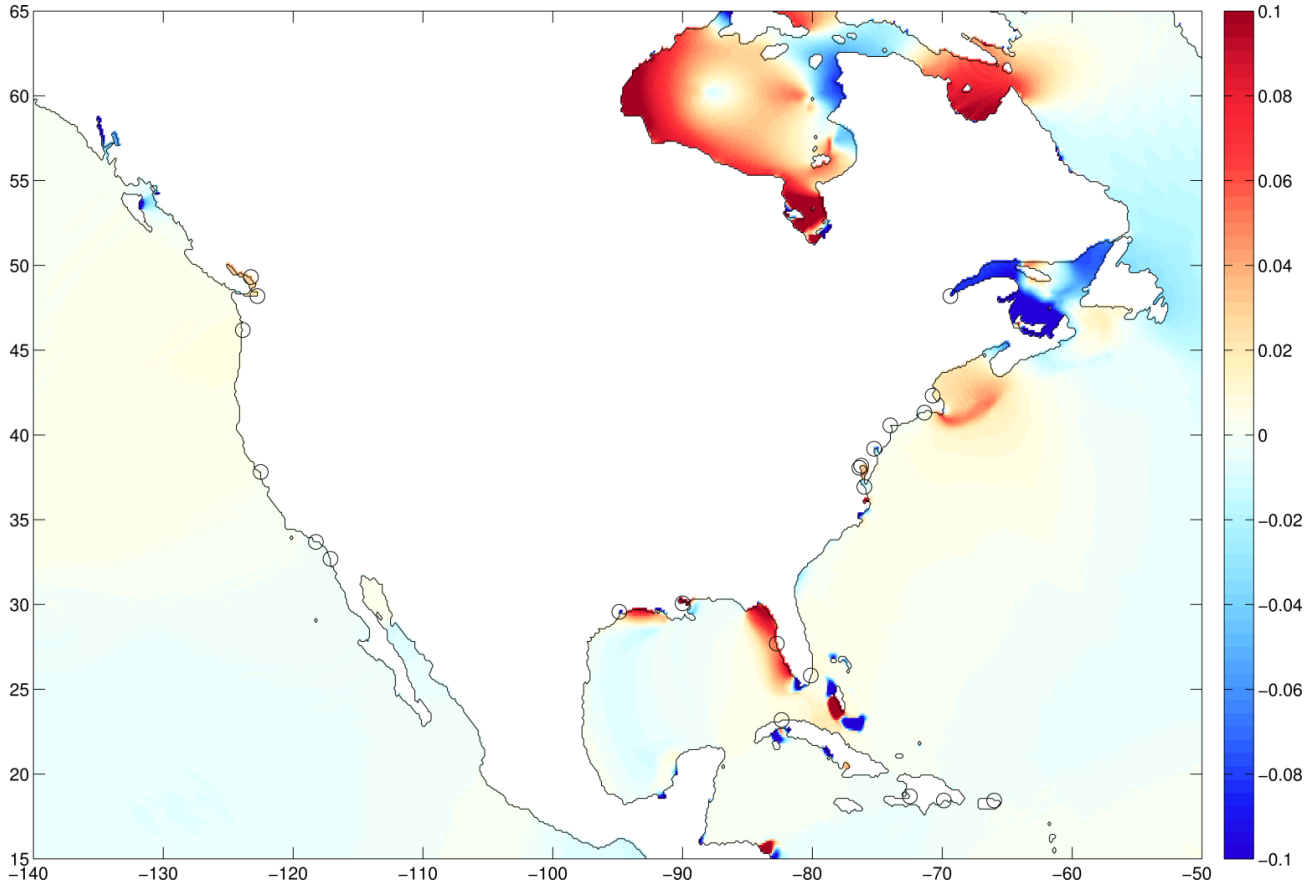

Figure 3.15. North American change in MHW (m) with 2m of uniform SLR assuming a fixed present day coastline (+2UF) (increases - red, decreases - blue). For coastal city changes, marked by the black circles, see Table 3.5 and 3.6. (Regional zoom of Figure 3.9)

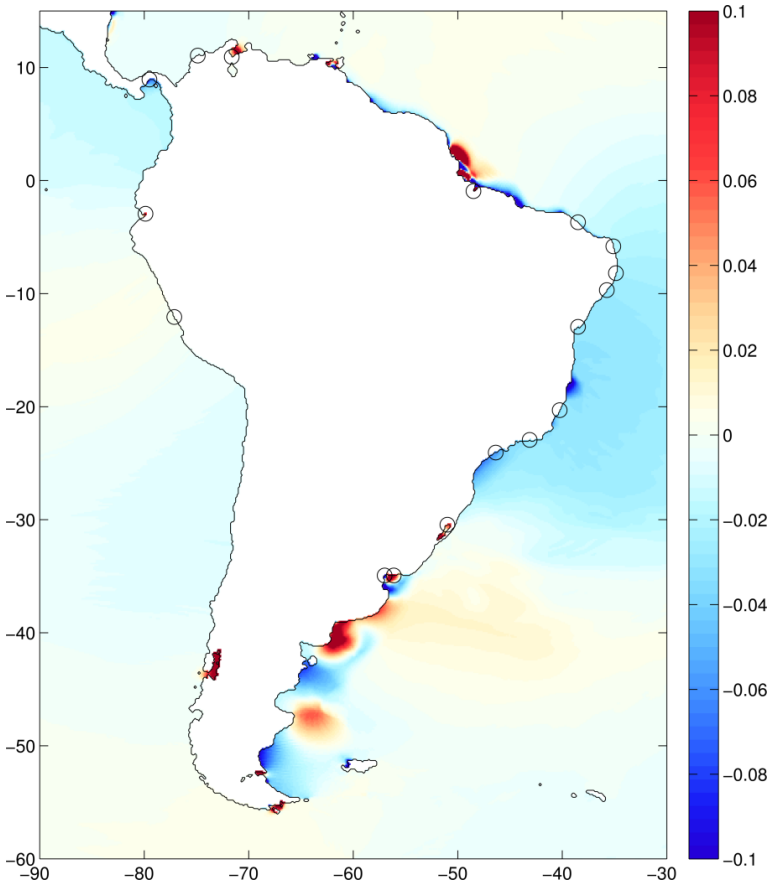

Figure 3.16. South American change in MHW (m) with 2m of uniform SLR assuming a fixed present day coastline (+2UF) (increases - red, decreases - blue). For coastal city changes, marked by the black circles, see Table 3.5 and 3.6. (Regional zoom of Figure 3.9)

the small but widespread decreases in MHW on the northwest and southwest coast of Africa and in the Gulf of Aden (Somalia). Figure 3.13 shows the substantial MHW response to uniform SLR in Asia. Details of the changes are complex but areas of substantial MHW increase occur on the northwest coast of India, eastern coast of Bangladesh, Gulf of Martaban (Burma), northern and eastern Gulf of Thailand, Strait of Malacca (Malaysia), east coast of Sumatra, coast of Central Kalimantan, East Malaysia, southern coast of Papua, Gulf of Tonkin (Vietnam), Strait of Taiwan and the East China Sea. The areas of substantial decrease are the western coast of Bangladesh, Andaman Sea, western Gulf of Thailand, southeast coast of Vietnam, West and South Kalimantan, western Bali Sea and the northern South China Sea. Figure 3.14 illustrates significant MHW changes, particularly on the north coast of Australia. MHW increases occur on the north coast of Western Australia, the southern and western Gulf of Carpentaria, Torres Strait, east coast of Queensland and the Bass Strait. Decreases occur on the northwest coast of Western Australia, central north coast of the Northern Territory and the eastern Gulf of Carpentaria. Figure 3.15 shows a marked MHW response to SLR on the Atlantic coast of North America. Pronounced MHW increases occur in the Hudson Bay, eastern Hudson Strait, the north and northeast Gulf of Mexico; decreases occur in the western Hudson Strait, Gulf of St. Lawrence and around The Bahamas and the southern side of Cuba. The final regional plot, Figure 3.16 again reveals a strong MHW response on the Atlantic coast of South America. Areas of MHW increase occur on the northwest coast of Venezuela, north coast of Brazil, southern coast of Uruguay, sections of the Patagonian Shelf and the Gulf of Corcovado (Chile) whereas decreases occur along the coast of Guyana, Suriname and French Guiana, the northeast and east coast of Brazil and sections of the Patagonian Shelf.

Table 3.6 shows the 40 largest MHW changes at coastal cities for the +2UF scenario. At 10 cities MHW changes of ≥20cm or ≤-20cm occur, with the largest increase (33cm) at Rangoon and the largest decrease (-27cm) at Ho Chi Minh City. The largest increase and decrease at locations with top 20 population exposure are 25cm at Dhaka and -27cm at Ho Chi Minh City. The largest increase and decrease at locations with top 20 asset exposure are 14cm at New Orleans and -23cm at Guangzhou Guangdong. Table 3.6 also shows the MHW change at these cities with 0.5m and 1m SLR. At all the cities

Table 3.6. Changes in MHW and Maximum Range over a 15 day period with 0.5, 1 and 2m of Uniform SLR assuming a fixed present day coastline (UF). This subset of 40 of the 136 coastal cities with populations >1 million is based on the locations with the 40 largest changes in MHW with 2m SLR. Stars after the change value indicate a non-proportional response (outside ± 10%) with respect to the 0.5m SLR change scaled according to the SLR.

	Present Day Exposure Ranking		MHW (cm)						Max Range (cm)					
COUNTRY, City/Agglomeration	Population	Asset	Control	+0.5UF	+1UF		+2UF		Control	+0.5UF	+1UF		+2UF	
ARGENTINA, Buenos Aires	64	52	98	-7	-12	*	-15	*	312	-20	-35	*	-46	*
AUSTRALIA, Melbourne	100	74	74	2	4		7		269	4	8		17	
BANGLADESH, Chittagong	39	72	147	3	7	*	16	*	433	8	19	*	43	*
BANGLADESH, Dhaka	14	43	134	6	13		25		393	18	35		71	
BRAZIL, Belém	72	79	233	9	16	*	28	*	614	26	48		83	*
CANADA, Montréal	84	55	182	0	1	*	-8	*	571	12	23		2	*
CHINA, Dalian	55	63	67	3	6		12		197	10	21		47	*
CHINA, Fuzhou Fujian	42	48	234	5	10		22		704	12	26		54	
CHINA, Guangzhou Guangdong	2	11	121	-7	-12	*	-23	*	480	-30	-62		-120	
CHINA, Shenzen	18	31	100	-2	-4	*	-11	*	395	-15	-35	*	-74	*
CHINA, Hangzhou	92	108	166	4	8		16		520	11	21		42	
CHINA, Ningbo	34	40	68	8	15		28		232	24	46		88	
CHINA, Qingdao	57	65	93	2	5		9		301	5	9		19	
CHINA, Shanghai	3	13	205	-6	-11		-21	*	623	-15	-31		-59	
CHINA, Taipei	49	59	85	4	8		16		276	10	20		42	
CHINA, Tianjin	12	25	67	4	7		12	*	225	18	33		60	*
CHINA, Xiamen	36	44	212	4	7		15		640	8	17		36	
CHINA, Yantai	115	119	33	0	1	*	7	*	118	5	11	*	28	*
CHINA, Zhanjiang	40	45	112	-4	-7	*	-12	*	435	-20	-39		-69	*
NORTH KOREA, Namp'o	87	121	167	3	5		12	*	548	9	18		37	
DENMARK, Copenhagen	82	53	27	8	15		9	*	67	21	36	*	29	*
ECUADOR, Guayaquil	26	41	152	3	5	*	7	*	428	10	17	*	23	*
GUINEA, Conakry	70	113	156	-7	-13	*	-21	*	435	-20	-35	*	-57	*
INDIA, Calcutta	6	22	127	-3	-6		-12	*	373	-9	-17		-31	*
INDIA, Bombay	1	17	148	-2	-5		-8	*	489	-5	-10		-16	*
INDIA, Surat	24	46	228	2	4		9	*	759	7	15		32	
INDONESIA, Palembang	48	73	76	6	10	*	18	*	192	13	24		43	*
INDONESIA, Surabaya	68	88	194	-7	-13		-25		651	-17	-33		-69	
IRELAND, Dublin	95	62	129	3	6		12		363	8	17		34	
JAPAN, Hiroshima	44	24	175	-3	-5		-10	*	539	-8	-15		-28	*
KUWAIT, Kuwait City	101	84	99	2	5	*	9	*	384	10	22		36	*
MYANMAR, Rangoon	22	60	158	8	16		33		471	23	46		92	
NETHERLANDS, Rotterdam	17	7	131	0	-3	*	-8	*	376	0	-7	*	-17	*
PANAMA, Panama City	99	109	237	-2	-4		-7		662	-4	-10		-19	
SOUTH KOREA, Inchon	43	30	353	4	7		13		1045	11	21		37	*
SINGAPORE, Singapore	96	75	31	2	4		8	*	105	5	10		20	
USA, Houston	67	36	65	1	-3	*	-15	*	213	6	-9	*	-31	*
USA, New Orleans	10	3	16	3	7	*	14	*	46	8	21	*	41	*
URUGUAY, Montevideo	94	96	20	3	6	*	11	*	58	12	25		48	
VIETNAM, Ho Chi Minh City	5	27	128	-9	-15	*	-27	*	480	-26	-48		-95	*

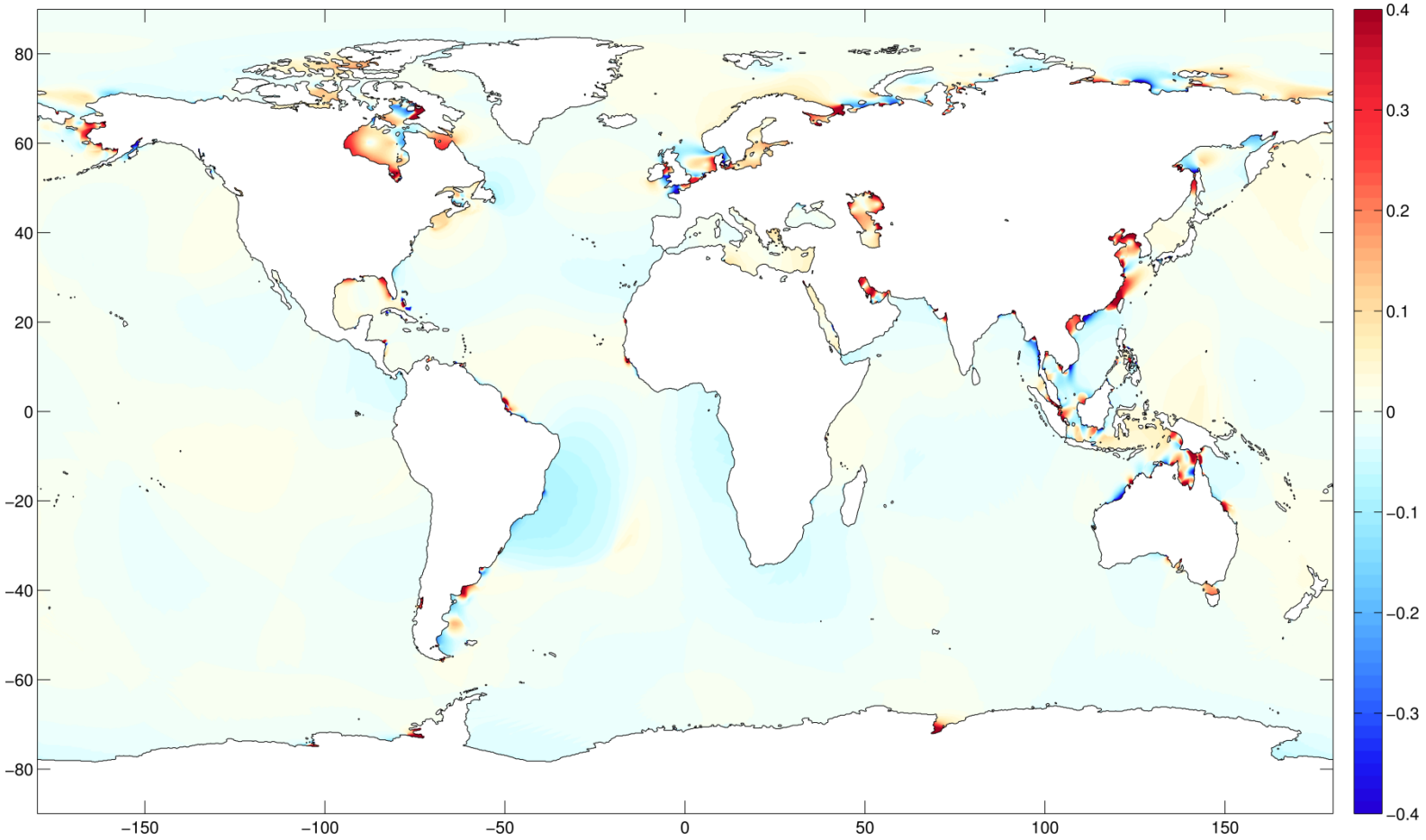

Figure 3.17. Change in maximum tidal range (m), over the 15 day SSH reconstruction based on the four tidal constituents, with 2m of uniform SLR assuming a fixed present day coastline (+2UF) (increases - red, decreases - blue). For coastal city changes see Table 3.5 and 3.6.

shown except Montreal, Copenhagen and Houston the MHW changes are of the same sign and increase incrementally from 0.5m to 1m and from 1m to 2m SLR. With 1m SLR there are 13 cities with MHW changes of ≥10cm or ≤-10cm, with the largest increase (16cm) again at Rangoon and the largest decrease (-15cm) again at Ho Chi Minh City. With 0.5m SLR there are 13 cities with MHW changes of ≥5cm or ≤-5cm, with the largest increase (9cm) at Belem and the largest decrease (-9cm) again at Ho Chi Minh City. Some locations, such as Adelaide (Table 3.5), do not appear in Table 3.6 as significant constituent changes oppose one another causing the MHW change to be small.

The maximum range changes in the +2UF scenario (Figure 3.17) have an almost identical spatial pattern to the MHW changes (Figure 3.9), although it should be noted that the absolute value of the change is much larger (the colour bar limits differ). Table 3.6 shows that the maximum range changes with 2m SLR are >40cm or <-40cm (limits of Figure 3.17) at 21 cities. Large increases are observed at Rangoon (92cm), Ningbo (88cm) and Belem (83cm) whereas large decreases are seen at Guangzhou Guangdong (-120cm), Ho Chi Minh City (-95cm) and Shenzen (-74cm). As with MHW changes, at all locations except Montreal, Copenhagen and Houston the maximum range changes are of the same sign and increase incrementally from 0.5m to 1m and from 1m to 2m SLR. With only 0.5m SLR maximum range changes are still substantial, with changes of ≥25cm or ≤-25cm (50% of the SLR imposed) occurring at 3 cities.

3.4.2 Effect on tides of including coastal recession with uniform SLR

The MHW changes presented in Section 3.4.1 for +2UF (Figure 3.9) can be compared to those obtained with the same SLR but allowing recession of the coastline in areas of low lying land (Figure 3.10). Large scale differences in the tidal response can be seen between the two coastline assumptions, with many MHW changes swapping sign when coastal recession is permitted. Areas where MHW increases become decreases with coastal recession are Hudson Bay, eastern Hudson Strait, Gulf of Maine, northeast Gulf of Mexico, Gulf of Corcovado, the Irish Sea, eastern North Sea, northern Persian Gulf, east coast of West Malaysia, northern Strait of Malacca, north coast of Java, south coast of Papua and Papua New Guinea, parts of the East China Sea, southern Gulf of Carpentaria and the Torres Strait. Conversely, areas where MHW decreases become increases with coastal recession include the eastern Hudson Bay,

Labrador Sea (Canada), northern Gulf of St. Lawrence, coast of Suriname, east coast of Brazil, west coast of Scotland, Skagerrak, southwest and east coast of Africa, Arabian Sea and the western and northern coast of the Northern Territory. Other areas maintain changes of the same sign and a similar magnitude in both coastal conditions: examples are the southern Gulf of St. Lawrence, sections of the Patagonian shelf, western English Channel and Bass Strait. In some regions the sign of the MHW change remains the same but the magnitude is amplified (e.g. northeast coast of Brazil, southern Patagonian Shelf, Baltic Sea, northwest coast of India, Gulf of St. Vincent (Australia) and Bass Strait). It is important to note that in the coastal recession SLR cases there are areas inland of the original coastline that now experience tides for the first time. These areas have their (now calculable) MHW value plotted necessarily on the positive part of the Figure 3.10 differences colour scale, although only the largest areas are visible (e.g. near the Amazon and southern Papua). Regional enlargements of Figure 3.10 allowing closer comparison with their fixed coastline counterparts (Figure 3.11-3.16) can be found in Appendix 3.4.

The changes in the four tidal constituents, MHW and maximum range at 40 coastal cities for the +2UR scenario are given in Table 3.5. The changes with 2m SLR and a fixed coastline (+2UF) were presented in Section 3.4.1 so the focus here will be where changes are substantially different in the coastal recession scenario (+2UR). There are still substantial changes to the M_2 constituent. There are now 20 locations where M_2 amplitude changes of ≥20cm or ≤-20cm occur, 12 of which are at new locations compared to the fixed coastline case. Of these 20 substantial changes, 16 are decreases in the recession scenario (compared with 6 from 14 in the fixed coastline scenario). The largest M_2 increase and decrease with recession is now 154cm at Montreal and -142cm at Belem. Changes to the amplitude of the S_2 constituent of ≥10cm or ≤-10cm occur at 15 locations, 8 of which are at new locations compared to the fixed coastline case. Of these 15 substantial changes, 12 are decreases in the recession scenario (compared with only 7 from 12 in the fixed coastline scenario). The largest S_2 increase and decrease with recession is now 38cm at Adelaide and -92cm at Montreal. With recession, significant (≥5cm or ≤-5cm) change in K_1 amplitude occurs at 3 locations where with a fixed coastline the change was insignificant: Porto Alegre (8cm), Surabaya (6cm) and Ho Chi Minh City (-15cm). At New Orleans the change in K_1 was significant in both scenarios

(12cm in recession case). The SLR induced change in the O_1 constituent with coastal recession is significant (≥5cm or ≤-5cm) at 4 locations where with a fixed coastline the change was insignificant: Buenos Aires (-6cm), Porto Alegre (14cm), Rotterdam (-5cm) and Ho Chi Minh City (-10cm). At New Orleans the change was again significant in both scenarios (8cm in recession case). With coastal recession, MHW change of ≥20cm or ≤-20cm now occurs at 18 locations, 13 of which are at new locations compared to the fixed coastline. Of these 18 substantial changes, 14 are decreases in the recession scenario (compared with 5 from 10 in +2UF). The largest MHW increase and decrease with recession is now 66cm at Montreal and -131cm at Belem. With coastal recession the largest MHW increase and decrease at locations with top 20 population exposure are respectively 16cm at New Orleans and -43cm at Calcutta. The largest MHW increase and decrease at locations with top 20 asset exposure are 16cm at New Orleans and -96cm at Hamburg. Maximum range changes are >40cm or <-40cm at 26 cities: large maximum range increases are seen at Montreal (150cm), Hangzhou (72cm) and Porto Alegre (65cm), whilst large maximum range decreases are predicted at Belem (-340cm), Hamburg (-247cm) and Buenos Aires (-195cm).

To assist in explaining these changes in the tide with SLR and different coastline assumptions, energy dissipation through bed friction was calculated. The present day tide energy dissipation plots (not shown) showed good agreement with previously published plots (e.g. Figure 8 of Lyard et al. (2006)). The change in energy dissipation from the four tidal constituents with the +2UF and +2UR scenarios is given in Figure 3.18 and 3.19 respectively. Figure 3.18 shows there to be reduced (increased) frictional energy dissipation at the bed in areas of reduced (increased) MHW (Figure 3.9). This is also largely true of the respective plots (Figure 3.19 and 3.10) for +2UR. Noteworthy differences in the change in energy dissipation between +2UF and +2UR scenarios include regions such as Hudson Bay, Gulf of St. Lawrence and Gulf of Maine, the coast of Guyana and Suriname, Celtic and North Seas, Persian Gulf, the northwest coast of Australia, Gulf of Carpentaria, East China Sea and Bering Sea.

Table 3.7 shows the MHW changes again for 2m uniform SLR (both with a fixed coastline and allowing coastal recession) as well as for 5m and 10m uniform SLR. For the fixed coastline the tidal change is of the same sign and incrementally increasing with SLR at 24 out of 40 cities. With the fixed

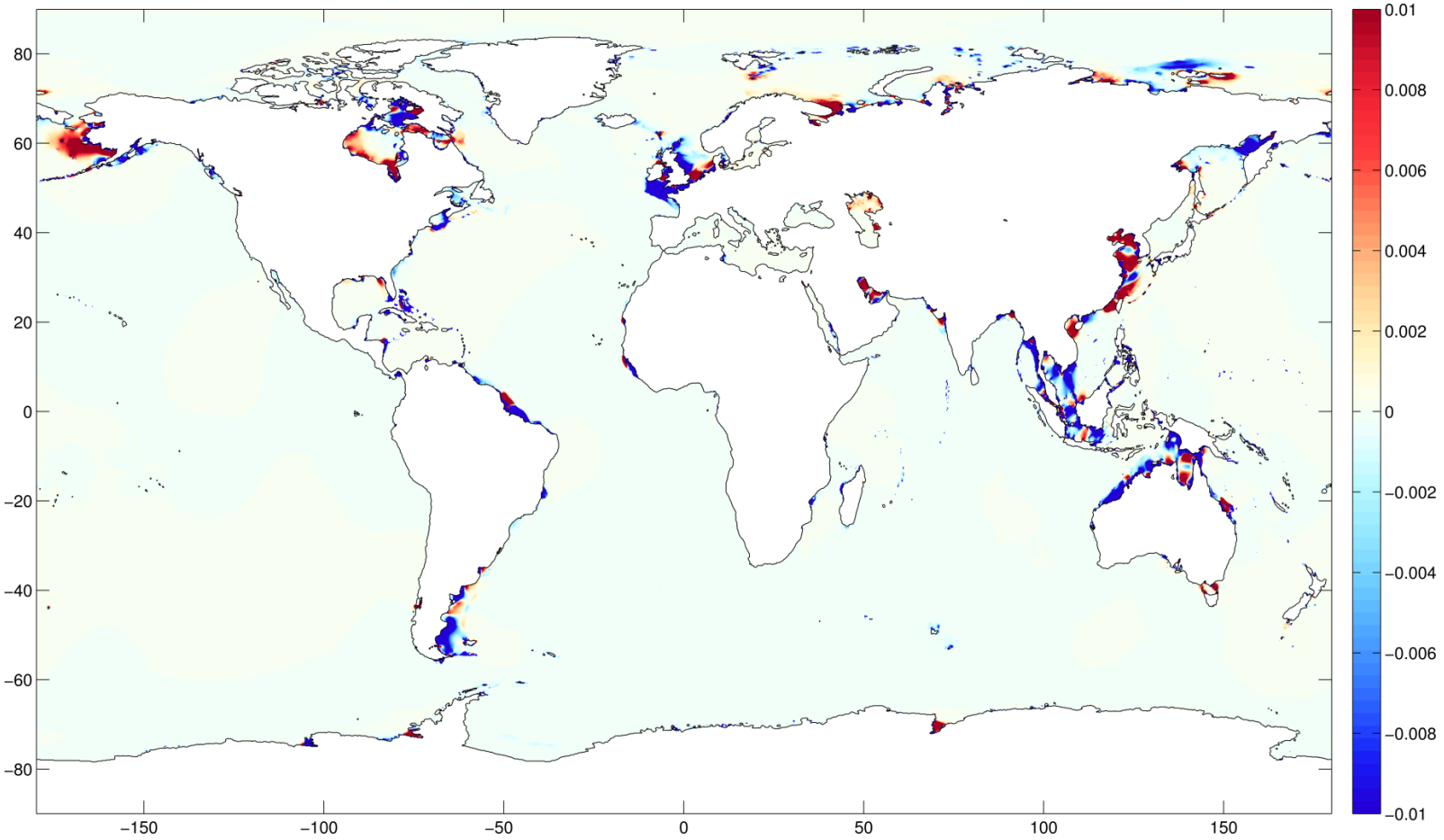

Figure 3.18. Change in energy dissipation at the bed (W/m^2) over a 15 day reconstruction period (for 4 constituents) with 2m of uniform SLR assuming a fixed present day coastline (+2UF).

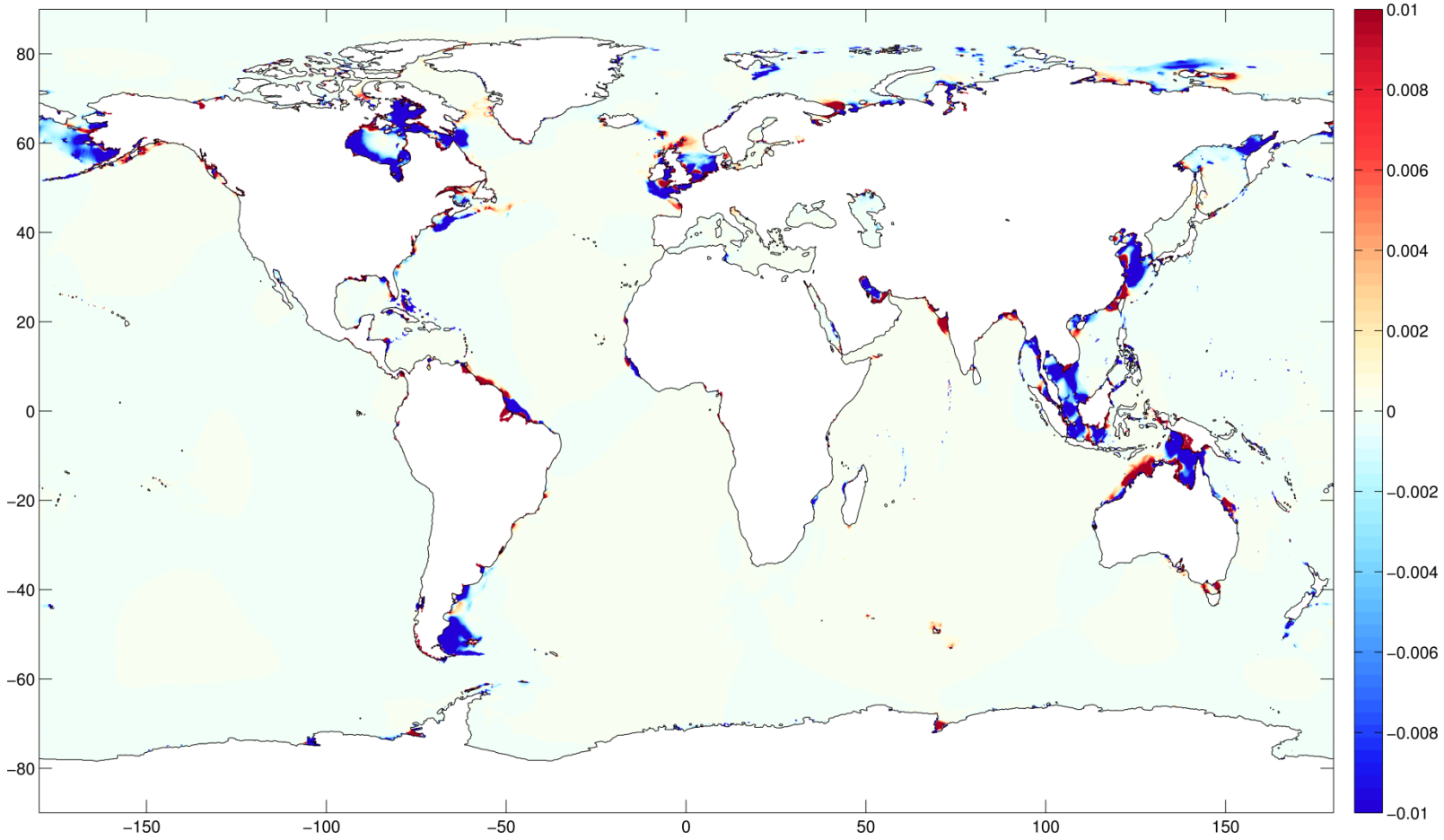

Figure 3.19. Change in energy dissipation at the bed (W/m^2) over a 15 day reconstruction period (for 4 constituents) with 2m of uniform SLR permitting coastal recession of the coastline except around Antarctica (+2UR). For newly wet areas in the SLR scenario new areas of dissipation are plotted as positive values.

Table 3.7. Changes in MHW with 2, 5 and 10m of Uniform SLR assuming a fixed present day coastline (UF) and permitting the coastline to recede (UR). This subset of 40 of the 136 coastal cities with populations >1 million is based the same criteria as Table 3.5. Stars after the change value indicate non-proportional response (outside ± 10%) with respect to the 0.5m SLR change scaled with the SLR.

	Present Day Exposure Ranking		MHW (cm)													
COUNTRY, City/Agglomeration	Population	Asset	Control	+2UF		+2UR		+5UF		+5UR		+10UF		+10UR		
ARGENTINA, Buenos Aires	64	52	98	-15	*	-64	*	-5	*	-79	*	48	*	-68	*	
AUSTRALIA, Adelaide	123	103	86	0	*	17	*	28	*	19	*	54	*	26	*	
BANGLADESH, Chittagong	39	72	147	16	*	-13	*	53	*	1	*	115	*	-1	*	
BANGLADESH, Dhaka	14	43	134	25		-1	*	70	*	-41	*	133		-47	*	
BANGLADESH, Khulna	23	54	87	-4	*	19	*	-8	*	9	*	-8	*	-8	*	
BRAZIL, Belém	72	79	233	28	*	-131	*	51	*	-139	*	101	*	-150	*	
BRAZIL, Porto Alegre	78	83	14	7		18	*	6	*	21	*	17	*	40	*	
CAMEROON, Douala	110	128	70	-3	*	-16	*	-4	*	5	*	7	*	17	*	
CANADA, Montréal	84	55	182	-8	*	66	*	-37	*	113	*	-49	*	21	*	
CHINA, Dalian	55	63	67	12		-3	*	34	*	7	*	72	*	17	*	
CHINA, Fuzhou Fujian	42	48	234	22		6	*	62	*	20	*	113	*	38	*	
CHINA, Guangzhou Guangdong	2	11	121	-23	*	-19	*	-40	*	-30	*	-34	*	-61	*	
CHINA, Shenzen	18	31	100	-11	*	-8	*	-24	*	-17	*	-17	*	-40	*	
CHINA, Hangzhou	92	108	166	16		25	*	37	*	22	*	66	*	-75	*	
CHINA, Ningbo	34	40	68	28		20	*	62	*	34	*	110	*	21	*	
CHINA, Shanghai	3	13	205	-21	*	-22		-41	*	-29	*	-33	*	-79	*	
CHINA, Taipei	49	59	85	16		8	*	45	*	26	*	89	*	45	*	
CHINA, Tianjin	12	25	67	12	*	1	*	31	*	-21	*	38	*	-47	*	
CHINA, Xiamen	36	44	212	15		2	*	45	*	31	*	86	*	26	*	
CHINA, Zhanjiang	40	45	112	-12	*	-7	*	-22	*	-20	*	-15	*	-35	*	
NORTH KOREA, Namp'o	87	121	167	12	*	-6	*	37	*	8	*	87	*	9	*	
DENMARK, Copenhagen	82	53	27	9	*	15	*	-21	*	-8	*	-8	*	-17	*	
ECUADOR, Guayaquil	26	41	152	7	*	-71	*	-1	*	-91	*	-20	*	-73	*	
GERMANY, Hamburg	37	18	156	-1	*	-96	*	8	*	-143	*	32	*	-137	*	
GUINEA, Conakry	70	113	156	-21	*	-15	*	-34	*	-31	*	-49	*	-46	*	
INDIA, Calcutta	6	22	127	-12	*	-43	*	-23	*	-36	*	-37	*	-40	*	
INDIA, Surat	24	46	228	9	*	26	*	26	*	58	*	60	*	66	*	
INDONESIA, Palembang	48	73	76	18	*	-10	*	36	*	-9	*	61	*	6	*	
INDONESIA, Surabaya	68	88	194	-25		-50	*	-52	*	-57	*	-86	*	-98	*	
IRELAND, Dublin	95	62	129	12		-22	*	29		-29	*	54	*	-19	*	
JAPAN, Hiroshima	44	24	175	-10	*	-58	*	-22	*	-45	*	-46	*	-15	*	
MALAYSIA, Kuala Lumpur	35	33	127	6	*	-15	*	9	*	-20	*	5	*	-16	*	
MYANMAR, Rangoon	22	60	158	33		-6	*	85		-21	*	168		-12	*	
NETHERLANDS, Amsterdam	15	6	76	7	*	-33	*	9	*	-22	*	23	*	-10	*	
NETHERLANDS, Rotterdam	17	7	131	-8	*	-69	*	-18	*	-72	*	-11	*	-65	*	
SOUTH KOREA, Inchon	43	30	353	13		-10	*	26	*	4	*	0	*	-32	*	
UNITED KINGDOM, Glasgow	91	68	133	5	*	-29	*	14	*	-43	*	26	*	-33	*	
USA, Houston	67	36	65	-15	*	-30	*	-26	*	-32	*	-39	*	-45	*	
USA, New Orleans	10	3	16	14	*	16	*	24		6	*	20	*	1	*	
VIETNAM, Ho Chi Minh City	5	27	128	-27	*	-46	*	-41	*	-70	*	6	*	-74	*	

coastline a number of cities show larger MHW changes with 5m SLR than with 10m SLR. For the coastal recession case, the tidal change is only of the same sign and incrementally increasing with SLR at 15 from the 40 cities. The effects of these higher SLR scenarios contrast with the MHW changes analysed in Section 3.4.1 (and Table 3.6) for lower SLR fixed coastline scenarios where 37 cities had changes of the same sign and increased monotonically with SLR. In the 5m and 10m SLR scenarios, MHW changes with the two different coastal assumptions are also substantially different. With +5UR, 7 of the 9 substantial (>10% of the SLR imposed) MHW changes were decreases (compared with 1 of 6 in +5UF) and with +10UR 2 of 2 substantial MHW changes were decreases (compared with 0 of 6 in +10UF). In the UF scenarios, the largest MHW increases all occur at Rangoon, whilst the largest decreases occur at Ho Chi Minh City with +2UF, and at Surabaya with +5UF and +10UF. For +2UR and +5UR, the largest increases occur at Montreal whereas the largest increases are at Surat with +10UR; the largest decreases are at Belem for +2UR and +10UR and at Hamburg for +5UR.

3.4.3 Percentage MHW changes and proportionality of the tidal response

In addition to the absolute changes presented in Sections 3.4.1 and 3.4.2 the tidal change as a percentage of the present day (Control) tide is of interest as it allows identification of regions where changes are large with respect to their original tidal amplitude. Here we focus on the percentage MHW changes with 1m, 2m and 5m of uniform SLR assuming a fixed coastline. The percentage MHW change with 1m SLR is shown in Figure 3.20. The regions with a large (>20%) percentage MHW response are parts of Hudson Bay, Kattegat, Baltic Sea, eastern Kara Sea (Russia), Laptev Sea and East Siberian Sea as well as the Chukchi (Alaska) and northern Bering Seas. With 2m SLR (Figure 3.21) large percentage MHW changes also become pronounced in the Gulf of St. Lawrence, along the coastline of the Gulf of Mexico, eastern North Sea, southern central Mediterranean Sea, Persian Gulf, Strait of Malacca, Gulf of Carpentaria and Beaufort Sea (Alaska). With 5m SLR (Figure 3.22) large percentage MHW changes now also occur across most of Hudson Bay, the western South Atlantic, central Red Sea (Saudi Arabia), Java Sea, Gulf of Thailand, East China Sea and Sea of Japan, southern Barents Sea and Canadian Archipelago. The

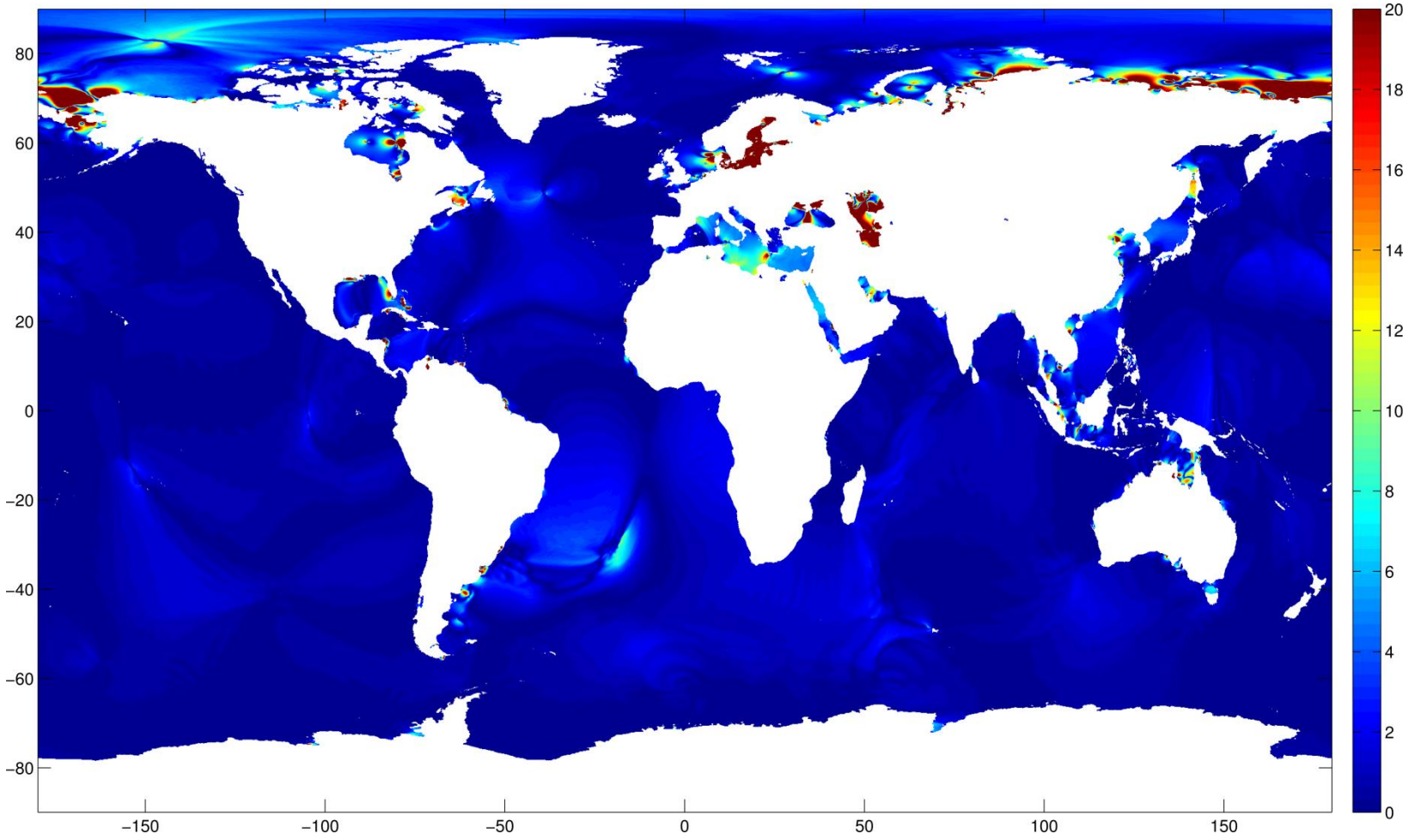

Figure 3.20. Modulus of MHW change with 1m of uniform SLR assuming a fixed present day coastline (+1UF) as a percentage of the control MHW. Limits 0 - 20%.

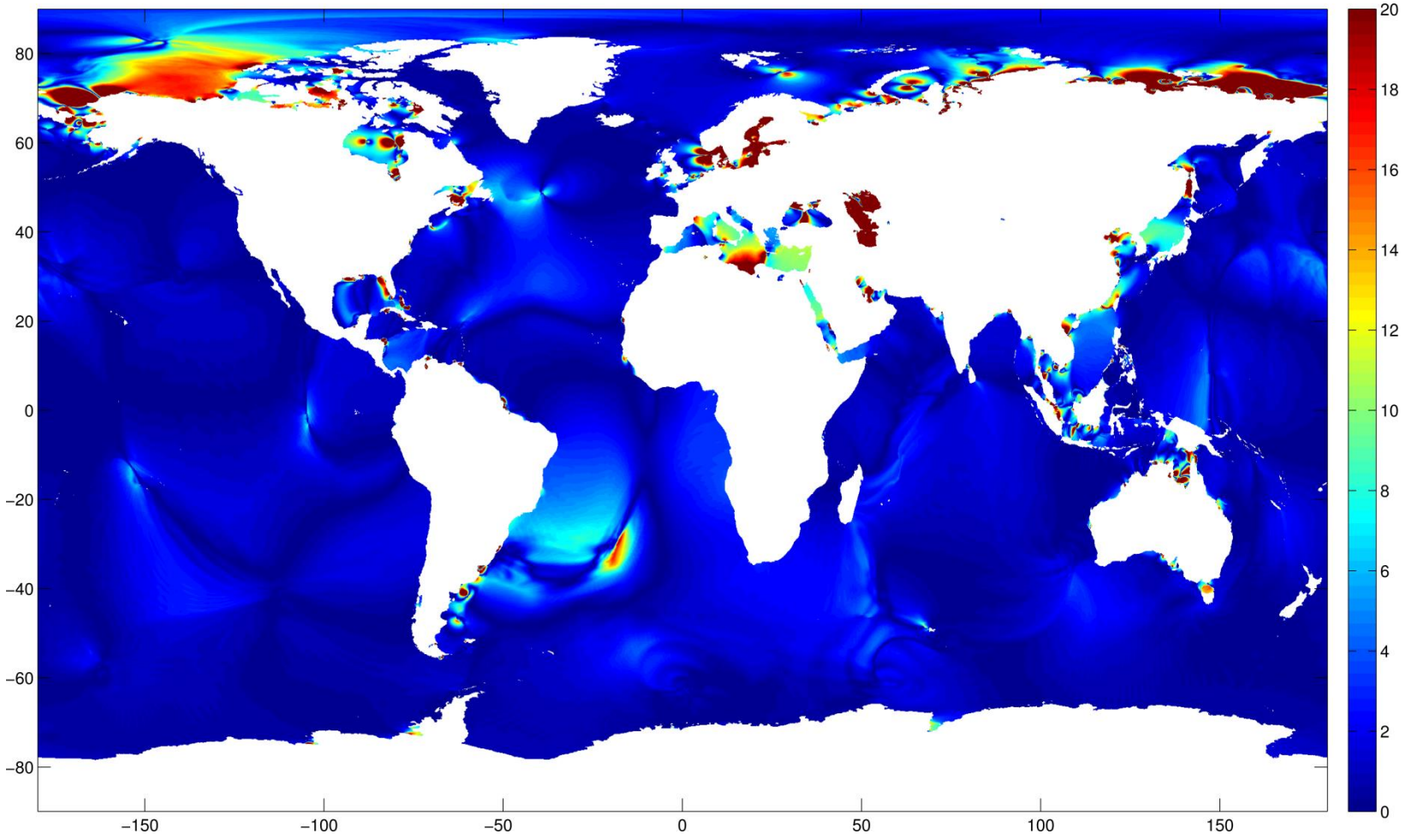

Figure 3.21. Modulus of MHW change with 2m of uniform SLR assuming a fixed present day coastline (+2UF) as a percentage of the control MHW. Limits 0-20%.

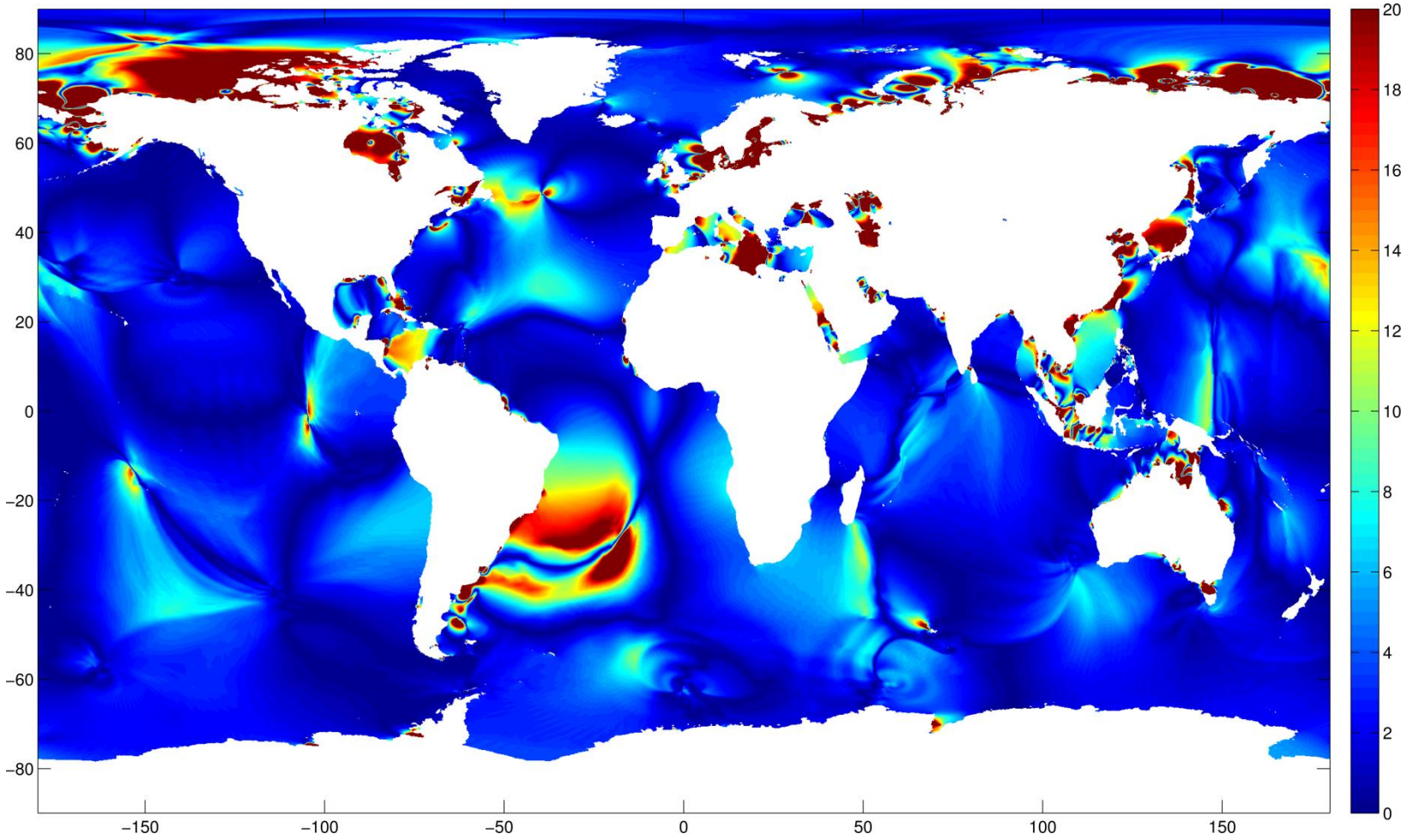

Figure 3.22. Modulus of MHW change with 5m of uniform SLR assuming a fixed present day coastline (+5UF) as a percentage of the control MHW. Limits 0-20%.

colour scales of Figure 3.20-3.22 are not scaled proportionally to the SLR imposed, and it is not surprising that there are more areas with large percentage MHW changes in the 5m SLR scenario. In addition to these plots all the tables showing tidal amplitude changes at cities give the control amplitude for the particular property before the change itself. This allows an assessment of cities where the tidal change is large relative to its control amplitude: for example, in Table 3.6 with 2m SLR the MHW change at Ningbo is 28cm (~41% of the 68cm Control MHW).

Using the definition of proportional tidal change (see Section 3.3.3) Table 3.8 provides a global overview of the proportionality of change at points with significant (>5cm or <-5cm) MHW change for +1UF, +2UF, +5UF and +10UF. Table 3.8 shows that the portion of cells displaying a proportional change decreases with SLR. Conversely, the portion of cells classified as strongly non-proportional (ratios of <0, 0-0.5 and 1.5+) generally increases with SLR. The largest category of model cells is proportional for both 1m and 2m SLR, and that mode moves towards higher proportionality ratios with further SLR: in other words changes are proportionally smallest at lower SLR scenarios and changes become increasingly above proportional at higher SLR scenarios.

Table 3.8. Percentage of total significant (>+/ <- 5cm) MHW change cells in each proportionality category for various uniform SLR scenarios with a fixed coastline assumption (UF) (geographic distribution of points given in Figure 3.23-3.34). The proportionality ratio for each cell is given by the ratio of the MHW change for the SLR scenario to the 0.5m SLR MHW change which is then normalised for each SLR scenario so that proportional change is given by a ratio of 1 (± 0.1). Ratio values <0.9 (>1.1) or <0 show a below (above) proportional change or sign change of the MHW response in the SLR scenario.

	Percentage of Sig. MHW Response Cells in each Proportionality Category (%)			
Norm. Proportionality Ratio	+1UF	+2UF	+5UF	+10UF
<0 (Sign Change)	1	4	9	19
0- 0.5	1	3	6	6
0.5- 0.9	24	27	19	18
0.9- 1.1 (Proportional)	61	34	19	11
1.1- 1.5	9	19	25	10
1.5+	4	12	21	37
Total Sig. Cells (>+/ <- 5cm)	12871	32166	104106	278050

The spatial distributions of the significant MHW change points (analysed in Table 3.8) for +1UF are shown in Figure 3.23, 3.25, 3.27, 3.29, 3.31 and 3.33.

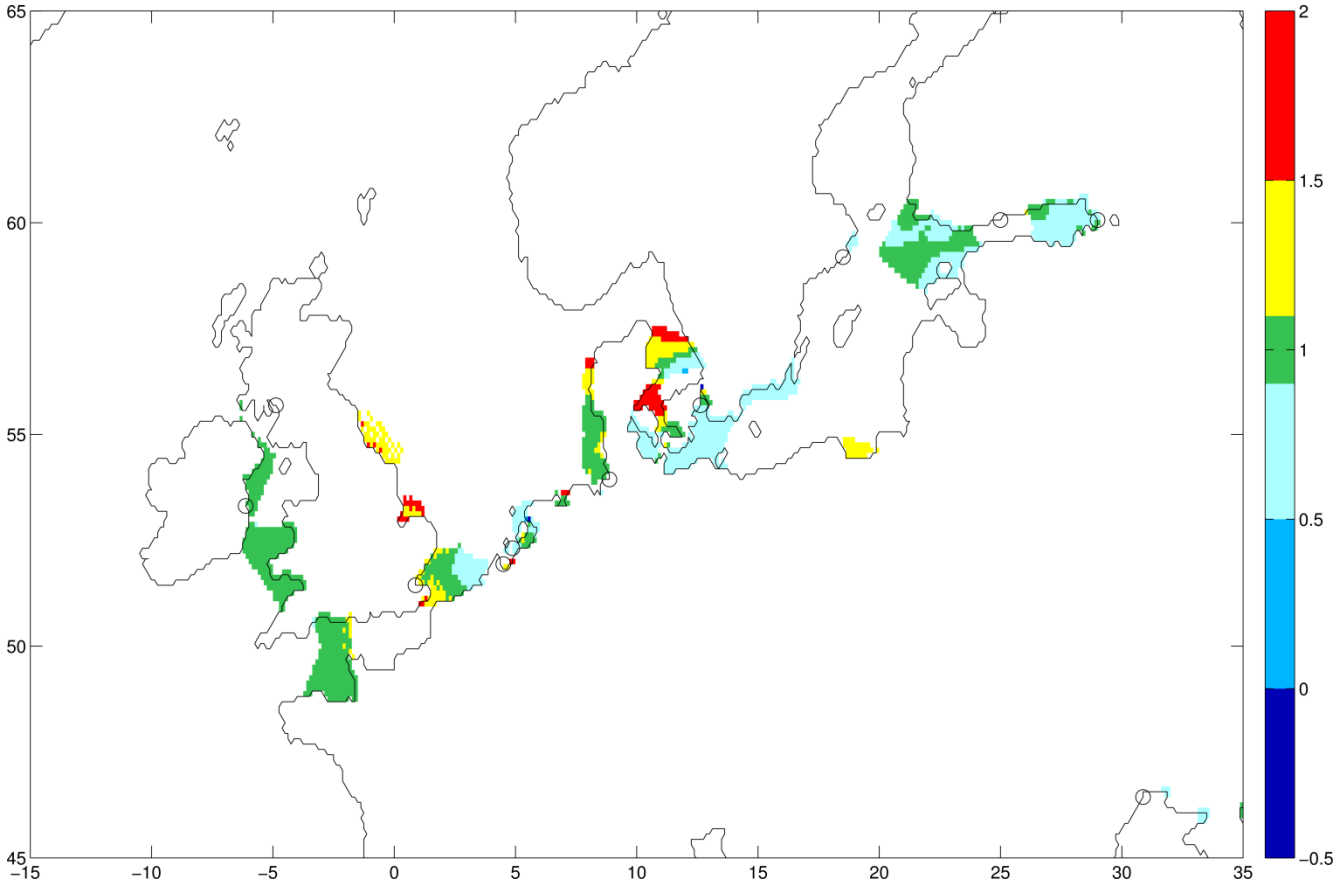

Figure 3.23. European normalised proportionality ratio of the significant MHW change with 1m uniform SLR (+1UF) to the MHW change with 0.5m uniform SLR (+0.5UF) assuming a fixed coastline. Proportional change is given by a ratio of 1 (± 0.1). Ratio values <0.9 (>1.1) or <0 show a below (above) proportional change or sign change of the MHW response in the SLR scenario. Insignificant MHW Changes (<+/ >- 5cm) are masked out. Black circles mark coastal cities.

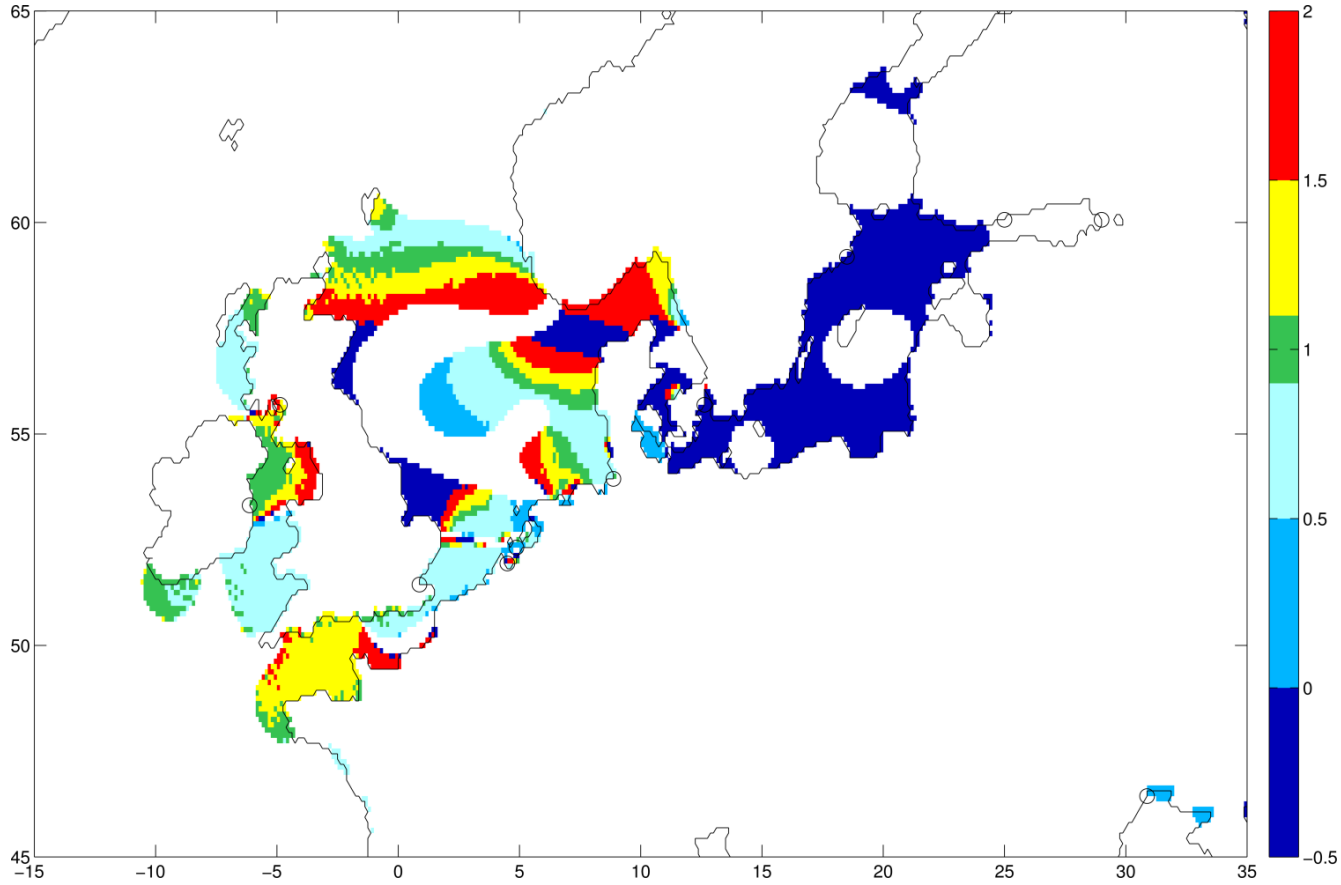

Figure 3.24. European normalised proportionality ratio of the significant MHW change with 5m uniform SLR (+5UF) to the MHW change with 0.5m uniform SLR (+0.5UF) assuming a fixed coastline. Proportional change is given by a ratio of 1 (± 0.1). Ratio values <0.9 (>1.1) or <0 show a below (above) proportional change or sign change of the MHW response in the SLR scenario. Insignificant MHW Changes (<+/ >- 5cm) are masked out. Black circles mark coastal cities.

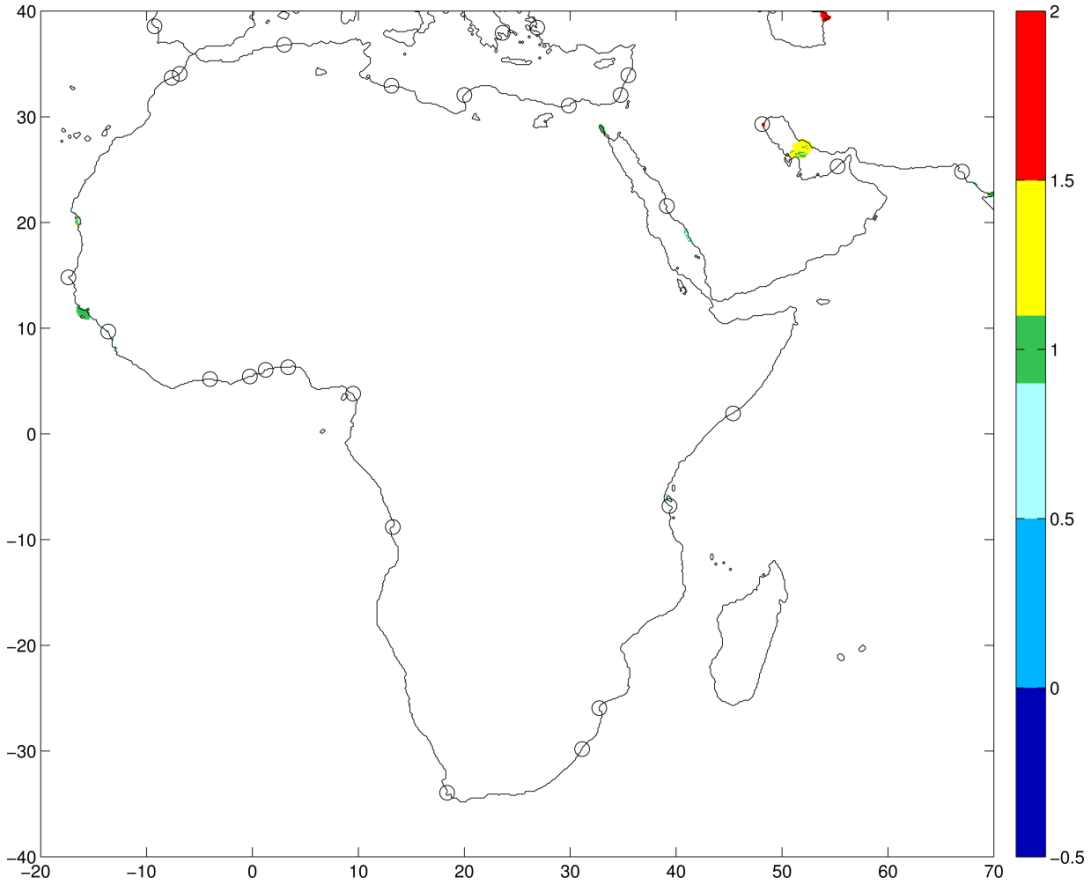

Figure 3.25. African normalised proportionality ratio of the significant MHW change with 1m uniform SLR (+1UF) to the MHW change with 0.5m uniform SLR (+0.5UF) assuming a fixed coastline. Proportional change is given by a ratio of 1 (± 0.1). Ratio values <0.9 (>1.1) or <0 show a below (above) proportional change or sign change of the MHW response in the SLR scenario. Insignificant MHW Changes (<+/ >- 5cm) are masked out. Black circles mark coastal cities.

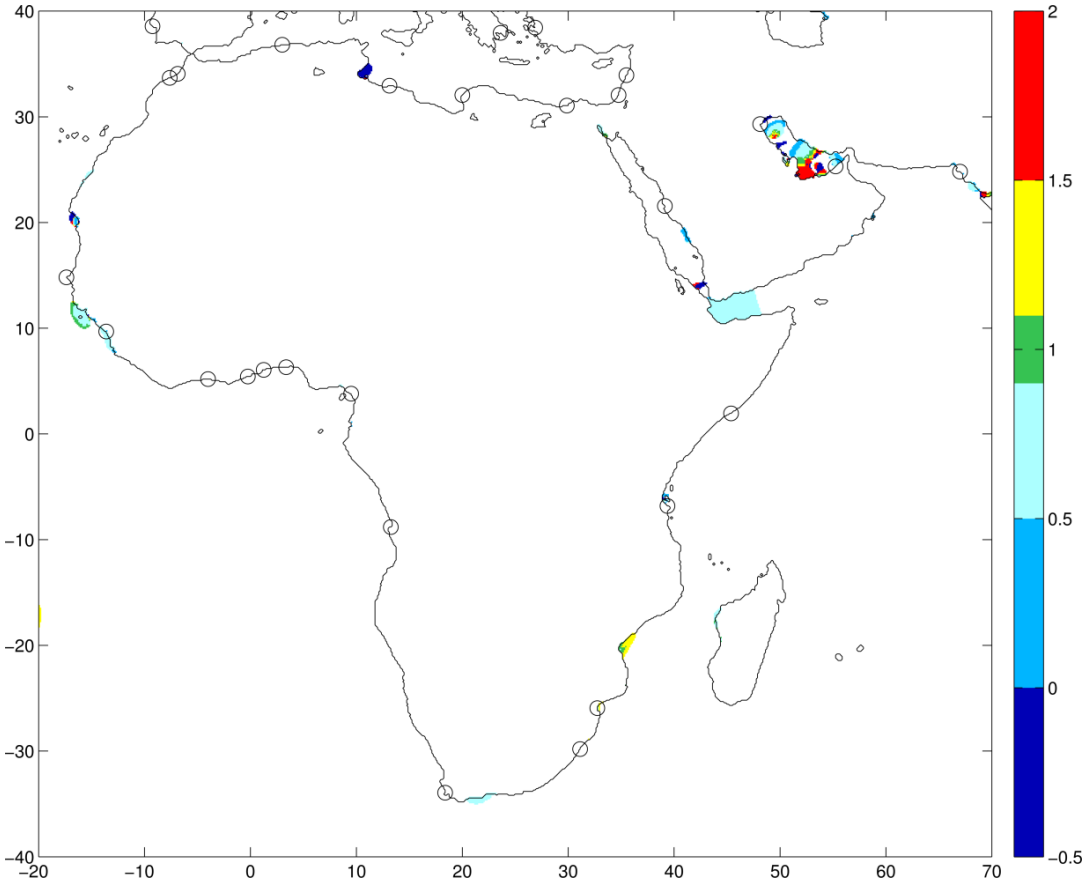

Figure 3.26. African normalised proportionality ratio of the significant MHW change with 5m uniform SLR (+5UF) to the MHW change with 0.5m uniform SLR (+0.5UF) assuming a fixed coastline. Proportional change is given by a ratio of 1 (± 0.1). Ratio values <0.9 (>1.1) or <0 show a below (above) proportional change or sign change of the MHW response in the SLR scenario. Insignificant MHW Changes (<+/ >- 5cm) are masked out. Black circles mark coastal cities.

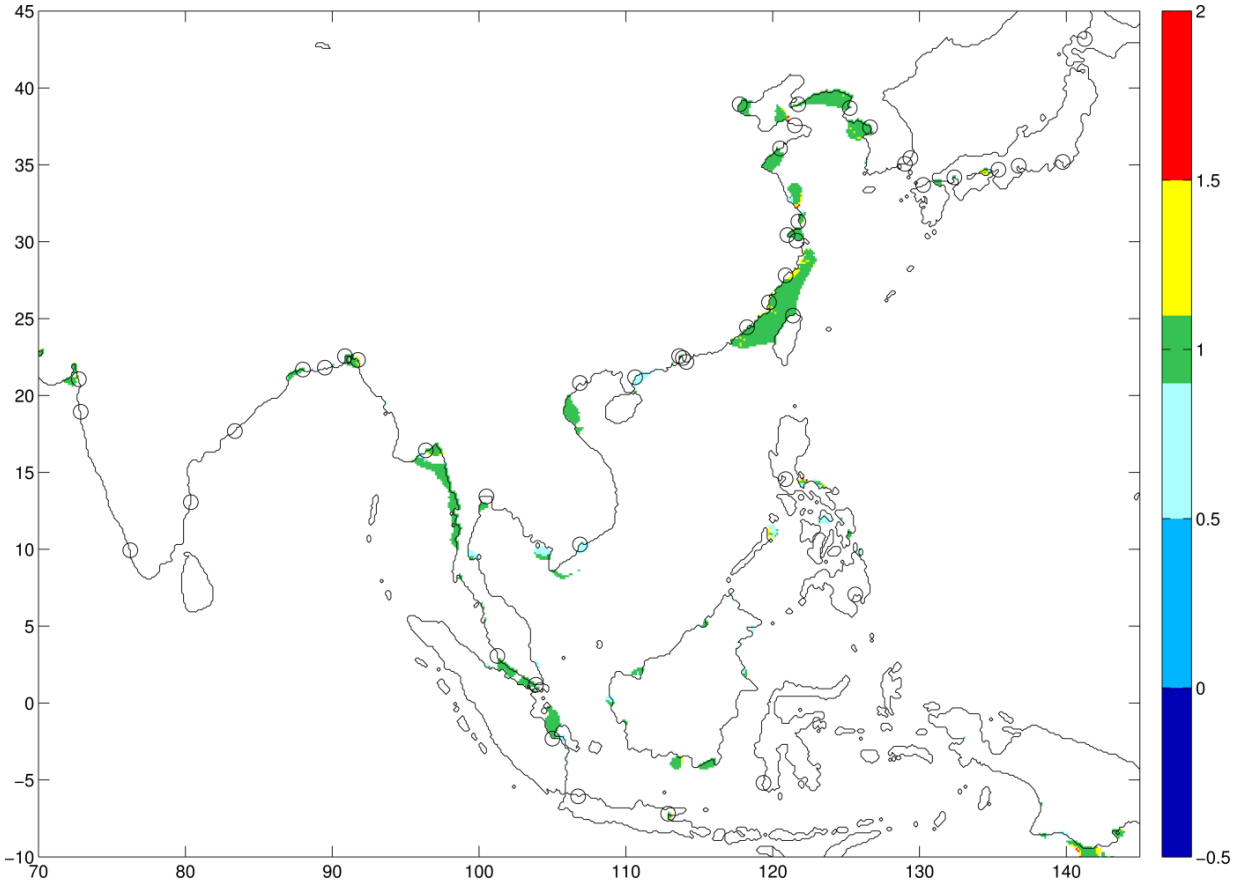

Figure 3.27. Asian normalised proportionality ratio of the significant MHW change with 1m uniform SLR (+1UF) to the MHW change with 0.5m uniform SLR (+0.5UF) assuming a fixed coastline. Proportional change is given by a ratio of 1 (± 0.1). Ratio values <0.9 (>1.1) or <0 show a below (above) proportional change or sign change of the MHW response in the SLR scenario. Insignificant MHW Changes (<+/ >- 5cm) are masked out. Black circles mark coastal cities.

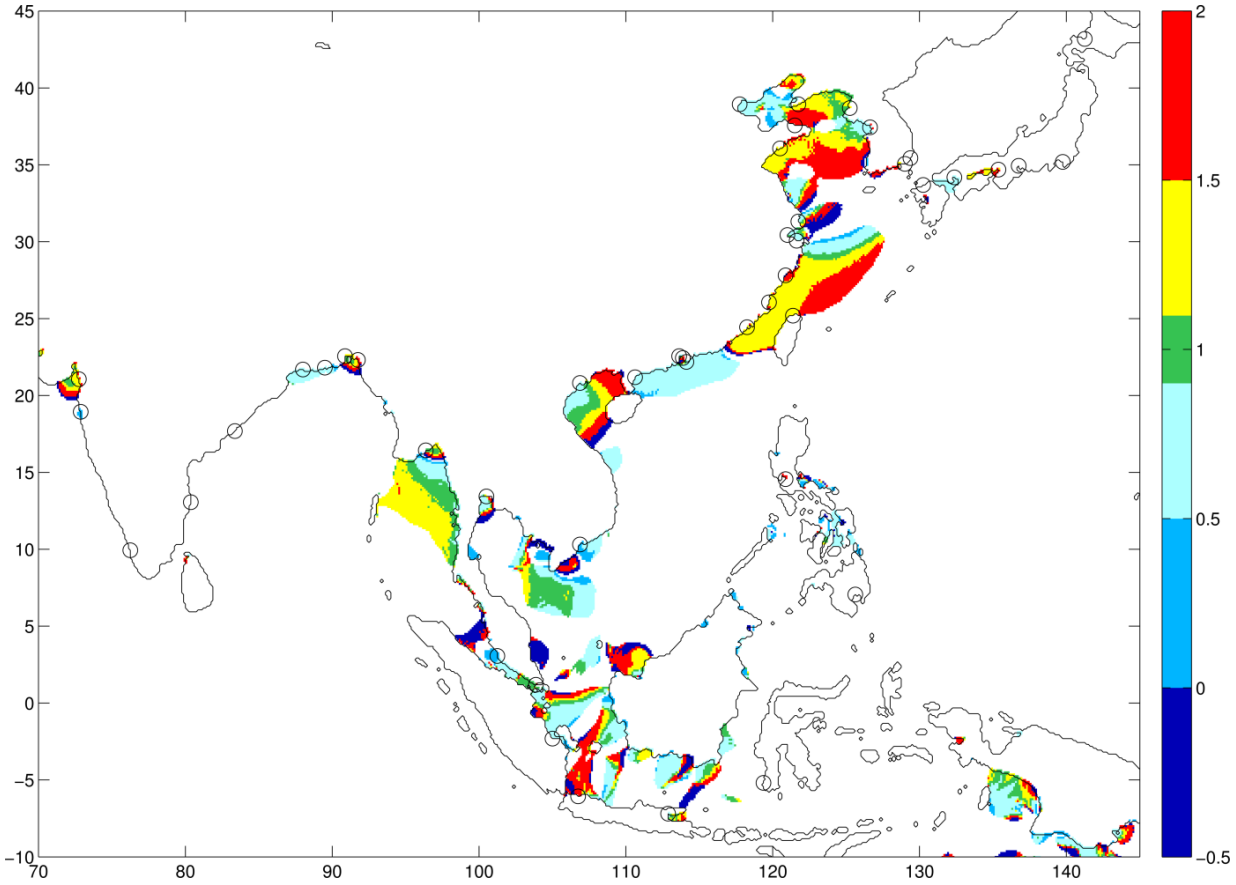

Figure 3.28. Asian normalised proportionality ratio of the significant MHW change with 5m uniform SLR (+5UF) to the MHW change with 0.5m uniform SLR (+0.5UF) assuming a fixed coastline. Proportional change is given by a ratio of 1 (± 0.1). Ratio values <0.9 (>1.1) or <0 show a below (above) proportional change or sign change of the MHW response in the SLR scenario. Insignificant MHW Changes (<+/ >- 5cm) are masked out. Black circles mark coastal cities.

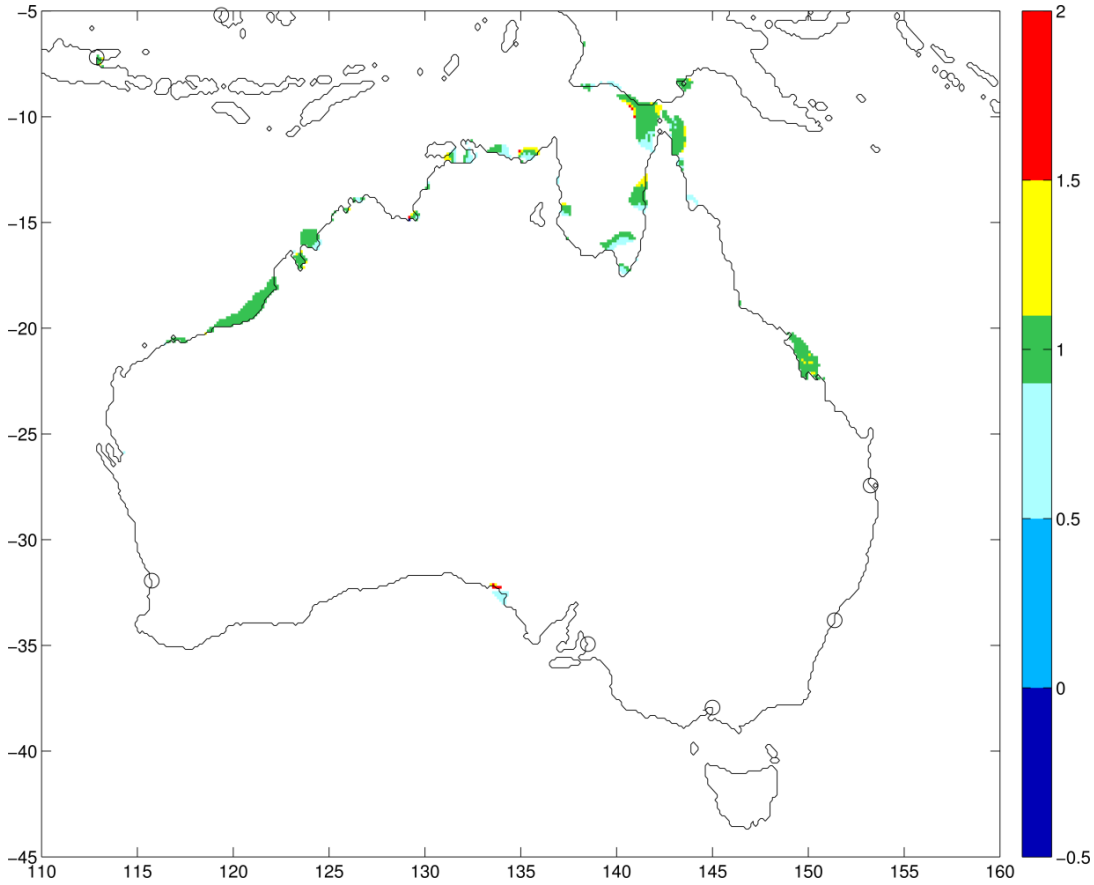

Figure 3.29. Australian normalised proportionality ratio of the significant MHW change with 1m uniform SLR (+1UF) to the MHW change with 0.5m uniform SLR (+0.5UF) assuming a fixed coastline. Proportional change is given by a ratio of 1 (± 0.1). Ratio values <0.9 (>1.1) or <0 show a below (above) proportional change or sign change of the MHW response in the SLR scenario. Insignificant MHW Changes (<+/ >- 5cm) are masked out. Black circles mark coastal cities.

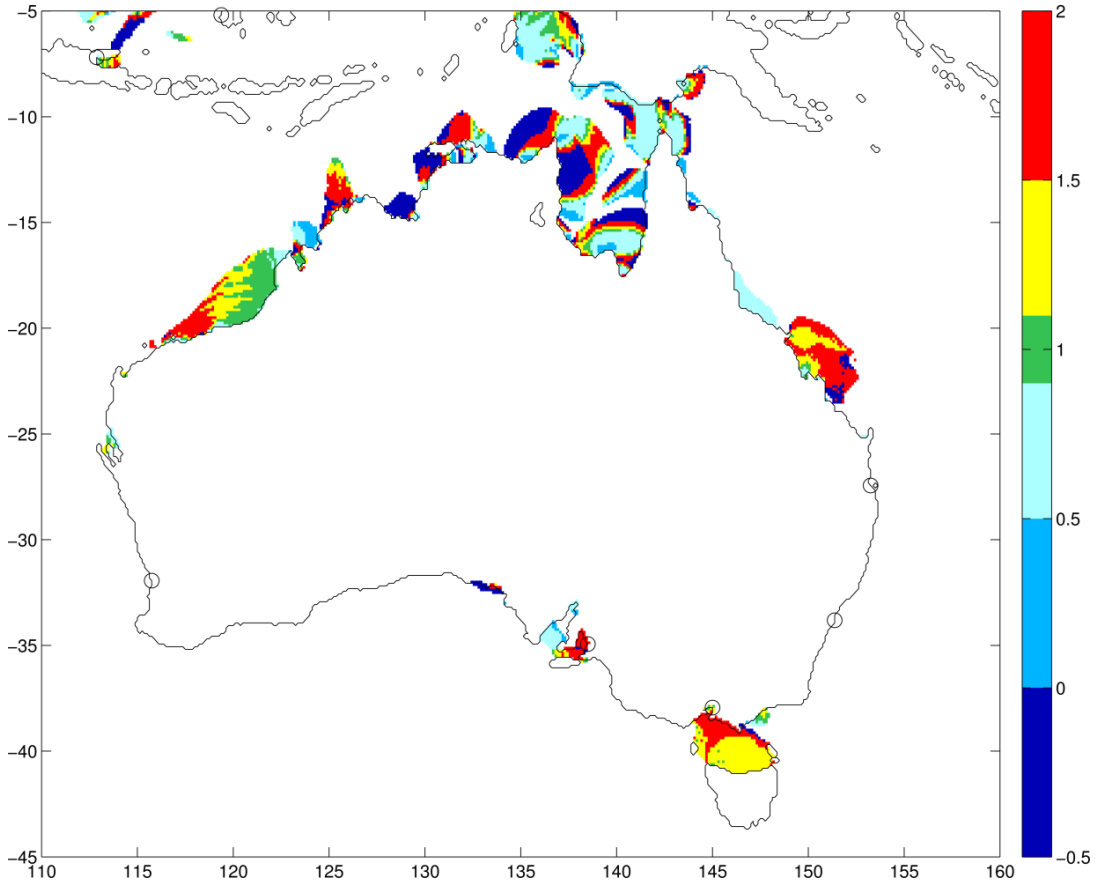

Figure 3.30. Australian normalised proportionality ratio of the significant MHW change with 5m uniform SLR (+5UF) to the MHW change with 0.5m uniform SLR (+0.5UF) assuming a fixed coastline. Proportional change is given by a ratio of 1 (± 0.1). Ratio values <0.9 (>1.1) or <0 show a below (above) proportional change or sign change of the MHW response in the SLR scenario. Insignificant MHW Changes (<+/ >- 5cm) are masked out. Black circles mark coastal cities.

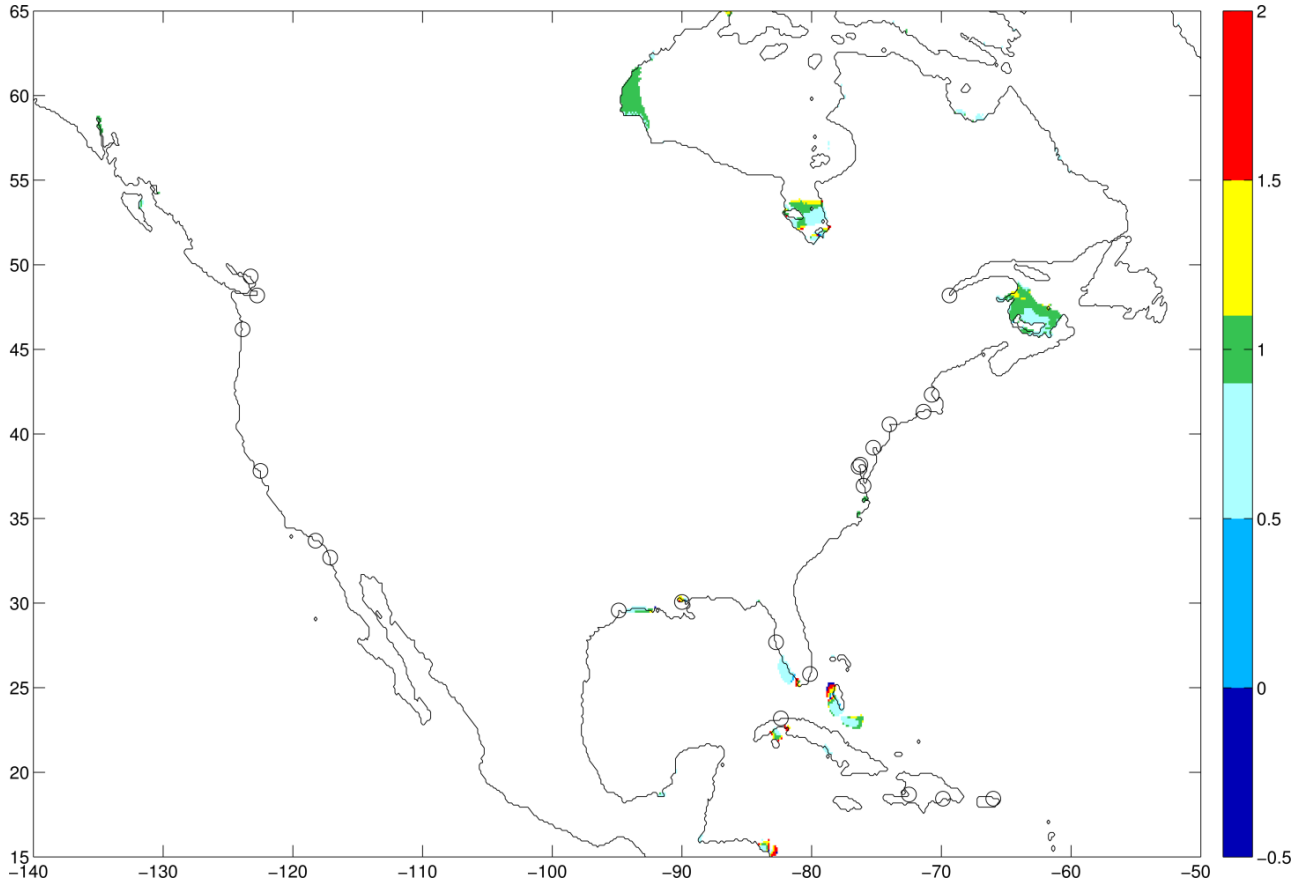

Figure 3.31. North American normalised proportionality ratio of the significant MHW change with 1m uniform SLR (+1UF) to the MHW change with 0.5m uniform SLR (+0.5UF) assuming a fixed coastline. Proportional change is given by a ratio of 1 (± 0.1). Ratio values <0.9 (>1.1) or <0 show a below (above) proportional change or sign change of the MHW response in the SLR scenario. Insignificant MHW Changes (<+/ >- 5cm) are masked out. Black circles mark coastal cities.

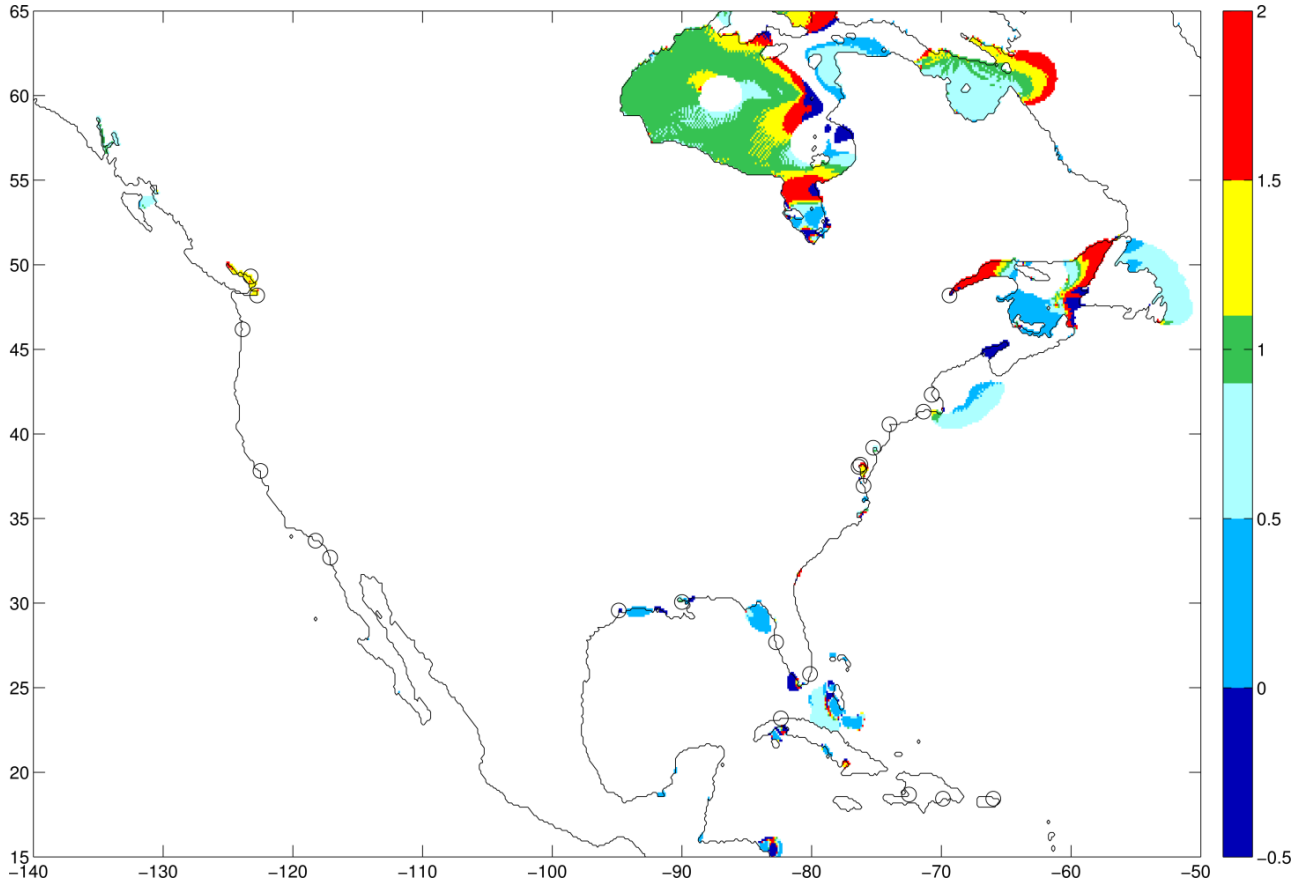

Figure 3.32. North American normalised proportionality ratio of the significant MHW change with 5m uniform SLR (+5UF) to the MHW change with 0.5m uniform SLR (+0.5UF) assuming a fixed coastline. Proportional change is given by a ratio of 1 (± 0.1). Ratio values <0.9 (>1.1) or <0 show a below (above) proportional change or sign change of the MHW response in the SLR scenario. Insignificant MHW Changes (<+/ >- 5cm) are masked out. Black circles mark coastal cities.

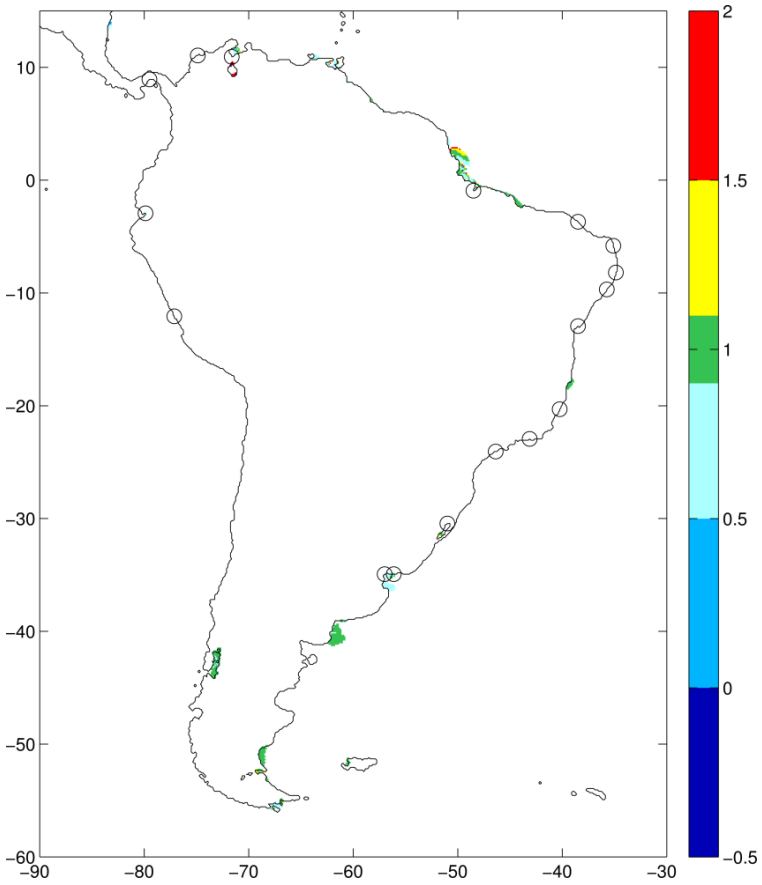

Figure 3.33. South American normalised proportionality ratio of the significant MHW change with 1m uniform SLR (+1UF) to the MHW change with 0.5m uniform SLR (+0.5UF) assuming a fixed coastline. Proportional change is given by a ratio of 1 (± 0.1). Ratio values <0.9 (>1.1) or <0 show a below (above) proportional change or sign change of the MHW response in the SLR scenario. Insignificant MHW Changes (<+/ >- 5cm) are masked out. Black circles mark coastal cities.

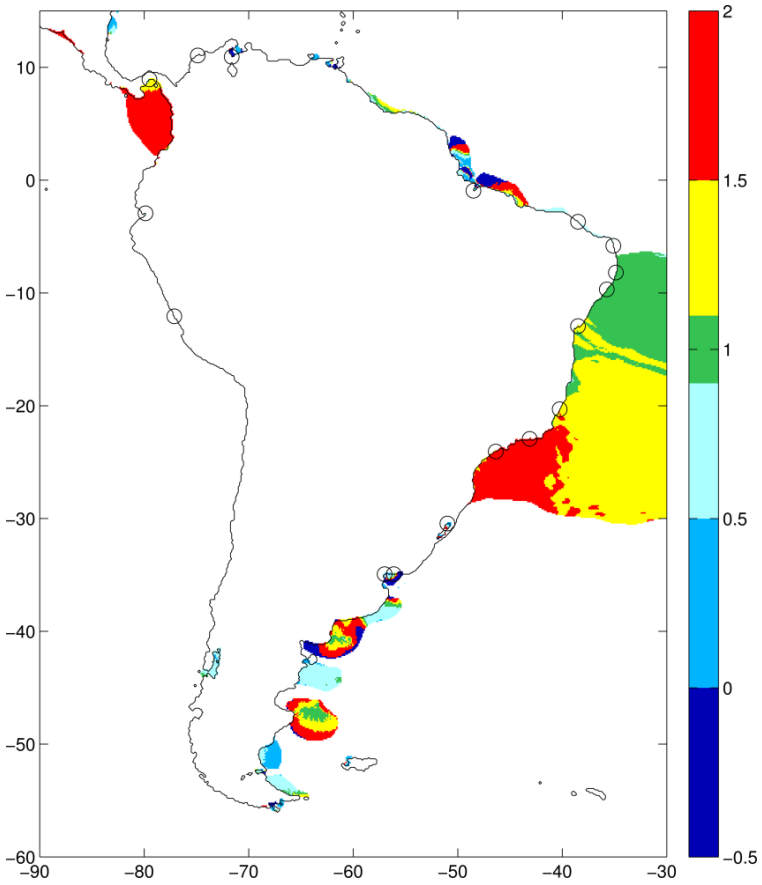

Figure 3.34. South American normalised proportionality ratio of the significant MHW change with 5m uniform SLR (+5UF) to the MHW change with 0.5m uniform SLR (+0.5UF) assuming a fixed coastline. Proportional change is given by a ratio of 1 (± 0.1). Ratio values <0.9 (>1.1) or <0 show a below (above) proportional change or sign change of the MHW response in the SLR scenario. Insignificant MHW Changes (<+/ >- 5cm) are masked out. Black circles mark coastal cities.

Corresponding distributions for +5UF are shown in Figure 3.24, 3.26, 3.28, 3.30, 3.32 and 3.34. +5UF is presented, rather than +10UF, as it is considered more plausible in the context of long timescale SLR (Church et al., 2014). Not surprisingly there are larger areas where the MHW changes exceed ±5cm in the 5m SLR plots than in the corresponding plots for only 1m of SLR. This is supported by the total numbers of significant cells in Table 3.8 (~13,000 with 1m SLR compared with ~104,000 with 5m SLR). The masking employed in the figures ensures that proportionality ratios are only shown at points with significant MHW change.

Figure 3.23 and 3.24 show the proportionality of MHW changes for Europe with 1m and 5m SLR. Changes that are proportional with 1m SLR in the Celtic Sea and western English Channel become slightly below and above proportional respectively with 5m SLR. In the southern North Sea, the near proportional and proportional changes with 1m SLR become below proportional with 5m SLR. In the rest of the North Sea, with 5m SLR, large new areas experience significant MHW change in a variety of proportionality ratio categories. In the Baltic Sea regions of proportional and near proportional change with 1m SLR become areas of sign change with 5m SLR.

Figure 3.25-3.34 show these same proportionality characteristics for Africa, Asia, Australia, North and South America. Generally the changes around the African coast are proportional or near proportional with 1m SLR and become less proportional with 5m SLR. Asia shows a similar trend with extensive proportional areas becoming non-proportional with 5m SLR. Around Australia and South America changes are proportional or slightly below proportional with 1m SLR. On the central north coast of Australia changes with 5m SLR show a variety of proportionality ratios whereas changes on the northwest coast of Western Australia, east coast of Queensland and Bass Strait are largely above proportional. South American changes become more non-proportional with 5m SLR, additionally large new areas of proportional and above proportional change extend from the central Brazilian coastline. In North America changes in the Gulf of Mexico are largely non-proportional with 1m SLR and become more so with 5m SLR, changes are largely proportional in the southern Gulf of St. Lawrence with 1m SLR and the Hudson Bay with 5m SLR. Other localised features to note include the areas of strongly above proportional change with 5m SLR in the Persian Gulf, northwest South China Sea, parts of the East China

Sea, west Java Sea, east and west Gulf of St Lawrence, west coast of Columbia, southeast coast of Brazil, and parts of the Patagonian Shelf.

In Table 3.5-3.7, non-proportionality of the changes in the tidal properties presented for individual port cities is indicated by the stars after the change value. Using the full versions of these tables with all 136 coastal city results (see Appendix 3.1) the percentage of cities with non-proportional change for each tidal property and SLR scenario is given in Table 3.9. Similarly to the MHW results in Table 3.8 all properties have a tendency towards non-proportionality with increasing SLR. This is summarised in the increasing mean values (as SLR increases). The low K_1 constituent mean across the SLR scenarios shows it to be the most proportional property; conversely the high S_2 mean shows it to be the least proportional property. In Table 3.6 and 3.7 the same trend towards more non-proportional changes (stars) at the higher SLR is shown.

Table 3.9. Percentages of all the 136 coastal cities analysed where the change in tidal constituent, MHW or maximum range is defined as non-proportional (>+/ <- 10%) with respect to the scaled 0.5m SLR change. Mean values for constituents, MHW and maximum range as well as for each uniform fixed coastline (UF) SLR scenarios are given.

	Percentage of 136 Coastal Cities with Non-Proportional Change (%)				
Property	+1UF	+2UF	+5UF	+10UF	Mean
M2	56	79	89	93	79
S2	71	85	93	93	85
K1	43	72	88	93	74
O1	63	82	90	90	81
MHW	57	79	94	93	81
Max Range	51	74	89	93	77
Mean	57	79	90	93	

The equivalents of Table 3.8 and 3.9 showing the proportionality for the coastal recession SLR scenarios are Table 3.10 and 3.11 respectively. The proportionality ratio is defined as the ratio of the change in the tidal property (for a given scenario) to its change in the +0.5UF or +0.5UR case as appropriate (ratio is then normalised by the SLR scenario). There are no domain changes in the +0.5UR or +1UR cases (only the coastal shallowing effect discussed in Section 3.7.2). The +0.5UR tidal changes are therefore largely identical to the +0.5UF changes so comparing proportionality for the two coastal setups using near identical baselines is meaningless. As the +1UR scenario also entails no

domain change its proportionality results in Table 3.10 and 3.11 are similar to the +1UF case. For +2UR, +5UR and +10UR scenarios (where substantial domain changes do occur) the results are almost entirely non-proportional. In these cases the numerator of the ratio is significantly affected by domain changes whilst the denominator is not; the recession proportionality values are therefore biased and valid comparison with the fixed coastline case is not possible.

Table 3.10. Percentage of total significant (>+/ <- 5cm) MHW change cells in each proportionality category for various uniform SLR scenarios with a coastal recession assumption (UR). The proportionality ratio for each cell is given by the ratio of the MHW change for the SLR scenario to the 0.5m SLR MHW change which is then normalised for each SLR scenario so that proportional change is given by a ratio of 1 (± 0.1). Ratio values <0.9 (>1.1) or <0 show a below (above) proportional change or sign change of the MHW response in the SLR scenario.

	Percentage of Sig. MHW Response Cells in each Proportionality Category (%)			
Norm. Proportionality Ratio	+1UR	+2UR	+5UR	+10UR
<0 (Sign Change)	1	65	54	41
0- 0.5	0	2	5	6
0.5- 0.9	16	6	9	8
0.9- 1.1 (Proportional)	67	2	3	2
1.1- 1.5	11	5	4	4
1.5+	5	20	26	39
Total Sig. Cells (>+/ <- 5cm)	11894	71857	116600	282786

Table 3.11. Percentages of the all 136 coastal cities analysed where the change in tidal constituent, MHW or maximum range is defined as non-proportional (>+/ <- 10%) with respect to the scaled 0.5m SLR change. Mean values for constituents, MHW and maximum range as well as for each uniform coastal recession SLR scenario (UR) are given.

	Percentage of 136 Coastal Cities with Non-Proportional Change (%)				
Property	+1UR	+2UR	+5UR	+10UR	Mean
M2	49	98	98	99	86
S2	68	97	98	95	89
K1	40	90	94	94	80
O1	68	99	97	98	91
MHW	53	98	99	96	86
Max Range	51	95	99	97	85
Mean	55	96	97	96	

Tidal change symmetry about the present day SL was tested by comparing the 2m SLF and 2m SLR changes. In the -2UA case the coastline is allowed to advance so one might expect it to be fairly symmetrical with the +2UR case.

The MHW change with -2UA is shown in Figure 3.35 and whether this is inversely correlated with +2UF or +2UR MHW change can be assessed qualitatively by comparison with Figure 3.9 and 3.10. In most areas the -2UA scenario has spatial patterns and magnitudes of change that are similar but of opposing sign to the +2UF results. There are some limited areas such as the Hudson Strait, Gulf of Mexico, eastern North Sea, East China Sea where the symmetry is better with the +2UR MHW change. Table 3.12 gives MHW change at 40 cities with -2UA as well as the two coastal conditions for 2m SLR for comparison. At 37 of the 40 locations a change of the opposing sign to the

Table 3.12. Changes in MHW with 2m of Uniform SLF permitting the coastline to advance (-2UA). To assess whether the changes are symmetrical about the present day (Control) MHW the changes with 2m Uniform SLR are also shown, assuming both fixed coastline (+2UF) and coastal recession (+2UR). This subset of 40 of the 136 coastal cities with populations >1 million is based on the largest MHW changes with 2m SLF (cities where the representative model cell dries with SLF are not able to be included in the top 40).

	Present Day Exposure Ranking		MHW (cm)			
COUNTRY, City/Agglomeration	Population	Asset	Control	+2UF	+2UR	-2UA
AUSTRALIA, Adelaide	123	103	86	0	17	-7
AUSTRALIA, Brisbane	86	61	64	-1	-3	6
AUSTRALIA, Melbourne	100	74	74	7	10	-4
BANGLADESH, Chittagong	39	72	147	16	-13	-6
BANGLADESH, Dhaka	14	43	134	25	-1	-17
CANADA, Montréal	84	55	182	-8	66	56
CHINA, Dalian	55	63	67	12	-3	5
CHINA, Fuzhou Fujian	42	48	234	22	6	-16
CHINA, Hangzhou	92	108	166	16	25	-12
CHINA, Ningbo	34	40	68	28	20	-17
CHINA, Shanghai	3	13	205	-21	-22	8
CHINA, Taipei	49	59	85	16	8	-12
CHINA, Tianjin	12	25	67	12	1	-7
CHINA, Xiamen	36	44	212	15	2	-5
CHINA, Yantai	115	119	33	7	-5	8
CHINA, Zhanjiang	40	45	112	-12	-7	27
CHINA, HONG KONG SAR, Hong Kong	41	20	70	-5	-2	8
NORTH KOREA, Namp'o	87	121	167	12	-6	9
DENMARK, Copenhagen	82	53	27	9	15	-17
ECUADOR, Guayaquil	26	41	152	7	-71	-11
INDIA, Calcutta	6	22	127	-12	-43	10
INDONESIA, Jakarta	21	39	52	-4	0	6
INDONESIA, Palembang	48	73	76	18	-10	-17
INDONESIA, Surabaya	68	88	194	-25	-50	23
IRELAND, Dublin	95	62	129	12	-22	-12
JAPAN, Hiroshima	44	24	175	-10	-58	11
KUWAIT, Kuwait City	101	84	99	9	-13	-8
MOZAMBIQUE, Maputo	66	112	101	-4	-2	4
NETHERLANDS, Amsterdam	15	6	76	7	-33	59
NETHERLANDS, Rotterdam	17	7	131	-8	-69	-21
PHILIPPINES, Manila	53	66	55	-2	-4	-6
SOUTH KOREA, Inchon	43	30	353	13	-10	16
SWEDEN, Stockholm	128	115	14	3	3	-9
UKRAINE, Odessa	61	67	10	-4	-4	16
UNITED ARAB EMIRATES, Dubai	38	23	52	3	-6	-11
USA, New York-Newark	7	2	55	0	-7	6
USA, Philadelphia	47	21	73	-5	4	17
USA, Virginia Beach	27	10	35	-2	-4	5
URUGUAY, Montevideo	94	96	20	11	3	19
VIETNAM, Ho Chi Minh City	5	27	128	-27	-46	42

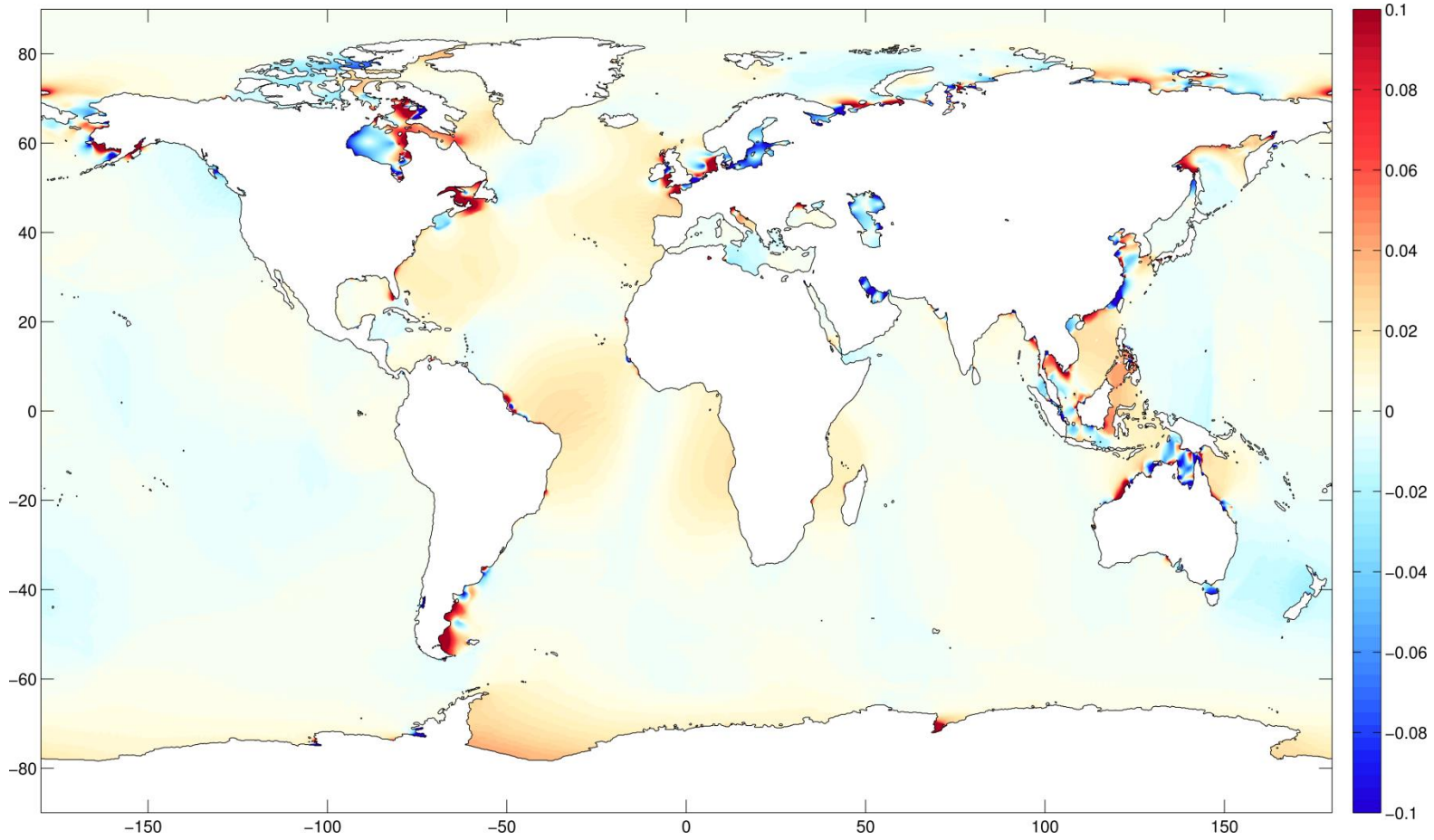

Figure 3.35. Change in MHW (m) with a 2m uniform SLF permitting the coastline to advance (-2UA) (increases- red, decreases- blue). For coastal city changes see Table 3.12. To assess symmetry of MHW change about present day SL compare with Figure 3.9 and 3.10.

-2UA change can be found in one of the two 2m SLR coastal setups, suggesting fairly a fairly symmetric tidal change. The -2UA change is more symmetrical with the +2UF scenario at 26 locations and with +2UR case at the other 14.

3.4.4 Effect on MHW of non-uniform SLR due to IER

This section describes the tidal response to non-uniform perturbations of the SLR resulting from IER. Three scenarios are chosen, all of which imply a 2m global MSLR. The three scenarios have distinct spatial fingerprints based on ice sheet melt contributions that are (1) 100% (2m) from Greenland, (2) 100% (2m) from Western Antarctic and (3) 50% (1m) from Greenland and 50% (1m) from Western Antarctica. These are shown in Figure 3.36, 3.37 and 3.38. The SLR fingerprint for the Greenland melt scenario (Figure 3.36) shows SLR to be above average in the southern hemisphere with peak SLR occurring in the South Atlantic and southeast Pacific Ocean; in the northern hemisphere SLR is below average in the North Atlantic and Arctic Ocean with another area of peak SLR in the northwest Pacific. The fingerprint for the Western Antarctic melt scenario (Figure 3.37) shows below average SLR in the Southern Ocean particularly in the southwest Atlantic and southern Pacific, peak SLR occurs in the central Indian Ocean, northeast Pacific and northwest Atlantic, the northern hemisphere experiences average or above average SLR. The combined fingerprints with 1m SLR from each ice sheet (Figure 3.38) shows below average SLR in the southwest Atlantic, southern Pacific, northern North Atlantic and Arctic Oceans; above average SLR largely occurs between the tropics with peak SLR in the north Pacific, South Atlantic and Indian Oceans.

The effect on the MHW of these three IER SLR perturbations is initially assessed with a fixed present day coastline but allowing coastal advancement (drying where SLFs). The +2UF MHW changes were thoroughly described in Section 3.4.1 but here we focus on regions where non-uniform SLR causes deviations from these changes. In the Greenland melt case (+2NUGF) the MHW response (Figure 3.39) differs from the uniform SLR response (Figure 3.9) in Hudson Bay (Northwest Passages) where the sign of change becomes negative (positive), the Gulf of St. Lawrence and Gulf of Maine where the sign of the change becomes positive and negative respectively and weakens in intensity. On the European Shelf and along the north coast of Russia the intensity of the changes are substantially reduced. Slight reductions (increases) in intensity occur in the

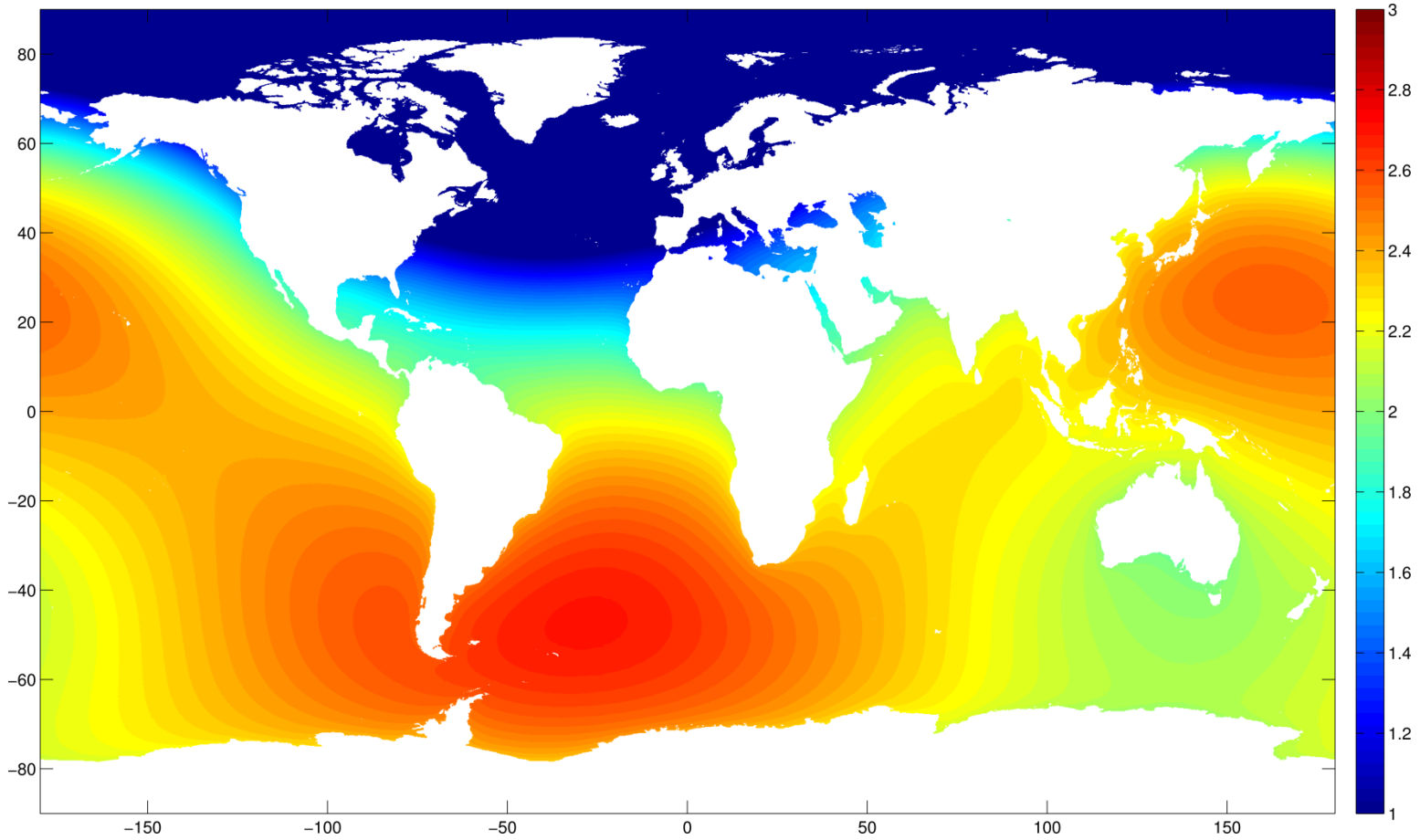

Figure 3.36. The SLR perturbation (m) applied to the model for the 2m average SLR non-uniform initial elastic response scenario with uniform ice sheet melt in Greenland (+2NUG). In the near field of the area of the mass loss SL change can be negative. Data courtesy of Mitrovica et al. (2001).

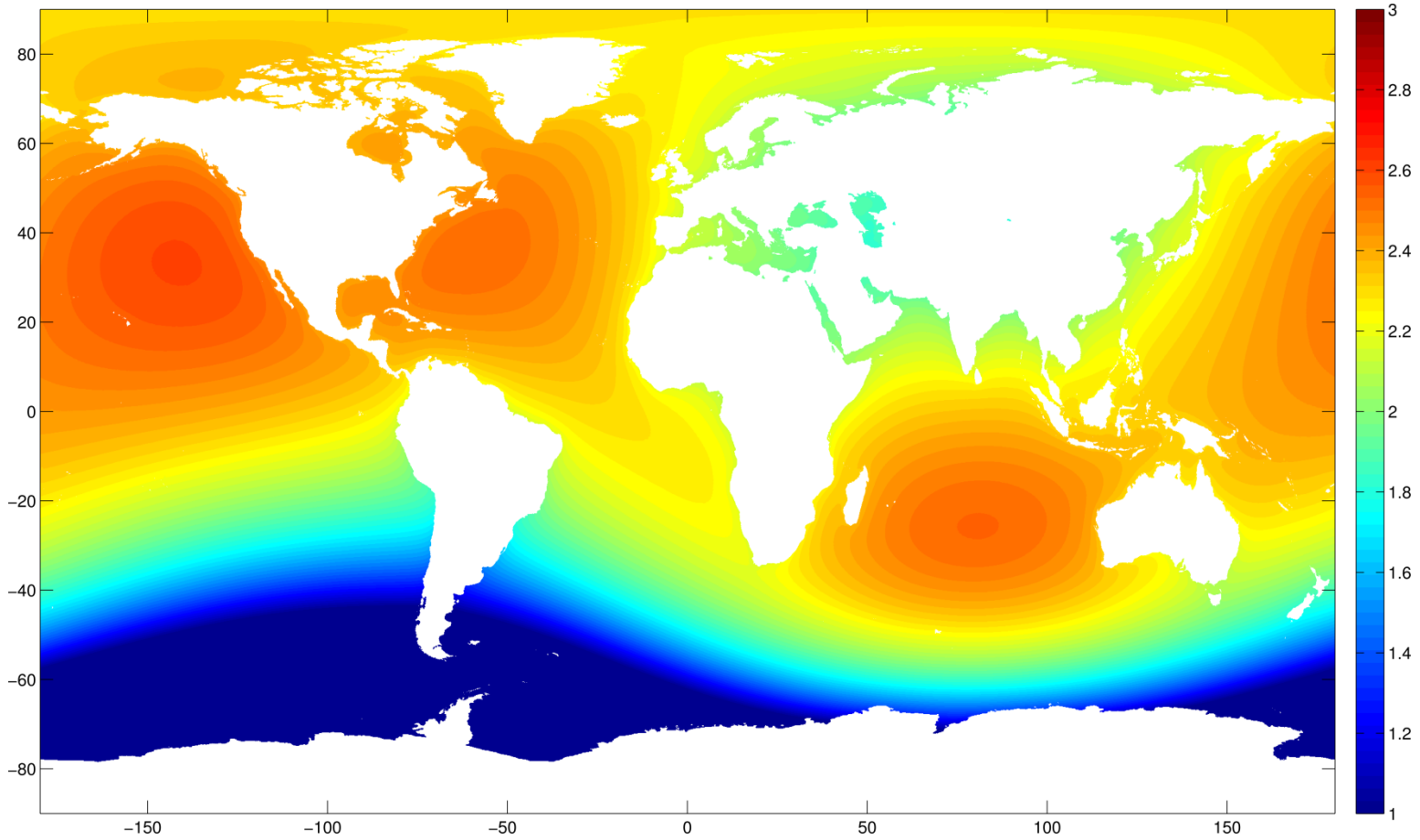

Figure 3.37. The SLR perturbation (m) applied to the model for the 2m average SLR non-uniform initial elastic response scenario with uniform ice sheet melt in Western Antarctica (+2NUWA). In the near field of the area of the mass loss SL change can be negative. Data courtesy of Mitrovica et al. (2001).

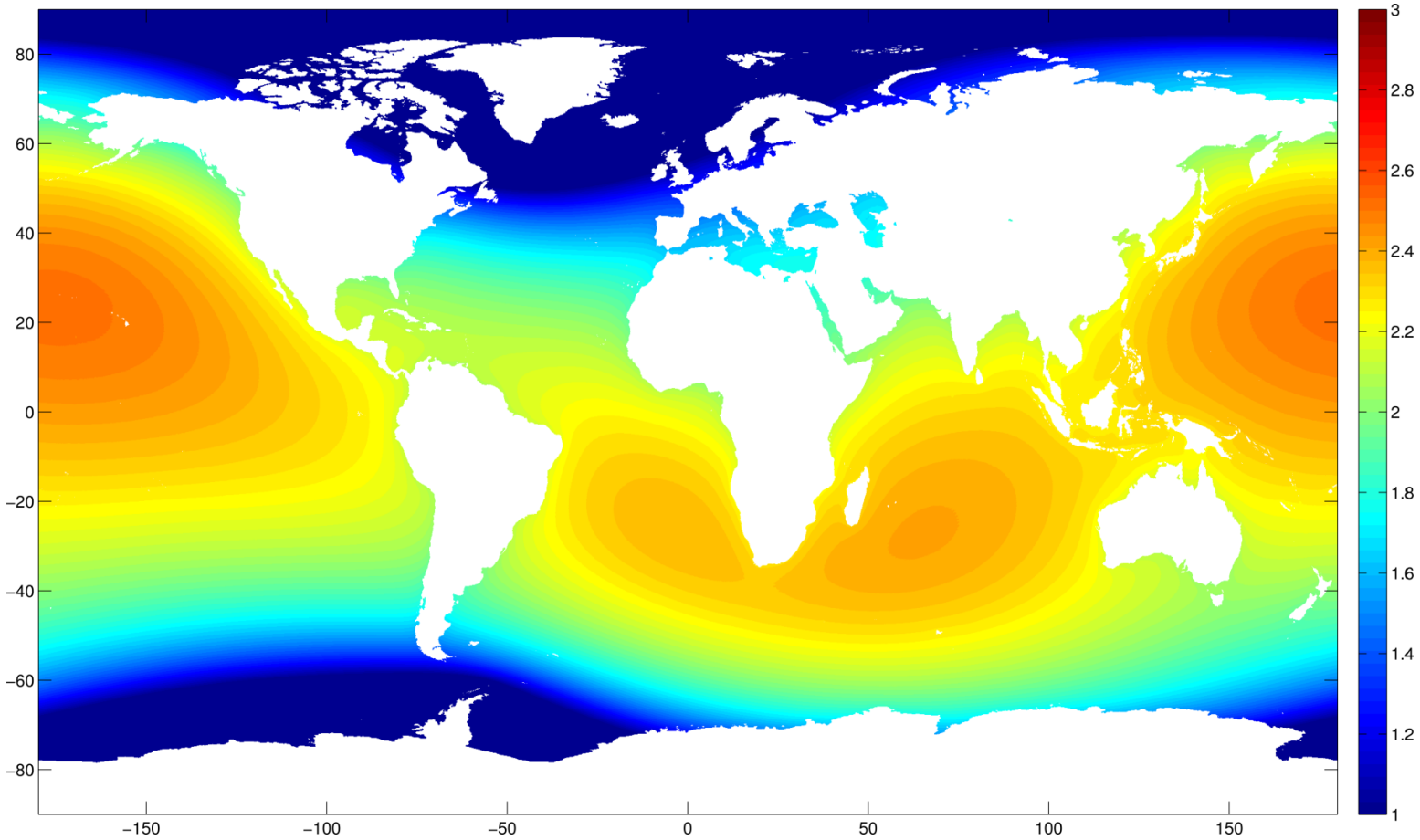

Figure 3.38. The SLR perturbation (m) applied to the model for the 2m average SLR non-uniform initial elastic response scenario with uniform ice sheet melt in both Greenland (1m) and Western Antarctica (1m) (+2NUB). In the near field of the areas of the mass loss sea-level change can be negative. For coastal city SLR values see Table 3.4. Data courtesy of Mitrovica et al. (2001).

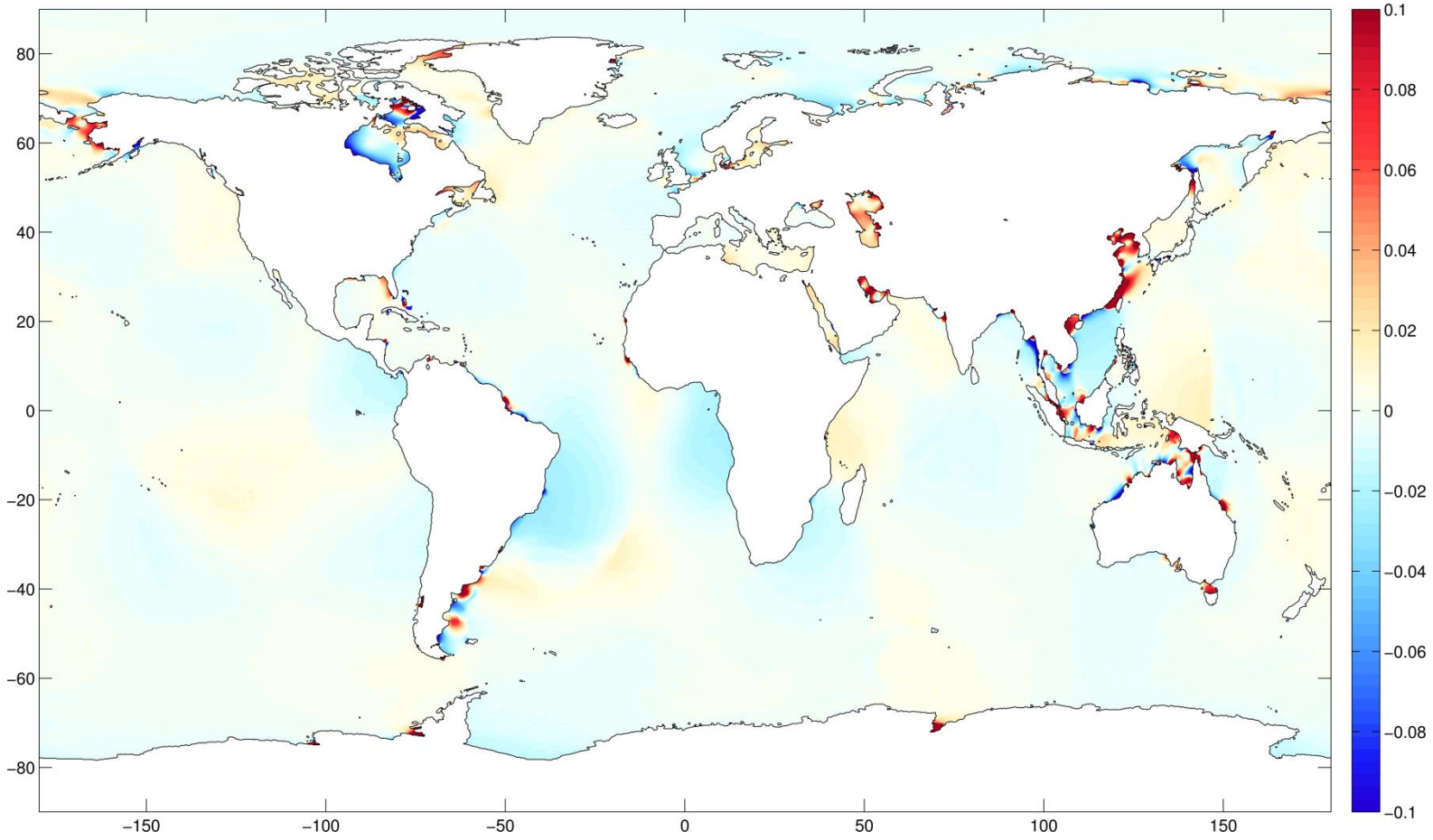

Figure 3.39. Change in MHW (m) with an average of 2m of non-uniform SLR from Greenland (Figure 3.36) assuming a fixed coastline (+2NUGF) (increases- red, decreases- blue). For coastal city changes see Table 3.13.

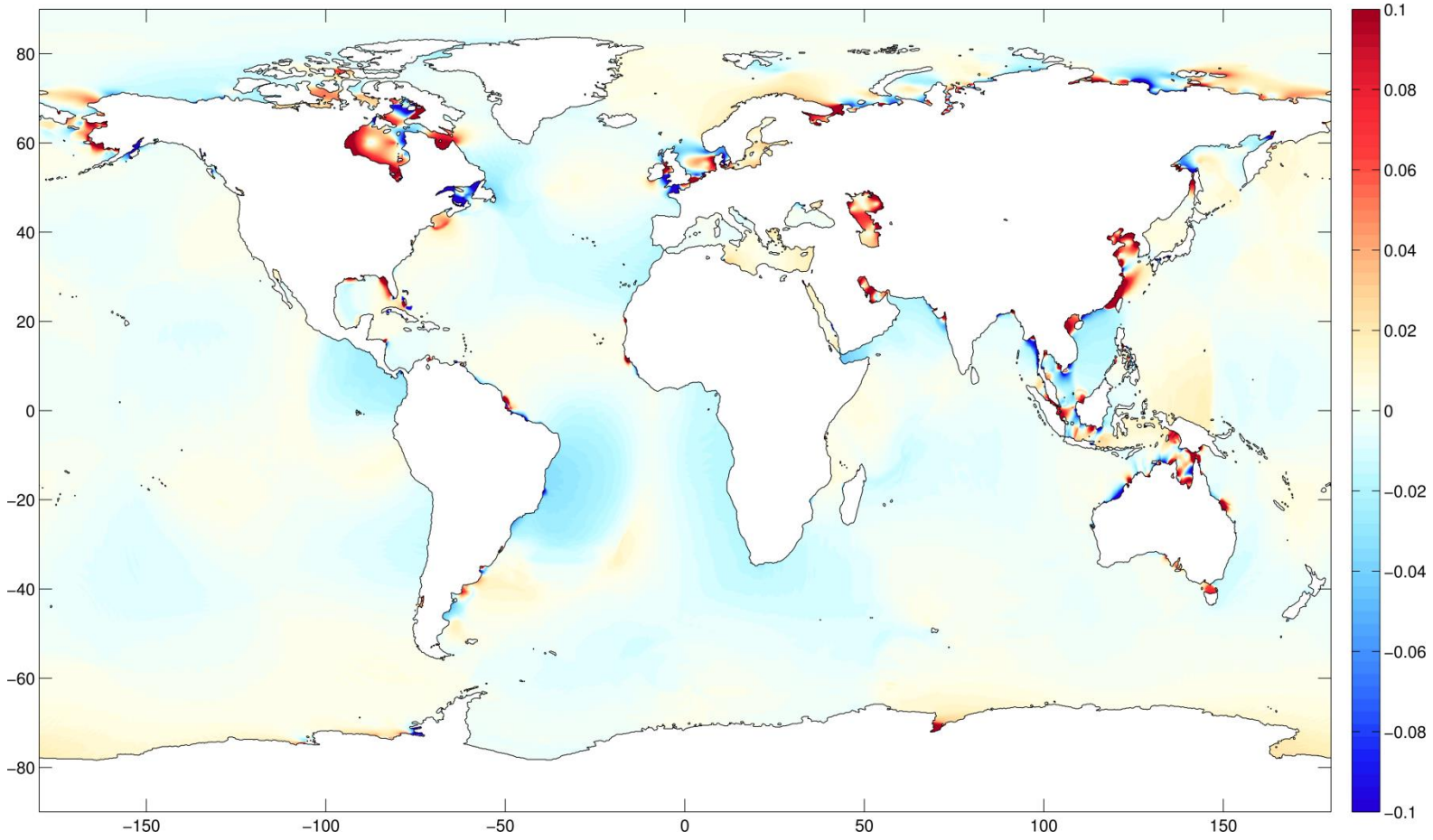

Figure 3.40. Change in MHW (m) with an average of 2m of non-uniform SLR from Western Antarctica (Figure 3.37) assuming a fixed coastline (+2NUWAF) (increases- red, decreases- blue). For coastal city changes see Table 3.13.

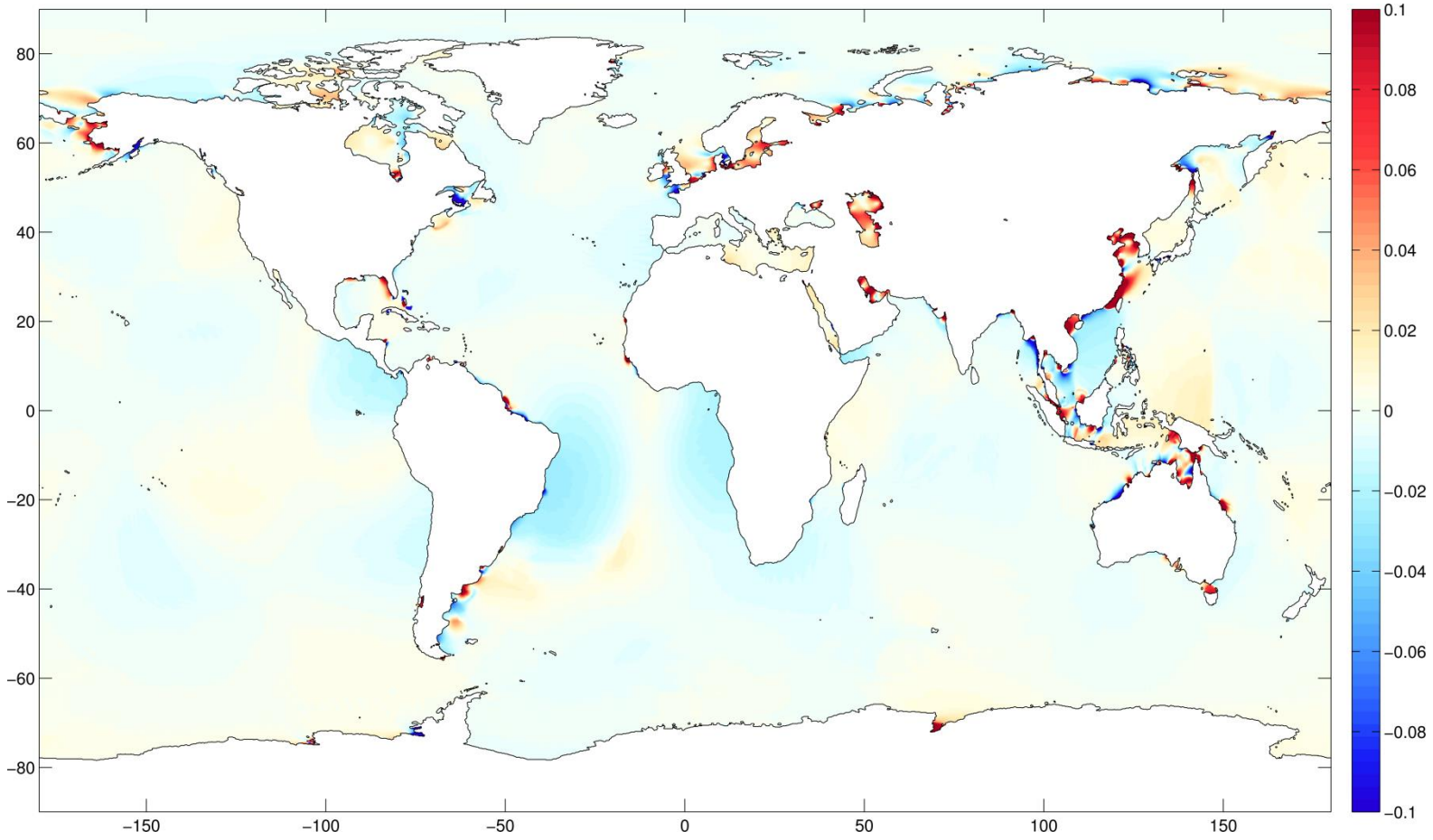

Figure 3.41. Change in MHW (m) with an average of 2m of non-uniform SLR from both Greenland and Western Antarctica (Figure 3.38) assuming a fixed coastline (+2NUBF) (increases- red, decreases- blue). For coastal city changes see Table 3.13.

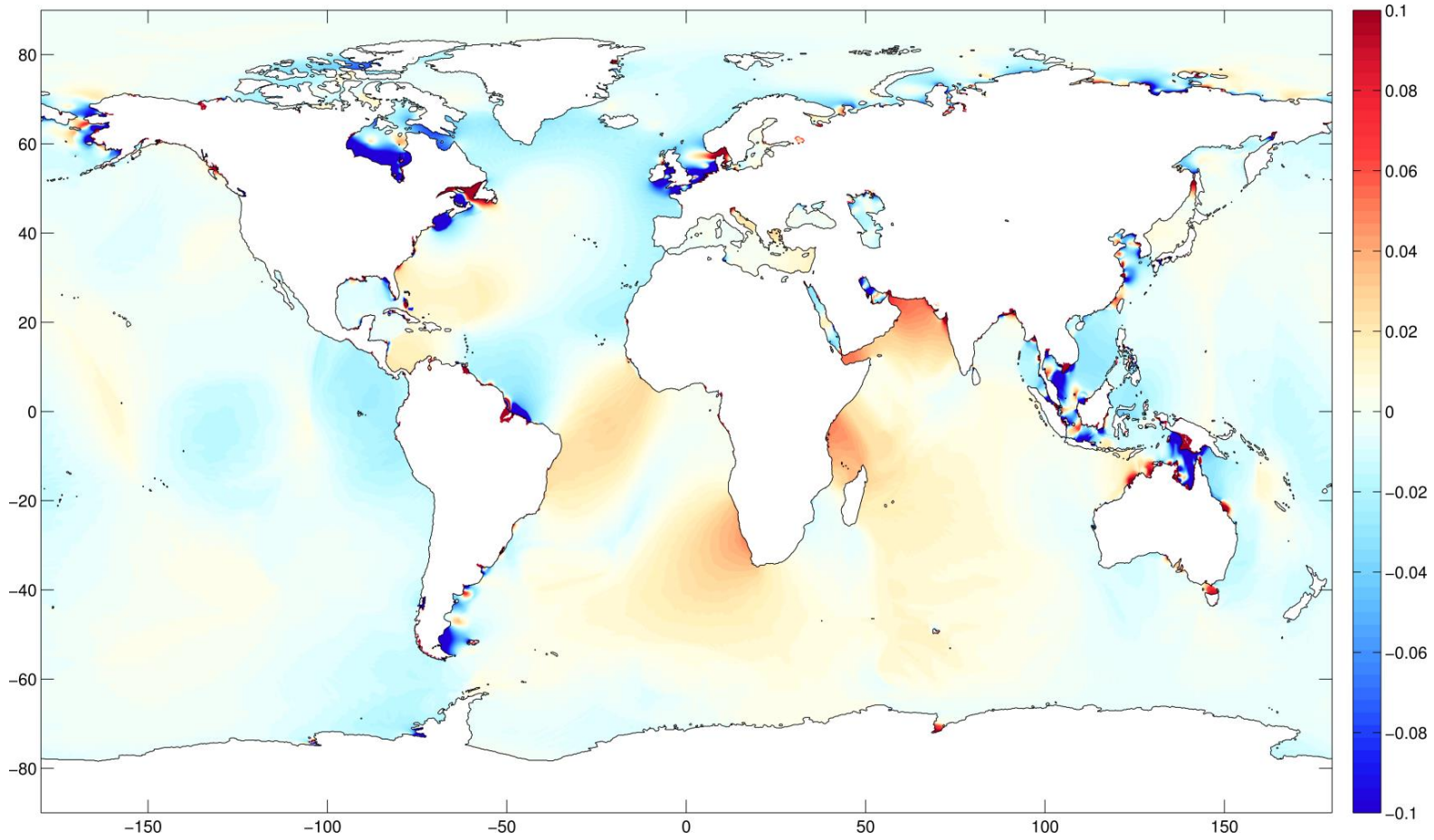

Figure 3.42. Change in MHW (m) with an average of 2m of non-uniform SLR from both Greenland (1m) and Western Antarctica (1m) (Figure 3.38) permitting recession of the coastline, except around Antarctica (+2NUBR) (increases- red, decreases- blue). For coastal city changes see Table 3.13. Newly wet areas with SLR give the now calculable MHW values on the positive part of the colour scale.

Table 3.13. Changes in MHW with a global average of 2m SLR distributed non-uniformly according to initial elastic response sea-level fingerprints (Figure 3.36, 3.37 and 3.38) associated with uniform melt of either the Greenland (+2NUGF), Western Antarctic (+2NUWAF) or Both (+2NUBF) of these two ice sheets. A scenario with melt from Both ice sheets that permits coastal recession with SLR (+2NUBR) is also included. MHW change values with 2m uniform SLR for fixed (+2UF) and receding coastlines (+2UR) are provided for comparison. This subset of 40 of the 136 coastal cities with populations >1 million is based the same criteria as Table 3.5.

	Present Day Exposure Ranking		MHW (cm)						
COUNTRY, City/Agglomeration	Population	Asset	Control	+2UF	+2NUGF	+2NUWAF	+2NUBF	+2UR	+2NUBR
ARGENTINA, Buenos Aires	64	52	98	-15	-17	-13	-15	-64	-63
AUSTRALIA, Adelaide	123	103	86	0	2	3	2	17	4
BANGLADESH, Chittagong	39	72	147	16	18	16	17	-13	-17
BANGLADESH, Dhaka	14	43	134	25	28	26	27	-1	-40
BANGLADESH, Khulna	23	54	87	-4	-4	-4	-4	19	16
BRAZIL, Belém	72	79	233	28	27	29	28	-131	-140
BRAZIL, Porto Alegre	78	83	14	7	7	6	7	18	19
CAMEROON, Douala	110	128	70	-3	-3	-2	-3	-16	-16
CANADA, Montréal	84	55	182	-8	8	-18	1	66	74
CHINA, Dalian	55	63	67	12	14	12	13	-3	-5
CHINA, Fuzhou Fujian	42	48	234	22	26	22	24	6	-1
CHINA, Guangzhou Guangdong	2	11	121	-23	-26	-24	-25	-19	-18
CHINA, Shenzen	18	31	100	-11	-14	-12	-13	-8	-7
CHINA, Hangzhou	92	108	166	16	19	17	18	25	19
CHINA, Ningbo	34	40	68	28	32	29	31	20	17
CHINA, Shanghai	3	13	205	-21	-23	-22	-23	-22	-19
CHINA, Taipei	49	59	85	16	19	17	18	8	5
CHINA, Tianjin	12	25	67	12	13	12	13	1	-3
CHINA, Xiamen	36	44	212	15	19	16	17	2	19
CHINA, Zhanjiang	40	45	112	-12	-13	-12	-13	-7	-6
NORTH KOREA, Namp'o	87	121	167	12	14	12	13	-6	-6
DENMARK, Copenhagen	82	53	27	9	4	8	17	15	-4
ECUADOR, Guayaquil	26	41	152	7	7	7	7	-71	-70
GERMANY, Hamburg	37	18	156	-1	-1	0	3	-96	-99
GUINEA, Conakry	70	113	156	-21	-19	-23	-22	-15	-16
INDIA, Calcutta	6	22	127	-12	-12	-11	-12	-43	-40
INDIA, Surat	24	46	228	9	14	7	11	26	22
INDONESIA, Palembang	48	73	76	18	19	20	19	-10	-21
INDONESIA, Surabaya	68	88	194	-25	-27	-29	-29	-50	-50
IRELAND, Dublin	95	62	129	12	-2	14	6	-22	-28
JAPAN, Hiroshima	44	24	175	-10	-11	-11	-11	-58	-68
MALAYSIA, Kuala Lumpur	35	33	127	6	7	7	7	-15	-20
MYANMAR, Rangoon	22	60	158	33	36	34	35	-6	-2
NETHERLANDS, Amsterdam	15	6	76	7	4	7	6	-33	-41
NETHERLANDS, Rotterdam	17	7	131	-8	2	-9	-4	-69	-75
SOUTH KOREA, Inchon	43	30	353	13	15	13	14	-10	-6
UNITED KINGDOM, Glasgow	91	68	133	5	0	6	2	-29	-36
USA, Houston	67	36	65	-15	-15	-13	-15	-30	-34
USA, New Orleans	10	3	16	14	11	16	14	16	17
VIETNAM, Ho Chi Minh City	5	27	128	-27	-30	-30	-30	-46	-57

Gulf of Mexico (on the Patagonian Shelf and East China Sea). The MHW change in the Western Antarctic melt case (+2NUWAF) (Figure 3.40) is for the most part almost identical to the uniform SLR response (Figure 3.9) except for a substantial reduction in the intensity of the response on the Patagonian Shelf and slight increases in intensity of the Gulf of Mexico, Maine and St. Lawrence and Hudson Strait and Bay changes. The MHW change in the IER scenario with melt from both ice sheets (+2NUBF) (Figure 3.41) differs from the uniform scenario (Figure 3.9) in that the response in Hudson Bay, the Hudson Strait and Northwest Passages is almost entirely diminished, the response in the Gulf of St. Lawrence and on the European Shelf is substantially reduced with some change in sign in the North Sea; furthermore slight reductions in intensity also occur along the north coast of Russia and on the Patagonian Shelf. In all three IER SLR scenarios the MHW change within 30 degrees of the equator is largely consistent. This means regions such as Asia experience substantial changes to tidal characteristics, regardless of the IER scenario, whereas the effect of SLR on tides in higher latitude areas is more IER scenario dependent.

In some regions the differences between the uniform and non-uniform SLR scenarios are too small to identify by comparison of the MHW plots. The MHW change values at large coastal cities are therefore presented in Table 3.13. To complement this table the SLR imposed at the city location in each of the IER scenarios is given in Table 3.4. The values for cities such as Montreal confirm the large differences that are observed between all three IER scenarios and the uniform SLR case (which was -8cm): the IER results for Montreal were respectively a change in sign (8cm), intensification (-18cm) and reduction (1cm) for the +2NUGF, +2NUWAF and +2NUBF scenarios. In the Gulf of Mexico, values from New Orleans show a slight decrease (11cm) and increase (16cm) respectively from the Greenland and Western Antarctic melt scenarios compared to the uniform response (14cm). The tabulated values for Dublin exemplify the substantial changes on the European Shelf between the IER scenarios with the intensity of the uniform change (12cm) being substantially reduced (-2cm), similar (14cm) and reduced (6cm) for +2NUGF, +2NUWAF and +2NUBF. At all 22 Asian cities the uniform SLR MHW changes either remain the same or are intensified in all three IER scenarios.

Other noticeable differences from the uniform SLR MHW changes (for at least one IER scenario) can be seen at Copenhagen, Surat, Rotterdam and Glasgow.

Looking at the local SLR at the cities in each IER scenario (Table 3.4) it is interesting to note that most of the locations with large MHW differences are also those that experience the largest deviations from the MSLR of 200cm. Higher than global MSLR in the non-uniform SLR scenarios in addition to augmented tidal changes could pose substantially increased flood risk: for example, a uniform SLR of 200cm and MHW increase of 28cm at Ningbo becomes a SLR of 233cm and MHW increase of 32cm in the Greenland melt scenario.

To assess the tidal response associated with non-uniform SLR and also permitting coastal recession, a 2m average SLR scenario with 1m of melt from each of the ice sheets allowing coastal recession with SLR (as well as drying where SLFs) was tested. The MHW change under this +2NUBR scenario (Figure 3.42) can be compared with the MHW change for the +2UR scenario (Figure 3.10). The substantial differences with the uniform SLR change are in the Northwest Passages, northern Hudson Bay and Strait where the intensity of the MHW decrease is reduced. The substantial increases in the Labrador Sea (seen in Figure 3.10) become small decreases; the area of decrease in the Gulf of Maine no longer extends southeast into the Atlantic; on the European Shelf the areas of decrease become more pronounced and more widespread, and the slight increases in the Baltic and southern Barents Sea are diminished. The intensity of changes in the Caribbean Sea, on the Patagonian Shelf, coastline of Africa, Gulf of Aden, Arabian Sea, Strait of Taiwan and Sea of Okhotsk are all reduced slightly. Table 3.13 shows the differences between the +2UR and the +2NUBR scenarios. The differences between changes in the Uniform and Both scenarios are larger for coastal recession than for the fixed coastline case. With a fixed coastline the difference between the uniform SLR and IER Both scenarios is ≥5cm at only 3 of 40 cities whereas allowing coastal recession the difference is ≥5cm at 16 of 40 cities. The three largest differences between the +2UR and +2NUBR scenarios occur at Dhaka (-1cm to -40cm), Copenhagen (15cm to -4cm) and Xiamen (2cm to 19cm). The inclusion of non-uniform SLR in the coastal recession scenario significantly augments the large uniform changes at Belem, Montreal, Dublin, Hiroshima, Amsterdam, Rotterdam, Glasgow and Ho Chi Minh City. The coastal condition is shown to be as important in the IER scenario as it was for Uniform SLR. In the +2NUBF scenario there are 10 substantial (≥20cm or ≤-20cm) changes (5 of which are

decreases), whereas in the +2NUBR scenario, 18 are substantial (16 being decreases). These +2NUBF and +2NUBR scenarios show there to be a larger number of substantial changes (with a greater portion of them being decreases) when coastal recession is included - the same pattern identified in the uniform 2m SLR scenarios (Section 3.4.2).

3.4.5 Implications for marine renewable energy

The criteria for a presently viable location for tidal energy extraction given in Section 3.3.3 were used to create a mask that was then applied to the maximum range change results given in (Figure 3.17). Regional plots with this mask applied were created using the maximum range change with +2UF. The European plot in Figure 3.43 indicates that under this SLR scenario there are large decreases in available future energy in the Gulf of St. Malo (France), Bristol Channel (England), west coast of Scotland and east coast of England; increases are suggested in the eastern English Channel, eastern Irish Sea and north coast of East Anglia. Other global regions (not shown) viable for tidal power that are affected in this SLR scenario are the east of the Gulf of Martaban, west coast of South Korea, north coast of Western Australia, northeast Sea of Okhotsk, Northwest Passages, east Gulf of Alaska, northeast coast of Brazil, San Matias Gulf and southern Patagonian Shelf which all show decreases. On the other hand, increases in energy generating potential are predicted to be in the north of the Gulf of Martaban, Strait of Taiwan, northwest coast of South Korea, northeast coast of Western Australia, east coast of Queensland, Bay of Fundy, eastern Hudson Strait and the Gulf of Corcovado. It should be noted that the trends in the maximum tidal range are sometimes dependent on both the SLR scenario and the coastline assumption (e.g. the tidal response in the Hudson Strait).

3.4.6 Comparison of the modelled tidal changes with previous studies

Extensive comparison of the OTISmpi tidal changes in response to different SLR scenarios with results from other studies has been made. Figure 3.45 illustrates the OTISmpi M_2 tidal change with +2UF allowing direct comparison with previous regional modelling results (Figure 2.4). Comparison shows good agreement between the global and regional models particularly in the English Channel, Celtic Sea, Irish Sea and southern North Sea. The model results only

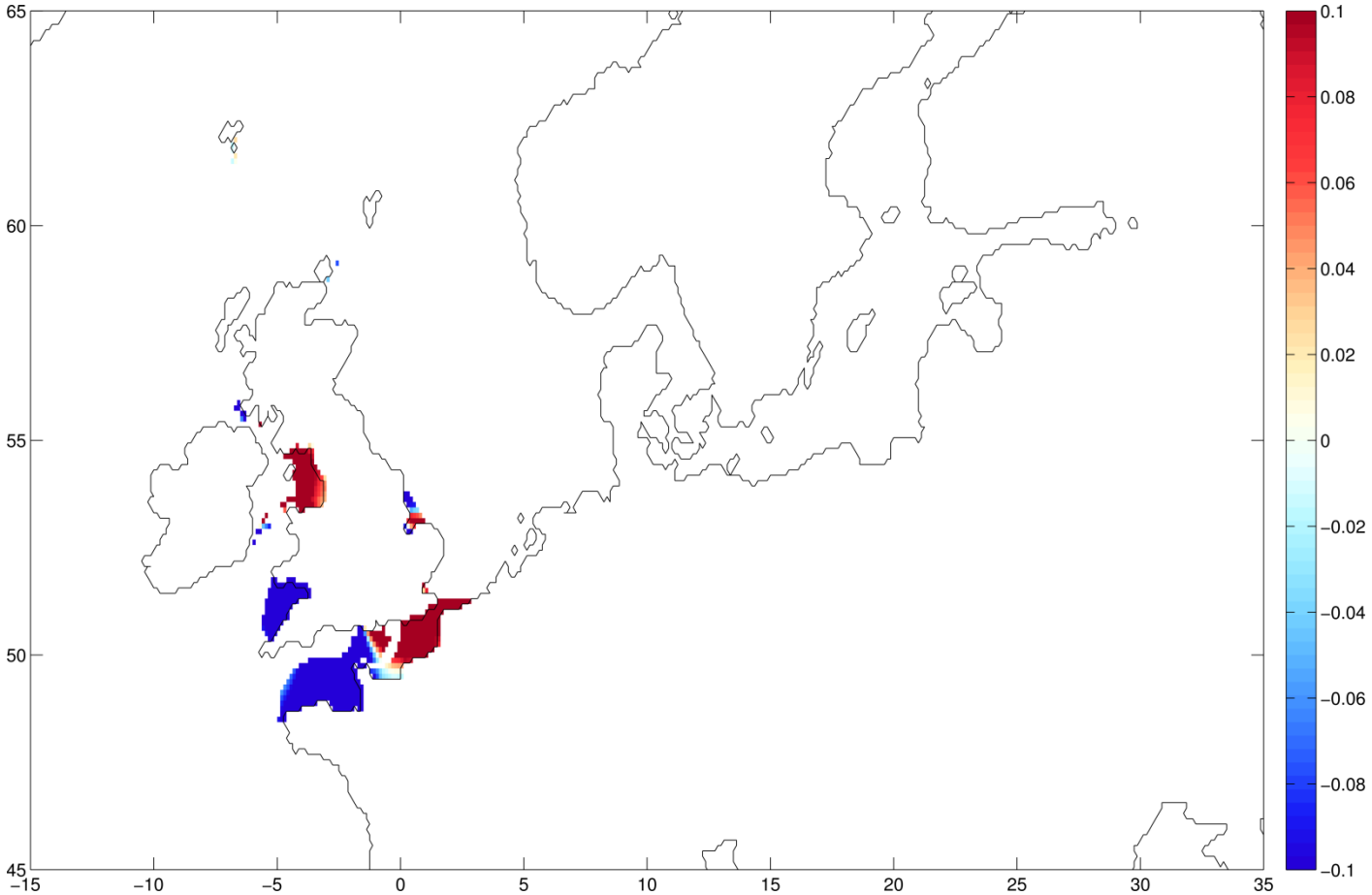

Figure 3.43. European change in maximum range (m), over the 15 day SSH reconstruction based on the four tidal constituents, with a 2m uniform SLR assuming a fixed coastline (+2UF) (increases- red, decreases- blue) for those locations found to be presently viable for tidal renewable energy (either 25-100m depth and peak current velocities >2m/s or with a MTR> 5m).

diverge in the Skagerrak and Kattegat where there is a change in sign of the M_2 constituent response between the models. However the global model domain differs in that it includes the Danish Straits and Baltic Sea, whereas the regional model does not.

The M_2 constituent response for a +5UF scenario (using a different setup of the OTISmpi model) was published in Figure. 6c of Green (2010). To allow direct comparison Figure 3.44 shows the M_2 amplitude change for this Chapter's +5UF scenario on the same colour scale. Broadly the two simulations show a similar M_2 response, however details differ. The results of Green (2010) suggest smaller changes in the Gulf of St. Lawrence, east coast of Brazil, Patagonian Shelf, southern Barents Sea, western Indian Ocean, northern Sea of Japan and eastern Bering Sea. There are also larger changes presented by Green (2010) in the Labrador Sea and eastern South Atlantic. These relatively small discrepancies are almost certainly attributable to various differences in the setup and choices of parameters (domain extent, resolution, included tidal constituents and self-attraction and loading correction) for the two model studies.

Additional figures for the European Shelf, Bohai Sea and Gulf of Maine plotted to allow direct comparisons of the OTISmpi results with those from other studies, such as Flather et al. (2001), Pickering et al. (2012), Ward et al. (2012), Pelling et al. (2013a; 2013b) and Pelling and Green (2013), can be found in Appendix 3.5.

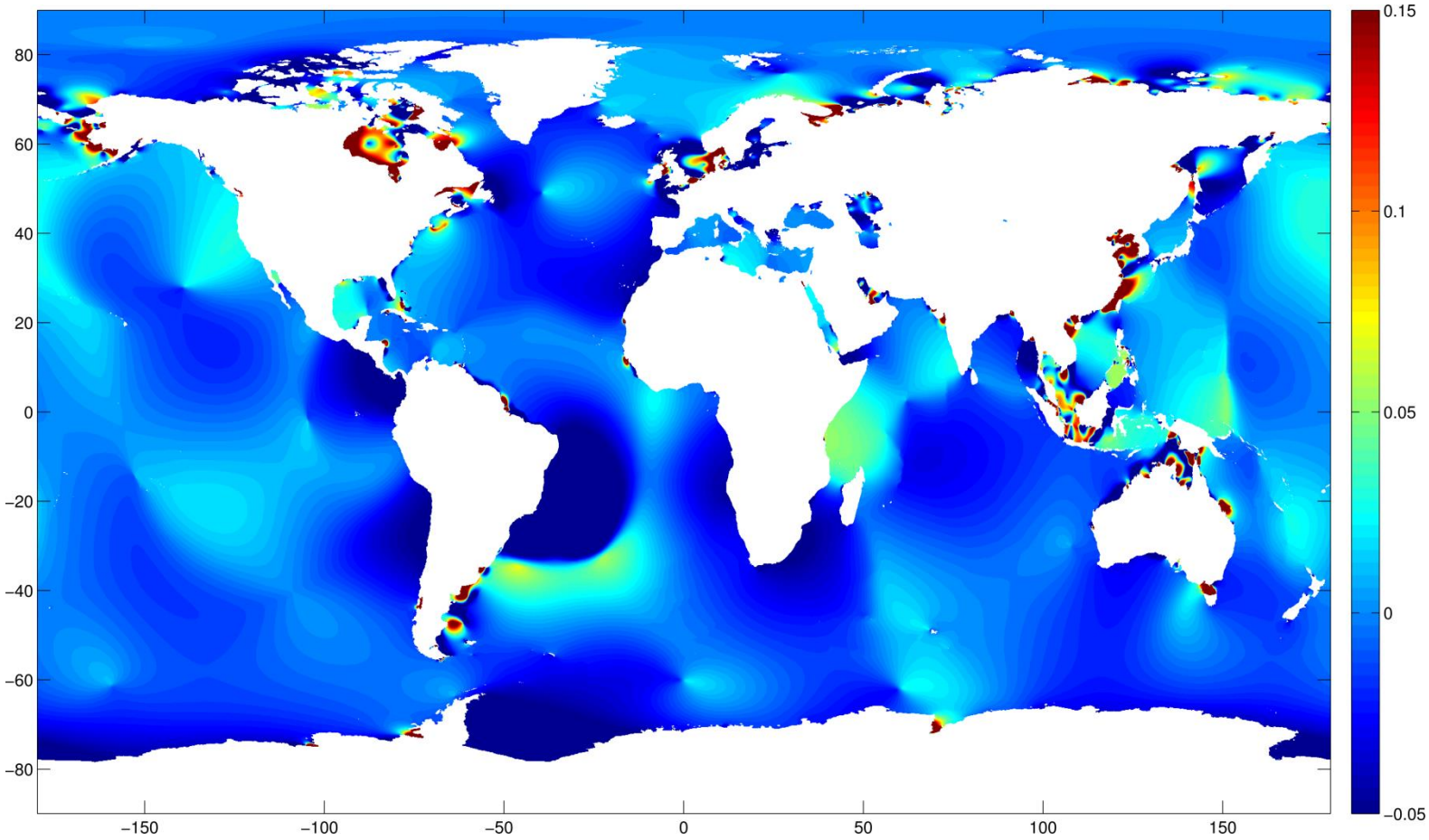

Figure 3.44. Change in M_2 (m) with a 5m uniform SLR assuming a fixed coastline (+5UF) (increases - red, decreases - blue). Plotted on same colour scale as Fig. 6c of Green (2010) for direct comparison. Note OTISmpi model setups in the two investigations differ in the extent of domain, resolution, run length, forcing constituents, SAL correction, etc.

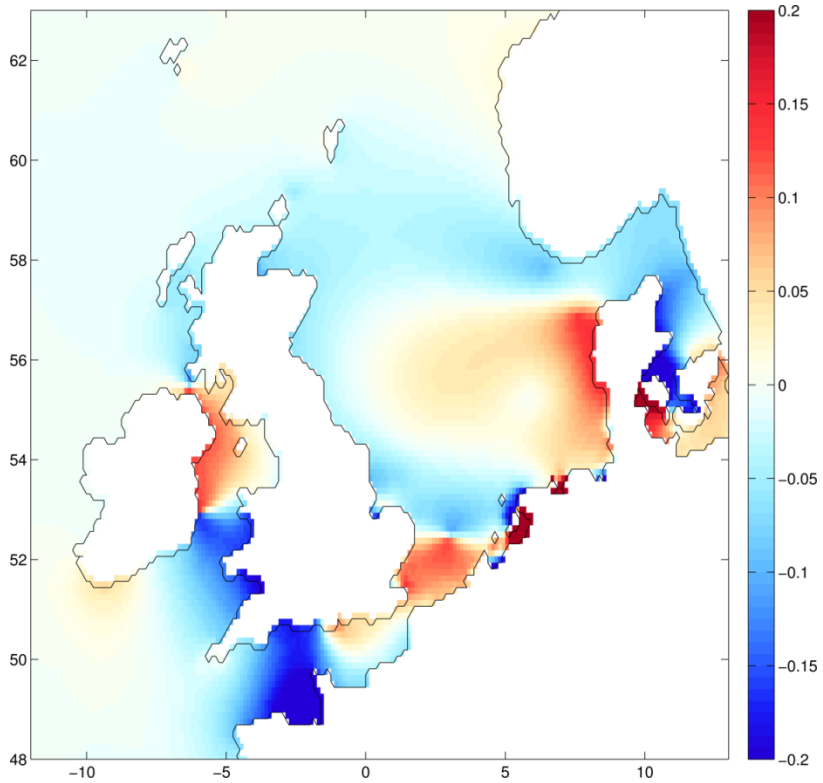

Figure 3.45. European change in M_2 amplitude (m) with a 2m uniform SLR assuming a fixed coastline (+2UF) (increases - red, decreases - blue) for direct comparison with the regional model result, Figure 2.4. (Regional zoom of Figure 3.2)

3.5 Discussion

3.5.1 Discussion of tidal changes

The results presented here show that future SLR will significantly affect global tides. Evaluation of the different uniform SLR scenarios with fixed coastlines or with coastal recession, as well as non-uniform SLR patterns, allows qualitative ranking of these influencing factors on the tidal change. The most important factor causing tidal change is the amount of SLR imposed. Following that is the inclusion (or not) of coastal recession with SLR, and the smallest effect on the tidal change is the global pattern of non-uniform SLR represented here by the IER scenarios. This ranking is based on the fact that SLR causes the coastal recession: should the coastline change without SLR (e.g. due to large scale land reclamation, erosion or managed retreat) then coastal recession may potentially be as important a factor as the SLR itself.

The changes in tidal constituents presented in section 3.4.1 showed the two semidiurnal constituents in some areas to exhibit changes of opposing signs whilst in others changes were of the same sign. When considering the phasing of these constituents the consequence of the opposing (same) signs of change is a reduced (increased) effect on the spring tidal amplitude and increased (reduced) effect on the neap tidal amplitudes. Both positive and negative changes have implications for flood risk but in different ways. Positive, same sign changes would cause an increase in the spring tidal HWs increasing the height of extreme water levels. Opposing sign changes can potentially increase the neap tidal range, thus raising the average tidal range which may have consequences when combined with other flood drivers (e.g. storm surge or river flow). Changes in spring and neap HWs will often be larger than the MHW changes presented; they can be found by respectively summing and taking the difference of the M_2 and S_2 changes (Table 3.5). For example with at Ningbo in the +2UF scenario the MHW increase is 28cm however the increase in spring HW (not shown) is 45cm. At Montreal the MHW decrease is -8cm however the neap HW increases by 58cm. An estimate of the change in the maximum HW (analogous to spring or tropic tides), assuming the range change is symmetrical about MSL, can be found by halving the maximum range change values (e.g. for Ningbo this gives a 44cm increase in maximum HW). Generally

spatial characteristics of maximum range change follow those of MHW change; exceptions to this such as the Gulf of St. Lawrence and the Bay of Fundy seem to be present when M_2 and S_2 constituent changes are of opposing signs.

The reason why the M_2 and S_2 constituents respond in opposite ways with the same SLR scenario in certain regions may be due to an alteration in the natural period of oscillation. For example, in the English Channel for the +2UF scenario the M_2 constituent amplitude decreases whereas the S_2 amplitude increases. This might suggest that the natural period of oscillation for the English Channel is moving away from the M_2 period and towards the S_2 period. The English Channel resonance is described by a half-wave oscillator through Merian's formula ($T=2L/\sqrt{gh}$) (Merian, 1828). Based on the model topography we calculate a channel length (L) of 476.6km and an average depth (h) of 47.4m. A 2m SLR would change T for this channel from 12.28hrs to 12.03hrs, which brings the natural period closer to that of S_2 (12hr) and further from M_2 (12.42hrs). It is interesting to note that the changes to the diurnal K_1 and O_1 constituents (Table 3.5 +2UF) are of the same sign at 39 of 40 cities. These lower frequency constituents with the periods of 23.94hrs (K_1) and 25.82hrs (O_1) have less tendency to exhibit changes of opposite signs. The diurnal constituent changes with the same sign will have the greatest effect on HW when diurnal tides are at their maximum during tropic tides.

In this Chapter we have focused largely on the 2m SLR scenario because (1) it represents a high end scenario for SLR, (2) the characteristics of the changes are largely representative of those for 0.5m and 1m SLR, and (3) the SLR is large enough to test domain changes with coastal recession. The Baltic is identified as a region where MHW change with 2m SLR is not indicative of the change with 1m SLR; the increase in MHW with 1m SLR (not shown, see Copenhagen Table 3.6) is larger than that with 2m SLR. This could be due to a change in the tidal energy entering the Baltic Sea through the Kattegat due to the differing North Sea responses in the two SLR scenarios; additionally the natural oscillatory period of the Baltic Sea might be closest to the M_2 tidal period with 1m SLR.

The majority of the large MHW responses to SLR are in shelf seas, with the sign of change varying spatially on shelves with multiple amphidromes. In contrast to this are the smaller magnitude but far greater horizontal length scale MHW

decreases which extend across the Atlantic Ocean from northwestern and southern Africa and eastern Brazil (see Figure 3.9). As the relative depth change in these deep ocean areas is small the changes are more likely to result from a change in the interaction between the shelf and deep ocean tide. Arbic et al. (2009) show that resonant deep ocean tides are strongly affected by resonant shelves, generally causing reductions to the tide and that this back effect is greater for a weakly damped shelf. Reductions in the energy dissipation at the bed (and hence damping) on various shelf seas adjacent to these widespread areas of decrease (Figure 3.18) are evident (e.g. European Shelf, Gulf of Guinea (Cameroon), Mozambique Channel and the continental shelves adjacent to Guinea and Brazil). These reductions in shelf damping could, as suggested, be causing the widespread decreases in ocean tide through an increase in the back effect of the resonant shelf on the deep ocean. Another basin wide feature is the larger tidal response along the east coast of the Americas compared to the west. This may arise from a combination of the more limited spatial extent of shallow shelf seas on the west coast and the natural modes of oscillation for the two oceans (see Platzman et al., 1981).

Although coastal recession affects the tidal change estimates substantially, the two coastline setups (fixed and recession) represent the limits of the problem. Whether the coastline is permitted to recede globally in 100 to 200 years depends on complex regional future socio-economics and coastal management practices that cannot be easily predicted. Coastal recession will have substantial flood impacts for coastal communities even though the substantial tidal changes in wet areas in both the present day and recession SLR scenarios were found to be predominately decreases (14 of 18 substantial MHW changes in +2UR compared with 5 of 10 in +2UF). The larger number of cities with significant MHW decreases in the +2UR case is clear from the cumulative frequency distributions (CFDs) presented in Appendix 3.3. The results also showed there to be tendency for the MHW changes to swap sign between the two coastline scenarios: this is particularly important for flood risk. In the areas listed in Section 3.4.2 where MHW change switches from an increase to a decrease (when coastal recession is permitted) there is a strong argument to prefer managed retreat because by choosing to engineer large scale sea walls (fixed coastline) the tidal amplitude is amplified (and no longer reduced) with SLR. Furthermore, by engineering sea walls in these regions to protect against

the SLR (and consequently amplified tide) the residual risk in the event of a failure of the defences is also increased (e.g. Hanson et al., 2011). Conversely, for those coastlines where, in the recession case but for the same imposed SLR, MHW increases rather than decreases (fixed coastline) there might be a better case for hard engineering schemes like sea walls. As the tidal response is shown to be dependent on both the SLR and the coastline management one can use the coastal management to influence the tidal response and potentially offset and mitigate the SLR.

Coastal recession can have a substantial effect on the natural period (T) of oscillation of a channel. Using the English Channel half wavelength resonance example given earlier, a hypothetical increase in the channel length of just two grid cells (~28km) with 2m SLR causes an increase in period approximately twice as large as the decrease caused by 2m SLR alone. The tendency for the tidal changes to swap sign between the +2UF and +2UR scenarios could be due to the fact that SLR alone decreases T whereas SLR plus recession increases it. Furthermore the effect of recession on T will be further amplified for areas governed by quarter wavelength resonances ($T=4L/\sqrt{gh}$) such as the Bay of Fundy and the Bristol Channel where one finds the world's largest tides. The tidal changes swapping sign between the +2UF and +2UR scenarios in deep water regions such as the Atlantic is explicable through the same reasoning. In fact a simple scaling argument shows the effect of domain change with coastal recession on T in the deep ocean is at least as important as that of SLR. For example in 2000m deep water the dynamic effect of 2m SLR is to increase $c=\sqrt{gh}$ by 0.07m/s, tidal forcing periods are fixed, so the M_2 constituent wavelength must also increase by approximately 3.1km. This dynamic effect is less than a quarter the length of a grid cell (~14km), the minimum increment by which basin geometry can be increased with coastal recession.

The change in energy dissipation at the bed with +2UF and +2UR generally show reductions in energy dissipation where MHW is reduced and increases where MHW is increased. This result implies that the tidal changes cause the dissipation change and not vice versa; if the dissipation were the cause of the tidal changes the increased dissipation would coincide with reductions in the tidal amplitude. This suggests that generally resonance is more important than dissipation in driving the tidal changes.

Regions with MHW changes >20% of the control MHW under various SLR scenarios are listed in Section 3.4.3. The Baltic Sea and the seas around the coastline of the Arctic Ocean show particularly large percentage changes. Although the absolute change in these regions is not unusually large the tidal amplitude in the control is small so changes are large in percentage terms. Relative changes are more significant in these regions that currently have small tides so adaption measures may be less developed than for regions already experiencing large tides. The spatial variability of the percentage MHW response across the global domain shows that tidal changes with SLR are not a simple function of the present day tidal amplitude.

Changes in all tidal properties are shown to be increasingly non-proportional with increasing SLR, with a tendency towards an above proportional MHW response with higher SLR. There are a number of reasons why tidal changes are not expected to be proportional (i.e. scalable with SLR): (1) as the tidal wave speed increases with SLR, and the amphidromic points are shifted, the response at the coast is not a simple function of SLR; (2) the movement of the amphidrome is two dimensional and the curvature of corange lines leads to a complex response; (3) as an amphidrome moves past a fixed coastal point with SLR the amplitude will first decrease (as it gets closer) then increase (as it moves away); (4) bathymetric and topographic slopes are not constant (as shown by non-proportional land areas newly wetted areas in UR scenarios- Section 3.3.2). The increasing portions of the points with significant MHW change that are above proportional with increasing SLR suggests that the MHW response is proportionally smaller at low SLR values and changes in an increasingly above proportional manner with higher SLR. There is an obvious limit when considering tidal amplitude decreases (in that as they approach a zero tidal amplitude the decrease cannot continue to scale with SLR) which is illustrated by the negative quadrant of the +5UF and +10UF MHW change CFDs presented in Appendix 3.3. We acknowledge that the response being increasingly non-proportional with higher SLR may be influenced by the chosen definition of proportionality (since the higher SLR scenarios are further from the 0.5m SLR used as the baseline). Even so, the results emphasise that interpolation or extrapolation of the tidal changes from one SLR scenario to another will often be a poor assumption for planning purposes.

The non-uniform SLR from IER shows particular influence on the tidal response where it causes a positive or negative deviation from the average SLR in a coastal region, resulting in a respective amplification or weakening of the tidal response. In some scenarios, such as the Western Antarctica melt case, IER causes peaks of above average SLR in the mid ocean (e.g. Indian Ocean Figure 3.37); this has a negligible effect on the tidal response there. Where all three IER scenarios result in above average SLR in coastal regions (e.g. Asia) then the tidal response is substantial regardless of the IER scenario. Where tidal response is positive, IER compounds the effect with both a larger tidal amplitude increase and an above average SLR. This compounding effect occurs at many Asian cities (e.g. Ningbo) with the MHW increase being augmented by (of the order) a few cm and the SLR increasing above the average (of the order) 20cm in the IER scenarios compared with the uniform SLR scenarios. The primary effect on flood risk resulting from IER will be the increase in SLR above the average (which is approximately an order of magnitude larger than the amplification of tidal changes it causes). Higher latitude regions such as the European and Patagonian shelves and Hudson Bay have tidal responses which are much more dependent on the particular IER scenario. For high latitude regions the relative proportions of the melt from the two ice sheets will have a substantial effect of the degree of tidal alteration (as well as the SLR) experienced. Studies such as Shepherd et al. (2012) which use multiple datasets to constrain mass loss from the ice sheets are therefore crucial.

From the differences between the MHW changes in the IER scenarios we can also see that it is the regionally imposed SLR that drives the resulting tidal changes. If the change was determined by the global mean value there would be no difference between the tidal changes under different IER scenarios. This fairly localised effect of SLR on the tide means that spatially variable SLR caused by other processes, the projections of which are uncertain (Slangen et al., submitted), are also likely to influence the extent of regional tidal changes. It is also clear from our results that IER affects the SLR at ocean basin spatial scales, consequently influencing the deep ocean tides on sub-basin scales and the shelf sea tides on very short spatial scales.

The differences between +2UR and +2NUBR are larger than between +2UF and +2NUBF. This is most likely due to the SLR over large areas being >2m in the +2NUB cases rather than exactly 2m in the +2U cases. As the source

bathymetry is given to the nearest meter, and depths must be <0m to be considered wet, then any small increment of SLR above exactly 2m in the +2NUBR case causes a whole group of new cells to wet. The non-uniform SLR in the IER scenario is therefore also having an effect on the degree of coastal recession whereas in the fixed case it is not, causing the differences between +2UR and +2NUBR to be greater than those of +2UF and +2NUBF. Using Table 3.3 to take the average newly wetted grid cell size for +2NUBR (151km^2) and +2UR (136km^2) illustrates a tendency for the newly wetted cells in +2NUBR to be equatorial (larger cell area) rather than evenly spread across the domain.

In many regions where tidal streams represent a viable energy resource (e.g. Pentland Firth, Menai Strait) the tidal currents are strong and rectilinear. Over the scale of interest there is no significant horizontal gradient of current, so the one-dimensional momentum equation reduces to a balance between the horizontal elevation gradient and bed friction, which is normally expressed as a quadratic parameterisation (e.g. $g.dz/dx = Cd\ U\ |U|/h$). If one considers the sea surface slope over some constant distance, dx, then this simplification leads to an expression where depth-averaged currents will change as the square root of the sea surface slope (i.e. $\Delta U = C\sqrt{(\Delta dz/dx)}$). One arrives at exactly the same relationship if considering open channel flow as favoured by engineers. Manning's equation (1891) expresses the depth-averaged velocity as proportional to the square root of the hydraulic slope. It follows that any change in tidal elevation will affect tidal streams in this way, and – as a simple approximation – a 10% change in elevation amplitude would result in a 3% change in current amplitude. The results for maximum range changes at sites viable for new renewable energy extraction are therefore also indicative of associated changes in currents which are of direct importance for energy extraction. The potential alteration of the amount of available tidal energy with SLR must be taken into account when assessing future tidal energy resources. These alterations would affect cost-benefit analyses (CBA) for tidal installations which typically have operational lifetimes of 25-120 years.

Comparison of the European OTISmpi M_2 tidal changes with 2m SLR (Figure 3.45) to those of the regional modelling study (Chapter 2) shows good agreement. Furthermore, this global study shows that changes in the global model on the shelf edge (in the vicinity of the regional model's open boundary) are negligible. This supports the assumption (in the previous regional

modelling study) of maintaining constant tidal forcing at the open boundary with SLR. The weaker agreement between the two models with 10m SLR (see Appendix 3.5) suggests that this assumption will break down at very high SLR scenarios. Owing to the validity of the open boundary assumption, the higher resolution, and the more realistic Dutch coastline schematisation in the regional model, the changes for +2UF presented in Chapter 2 are likely to be better projections than those from OTISmpi. The differing spatial patterns of the M_2 change in the North Sea between 2m and 10m SLR in the global model (see Appendix 3.5) support the Chapter 2 conclusion that M_2 response is non-proportional in the North Sea.

Globally the results of our model are generally comparable with those of other studies (e.g. Green, 2010). Other regional comparisons for the European Shelf (see Appendix 3.5) show fairly similar patterns of M_2 amplitude change to Ward et al. (2012) for +2UR and +5UR cases, and similar patterns of M_2 amplitude change to Pelling et al. (2013b) for +2UR and +2UF cases. Comparisons of M_2 amplitude change with Pelling et al. (2013a) for the Bohai Sea shows a fairly similar response for the +2UR case but poorer agreement for the +2UF case where change outside the regional model's domain appear to influence the OTISmpi Bohai Sea response. The response of the astronomic tidal range in the Gulf of Maine is of the same sign as the regional modelling results of Pelling and Green (2013) for 1, 2 and 5m SLR cases with both fixed coastlines and coastal recession, however changes in the upper reaches of the Bay of Fundy were not replicated in the global model due to lower resolution.

3.5.2 Implications of the changes

The principal implication of altered tidal amplitudes with SLR is for future coastal flood risk. With 1m SLR, the high end of the process based AR5 estimates for 2100 (Church et al., 2014), an increase or decrease in MHW ≥10cm or ≤10cm occurs at 13 of the coastal cities analysed with populations >1 million in 2005. An increase or decrease of 10cm may seem manageable, however, when considering the effect on the return period of a certain extreme water level the impact is clear. The relationship of return period and extreme water levels is log-linear; this means a relatively small change in water level can cause a large change in the return period. This was demonstrated by Haigh et al. (2011) using a generalised extreme value distribution, where a SLR of only

12cm (from 1990 to 2100) caused the 1 in 100yr water level for 9 English Channel ports to reduce, on average, to become a 1 in 10yr event. A more conservative estimate, particularly in tidally dominated regions (Haigh et al., 2010b), of the change in return period with SLR or tidal amplitude change is obtained by fitting a Gumbel distribution to the detrended annual maximum water levels. This simple assessment estimates that the MHW increases with 1m SLR at Dhaka (13cm), Ningbo (15cm), Xiamen (7cm) and New Orleans (7cm) would reduce the return period of a the 1 in 100 yr water level to 1 in 60yr, 1 in 60yr, 1 in 63yr and 1 in 73yr events respectively. If the MHW increase and the SLR are taken into account the return period at all four cities decreases to less than a 1 in 2yr event. The effect of the SLR, or of any tidal change, on the return period is determined by the slope of the return period curve; steep return period curves such as the one presented by Xu and Huang (2011) for Shanghai will require a larger SLR or tidal change to substantially alter the return period and vice versa.

The uniform offset of the return period curve to account for SLR or a MHW change assumes that the change in the tide does not affect the local dynamics of the surge climatology and hence the extreme value statistics. It is possible that altered tidal amplitudes may have an effect on the surge propagation through tide-surge interaction (Horsburgh and Wilson, 2007). For example, regions with increased tidal range may cause less efficient surge generation on average, reducing surge height statistics. These second order effects mean the effect of tidal alterations on return period curves are likely to be more complex than the simple vertical offset of the curve as applied earlier. The effect of altered tidal characteristics on surges requires further investigation.

Currently national impact assessments such as the UKCP09 (Lowe et al., 2009) do not make an allowance for future tidal changes with SLR. However, results from this study, as well as (Chapter 2) and other supporting studies (de Ronde, 1986; Flather et al, 2001; Greenberg et al., 2012; Pelling and Green, 2013; Pelling et al. 2013a; Pelling et al., 2013b), suggest an allowance should be included in coastal impact assessments for all countries. The Dutch Delta Committee make a 10% allowance of the SLR imposed for the indirect effect of SLR on surges and any other effects (e.g. dredging and port alterations). For this to be sufficient the other factors and tidal change must not exceed 10% of the SLR. Our results show that changes >10% of the SLR imposed are possible

thus with the addition of the other effects the 10% allowance may be too small in places. Conversely, where SLR causes tidal decreases the 10% allowance may lead to over engineering of defences. Future work will aim to assess the national population and asset exposure resulting from SLR and tidal changes using the DIVA socio-economic impact and vulnerability model (Vafeidis et al. 2008).

In addition to having implications for future tidal renewable resources, changes in the tidal currents will have implications for the positions and intensity of tidal mixing fronts. Some analysis (Section 4.2.5) using the Stokes numbers, the ratio of the frictional depth to the total water column depth (e.g. Souza, 2013), showed alterations in the positions of the fronts, particularly in the northwest Gulf of Alaska, Bering Sea and North Sea. In other locations such as the eastern Irish Sea and Bristol Channel large alterations to the Stokes number occur, however, these regions already have values in excess of unity in the control scenario and so the water column is already well mixed. An as yet unexplored area relating to changes in currents is the interaction of the tidal changes occurring in the shelf seas with ocean boundary currents.

Another possible feedback of tidal changes is on the rate of ice-calving in polar regions. An increased tidal range, such as those strong isolated MHW increases along the coast of Antarctica, might lead to an increased rate of ice-calving and hence SLR creating a positive feedback mechanism. The strong effect (~20%) of the spring-neap tide on the outflow of a key Antarctic ice streams has already been reported (Gudmundsson, 2006); changes to tidal characteristics could therefore reasonably be expected to influence the outflow of these streams which is pivotal in the rate of mass transport off the ice-sheets. Additionally, the tidal migration of the ice-sheet grounding line has been shown to modify sub-glacial melting and lubrication, with a migration of several kilometres during a tidal cycle (Sayag and Worster, 2013). Larger tidal ranges could therefore increase the area of the ice-sheet where basal melting can occur (as in Mueller et al., 2012) and feedback on the mass transfer, positively feeding back on the rate of SLR. It should also be noted that where tidal range decreases occur, negative feedback effects could be expected. The interaction between SL, polar tides and climate is further explored in Griffiths and Peltier (2009).

Tidal changes have implications for shipping; with increased range, lower LWs present a grounding risk (although this may be partially offset by the SLR itself). An additional difficulty is associated with higher HWs as tall ships may not be able to clear low bridges at HW when they have sufficient depth clearance below. Tidal changes in the Northwest Passages and Arctic Ocean also hold implications for shipping on newly opened routes arising due to ice melt.

3.5.3 Limitations of the study

We investigated the effect of including coastal recession with SLR on the tidal response. Owing to the 1m vertical resolution of the bathymetric and topographic GEBCO dataset we are only able to investigate the effect of recession at SLR scenarios greater than 1m. As the effect of recession on the tidal changes is shown to be significant at 2m SLR it would be of interest to investigate this for 0.5m and 1m SLR scenarios. This would require a dataset with higher vertical resolution (at least around MSL) and a tidal model with higher horizontal resolution allowing more subtle (and more realistic) alterations in the coastline particularly around estuaries and barrier islands. Neither does this study take account of direct anthropogenic influence on the position of the coastline. Presently this is particularly relevant along the Chinese coast where large scale land reclamation of tidal flats is taking place. Studies on this effect for the East China Seas show there to be both localised changes to tidal characteristics as well as far field effects on Korean coast tide (Song et al., 2013); and for the Bohai Sea show increased tidal sensitivity to SLR (Pelling et al., 2013a). Coastline changes not associated with SLR in these regions may (as suggested in section 3.5.1) have equal (or greater) importance to (than) SLR on the tidal response.

The GEBCO bathymetry coupled with the OTISmpi grid generation routine does not take account of areas of land below MSL protected by high, narrow coastal defences leading to an unrealistic representation of the Dutch coastline (as discussed in Section 3.3.2). As mentioned in Section 3.3.3, where coastal cities are located high up estuaries the nearest representative coastal cell was taken; for such locations (see list in Appendix 3.2) results should be interpreted with caution as potential differences between our projections and actual change at the city may occur. For example where the estuary is no longer tidal the

changes will be smaller and conversely tidal changes may be amplified by some estuarine geometries. Where we consider future renewable energy resources no assessment is made here of the joint effect of the SLR and the tidal energy extraction by the device itself which may be relevant.

The harmonic analysis used here only includes the primary tidal constituents M_2, S_2, K_1 and O_1; although higher harmonic tides will be generated within the model at this resolution they are not analysed. It has been shown (Chapter 2; Ward et al., 2012) that changes in higher harmonics on, for example, the European Shelf with SLR are non-negligible. It is a limitation therefore that the reconstruction on which the MHW is based does not include higher harmonics.

Changes in energy dissipation at the bed with SLR are presented here, however any changes in the internal tidal dissipation through the internal wave (IW) drag scheme (Zaron and Egbert, 2006) are not shown. Equation 6 of Zaron and Egbert (2006) shows the IW drag simulated to vary with both SLR and changing tides through the dependent variables of depth and volume transport (U and NU SLR cases) and the square of the topographic slope (NU SLR cases). Egbert et al. (2004) briefly consider the effect of changes to the ocean stratification (through a doubling of the IW drag) and find there to be an effect on tidal amplitude. Furthermore Mueller (2012) finds that a 10m change in the mixed layer depth leads to a 1-2% change in tidal transports. Investigation of alterations to the tide with potentially increased future stratification due to climate change not assessed in this study would be worthwhile.

Finally, there are assumptions inherent in the IER SL fingerprints predictions: for example, the mass loss being uniform across the ice-sheet. Mitrovica et al. (2011) show the sensitivity of the fingerprints to this assumption to be limited to the near field. Additionally the SL fingerprints do not include the effect of the long-term viscous flow in the mantle or the steric SL effects of the ice mass loss. All SLR scenarios presented here do not include vertical land movement. This has to be incorporated subsequently for making engineering decisions, as is also the case for regional SLR projections (Katsman et al., 2011) and is performed for UKCP09 projections (Lowe et al., 2009).

3.6 Conclusions

This Chapter investigates the effect of future SLR on the global tides. We employed a global tidal model (Egbert et al., 2004), making refinements to the model setup to achieve improved representation of the present day tides and ensuring an appropriate physical setup for the future SLR perturbations. Various SLR scenarios are imposed including uniform and non-uniform patterns due to IER as well as comparing cases with fixed coastlines and permitting coastal recession. The main conclusions are listed below:

1) The tides in shelf seas across the globe change significantly with SLR, with substantial localised tidal responses to plausible projections of SLR. The responses are significant on the east coast of the Americas, northwest Europe, north coast of Russia, across Asia and Australasia.

2) The tidal response is complex and exhibits spatially coherent increases and decreases in tidal amplitude.

3) Significant changes in the semidiurnal constituents (M_2 and S_2) with SLR occur in most shelf seas globally, whereas large changes in the diurnal tidal response (K_1 and O_1) are limited to seas around Asia.

4) The changes in semidiurnal constituents are often of the same sign (and will thus be additive during spring tides) but can also show opposing responses. This phenomena is explained in terms of the natural oscillation period of individual channels and basins.

5) The difference in the effect on the tidal response between including coastal recession with SLR versus assuming a fixed coastline is substantial. Permitting coastal recession amplifies the tidal response. However, more of the substantial changes become amplitude decreases in the recession case. New tidal areas due to coastal recession will however have flood risk implications.

6) The response of the tidal constituents, MHW and maximum range is shown to be non-proportional to the SLR imposed in many areas. With higher SLR a tendency towards above proportional MHW response is shown, suggesting a magnification of the tidal response at higher SLR.

7) The inclusion of non-uniform SLR due to IER has a modest effect on the tidal response when compared with the uniform scenarios. The tidal response is most dependent on the IER scenario at high latitudes where it is amplified in the far field and diminished in the near field of the ice-mass loss in the Greenland and Western Antarctic melt scenarios. Within 30 degrees of the equator all IER scenarios tend to amplify the tidal response owing to the above average SLR in the fingerprint. At Asian cities the effect of all three IER scenarios is only to exacerbate the tidal response in addition to causing above average SLR. The influence of permitting coastal recession and IER results in greater differences with the uniform scenario than for the fixed coastline case.

8) The analysis at 136 coastal cities with populations >1 million predicts MHW changes exceeding ±10% of the SLR imposed at 13, 13 and 10 cities with +0.5UF, +1UF and +2UF respectively and at 18 cities with +2UR.

Projections of relative SLR for coastal management purposes consider global, and regional SL components (Slangen et al., submitted) as well as vertical land movements (Nicholls et al., 2014). This Chapter suggests that the patterns of MHW changes presented here should also be included in these analyses and that national adaptation approaches to SL change should not assume tidal changes to be negligible. Given the importance of non-uniform SLR patterns for tidal changes shown in our results future assessments of tidal changes should look to include additional components of regional SLR (as well as IER) in the depth perturbations. Understanding tidal changes for the 0.5m and 1m SLR scenarios presented here, comparable to the mid to high end IPCC RCP scenarios for global SLR in 2100, is particularly important as it is relevant for coastal management. For the larger SLR cases considered here, which may occur on longer time timescales, adaptive management approaches to the problem are probably more appropriate in terms of including this factor as an additional uncertainty (e.g. Ranger et al., 2013).

The strong effect of coastal recession on the modelled tidal response suggests that an engineering approach to influence the change in the tide with SLR through coastal management practises is possible. In some locations allowing coastal recession or imposing large scale sea walls can lead to reduced tidal amplitude with SLR which can be used to reduce coastal flood risk. Although allowing coastal recession on large scales may be possible it is recognised that

feasibility may be an issue in other areas requiring large scale sea walls. To assess coastal management strategies using combinations of fixed coastlines and allowing retreat, one must make explicit simulations (rather than taking results from one of the two coastline scenarios presented here). This could be further investigated at a range of scales linking these global results down to shoreline management scales (Nicholls et al., 2013).

From an alternate perspective, that of the marine renewable energy planner, tidal amplitude (and current) increases are beneficial and decreases potentially problematic. It is suggested that when planning tidal renewable energy projects with long intended lifetimes, such as 120 years for the Severn barrage scheme, the potential future alteration to the tide by SLR should be considered, as the site may become more or less productive in the future.

Finally, given the substantial research effort into future SLR and its impacts, we suggest that further studies refining predictions of future tidal changes would be worthwhile. The global results presented here could be used as boundary conditions for very high resolution regional tidal models and as computational power increases higher resolution global simulations will also become possible.

3.7 Appendix A

3.7.1 Description of accompanying material, Appendices 2 and 3:

The Accompanying Materials CD includes the following animations (these will also later be included with the online version of this paper):

- Animation of SSH (Eq. 3) of present day tides: (a) 3 day and (b) 15 day versions (.avi compatible with WM12+ /VLC players)

The Appendices to this Chapter include:

- Appendix 2: A document describing the porting, optimising and benchmarking of OTISmpi on the local compute cluster.

- Appendix 3.1: Full tables of all 136 largest coastal city results (extensions of Table 3.4, 3.5, 3.6, 3.7, 3.12 and 3.13).

- Appendix 3.2: Table of the latitude, longitude position of the model grid points used to represent the cities and flags for city centres far from this grid point (e.g. up an estuary) and the University of Hawaii Sea-Level Centre (UHSLC) tide gauge stations used for the return periods analysis.

- Appendix 3.3: CFDs of the MHW changes at all 136 cities comparing all UF scenarios, and +2UF and +2UR scenarios (all changes normalised to 1m SLR).

- Appendix 3.4: Regional enlargements of Figure 3.10- MHW change for +2UR- for comparison with Figure 3.11-3.16.

- Appendix 3.5: OTISmpi results plotted regionally on colour scales for direct comparison with previous studies.

3.7.2 Explanation of variations in SLR in coastal recession scenarios

In the recession cases lower SLR and occasional SLF values (e.g. Table 3.4) are caused by the SLR perturbation applied to the GEBCO dataset (before the land masking is performed) bringing new, shallow, depth values into the average (up to 56 GEBCO points). Only values below MSL are included in the average so with, for example, 2m SLR the average would now include a number of new 1m depth values (previously 1m high land). Depending on the number of new shallow points the effect on the average is either to cause less SLR than intended or a SLF. The other factor that can lead to less than the intended SLR at the coast in the recession scenarios is the 2m minimum depth applied to the bathymetry after the perturbation. For example if the control model cell average depth is 1m it will be reset to 2m, when 2m SLR is applied to the control depth it will be 3m leading to an actual imposition of only 1m SLR rather than the 2m in this scenario. These limitations only occur very close to the coast, the SLR imposed over the vast majority of the model domain is the intended value.

3.7.3 MHW method development explanation

Initially a MHW method was developed that takes the average of all peaks over a 15 day SSH reconstruction based on the four tidal constituents (Eq. 3). The limitation of this method is that wherever a peak exists on the tidal curve, even short lived secondary maxima close to LW, they are erroneously taken into the

average. This leads to unphysical spiral patterns in the MHW field often in the vicinity of tidal amphidromes. The second MHW method was to use the form factor (ff), see Eq. A1, in order to determine whether to take the single highest maximum (diurnal regions ff<1.5) or two highest maxima (semidiurnal regions ff>1.5) per tidal day and then take the average of these (NaN values were inserted where insufficient maxima exist).

$$ff_i = \left(\frac{Hm_{iK1} + Hm_{iO1}}{Hm_{iM2} + Hm_{iS2}} \right) \quad \text{(A1)}$$

where the ff is the ratio of the sum of the amplitudes of the diurnal constituents to the sum of the semidiurnal constituents. This has the advantage of omitting low secondary peaks in the tidal curve from the mean but the limitation, as shown in Figure 3.46, of introducing sharp unphysical MHW transitions in mixed tidal regions where the ff value goes from diurnal to semidiurnal and the number of maxima per tidal day changes. The solution to this, shown in Figure 3.47, was to identify an optimal percentile of the ranked SSH time series to represent MHW globally. Using the MHW from the ff method the optimum local percentile for each point was found and a global mean taken, giving the 88.8th percentile. To spatially smooth the field slightly the mean of a range (± 1 percentile) about the 88.8th percentile was taken. Some example points where the optimum local percentile is >2 SDs of the global percentile field from the optimum mean global percentile are shown in Figure 3.48a-d. Locations where the ff MHW includes particularly low (high) peaks can be seen in Figure 3.48a-c (Figure 3.48d). A similar method was used to identify the optimum percentile for mean low water, found to be the 10.8 percentile. For more details on MHW methods see (Haigh et al., in prep.).

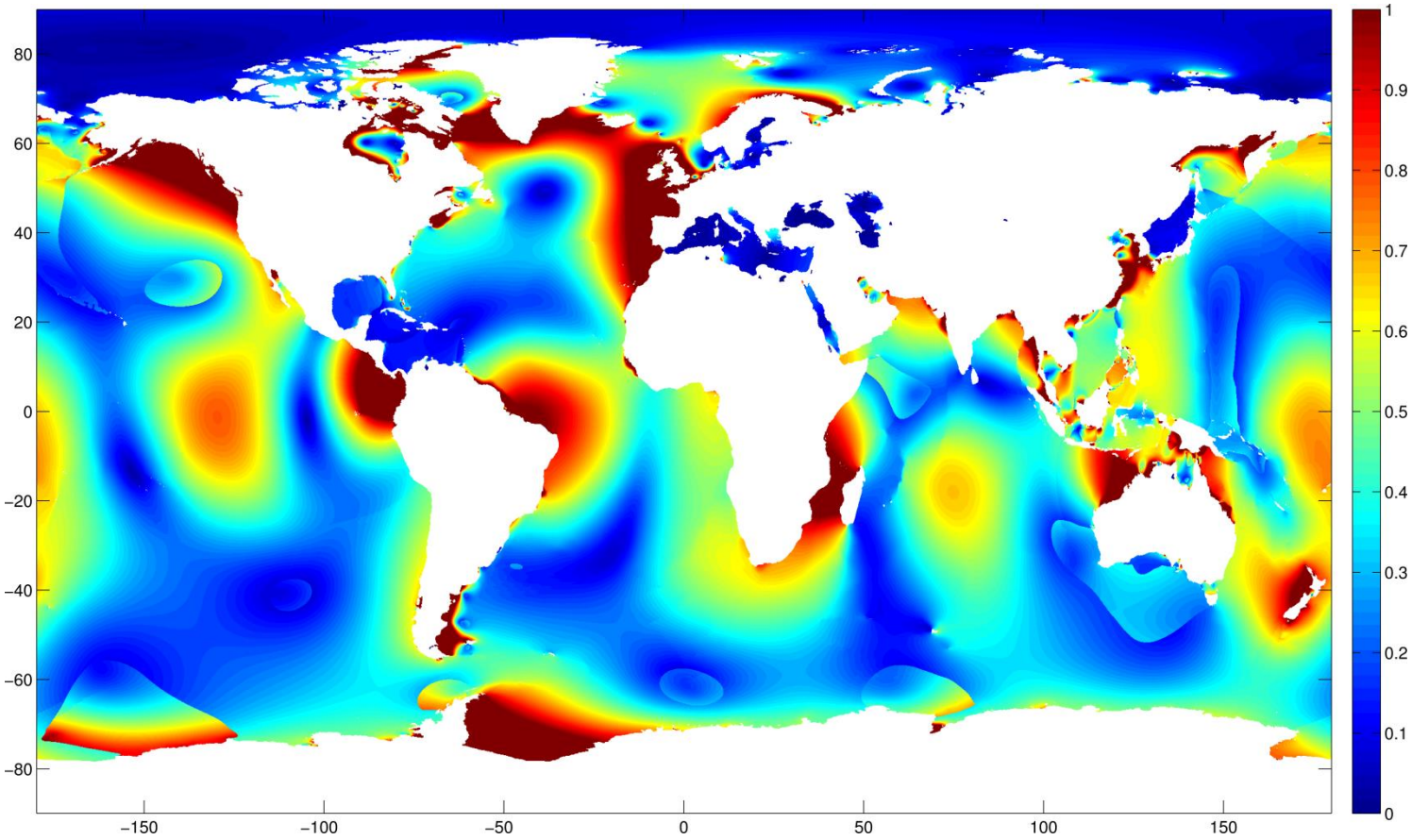

Figure 3.46. Present day MHW (m) from analysis of a 15 day reconstruction of SSH for each grid point (from the four tidal constituents) using a slope analysis method to identify peaks then taking the average of the highest peak (where diurnal - form factor < 1.5) or two peaks (where semidiurnal - form factor > 1.5) per day. Steps in the field are clear where the form factor transitions from diurnal to semidiurnal.

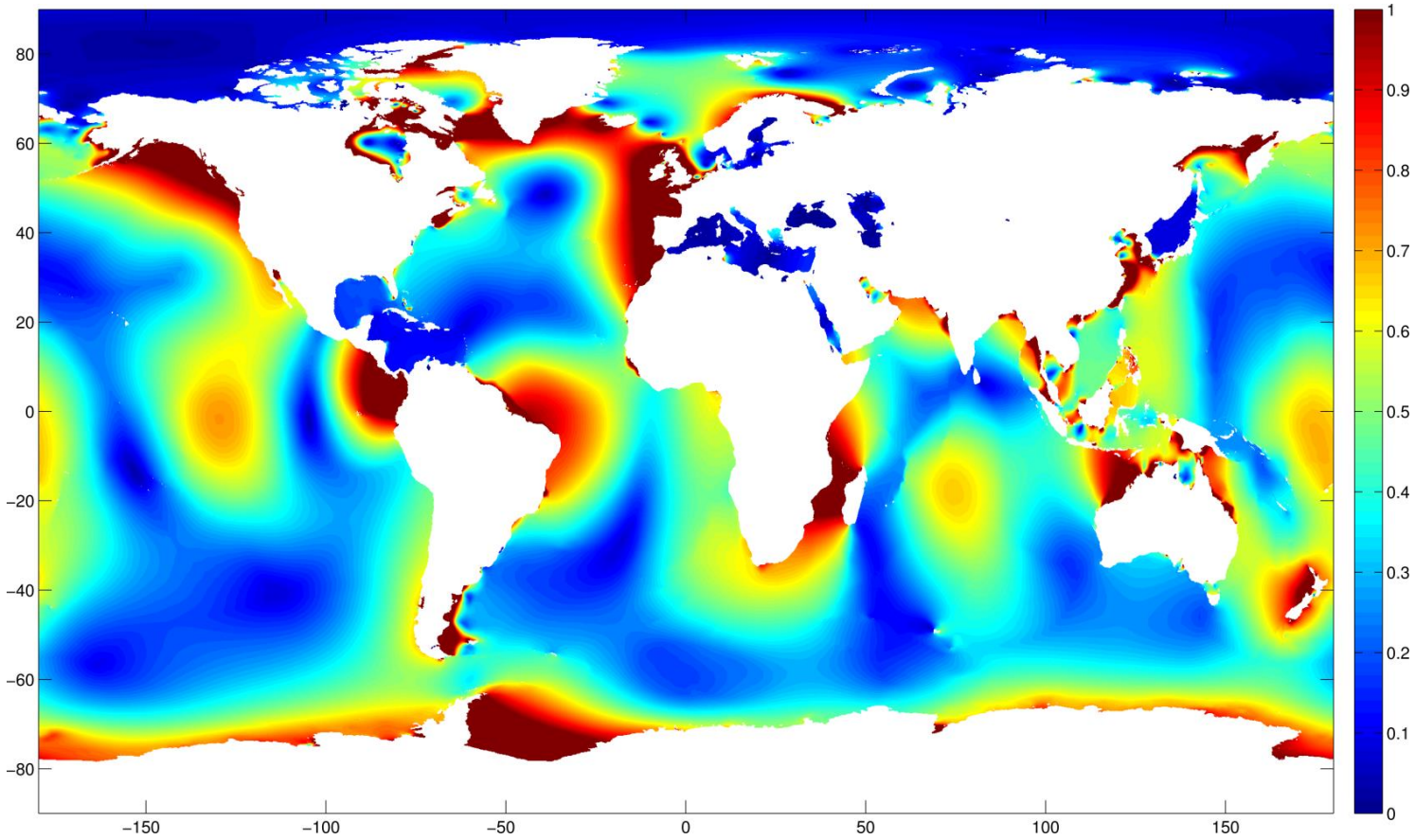

Figure 3.47. Present day MHW (m) from analysis of a 15 day reconstruction of SSH for each grid point (from the four tidal constituents) using the mean of the 87.8-89.8th percentile of the SSH for the whole period. The 88.8th percentile was found to be the optimum mean percentile to represent MHW based on point by point comparison with the MHW as obtained in Figure 3.46, the ± 1% range around that percentile mildly smooths the field. This method used for all MHW results.

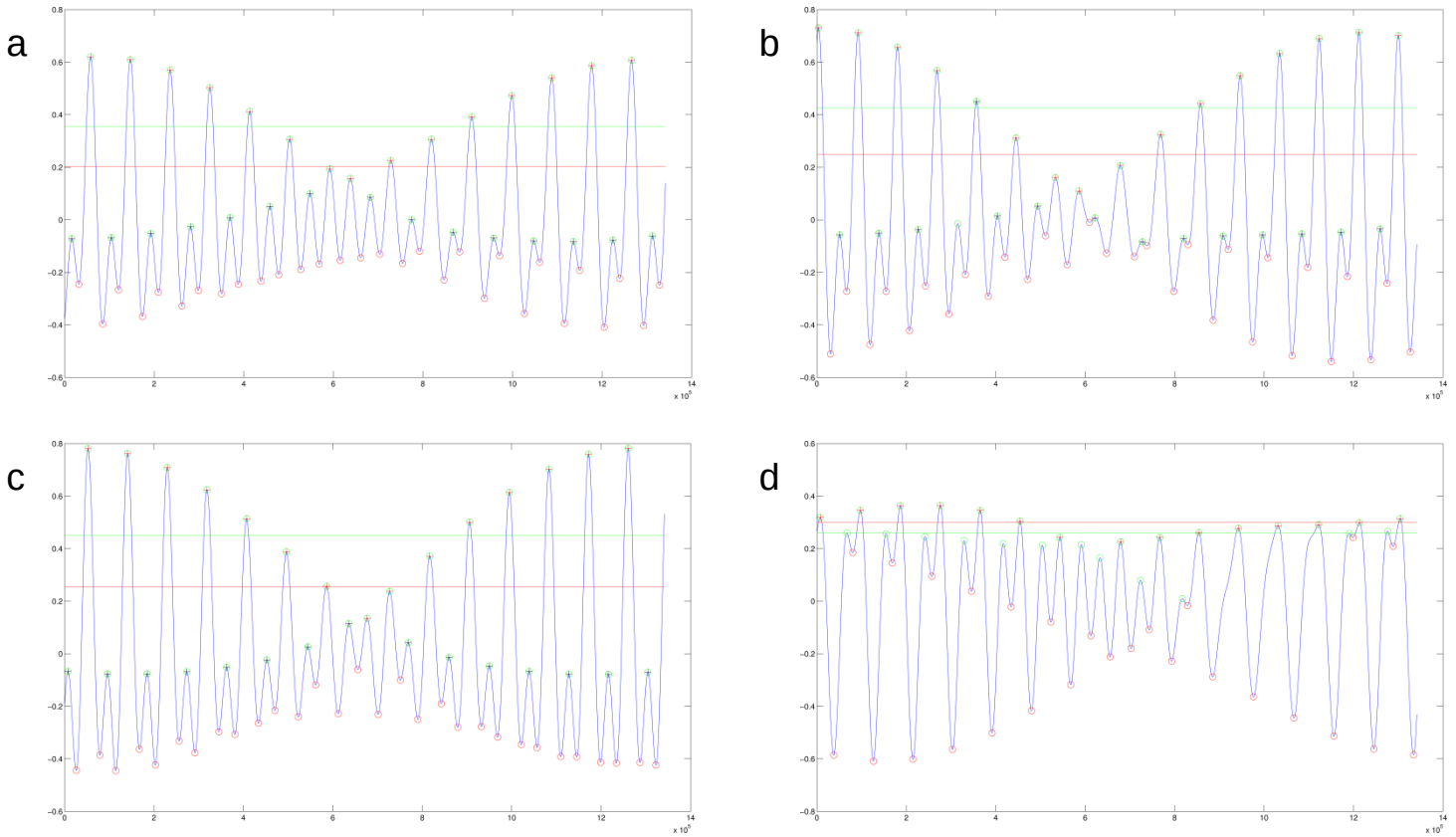

Figure 3.48a-d. 15 day SSH reconstructions (m) for mixed semidiurnal tides at locations south of Australia (a), east of Africa (b) and East Pacific (c), and mixed diurnal tides in NW Pacific (d). The red line shows the MHW calculated by the slope and form factor method (Figure 3.46) and the green line the MHW by the 88.8th percentile method (Figure 3.47). Points taken into the slope MHW are the red and black (semidiurnal) or red (diurnal) crosses. These **points represent outlier locations where the local optimum percentile was >2σ** from the global mean percentile of 88.8 (i.e. where slope and percentile MHW methods differ the most).

4. Potential implications of changing tides resulting from sea-level rise

This Chapter has been prepared primarily to extend the implication discussions of Chapters 2 and 3. An adapted version of this text may later be submitted for publication in Global Environmental Change or Environmental Research Letters.

4.1 Abstract

After establishing in the preceding Chapters that future sea-level rise will cause significant changes in global and regional tides, this Chapter discusses the wide range of potential implications. The discussion focuses particularly on the potential impacts along European coastlines and the coastal seas. Regular reference to the results of Chapter 2 will be drawn to quantify the likely changes. This Chapter highlights the importance of the effect of future sea-level rise on the tides by exploring the impacts of these changes for coastal flooding, renewable energy generation, nuclear power generation and water reliant industry, sediment transport, dredging and shipping, tidal mixing fronts and intertidal habitats.

4.2 Discussion

The changes in the tides caused by SLR presented in Chapter 2 and 3 can significantly influence each of the following:

1) Coastal flooding

2) Renewable energy generation

3) Nuclear power generation and water reliant industry

4) Sediment transport, dredging and shipping

5) Tidal mixing fronts

6) Intertidal habitats

This chapter discusses some of these implications with a focus on European Shelf implications many of which are also relevant globally; additionally global examples will also be given.

4.2.1 Coastal Flooding

Coastal flood risk at major coastal cities will be influenced by changes to tidal amplitude caused by future SLR. For example under a scenario with 2m of SLR and a fixed coastline, two major European cities (Chapter 2) and ten major global cities (Chapter 3) will experience tidal HW changes >10% of the SLR itself. These HW changes include both increases and decreases with SLR; regions with HW increase will augment the flood risk increase from the SLR itself and conversely regions with HW decrease will diminish the flood risk increase from the SLR. Tidal changes were also shown to be very sensitive to the coastal management practices, either maintaining fixed coastlines or allowing coastal recession with SLR (Chapter 3.4.2); this is an additional factor to consider when assessing future flood risk associated with tidal alterations due to SLR.

Currently the approach to both overall flood defence strategy and, within this, the allowance for alterations in the tide differs between the UK and the Netherlands. As part of the 'making space for water' strategy (http://archive.defra.gov.uk/environment/flooding/documents/policy/strategy/strategy-response1.pdf) the UK aim to defend coastlines against the 1 in 100year flood event, allowing managed retreat in some areas. In the Thames Estuary 2100 (TE2100) and UK Climate Projections 2009 (UKCP09) projects no allowance was made for future tidal alterations. The tide and surge simulations used present day bathymetry and the direct effect of SLR was included by a linear addition to the future climate surge levels (Lowe et al., 2009). In the Netherlands, according to what has traditionally been a 'hold the line' approach to flood strategy, Dutch law requires a 1 in 4,000year to 1 in 10,000year coastal safety level for the average exceedance probability (Kabat et al., 2009). The Dutch Delta Committee assessment method makes a uniform allowance of ~+10% of the SLR scenario for future tidal alterations in addition to a linear inclusion of the SLR itself (Vellinga et al., 2009). The Dutch ministry for water management, Rijkswaterstaat, make a 0.05m allowance (~+10% of the 0.6m SLR scenario for 2100) for any changes to HW. Rakhorst (2005) states

that the majority of tidal amplitude changes observed to date on the Dutch coast can be explained by anthropogenic influences including dredging, harbour creation, tidal inlet closure, other engineering schemes and natural tidal variability. The 0.05m (~+10% of SLR) allowance is intended to cover all of these factors as well as the effect of SLR on the tide, however this thesis shows the later can be >+10% in its own right (Table 2.3, 3.6 and 3.7). The 0.05m allowance is also uniform along the Dutch coast however our results show that on length scales less than that of the Dutch coast tidal changes switch from increases to decreases. For these reasons the UK (no allowance) and Dutch (uniform +~10% of SLR for all tidal alterations) allowances are shown by our results to be unsuitable for sustainable coastal defence policy. Based on our similar conclusions regarding the magnitude and short spatial length scale non-uniformity of the tidal response along global coastlines (Chapter 3), the same conclusion can be drawn globally for other national flood risk assessments applying similar allowances. Additionally for the North Sea between 2m and 10m SLR (Chapter 2) and globally between 1m and 5m SLR (Chapter 3.4.3) the tidal changes are shown not to be proportional to the SLR imposed so any allowance which is based on some percentage of the SLR will also be unsuitable. Both the omission of an allowance or a uniform percentage of SLR allowance will lead to costly over engineering in certain locations (where tides decrease) and, more concerning, other locations being left more exposed than the legislative safety level requires (where tides increase).

As higher SLR scenarios (≥1m by 2100) become increasingly plausible the importance of properly including the larger associated tidal changes becomes ever more apparent. Here we suggest that the best way of making a suitable allowance for changes in tides caused by SLR is to explicitly model the tide for the SLR scenario under consideration and impose a spatially non-uniform allowance for the change in tidal amplitude along the coast. There are two methods of including these tidal change allowances into future estimates of extreme sea levels (ESLs). The first, more basic method, (as was demonstrated in Chapter 3.5.2) is to make a linear offset to the present day return period curve in line with the tidal change, in the same way as is currently done to include SLR itself in return period estimates (Nicholls and Wilson, 2001). Including offsets to the return period curve for both SLR and the tidal change allows the coastal planner to see the first order combined effect of SLR and

tidal change on ESLs. Ongoing work with the DIVA socio-economic impact and vulnerability model (Vafeidis et al. 2008) aims to include changes to the ESLs in exactly this way. In this work the surge climatology is assumed to remain unaltered by the changing tide and linear additions for the SLR itself as well as for the MHW change are made to each of the return periods (from 1 in 1 year to 1 in 1000 year) for each of the coastal segments in the global database. This work aims to assess the importance of tidal alterations due to SLR for national population and asset exposure to flooding and erosion (amongst other tidally influenced risks). The work will also look to improve the DIVA model's database of present day tidal elevations with MTR data from OTISmpi, tidal data affects a number of different aspects of the model.

The first, linear offset, method assumes that altered tidal conditions do not influence the surge propagation and the associated distribution of extreme surge events through tide-surge interaction. It is known that the tide and meteorologically driven surge waves interact with each other in a complex non-linear manner (Flather and Khander, 1993) which causes higher probability of the largest non-tidal residuals avoiding HW (Horsburgh and Wilson, 2007). If tidal ranges are increased or decreased with SLR the probability of large residuals occurring near HW may be decreased (e.g. Cuxhaven) or increased (e.g. Bristol Channel), respectively; with the two components combining to alter the ESLs. The second, more advanced, method incorporates this physical mechanism by building on the skew surge joint probability method (SSJPM) by Batstone et al. (2013). The SSJPM uses a combination of tide gauge data around the UK to calculate ESLs and a model to dynamically interpolate the ESLs between the tide gauge stations around the complex coastal bathymetry. The Batstone et al. (2013) model simulations use tidally and meteorologically forced, as well as tidally forced 44year hindcast simulations in order to calculate tidal predictions and skew surge (the water level difference between maximum predicted HW and the maximum water level of the tide and surge). The ESLs from the model simulation are then adjusted using the error between tide gauge and model estimates of ESLs. To recalculate ESLs (as return periods) that include tidal alterations due to future SLR both of the simulations would have to be repeated, with the SLR perturbation applied to the original bathymetry, to obtain new probability distribution functions (PDFs) for both tide and skew surge. The tide and surge simulation would include the altered

tide and the altered tide-surge interaction; the tide only simulation would include just the altered tide. The skew surge derived from these simulations would then also include tidal changes and tide-surge interaction changes. The combination of the new skew surge PDF and altered tide PDF using SSJPM would provide new estimates of ESLs with an improved physical representation compared to those from the linear offset method. It would not be possible to adjust the model ESL estimates using the present day tide gauge data as in Batstone et al. (2013) as tide gauge data does not include the projected tidal alterations. Owing to this either no adjustment is made to the model estimates, or the same adjustment made for the present day ESLs is applied (assuming the errors are independent of tidal changes), or after the tidal changes are evident in the tide gauge data (e.g. in 50years time, depending on the rate of SLR) the SSJPM ESLs from the tide gauge data are recalculated and then the adjustment to the modelled ESLs reapplied. A key recommendation of this thesis is for all nations' future national flood assessments to include at least the first method and preferably the second method of including tidal alterations due to SLR so that flood assessments fully evaluate the combined tide, surge and SLR flood risk.

Owing to the complex non-linear nature of tide-surge interaction and the complexities of tide-SLR interaction numerical simulations are required in order to determine the net effect on ESLs of altered tidal phase and amplitude, SLR, and phase alteration of the largest residuals. Modelling by Pickering (2009) using the same model as in Chapter 2 identified tide-surge interaction showing that the DCSMv5 would be appropriate for such a study. Recent DCSMv5 simulations run for 1 year, including tidal and meteorological forcing, showed the effect of the tide-surge interaction on the alterations to tidal amplitudes to be very small (<1cm) (Firmijn Zijl, pers. comm). The effect of the altered tide on the surge elevations in these simulations remains to be analysed. Previous studies only at Immingham and with 0.5m SLR suggest the effect on ESLs is small (Lowe et al., 2001) and for multiple locations with 5m SLR find -0.2 to 0.1m changes to the surge elevations (de Ronde, 1993).

Taking Hamburg, one of the two aforementioned major European cities with substantial HW changes (for which a representative model location of Cuxhaven was analysed), the importance of localised factors can be seen. Hamburg lies 140km up the tidal Elbe Estuary from Cuxhaven at the mouth.

The estuary has a MTR of 3.6m (Muller-Navarra and Bork, 2011) and exhibits tidal amplification up its course (Weilbeer and Klopper, 2011). The increases in tidal amplitude we find at the mouth of the estuary will therefore be altered as the tide propagates up the estuary to Hamburg. The coastline geometry of the southeastern German Bight also causes some of the largest storm surges in the North Sea due to its funnelling effect (von Storch and Woth, 2008); additionally storm surges upstream in Hamburg are on average 1m higher than those at Cuxhaven (Grossmann et al., 2007). This storm surge risk combined with the Cuxhaven HW increases and estuarine tidal amplification mean it is likely that flood defences along the tidal stretch of the Elbe will require improvements in the future. The same will apply to many global coastal communities which lie up estuaries where progressive narrowing of the channel generally causes tidal amplitudes (H_o) to increase according to approximately $H_o^2 = \text{width}^{-1}$ (Pugh, 1987). The modelling presented in this thesis has insufficient resolution to quantify the upstream, estuarine effects of changing tides at the coast. Owing to the particular importance of these effects for the flood risk at major estuarine cities it is recommended that high resolution localised modelling is undertaken. This modelling should use sufficient resolution to properly represent the tidal propagation within the estuary and force with SLR scenario dependent tidal boundary conditions from the larger scale tidal models of Chapter 2 and 3. As the tidal changes are shown to be driven at a shelf scale it is only through downscaling from shelf or global tidal models to estuarine models that up estuary tidal effects can be properly quantified. Recent high resolution localised flood risk studies for cities such as Hamburg (Ge et al., 2013) are now recognising the non-linear influence of SLR on the tide (and surge) by including a SLR perturbation to their model bathymetry. This incorporates the SLR-tide interaction within their estuarine domain however such studies would benefit further from applying tidal alterations to their seaward boundary condition as described above.

The tide contains cyclic variability on a multitude of different timescales. For example the coincidence of the M_2 and S_2 tidal constituents generates the fortnightly spring tides which in locations where S_2 amplitude is large (e.g. Newport Table 2.3) can result in spring and neap amplitudes that differ by meters. On longer, twice yearly timescales, semidiurnal tides reach their maximum at the equinoxes when zero solar declination amplifies the S_2

amplitude leading to even larger spring tides. Another much longer period of variability is the 18.6year nodal tidal cycle, during which the M_2 amplitude, for example, deviates from its mean value by ~±3.7% (Pugh, 1987). These seasonal and nodal tidal variations are reflected in the analyses of ESLs (Weisse et al., 2013). It is within this context of cyclic natural tidal variability that the secular trends in tidal amplitudes presented in Chapters 2 and 3 will occur. This is important in two ways. Firstly in terms of the background natural tidal amplitude variability present; for example the spring-neap cycle amplitude variability will often be larger than the SLR induced secular amplitude changes we present. The longer nodal variations in the tide may present challenges for identifying secular tidal changes requiring datasets longer than 18.6years to distinguish the trends. This is an analogous challenge to identifying small (1mm) increments of SL change against a background of natural variability, Hughes and Williams (2010) suggest this will require >100 years of data where variability is large in the Kuroshio Extension but <12 years of data where variability is small in the tropical Atlantic. Secondly the secular amplitude trends we present will, after SLR has occurred, be present and superimposed on all phases of the natural variability of the tide. This means that when natural tidal forcing is close to a maximum the SLR induced amplitude change will also be present. In such instances amplitude changes caused by SLR will act to exacerbate or mitigate (depending on their sign) the high tidal levels present from the natural forcing. Combinations of near maximum tidal forcing and SLR induced tidal amplitude increases could lead to more severe flood risk, particularly in combination with an extreme meteorological event.

4.2.2 Renewable Energy Generation

Engineers planning tidal energy installations pay attention to the effect of the turbine or barrage on the localised stream flow and the back effects on the local tidal dynamics. The motivation for this is to achieve correct tidal array spacing to enable optimum power capture. The localised wake generated by a tidal device may be important (Blunden and Bahaj, 2007) however a vast number of tidal stream devices would be required to significantly alter the regional tidal dynamics. Modelling studies into the effect of large potential tidal barrage schemes on the tides show that barrages, such as that proposed for the Bristol Channel, could lead to small but noticeable far field effects in

remote locations such as the Bay of Fundy and Hudson Strait (Ian Walkington, pers. comm.). Engineers may not be aware of the potentially much more substantial alterations to tidal dynamics, range, velocities and hence available tidal energy caused by other external factors such as SLR. Tidal alterations of this kind should be considered in conjunction with the more localised effects of the extraction infrastructure itself.

Assessing future available tidal energy will require consideration of the alterations to tidal conditions resulting from SLR. It is therefore pragmatic that any CBA performed to assess the suitability of a site for a tidal power installation should include possible long term increases or decreases in the potential tidal energy associated with SLR. For example locations such as the Bristol Channel and St. Malo show substantial decreases in tidal range with future SLR. If these future range decreases, and associated decreases in current speed, are not included in the CBA then this could lead to costly overestimates of the net present value of the project by government bodies such as the Department of Energy and Climate Change and the Carbon Trust. As such the present results have relevance to Strategic Environmental Assessments for marine renewable energy included in the UK's (and other coastal countries' worldwide) Renewable Energy Strategy.

Simulations to assess the available wattage of energy at viable sites could explore a range of future SLR scenario trajectories and depending on the rate of SLR, the longevity of a tidal facility based on changing tidal conditions could be assessed. This would lead to a scenario based set of CBAs which could be used to select the appropriate investment level at any particular tidal site given the expected lifetime of the infrastructure as well the possible SLR and tidal alterations. It should be noted that tidal changes on the timescale of tidal stream project lifespans (~20 years) will be much smaller than those of tidal barrages (~120 years).

Based on the amplitude changes presented in Chapter 2 potentially key locations for future increases in available tidal energy will be Vlissingen, Harlingen, Cuxhaven and Dublin. The key locations where decreases in available tidal energy will be are the Gulf of St Malo, the Bristol Channel, Cherbourg, Plymouth, Dieppe and Immingham. This could have serious implications for calculated 'pay back' periods of existing tidal range (La Rance,

Gulf of St Malo) and tidal stream (Strangford Lough, northwest Irish Sea) and proposed tidal range (River Severn and Swansea Bay Bristol Channel) and tidal stream (Pentland Firth, north of Scotland) power plants. It may also cause present day assessments of tidal energy not to be valid for the future with altered tidal regimes due to SLR (e.g. European Commission, 1996; ABPmer et al., 2004; Myers and Bahaj, 2005; Blunden and Bahaj, 2006). Chapter 3.4.5 suggests that with 2m SLR and a fixed coastline currently viable tidal renewable sites, for either tidal stream or tidal barrage projects, will experience increases and decreases in maximum tidal range and hence energy generation potential. The specific European sites affected by tidal alterations are shown in Figure 3.43, similar plots for other regions globally are given in Figure 4.1-4.4 (Africa is not shown as there are no changes). It should be noted that a 10% reduction in amplitude would cause a 3% reduction in current velocity (see Chapter 3.5.1) which for tidal stream power, owing to the cubic relationship between current velocity and tidal hydraulic power density (Hardisty, 2008), would lead to a 9% reduction in power generation and for tidal barrage power, owing to the quadratic relationship between tidal amplitude and hydraulic power density (MacKay, 2008), would lead to a 19% reduction in power generation. It should be noted that an amplitude change in a semidiurnal tide will have approximately double the effect on tidal velocities of the same change in a diurnal tide owing to their relative forcing frequencies.

Whether an assessed site remains viable when including tidal alterations is dependent on the expected lifetime of the extraction project, the rate of SLR and the tidal sensitivity to SLR in this location. Clearly candidate sites with macrotidal conditions are particularly attractive for tidal barrage energy generation projects, these large amplitudes often occur where tides in estuaries and embayments are close to resonance (e.g. Gulf of St. Malo and Bristol Channel). These locations are shown to experience large decreases in tidal range with future SLR, as the semidiurnal components of the tide move away from resonance. Initially SLR may move the tide towards resonance although as SLR continues from that point it will then move it away from resonance. To avoid erroneously assuming a proportional tidal response between 0 and 2m SLR a number of interim SLR scenarios using the regional DCSMv5 model would allow quantification of future tidal evolution patterns (as was done for the global model Chapter 3). As increased certainty is gained in

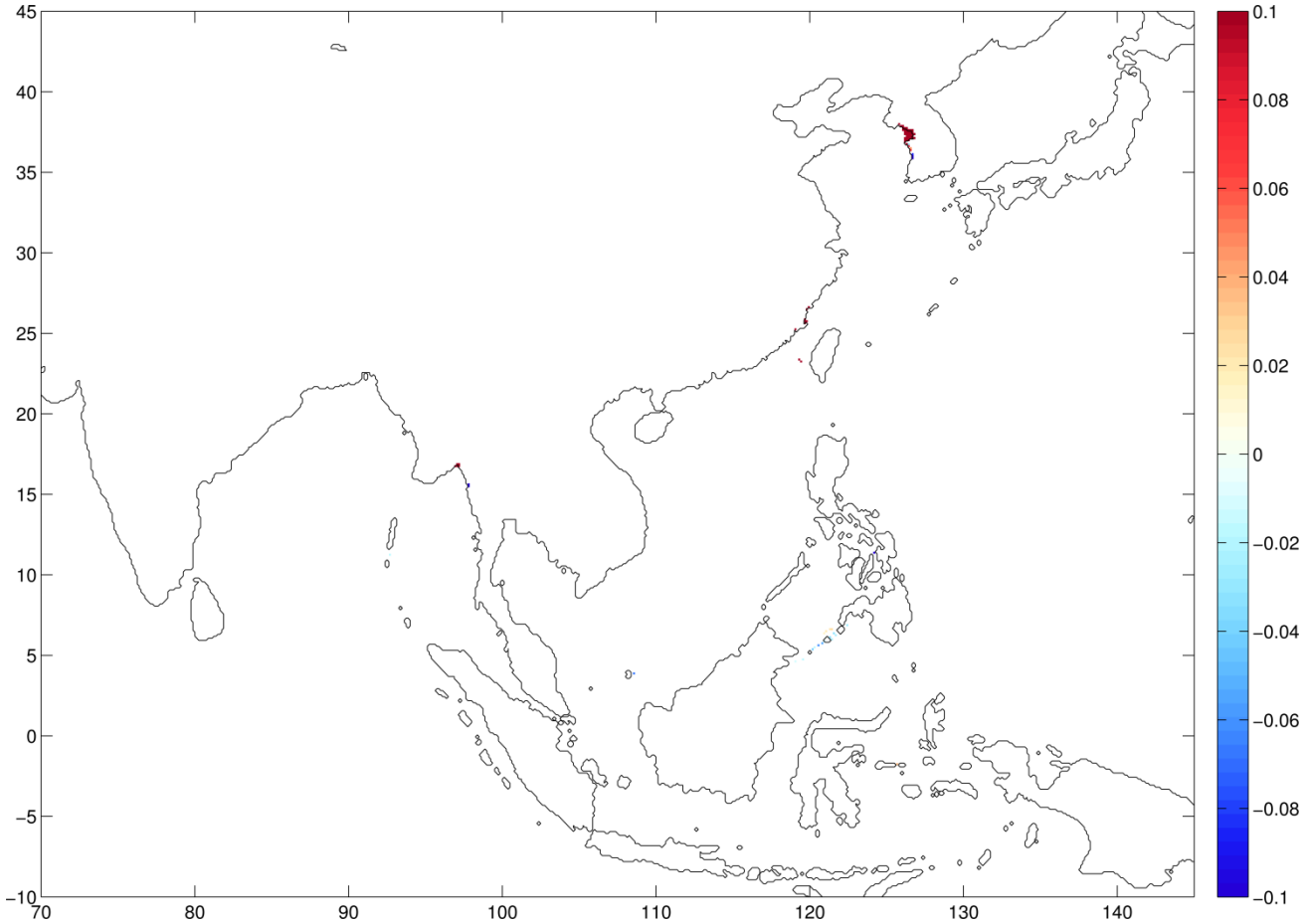

Figure 4.1. Asian change in maximum range (m), over the 15 day SSH reconstruction based on the four tidal constituents, with a 2m uniform SLR assuming a fixed coastline (+2UF) (increases- red, decreases- blue) for those locations found to be presently viable for tidal renewable energy (either 25-100m depth and peak current velocities >2m/s or with a MTR> 5m).

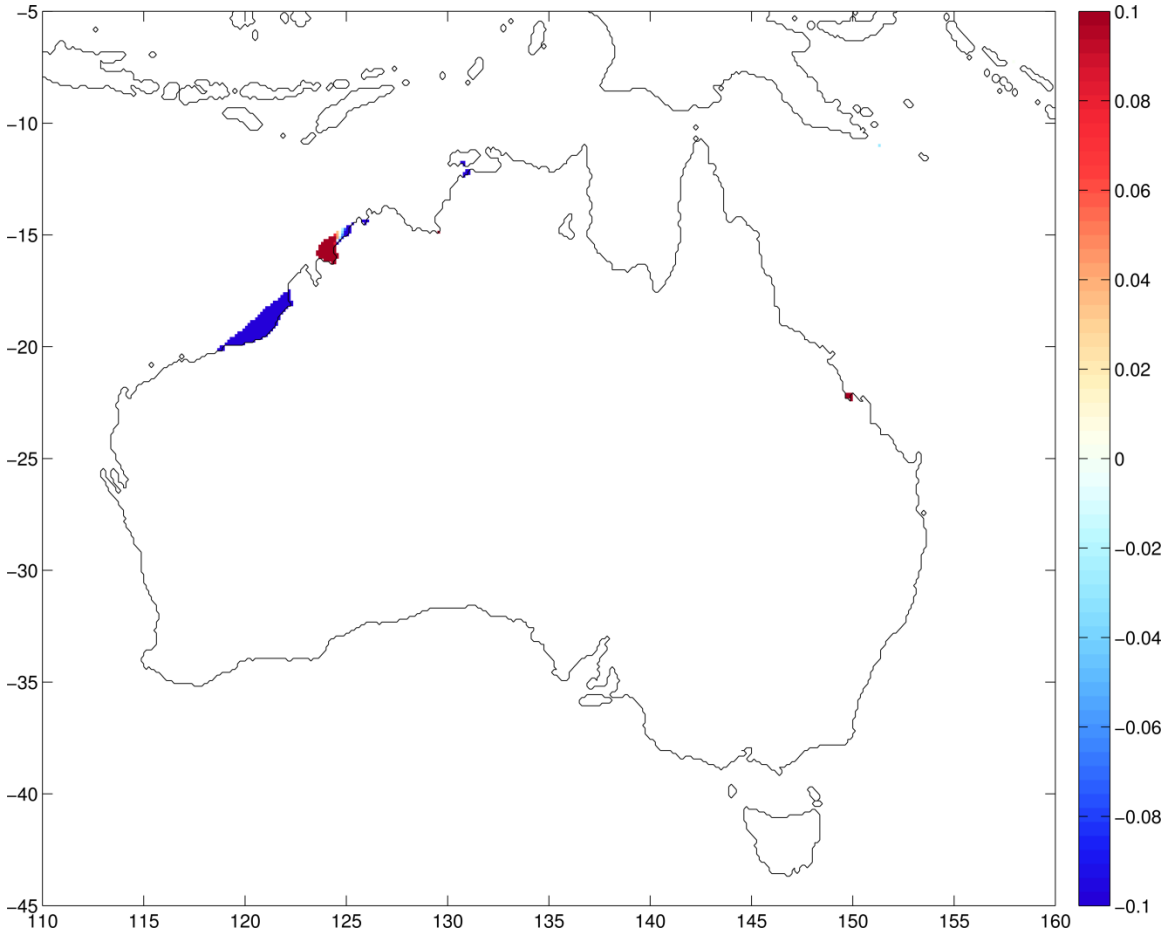

Figure 4.2. Australian change in maximum range (m), over the 15 day SSH reconstruction based on the four tidal constituents, with a 2m uniform SLR assuming a fixed coastline (+2UF) (increases - red, decreases - blue) for those locations found to be presently viable for tidal renewable energy (either 25 - 100m depth and peak current velocities >2m/s or with a MTR> 5m).

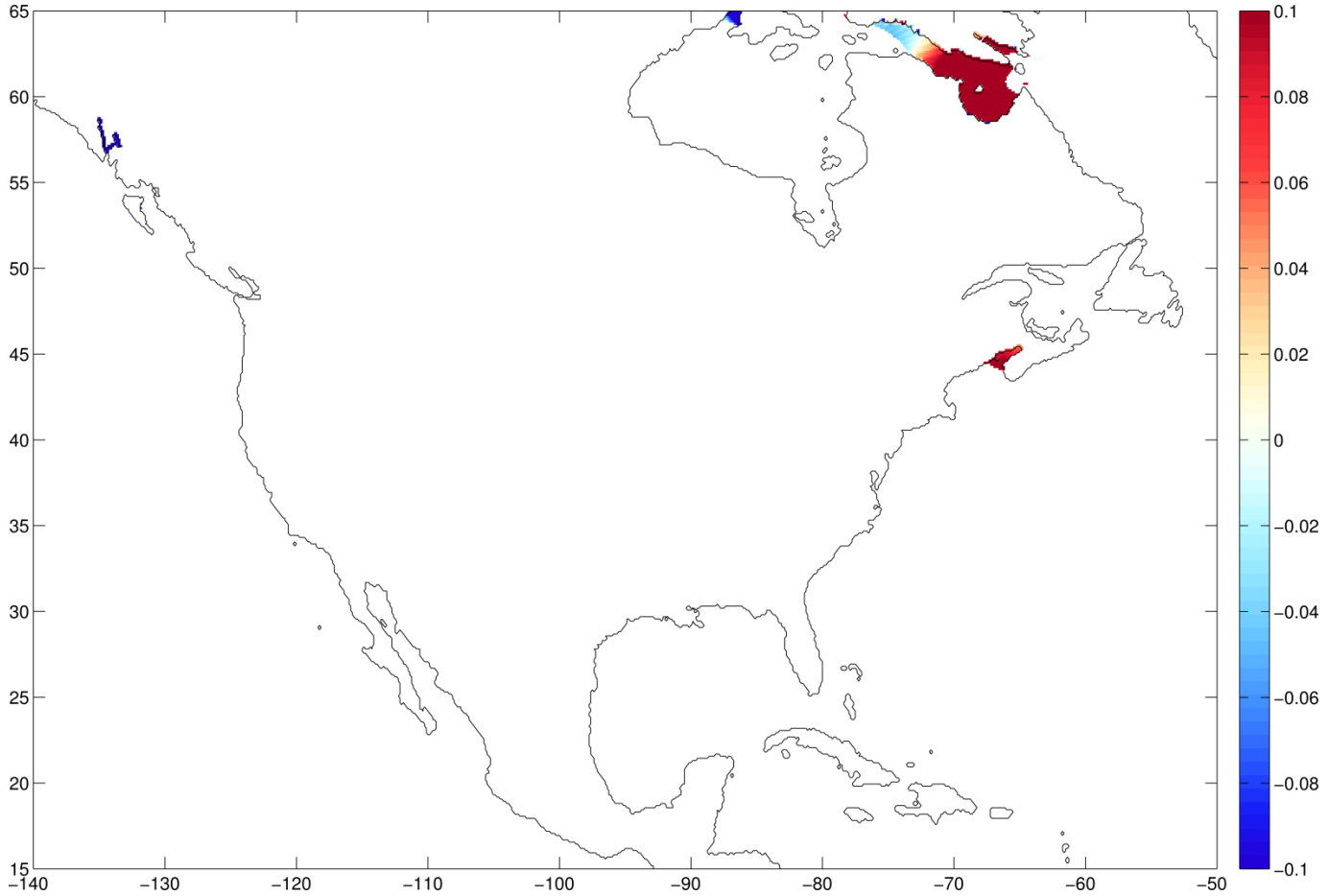

Figure 4.3. North American change in maximum range (m), over the 15 day SSH reconstruction based on the four tidal constituents, with a 2m uniform SLR assuming a fixed coastline (+2UF) (increases - red, decreases - blue) for those locations found to be presently viable for tidal renewable energy (either 25-100m depth and peak current velocities >2m/s or with a MTR> 5m).

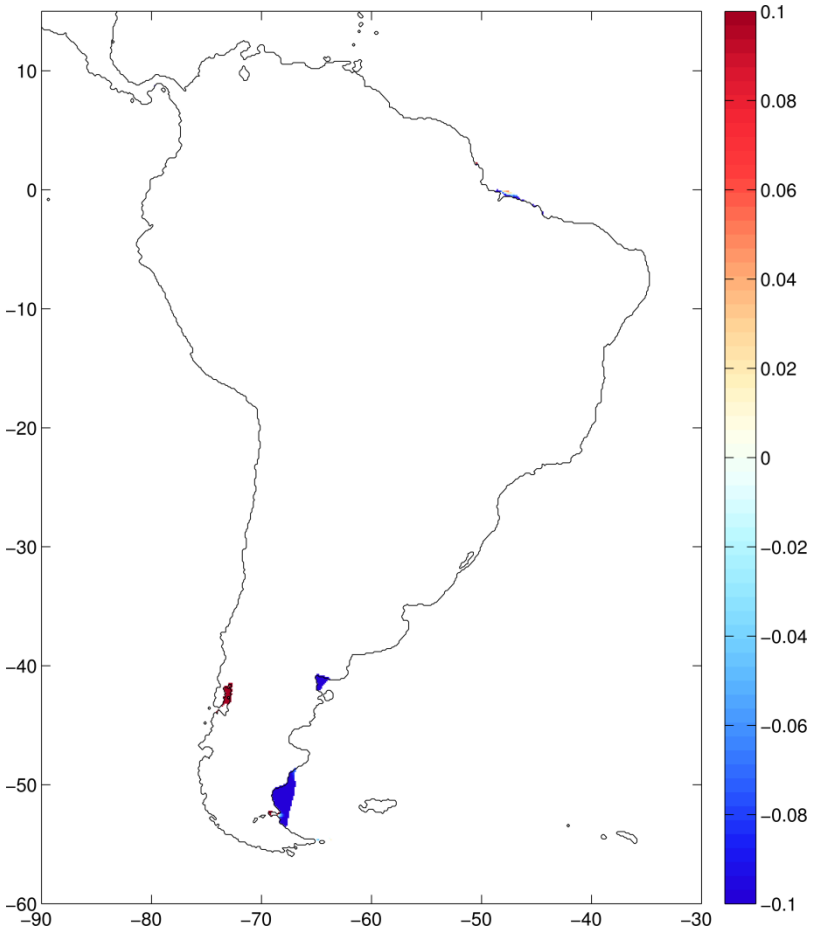

Figure 4.4. South American change in maximum range (m), over the 15 day SSH reconstruction based on the four tidal constituents, with a 2m uniform SLR assuming a fixed coastline (+2UF) (increases - red, decreases - blue) for those locations found to be presently viable for tidal renewable energy (either 25-100m depth and peak current velocities >2m/s or with a MTR> 5m).

the rate at which future SLR will occur, the SLR scenario based tidal predictions can be used to assess the present and future viability of a site for tidal energy generation. Tidal stream sites tend to be between islands and around headlands where tides are strong but not necessarily resonant; tides in these locations may be less sensitive to SLR.

In addition to the direct influence on future available tidal renewable energy there are also potential implications for other forms of offshore renewable energy such as wind farms. The long term evolution of bedforms, particularly sand waves, is of importance for the foundation requirements for wind turbines where long term alterations to tidal characteristics could, for example, lead to increased erosion and scour around the footings reducing stability. Sand waves are shown to be sensitive to both tidal asymmetry and water depth, both of which are altered with SLR (Jordan Mattieu, pers. comm.). Stronger tidal currents are shown to cause decay of sand waves with suspended transport dominating and weaker tidal currents causing sand waves to grow with bedload transport dominating (Tonnon et al. 2007). It is possible that alterations to sand waves by altered tidal conditions may in turn influence the formation of smaller surface bedforms altering the friction at the bed which may then feedback on the tides. Fully coupled hydrodynamic-morphology simulations are recommended to assess the importance of the feedback of changing bed morphology on the tides.

4.2.3 Nuclear power generation and other water reliant industry

In addition to direct implications for tidal energy generation, there are indirect implications for thermal power plants which constantly require water for ‘wet cooling’ purposes. Tidal range increases with SLR could lead to the exposure of the existing intakes at LW. Both uranium fuel and fossil fuel driven plants, making up 82% of current global electricity generation, require cooling water. Considering only the former, there are 185 operational nuclear facilities in wider Europe (January 2013) (European Nuclear Society, 2014) of these 27 are coastal and lie in the European domain modelled in Chapter 2. Those nuclear facilities which may be influenced by the particularly large tidal range changes presented in Europe include 3 British facilities in the Bristol Channel, 1 French facility near Cherbourg, 1 Dutch facility near Vlissingen, 3 German facilities in the southeastern German Bight and 1 Swedish facility on the east coast of the

Kattegat. Globally there are (January 2013) 437 nuclear power plants in 31 countries (European Nuclear Society, 2014) some of which may also be effected by tidal alterations. Further analysis of the tidal water levels and specifications of the intakes are required to establish how significant these range changes are in terms of duration of consistent supply of cooling water to power stations. In most cases, increases in even the maximum range are less than the SLR itself therefore the absence of available seawater at the intake seems unlikely. Furthermore extension of the intake pipes into deeper water would be fairly straightforward. A further potential complication of changes in tidal range is increased salt water intrusion into estuaries where industry and agriculture relies on a fresh water supply such as in the Loire (Winterwerp, 2013). This may lead to reductions in the length of time freshwater is available or potentially to a total lack of available fresh water from the estuary.

4.2.4 Sediment transport, dredging and shipping

The changes in tidal range presented will cause associated changes in current velocities and hence sediment transport; this in turn will have an impact on the coastal morphology.

The magnitude of sedimentation and erosion is correlated with bed shear stress and hence tidal velocity (Gerritsen and Berentsen, 1998). In those locations where tidal current velocities increase with SLR, bed shear stresses will increase and the kinetic energy acting to suspend bed material and transport it also increases (and vice versa where current velocities decrease). In Gerritsen and Berentsen (1998), as SLRs from -15m and -5m to present day SL erosion is found to decrease in the southern North Sea and increase in the German Bight with altered tidal dynamics. Assuming the tidal response to this SLR is proportional (unlikely to hold over such large SLR changes) these trends in erosion characteristics might be expected to continue as tidal dynamics are altered under future SLR. Jensen and Mudersbach (2005) consider changes in the observed tide with SLR and highlight the future implications for erosion problems in the Dutch Wadden Sea. Additionally a UK assessment of the impact of climate change on coastal erosion states that SLR is very likely to increase the rate of erosion along already eroding coasts and notes that long term future changes in the tidal regime due to SLR could also influence erosion (Masselink and Russell, 2013). Future work should look to couple the output

from our tidal simulations with coastal morphology models such as those considered in the ARCoES (Adaptation and Resilience of Coastal Energy Supply) project (http://www.arcc-network.org.uk/project-summaries/arcoes/). ARCoES aims to assess coastline vulnerability to flooding and erosion on long climate change timescales >100years, relevant to existing and planned coastal nuclear installations, these are long enough timescales that tidal amplitudes and currents can no longer be assumed constant with SLR; the impacts should therefore be assessed.

In estuaries (Bolle et al., 2010) and coastal lagoons (Araujo et al., 2008) detailed modelling assessments of the changes in the tidal asymmetry and the sediment exchange changes due to natural and anthropogenic alterations in the bathymetry have been made. Of particular importance is the tidal flood or ebb dominance and how it might change the sediment import or export respectively. The link between increased tidal propagation and increased suspended sediment concentrations (SSC) has been demonstrated for the Humber Estuary by Morris and Mitchell (2013). In the Humber Estuary the net sediment import per tide (100 tonnes) is only 0.08% of the total sediment exchanged during a tidal cycle (Townend and Whitehead, 2003); substantial, finely balanced estuarine sediment budgets such as this have the potential to be strongly influenced by tidal changes. At the mouth of the Western Scheldt in southern Holland increased depth due to dredging has led to greater export of sediment (Haecon, 2006) whereas in the central Scheldt it has led to increased import (Stikvoort et al., 2003). In the Stour and Orwell estuaries in the UK a significant increase in ebb dominance was found when dredging increased depth (Roberts et al., 1998) whereas in the Mersey the evolution of the bathymetry is much slower to respond (Lane, 2004). In a similar way, as estuaries are deepened by the process of SLR, alterations to the tidal asymmetry will change the net sediment transport. The depth change of an estuary may not be as large as the SLR itself as the estuary attempts to import sediment in order to maintain dynamic morphological equilibrium up to a point where there is no longer sufficient sediment supply or the rate of SLR is too great causing the estuary to drown (van Goor et al., 2003). At this point saltmarshes and spits are likely to receded or disappear as the morphology adjusts (Masselink and Russell, 2013). It is also important to note that tidal pumping in the near shore will change. This is a non-linear process which can

drive sediments landwards depending on the asymmetry in the tidal velocities. This asymmetry (flood or ebb dominance) depends on the relative phase and amplitudes of the M_2, M4 and M6 constituents (Dyer, 1997) which have all been shown to be sensitive to SLR in Chapter 2. Any transition in the tides from a standing wave to progressive wave would also have implications for saltmarsh growth or depletion. A progressive tidal wave has a velocity minimum (slack water) midway between high and low water whereas a standing wave has velocity minimum at high and low water influencing sediment transport (Pugh, 1987). Furthermore changes to the tidal range in estuaries will alter the volume of water exchanged between the estuary and the coastal waters, the tidal prism. This will in turn alter the residence time for pollutants in the estuary which are dependent on the tidal prism volume (Dyer, 1997).

Many estuaries bordering the European coastline are fundamental arteries for passage of shipping to major ports stimulating local and national economies. Therefore there is a requirement to dredge these estuaries so that they are deep enough to remain passable for ships. The estuary of the River Elbe in Germany, for example, connects the southeast German Bight at Cuxhaven to the major port city of Hamburg. For 140km a minimum depth of 13.5m is maintained (Muller-Navarra and Bork, 2011), the afore mentioned possible increase in erosion in the German Bight, as well as the increased tidal range at Cuxhaven (with lower LW) and increase in MSL could lead to alterations in the sediment transport (import and morphology), the channel depth and hence the dredging requirement for such channels. Changes to the tidal currents will also affect navigation pathways. Navigation on the River Elbe is very dependent on water levels influenced by tides and wind setup, with extended periods of LW reducing the length of the tidal cycle suitable for passage of deep draft vessels (Muller-Navarra and Bork, 2011). Plans to slow the hydrodynamic regime of the Elbe to subdue the disadvantageous sediment transport patterns (von Storch and Woth, 2008) could be inhibited by increased tidal range due to SLR. Some large modern container ships in the Elbe have clearances with the seabed of <1m so dredging requirements have very fine tolerances in the context of changes in depth, sediment transport and tidal range with SLR.

Winterwerp (2013) shows the tidal range evolution over the last century at five European ports with long narrow channels where deepening and narrowing by dredging and canalization has led to substantial (order meters) increases in

tidal range. These increased tidal ranges have caused problems with salt water intrusion, water quality and lowering of the ground water table. The Ems and Loire estuaries are now classified as hyper-turbid with high SSCs (Winterwerp, 2011). The Ems River in the Wadden Sea has been heavily dredged (1.5Mton/year) as well as having the entrance and lower reaches deepened by ~2m this has increased the tidal asymmetry and tidal pumping of fine sediments leading to increased turbidity further upstream in the estuary. This has had a catastrophic influence on the ecology of the estuary, it is expected that further deepening of the estuary by SLR and potential increased tide could further exacerbate the turbidity driven ecological problems. Analytical solutions (Winterwerp, 2013) show in convergent channels with no intertidal area the flood dominance of the tidal asymmetry increases rapidly as channel water depth increases (by dredging or SLR) between 3-7m; in channels with larger intertidal areas tidal asymmetry is more resilient to depth increases. These analytical solutions and observations of how the effect of estuarine channel deepening by dredging causes increasing tidal range and effects SSC are a good proxy for the likely effects of future SLR and increased tidal ranges at the mouths of estuaries presented here.

Some ports such as Amsterdam are dependent on extensive lock systems as well as discharge sluices and pumping stations (at IJmuiden) to create safe passage for shipping from the coast inland and to manage the landward water levels (Swinkels et al., 2010). These locks were designed based on present day MSL and tidal range. Change in tidal range at such locations as well as SLR itself may change the length of the window of opportunity where such locks are operable and the volume of water able to be discharged through sluices (and hence the pumping requirements). Some docks have very narrow tolerances for vessel draft over the dock sills so changes to MSL and tidal range may be particularly important especially given the substantial costs of altering the height of the dock sill. Similarly increases in HW may cause difficulties for tall shipping where there is limited clearance below bridges at HW when water depth is sufficient for their passage (especially if the estuary is importing sediment with SLR so SLR is not increasing depth). The relevance of this problem is substantiated by the installation of real time air gap monitoring sensors on a number of US bridges (NOAA, 2008). In an alternative scenario if the channel has sufficient depth but shipping can only clear the bridge at LW,

SLR and reductions in tidal range may reduce the number of LWs where successful passage is possible. Reductions in MTR could also cause difficulty where the HW is used to gain the clearances with the seabed necessary to enter the harbour; at these locations more dredging may be required (although this problem may be offset as the SLR itself is often larger than the MTR decrease).

4.2.5 Tidal mixing fronts

Primary productivity is high in the seasonally stratified areas of the European Shelf as well as many other shelf seas globally. In addition to the seasonality in the heat fluxes and wind, the tidally induced turbulence and hence vertical mixing plays a substantial role in the position of the 4 main European tidal fronts. The Simpson and Hunter criteria (1974) can be used to quantify whether a water column will be vertically well mixed or stratified, according to h/u^3 where h is depth and u is the current velocity vector. As tidal amplitudes are altered with SLR the tidal current velocities will also be altered. This could in turn alter the tendency for a location to be stratified or well mixed thus altering the position of tidal mixing fronts.

This has been demonstrated for various fronts globally using a similar criterion, the Stokes Number (Souza, 2013), derived from current velocities and depths from the present day and 2m SLR coastal recession simulations (+2UR) presented in Chapter 3. Stokes numbers in excess of unity indicate a well-mixed water column. Comparative Stokes number plots are shown for various shelf seas. In the northwest Gulf of Alaska and the Bering Sea (Figure 4.5) 2m SLR reduces the well mixed area in the Kotzebue Sound and along the coastline to its west as well as in the Norton Sound. The Gulf of Maine (Figure 4.6) shows larger well mixed areas with 2m SLR in the upper Bay of Fundy and along the central coast of Maine. Well mixed areas in the Irish Sea (Figure 4.7) increase with 2m SLR in the Firth of Clyde and along the southeast coast of Ireland. Substantial decreases in the well mixed area with 2m SLR in the North Sea (Figure 4.8) are shown in the German Bight and in the East China Seas (Figure 4.9) there are smaller decreases offshore to the east of Ningbo.

The stratification of the water column in shelf seas plays an important role in primary productivity and hence draw down of atmospheric CO2 through the carbon pump (Thomas et al., 2004). Where large tidal range decreases occur

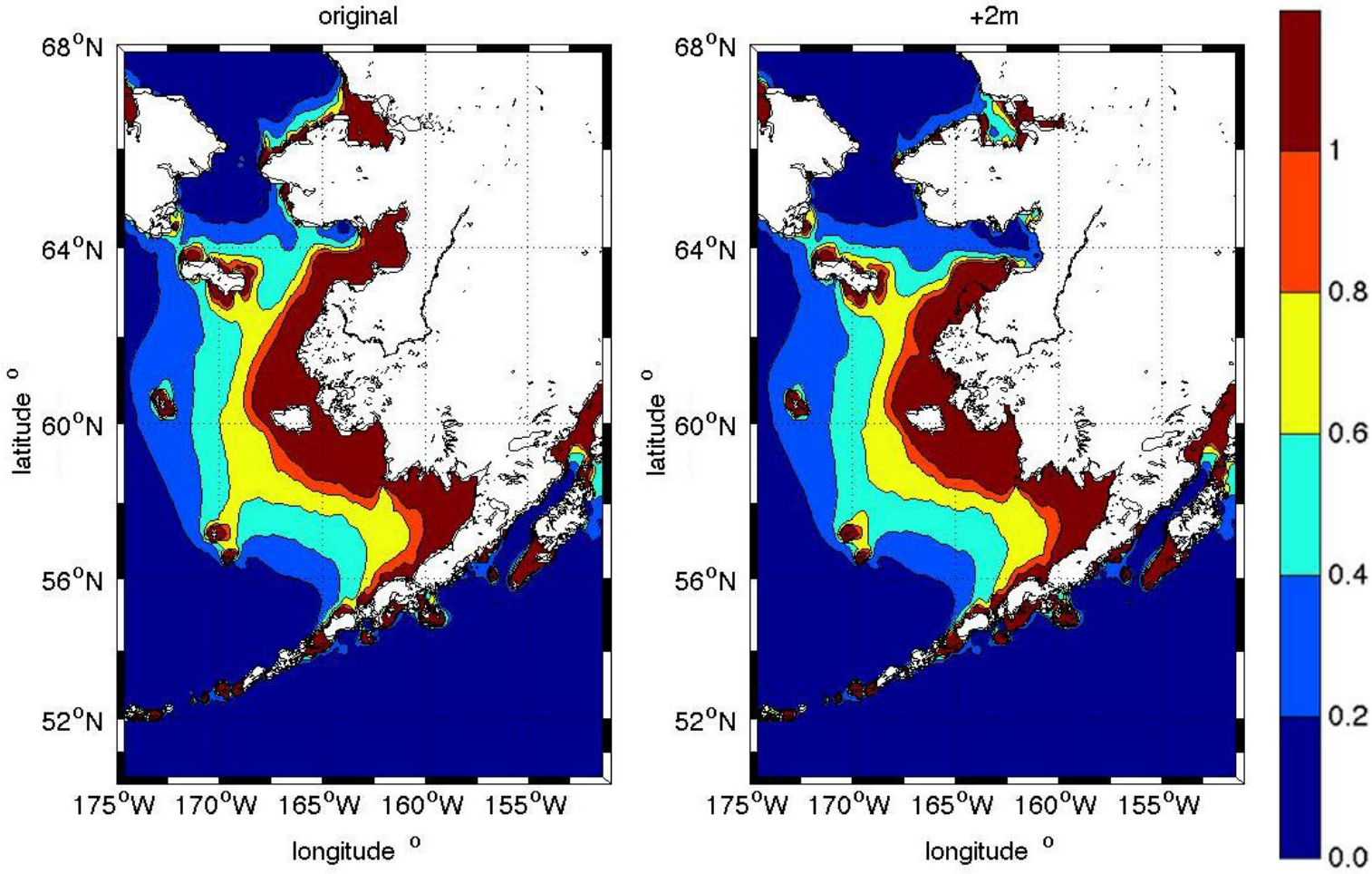

Figure 4.5. Gulf of Alaska Stokes number plots based on currents and depths from the present day (original) and the 2m uniform SLR coastal recession (+2m) scenarios. A value in excess of unity indicates a well mixed water column.

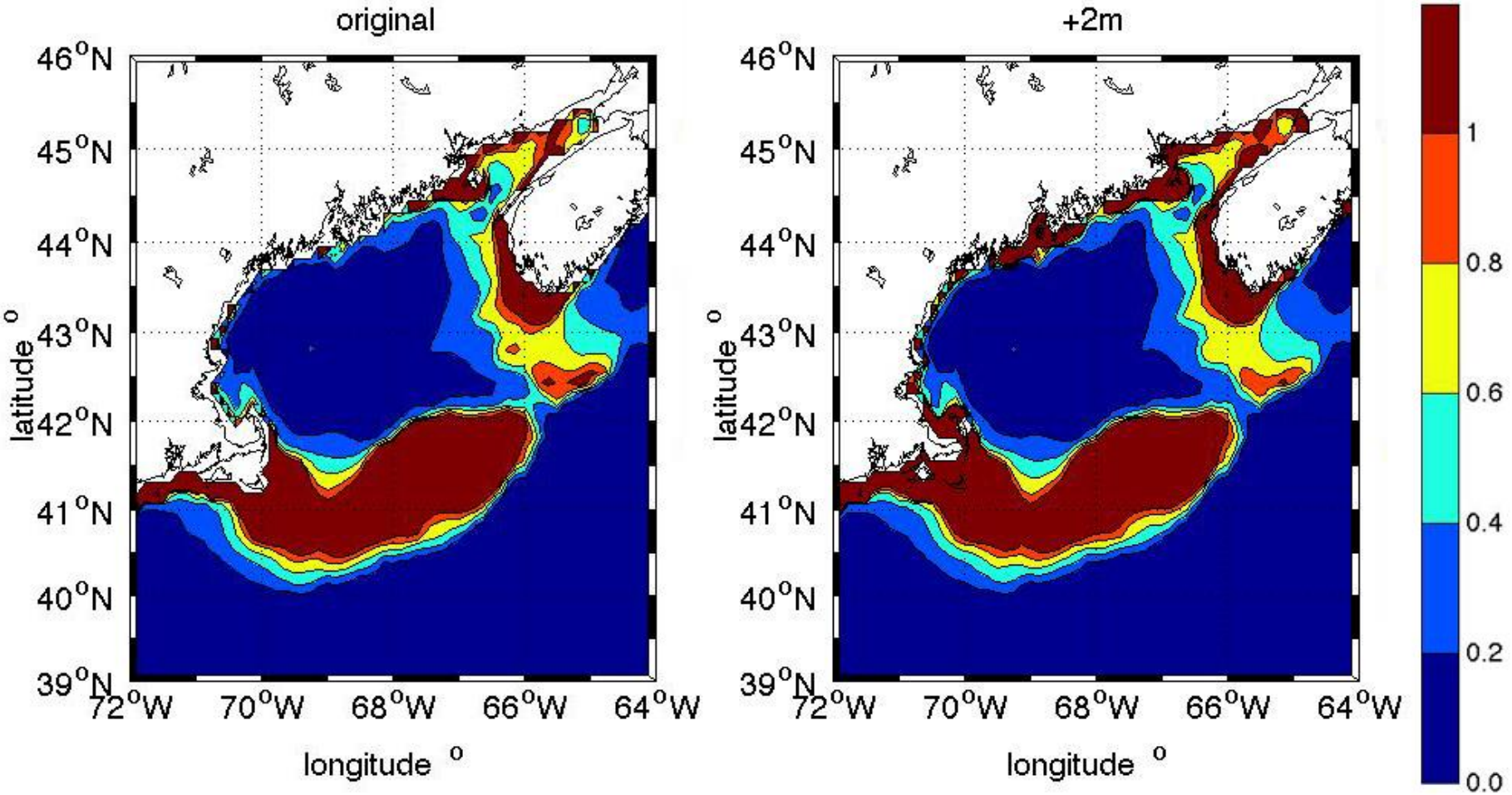

Figure 4.6. Gulf of Maine Stokes number plots based on currents and depths from the present day (original) and the 2m uniform SLR coastal recession (+2m) scenarios. A value in excess of unity indicates a well mixed water column.

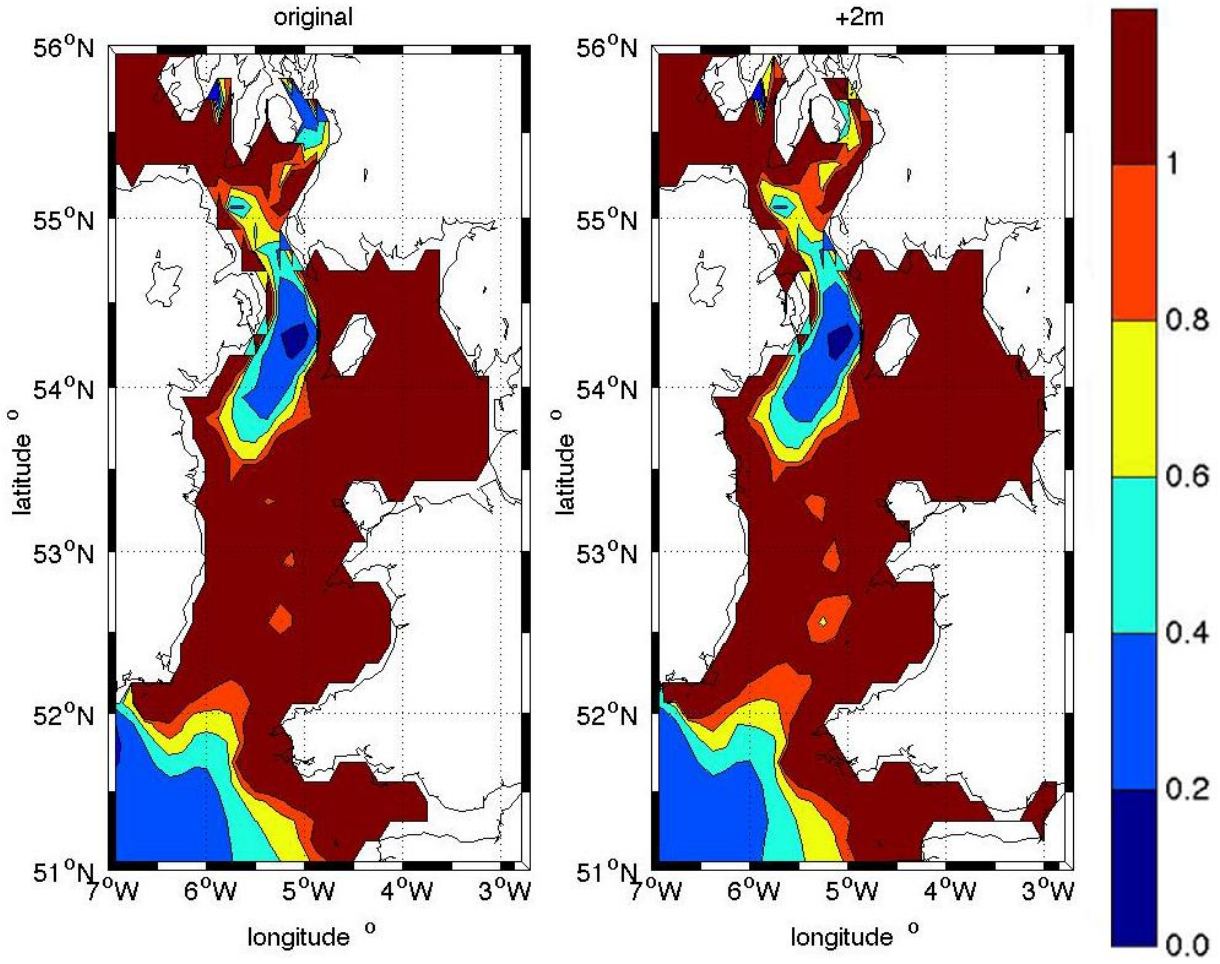

Figure 4.7. Irish Sea Stokes number plots based on currents and depths from the present day (original) and the 2m uniform SLR coastal recession (+2m) scenarios. A value in excess of unity indicates a well mixed water column.

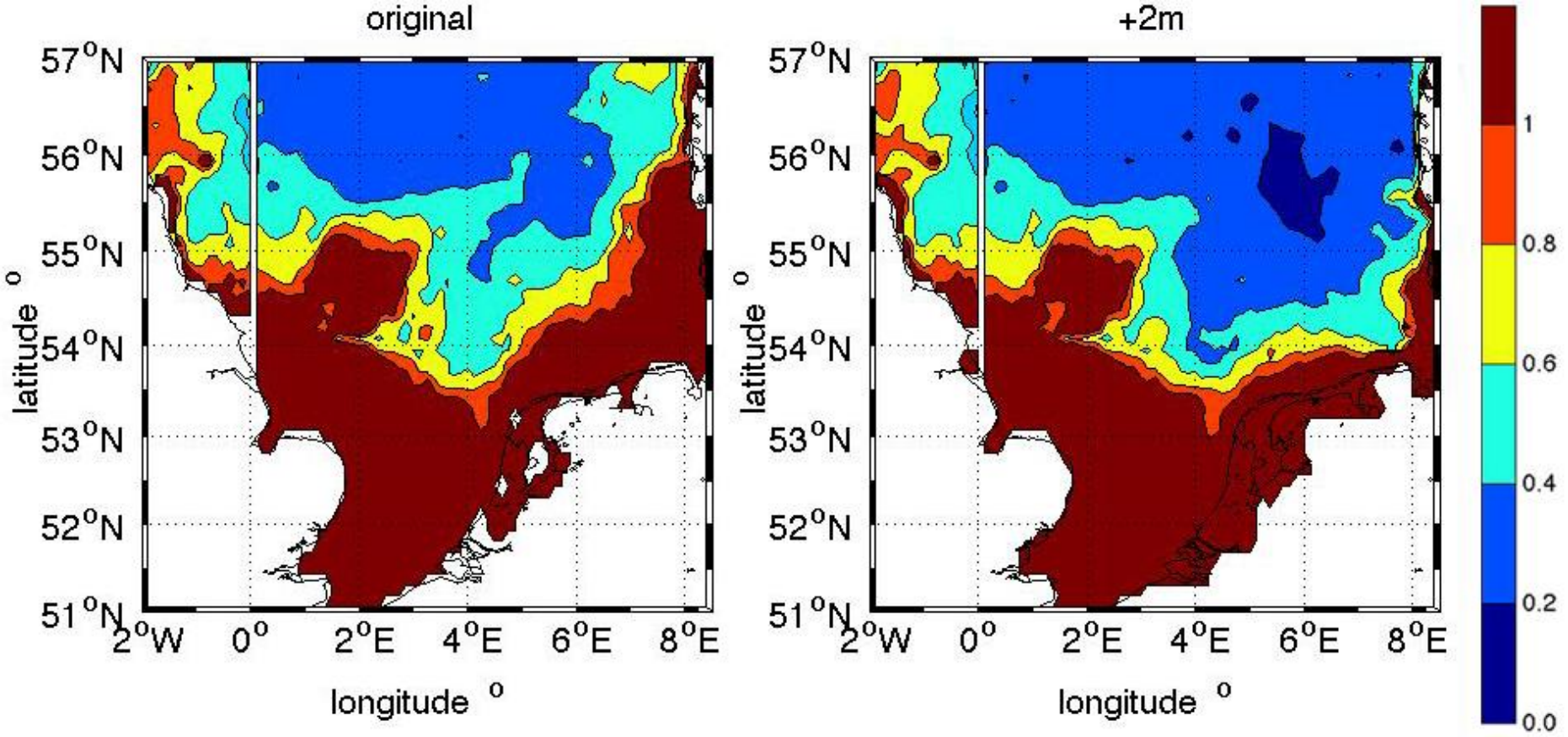

Figure 4.8. North Sea Stokes number plots based on currents and depths from the present day (original) and the 2m uniform SLR coastal recession (+2m) scenarios. A value in excess of unity indicates a well mixed water column.

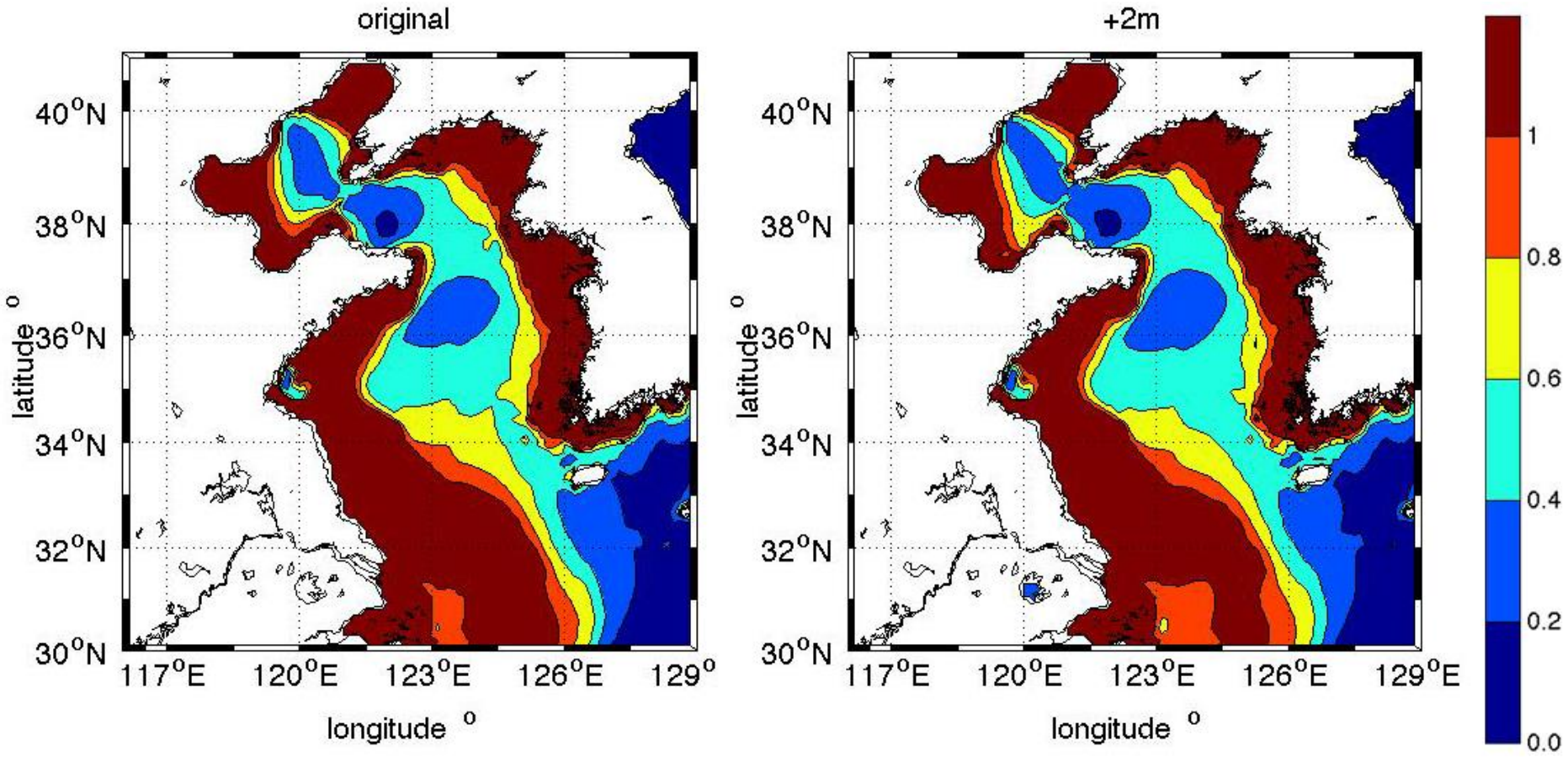

Figure 4.9. East China Sea Stokes number plots based on currents and depths from the present day (original) and the 2m uniform SLR coastal recession (+2m) scenarios. A value in excess of unity indicates a well mixed water column.

tidal currents will become weaker and the tidal front will shift towards the region of range decrease reducing the spatial extent of the well mixed water (and vice versa). These shelf wide changes in the distribution and proportion of stratified waters as well as tidal fluxes onto and off the shelf could change the amount of CO2 drawn down, sequestered and exported for storage in the deep ocean. An additionally variable in the future climate where these tidal changes occur is the potential for an increase in the heat flux with global climate change. In regions where tidal range is reduced this would compound the tidal effect further increasing the tendency for a stratified water column. In regions of tidal range increase, increased future heat flux would act to offset the increased vertical tidal mixing.

In the vicinity of estuaries, regions of freshwater influence (ROFIs) can dominate the stratification rather than the spatially uniform buoyancy input from heating. The discharge of freshwater from estuaries influencing the stratification can vary on timescales of days, much shorter than that of the seasonal heat flux variability. In ROFIs the future buoyancy-stirring competition determining the stratification will depend on alterations to estuarine discharge of freshwater with altered precipitation characteristics as well as alterations to the tides with SLR.

It is important to note that the stirring depends on the cube of the tidal current speed so small alterations to current velocities will have a cubic relationship with the stirring (Simpson, 1998). Furthermore the change in stratification and hence primary productivity of our coastal seas (Sharples, 2008) may have implications for species of higher trophic levels such as fish and apex predators such as birds which in turn depend on seasonal phytoplankton blooms (Scott et al., 2010; Embling et al., 2012; Scott et al., 2013). Additionally altered tidal currents ellipses may influence the migratory fish species which depend on these currents, such as Plaice in the southern North Sea (Walker et al., 1978). Another species shown to be sensitive to the position of tidal mixing fronts, particularly the baroclinic flows of the Irish Sea gyre, is the Norwegian Lobster (Nephrops norwegicus) which during the larval stage depends on their retention in close proximity to an area of muddy substrate for settlement and during the postlarval stage for burrowing (Hill et al., 1996; Horsburgh and Hill, 2003). Any change in the advection of the sediments used for burrowing or the baroclinic flows which retain the larvae in the vicinity

could have a detrimental effect on the stocks of Nephrops which are of an estimated value of £10million/yr to the Irish economies (Seafish, 2007) and £84million to the Scottish economy (Scottish Government, 2012). If effects were to act on these higher tropic levels there is potential for impacts on European marine fisheries and aquaculture.

4.2.6 Intertidal habitats

Changes in the MSL and the MTR will hold implications for those species which live in the intertidal zone. The SLR will shift the intertidal zone inshore and the changes in the tidal range will alter the spatial extent of the littoral zone, the current speeds, the bed type, the emersion/submersion curves and the position of areas exposed during daylight. The natural response of estuaries to SLR is landward migration, where coastal defences prevent this the seaward edge of marshes and lower part of the intertidal zone still erode, leading to a narrowing of the intertidal zone also known as coastal squeeze (Masselink and Russell, 2013). In such cases a managed realignment of the coastal flood defences will be required if the intertidal habitat is to be maintained. Coastal squeeze will be a particular problem along coastlines with hard engineering schemes in place such as in the Netherlands where dykes prevent landward intertidal zone migration.

There are many important intertidal habitats around European shorelines which could be affected. Coastal habitats on rocky shores, estuaries and saltmarshes are all strongly influenced by tidal conditions (Pugh, 1987). The Dutch and German Wadden Sea, for example, is a Ramsar wetland of international importance (1987) and a UNESCO world heritage site (2009) with a rich biodiversity of ecology living in the intertidal zone. Substantial changes to the MSL and tidal range could have large impacts in these extensive flat intertidal habitats which are home to over 10,000 species of flora and fauna as well as being a key haven for 10-12 million migratory birds per annum. Species which will be particularly strongly influenced will be those which lack adaptive and migratory capacity. If SLR rates are high and tidal ranges increased, the sedimentation-erosion balance in vegetated saltmarshes (Bos et al., 2007) may be pushed out of equilibrium, causing habitat loss. Additionally the ecosystem engineering capability of the flora and fauna could be affected by changing tides which would have associated consequences for biodiversity (Bouma et al.,

2009). One such example of an ecosystem engineer is the burrowing marine polychaete worm, Lanice conchilega, this worm has been shown to reduce the near bottom flow velocities and increase the sedimentation rates in ecologically sub-optimal regions of the intertidal zone (Rabaut et al., 2007). The reduction of habitat for such poltchaetes by coastal squeeze and reduced tidal range could lead to, amongst a variety of ecological impacts, the removal of nursery habitats in high velocity environments for macrobenthic fauna such as the juvenile flatfish (Rabaut et al., 2013). The existing spring-neap variation in the intertidal inundation (abiotic stress) causes differing intertidal elevations to experience differing inundation periods and frequencies. These abiotic stresses from tidal inundation characteristics could change with future SLR which will have implications for species whose physiologies are more adapted to aquatic or terrestrial conditions (Bouma et al., 2009). Where the abiotic stresses (including tidal range) are reduced biotic stresses will become more important (and vice versa) (Bertness, 2007). The importance of the tide in coastal marshes for feeding of wading birds is well established (Piersma et al. 2005). More recently the tidal importance for the homerange area required during the stopover of migrating land based birds has also been shown, with the potential for reduced carrying capacity with SLR and tidal changes (Arizaga et al., 2013). It should be noted that increased tidal range in some areas could also lead to enlargements of important intertidal habitats.

Globally diverse habitats such as mangroves (tropical and subtropical climates), saltmarshes (temperate climates) and corals, which are all also engineered by their inhabitants (Bertness, 2007), might be negatively impacted by SLR and alterations to the tide occurring too quickly for the biology to keep pace. Colonisation of sandbars and riverbanks occurs under low flow conditions which may no longer exist in regions of tidal range increase. This colonisation protects the sediment from erosion and allows further increases in plant growth increasing the stability of the sediment through biogeomorphic interactions (Balke, 2013). In vegetated biogeomorphic systems a gradual increase in environmental stress or disturbance frequency (with increased tidal velocities) could cause sudden loss of vegetation removing the biogeomorphic feedbacks; for vegetation to re-establish itself the tidal conditions would need to revert to their original state. Mangroves and saltmarshes occur in the upper intertidal zone. The settling and survival of mangrove and saltmarsh seedlings

depend on short disturbance free periods called windows of opportunity in order for roots to develop; these are limited by small scale physical disturbance by tidal inundation and wave induced sediment dynamics (Balke et al., 2011). These disturbances are the main bottleneck to seedling establishment and changes to these drivers (including tides) could alter colonisation by pioneer species influencing the possibilities for habitat management and restoration in some areas (Balke et al. , 2011). Seedling establishment at lower intertidal elevations is dependent on there being periods of no inundation which would be reduced by SLR and reduced tidal range (Balke, 2013).

Beach habitats may also be affected by SLR and changing tides. Areas where landward migration or increased erosion occurs may lead to mitigation attempts through beach nourishment programs which result in steeper beach slopes and reduction of subtidal and intertidal habitat. Loss of intertidal habitats such as saltmarshes and beaches or reduction of subtidal living zones could have severe consequences for countries to comply with, for example, the European Union Water Framework Directive and Marine Framework Directives. An additional implication of habitat loss in the coastal zone (e.g. mangroves) is the loss of their natural contribution to coastal flood defences.

4.2.7 Conclusion

The foregoing discussion highlights the pervasive influence of tides on many aspects of human activity from commerce to coastal protection to ecosystem services. We have long understood the importance of tides but this work illustrates that changes to tides – globally, regionally and locally – are as important. As mankind moves into an era of adaptation to our changing climate we should consider changes to tides as another factor in our adaptation strategies.

5. Conclusions

This thesis assessed the effect of future SLR on the European Shelf and global tides using both regional and global tidal models. This section discusses the relationship of the regional and global model results before summarising the key conclusions.

Section 3.4.6 makes comparison of the regional and global model results for M_2 tidal amplitude changes on the European Shelf and shows good agreement across most of the domain with 2m SLR and a fixed coastline (+2UF). There is a lack of agreement, with differing signs of amplitude change, in the Skagerrak and Kattegat between the two models. This is most likely a result of the Danish Straits being open or the Dutch coastline being poorly schematised in the global model. Appendix 3.5 shows the agreement between the two models to be better for +2UF, with only the aforementioned disagreement, than for +10UF where there is disagreement in the North Sea. The reduced agreement at 10m SLR suggests that the assumption of constant open boundary forcing in the regional model is beginning to break down. Both the regional and global models show differing patterns of M_2 amplitude response between 2m and 10m SLR, indicating the tidal response is non-proportional to the SLR imposed. There are differences in the spatial characteristics between the two models; the regional model suggests non-proportional response in the North Sea whereas the global model suggests non-proportional response in the Skagerrak and Kattegat. Despite some differences between them, the predictions of the two models of tidal changes on the European Shelf are useful for different purposes. To estimate tidal changes with +2UF SLR the regional model results (Chapter 2) supersede those of the global model as the regional simulation is higher resolution (1/12˚ not 1/8˚) and the Dutch coastline is better schematised. For higher SLR scenarios, such as +5UF and +10UF, where the assumption of constant tidal forcing at the open boundary of the regional model becomes more questionable the results from the global model (Chapter 3) may be preferable. Finally to evaluate SLR scenarios with a fixed coastline or coastal recession only the global model results can be used.

In the Introduction (Section 1) a number of key research questions were posed, below the conclusions of the thesis Chapters are related to these questions.

i) Contrary to previous European Shelf studies the tidal changes with SLR are found to be substantial in many regions both in Europe and globally. The fully forced regional simulations show M_2 amplitude changes with 2m SLR exceeding ±5cm at 13 of the 32 ports analysed. The spring tidal amplitude changes at these ports are even more substantial ranging from -49cm to +35cm with 2m SLR. In the global model 0.5m, 1m and 2m SLR scenarios with a fixed coastline cause MHW changes exceeding ±10% of the SLR imposed at 13, 13 and 10 of the 136 major coastal cities analysed respectively. Inclusion of coastal recession with 2m SLR (+2UR) results in a more substantial MHW response, exceeding ±10% of the SLR at 18 of the major cities. Assessing the changes in the maximum tidal range (spring and tropic tidal ranges) with +2UF SLR shows changes exceeding ±20% of the SLR imposed at 21 cities, ranging from -120cm to 92cm.

ii) The regional model shows the largest tidal alterations to occur in resonant or near resonant areas such as the Bristol Channel and Gulf of St Malo as well as in expansive areas of shallow water such as the German Bight. It also shows changes in spring HW exceeding +10% of the 2m SLR at two major European cities. The global model shows these changes will occur in shelf seas globally with a widespread global response of the shelf sea semidiurnal tides and a diurnal tidal response confined to Asian shelf seas. These changes will alter MHW and maximum tidal range in close proximity to major coastal cities, as described in (i), resulting in changes to future coastal flood risk as well as the other implications of changing tides discussed in Chapter 4.

iii) Both regional and global models show tidal changes with SLR to be spatially non-uniform with strong increases and decreases in amplitude irrespective of which tidal property is assessed (semidiurnal or diurnal constituents, MHW or maximum tidal change). These strong changes in shelf seas vary on short spatial scales consistent with the migration of amphidromic points. Changes in the deep ocean tides through resonant interplay of shelf and deep ocean tides leads to tidal changes that are more uniform over larger spatial areas.

iv) The regional model suggests that M_2 tidal amplitudes (and phases) change non-proportionally with respect to the imposed SLR between 2m and 10m. The more extensive analysis of proportionality for the global model results reveals an increasingly non-proportional tidal response with increasing SLR in all tidal

properties. The MHW response is shown to be increasingly above proportional with further SLR. The CFD plots for MHW changes at the 136 coastal cities in Appendix 3.3 suggest that tidal amplitude decreases saturate at higher SLR; that is as the amplitude decreases towards zero the decreases cannot continue to scale. To assess the proportionality of the tidal change more fully in the regional model additional intermediary scenarios between 2m and 10m should be tested and the SLR thresholds for non-proportional change identified.

v) The assumption of constant open boundary forcing with SLR for the regional European Shelf model is shown to be fair for 2m SLR because the tidal changes in the vicinity of the models open boundary are negligible in the global simulations and the characteristics of tidal changes within the domain show good agreement between the two models and are therefore not sensitive to this assumption. At 10m SLR these two statements cannot be made so definitively and the assumption is therefore becoming questionable. For other regional models the general principle can be applied that this assumption is justifiable for plausible SLR scenarios (up to 2m SLR) as long as the model's open boundary is in deep water and the tide in this location is dominated by the incoming deep ocean tide.

vi) Between the regional and global studies the tidal changes were assessed using an array of tidal properties including tidal constituents, spring and neap amplitudes, MHW, maximum tidal range and percentage change relative to the present day amplitude of these properties. The changes in M_2 and S_2 constituents in the regional model were often shown to be correlated and are therefore additive during spring tides. The spring tidal changes are generally larger than those of M_2 or neap tides. The global model shows this correlation to be true in most shelf seas globally with a limited number of areas having differing M_2 and S_2 signs resulting in larger neap tides. The MHW property provides an assessment of the compound effect of the changes in the four tidal constituents over spring-neap or tropic-equatorial tidal cycles. MHW changes are particularly useful when assessing changes to ESLs through the combination of the tide, surge and SLR. The maximum tidal range property is important when looking at the global results as some regions are dominated by diurnal tides where tropic tides (not springs) cause the highest water levels. This property allows comparable analysis regardless of which tidal species dominates. The tidal changes as a percentage of the original amplitudes are

shown to be large in regions with small present day tides such as microtidal environments or near amphidromes. This thesis focused on the effect of SLR on the dominant tidal constituents regionally and globally. Initial investigation of shallow water tides in the regional model suggests changes in higher harmonics with SLR could also be significant. Further work should assess tidal changes in a fuller set of tidal constituents including, for example, N_2 and P_1 as well as the quarter, sixth and eighth diurnal species of shallow water tides.

vii) The global model results show the inclusion of coastal recession with SLR to have a profound effect on the tidal response, often resulting in a change of the sign of the response. There is also an increasing tendency towards amplitude decreases when recession is included; for example of the 13 substantial tidal changes at major coastal cities with 2m SLR and a fixed coastline only 5 were decreases whereas of the 18 with 2m SLR and coastal recession 14 were decreases. The important implication of this result is that coastal management practices could be used strategically to influence the tidal amplitudes, using amplitude decreases to offset part of the SLR. This investigation tests the two limits of the problem, no recession and total recession globally. Further work should look to explore the boundless range of intermediary scenarios to test the effects of different combinations of coastal management strategies.

viii) Generally the difference in the tidal response between the uniform SLR and non-uniform IER SLR is modest, particularly where differences from the MSLR are small. At high latitudes however, where non-uniform SLR differs substantially from the global mean in these fingerprints, the alteration to the tidal response with uniform SLR is significant. The tidal response (both amplitude increases and decreases) is amplified in the far field of the ice mass loss where there is above average SLR and diminished in the near field where there is below average SLR. Whether the amplification occurs in northern or southern hemisphere high latitudes depends on the ice mass loss scenario Western Antarctica or Greenland respectively. In all IER SLR scenarios, including ice mass from both sources, Asia gets above average SLR and hence always experiences an amplified tidal response. As uncertainty is reduced over the patterns of future SLR from other processes further work should evaluate the combined effect of multiple non-uniform SLR fingerprints on the tides using the global methodology developed here.

The results of this thesis, as discussed further in Chapter 4, suggest that tidal changes with future SLR should be incorporated into future national assessments of: flood risk, renewable energy generation potential, cool water supply for industry (including the energy sector), coastal erosion, dredging requirements, shelf sea primary productivity and intertidal habitat alterations. This work fits into the context of the global effort to predict and understand the effects of future climate change. It is hoped that this thesis represents a significant contribution to advancing the knowledge and science of future sea-levels; particularly the lesser recognised effect of future SLR on tides.

Appendices

Appendix 1.1- European Port Tidal Curves (M_2 Runs)

Tidal curves for 0, 2 and 10 m SLR for all 32 ports from day 8.5-10 of the M_2 forced simulations (allowing comparison with tidal curves presented in other studies).

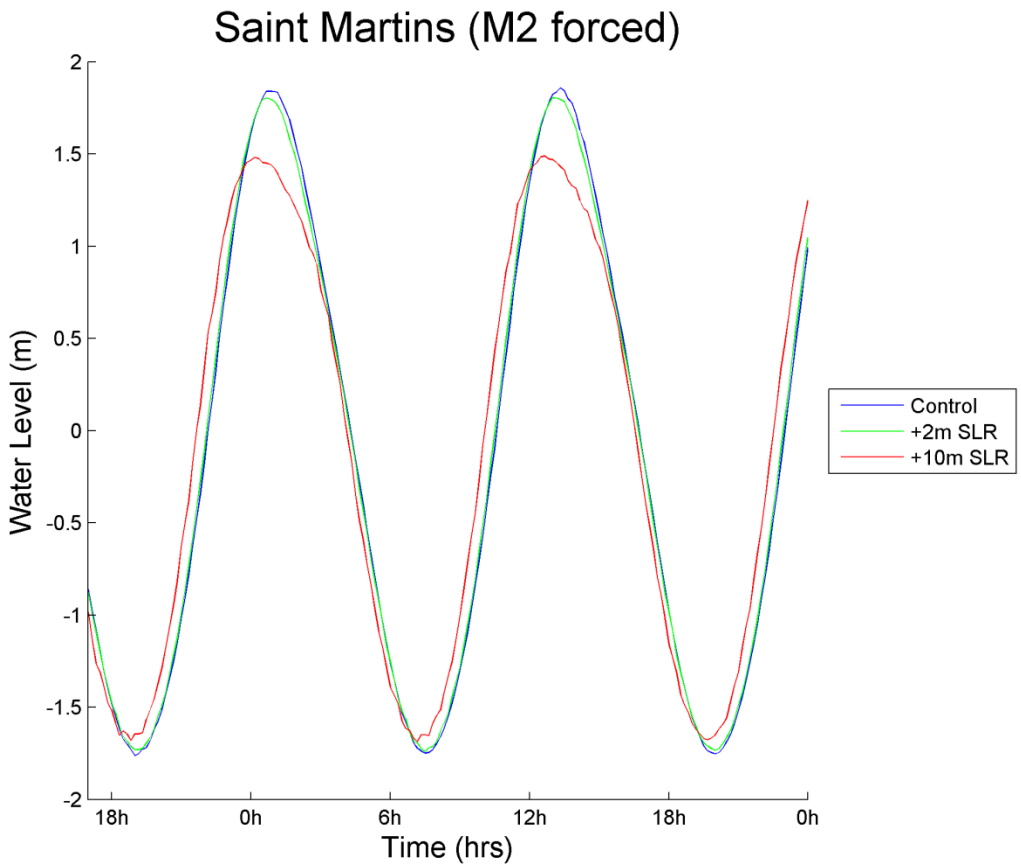

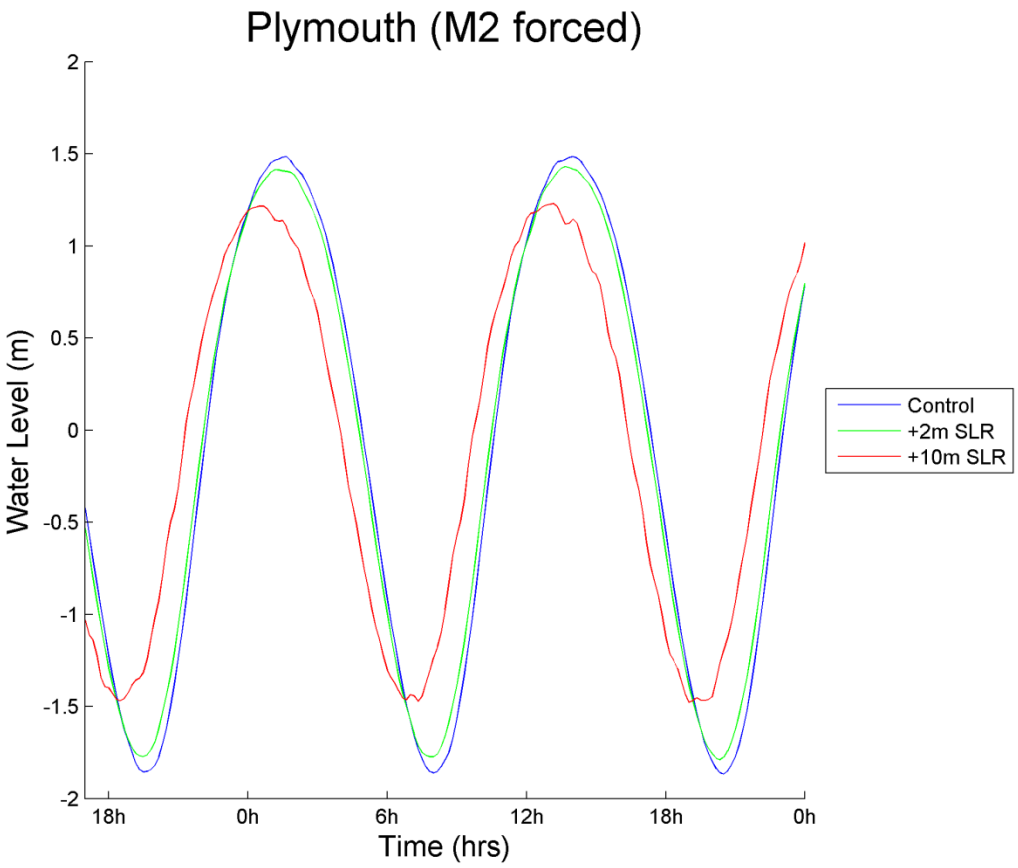
Plymouth (M2 forced)
Water Level (m)
Time (hrs)
Control
+2m SLR
+10m SLR
2
1.5
1
0.5
0
-0.5
-1
-1.5
-2
18h
0h
6h
12h
18h
0h

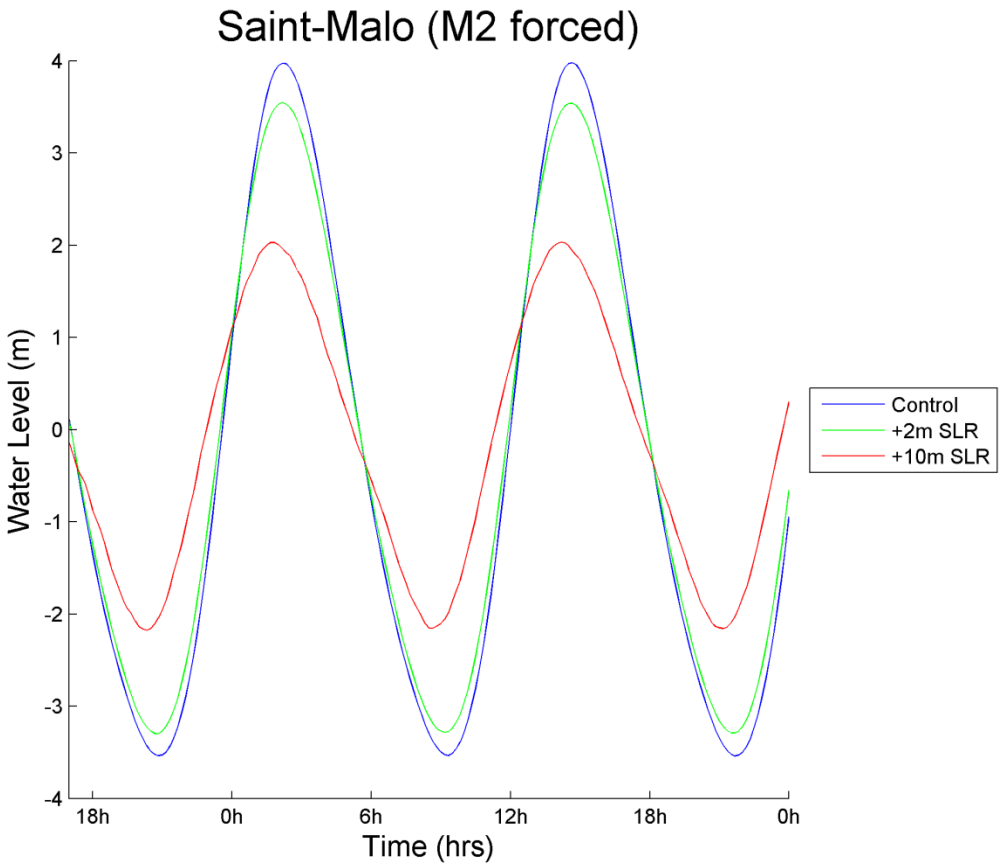
Saint-Malo (M2 forced)
Water Level (m)
Time (hrs)
Control
+2m SLR
+10m SLR
4
3
2
1
0
-1
-2
-3
-4
18h
0h
6h
12h
18h
0h

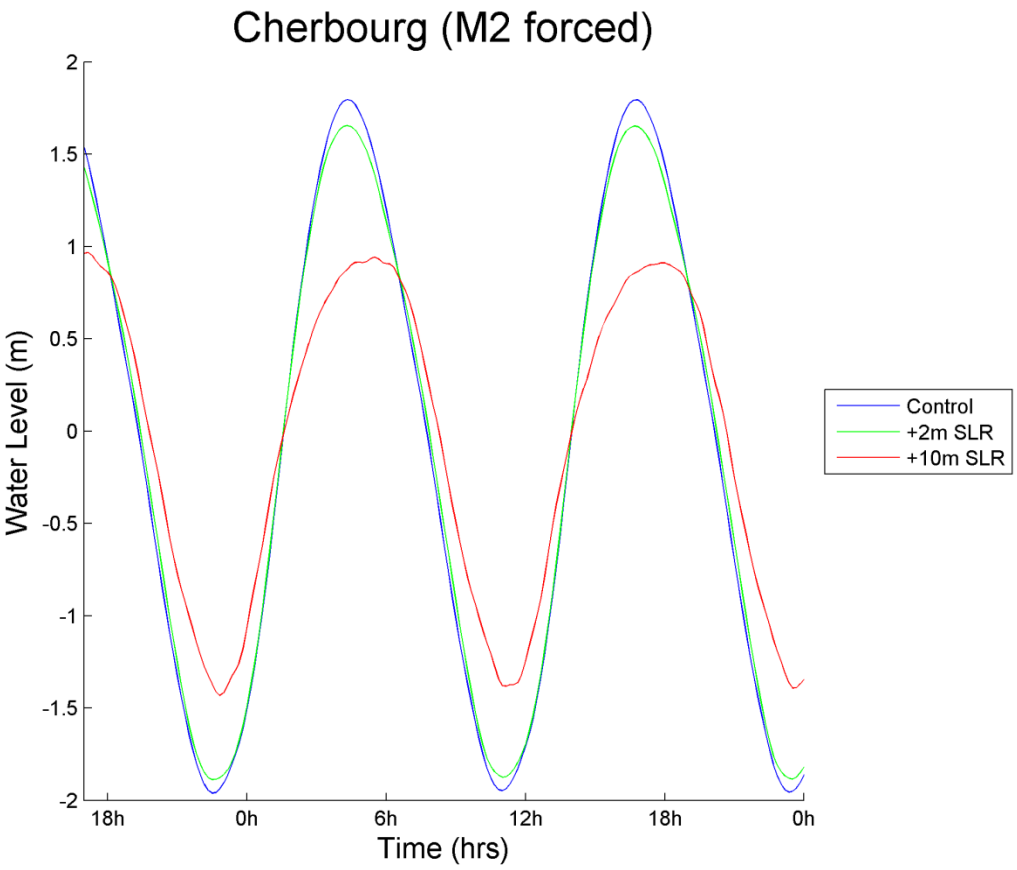
Cherbourg (M2 forced)
Water Level (m)
Time (hrs)
2
1.5
1
0.5
0
-0.5
-1
-1.5
-2
18h
0h
6h
12h
18h
0h
Control
+2m SLR
+10m SLR

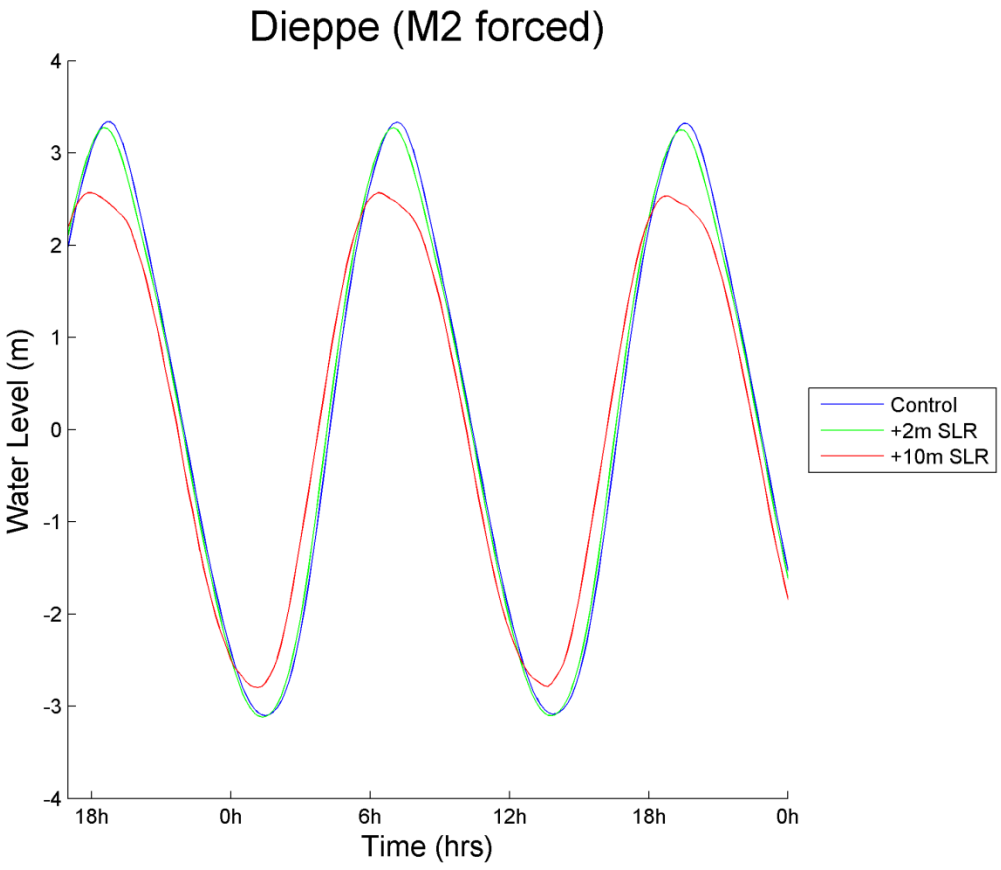
Dieppe (M2 forced)
Water Level (m)
Time (hrs)
4
3
2
1
0
-1
-2
-3
-4
18h
0h
6h
12h
18h
0h
Control
+2m SLR
+10m SLR

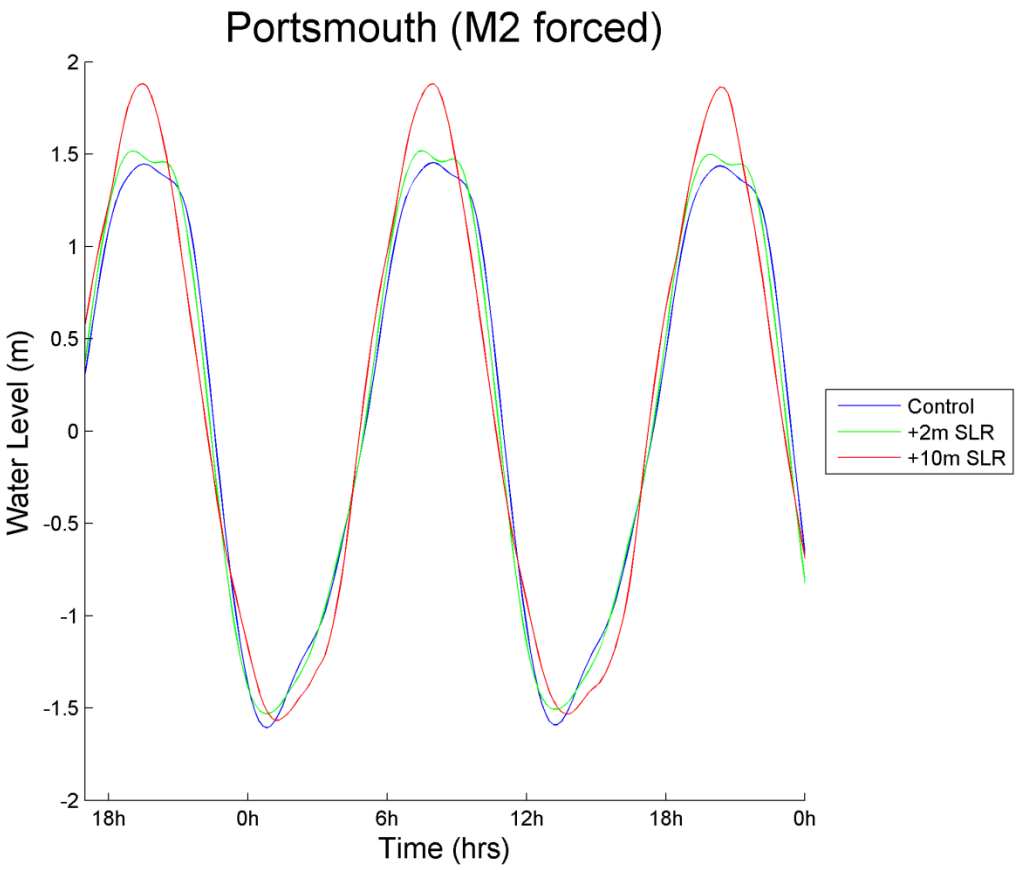
Portsmouth (M2 forced)
Water Level (m)
2
1.5
1
0.5
0
-0.5
-1
-1.5
-2
18h
0h
6h
12h
18h
0h
Time (hrs)
Control
+2m SLR
+10m SLR

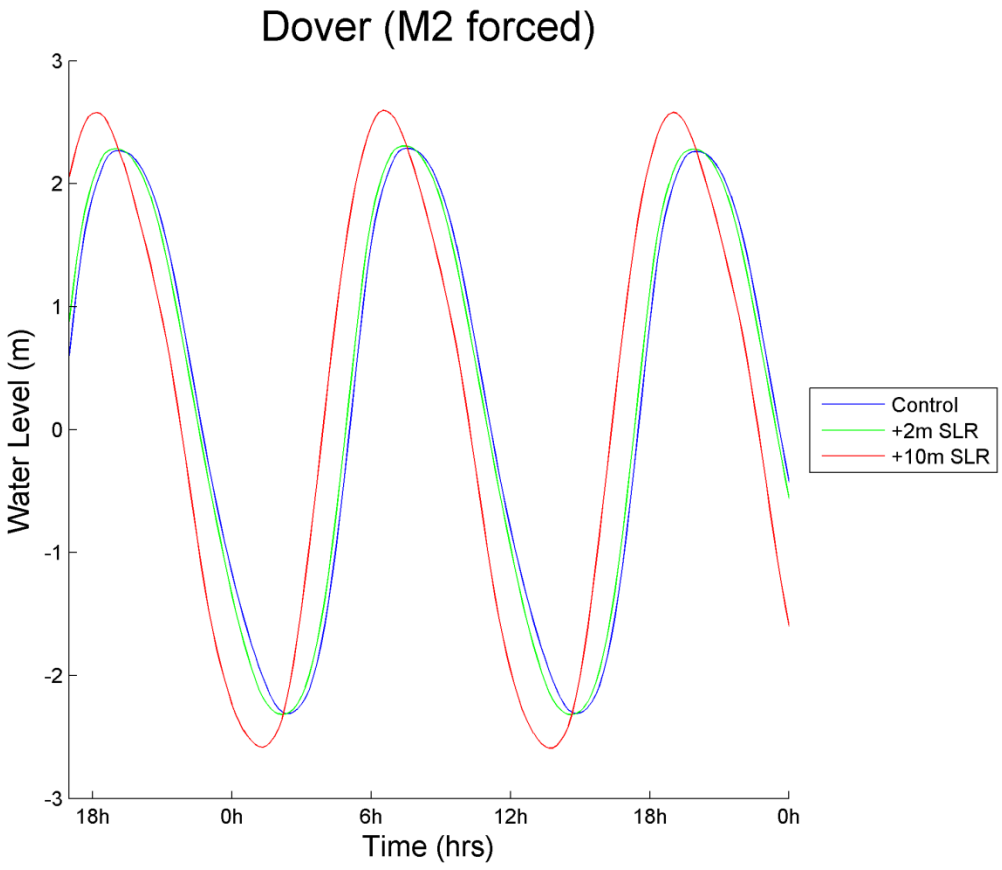
Dover (M2 forced)
Water Level (m)
3
2
1
0
-1
-2
-3
18h
0h
6h
12h
18h
0h
Time (hrs)
Control
+2m SLR
+10m SLR

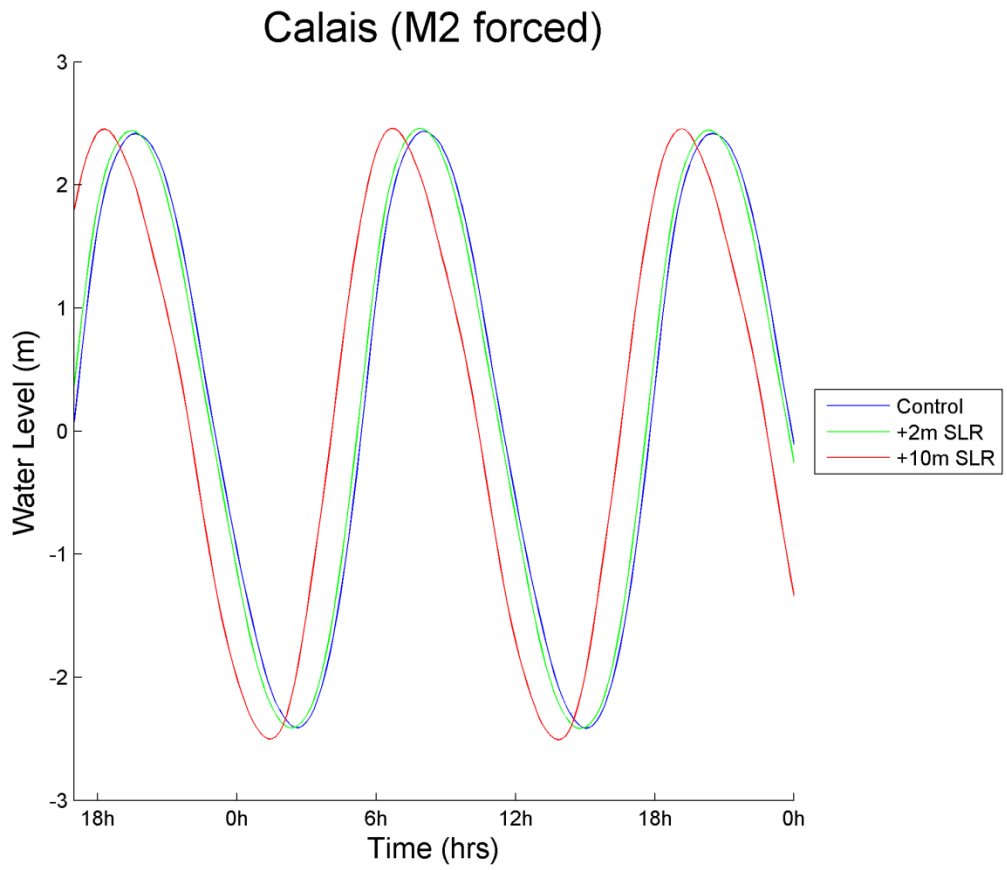
Calais (M2 forced)
Water Level (m)
3
2
1
0
-1
-2
-3
18h
0h
6h
12h
18h
0h
Time (hrs)
Control
+2m SLR
+10m SLR

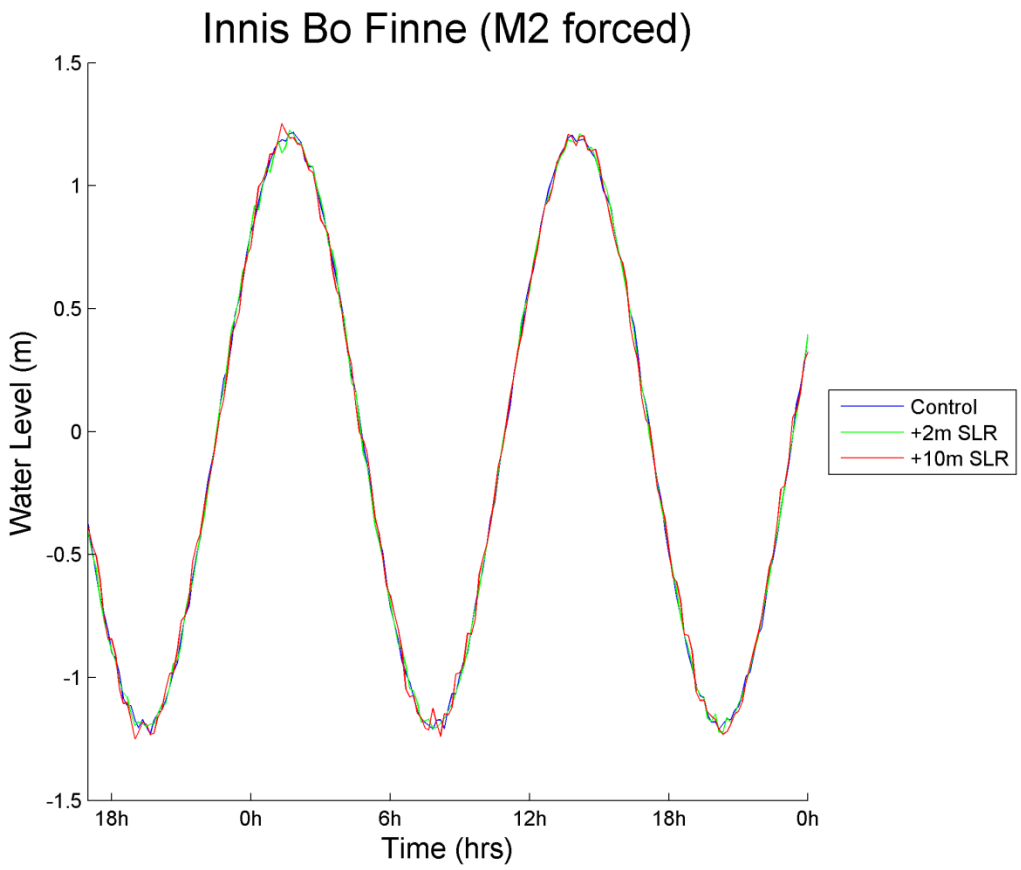
Innis Bo Finne (M2 forced)
Water Level (m)
1.5
1
0.5
0
-0.5
-1
-1.5
18h
0h
6h
12h
18h
0h
Time (hrs)
Control
+2m SLR
+10m SLR

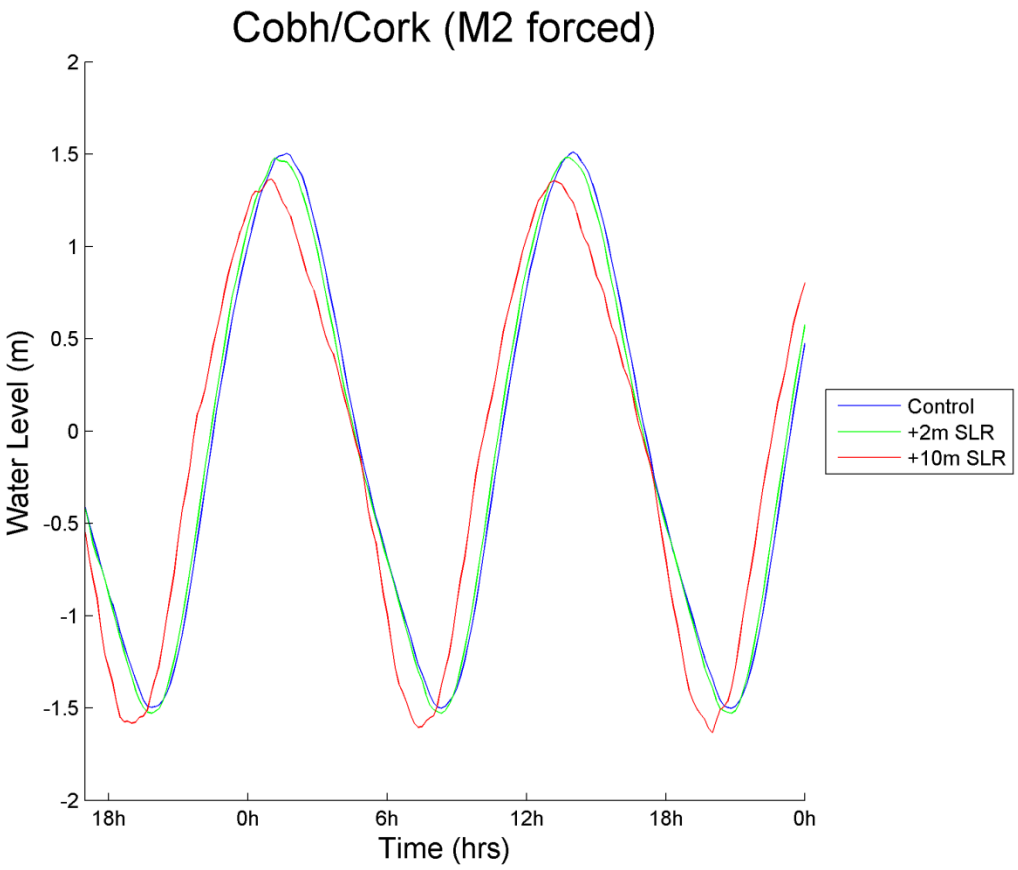
Cobh/Cork (M2 forced)
Water Level (m)
2
1.5
1
0.5
0
-0.5
-1
-1.5
-2
18h
0h
6h
12h
18h
0h
Time (hrs)
Control
+2m SLR
+10m SLR

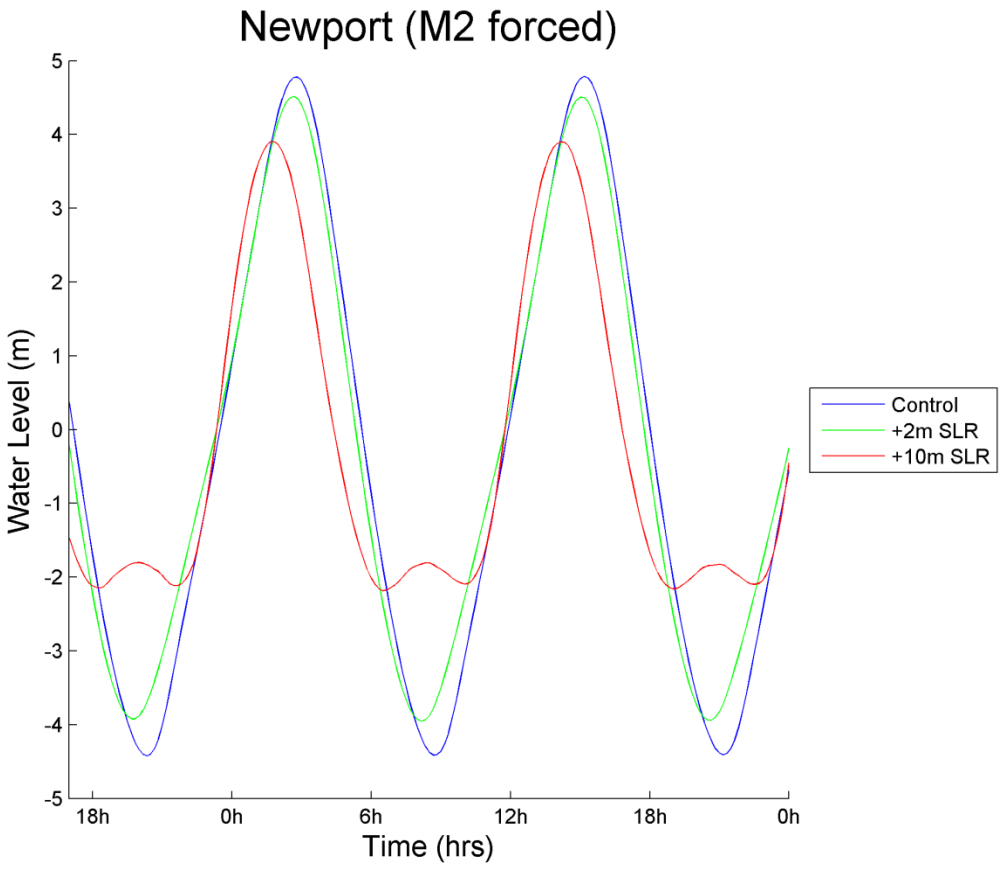
Newport (M2 forced)
Water Level (m)
5
4
3
2
1
0
-1
-2
-3
-4
-5
18h
0h
6h
12h
18h
0h
Time (hrs)
Control
+2m SLR
+10m SLR

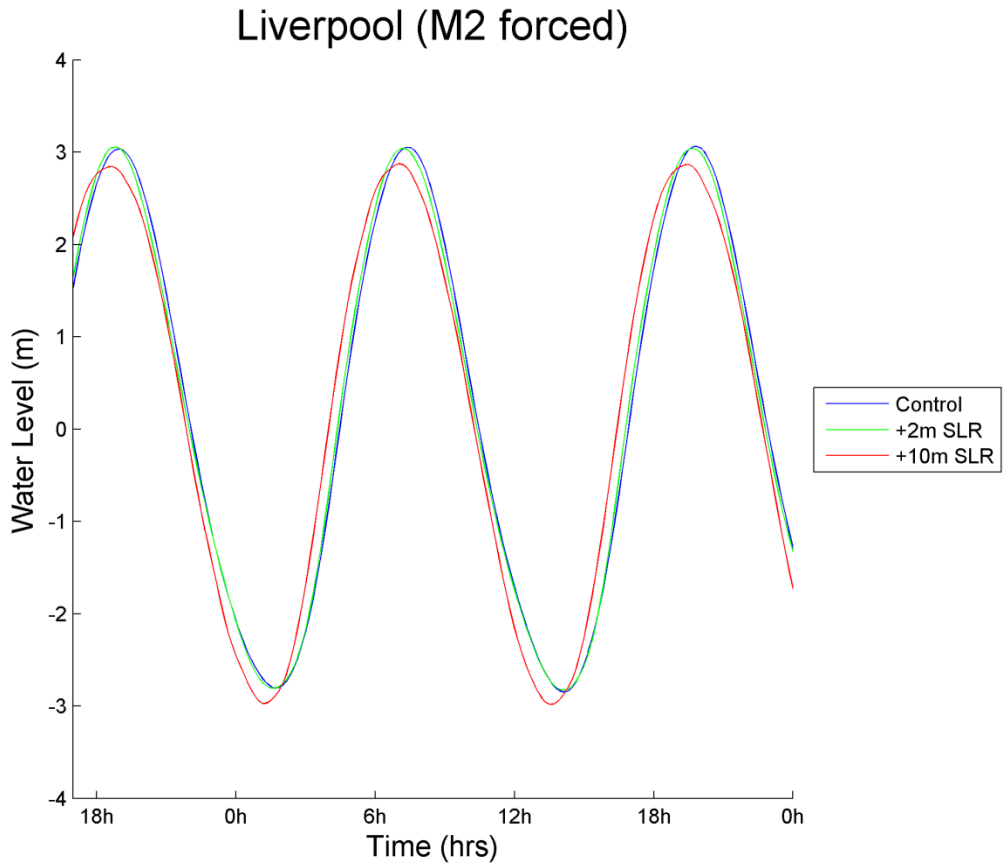
Liverpool (M2 forced)
Water Level (m)
Time (hrs)
4
3
2
1
0
-1
-2
-3
-4
18h
0h
6h
12h
18h
0h
Control
+2m SLR
+10m SLR

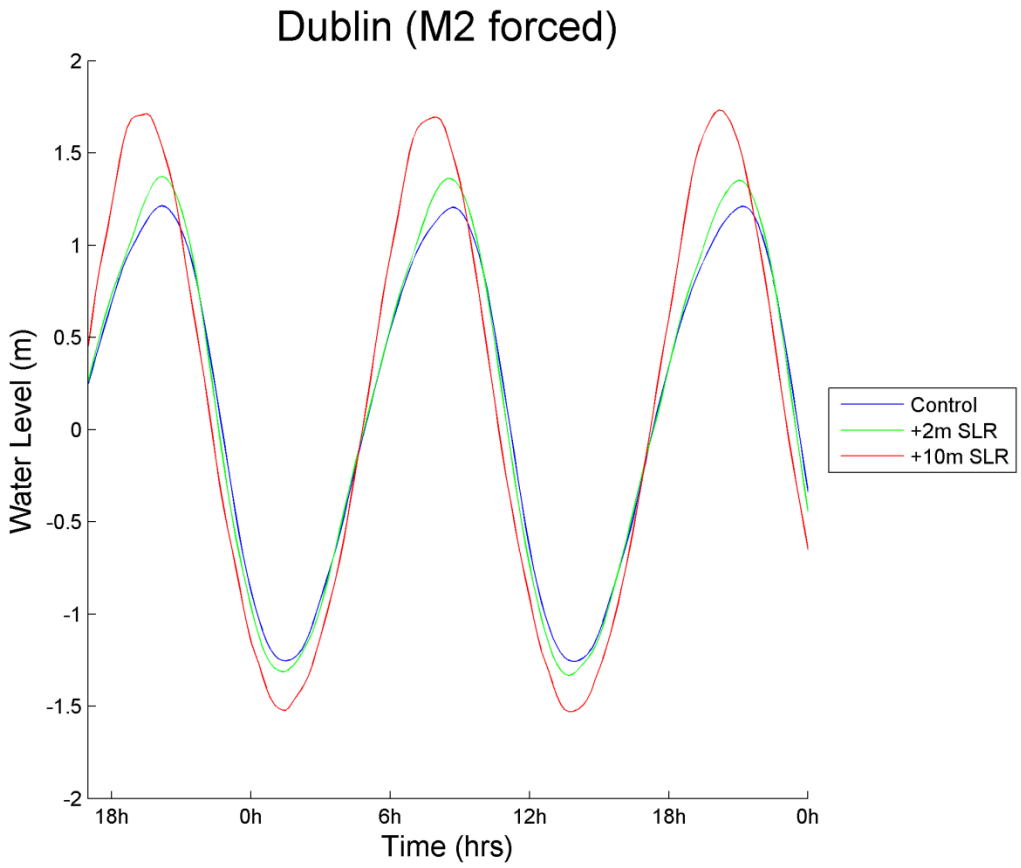
Dublin (M2 forced)
Water Level (m)
Time (hrs)
2
1.5
1
0.5
0
-0.5
-1
-1.5
-2
18h
0h
6h
12h
18h
0h
Control
+2m SLR
+10m SLR

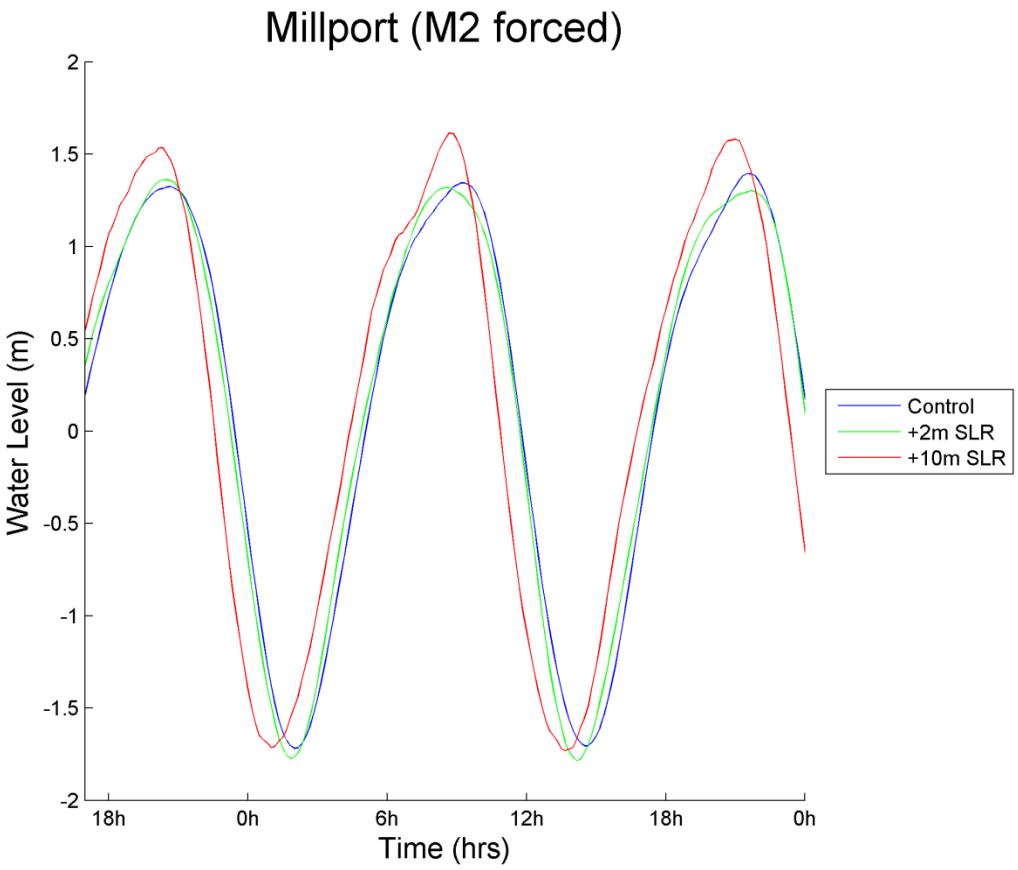
Millport (M2 forced)
Water Level (m)
2
1.5
1
0.5
0
-0.5
-1
-1.5
-2
18h
0h
6h
12h
18h
0h
Time (hrs)
Control
+2m SLR
+10m SLR

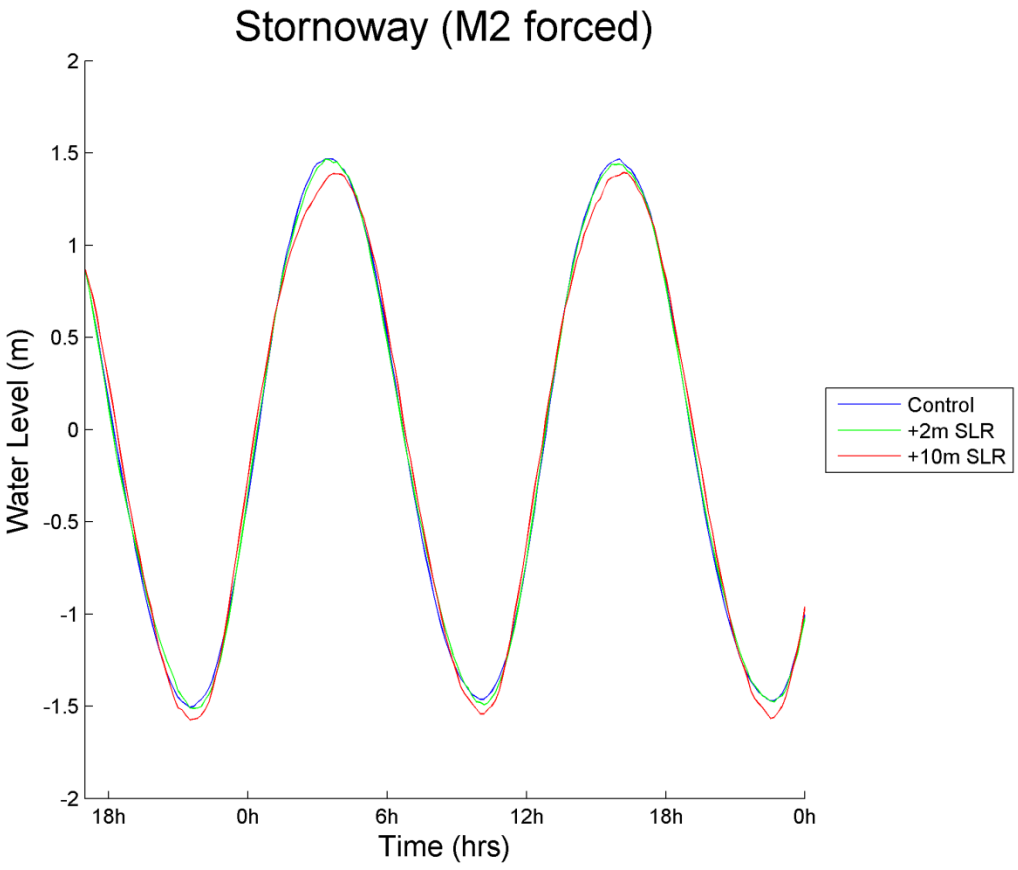
Stornoway (M2 forced)
Water Level (m)
2
1.5
1
0.5
0
-0.5
-1
-1.5
-2
18h
0h
6h
12h
18h
0h
Time (hrs)
Control
+2m SLR
+10m SLR

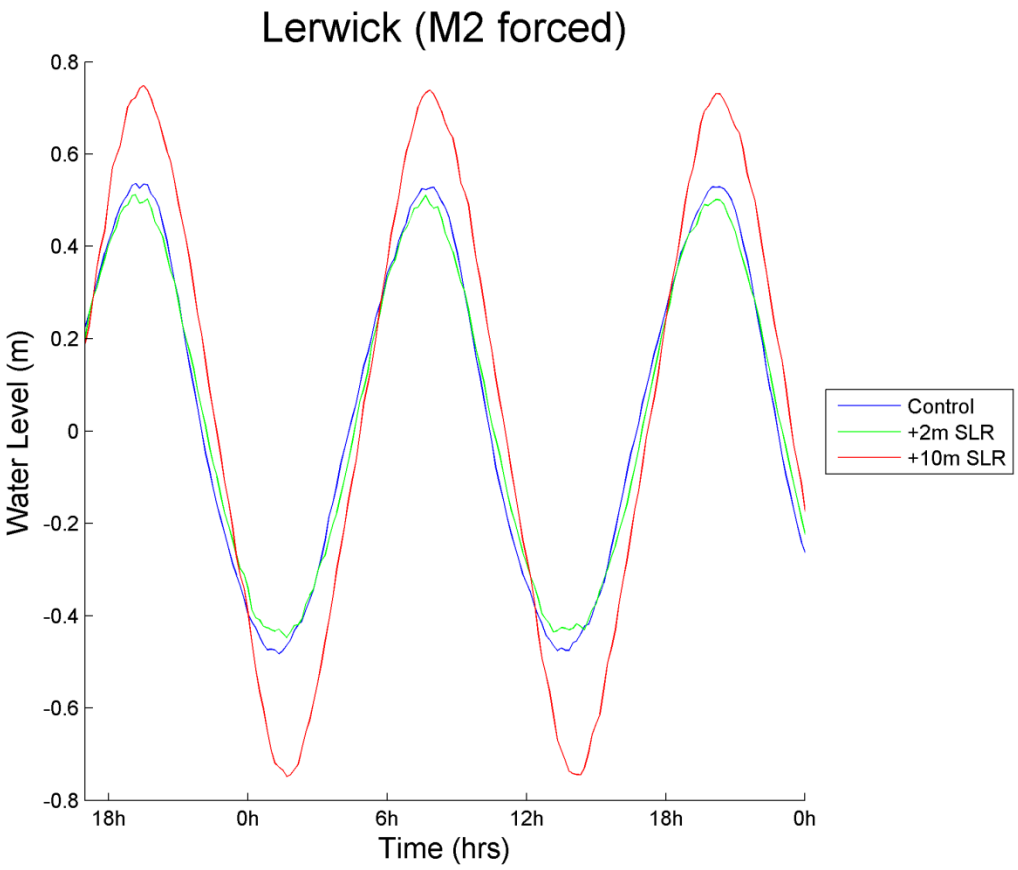
Lerwick (M2 forced)
Water Level (m)
0.8
0.6
0.4
0.2
0
-0.2
-0.4
-0.6
-0.8
18h
0h
6h
12h
18h
0h
Time (hrs)
Control
+2m SLR
+10m SLR

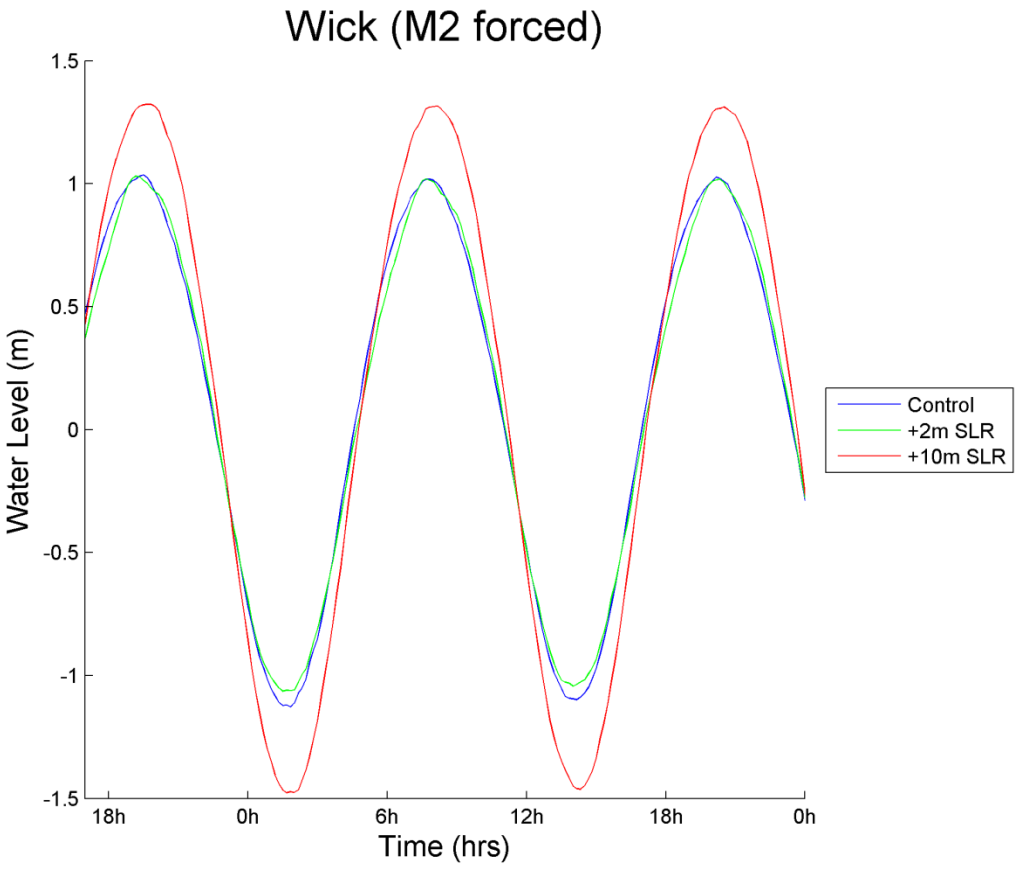
Wick (M2 forced)
Water Level (m)
1.5
1
0.5
0
-0.5
-1
-1.5
18h
0h
6h
12h
18h
0h
Time (hrs)
Control
+2m SLR
+10m SLR

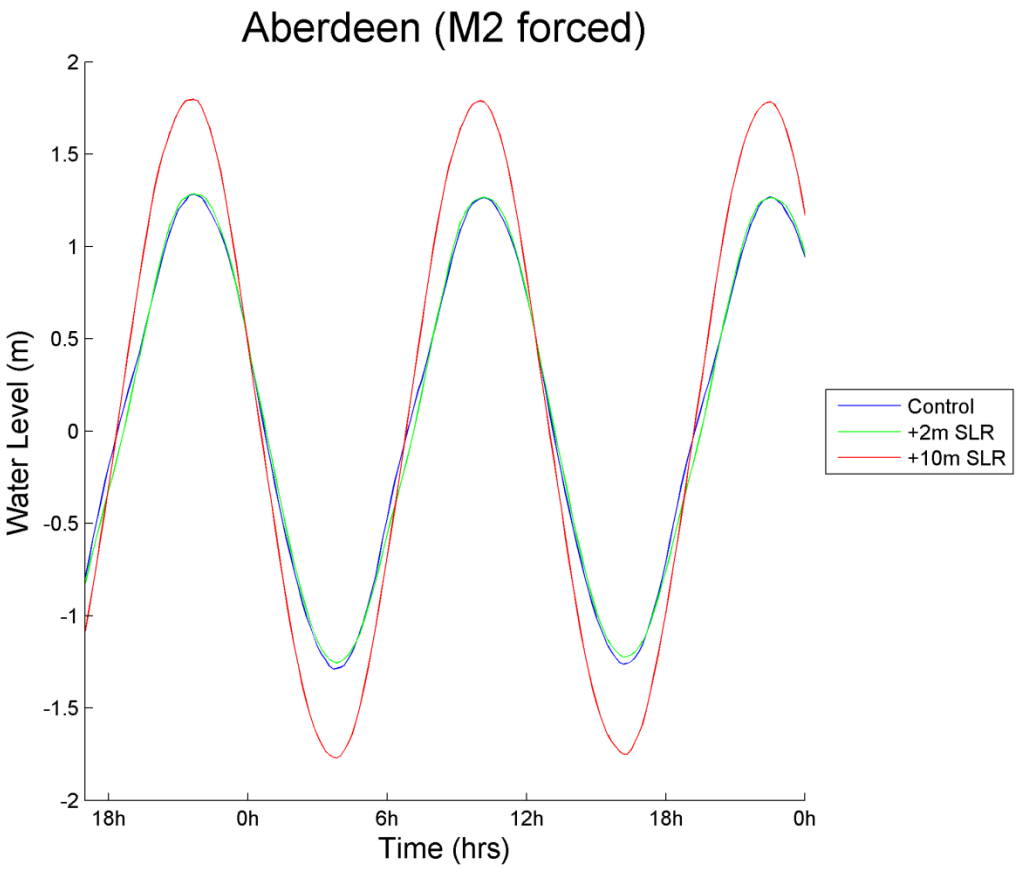
Aberdeen (M2 forced)
Water Level (m)
Time (hrs)
Control
+2m SLR
+10m SLR
2
1.5
1
0.5
0
-0.5
-1
-1.5
-2
18h
0h
6h
12h
18h
0h

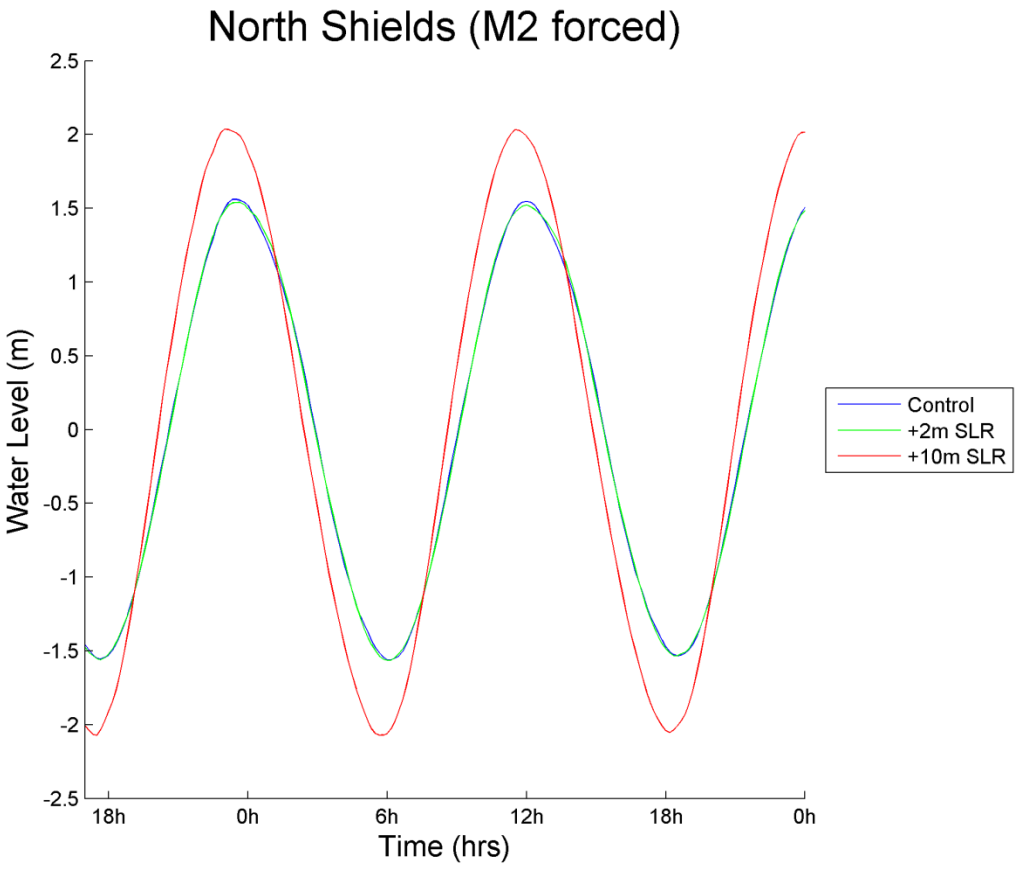
North Shields (M2 forced)
Water Level (m)
Time (hrs)
Control
+2m SLR
+10m SLR
2.5
2
1.5
1
0.5
0
-0.5
-1
-1.5
-2
-2.5
18h
0h
6h
12h
18h
0h

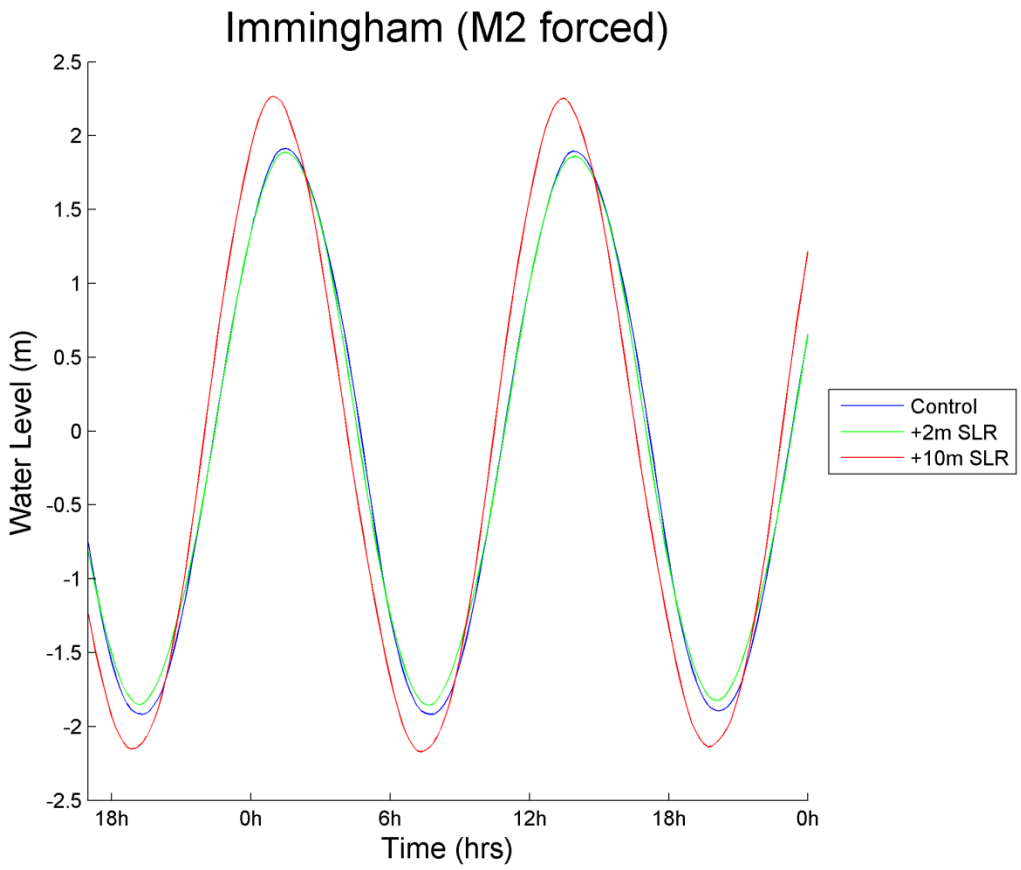
Immingham (M2 forced)
Water Level (m)
2.5
2
1.5
1
0.5
0
-0.5
-1
-1.5
-2
-2.5
18h
0h
6h
12h
18h
0h
Time (hrs)
Control
+2m SLR
+10m SLR

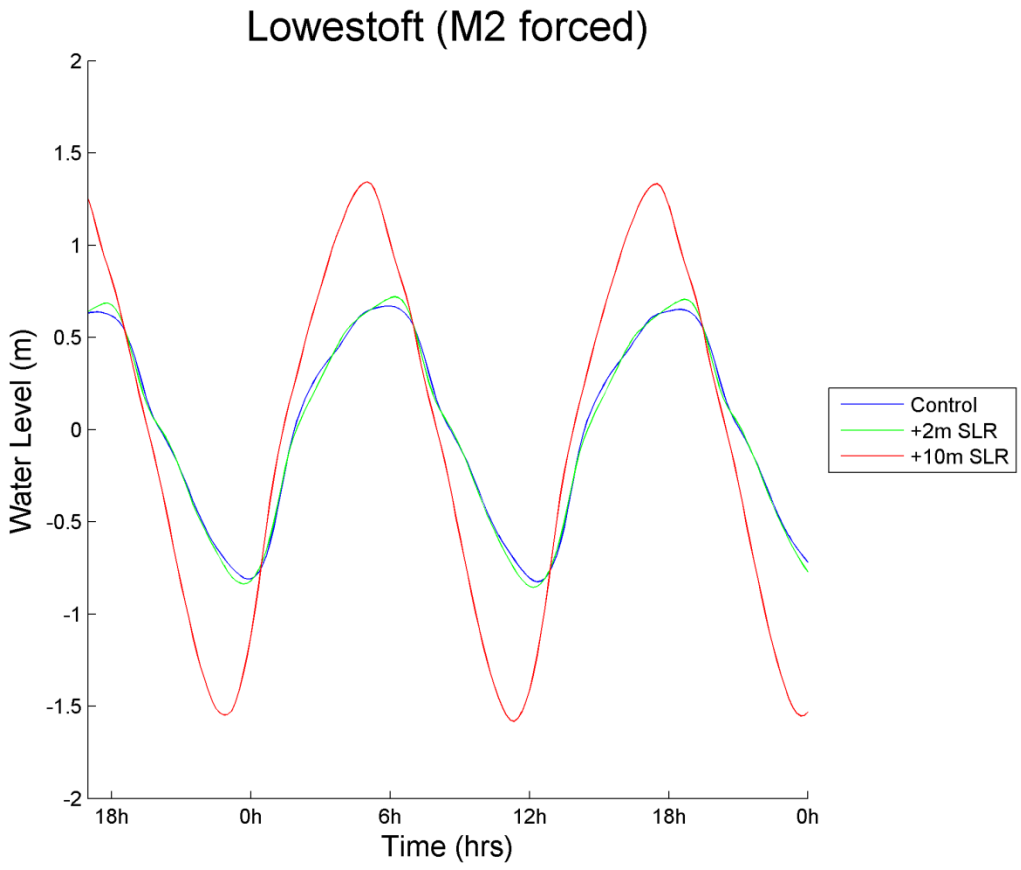
Lowestoft (M2 forced)
Water Level (m)
2
1.5
1
0.5
0
-0.5
-1
-1.5
-2
18h
0h
6h
12h
18h
0h
Time (hrs)
Control
+2m SLR
+10m SLR

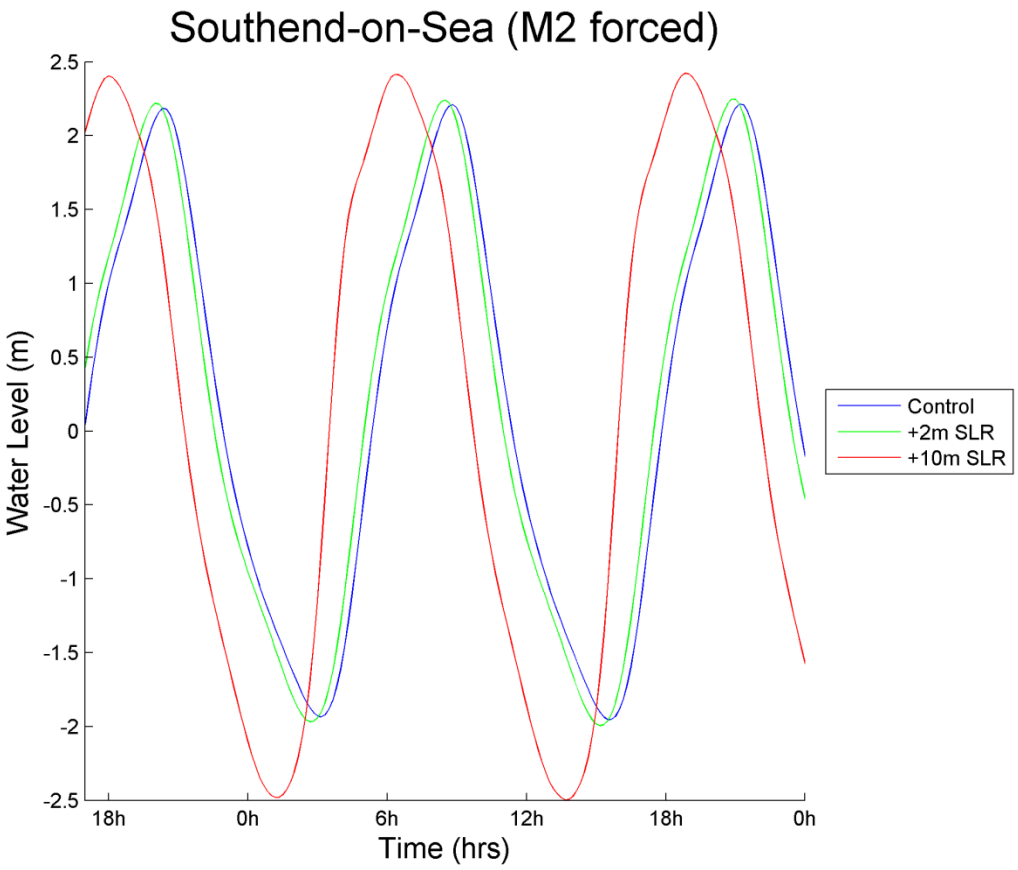
Southend-on-Sea (M2 forced)
Water Level (m)
Time (hrs)
Control
+2m SLR
+10m SLR
2.5
2
1.5
1
0.5
0
-0.5
-1
-1.5
-2
-2.5
18h
0h
6h
12h
18h
0h

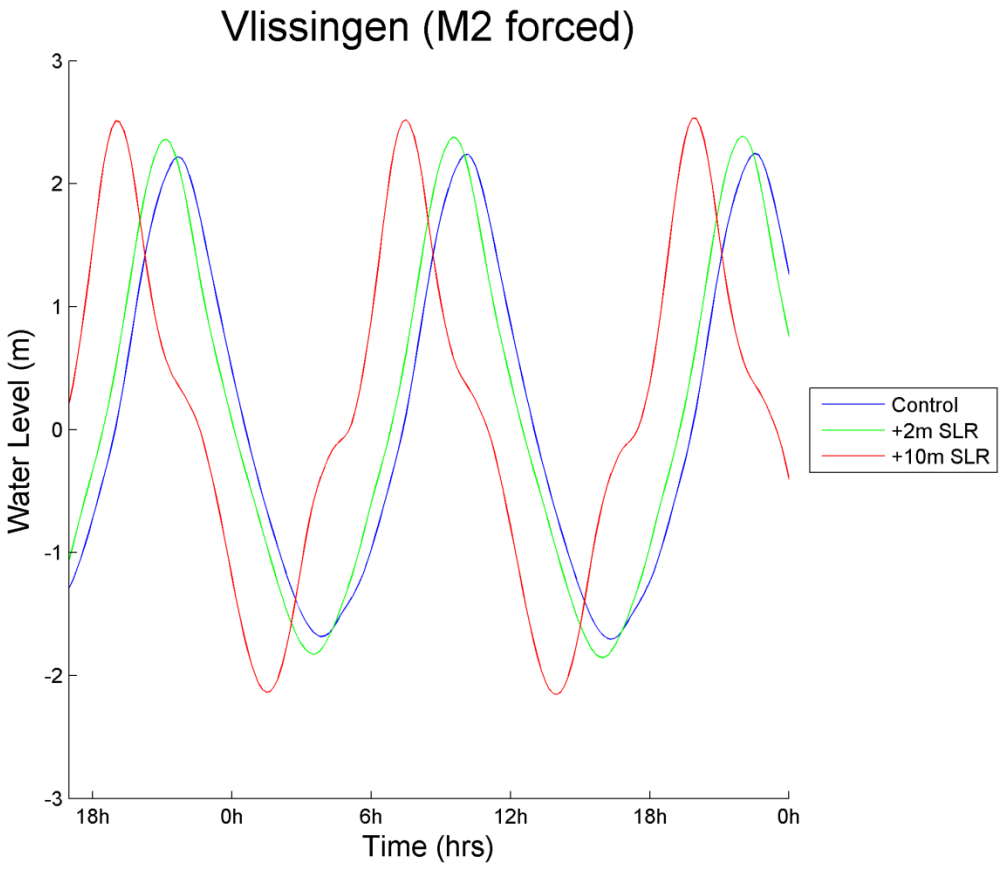
Vlissingen (M2 forced)
Water Level (m)
Time (hrs)
Control
+2m SLR
+10m SLR
3
2
1
0
-1
-2
-3
18h
0h
6h
12h
18h
0h

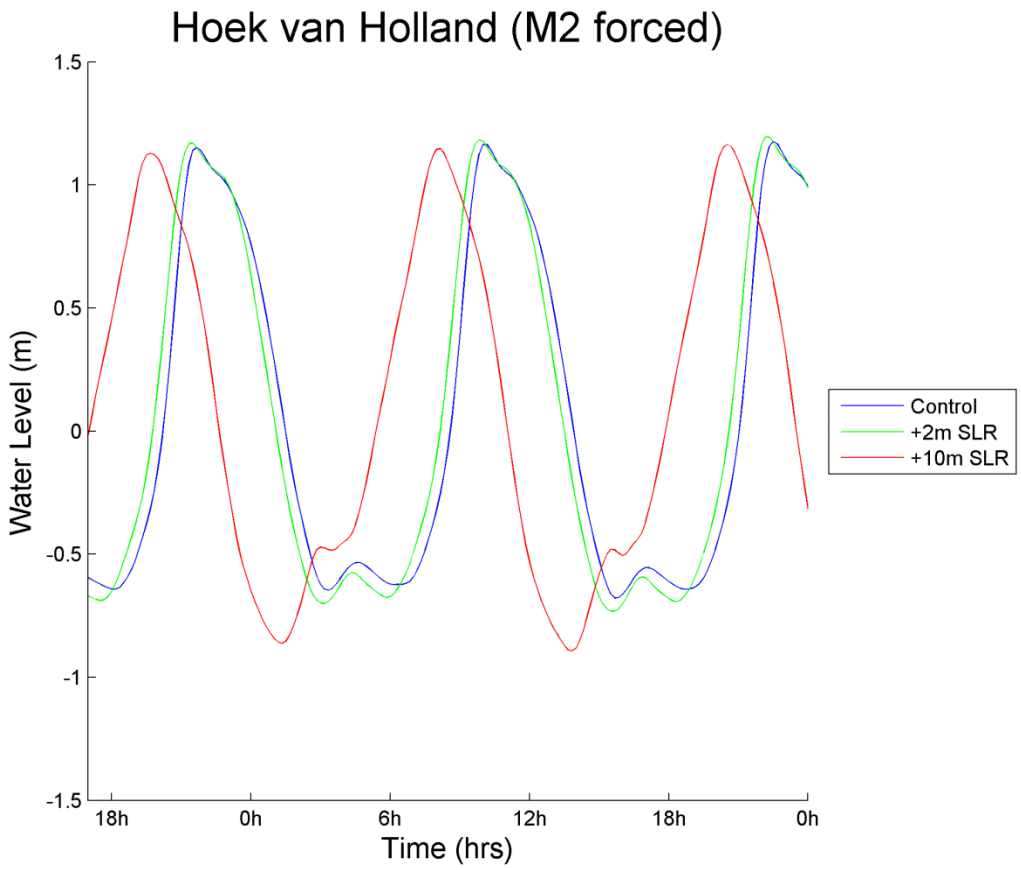
Hoek van Holland (M2 forced)
Water Level (m)
1.5
1
0.5
0
-0.5
-1
-1.5
18h
0h
6h
12h
18h
0h
Time (hrs)
Control
+2m SLR
+10m SLR

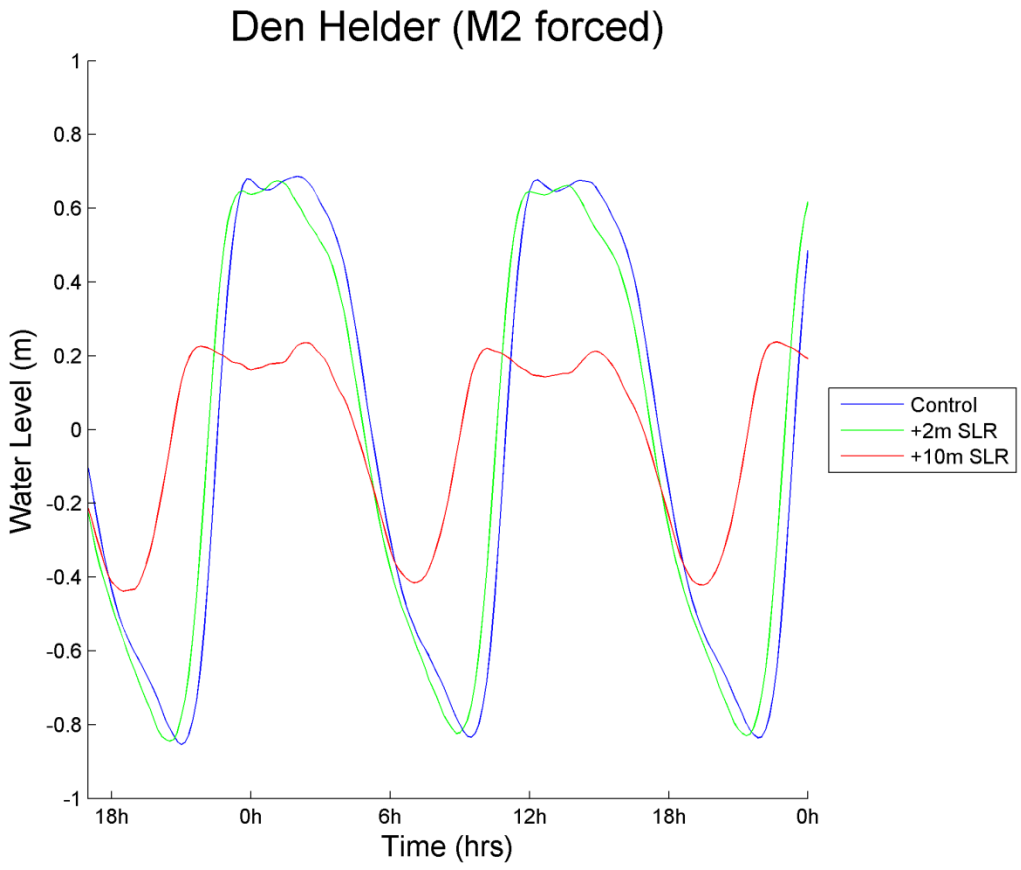
Den Helder (M2 forced)
Water Level (m)
1
0.8
0.6
0.4
0.2
0
-0.2
-0.4
-0.6
-0.8
-1
18h
0h
6h
12h
18h
0h
Time (hrs)
Control
+2m SLR
+10m SLR

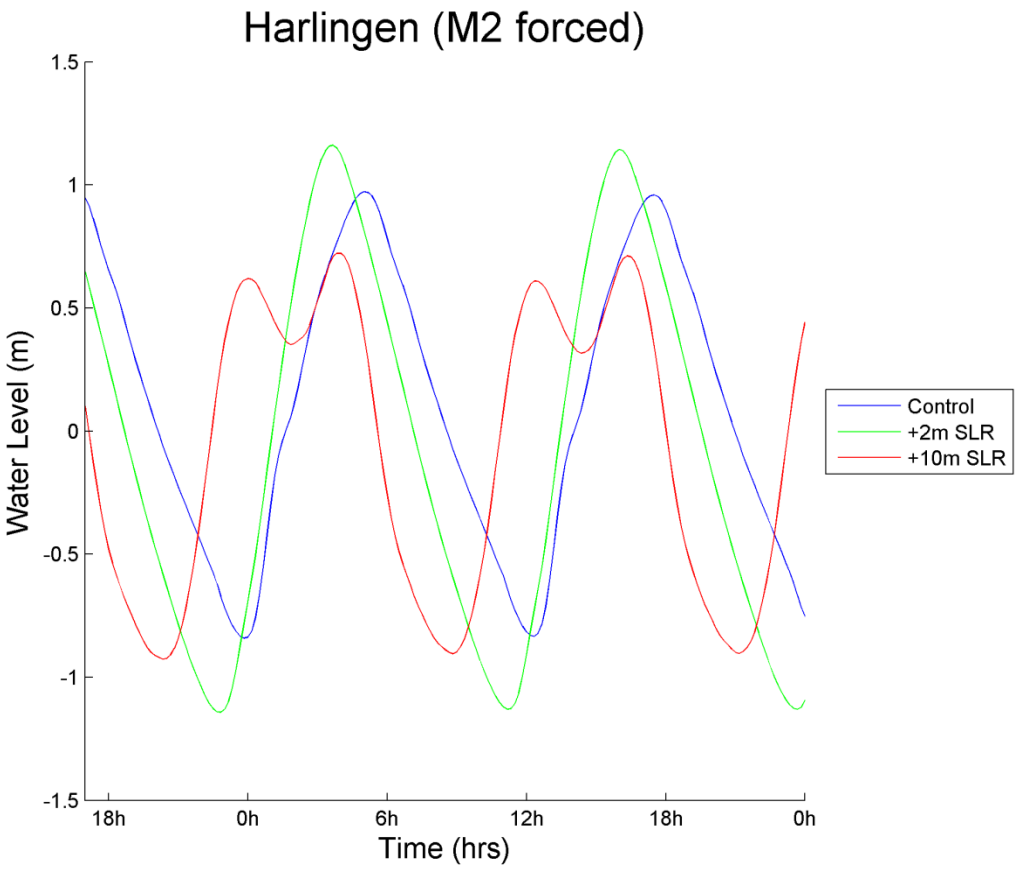
Harlingen (M2 forced)
Water Level (m)
1.5
1
0.5
0
-0.5
-1
-1.5
18h
0h
6h
12h
18h
0h
Time (hrs)
Control
+2m SLR
+10m SLR

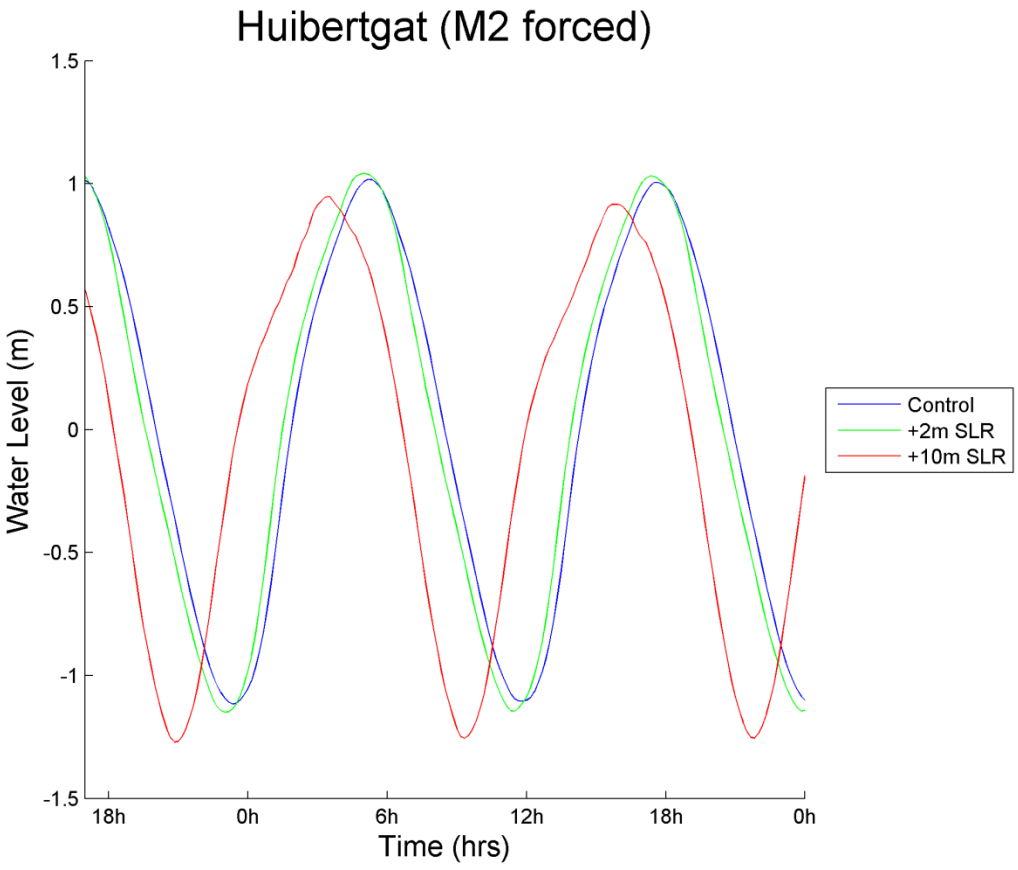
Huibertgat (M2 forced)
Water Level (m)
1.5
1
0.5
0
-0.5
-1
-1.5
18h
0h
6h
12h
18h
0h
Time (hrs)
Control
+2m SLR
+10m SLR

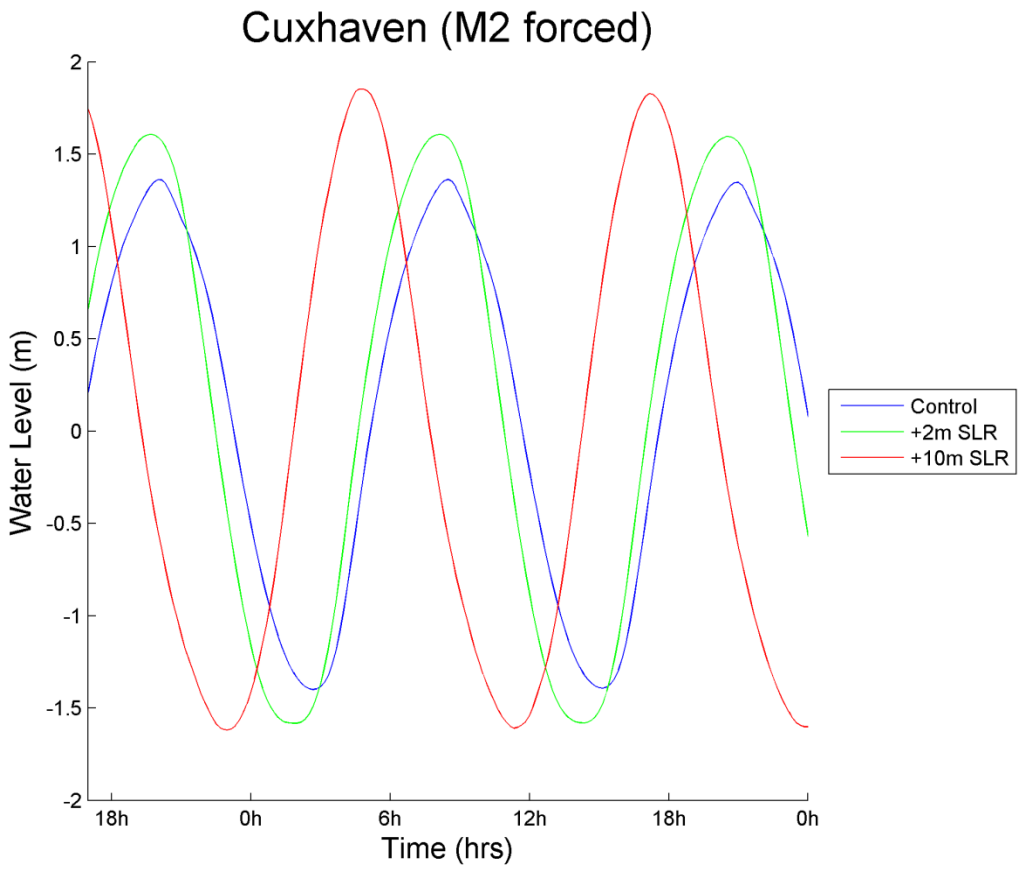
Cuxhaven (M2 forced)
Water Level (m)
Time (hrs)
2
1.5
1
0.5
0
-0.5
-1
-1.5
-2
18h
0h
6h
12h
18h
0h
Control
+2m SLR
+10m SLR

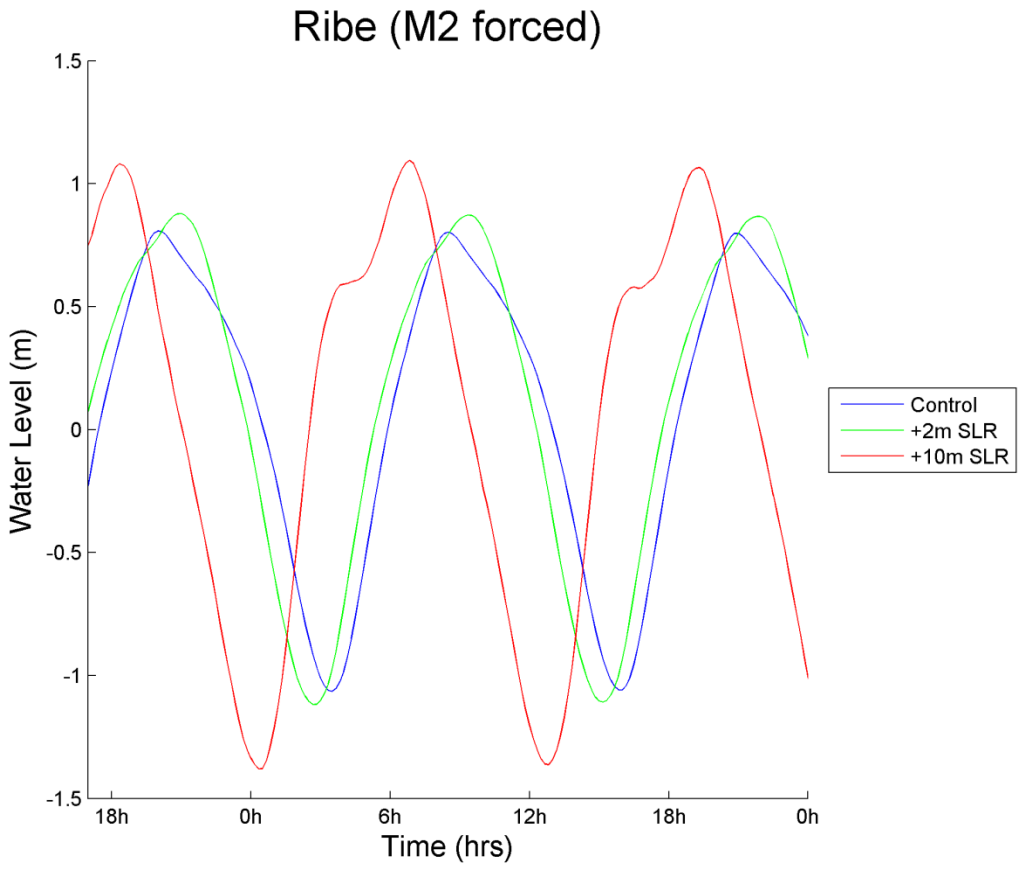
Ribe (M2 forced)
Water Level (m)
Time (hrs)
1.5
1
0.5
0
-0.5
-1
-1.5
18h
0h
6h
12h
18h
0h
Control
+2m SLR
+10m SLR

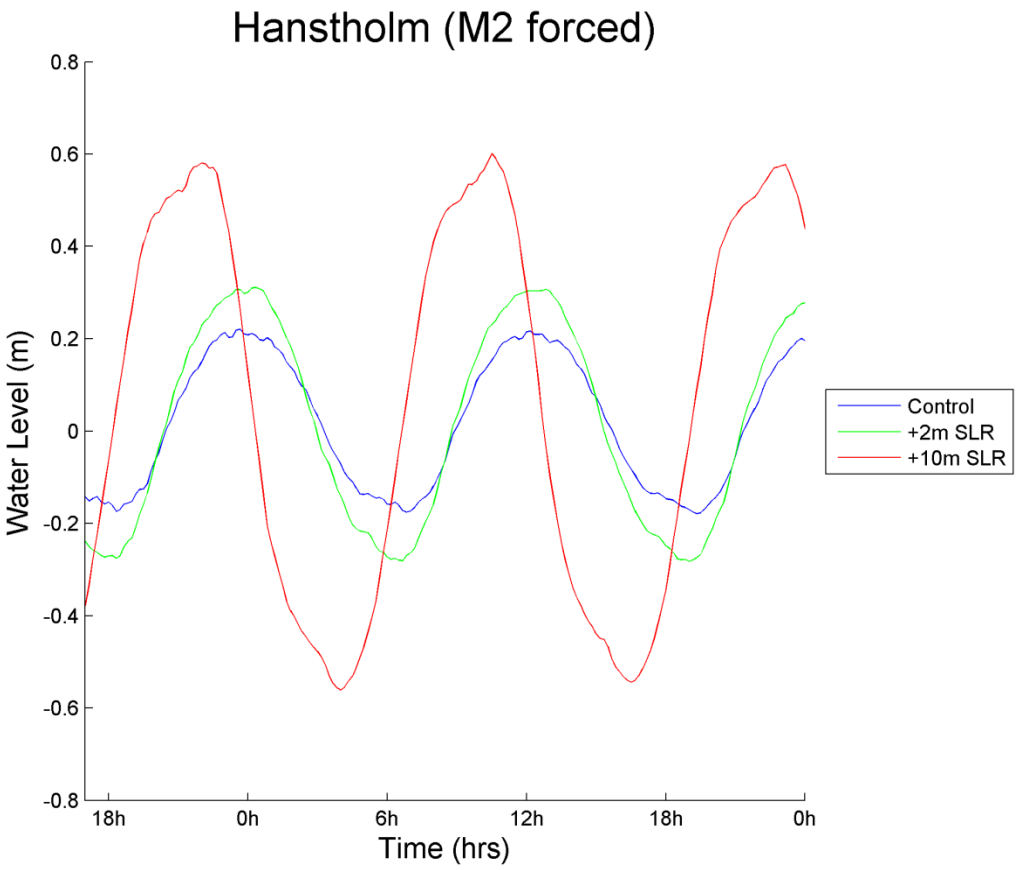
Hanstholm (M2 forced)
Water Level (m)
0.8
0.6
0.4
0.2
0
-0.2
-0.4
-0.6
-0.8
18h
0h
6h
12h
18h
0h
Time (hrs)
Control
+2m SLR
+10m SLR

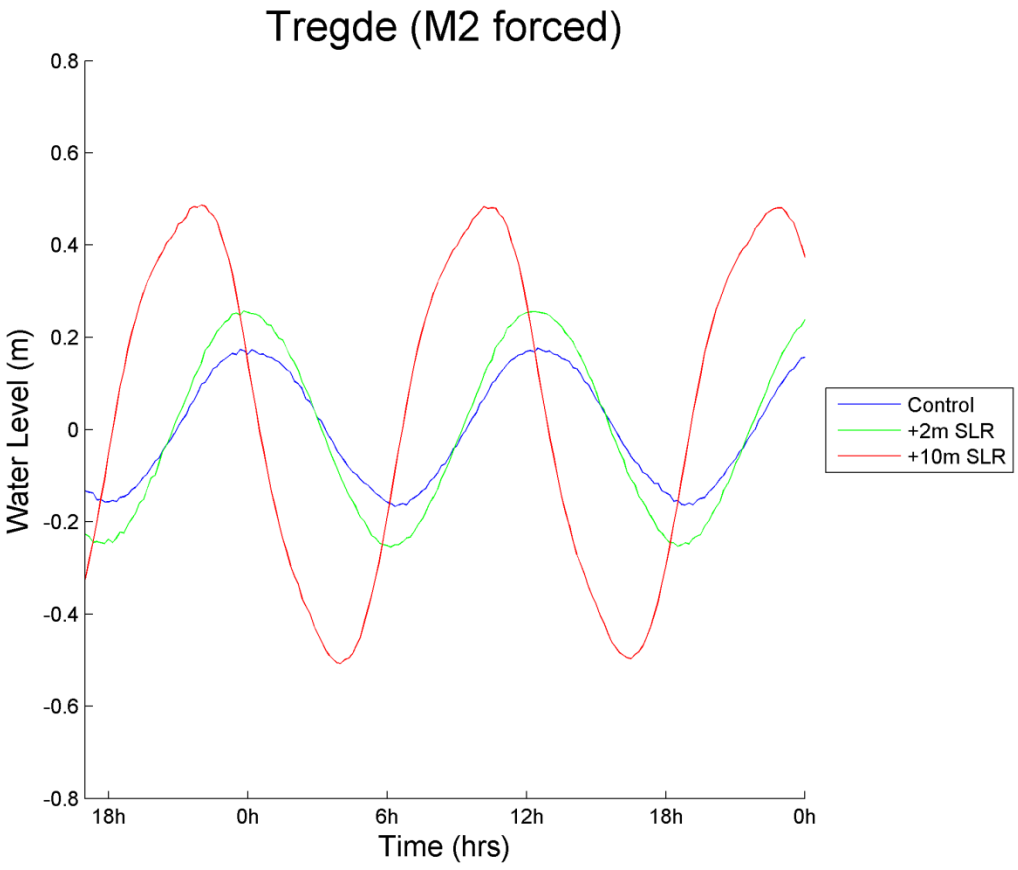
Tregde (M2 forced)
Water Level (m)
0.8
0.6
0.4
0.2
0
-0.2
-0.4
-0.6
-0.8
18h
0h
6h
12h
18h
0h
Time (hrs)
Control
+2m SLR
+10m SLR

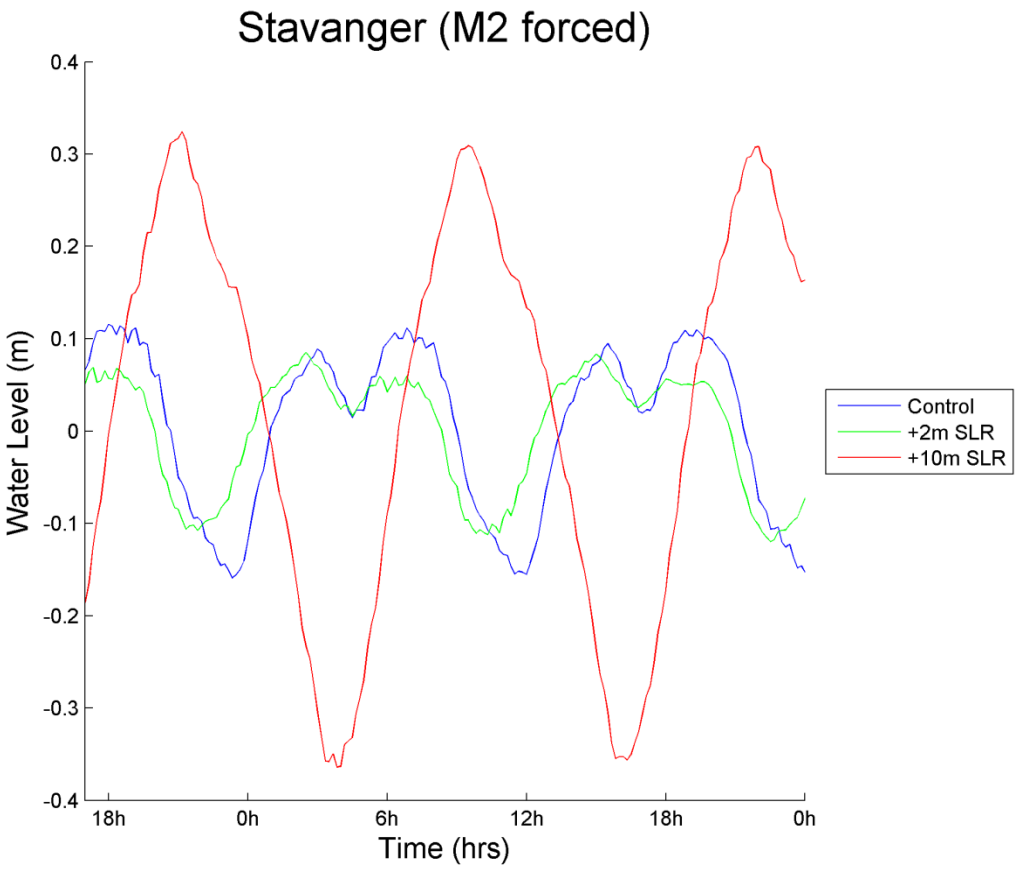
Stavanger (M2 forced)
Water Level (m)
0.4
0.3
0.2
0.1
0
-0.1
-0.2
-0.3
-0.4
18h
0h
6h
12h
18h
0h
Time (hrs)
Control
+2m SLR
+10m SLR

Appendix 1.2- European Port Tidal Curves (Full Runs)

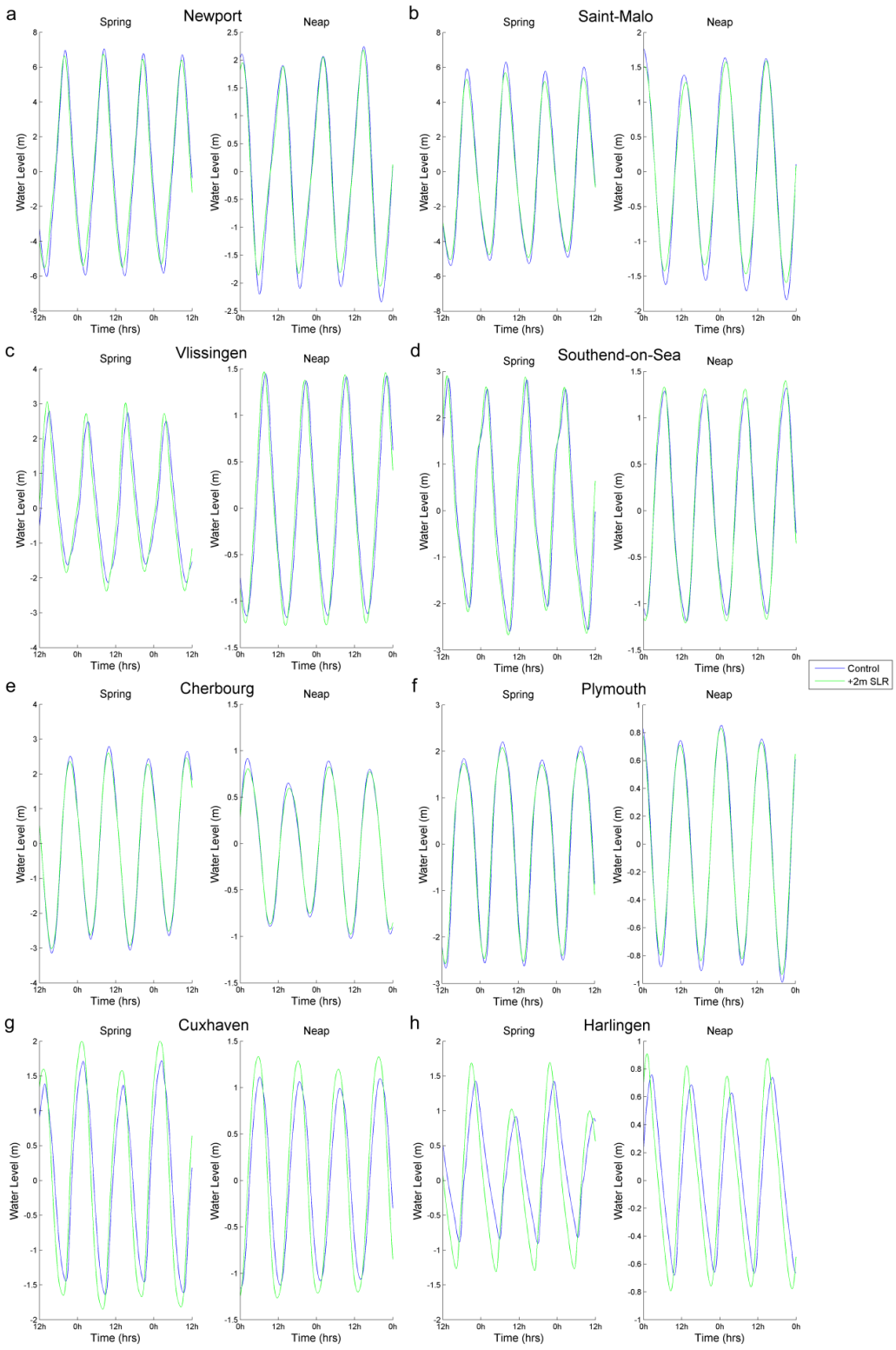

Figure 4.12. Tidal curves from Full Runs at 8 ports where key changes occur. Two sea-level scenarios are shown 0m (blue line) and 2m SLR (green line) Note that the limits of the y-axis are not normalised and ports are listed in the same order as Figure 2.6.

Tidal curves for 0 and 2 m SLR for all 32 ports from days 14-16 (Spring Tide) and days 22-24 (neap tide) of the fully forced simulations (allowing comparison with tidal curves presented in other studies).

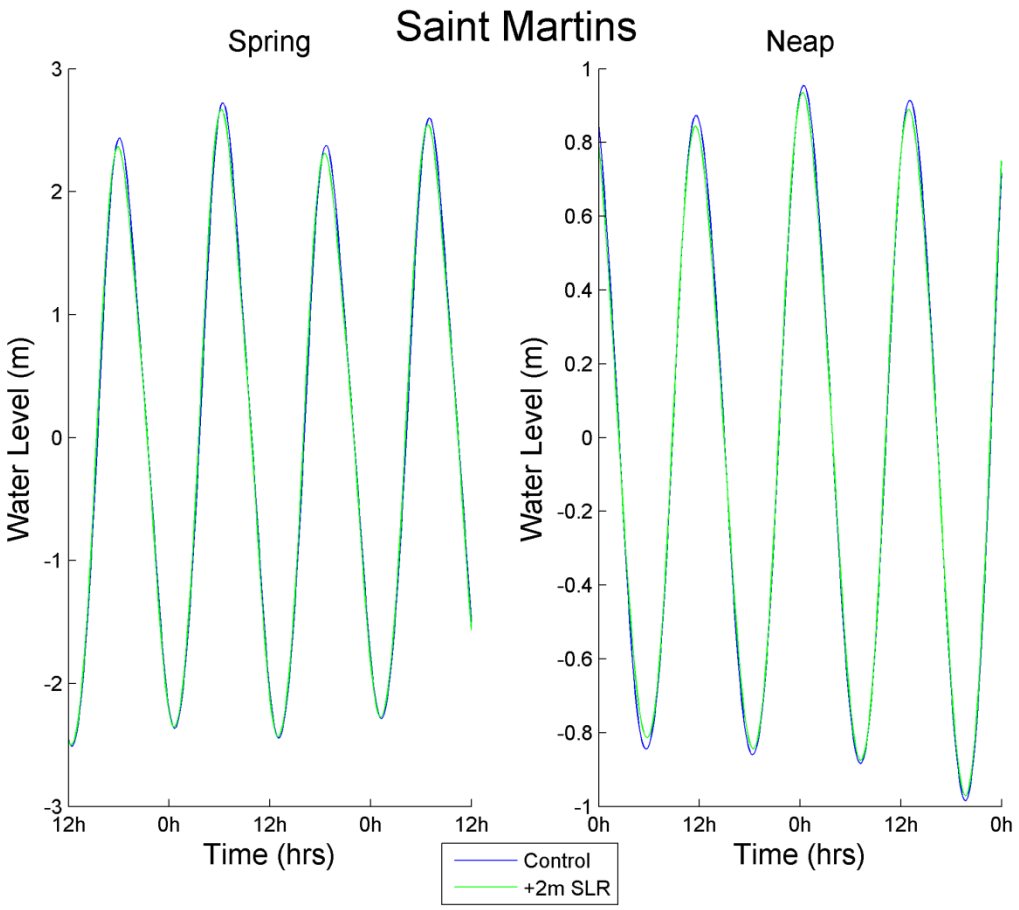

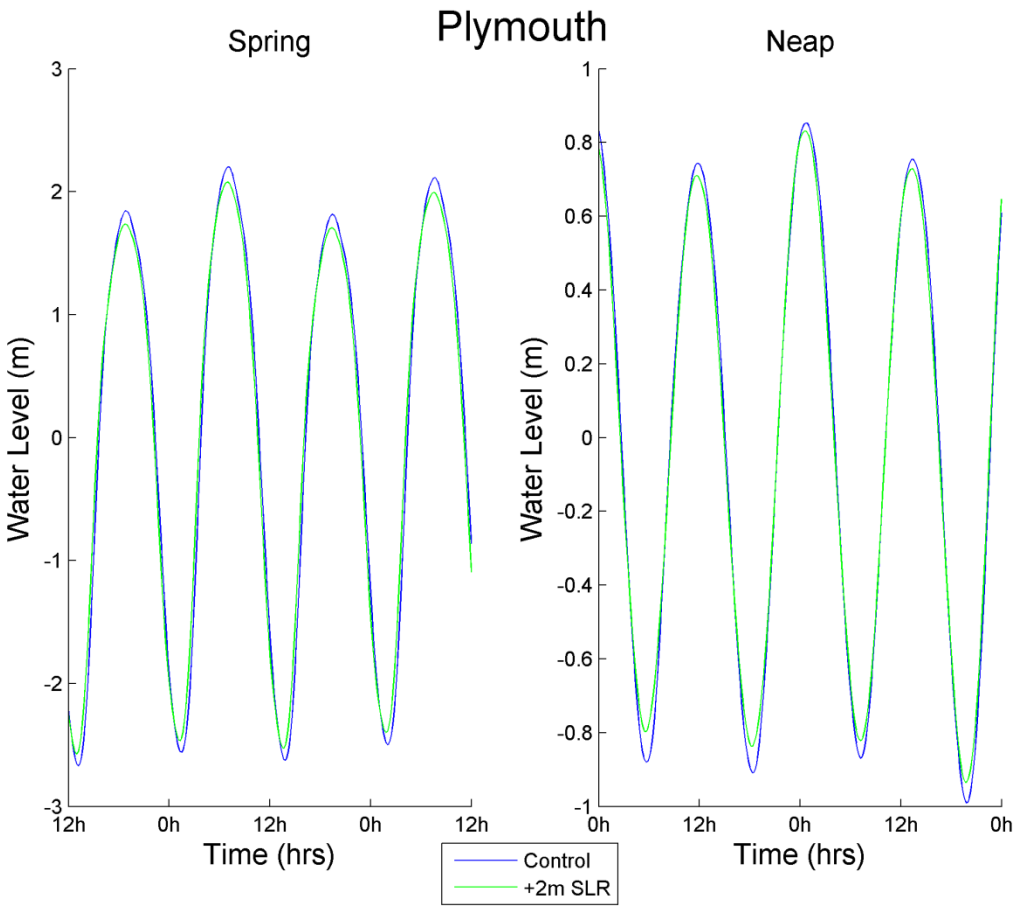
Plymouth
Spring
Neap
Water Level (m)
Time (hrs)
12h
0h
Control
+2m SLR

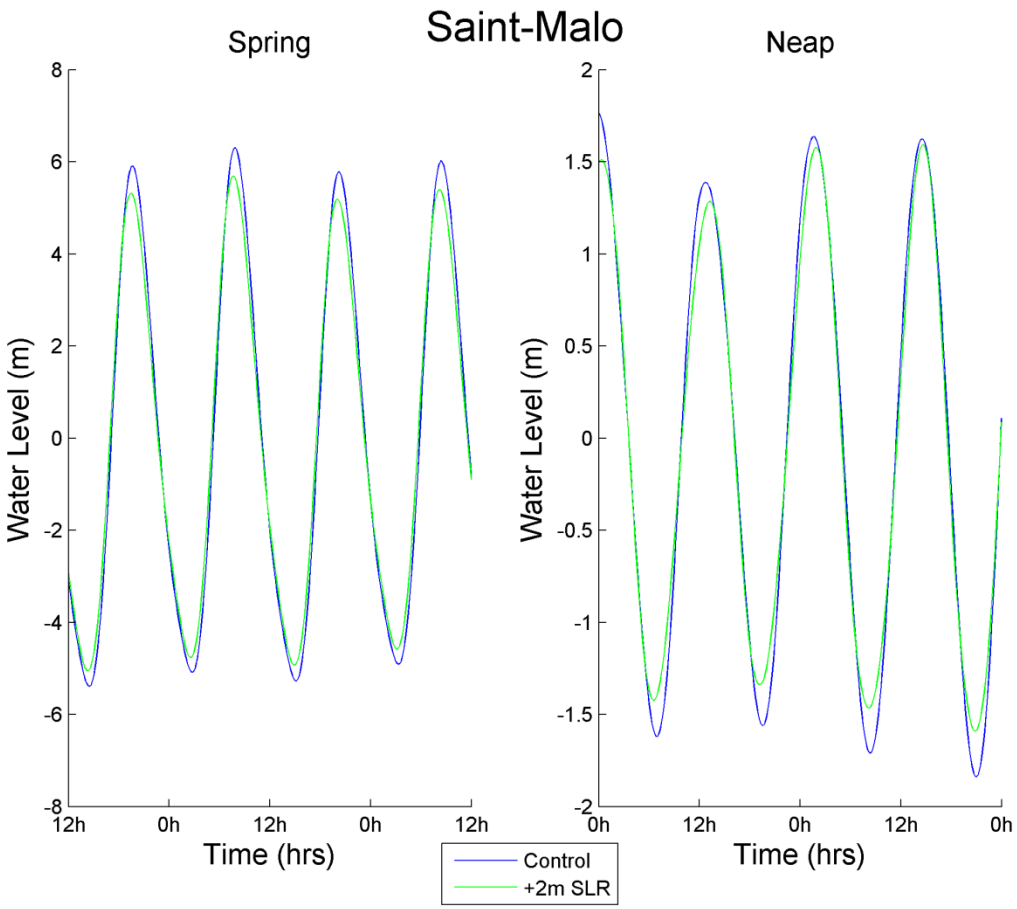
Saint-Malo
Spring
Neap
Water Level (m)
Time (hrs)
12h
0h
Control
+2m SLR

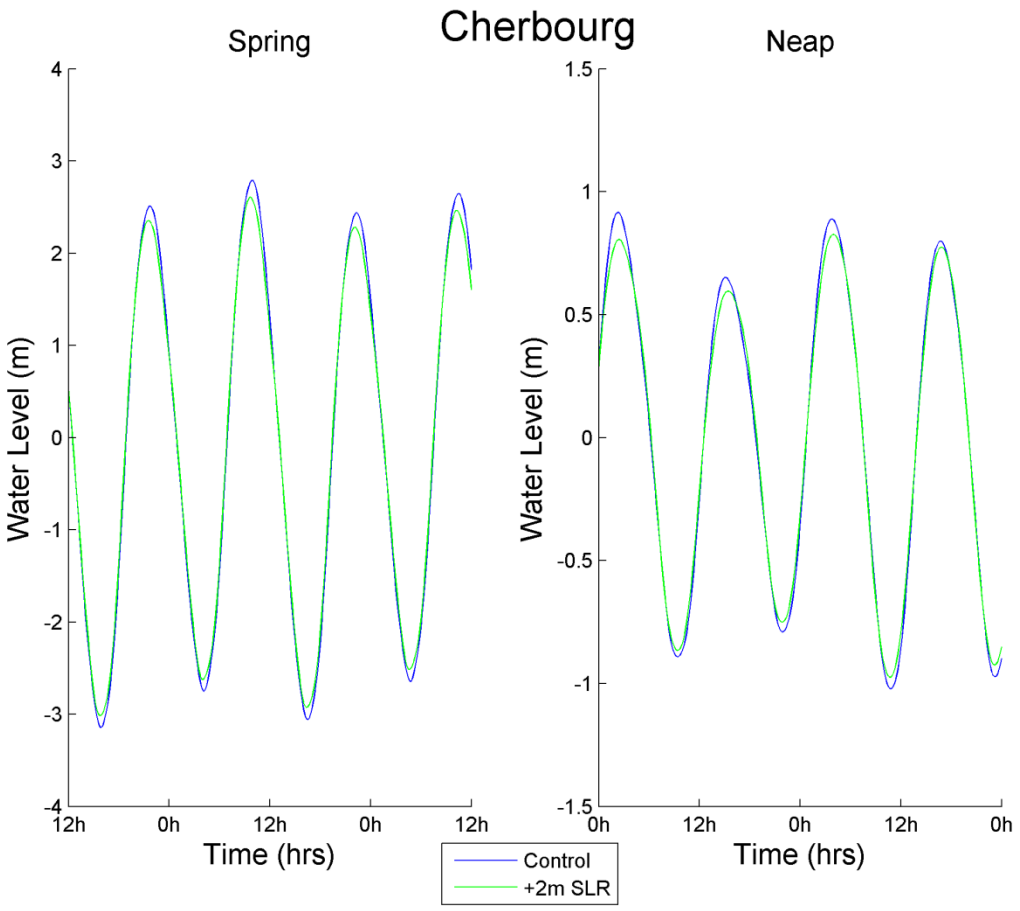
Cherbourg
Spring
Neap
Water Level (m)
Time (hrs)
12h
0h
Control
+2m SLR

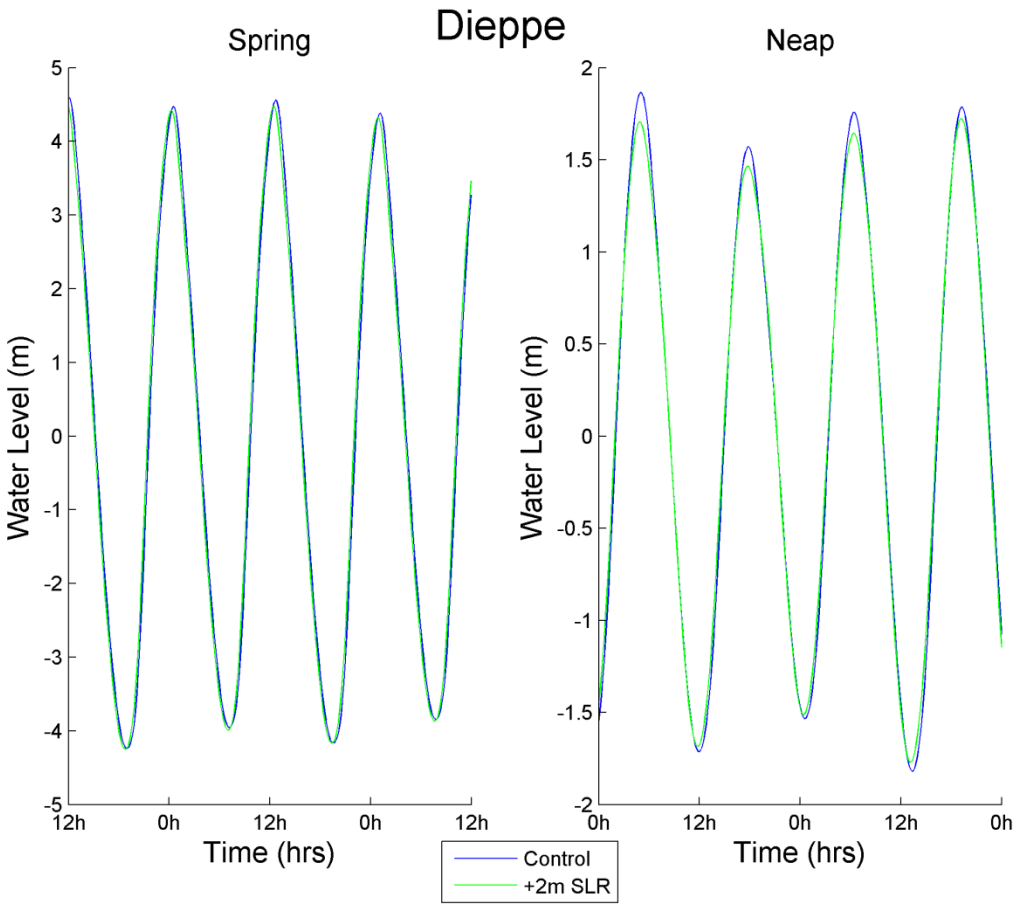
Dieppe
Spring
Neap
Water Level (m)
Time (hrs)
12h
0h
Control
+2m SLR

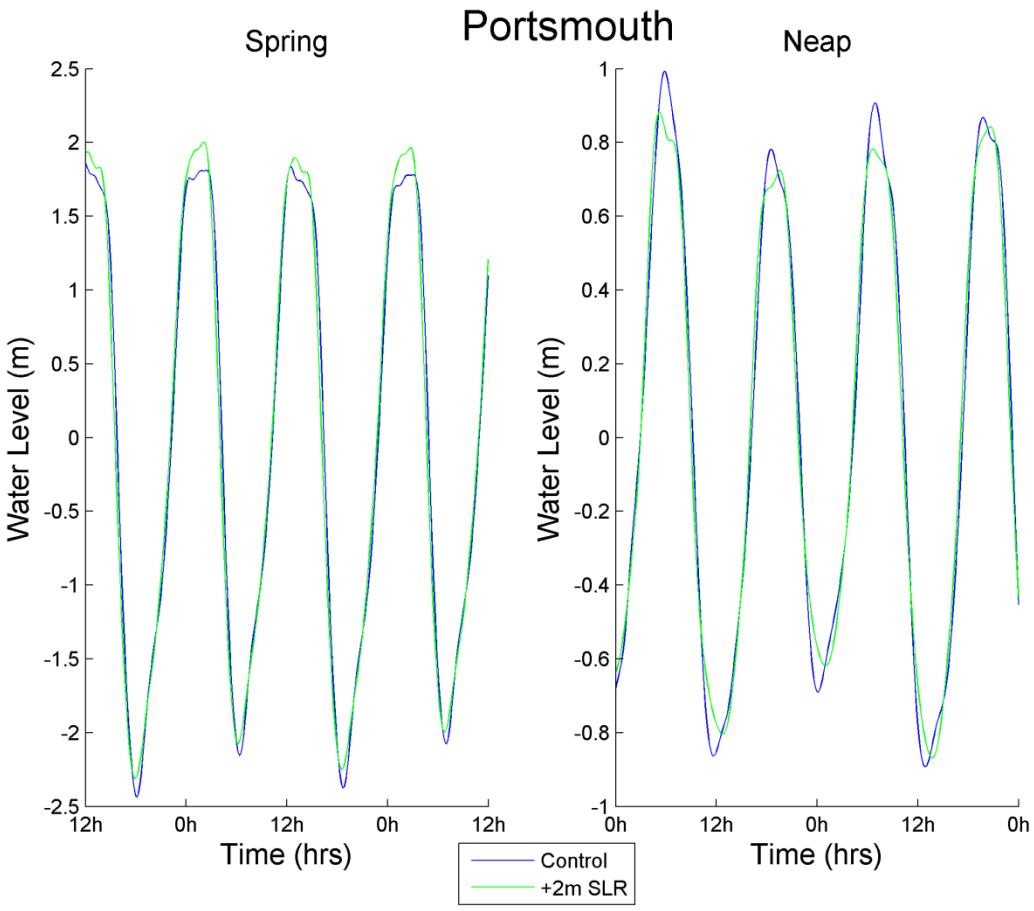
Portsmouth
Spring
Neap
Water Level (m)
Time (hrs)
12h
0h
Control
+2m SLR

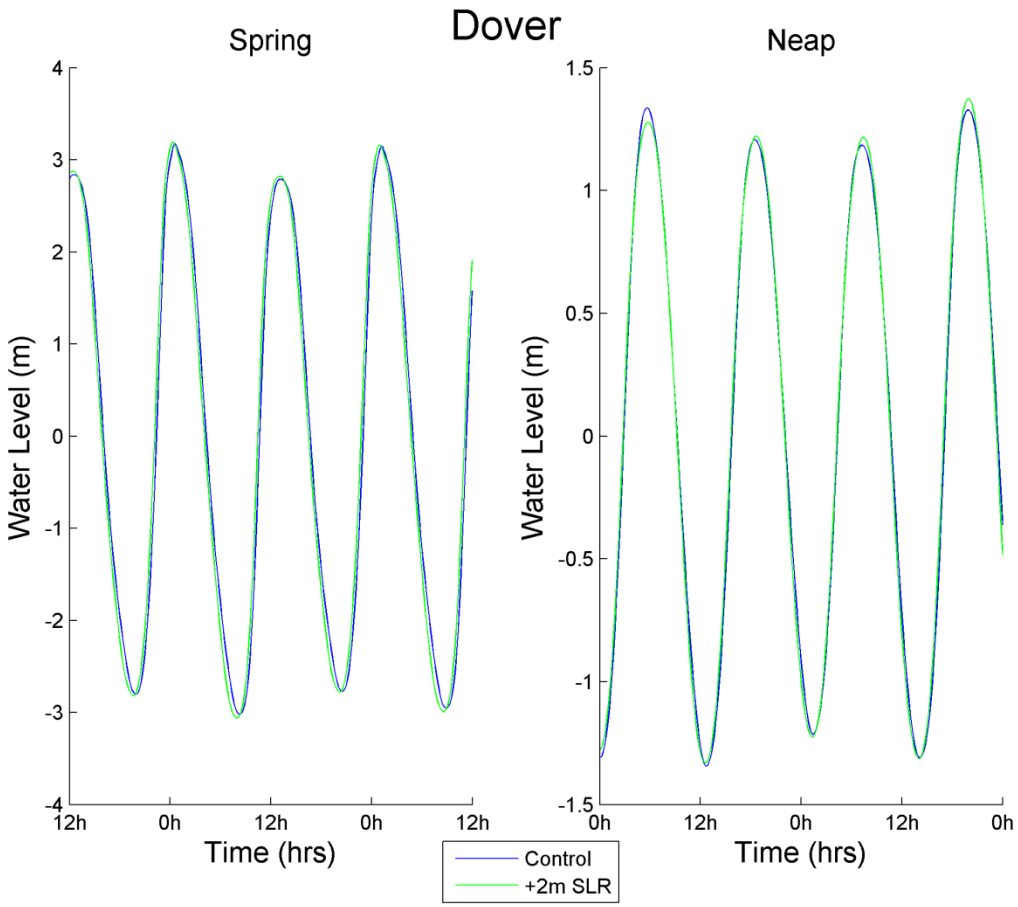
Dover
Spring
Neap
Water Level (m)
Time (hrs)
12h
0h
Control
+2m SLR

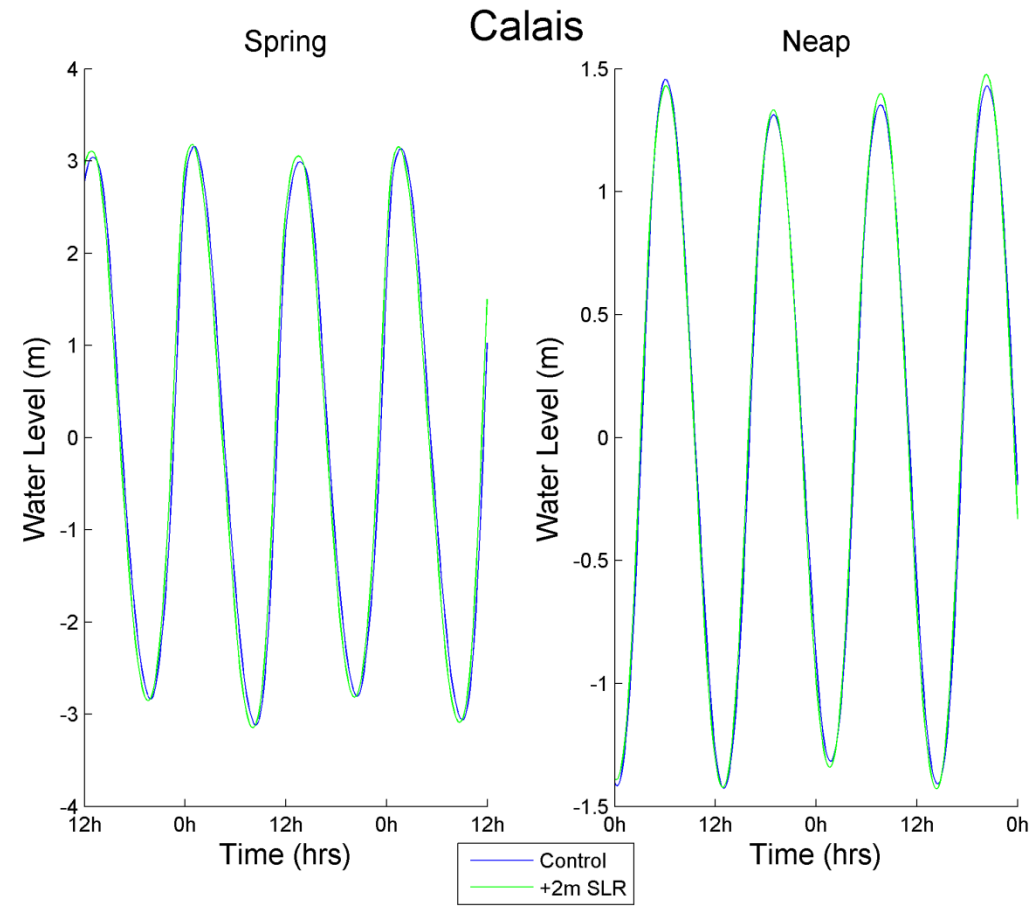
Calais
Spring
Neap
Water Level (m)
Time (hrs)
12h
0h
Control
+2m SLR

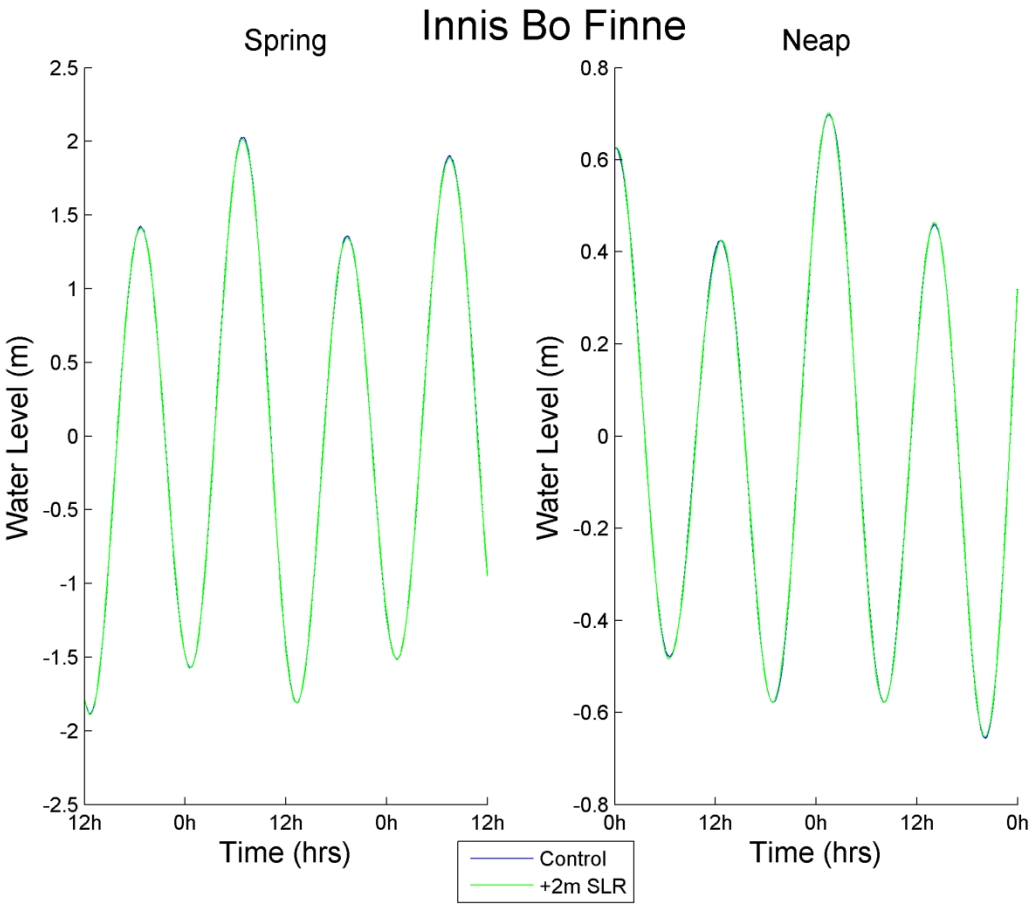
Innis Bo Finne
Spring
Neap
Water Level (m)
Time (hrs)
12h
0h
Control
+2m SLR

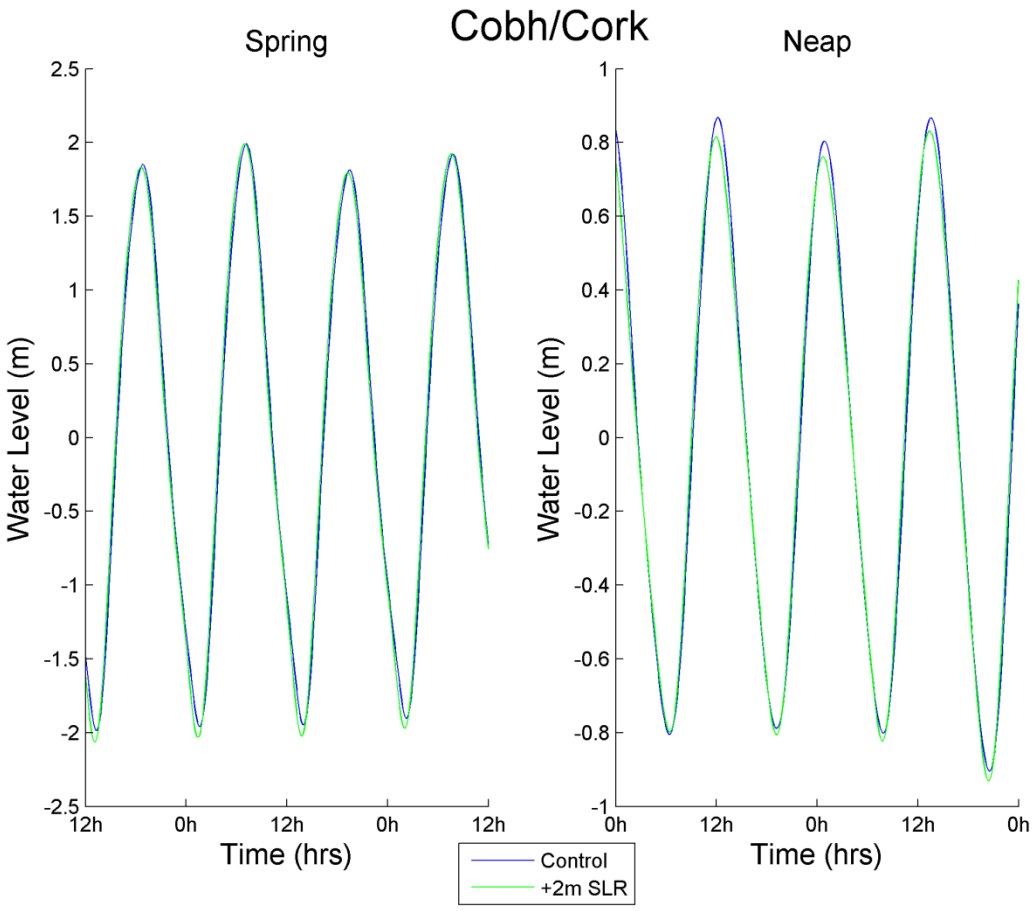
Cobh/Cork
Spring
Neap
Water Level (m)
Time (hrs)
12h
0h
Control
+2m SLR

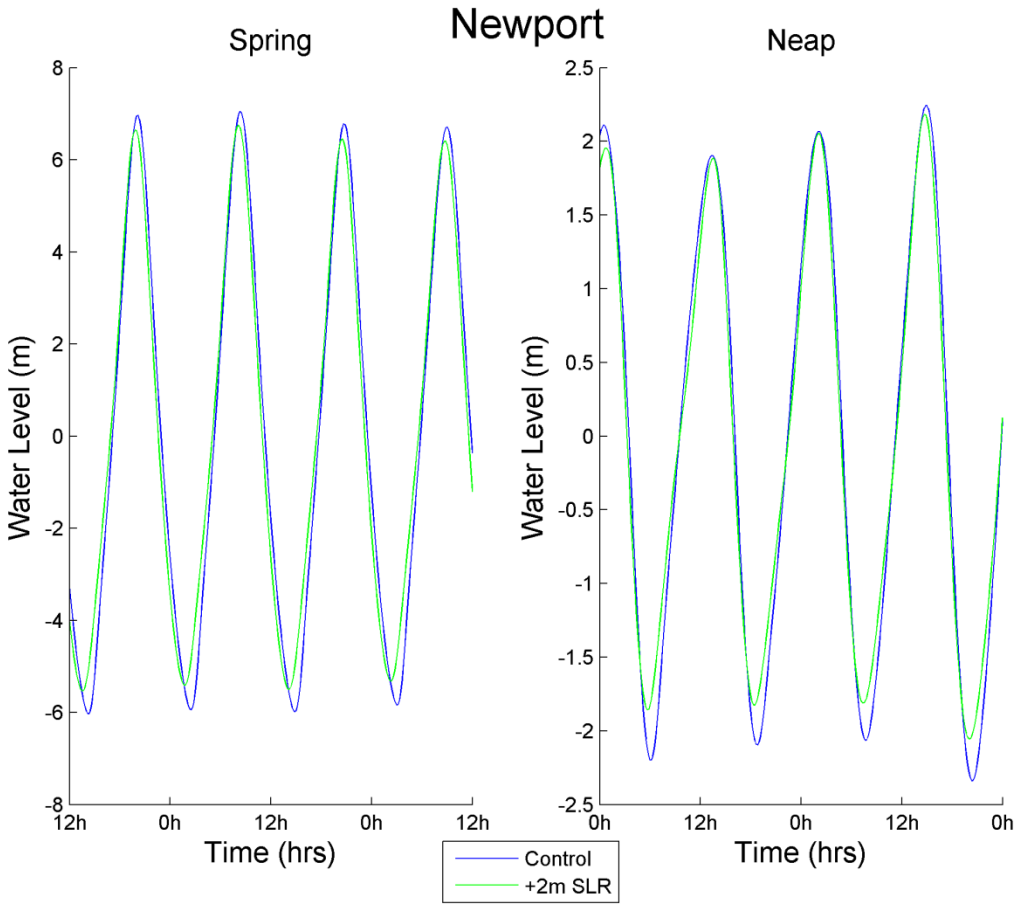
Newport
Spring
Neap
Water Level (m)
Time (hrs)
12h
0h
Control
+2m SLR

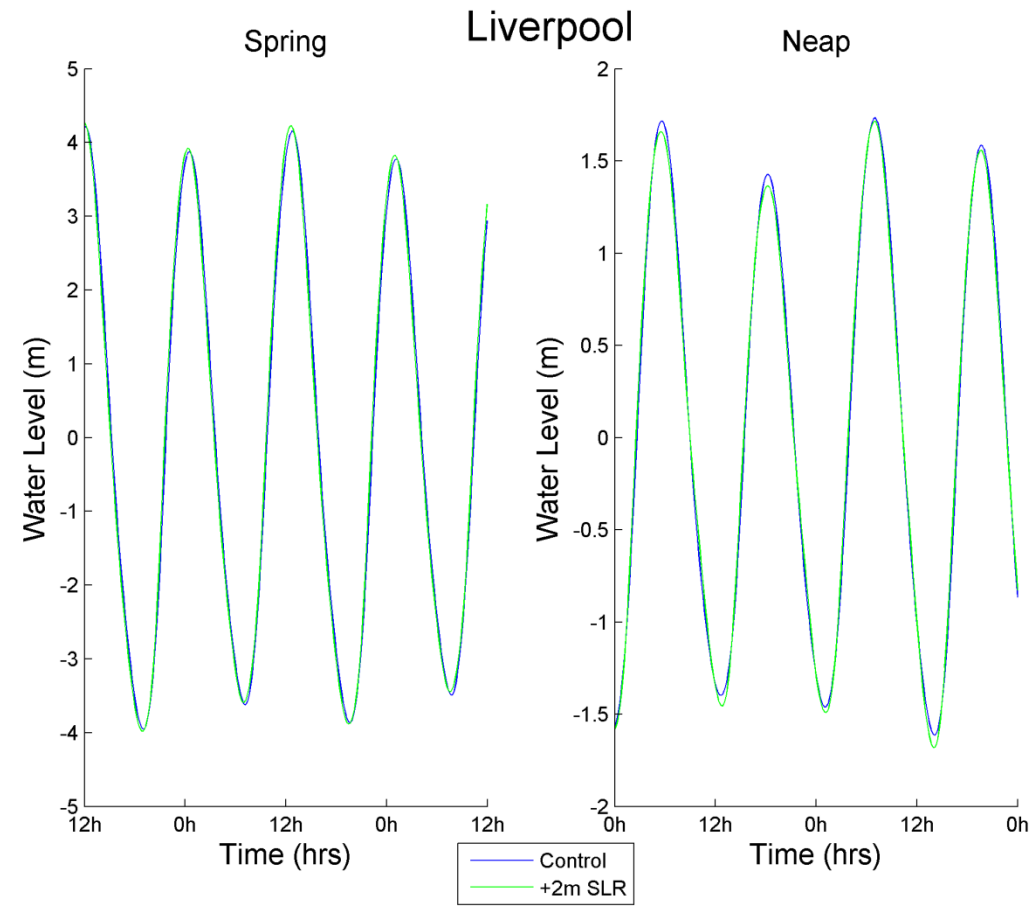
Liverpool
Spring
Neap
Water Level (m)
Time (hrs)
12h
0h
Control
+2m SLR

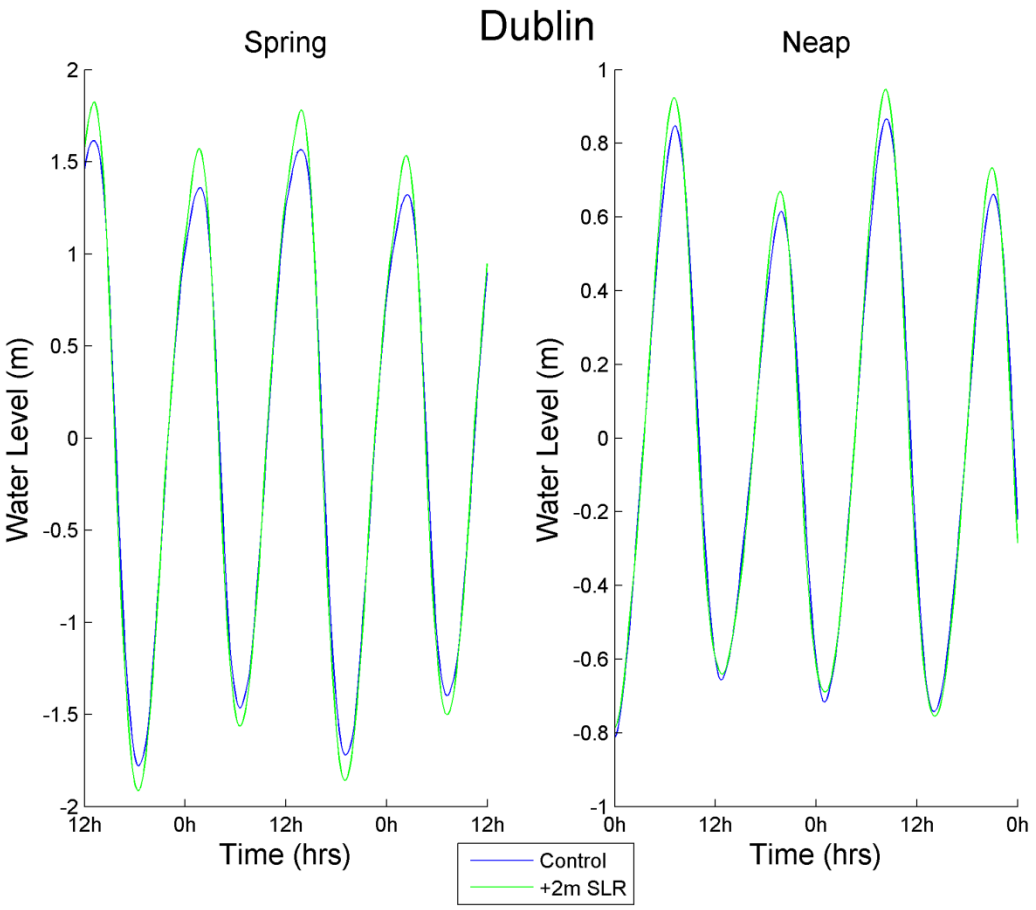
Dublin
Spring
Neap
Water Level (m)
Time (hrs)
12h
0h
Control
+2m SLR

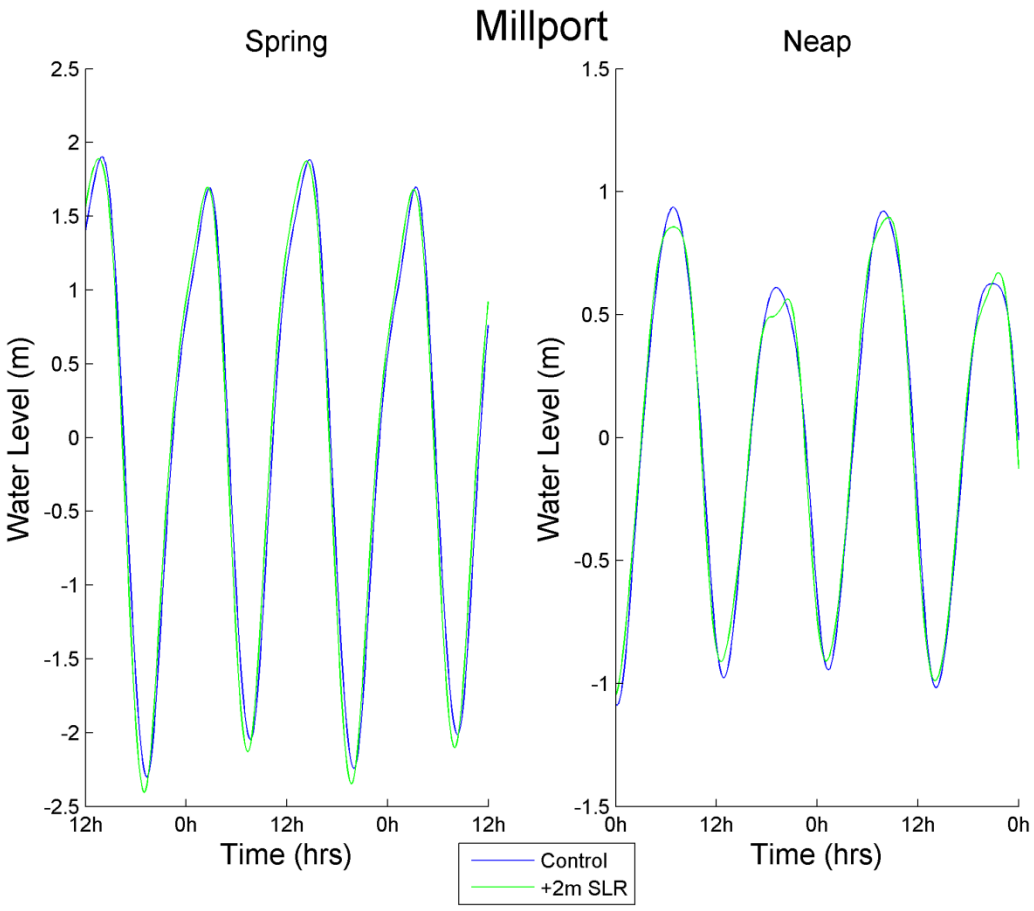
Millport
Spring
Neap
Water Level (m)
Time (hrs)
12h
0h
Control
+2m SLR

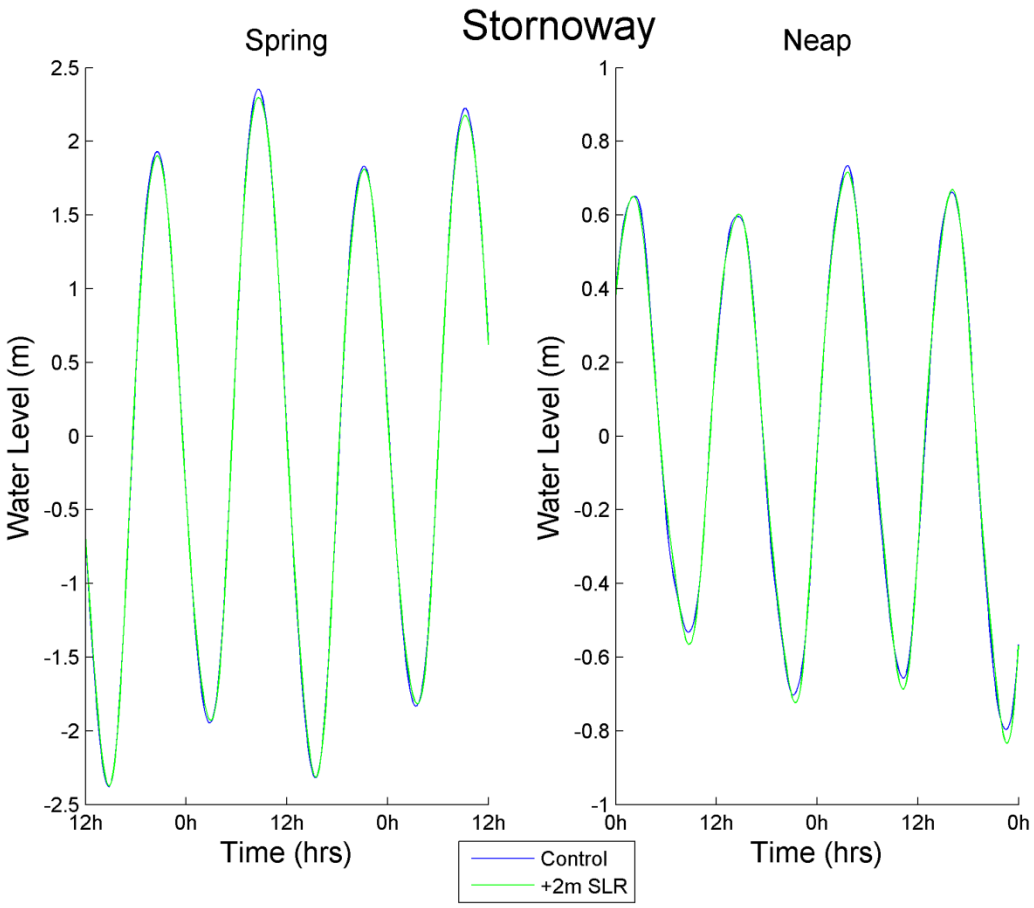
Stornoway
Spring
Neap
Water Level (m)
Time (hrs)
12h
0h
Control
+2m SLR

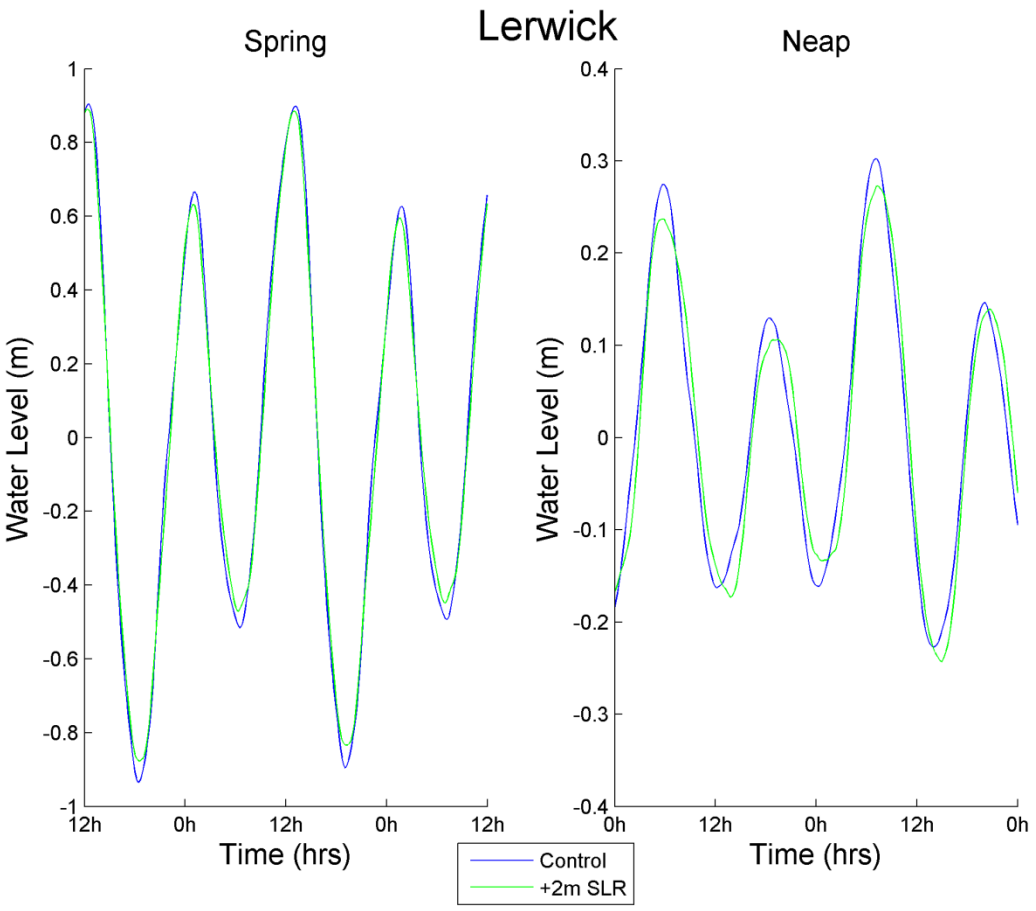
Lerwick
Spring
Neap
Water Level (m)
Time (hrs)
12h
0h
Control
+2m SLR

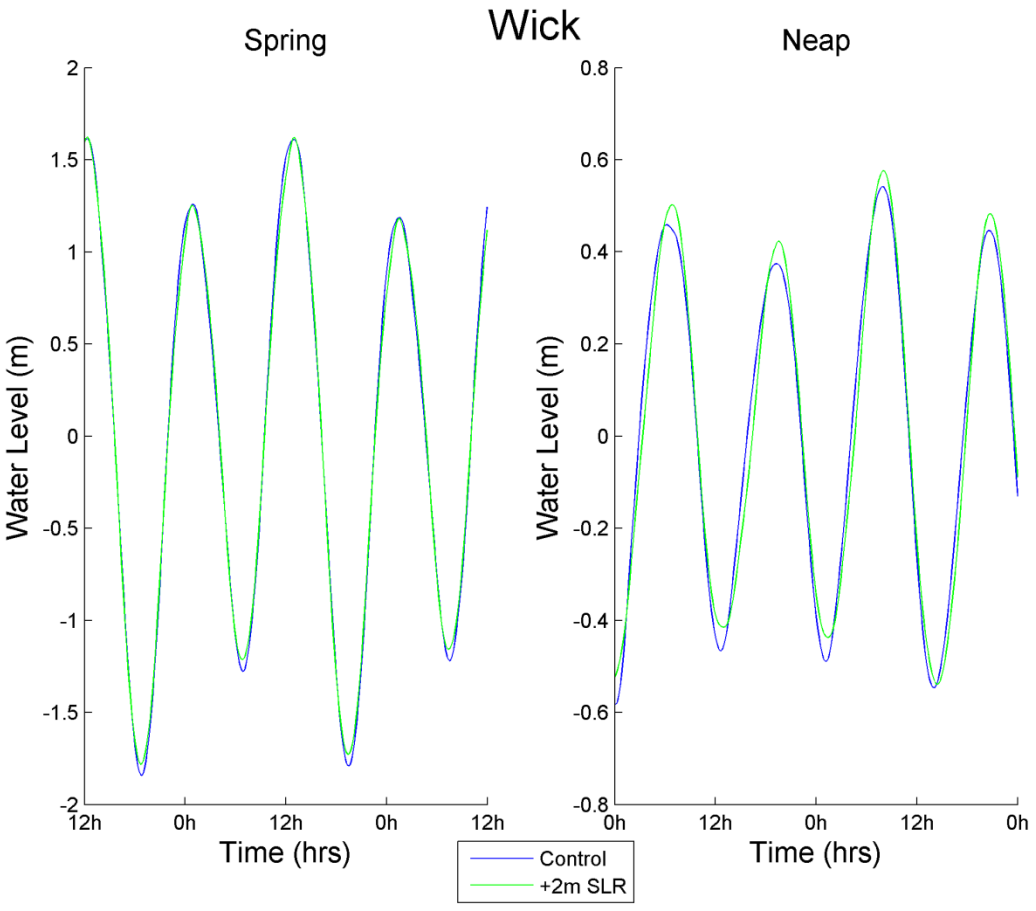
Wick
Spring
Neap
Water Level (m)
Time (hrs)
12h
0h
Control
+2m SLR

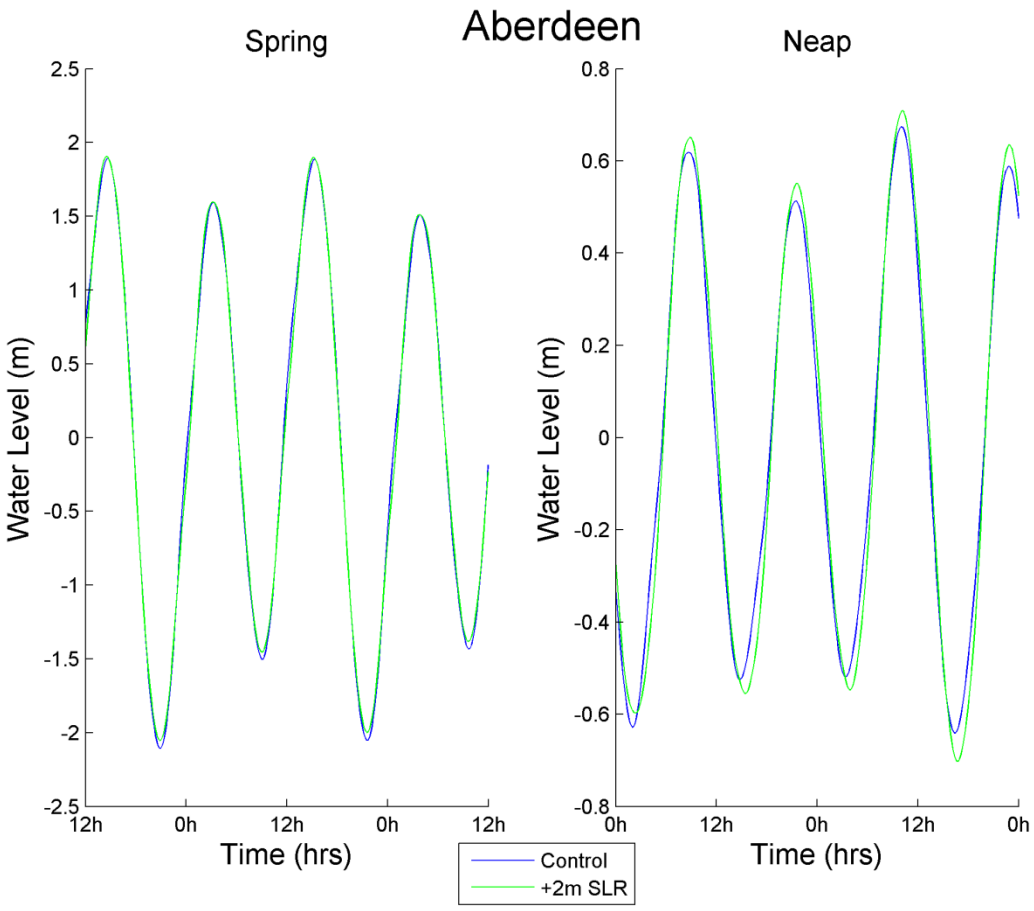
Aberdeen
Spring
Neap
Water Level (m)
Time (hrs)
12h
0h
Control
+2m SLR

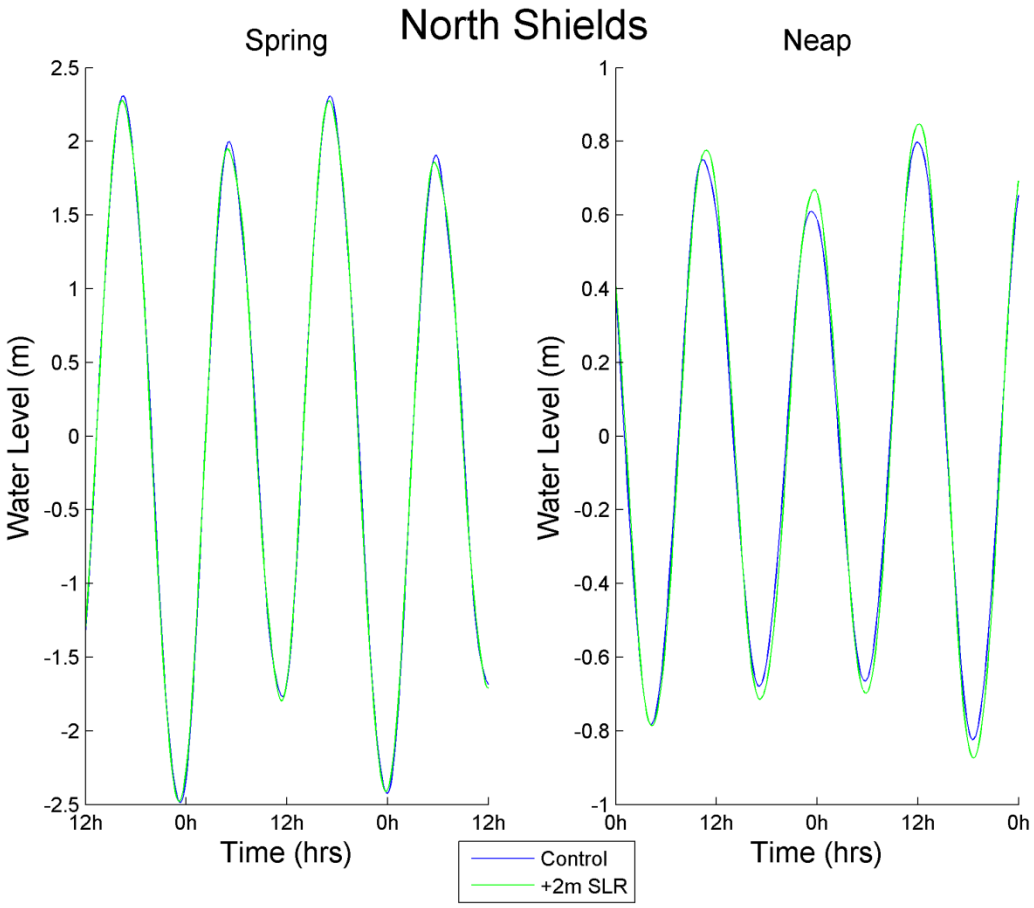
North Shields
Spring
Neap
Water Level (m)
Time (hrs)
12h
0h
Control
+2m SLR

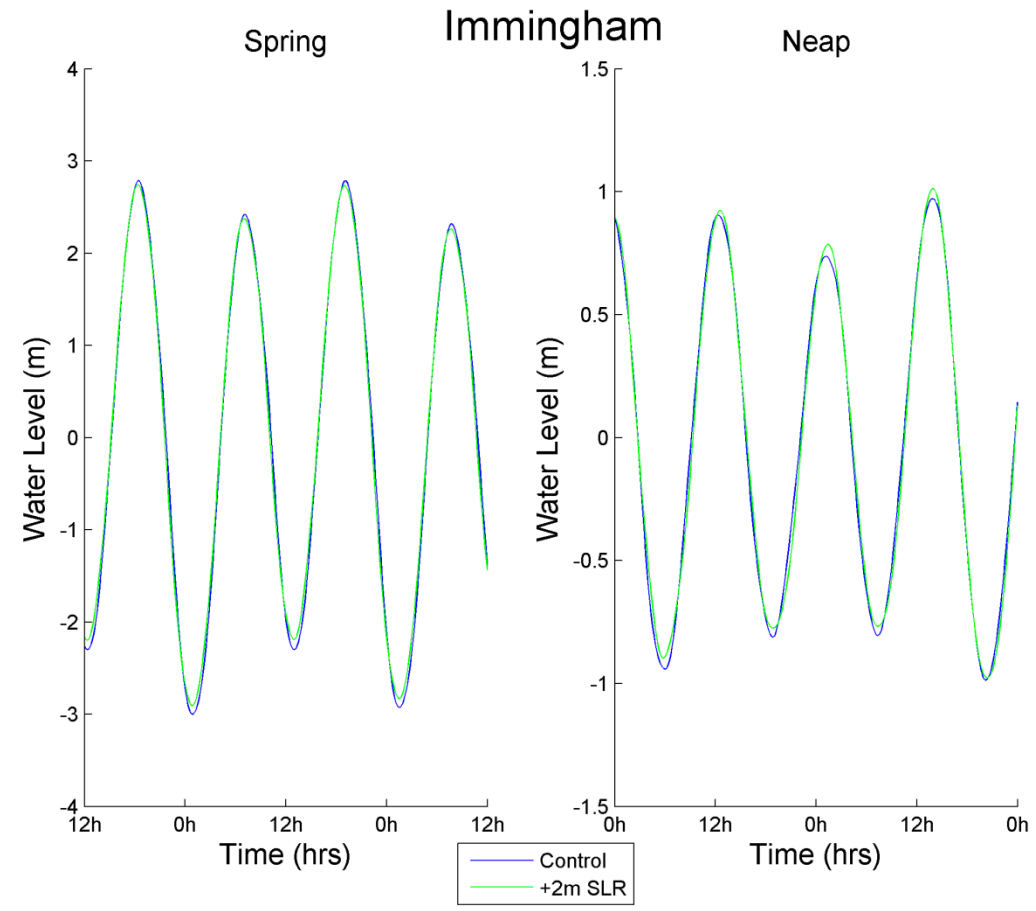
Immingham
Spring
Neap
Water Level (m)
Time (hrs)
12h
0h
Control
+2m SLR

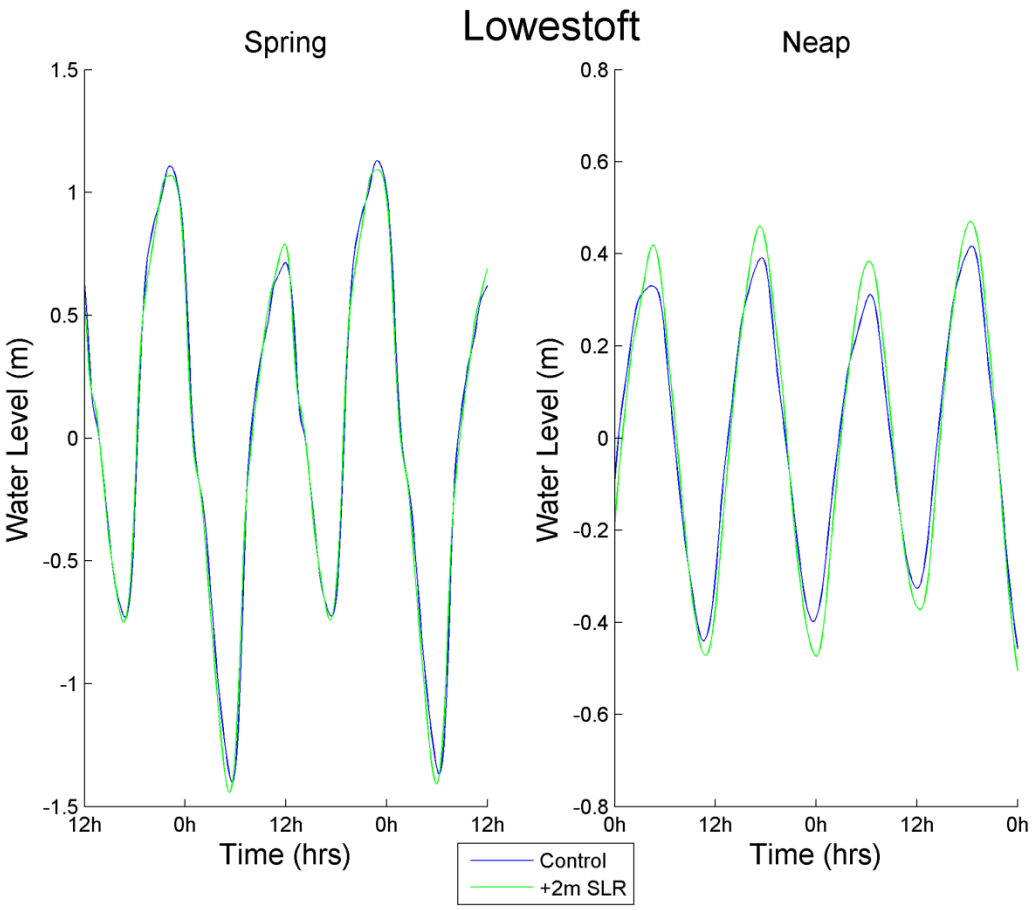
Lowestoft
Spring
Neap
Water Level (m)
Time (hrs)
12h
0h
Control
+2m SLR

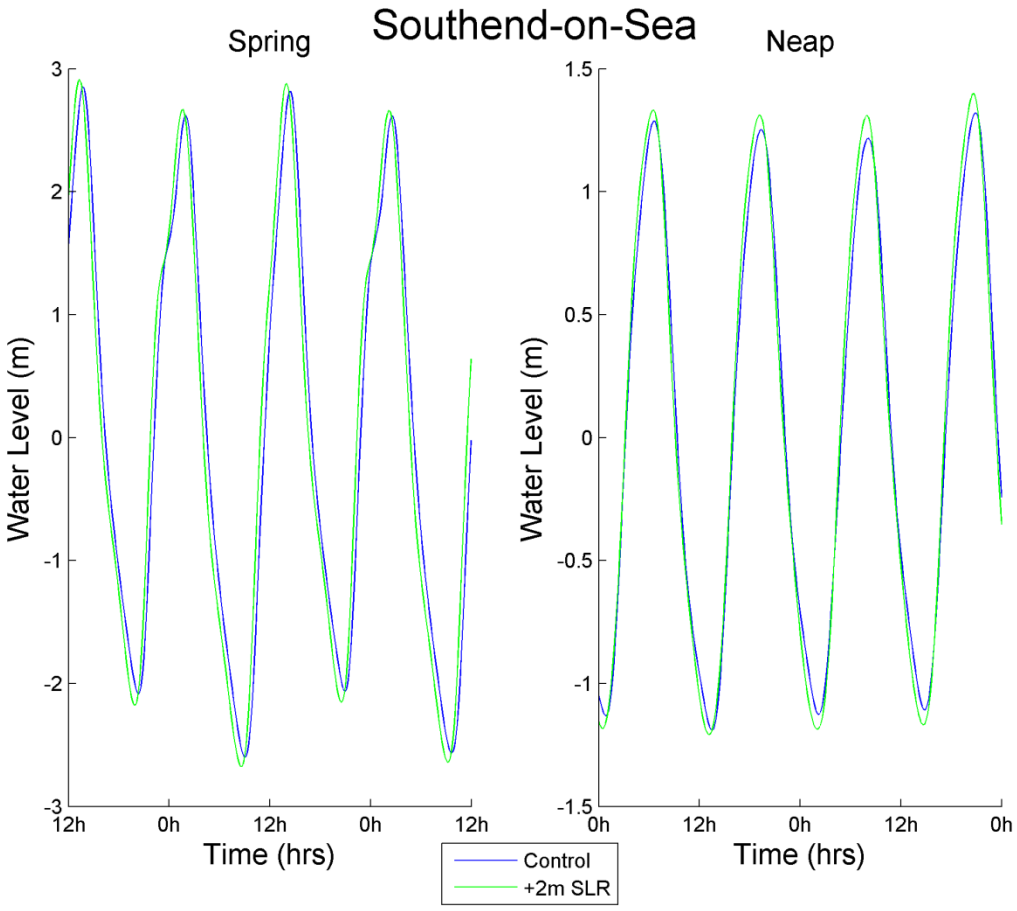
Southend-on-Sea
Spring
Neap
Water Level (m)
Time (hrs)
12h
0h
Control
+2m SLR

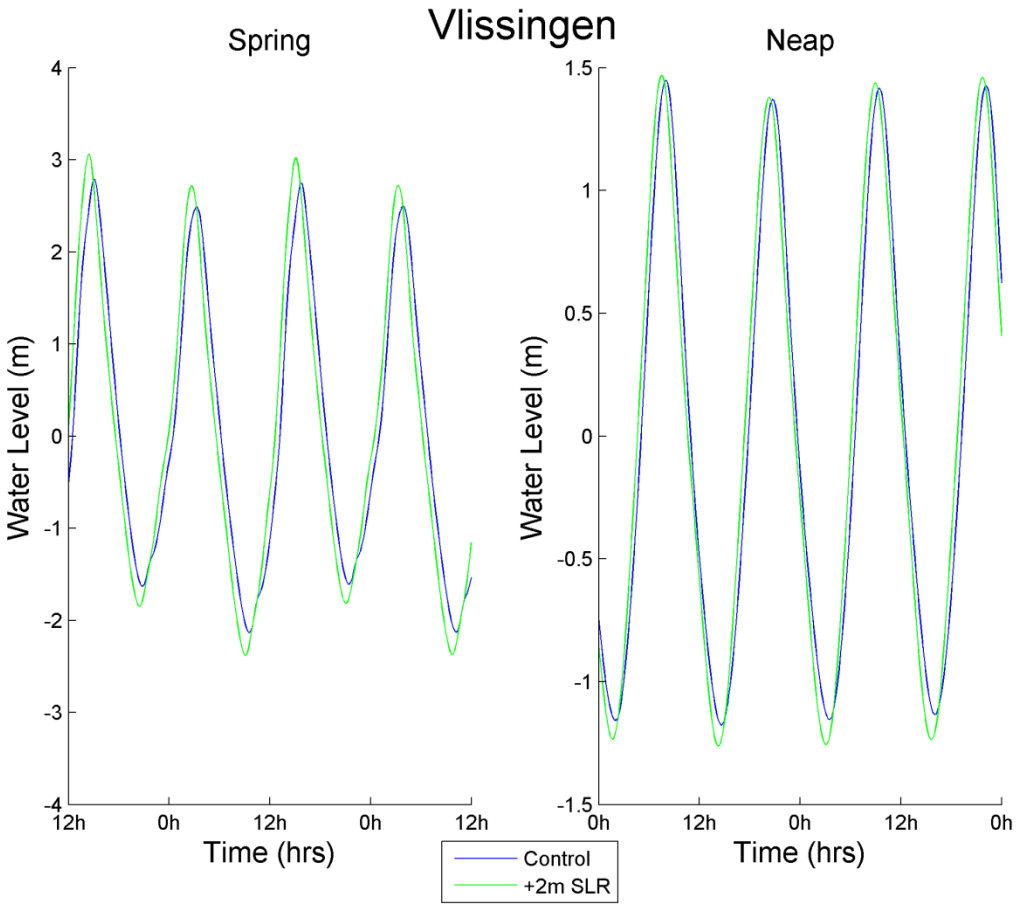
Vlissingen
Spring
Neap
Water Level (m)
Time (hrs)
12h
0h
Control
+2m SLR

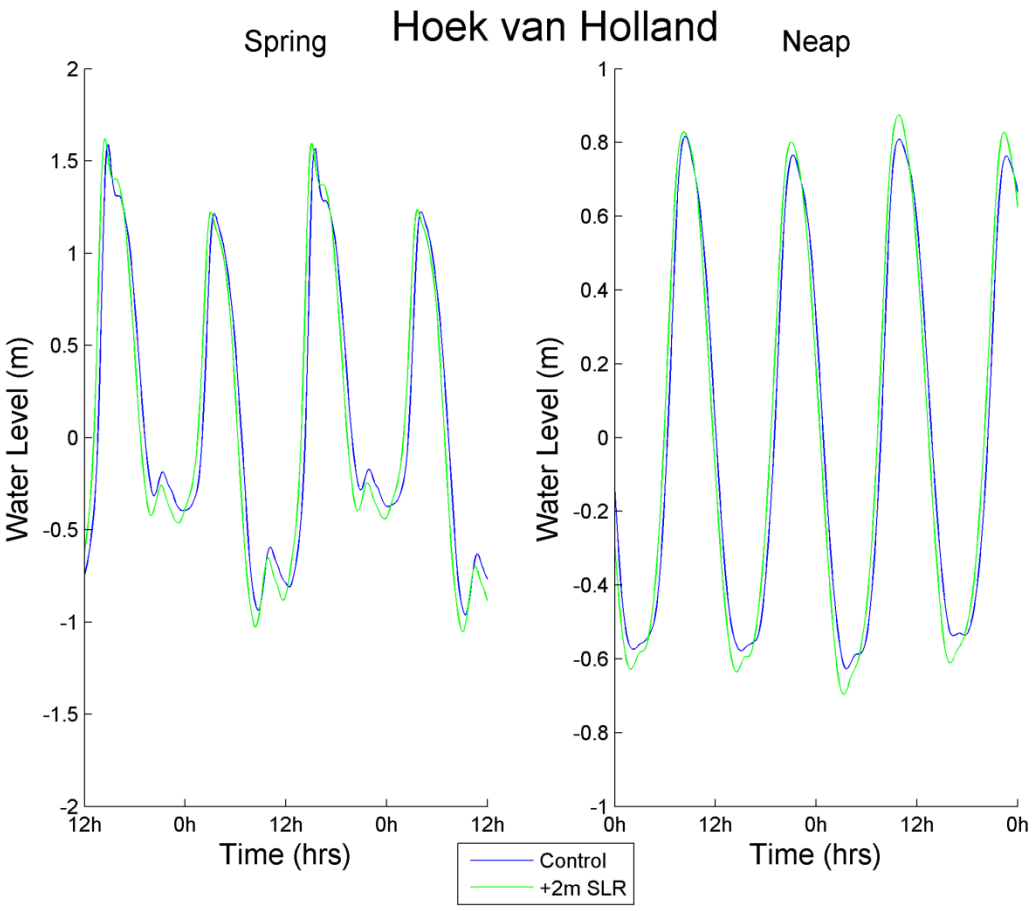
Hoek van Holland
Spring
Neap
Water Level (m)
Time (hrs)
12h
0h
Control
+2m SLR

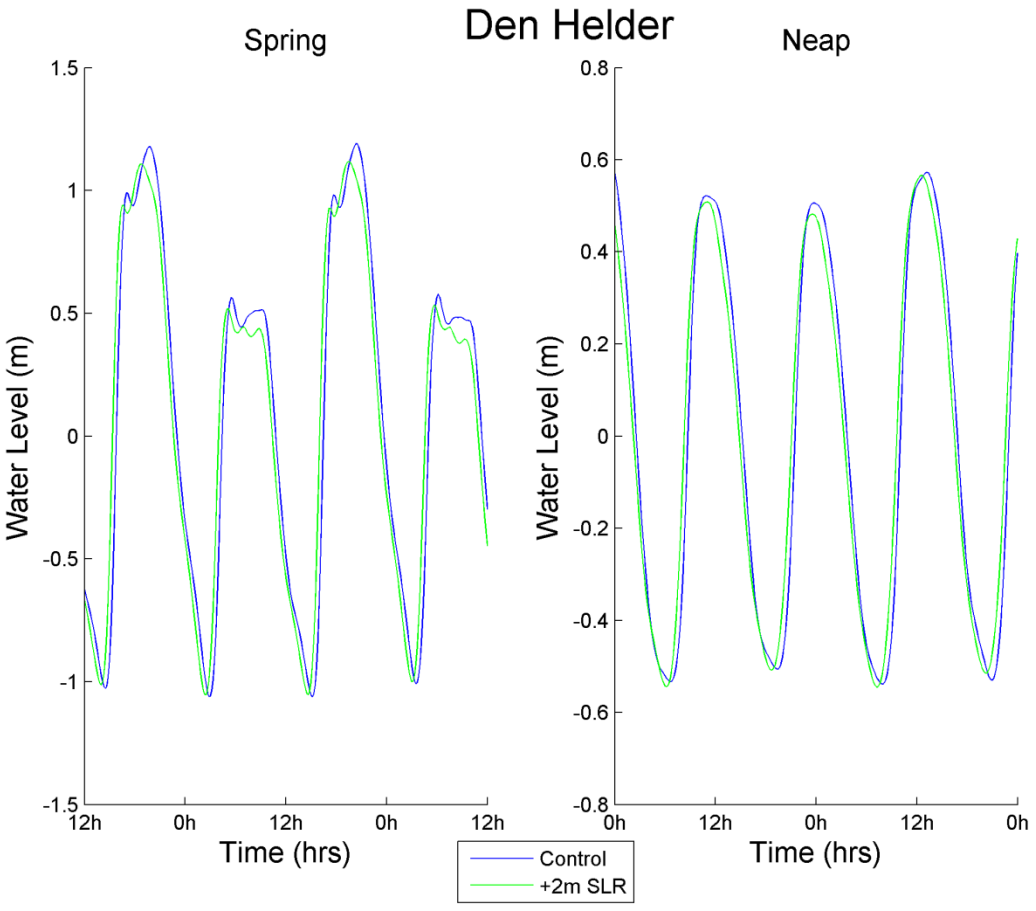
Den Helder
Spring
Neap
Water Level (m)
Time (hrs)
12h
0h
Control
+2m SLR

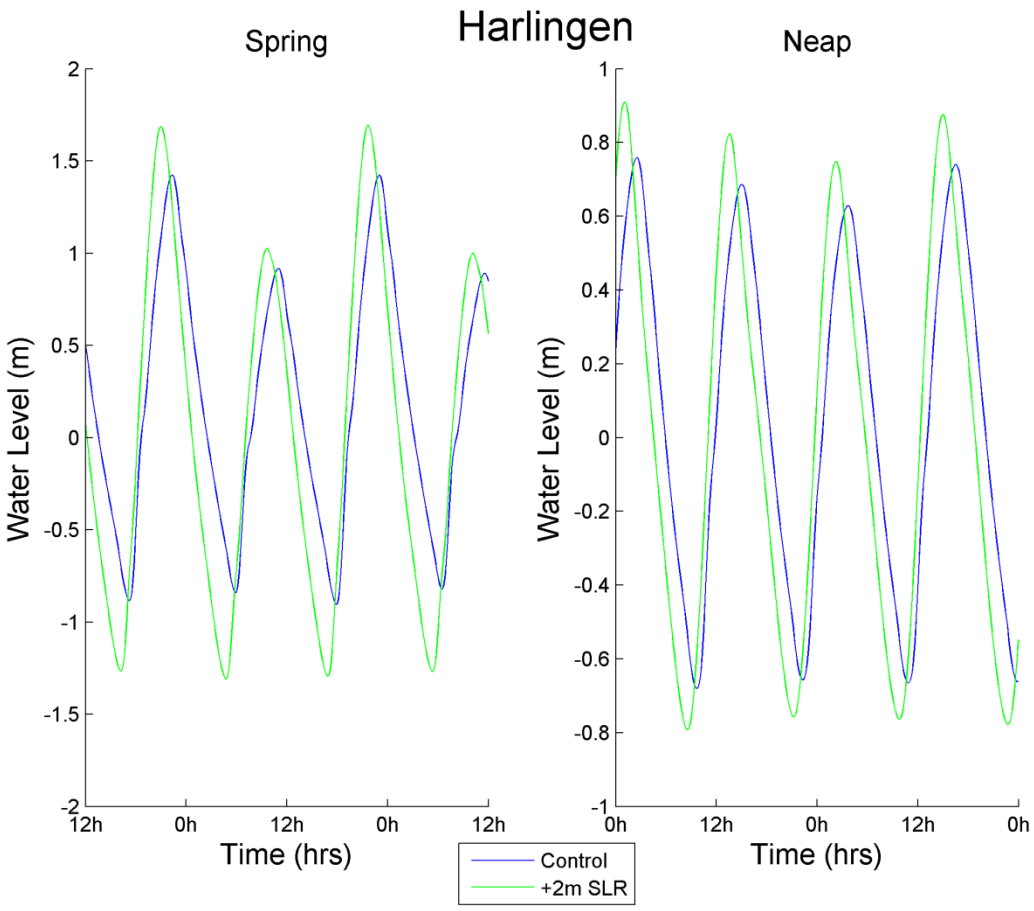
Harlingen
Spring
Neap
Water Level (m)
Time (hrs)
12h
0h
Control
+2m SLR

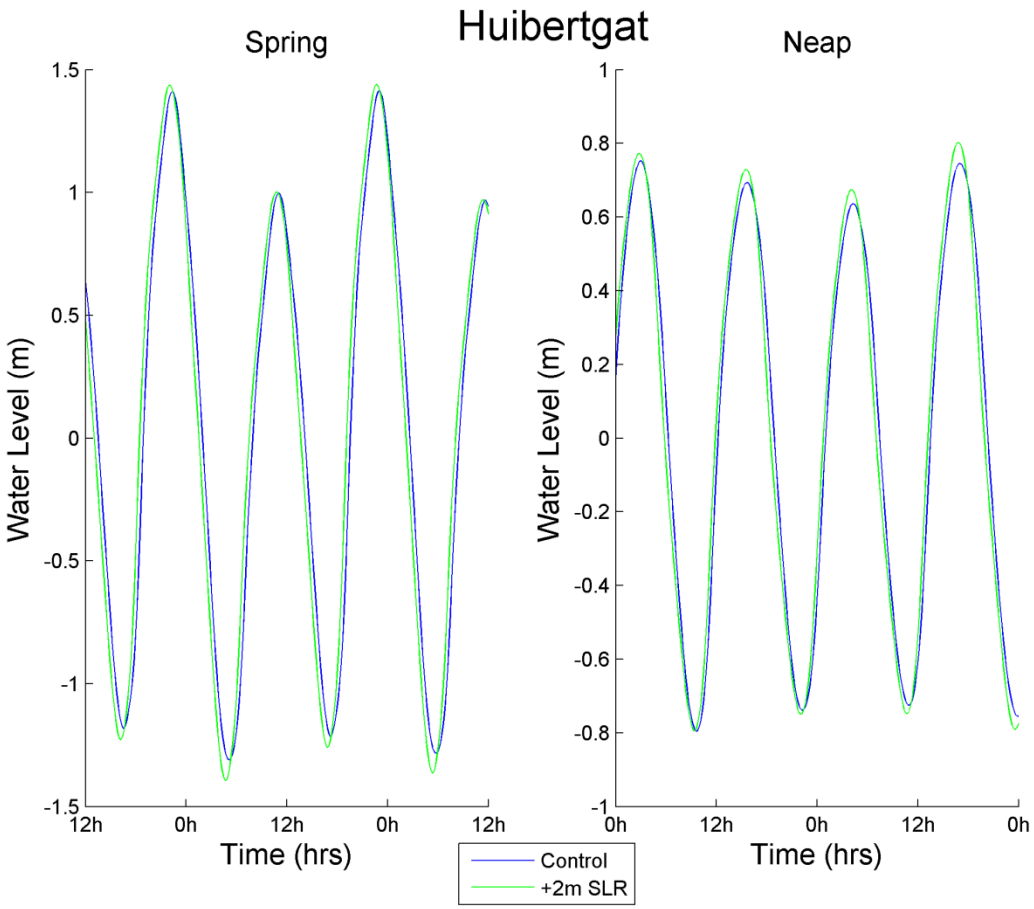
Huibertgat
Spring
Neap
Water Level (m)
Time (hrs)
12h
0h
Control
+2m SLR

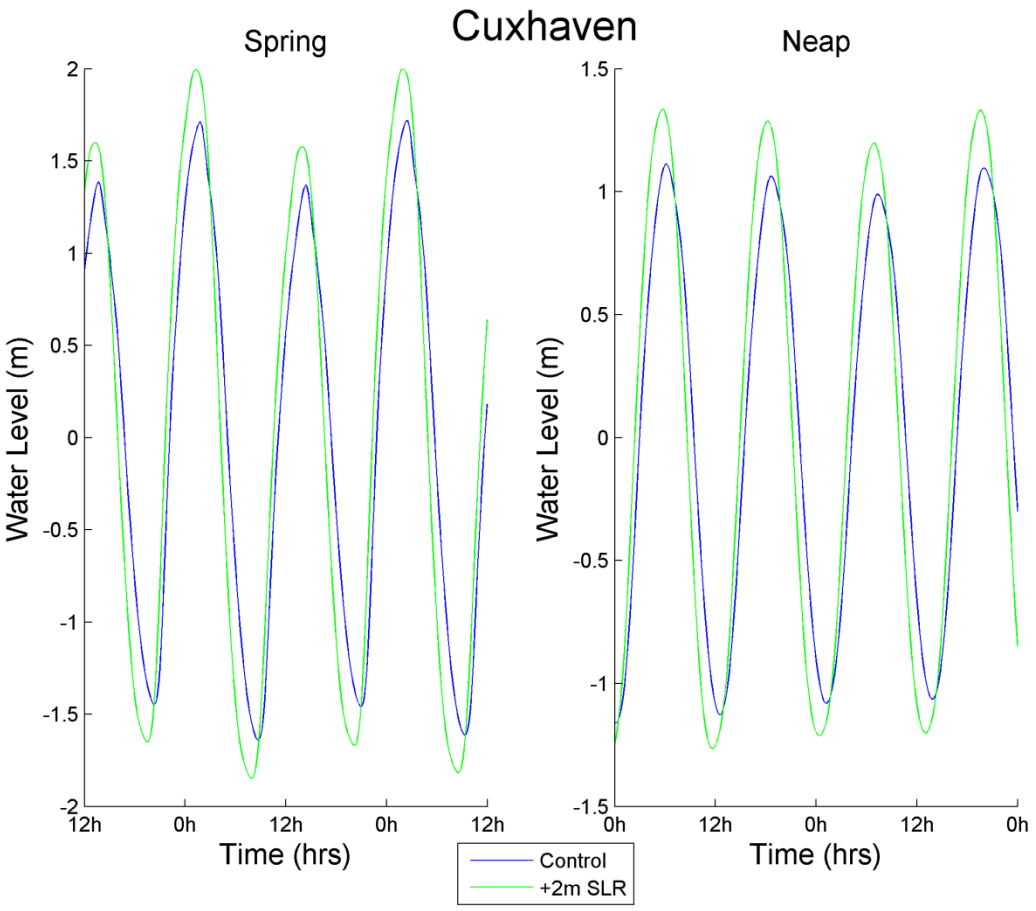
Cuxhaven
Spring
Neap
Water Level (m)
Time (hrs)
12h
0h
Control
+2m SLR

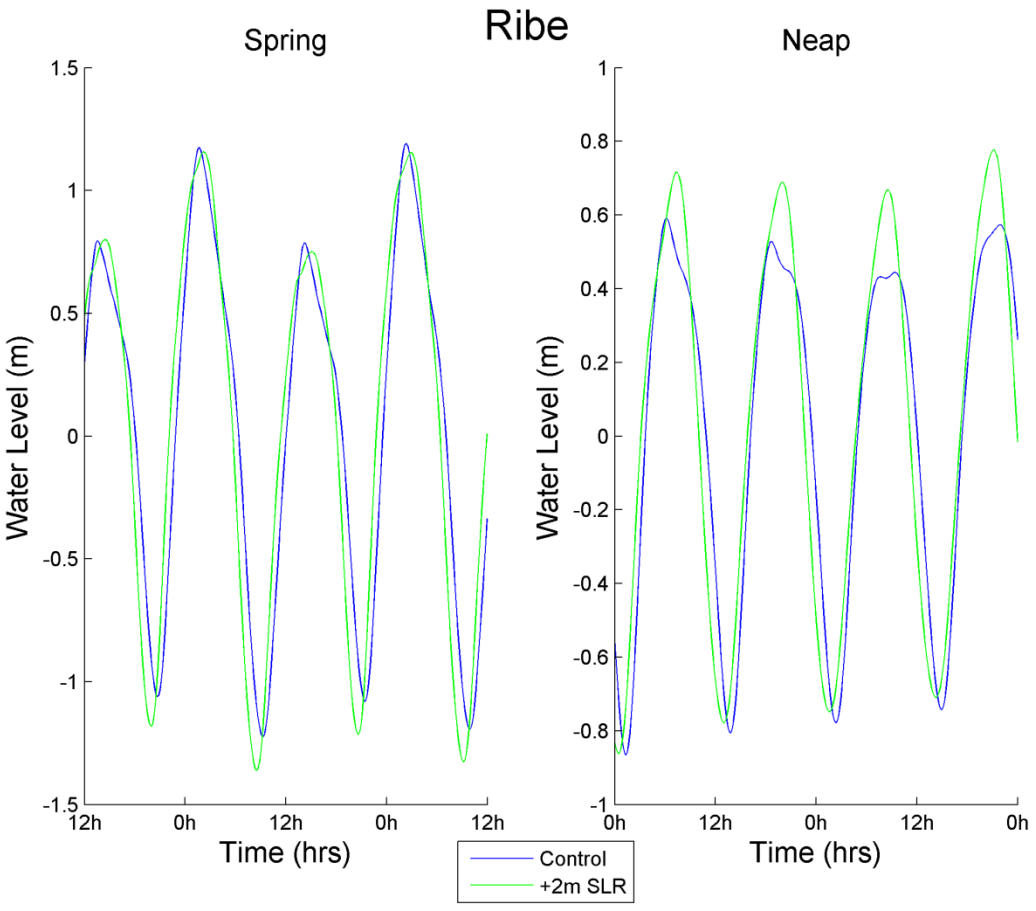
Ribe
Spring
Neap
Water Level (m)
Time (hrs)
12h
0h
Control
+2m SLR

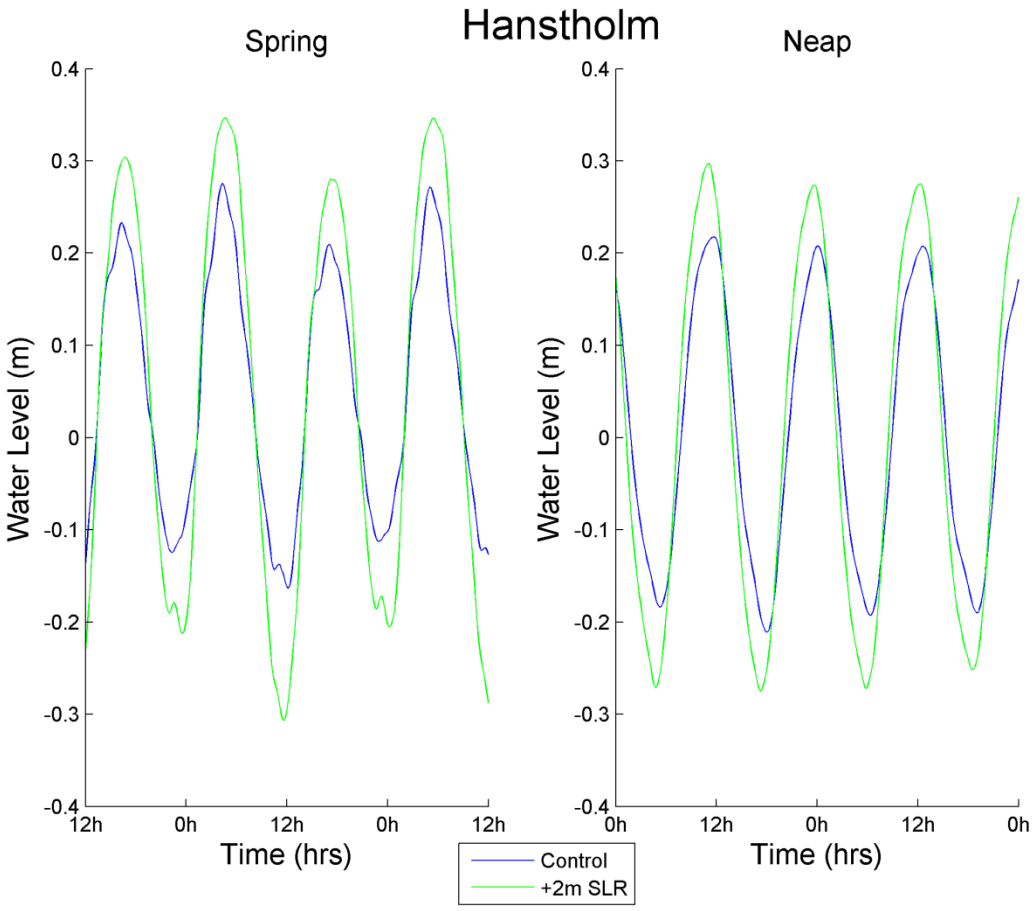
Hanstholm
Spring
Neap
Water Level (m)
0.4
0.3
0.2
0.1
0
-0.1
-0.2
-0.3
-0.4
12h
0h
12h
0h
12h
Time (hrs)
Control
+2m SLR

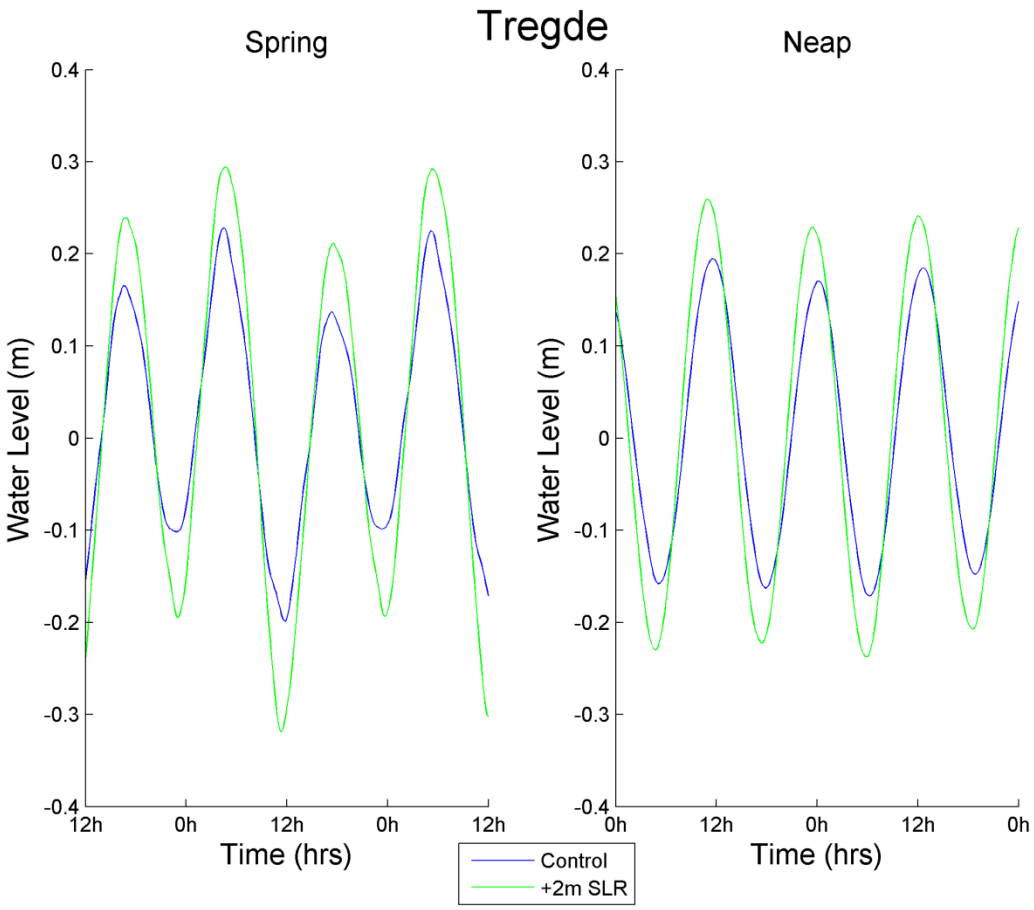
Tregde
Spring
Neap
Water Level (m)
0.4
0.3
0.2
0.1
0
-0.1
-0.2
-0.3
-0.4
12h
0h
12h
0h
12h
Time (hrs)
Control
+2m SLR

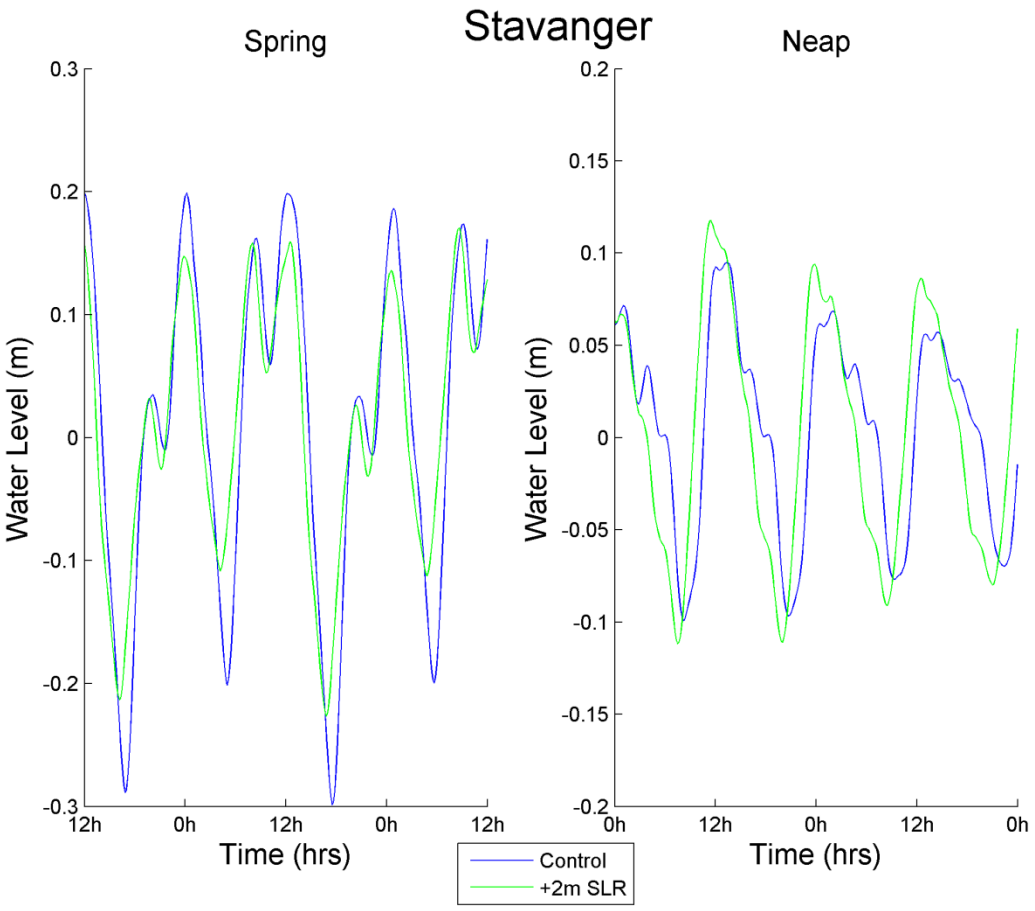
Stavanger
Spring
Neap
Water Level (m)
Time (hrs)
12h
0h
Control
+2m SLR

Appendix 2 - Porting to, and Optimising and Benchmarking of the OTISmpi Global Tidal Model on the NOCS Altix ICE Cluster (Nautilus)

Purpose of this Appendix

To:

- document lessons learnt from porting, optimisation and benchmarking of OTISmpi for future reference.

- record limitations of the present version of OTISmpi and highlight areas for potential future improvement.

- communicate the potential of OTISmpi for future studies.

A2.1 Versions and users of the OTISmpi model

The OTISmpi forward global tidal model (GTM) has its name derived from the related data assimilative tidal model, OTIS (OSU Tidal Inversion Software). OTISmpi was written by Gary Egbert, Lana Erofeeva at OSU, Richard Ray and Bruce Bills (NASA Goddard Flight Centre, Greenbelt, Maryland).

The code discussed in this Appendix was obtained directly from Lana Erofeeva at OSU and then developed to create the present version (OTISmpi_altix). When verifying the port of the model two further versions of the model were obtained from OSU which included different simulation setups and tidal results for benchmarking.

The OTISmpi code can be compiled into three different executables: fwd_ts, fwd_ts_fast and fwd_ts_NPG. The first two executables have a near global domain with open boundary conditions prescribed at high latitude in the northern Arctic (to avoid a singularity associated with grid line convergence); amongst other things they differ in the time stepping routines used. The fwd_ts_NPG executable is a truly non-data assimilative GTM with a fully global domain using a rotated co-ordinate system (avoiding the singularity by locating the co-ordinate North Pole in the Greenland land mass). All three model executables are compiled in a very similar way, with some code being common to all of them; where comments in this Appendix are specific to a particular executable the distinction will be made.

Aside from the developers of the model mentioned above the main users of the model are:

Mark Pickering - National Oceanography Centre Southampton

Edward Zaron - University of Portland, USA

Mattias Green - University of Bangor, UK

Holly Pelling - University of Bangor, UK

A2.2 **Overview of OTISmpi model's directory structure**

OTISmpi_altix / bin

/ comm /

/ DB /

/ include /

/ local / GLOB8 / exe

/ include

/out

/prm

/ GLOB8npg / (same subdirectories as GLOB8)

/ src / fwd_ts

/ oo

/ par

/ sal

/ utils

Quick Start

Once the model is correctly ported to your architecture a compile should be as simple as:

1) In /bin type make linux.all

2) In /comm type make all

3) In /utils type make all

4) In either of the sub directories of /local/GLOB8/exe or /local/GLOB8npg/exe

type make mpi.fwd_ts or make mpi.fwd_ts_NPG respectively

For more information on Quick Start see section A2.4.1

A2.3 Porting the OTISmpi model

A2.3.1 System Requirements

This appendix describes the port of the code to a specific Linux environment with the hope that much of the advice will be platform independent.

The code requires the LAPACK and BLAS libraries which are standard high-level linear algebra libraries available on most Linux platforms (contact your local system administrator to determine the correct paths to these libraries). On Nautilus we use the Intel Math Kernel Library for reasons of efficiency.

The compilers used in this case are the Intel ifort and icc v11.1 compilers. It should be noted that builds with other compilers, such as the Portland group compilers, at other sites have also been performed successfully.

The code is written in Fortran 77, 90, 95 as well as in C. Therefore compilers for both Fortran and C code are required.

The model also requires Message Passing Interface (MPI) libraries. The code for all three versions of OTISmpi (section A2.1) must be compiled as MPI-enabled executables even if it is only run on a single core after compilation.

The /bin codes require netCDF libraries. Here version /netcdf-3.6.3/altix_opt is used.

The memory requirement for 1/8 x 1/8 degree global simulations is estimated to be 1.28 Gbtyes and as will be presented in section A2.5 the model performance benefits from large numbers (order 200) of compute cores but can be run on a single core.

A2.3.2 Source and destination computing platforms

The copy of OTISmpi was obtained directly from OSU, kindly provided by Lana Erofeeva.

The source copy of the model was running under a Linux operating system, using the Portland group pgf90 compiler. The model runs are often computed on workstation scale machines with up to 8 cores. The MPI used was MPICH2.1.

The destination computing platform is the National Oceanography Centre Southampton's Linux Cluster (a SGI Altix ICE 8200), called "Nautilus". The destination architecture has a different chipset as well as different compilers. Additionally jobs are run on compute nodes with up to 8 cores per node. These compute nodes are accessed via login nodes on the cluster where the MPI job is submitted from. Each node has 2 processors with 4 cores, each processor has two pairs of cores which share 6MB of cache memory (see NOCS Nautilus manual for more details). The MPI implementation used is mpt/2.03 provided by SGI.

A2.3.3 The multi stage compilation, in principle

As outlined in the quick start in section A2.2, it should be possible to obtain an executable version of the mode with default settings with four make commands.

In reality there were a number of alterations required to the makefiles in each of the four subdirectories to obtain a clean build of the model. An overview of the alterations and solutions is given in section A2.3.4.

A2.3.4 Bugs revealed during initial compilation attempts and their solutions

During the model compilation a number of bugs where located using the flags given in section A2.3.7. The most significant of these are listed below:

The variable ‘ARCH’ in the makefiles should always equal ‘Linux’. This allows the correct set of compile flags and libraries to be selected in the makefile.

When using the Intel 11.1 compilers it was found to be important to use static linking in /bin makefile (dynamic linking seemed to throw up error messages).

The mcmodel=medium flag was removed from the compiler options as it is only required when memory requirements exceed 2 Gbtyes and at the present 1/8 x 1/8 degree resolution the model only requires ~1.28 Gbytes.

The ifort compiler behaves slightly differently than the Portland Group compiler when it comes to preprocessing *.F Fortran routines into *.f files and then *.o files. An alteration was made to the makefile so that the Intel compiler creates *.o files directly from *.F files. The alteration to the Portland makefile was simply changing the -F flag to -fpp (as shown in section A2.5.2).

Some incompatibilities of the Fortran language ages were highlighted by the port to the Nautilus Cluster. For example in the routine ‘wave_load.f90’ line continuations used ‘*’ characters which threw up errors at compile time; these were therefore replaced with the more common ‘&’ continuations. Additionally comment lines were indicated by ‘*’ characters; these were replaced with ‘!’ characters in this and other routines. Furthermore any instances of the -std90 compile flag were removed to prevent the compiler enforcing the Fortran 90 language standard which with the various vintages of Fortran used resulted in the generation of error messages. In ‘constit_in.f’ some tab-like bits of formatting not processable by the Intel compiler were removed.

In the /comm makefile the variable ‘CC’ was set to ‘icc’. Additionally ‘libs’ was changed to ‘-lmpi’, removing the ‘-static’ linking for the MPI library only.

A2.3.5 Bugs revealed at runtime and their solutions

This section contains errors and solutions found at the point of running the executable. The alphanumerical output of the model at runtime is piped to a text file where these warnings or errors are collected.

The routine ‘SALset.f’ gives an error that CONSTITO has a value of 11 and ‘ncMax’ (the maximum number of constituents) is only set to 10. ncMax was therefore changed to 50 to accommodate any foreseeable increase in the number of tidal constituents the user might like.

It was also found in the /comm. and /utils makefiles that the variable 'AR' should equal '-xiar'.

At this stage a MPI build of the model executables could be run on a single core to completion providing tidal solutions; the next challenge was to run the executable across multiple cores.

A2.3.6 Challenges with running executable on more than one core (MPI)

Although not apparent when reading the makefiles, the model will not run, if you attempt to turn off the MPI using the _NOMPI flag. For even a single core computation the MPI flag must be left on. This is due to some of the MPI library paths being 'hard wired' in some of the routines (e.g. b_cast.F). It would be desirable to fix this issue in future developments of the model.

One key consideration is that many of the routines contained explicit pathways to mpif.h which are specific to the compute platform the build was being made on. These must be changed to the correct path to the MPI libraries on the local machine. If another port of the model is required one can identify all the routines and lines which need altering using grep -r mpif.h. If desired, these references could be removed by the pre-processor after suitable changes to the code.

Either ensure all pathways to libraries such as mpi.h and mpif.h in /comm and /src/par are the same (do not use two different versions of the libraries), or as is now the case rather than using explicit paths to the MPI libraries we write '-INCLUDE mpif.h' in the code and use '-I' statements in the makefiles. For the C programming language makefiles '-I.' was also required.

Additionally when running on multiple cores one must supply the PBS job scheduler with a job script which requests multiple cores. Examples of this are given in section A2.4.2 and the section A2.8.3 jobscripts.

Even using the extensive debugging options in section A2.3.7, locating the problem with the MPI was challenging and runs would go partway through the initialisation before giving a Segmentation Fault.

To address this recurrent and frustrating problem a number of MPI options were added to the jobscript to aid the debugging including 'MPI_COREDUMP ALL' and after the mpirun command 'MPI_UNBUFFERED_STDIO'. This gave a

more verbose output from each of the threads allowing identification of the source of the segmentation fault problem. The issue was three lines in the fwd_ts*.f programs themselves where parameter values were being broadcast and later attempts on the receiving core to unpack the value into the parameter variable caused an inevitable segmentation fault. By definition parameter values cannot be reset in Fortran so the broadcast of variables ‘a’, ‘eps_rewet’ and ‘ilglobe’ were removed.

After a number of successful production runs up to mid April 2013 the model began to fail giving MPI error messages relating to a failure to call MPI_Finalize. In the process of debugging this error a number of changes were made. A harmless divide by 0 in ZEQset_NPG.f was corrected. The internal tide code in fwd_ts_NPG.f was found to be being performed by all processors not just the root processor so an ‘if parrank=parroot’ logical loop was put around this code. Subroutine chdec in /src/fwd_ts/ts_subs.f was rewritten to use enddo statements rather than statement number ends to the loops. It was suspected that the MPI error was stemming from a race condition during the ‘tidy up’ phase of the model code for this reason a number of MPI barriers were inserted into the end of fwd_ts_NPG.f.

On analysis of the u and v transport fields outputted to the binary file /out/u0.it5 it was discovered that the v field had horizontal lines of anomalous values in the field with a vertical offset analogous to the domain decomposition boundaries. An error when reconstructing the v field from the results of each subdomain was found where anomalous ghost points were incorrectly getting saved over the correct values from the processor below. This required alteration of the /src/par/assemble_real3D.F routine. This was not an error in the transports in the model run itself but just the way in which they were saved into the model output.

A2.3.7 Debugging flags for makefiles

It is recognised that the debug flags are specific to the Intel 11.1 compiler (ifort) used on this platform however the flags used during debugging are listed below:

#DEBUGS = -check all -ftrapuv -warn all,nointerfaces,notruncated_source -debug all -mp1 -fpe0 -g –traceback

It is recommended to compile any new port of the model with these or analogous flags for an alternate compiler, prior to any production run with the model.

A2.4 Running the OTISmpi model

A2.4.1 Regular compilation of the model (post porting and debugging)

Section A2.3 includes an outline of a build of OTISmpi which produces no error messages at compile time. It is at this stage that the debug flags can be commented out and normal compilation of the model can be undertaken.

A further tip is that the contents of /bin, /comm and /utils only need compiling once, whereas for each /local/ instance of the model the compile must be repeated for each new model setup in order to incorporate the most recent model settings.

The user should note that by default all calculations are performed using single precision values. The benchmarking in section A2.6 indicates reproduction of the solutions with a high degree of accuracy, however the option is there to compute at double precision as is the norm in many scientific calculations. It is recommended that further understanding of exactly which parts of the calculation are done at which level of precision and the effect of this on the solution accuracy is explored.

Also note the /GLOB8npg/include/gridsize.h and /nc.h files which should be used to specify the grid size and number of tidal constituents required respectively. The tidal constituents to include are specified in the control file /prm/constituents.

A2.4.2 Running the executable: jobscripts and command line arguments

An example jobscript for a multi core run of the fwd_ts (excludes high latitude Arctic) and fwd_ts_NPG executable (fully global) on multiple cores can be found in section A2.8.3.

There is also a fwd_ts_fast executable which uses a more efficient time stepping routine; this has been run successfully but is not focused on in this Appendix as for this investigation the fully global model was required. The

compilation and execution of fwd_ts_fast is very similar to the fwd_ts or fwd_ts_NPG executables.

One must ensure that all the required input files are located in /DB for the executable to avoid runtime errors. Owing to dependencies of this nature the directory structure outlined in section A2.2 should be maintained with the executable always run in /local/*/exe so that relative paths are correct.

There are a variety of command line arguments which can be fed into the model via the mpirun command to alter the model setup from its defaults at runtime. Some of the important flags are outlined below:

-r <string> This argument names the run's output files with the name specified in the string. Can usefully be used to name the iteration of SAL the results relate to.

-T This argument overrides the default runtime (if there is one) for the particular executable and is specified in megaseconds (decimal values are accepted). 1 model day is 0.0864 megaseconds.

-H This argument specifies the period of the run over which harmonic analysis should be performed (from the end of the run backwards); it is also specified in megaseconds. The -H value must be less than the -T value and should allow for full model spin up (for the 4 consistent, 1/8 degree resolution setup we found spin up time to be approximately 30-40 days). The length of the harmonic analysis required will depend on the tidal constituents the model is forced with and analysed for according to the Rayleigh Criterion.

-t This flag applies a uniform 10% reduction to the horizontal pressure gradients (* 0.9) in the hydrodynamics in order to make an allowance for SAL. If this flag is not set the TOPEX/Poseidon derived SAL correction file /DB/otis_sal is picked up by default at runtime and used instead (this gives superior results for iteration 0 of the model if your run does not need to be independent of present day data however SAL iterations cause validation statistics to converge with uniform initialisation of SAL). The -t flag and then a filename specifies an alternative SAL correction file. It is the combination of the -t<input filename string> and the otis_salC program which facilitates the modified iterative scheme for SAL which is used in this investigation (Egbert et al., 2004). The process used is:

i) to run the 0th iteration of the model with just -t specified to initialise the SAL with the uniform correction.

ii) The tidal solution obtained (h0.it1) from iteration 0 it is then regridded from the distorted model grid to the regular grid (h0.it1_c) using the Matlab routine 'solNP4_it1.m' (adapted from solNP4.m from OSU) and then passed to the otis_salC program, run in the /out directory.

iii) otis_salC outputs the new SAL correction file (h0.it1_c_sal) which is used as input to the 1st iteration of the SAL scheme using the -t<filename> approach.

N.B. In order to obtain the best performance from the modified iterative scheme for SAL all subsequent iterations (1st iteration onwards) must also include the -C flag so that the uniform correction is applied as well as the additional correction file calculated by otis_salC (otherwise -t filename applies only the correction file which yields poor results).

iv) This process (i-iii) is then repeated for as many iterations of the SAL as the user required. With the 4 constituent fully global 50 day, 20 day harmonic analysis setup we used we found validation statistics to converge after 4 iterations of this scheme (5 model runs).

-I The internal wave (IW) parameterisations are activated using this flag. Here we use the Zaron and Egbert (2006) scheme which is selected using -I<negative value>. The negative value itself is a scaling factor for the IW drag applied; although various scaling factors were tested a value of -1 (no scaling) was used in this investigation. Additionally the -I flag can be used to select the Egbert IW parameterisation which takes the array of IW drag coefficients from a pre-processed observation based file.

-w This flag can be used to activate the drying-rewetting scheme including a non-linear continuity term. This scheme only allows wet cells defined when the model is at rest to dry and then rewet, there is no allowance for wetting and drying of the cells landward of the coastline which acts as a closed boundary (the grid generation routine removes all land topography). The model default is for drying-rewetting to be off, here we leave off as it seems to only affect the quality of the validation statistics very subtly and adds a factor of approximately one third to the run time.

-k This flag followed by a numeric value can be used to change the bed drag coefficient. By default this is 0.003. Here we keep the default value. Testing of sensitivity of the tidal solution to this value should be undertaken after all other frictional processes such as IW are included in the model setup

-h This flag allows the minimum model cells depth to be reset from the 2m default value (which we use in this study).

There are numerous other command line arguments which can be found in the first few hundred lines of /src/fwd_ts/ fwd_ts.f or /fwd_ts/fwd_ts_NPG.f. It does not appear to matter in which order the command line arguments (flags) are specified.

A2.4.3 Offline routines associated with OTISmpi

otis_salC: in directory /bin/ (but run from /local/*/exe) is used to generate a SAL correction file for the model as described in section A2.4.2.

mk_grid: in directory /bin/ (but run from /local/*/exe) generates grid of model bathymetry based on chosen source bathymetry which for benchmarking is the GEBCO One Minute dataset version 1 and for the production runs is version 2 of the same dataset. To get a fwd_ts_NPG grid which matches the OSU benchmark the latitude and longitude limits supplied must be -89.9375, 89.9375 and 0.125, 360 respectively (/include/gridsize.h must also be edited to 2880 x1440). It was this that was used to introduce SL changes to the bathymetry, there are multiple versions of this routine for adding uniform and non-uniform SL and imposing a fixed coastline or allowing coastal recession. For a guide to these new versions see /src/oo/Index_to_mk_grid_versions.f90. This routine originally generated depths to the nearest integer value in meters; this has been improved to allow decimal changes in SL which also required alterations to an associated routine ‘subs_nc.f90’. This routine also performs the land-ocean masking for the model. Making more than a 1/9 degree resolution model requires this program and any libraries to be compiled with mcmodel=medium as array memory requirements exceeds 2 Gbytes.

A2.4.4 Useful preprocessing and postprocessing Matlab routines from OSU

All Matlab routines should be run from the /local/*/exe directory with '../../../matlab' added to the Matlab path. Further details on the usage of these routines can be found in the comments and code in the mfile itself.

grd_in.m: reads binary file of depth data and the ocean mask produced by mk_grid

shgr.m: reads and plots the binary grid file in ../out

gridNP.m: regrids the regular bathmetric grid from mk_grid to the distorted grid required by the fwd_ts_NPG version of the model. It requires an even number of longitudinal grid points (fails with odd number of longitudinal points). This is also where the timestep of the model is set (2s for fully global model at 1/8 degree resolution as recommended by mk_grid, smaller for higher resolution)

solNP4.m: allows for regridding of the binary output files of the tidal solutions on the distorted grid to a regular grid binary file for further plotting or processing (various versions of this routine exist for different numbers of tidal constituents and different input file filenames for each of the SAL iterations).

h_in.m: reads in the tidal elevations from the binary model output for the constituent number specified in the argument list.

u.in: this routine obtains the u and v transports from the model output binaries. Each transport is specified as a complex number where the modulus is the total magnitude which must be divided by the model depth to obtain depth average current velocities.

hPlot.m: creates cotidal plots for the tidal elevations and phases of each of the modelled tidal constituents obtained by harmonic analysis during the model run. A GUI is used to select the h0.* file to plot. The plot created allows you to select which constituent to view, the Matlab variables then relate to that constituent and can be used to save constituent phase and amplitude for further processing.

A2.5 Optimisation of the OTISmpi model

A2.5.1 Justification

Initial single core compiler optimised runs showed the not fully global model (more efficient than the fully global model) to take 6 hours of wall time to run one model day at 1/8th degree resolution. Given that the benchmark run required 46 model days to be computed the requirement for speedup through improved parallelism was clear. The Nautilus cluster has a 12 hour wall clock limit so 2 days of the above setup was the maximum obtainable before running the model in parallel.

OTISmpi also currently lacks the ability to do model dumps and restarts, so a model run must go from rest to completion within the 12 hour limit. This further strengthened the requirement to look at the scalability of the code across numerous cores.

A2.5.2 Single core compiler optimisations

Again compiler flags are specific to the Intel11.1 compiler but for a point of reference the optimisation flags used in the makefiles are:

FFLAGS= ${DEBUGS} -fpp -xSSSE3 -O3 -ipo

-fpp has already been discussed in section A2.3.4

-xSSSE3 optimises the executable specifically for the instruction set on the chips in the Nautilus cluster.

-O3 turns on a number of optimisation functions which the compiler puts into place automatically.

-ipo this turns on interprocedural optimisation between files. It is a more aggressive level of optimisation than -ip and yields ~33% speedup.

These optimisations yielded a 2.6x speedup of the single core simulation. Although this is a substantial improvement much more speedup was required to run the model for order tens to hundreds of days considering the 12 hour wall time limit. With the optimisations above the fully global fwd_ts_NPG could now be run for 1 model day in 9 hours.

N.B. The –align flag was also tested but this was rejected as it made no run speed improvements. The fwd_ts_fast executable was found to run 32% faster than the other not fully global fwd_ts executable however as fully global runs are required for this investigation testing with fwd_ts and fwd_ts_fast was discontinued. The fully global fwd_ts_NPG domain setup is selected as it has no prescribed open boundaries and therefore can be used for SL perturbation experiments without present day data assimilation constraining the calculation.

A2.5.3 Scalability of the code to multiple cores, node under population

To obtain the necessary speedup a large number of scalability experiments were undertaken using OTISmpi's inbuilt horizontal domain decomposition.

As mentioned previously a compute node on Nautilus has 8 cores, with pairs of cores sharing 6MB of cache. Commonly, computationally expensive models (such as NEMO and MITgcm) are found to perform best by under populating the node i.e. running the code across 4 of the 8 processors so that there is no contention for memory bandwidth. For this reason various degrees of node under population were tested from using one core per node to a fully populated 8 core per node simulation.

The results are presented in the tables below; the maximum number of nodes (8 cores per node) is 32 for any one run. The simulation length is 1 day and includes both initialisation and closure phases of the model run saving the tidal solutions.

Program: fwd_ts_NPG Simulation: 1 day

Cores per node = 1

Active Cores	Wall time Mins	Wall time Secs	Total Secs	Speed up
1	540	6	32406	1.0
2	267	31	16051	2.0
4	133	20	8000	4.1
8	61	58	3718	8.7
16	24	45	1485	21.8
32	10	27	627	51.7

Cores per node = 2

Active Cores	Wall time Mins	Wall time Secs	Total Secs	Speed up
2	359	10	21550	1.5
4	178	10	10690	3.0
8	81	23	4883	6.6
16	31	2	1862	17.4
32	12	33	753	43.0
64	5	45	345	93.9

Cores per node=4					Cores per node=8				
Active Cores	Wall time Mins	Secs	Total Secs	Speed up	Active Cores	Wall time Mins	Secs	Total Secs	Speed up
4	346	27	20787	1.6	**8**	337	35	20255	1.6
8	171	44	10304	3.1	**16**	149	41	8981	3.6
16	79	6	4746	6.8	**32**	59	48	3588	9.0
32	28	29	1709	19.0	**64**	21	29	1289	25.1
64	11	49	709	45.7	**128**	9	40	580	55.9
128	5	42	342	94.8	**256**	3	44	224	144.7

These runs include all of the compiler optimisations outlined in section A2.5.2 (with 1 day on one core taking ~9hours or 540 mins). The results show that for this model node under population using 1, 2 or 4 cores per node does not yield the greatest speed up. The optimal speed up is obtained using fully populated nodes. This is shown by the 3m 44s result in the bottom right of the table using 256 cores.

It should be noted that initialisation and closure phases only have to be performed once for a run no matter whether it is one day or many days so one might expect slightly better than 3m 44s per day of the fully global executable when running multiple days. If one simply divides the wall time limit (12 hours) by 3m 44s you get an estimate of 192.9 model days being possible, however empirical tests show that in fact 242.2 days are possible in the walltime limit owing to the reduction of this initialisation and closure overhead per modelled day.

N.B. Additionally some alternative processor maps were tried in terms of the order in which the node is populated, however these yielded no significant speedup.

A2.5.4 Profiling

An open source, portable and MPI compatible profiler recommended by the Numerical Algorithms Group (NAG) called Scalasca was chosen. A standard test case of a 64 core (8 node), 1 day simulation was chosen as it uses a reasonable level of parallelism and provides sufficient runtime (~24 mins) to give robust profiling statistics whilst maintaining manageable turnaround times. The profiling showed:

- The cost of the MPI calls in the program was an acceptable proportion of the total runtime, given the speed up it enables, at around 7%.

- The majority of the rest of the time, ~85%, is spent in the timestepping routine itself (rather than the subroutines it calls).

- The MPI overhead increases as the number of cores used is increased but not to the point of inefficiency.

These results suggest that paying special attention to optimising the 500 line timestepping routine (/src/fwd_ts/tstep_fast.f) may yield some worthwhile benefits in future work. This would require line level profiling of this routine, which SCALASCA does not yet automatically provide.

A2.5.5 Present run duration capabilities and the PBS job scheduler

The table below shows the estimated number of days for runs taking into account the restrictions of the general queue on Nautilus. Empirical tests show these values represent conservative estimates for the fully global model (fwd_ts_NPG).

Program: fwd_ts_NPG (8 cores per node)

Day (07:00-18:00)

Queue Name	Time Allowed (mins)	No. of Runs		Nodes	Max Days Per Run	Cumulative Days
general_s	120	1	OR	32	32.1	32.1
	120	2	OR	16	12.4	24.8
	120	4		8	5.6	22.3
general_t	720	1	AND	8	33.5	33.5
	720	1		4	12.0	12.0
general_b	720	4	OR	2	4.8	19.2
	720	8		1	2.1	17.1

Night (18:00-07:00)

Queue Name	Time Allowed (mins)	No. of Runs		Nodes	Max Days Per Run	Cumulative Days
np_general_l	720	1	OR	32	192.9	192.9
	720	2	OR	16	74.5	149.0
	720	4		8	33.5	134.1
(and those above)						

Rather than running for order 200 days which was not necessary for the spin up of the model or harmonic analysis the speedup was used to increase the complexity of the model setup. For example the inclusion of additional tidal constituents was found to increase the runtime linearly.

A2.6 Verifying the port with results- Benchmarking

A2.6.1 Benchmark tidal solutions and run setup

OSU kindly provided two sets of OTISmpi runs (with solutions) enabling us to verify the tidal solutions from our runs of OTISmpi on the Nautilus cluster.

The set of these which were concentrated on were a 46.3 day run of fwd_ts at 1/8 degree resolution with a 23.15 day harmonic analysis, and a 10.42 day run of fwd_ts_NPG with a 3.48 day harmonic analysis (for reference these are Nautilus runs /fibre /055 and /056 respectively and OSU runs /working/OTISmpi_bench). The model was forced with the M_2 and K_1 constituents and analysed for the same two constituents.

N.B. The runs performed at OSU were always on 4 cores and sometimes took ~60hours of wall time to run. The other benchmark runs were shorter run lengths of ~5 days and were not extensively compared.

A2.6.2 Online Energetics (Core no. Dependant)

In addition to comparing the tidal solutions themselves it was desirable to compare the online energy statistics which the model prints out during the run. These are kinetic, potential and total energy. This has not been possible as the values are not truly global, they in fact only calculate the energy values for the first processor (proc. 0). This is less than ideal as the Nautilus benchmarking runs use 64 cores and the OSU ones only 4, the area of ocean is therefore different for proc. 0 and the energy statistics are not comparable. The fact that the energy statistics are only for one small part of the domain also makes model spin up hard to evaluate.

One other very small core number dependence became clear when running the not fully global fwd_ts executable. The phase lines in tidal solutions in the high latitude Artic Ocean (close to the open boundary) move slightly between different numbers of cores. This suggests there may be a small issue with how the open boundary is prescribed on different numbers of cores.

A2.6.3 Excessive amplitudes in ported model

It was discovered that the amplitudes in the fwd_ts_fast and fwd_ts_NPG model runs were approximately double what they should be when compared with the

benchmark tidal solutions from OSU. This problem was not found in the fwd_ts executable which qualitatively replicated the OSU benchmark tidal solutions with a good degree of accuracy.

The problem was therefore something common to fwd_ts_fast and fwd_ts_NPG. Using the sdiff command all of the Fortran and C code was compared between the Nautilus and OSU benchmark versions. This showed the changes as described in previous sections only with no apparent anomalies. Tests were also made to see if this was a core number dependency problem which it was not.

It was found that the lack of a default logical value for a variable 'l_SalC' in the fwd_ts_fast and fwd_ts_NPG codes meant that the SAL correction was not properly applied (beta=0.9). Once a default value of false was put in the correction was implemented in the same way as in the benchmark runs (beta=1.0) and the tidal solutions were qualitatively identical to the benchmarks for these executables.

Problems of this nature encouraged us to put more printouts in the model initialisation stage of key input parameters, such as beta. This remains an ongoing policy as new key input parameters are discovered.

A2.6.4 Degree of tidal solution reproducibility

Once the problems discussed in section A2.6.3 were dealt with direct quantitative comparison was made between the Nautilus and the OSU tidal solutions.

To find the largest differences between the Nautilus and benchmark tidal solutions the differences between the amplitudes for M_2 and K_1 tidal components were taken and the maximum and minimum differences calculated.

For the fwd_ts tidal solutions the M_2 amplitude difference range was -0.0493m to 0.1289m and for K_1 -0.0075m to 0.0060m.

For the fwd_ts_NPG tidal solutions the M_2 amplitude difference range was -0.00013m to 0.00005m and for K_1 -0.00016m to 0.00018m.

The fwd_ts results are slightly less accurate owing to differences near the Arctic Ocean open boundary as mentioned in section A2.6.2. The fwd_ts_NPG results are very close to the OSU benchmark solution and given that the level of precision which we are interested in this study are order centimetres to meters this is seen as a very acceptable replication of the benchmark solutions. Various reasons may exist for the small remaining differences in fwd_ts_NPG such as differing chips between machines, differing compilers and levels of optimisation.

a) OSU, fwd_ts_NPG, M_2 tide, 69hrs b) Nautilus, fwd_ts_NPG, M_2 tide, 2.5hrs

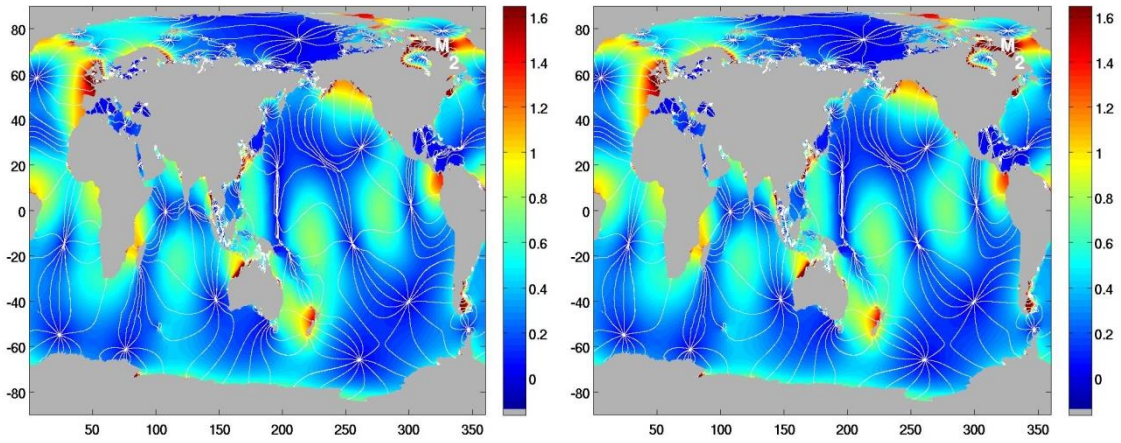

A2.7 Notes on References

There are a number of reports, manuals and published papers that relate in some way to the forward Global Tidal Model OTISmpi. Mostly this literature is specific to the OTIS or OTISoo, the data assimilative tidal model and therefore has not been referenced in this Appendix to avoid confusion. Often nomenclature between the OTISmpi and OTIS is shared in terms of routines and compilation steps so use of the OTIS documentation to aid in the use of OTISmpi should be treated with a degree of caution. The main paper relating to OTISmpi is Egbert et al. (2004) and details of the internal wave drag parameterisation used in our production runs can be found in Zaron and Egbert (2006).

A2.8 Supplementary Material

A2.8.1 Documentation received with the model

Comments on usage of OTISmpi (05.30.2011) by Lana Erofeeva

1. TO COMPILE the package
Since OTISmpi consist of different parts, written by different persons,
compilation is done in 4 steps with separate makefiles
 - in OTISmpi/bin do
make linux.all
- in OTISmpi/comm do
make all
- in OTISmpi/utils do
make all
This will provide set of executables and libraries, which do not need
to be recompiled for every local area
- in OTISmpi/local/GLOB8/exe try
make mpi.fwd_ts
make mpi.fwd_ts_fast
make mpi.fwd_ts_NPG
This will creat set of mpi executables for a particular area, i.e. GLOB8

Try to compile and run fwd_ts_fast or fwd_ts

2. To create new local area set_up
from OTISmpi do:
crd <new_area_name>
cd local/<new_area_name>
NOTE! Further paths are given relative OTISmpi/local/<new_area_name>/exe
Then run
mk_grid
This will create bathymetry grid in ../prm/grid
Please, see online OTISoo manual on details
After this you need to edit ../include/gridsize.h for n,m
from mk_grid prompt
Edit ../prm/constituents for desired constituents. Format of the files
should be (old style, not supported in OTISoo)
<number of constituents>
constituent 1
constituent 2
...
For example, if you need 2 constituents m2 and k1, the file content
will be:
2
m2
k1
Edit ../include/nc.h for the number of constituents
Then make executables for this particular area, i.e.
make mpi.fwd_ts
make mpi.fwd_ts_fast
make mpi.fwd_ts_NPG

Make open boundary by running
ob_eval
File ../prm/obc will be created
Try to run fwd_ts(_fast) using one of scripts js1, js_SAL,

which might need to be modified for your local environment
/compiler first.

3. Rotated coordinates
First rotated grid should be created by running matlab script
gridNP from OTISmpi/local/<area_name>/exe
Obviously no OBC are needed for this case.
Try to run fwd_ts_NPG
Smaller step might be needed

++
++++++++++
++++ Old comments
++
Lana, March 2009

Merging OTISmpi and Gary's iterSAL procedure:

DONE:

1. MPI version of Gary's original code in
/home/gauss/egbert/project/BILLS/GLOB8/FWD_TS

I kept ALL GARY's command line options.
He needs to explain them himself
(especially when they require some extra input
files).

To compile for MPI go to OTISmpi/local/GLOB8/exe and do
make mpi.fwd_ts_fast

If grid size and # of constituent changed
(in OTISmpi/local/GLOB8/include/gridsize.h and nc.h)
fwd_ts_fast needs to be recompiled
For now everything is compiled for GLOB8 case and
2 constituents m2 and k1 (see control file
../prm/constituents)

Source codes for fwd_ts_fast are in
OTISmpi/src/fwd_ts

2. Simple script js_SAL edited to run on one machine
(though on multiple processors) and in one directory.
Outputs are in OTISmpi/local/GLOB8/out

A2.8.2 Nautilus Makefiles

A2.8.2.1 /bin/Makefile

```
####    Lana's makefile. Last modified 22.09.2011 (MDP)#################
# EXAMPLES of  usage:                                   #
#       1. To make an executable on Sun Station type:           #
```

```
#                   make <name>                          #
#                     OR                               #
#                   make ss.<name>                       #
#                                                      #
#      2. To make an executable on linux, type:                  #
#                   make linux.<name>                    #
#                                                      #
#  CHECK YOUR LIBRARIES PATHS AND COMPILER OPTIIONS!!!             #
########################################################################
###########
############## COMMON DEFINITIONS
#####################################
########################################################################
###########
#########
ARCH = $(uname -s)
#ARCH = $(shell uname -s)
#echo $(ARCH)
# Edited version of original loops
########################################################################
###########
ifeq ($(ARCH),Linux)
# Intel 11.1 Compiler
endif
# Jeffs q-gcm xSSE2.ifort11.1 LAPACK and BLAS stuff (edite
#
FC = ifort
# NetCDF:
# -------
NCDIR = /sata/working/jeff/packages/netcdf/netcdf-3.6.3/altix_opt
#NCDIR = /sata/working/jeff/packages/netcdf/netcdf-
3.6.3/altix/intel11.1/mcmedium
NCLIB = ${NCDIR}/lib
NCINCLUDE = ${NCDIR}/include
netcdfLIB= -L$(NCLIB) -lnetcdf
#
# LAPACK/BLAS:
# ------------
# Access to LAPACK/BLAS via the Intel MKL library:
# For workstations, architecture = Intel 64 -> use /lib/em64t
# For Q-GCM, MKL function domains required = BLAS, LAPACK
# MKL now has layered model concept: need to specify Interface, Threading,
#                            Computation and Run-time library
# version for OpenMP parallelism:
# To ensure efficiency and safe parallelism, we want
# static linking of a thread-safe version of the library
# See http://software.intel.com/en-us/articles/intel-mkl-link-line-advisor/
MKLDIR = /sw/Intel/fce/11.1.072/mkl
#MKLDIR = /sw/Intel/fce/10.1.021/mkl
MKLPATH = ${MKLDIR}/lib/em64t
MKLINCLUDE = ${MKLDIR}/include
# START OVER of the line below
```

```
linuxLIB = -L${MKLPATH} -I${MKLINCLUDE} -Wl,--start-group
${MKLPATH}/libmkl_intel_lp64.a ${MKLPATH}/libmkl_sequential.a
${MKLPATH}/libmkl_core.a ${MKLPATH}/libmkl_blacs_intelmpi_lp64.a -Wl,--end-
group -lpthread
# CHECK THE NEW LINE BELOW MIGHT BE MUNGED START OVER (just noticed
uses mixture of ( and { .... error? jeff= {
#linuxLIB = -L$(MKLPATH) -I${MKLINCLUDE} -Wl,--start-group -lmkl_intel_lp64 -
lmkl_sequential -lmkl_core -lmkl_blacs_intelmpi_lp64 -Wl,--end-group -lpthread
# Suggested options for MPI:   !!    -L$(MKLROOT)/lib/intel64 -
lmkl_scalapack_lp64  -Wl,--start-group -lmkl_intel_lp64 -lmkl_sequential -
lmkl_core -lmkl_blacs_intelmpi_lp64 -Wl,--end-group -lpthread
#linuxLIB = -L${MKLPATH} -I${MKLINCLUDE} -Wl,--start-group
${MKLPATH}/libmkl_intel_lp64.a ${MKLPATH}/libmkl_sequential.a
${MKLPATH}/libmkl_core.a -Wl,--end-group -lpthread
# version for single-thread testing:
# For the sequential version, no RTL should be needed, but the
# POSIX thread library (pthread) will be needed for thread-safety
# must provide something here
# Alternative workstation access to LAPACK/BLAS using the NAG library
# LAPACK = -L${NAGDIR} -lnag_nag

# Original LAPACK and BLAS stuff
#ssLIB=
# ssLIB= -lm /usr/local/lib/liblapack.a /usr/local/lib/libblas.a \
#       /usr/lang/lib/libF77.so

#linuxLIB=-llapack -lblas
srcDIR= ../src/oo/
srcSAL= ../src/sal/
# Original setup from Lana (note ssLIB is not used in this makefile)
#ssLIB=
##ssLIB= -lm /usr/local/lib/liblapack.a /usr/local/lib/libblas.a \
#       /usr/lang/lib/libF77.so
#linuxLIB=-llapack -lblas
#netcdfLIB=-lnetcdf
#srcDIR= ../src/oo/
#srcSAL= ../src/sal/
######## SOURCE FILES
#####################################################
ob_eval_SRC=$(srcDIR)ob_eval.f90 $(srcDIR)Constit.f90
$(srcDIR)def_sparsedf.f90 \
        $(srcDIR)dc_subs.f90 $(srcDIR)interp_driver.f90  \
        $(srcDIR)grid_subs.f90 $(srcDIR)LTEco.f90
ob_eval_obj = ob_eval.o Constit.o def_sparsedf.o dc_subs.o interp_driver.o \
             grid_subs.o LTEco.o
ob_eval_INC = ../include/constit_f90.h ../include/constants_f90.h
../include/derived_types.h
#############################################################
############
mk_grid_SRC=$(srcDIR)mk_grid.f90 $(srcDIR)subs_nc.f90
mk_grid_obj=mk_grid.o subs_nc.o
mk_grid_INC=-I$(NCINCLUDE)
```

```
#############################################################
###############
Fwd_fac_SRC =  $(srcDIR)Fwd_fac.f90 $(srcDIR)Sfact.f90 $(srcDIR)CDG.f90 \
        $(srcDIR)LTEco.f90 $(srcDIR)ATGF.f90 $(srcDIR)interp_driver.f90\
        $(srcDIR)z_uv.f90 $(srcDIR)Constit.f90 $(srcDIR)def_sparsedf.f90\
        $(srcDIR)makeE.f90 $(srcDIR)Glob_case.f90 $(srcDIR)ZEQset_NPG.f90\
        $(srcDIR)dc_param_subs.f90 $(srcDIR)SAL_set.f90
$(srcDIR)dc_subs.f90\
         $(srcDIR)grid_subs.f90
Fwd_fac_obj = Fwd_fac.o Sfact.o CDG.o Constit.o interp_driver.o\
       LTEco.o ATGF.o z_uv.o makeE.o ZEQset_NPG.o\
       Glob_case.o dc_param_subs.o SAL_set.o def_sparsedf.o  \
       dc_subs.o grid_subs.o
Fwd_fac_INC = ../include/constit_f90.h ../include/constants_f90.h\
            ../include/derived_types.h
#############################################################
###############
Fwd_fac_b_SRC =  $(srcDIR)Fwd_fac_b.f90 $(srcDIR)Sfact_b.f90
$(srcDIR)CDG.f90 \
        $(srcDIR)LTEco.f90 $(srcDIR)ATGF.f90 $(srcDIR)interp_driver.f90\
        $(srcDIR)z_uv.f90 $(srcDIR)Constit.f90 $(srcDIR)def_sparsedf.f90\
        $(srcDIR)makeE.f90 $(srcDIR)Glob_case_b.f90
$(srcDIR)ZEQset_NPG.f90\
        $(srcDIR)dc_param_subs.f90 $(srcDIR)SAL_set.f90
$(srcDIR)dc_subs.f90\
        $(srcDIR)BDS.f90 $(srcDIR)BDSc.f90 $(srcDIR)spMatProd.f90 \
        $(srcDIR)BDS_util.f90  $(srcDIR)grid_subs.f90
Fwd_fac_b_obj = Fwd_fac_b.o Sfact_b.o CDG.o Constit.o def_sparsedf.o\
       LTEco.o interp_driver.o ATGF.o z_uv.o makeE.o dc_subs.o \
       Glob_case_b.o dc_param_subs.o SAL_set.o grid_subs.o \
       BDS.o BDSc.o spMatProd.o BDS_util.o  ZEQset_NPG.o
Fwd_fac_b_INC = ../include/constit_f90.h ../include/constants_f90.h\
            ../include/derived_types.h
#############################################################
###############
mk_g_ll_SRC=$(srcDIR)mk_g_ll.f90 $(srcDIR)grid_subs.f90
$(srcDIR)dc_subs.f90 \
          $(srcDIR)Constit.f90
mk_g_ll_INC=../include/constants_f90.h ../include/derived_types.h
mk_g_ll_obj= mk_g_ll.o grid_subs.o dc_subs.o  Constit.o
#############################################################
################
otis_salC_SRC=$(srcSAL)otis_salC.f90 $(srcSAL)wave_sal.f90
$(srcSAL)spherpak3.2.f
otis_salC_INC=
otis_salC_obj= otis_salC.o wave_sal.o spherpak3.2.o
#############################################################
###############
otis_load_SRC=$(srcSAL)otis_load.f90 $(srcSAL)wave_load.f90
$(srcSAL)spherpak3.2.f
otis_load_INC=
otis_load_obj= otis_load.o wave_load.o spherpak3.2.o
```

```
#################################################################
###############
# INSTRUCTIONS FOR MAKING THE EXECUTABLES:
#################################################################
################
linux.Fwd_fac: $(Fwd_fac_SRC) $(Fwd_fac_INC)
	make linux90 "SI=Fwd_fac"
#-----------------------------------------------------------------------
linux.Fwd_fac_b: $(Fwd_fac_b_SRC) $(Fwd_fac_b_INC)
	make linux90 "SI=Fwd_fac_b"
#-----------------------------------------------------------------------
linux.ob_eval: $(ob_eval_SRC) $(ob_eval_INC)
	make linux90 "SI=ob_eval"
#-----------------------------------------------------------------------
linux.mk_grid: $(mk_grid_SRC) $(mk_grid_INC)
	make linuxnc "SI=mk_grid" "INC=$(mk_grid_INC)"
#-----------------------------------------------------------------------
linux.mk_g_ll: $(mk_g_ll_SRC) $(mk_g_ll_INC)
	make linux90 "SI=mk_g_ll"
#-----------------------------------------------------------------------
linux.otis_salC: $(otis_salC_SRC)
	make linuxs "SI=otis_salC"
#-----------------------------------------------------------------------
linux.otis_load: $(otis_load_SRC)
	make linuxs "SI=otis_salC"
#	 Jeff swapped as it seemed like an error
#	 make linuxs "SI=otis_load"
#-----------------------------------------------------------------------
linux.all:
	make linux90 "SI=Fwd_fac"
	make linux90 "SI=Fwd_fac_b"
	make linux90 "SI=mk_g_ll"
	make linux90 "SI=ob_eval"
	make linuxnc "SI=mk_grid"
	make linuxs "SI=otis_salC"
	make linuxs "SI=otis_load"
#########  RULES
#############################################################
.SUFFIXES :
.SUFFIXES : .o .f90 .f

F90SRC = $(SI)_SRC
INC = $(SI)_INC
obj = $($(SI)_obj)

.f90.o:
	@ln -f -s $< $(<F)
	$(FC) -c $(FLAGS) $(<F)
######### EXE
#################################################################
exelinux:  $(SRC) $(OBJ) $($(INC)) makefile
	$(FC) $(FLAGS) -o $(EXE) $(obj) $(linuxLIB)
	@rm *.f*
```

```
	@rm *.o
exelinuxnc:  $(SRC) $(OBJ) $($(INC)) makefile
	$(FC) $(FLAGS) -o $(EXE) $(obj) $(linuxLIB) $(netcdfLIB)
	@rm *.f*
	@rm *.o
exelinuxs:  $(SRC) $(OBJ) $($(INC)) makefile
	$(FC) -c $(FLAGS) ../src/sal/spherpak3.2.f
	$(FC) $(FLAGS) -o $(EXE) $(obj)
	@rm *.f*
	@rm *.o
#################################################################
#############
#### Linux targets
linux90:
	@$(MAKE) exelinux "EXE=$(SI)" "FC=ifort " "SRC=$($(F90SRC))" \
	"OBJ=$($(F90SRC):.f90=.o)" \
	"FLAGS= -static -fpp -xSSSE3 -O3 -ipo"
#	 "FLAGS= -static -fpp -xSSSE3 -O3 -ipo -check all -ftrapuv -warn
all,nointerfaces,notruncated_source -debug all -mp1 -fpe0 -g -traceback"
#	 "FLAGS= -static -fpp -xSSSE3 -O3 -ip"
#	 "FLAGS= -static -fpp -xSSSE3"
#	 "FLAGS= -static -fpp -xSSSE3 -mcmodel=medium"
#	 Note forgot to give -mcmodel=medium the -shared-intel option
##	  "FLAGS= -fast -Mbyteswapio -Mlarge_arrays -mcmodel=medium"
linuxnc:
	@$(MAKE) exelinuxnc "EXE=$(SI)" "FC=ifort" "SRC=$($(F90SRC))" \
	"OBJ=$($(F90SRC):.f90=.o)" "INC=$($(INC))" \
	"FLAGS= -static -fpp -xSSSE3 -O3 -ipo -I$(NCINCLUDE)"
#	 "FLAGS= -static -fpp -xSSSE3 -O3 -ipo -check all -ftrapuv -warn
all,nointerfaces,notruncated_source -debug all -mp1 -fpe0 -g -traceback -
I$(NCINCLUDE)"
#	 "FLAGS= -static -fpp -xSSSE3 -O3 -ip -I$(NCINCLUDE)"
#	 "FLAGS= -static -fpp -xSSSE3 -I$(NCINCLUDE)"
#	 "FLAGS= -static -fpp -xSSSE3 -mcmodel=medium -I$(NCINCLUDE)"
#	 Note forgot to give -mcmodel=medium the -shared-intel option
linuxs:
	@$(MAKE) exelinuxs "EXE=$(SI)" "FC=ifort" "SRC=$($(F90SRC))" \
	"OBJ=$($(F90SRC):.f90=.o)" \
	"FLAGS= -static -fpp -xSSSE3 -O3 -ipo"
#	 "FLAGS= -static -fpp -xSSSE3 -O3 -ipo -check all -ftrapuv -warn
all,nointerfaces,notruncated_source -debug all -mp1 -fpe0 -g -traceback"
#	 "FLAGS= -static -fpp -xSSSE3 -O3 -ip"
#	 "FLAGS= -static -fpp -xSSSE3"
## These flags below may work for make linux.otis_salC but will not work for
make linux.otis_load
##	 "FLAGS= -fpp -std90 -xSSE2 -fast -Mbyteswapio -Mlarge_arrays -
mcmodel=medium"
#################################################################
#############
```

A2.8.2.2) /comm./makefile

```
.SUFFIXES: .c .o

ARCH=$(shell uname -s)

#PREC = _DBL
PREC = _SGL

MPI = _MPI
#MPI = _NOMPI

# LAM flag is deprecated in NewComm.._SGL and .._DBL routines.
# f2c and c2f conversion is part of the MPI standard, so it should
# not be necessary to have a special flag for it.
#LAM = LAM_MPI
#LAM = NOLAM_MPI

rect_objs = Vertex.o RectGraph.o NewRectComm$(PREC).o

ifeq ($(ARCH),SunOS)
  CC=cc
  AR   = ar -r -v
  RANLIB= ranlib
  cdefs  = -I. -D$(ARCH) -D$(MPI) -D$(PREC)
  copt   = -I. -xO5 -fsimple=2 -native -dalign -xarch=v8 -xrestrict -Xa -mt
  libs   =
endif

ifeq ($(ARCH),AIX)
   ifeq ($(MPI),_MPI)
      CC   = mpcc
   else
      CC   = cc
   endif
   AR     = ar -r -v
   RANLIB = ranlib
   cdefs  = -I. -D$(ARCH) -D$(MPI) -D$(PREC)
   copt   = -O3 -qstrict -qarch=pwr4 -qalias=allp -qlanglvl=ansi
   libs   =
endif

ifeq ($(ARCH),Darwin)
   ifeq ($(MPI),_MPI)
      CC   = mpicc
#      MPI_INCL_PATH =
#      MPI_LIB = MacMPI_X.c
/System/Library/Frameworks/Carbon.framework/Carbon -I \
#       /Developer/Headers/FlatCarbon
   else
      CC   = cc
      MPI_INCL_PATH =
      MPI_LIB =
   endif
   AR     = ar -r -v
```

```
  RANLIB = ranlib
  cdefs  = -I. -D$(ARCH) -D$(MPI) -D$(PREC)
  copt   = -g -O3 -arch=g5 -ansi
  libs   = $(MPI_LIB)
endif

ifeq ($(ARCH),Linux)
#    CC    = mpicc
   CC    = icc
#   CC    = gcc
#   CC    = ifort
#   CC    = mpif90
  AR    = xiar -crv
#   AR    = ar -crv
  RANLIB= ranlib
  cdefs = -D$(ARCH) -I. -D$(MPI)
#   copt  = -O2 -I. -pgf90libs
#    DEBUGS = -check-uninit -ftrapuv -debug all -mp1 -g -traceback
#    copt  = ${DEBUGS}  -xT -O3 -ipo -I.
   copt  = ${DEBUGS}  -xSSSE3 -O3 -ipo -I.
#    copt  = ${DEBUGS}  -xSSSE3 -O3 -ip -I.
#    copt  = ${DEBUGS}  -xSSSE3 -O2  -I.
#    copt  = ${DEBUGS}  -xSSSE3 -mcmodel=medium -shared-intel -O2  -I.
#    copt  = ${DEBUGS} -O2 -I.
#     libs = -L/usr/mpi/mvapich-0.9.9/intel/lib/shared -lmpi
   libs = -lmpi
#    libs =
endif

ifeq ($(ARCH),IRIX64)
  CC   = cc
  AR   = ar vru
  RANLIB= ls
  cdefs= -D$(ARCH) -I.
  copt = -O3 -64 -mips4
  libs =
endif

all: gentorus libcomm$(MPI)$(PREC).a

###
###   Rectangle objects
###

Vertex.o: Vertex.c
	$(CC) $(copt) $(cdefs) Vertex.c -c

RectVertex.o: RectVertex.c
	$(CC) $(copt) $(cdefs) RectVertex.c -c

RectGraph.o: RectGraph.c
	$(CC) $(copt) $(cdefs) RectGraph.c -c
```

```
NewRectComm$(PREC).o: NewRectComm$(PREC).c
	$(CC) $(copt) $(cdefs) NewRectComm$(PREC).c -c

gentorus.o: gentorus.c
	$(CC) $(copt) $(cdefs) gentorus.c -c

###
###   Linking rules
###

gentorus: $(rect_objs) gentorus.o
	$(CC) $(copt) $(rect_objs) gentorus.o $(libs) -o gentorus $(TARGET)

libcomm$(MPI)$(PREC).a: $(rect_objs)
	$(AR) libcomm$(MPI)$(PREC).a $(rect_objs)
	$(RANLIB) libcomm$(MPI)$(PREC).a

clean:
	rm -f *.o gentorus libcomm*.a
```

A2.8.2.3) /utils/makefile

```
ifeq ($(ARCH),SunOS)
  CC   = cc
  AR   = ar -r -v
  RANLIB= ranlib
  cdefs= -D$(ARCH) -I.
  copt = -xO5 -fast -xarch=v8plusa -xchip=ultra2 -dalign -xrestrict=%all -
xunroll=4
  libs =
endif

ifeq ($(ARCH),Darwin)
  CC   = cc
  AR   = ar -r -v
  RANLIB= ranlib
  cdefs= -D$(ARCH) -D_NOMPI
  copt = -O2 -arch=ppc -I.
  libs =
endif

ifeq ($(ARCH),AIX)
  CC   = cc
  AR   = ar -r -v
  RANLIB= ranlib
  cdefs= -D$(ARCH) -D_MPI
  copt = -O2 -qarch=pwr3 -I.
  libs =
endif

ifeq ($(ARCH),Linux)
  CC    = icc
```

```
#   CC    = gcc
#   CC    = pgf90
  AR    = xiar -crv
#   AR    = ar -crv
  RANLIB= ranlib
  cdefs = -D$(ARCH)
#   DEBUGS = -check-uninit -ftrapuv -debug all -mp1 -g -traceback
  copt  = ${DEBUGS}  -xSSSE3 -O3 -ipo -I.
#   copt = -xSSSE3 -O3 -ipo -I.
#   copt = -xSSSE3 -O3 -ip -I.
#   copt = -xSSSE3 -O2  -I.
#    copt  = -O2 -I.
#   copt  = -O2 -I.
#   copt  = -O2 -I. -Mnomain
  libs =
endif

ifeq ($(ARCH),IRIX64)
  CC   = cc
  AR   = ar vru
  RANLIB= ls
  cdefs= -D$(ARCH) -I.
  copt = -O3 -64 -mips4
  libs =
endif

all: libutils.a nbits

timer.o: timer.c
	$(CC) $(copt) $(cdefs) timer.c -c

nbits.o: nbits.c
	$(CC) $(copt) $(cdefs) nbits.c -c

testnbits.o: testnbits.c
	$(CC) $(copt) $(cdefs) testnbits.c -c

precision.o: precision.c
	$(CC) $(copt) $(cdefs) precision.c -c

#
# Build unit testers and the library
#

nbits: $(objs) testnbits.o
	$(CC) $(copt) $(objs) testnbits.o $(libs) -o nbits

libutils.a: $(objs)
	$(AR) ./libutils.a $(objs)
	$(RANLIB) ./libutils.a

clean:
	rm -f *.o libutils.a nbits
```

A2.8.2.4) /local/GLOB8npg/exe/makefile

```
PREC=_SGL
#PREC=_DBL
MPI=_MPI
#MPI=_NOMPI
ARCH=$(shell uname -s)

#FFLAGS= -fpp -xSSSE3 -mcmodel=medium -shared-intel
#FFLAGS= -fpp -xSSE2 -mcmodel=medium
#FFLAGS= -static -fpp -xSSE2 -mcmodel=medium
#FFLAGS= -static -fpp -noform-main -nodefaultlibs -xSSE2 -mcmodel=medium
#FFLAGS= -static -fpp -xSSE2 -mcmodel=medium
#FFLAGS= -static -fpp -std90 -xSSE2 -mcmodel=medium
#FFLAGS = -O3 -fast -mcmodel=medium
#FFLAGS = -O -fast -Mbyteswapio -Mlarge_arrays -mcmodel=medium
#DEBUGS = -check all -ftrapuv -warn all,nointerfaces,notruncated_source -
debug all -mp1 -fpe0 -g -traceback
#FFLAGS= ${DEBUGS} -fpp -xSSSE3 -mcmodel=medium -shared-intel
#FFLAGS= ${DEBUGS} -fpp -xSSSE3
FFLAGS= ${DEBUGS} -fpp -xSSSE3 -O3 -ipo
CPPFLAGS = -D$(MPI) -DLINUX -D$(PREC) -D_64BIT
CFT = ifort

##############################################################
########
#mpiLIB= -L../../../utils -lutils -L../../../comm/ -lcomm_MPI$(PREC) -Mmpi
mpiLIB= -L../../../comm/ -lcomm_MPI$(PREC) -lmpi

ftDIR= ../../../src/fwd_ts/
pdir=../../../src/par/

fwd_SRC = tstep.f ts_subs.f constit.f checklim.f inner.f interp_rpx.f
BSI_weights.f

fwd_ts_SRC = main_fwd_ts.f fwd_ts.f lteco.f atgf.f SALset.f $(fwd_SRC)

fwd_ts_NPG_SRC = main_fwd_ts_NPG.f fwd_ts_NPG.f lteco_NPG.f ZEQset_NPG.f\
            SALset_NPG.f $(fwd_fast_SRC)

fwd_fast_SRC = tstep_fast.f ts_subs.f constit.f checklim.f inner.f interp_rpx.f
BSI_weights.f

fwd_ts_fast_SRC = main_fwd_ts.f fwd_ts_fast.f lteco_fast.f atgf.f SALset.f
$(fwd_fast_SRC)

par_SRC = kinds.F parallel_mod.F rect_comm_mod.F \
      domain_mod.F thread_mod.F assemble_real3d.F \
      distribute.F BHexchange.F b_cast.F
##############################################################
##############
```

```
 SRCS = $(fwd_ts_SRC) $(par_SRC)
 fwd_ts_OBJ =$(fwd_ts_SRC:.f=.o)
 fwd_ts_NPG_OBJ =$(fwd_ts_NPG_SRC:.f=.o)
 fwd_ts_fast_OBJ =$(fwd_ts_fast_SRC:.f=.o)
 par_OBJ = $(par_SRC:.F=.o)

.SUFFIXES: .o .f .F
.F.o:
	$(CFT) -c $(FFLAGS) $(CPPFLAGS) $(mpiFLAGS) $*.F
.f.o:
	$(CFT)  -c $(FFLAGS) $*.f

mpi.fwd_ts:
	make LNK
	make EXE
	make clean
mpi.fwd_ts_NPG:
	make LNK
	make EXE_NPG
	make clean
mpi.fwd_ts_fast:
	make LNK
	make EXEfast
	make clean
EXE: $(par_OBJ) $(fwd_ts_OBJ)
	$(CFT) -o fwd_ts $(FFLAGS) $(fwd_ts_OBJ) $(par_OBJ) $(mpiLIB)

EXEfast: $(par_OBJ) $(fwd_ts_fast_OBJ)
	$(CFT) -o fwd_ts_fast $(FFLAGS) $(fwd_ts_fast_OBJ) $(par_OBJ) $(mpiLIB)

EXE_NPG: $(par_OBJ) $(fwd_ts_NPG_OBJ)
	$(CFT) -o fwd_ts_NPG $(FFLAGS) $(fwd_ts_NPG_OBJ) $(par_OBJ) $(mpiLIB)

LNK:
	@ln -f -s $(pdir)/*.F .
	@ln -f -s $(ftDIR)/*.f .
clean:
	@rm *.f
	@rm *.F
	@rm *.o
#	 @rm *.mod
#	 @rm *genmod*
```

A2.8.3 Nautilus (PBS scheduler) jobscripts

/GLOB8/exe/ (near global) jobscript for benchmark ~46 day case on 64 cores

Filename: mark.pbsscript.64CPU_16NODE.DEFday [/fibre/055]

```
#!/bin/bash
#!
```

```
#PBS -N OTIS_GLOB8
#PBS -l select=16:ncpus=8:mpiprocs=4
#PBS -l place=scatter:excl
#PBS -l walltime=03:00:00
#PBS -q general
#PBS -W group_list=altix
#PBS -j oe

## PBS_O_WORKDIR = directory from which the batch job is launched.
### You should not have to change anything below this line ####
##############################################################
##

export MPT_HOME=/opt/sgi/mpt/mpt-2.03
export NC4_HOME=/sata/working/jeff/packages/netcdf/netcdf-3.6.3/altix_opt
#export NC4_HOME=/sata/working/jeff/packages/netcdf4/netcdf-
4.1.1/altix/intel10.1
#export HD5_HOME=/sata/working/jeff/packages/hdf5/hdf5-1.8.4-
patch1/altix/intel10.1
export IFT_HOME=/sw/Intel/fce/11.1.072
OCEANCORES=64

#! change the working directory (default is home directory)
cd $PBS_O_WORKDIR
#
echo Running on host `hostname`
echo Time is `date`
echo Directory is `pwd`
echo PBS job ID is $PBS_JOBID
echo This jobs runs on the following machines:
# Create a machine file for MPI
echo `cat $PBS_NODEFILE | uniq`
numnodes=`wc $PBS_NODEFILE | awk '{ print $1 }'`
#! Create a machine file for MPI
cat $PBS_NODEFILE | head -$numnodes > host.file.$PBS_JOBID

echo export
LD_LIBRARY_PATH=${MPT_HOME}/lib:${IFT_HOME}/lib/intel64:${NC4_HOME}/li
b
export
LD_LIBRARY_PATH=${MPT_HOME}/lib:${IFT_HOME}/lib/intel64:${NC4_HOME}/li
b
echo export PATH=${MPT_HOME}/bin:${PATH}
export PATH=${MPT_HOME}/bin:${PATH}
export PSM_SHAREDPORTS=1
echo export MPI_PPN=1
echo export MPI_PPN_CLIST="2-3-6-7-0-1-4-5"
echo export OMP_NUM_THREADS=1
export MPI_PPN=1
export MPI_PPN_CLIST="2-3-6-7-0-1-4-5"
export OMP_NUM_THREADS=1
#
#  Run the parallel MPI executable
```

```
#
  echo "Running time ${MPT_HOME}/bin/mpiexec_mpt -np " $OCEANCORES "
./fwd_ts -rit1 -T3.9744 -H1.9872"
#
  time ${MPT_HOME}/bin/mpiexec_mpt -np $OCEANCORES ./fwd_ts -rit1 >&
$PBS_O_WORKDIR/OTIS.$PBS_JOBID
#
  exit
```

/GLOB8npg/exe/ (fully global) jobscript for benchmark ~10 day case on 64 cores

Filename: mark.pbsscript.64CPU_16NODE.LANAday.NPG [/fibre/056]

```
#!/bin/bash
#!
#PBS -N OTIS_GLOB8
#PBS -l select=16:ncpus=8:mpiprocs=4
#PBS -l place=scatter:excl
#PBS -l walltime=02:30:00
#PBS -q general
#PBS -W group_list=altix
#PBS -j oe

## PBS_O_WORKDIR = directory from which the batch job is launched.
### You should not have to change anything below this line ####
##############################################################
##

export MPT_HOME=/opt/sgi/mpt/mpt-2.03
export NC4_HOME=/sata/working/jeff/packages/netcdf/netcdf-3.6.3/altix_opt
#export NC4_HOME=/sata/working/jeff/packages/netcdf4/netcdf-
4.1.1/altix/intel10.1
#export HD5_HOME=/sata/working/jeff/packages/hdf5/hdf5-1.8.4-
patch1/altix/intel10.1
export IFT_HOME=/sw/Intel/fce/11.1.072
OCEANCORES=64

#! change the working directory (default is home directory)
cd $PBS_O_WORKDIR
#
echo Running on host `hostname`
echo Time is `date`
echo Directory is `pwd`
echo PBS job ID is $PBS_JOBID
echo This jobs runs on the following machines:
# Create a machine file for MPI
echo `cat $PBS_NODEFILE | uniq`
numnodes=`wc $PBS_NODEFILE | awk '{ print $1 }'`
#! Create a machine file for MPI
cat $PBS_NODEFILE | head -$numnodes > host.file.$PBS_JOBID
```

```
echo export
LD_LIBRARY_PATH=${MPT_HOME}/lib:${IFT_HOME}/lib/intel64:${NC4_HOME}/li
b
export
LD_LIBRARY_PATH=${MPT_HOME}/lib:${IFT_HOME}/lib/intel64:${NC4_HOME}/li
b
echo export PATH=${MPT_HOME}/bin:${PATH}
export PATH=${MPT_HOME}/bin:${PATH}
export PSM_SHAREDPORTS=1
echo export MPI_PPN=1
echo export MPI_PPN_CLIST="2-3-6-7-0-1-4-5"
echo export OMP_NUM_THREADS=1
export MPI_PPN=1
export MPI_PPN_CLIST="2-3-6-7-0-1-4-5"
export OMP_NUM_THREADS=1
#
#  Run the parallel MPI executable
#
  echo "Running time ${MPT_HOME}/bin/mpiexec_mpt -np " $OCEANCORES "
./fwd_ts_NPG -rit1 -T0.9 -H.3 "
#
  time ${MPT_HOME}/bin/mpiexec_mpt -np $OCEANCORES ./fwd_ts_NPG -rit1 -
T0.9 -H.3 >& $PBS_O_WORKDIR/OTIS.$PBS_JOBID
#
  exit
~
```

A2.8.4 RODIN backup of model version described in this Appendix

A backup of the May 2012 version (i) of the Nautilus OTISmpi_altix port has been stored on RODIN (~1.5 Gbytes with results). Additionally the OSU benchmark described in section A2.6 (OTISmpi_bench) has been put in the same archive to enable future benchmarking post port. The most recent version of the model used for the production runs and SL experiments has been moved to the new NOCS Cluster (Mobilis) and will also be archived (ii).

The IDs for the RODIN archive tar files are:

i) NOCSDAT3305 (May 2012)

ii) NOCSDAT(t.b.c.) (June 2014)

Appendix 3.1 - Full Tables of Global Coastal City Tidal Changes

Full version of Table 3.5

	Present Day Exposure Ranking		M2 (cm)			S2 (cm)			K1 (cm)			O1 (cm)			MHW (cm)			Max Range (cm)		
COUNTRY, City/Agglomeration	Population	Asset	Control	+2UF	+2UR	Control	+2UF	+2UR	Control	+2UF	+2UR	Control	+2UF	+2UR	Control	+2UF	+2UR	Control	+2UF	+2UR
ALGERIA, Algiers	88	99	2	0 *	0 *	1	0 *	0 *	2	0	0 *	2	0 *	0 *	4	0 *	0 *	11	0 *	0 *
ANGOLA, Luanda	134	134	51	-3 *	0 *	24	0 *	0 *	5	0 *	0 *	4	0 *	0 *	54	-2 *	0 *	155	-5 *	1 *
ARGENTINA, Buenos Aires	64	52	78	-4 *	-51 *	68	-20 *	-47 *	13	-2 *	-3 *	22	0 *	-6 *	98	-15 *	-64 *	312	-46 *	-195 *
AUSTRALIA, Adelaide	123	103	54	-13 *	-31 *	73	13 *	38 *	23	-1 *	-1 *	21	0 *	-1 *	86	0 *	17 *	318	-4 *	11 *
AUSTRALIA, Brisbane	86	61	66	-1 *	-3 *	14	0 *	2 *	19	0 *	0	13	0 *	0 *	64	-1 *	-3 *	200	-2 *	-3
AUSTRALIA, Melbourne	100	74	74	8	11 *	28	2	2 *	26	-1	-1 *	23	-1	-1 *	74	7	10 *	269	17	20
AUSTRALIA, Perth	77	51	11	0 *	-1 *	1	0 *	1 *	17	0 *	0 *	15	0 *	0 *	25	0 *	-1 *	75	-1 *	-1 *
AUSTRALIA, Sydney	124	104	57	0 *	-2 *	8	1 *	1 *	15	0 *	0 *	12	0 *	0 *	55	-1 *	-2 *	165	1	-1 *
BANGLADESH, Chittagong	39	72	153	16 *	-13 *	49	5 *	-6 *	20	0 *	-1 *	8	0 *	0 *	147	16 *	-13 *	433	43 *	-37 *
BANGLADESH, Dhaka	14	43	140	26	-1 *	41	9	0 *	20	0	0 *	8	0 *	0 *	134	25	-1 *	393	71	-1 *
BANGLADESH, Khulna	23	54	88	-4 *	19 *	34	-1 *	6 *	16	0	1 *	5	0	0 *	87	-4 *	19 *	266	-9 *	51 *
BRAZIL, Santos	89	98	51	-9	5 *	52	0 *	-3 *	10	0 *	0 *	17	0 *	0 *	74	-6 *	1 *	244	-18 *	5 *
BRAZIL, Belém	72	79	251	28 *	-142 *	44	11	-23 *	9	1 *	-4 *	10	2 *	-4 *	233	28 *	-131 *	614	83 *	-340 *
BRAZIL, Fortaleza	107	110	103	-2	1 *	32	0 *	1 *	8	0	0 *	8	0 *	0 *	100	-2	1 *	291	-4 *	3 *
BRAZIL, Grande Vitória	31	35	56	-5	5 *	35	1 *	-1 *	8	0 *	0 *	13	0 *	0 *	65	-3 *	3 *	210	-9 *	6 *
BRAZIL, Maceió	105	106	82	-5	6 *	37	0 *	0 *	5	0 *	0 *	9	0 *	0 *	86	-4	4 *	251	-9	10 *
BRAZIL, Natal	93	102	85	-3	4 *	32	0 *	0 *	5	0	0 *	7	0 *	0 *	86	-2	4 *	250	-5	9 *
BRAZIL, Recife	81	86	83	-4	5 *	35	0 *	0 *	5	0	0 *	8	0 *	0 *	86	-3	4 *	250	-7	11 *
BRAZIL, Porto Alegre	78	83	6	1 *	3 *	10	9	12 *	5	0 *	8 *	9	1 *	14 *	14	7	18 *	50	18 *	65 *
BRAZIL, Rio de Janeiro	54	56	40	-5 *	3 *	34	1 *	-2 *	10	0 *	0 *	16	0 *	0 *	54	-3 *	1 *	185	-10 *	3 *
BRAZIL, Salvador	113	116	76	-4	10 *	37	1 *	0 *	5	0 *	0 *	10	0 *	0 *	81	-3	8 *	241	-8	20 *
CAMEROON, Douala	110	128	65	-3 *	-15 *	33	-1 *	-8 *	9	0 *	0 *	2	0	0 *	70	-3 *	-16 *	204	-8 *	-46 *
CANADA, Montréal	84	55	109	23 *	154 *	160	-35 *	-92 *	24	0 *	-2 *	25	1 *	-2 *	182	-8 *	66 *	571	2 *	150 *
CANADA, Vancouver	32	15	164	6 *	-4 *	49	1 *	-2 *	82	-1 *	-2 *	50	0 *	0 *	170	3 *	-9 *	619	11 *	-18 *
CHINA, Dalian	55	63	49	22	-1 *	15	4 *	-1 *	32	-2 *	-2	22	-1 *	-1 *	67	12	-3 *	197	47 *	-9 *
CHINA, Fuzhou Fujian	42	48	238	23 *	7 *	77	5 *	2 *	34	-1	-1 *	27	0	0 *	234	22	6 *	704	54	14 *
CHINA, Guangzhou Guangdong	2	11	116	-29 *	-29 *	60	-27 *	-13 *	48	-3 *	-4 *	38	-2 *	-3	121	-23 *	-19 *	480	-120	-94 *
CHINA, Shenzen	18	31	92	-17 *	-17	46	-18 *	-6 *	45	-2 *	-3 *	35	-1 *	-2 *	100	-11 *	-8 *	395	-74 *	-54
CHINA, Hangzhou	92	108	173	15	24 *	49	8	12 *	30	-1	1 *	24	-1 *	1 *	166	16	25 *	520	42	72 *
CHINA, Ningbo	34	40	64	35	21 *	19	10	6 *	26	1 *	2 *	20	0 *	1 *	68	28	20 *	232	88	60 *
CHINA, Qingdao	57	65	93	8	-3 *	34	3	3 *	21	1 *	2 *	17	1 *	2 *	93	9	0 *	301	19	3 *
CHINA, Shanghai	3	13	203	-22 *	-24	79	-5 *	-4 *	26	-1 *	-1 *	18	-2 *	-1 *	205	-21 *	-22	623	-59	-61
CHINA, Taipei	49	59	86	17	9 *	24	4 *	2 *	24	0	-1 *	19	0	0 *	85	16	8 *	276	42	21 *
CHINA, Tianjin	12	25	59	25 *	8 *	14	5 *	2 *	29	1 *	1	23	0 *	2 *	67	12 *	1 *	225	60 *	24 *
CHINA, Wenzhou	58	71	214	8 *	15 *	79	-2 *	4 *	31	0 *	0 *	24	0	0 *	216	5 *	15 *	648	12 *	39 *
CHINA, Xiamen	36	44	217	17 *	2 *	64	4 *	1 *	38	-2	-2 *	30	-1 *	-1 *	212	15	2 *	640	36	0 *
CHINA, Yantai	115	119	28	15 *	0 *	9	3 *	-1 *	18	-3	-1 *	11	-2	-1 *	33	7 *	-5 *	118	28 *	-5 *
CHINA, Zhanjiang	40	45	101	-13 *	-10 *	54	-21	-4 *	47	-2	-2 *	37	0 *	-1 *	112	-12 *	-7 *	435	-69 *	-34 *
CHINA, HONG KONG SAR, Hong Kong	41	20	47	-5 *	-4 *	23	-6 *	-1 *	39	-1	-2 *	30	0 *	-1 *	70	-5	-2 *	247	-25	-16 *
COLOMBIA, Barranquilla	129	129	4	0 *	4 *	4	0 *	0 *	10	0 *	0 *	7	0	0 *	13	0 *	2 *	45	0 *	8 *
CÔTE D'IVOIRE, Abidjan	20	58	42	0 *	1 *	19	0 *	0 *	8	0 *	0 *	2	0 *	0 *	44	0 *	1 *	130	-1 *	2 *
CUBA, Havana	133	132	15	1 *	0 *	4	1	0 *	8	0 *	0 *	9	0	0 *	20	1 *	-1 *	61	3 *	-2 *
NORTH KOREA, Namp'o	87	121	171	18	-7 *	53	3	0 *	46	-3 *	-2 *	31	-1 *	0 *	167	12 *	-6 *	548	37	-18 *
DENMARK, Copenhagen	82	53	29	9 *	16 *	4	4 *	1 *	1	0 *	0 *	1	0 *	0 *	27	9 *	15 *	67	29 *	36 *
DOMINICAN REPUBLIC, Santo Domingo	109	114	3	0 *	2 *	3	0 *	0 *	8	0 *	0 *	7	0 *	0 *	10	0 *	1 *	36	-1 *	3 *
ECUADOR, Guayaquil	26	41	157	5 *	-75 *	49	7 *	-19 *	11	0 *	-2 *	3	0 *	-1 *	152	7 *	-71 *	428	23 *	-193 *

	Present Day Exposure Ranking		M2 (cm)			S2 (cm)			K1 (cm)			O1 (cm)			MHW (cm)			Max Range (cm)		
COUNTRY, City/Agglomeration	Population	Asset	Control	+2UF	+2UR	Control	+2UF	+2UR	Control	+2UF	+2UR	Control	+2UF	+2UR	Control	+2UF	+2UR	Control	+2UF	+2UR
EGYPT, Alexandria	9	26	11	0 *	0 *	5	2 *	2	1	0 *	0 *	1	0 *	0 *	11	1 *	1 *	34	4	5 *
FINLAND, Helsinki	119	89	5	1 *	2 *	0	1 *	0 *	3	0 *	0 *	3	1 *	0 *	7	2 *	0 *	19	6 *	4
FRANCE, Marseille-Aix-en-Provence	102	78	3	0 *	0 *	1	0 *	0 *	2	0	0 *	1	0 *	0 *	3	0 *	0 *	11	1 *	0 *
GERMANY, Hamburg	37	18	167	-2 *	-104 *	35	4	-18 *	4	0 *	-1 *	11	2	-2 *	156	-1 *	-96 *	425	7 *	-247 *
GHANA, Accra	104	123	52	-1 *	0 *	25	0 *	-1 *	9	0 *	0 *	2	0 *	0 *	56	-1 *	0 *	162	-3 *	0 *
GREECE, Athens	127	118	9	0 *	0 *	3	1 *	1 *	1	0 *	0 *	1	0 *	0 *	8	0 *	0 *	25	1 *	1 *
GUINEA, Conakry	70	113	159	-21 *	-15 *	54	-8 *	-5 *	8	0 *	0	4	0 *	0 *	156	-21 *	-15 *	435	-57 *	-41 *
HAITI, Port-au-Prince	135	136	17	0 *	0 *	4	0 *	0 *	7	0 *	0 *	5	0 *	0 *	17	0 *	0 *	59	0 *	1 *
INDIA, Madras	46	70	33	-1 *	0 *	11	0 *	0 *	11	0 *	0 *	3	0 *	0 *	31	0 *	0 *	101	-1 *	-1 *
INDIA, Cochin	56	80	19	1	2 *	12	0 *	0 *	19	0 *	0 *	12	0	0 *	25	0 *	2 *	102	1	1
INDIA, Calcutta	6	22	125	-12 *	-40 *	50	-4 *	-21 *	17	0 *	0 *	5	0 *	0 *	127	-12 *	-43 *	373	-31 *	-119 *
INDIA, Bombay	1	17	123	-4 *	18 *	85	-6	-7 *	38	0	0 *	24	0	0 *	148	-8 *	9 *	489	-16 *	20 *
INDIA, Surat	24	46	200	11 *	39 *	123	4 *	-8 *	50	0 *	-1 *	35	0 *	-2 *	228	9 *	26 *	759	32	55 *
INDIA, Visakhapatnam	83	111	48	-1 *	0 *	17	0 *	0 *	13	0 *	0 *	3	0 *	0 *	46	-1 *	0 *	148	-1 *	0 *
INDONESIA, Jakarta	21	39	16	-6	-9 *	17	-2 *	-4 *	40	-2 *	2 *	25	-2 *	1 *	52	-4 *	0 *	163	-22	-14 *
INDONESIA, Palembang	48	73	16	1 *	-10 *	5	2 *	-3 *	50	15 *	-3 *	43	7 *	-3 *	76	18 *	-10 *	192	43 *	-18 *
INDONESIA, Surabaya	68	88	190	-22 *	-46 *	78	-14 *	-28 *	45	1	6 *	36	-1	4 *	194	-25	-50 *	651	-69	-136 *
INDONESIA, Ujung Pandang	118	126	26	2	-3 *	16	0	-4 *	29	0 *	1 *	23	0	2 *	38	1 *	-1 *	144	3	-15 *
IRELAND, Dublin	95	62	133	12	-24 *	36	5	-6 *	9	0 *	0	16	0 *	0 *	129	12	-22 *	363	34	-60 *
ISRAEL, Tel Aviv-Jaffa	136	135	15	0 *	0 *	6	3	3	2	0	0 *	1	0 *	0 *	16	2 *	1 *	48	6 *	6 *
ITALY, Naples	131	117	5	0 *	0 *	2	-1 *	0 *	2	0	0 *	1	0 *	0 *	5	-1 *	0 *	19	-2	0 *
JAPAN, Fukuoka-Kitakyushu	33	16	74	0 *	-1 *	32	0 *	1 *	20	0	0 *	16	0 *	0 *	79	-1	-1	260	-1 *	-1 *
JAPAN, Hiroshima	44	24	163	-9 *	-50 *	79	-4 *	-32 *	29	0	1 *	22	0 *	2 *	175	-10 *	-58 *	539	-28 *	-146 *
JAPAN, Nagoya	19	8	61	-2	-2 *	29	-1 *	0 *	26	0	-1 *	20	0	0 *	67	-1	-1 *	230	-5	-4 *
JAPAN, Osaka-Kobe	8	4	96	-7 *	-2 *	43	0 *	1 *	29	0 *	-1 *	22	0 *	0 *	102	-5 *	-1 *	340	-16 *	-2 *
JAPAN, Sapporo	121	100	6	0	0 *	2	0 *	0 *	8	0 *	0 *	8	0 *	0 *	10	0 *	0 *	39	2 *	2
JAPAN, Tokyo	11	5	34	0 *	1 *	18	0	1 *	26	0	0	21	0 *	0 *	43	0 *	1 *	162	0 *	5 *
KUWAIT, Kuwait City	101	84	93	12 *	-8 *	56	0 *	-13 *	35	5	-2 *	29	1 *	-1 *	99	9 *	-13 *	384	36 *	-46 *
LEBANON, Beirut	120	125	16	0 *	0 *	6	3	3	2	0	0 *	1	0 *	0 *	16	2 *	1 *	50	6 *	6 *
LIBYA, Banghazi	73	77	4	1	0 *	1	1 *	1 *	1	0 *	0 *	1	0 *	0 *	4	1 *	0 *	12	3 *	2 *
LIBYA, Tripoli	126	122	14	1 *	0 *	5	3 *	2 *	2	0 *	0 *	1	0 *	0 *	14	3	1 *	43	8 *	4 *
MALAYSIA, Kuala Lumpur	35	33	128	4 *	-16 *	42	6 *	-3 *	30	0 *	-1 *	15	0 *	-1 *	127	6 *	-15 *	396	22 *	-42 *
MOROCCO, Casablanca	75	97	121	-2 *	4 *	41	1 *	0 *	7	0 *	0	10	0 *	0 *	120	-1 *	3 *	347	-3 *	8 *
MOROCCO, Rabat	111	120	120	-2 *	5 *	40	1 *	1 *	7	0 *	0 *	10	0 *	0 *	119	-1 *	4 *	344	-3 *	11 *
MOZAMBIQUE, Maputo	66	112	92	-4 *	-1 *	50	-1 *	-2 *	1	0 *	0 *	7	0 *	0 *	101	-4	-2 *	294	-11	-6 *
MYANMAR, Rangoon	22	60	162	32	-8 *	54	13	1 *	20	1 *	0 *	9	1 *	0 *	158	33	-6 *	471	92	-13 *
NETHERLANDS, Amsterdam	15	6	84	7 *	-38 *	18	5 *	-7 *	6	0	-1 *	16	2	-4 *	76	7 *	-33 *	228	24 *	-94 *
NETHERLANDS, Rotterdam	17	7	144	-9 *	-75 *	29	2 *	-14 *	7	0 *	-2 *	20	1 *	-5 *	131	-8 *	-69 *	376	-17 *	-185 *
NEW ZEALAND, Auckland	116	92	118	0 *	0 *	30	0 *	0 *	6	0 *	0 *	2	0 *	0 *	112	0 *	0 *	305	0 *	-1 *
NIGERIA, Lagos	30	76	54	-1 *	0 *	27	0 *	-1 *	10	0 *	0 *	1	0 *	0 *	58	-1 *	0 *	171	-4 *	0 *
PAKISTAN, Karachi	69	105	74	-2 *	15 *	51	-2 *	-1 *	37	0 *	0 *	23	0 *	0 *	91	-2 *	10 *	313	-6 *	26 *
PANAMA, Panama City	99	109	237	-8	4 *	86	-1 *	-3 *	12	0 *	0 *	3	0	0 *	237	-7	2 *	662	-19	3 *
PERU, Lima	132	130	38	0 *	-2 *	7	0 *	-1 *	13	0	0 *	8	0 *	0 *	37	0 *	-2 *	119	1 *	-6 *
PHILIPPINES, Davao	130	131	57	1	-2 *	26	0 *	-1 *	18	0	-1 *	14	0 *	0 *	60	0 *	-2 *	214	1	-6 *
PHILIPPINES, Manila	53	66	41	-7 *	-12 *	14	-2 *	-2 *	40	-3 *	-4 *	33	-2 *	-4 *	55	-2 *	-4 *	219	-21 *	-36 *
PORTUGAL, Lisbon	71	57	117	-2 *	4 *	39	1 *	1 *	8	0 *	0 *	10	0 *	0 *	115	-1 *	4 *	335	-2 *	10 *

	Present Day Exposure Ranking		M2 (cm)			S2 (cm)			K1 (cm)			O1 (cm)			MHW (cm)			Max Range (cm)		
COUNTRY, City/Agglomeration	Population	Asset	Control	+2UF	+2UR	Control	+2UF	+2UR	Control	+2UF	+2UR	Control	+2UF	+2UR	Control	+2UF	+2UR	Control	+2UF	+2UR
PORTUGAL, Porto	103	82	120	-2 *	4 *	40	1 *	1	8	0 *	0 *	10	0 *	0 *	119	-1 *	3 *	345	-2 *	9 *
PUERTO RICO, San Juan	65	49	10	0 *	-1 *	1	-1 *	0 *	8	0	0 *	7	0 *	0 *	16	0 *	-2 *	46	-2 *	-1 *
SOUTH KOREA, Pusan	60	42	60	0 *	-2 *	25	0 *	0 *	6	0	0 *	3	0 *	0 *	61	0 *	-1 *	180	0 *	-3 *
SOUTH KOREA, Ulsan	117	95	24	-1 *	-1 *	10	0 *	0 *	4	0 *	0 *	5	0	0 *	25	0 *	-1 *	79	-1 *	-1 *
SOUTH KOREA, Inchon	43	30	364	12 *	-13 *	109	8 *	3 *	42	-2 *	-1 *	31	-1 *	0 *	353	13	-10 *	1045	37 *	-22 *
RUSSIA, St. Petersburg	45	38	15	3 *	7 *	0	3 *	1 *	5	0 *	0 *	4	2 *	0 *	14	3 *	7 *	40	18 *	16 *
SAUDI ARABIA, Jiddah	97	85	6	1 *	0 *	3	0 *	0 *	4	0	0 *	3	0	0 *	7	1 *	1 *	27	3 *	-1 *
SENEGAL, Dakar	90	124	49	0 *	-3 *	17	1 *	0 *	5	0 *	0	6	0 *	0 *	48	0 *	-2 *	146	2 *	-7 *
SINGAPORE, Singapore	96	75	34	7 *	-16 *	9	2	-4 *	8	1 *	3 *	5	2 *	7 *	31	8 *	-12 *	105	20	-28 *
SOMALIA, Mogadishu	114	133	55	2	4 *	37	-1 *	0 *	22	0 *	0 *	16	0 *	0 *	66	1 *	3 *	232	1 *	5 *
SOUTH AFRICA, Cape Town	112	107	58	-1 *	7 *	30	0 *	0 *	2	0 *	0 *	5	0 *	0 *	63	-1 *	6 *	182	-3 *	13 *
SOUTH AFRICA, Durban	98	93	69	-2 *	1 *	38	0 *	-1 *	1	0 *	0 *	6	0 *	0 *	77	-2 *	0 *	221	-4 *	0 *
SPAIN, Barcelona	108	81	1	0 *	0 *	1	0 *	0 *	1	0	0 *	1	0 *	0 *	2	0 *	0 *	8	1 *	0 *
SWEDEN, Stockholm	128	115	15	3 *	3 *	0	4 *	1 *	1	0 *	0 *	1	0 *	0 *	14	3 *	3 *	34	14 *	7 *
THAILAND, Bangkok	13	19	10	4	8 *	2	2 *	3 *	103	2 *	-7 *	61	2 *	0 *	117	2 *	-7 *	329	8 *	-14 *
TOGO, Lomé	50	90	53	-1 *	0 *	26	0 *	-1 *	10	0 *	0 *	1	0 *	0 *	57	-1 *	0 *	168	-3 *	0 *
TURKEY, Istanbul	62	64	0	0 *	0 *	0	0 *	0 *	0	0 *	0 *	0	0 *	0 *	0	0 *	0 *	1	0 *	0 *
TURKEY, Izmir	79	87	32	-2 *	-1 *	12	6 *	6 *	2	0 *	0 *	1	0 *	0 *	32	2 *	3 *	91	7 *	11 *
UKRAINE, Odessa	61	67	6	-1 *	-1 *	8	-5 *	-5 *	1	0 *	0 *	0	0 *	0 *	10	-4 *	-4 *	29	-12 *	-13 *
UNITED ARAB EMIRATES, Dubai	38	23	46	1 *	-6 *	29	1 *	-7 *	15	4	-2 *	14	1 *	-1 *	52	3 *	-6 *	189	13 *	-34 *
UNITED KINGDOM, Glasgow	91	68	138	5 *	-30 *	37	3 *	-10 *	8	0 *	0 *	15	0 *	0 *	133	5 *	-29 *	376	17 *	-79 *
UNITED KINGDOM, London	28	14	288	-3 *	-10 *	71	4 *	-9 *	8	0 *	0 *	21	0 *	-1 *	273	0 *	-12 *	752	3 *	-40 *
TANZANIA, Dar-es-Salaam	74	127	87	2	4 *	57	-1 *	1 *	19	0 *	0 *	14	0	0 *	99	1	5 *	324	3	9 *
USA, Baltimore	52	29	30	2 *	-2 *	1	1 *	1 *	10	1 *	-4 *	8	1 *	-3 *	32	3 *	-7 *	85	4 *	-10 *
USA, Boston	29	12	243	1 *	-16 *	21	5 *	-3 *	12	0 *	-1 *	12	0 *	0 *	225	1 *	-15 *	554	9 *	-37 *
USA, Houston	67	36	66	-25 *	-33 *	16	13 *	-3 *	18	-2 *	-2 *	18	-1 *	-2 *	65	-15 *	-30 *	213	-31 *	-84 *
USA, Los Angeles-Long Beach	59	32	66	0 *	-1 *	22	0 *	0 *	35	0 *	0	25	0 *	0 *	72	0 *	0	267	0 *	-2 *
USA, Miami	4	1	33	0 *	-4 *	2	1 *	1 *	4	0	0 *	4	0 *	0 *	30	1 *	-3 *	81	1 *	-6 *
USA, New Orleans	10	3	1	6 *	3 *	0	2	1 *	11	7 *	12 *	12	10	8 *	16	14 *	16 *	46	41 *	42 *
USA, New York-Newark	7	2	60	-1 *	-8 *	4	1 *	2 *	9	0	0	7	0 *	0 *	55	0 *	-7 *	147	-2 *	-13 *
USA, Philadelphia	47	21	81	-8 *	4 *	5	0 *	4 *	9	0 *	0 *	8	0 *	0 *	73	-5	4 *	190	-16 *	19 *
USA, Portland	106	69	106	1 *	0 *	37	0 *	-1 *	46	0 *	0 *	31	0 *	0 *	104	1 *	0 *	395	1 *	0 *
USA, Providence	63	34	35	0 *	-4 *	3	0 *	2 *	6	0 *	0 *	5	0 *	0 *	33	0 *	-4 *	88	-2 *	-2 *
USA, San Diego	125	94	66	0 *	-1 *	23	0 *	0 *	35	0 *	0	24	0 *	0 *	72	0 *	0 *	266	-1 *	-1 *
USA, San Francisco - Oakland	51	28	67	1 *	0 *	20	0 *	0 *	39	0 *	0	27	0 *	0 *	72	0 *	0 *	271	1 *	-1 *
USA, San Jose	122	91	67	1 *	0 *	20	0 *	0 *	39	0 *	0	27	0 *	0 *	72	0 *	0 *	271	1 *	-1 *
USA, Seattle	80	50	99	4	-11 *	28	1 *	-4 *	75	-1	-3 *	46	0 *	-1 *	121	2 *	-15 *	434	8	-37 *
USA, Tampa-St Petersburg	25	9	34	5 *	-9 *	12	4 *	-4 *	14	0 *	-1 *	14	0 *	-1 *	37	5 *	-10 *	132	19 *	-29 *
USA, Virginia Beach	27	10	38	-3 *	-4 *	2	0 *	1 *	7	0	0 *	5	0	0 *	35	-2 *	-4 *	94	-6 *	-9 *
USA, Washington, D C	76	47	27	3 *	4 *	1	1 *	1 *	10	1 *	-5 *	8	1 *	-3 *	29	3 *	-1 *	77	5 *	3 *
URUGUAY, Montevideo	94	96	5	22 *	15	5	11 *	8 *	9	0 *	-1 *	16	1 *	-1 *	20	11 *	3 *	58	48	29 *
VENEZUELA, Maracaibo	85	101	8	-6 *	-2 *	3	0 *	-1 *	30	9 *	7 *	26	-5 *	-6 *	42	2 *	3 *	118	2 *	-3 *
VIETNAM, Hai Phòng	16	37	15	-1 *	-3 *	8	-1	0 *	62	4	2 *	66	6	4 *	95	6	3 *	270	17	7 *
VIETNAM, Ho Chi Minh City	5	27	111	-31 *	-40 *	56	-14 *	-31 *	67	-2 *	-15 *	54	-3	-10 *	128	-27 *	-46 *	480	-95 *	-171 *

Full version of Table 3.6

	Present Day Exposure Ranking		MHW (cm)						Max Range (cm)					
COUNTRY, City/Agglomeration	Population	Asset	Control	+0.5UF	+1UF		+2UF		Control	+0.5UF	+1UF		+2UF	
ALGERIA, Algiers	88	99	4	0	0	*	0	*	11	0	0	*	0	*
ANGOLA, Luanda	134	134	54	-1	-1		-2	*	155	-2	-3		-5	*
ARGENTINA, Buenos Aires	64	52	98	-7	-12	*	-15	*	312	-20	-35	*	-46	*
AUSTRALIA, Adelaide	123	103	86	0	0	*	0	*	318	0	0	*	-4	*
AUSTRALIA, Brisbane	86	61	64	0	-1		-1	*	200	-1	-2		-2	*
AUSTRALIA, Melbourne	100	74	74	2	4		7		269	4	8		17	
AUSTRALIA, Perth	77	51	25	0	0		0	*	75	0	0	*	-1	*
AUSTRALIA, Sydney	124	104	55	0	0	*	-1	*	165	0	0	*	1	
BANGLADESH, Chittagong	39	72	147	3	7	*	16	*	433	8	19	*	43	*
BANGLADESH, Dhaka	14	43	134	6	13		25		393	18	35		71	
BANGLADESH, Khulna	23	54	87	-1	-2		-4	*	266	-3	-5		-9	*
BRAZIL, Santos	89	98	74	-1	-3	*	-6	*	244	-4	-8	*	-18	*
BRAZIL, Belém	72	79	233	9	16	*	28	*	614	26	48		83	*
BRAZIL, Fortaleza	107	110	100	0	-1		-2		291	-1	-2	*	-4	*
BRAZIL, Grande Vitória	31	35	65	-1	-2	*	-3	*	210	-2	-4	*	-9	*
BRAZIL, Maceió	105	106	86	-1	-2		-4		251	-2	-5		-9	
BRAZIL, Natal	93	102	86	-1	-1		-2		250	-1	-2		-5	
BRAZIL, Recife	81	86	86	-1	-1		-3		250	-2	-4		-7	
BRAZIL, Porto Alegre	78	83	14	2	3		7		50	4	10	*	18	*
BRAZIL, Rio de Janeiro	54	56	54	-1	-1	*	-3	*	185	-2	-4	*	-10	*
BRAZIL, Salvador	113	116	81	-1	-2		-3		241	-2	-4		-8	
CAMEROON, Douala	110	128	70	-1	-2		-3	*	204	-2	-5		-8	*
CANADA, Montréal	84	55	182	0	1	*	-8	*	571	12	23		2	*
CANADA, Vancouver	32	15	170	1	1		3	*	619	2	5		11	*
CHINA, Dalian	55	63	67	3	6		12		197	10	21		47	*
CHINA, Fuzhou Fujian	42	48	234	5	10		22		704	12	26		54	
CHINA, Guangzhou Guangdong	2	11	121	-7	-12	*	-23	*	480	-30	-62		-120	
CHINA, Shenzen	18	31	100	-2	-4	*	-11	*	395	-15	-35	*	-74	*
CHINA, Hangzhou	92	108	166	4	8		16		520	11	21		42	
CHINA, Ningbo	34	40	68	8	15		28		232	24	46		88	
CHINA, Qingdao	57	65	93	2	5		9		301	5	9		19	

COUNTRY, City/Agglomeration	Present Day Exposure Ranking		MHW (cm)						Max Range (cm)					
	Population	Asset	Control	+0.5UF	+1UF		+2UF		Control	+0.5UF	+1UF		+2UF	
CHINA, Shanghai	3	13	205	-6	-11		-21	*	623	-15	-31		-59	
CHINA, Taipei	49	59	85	4	8		16		276	10	20		42	
CHINA, Tianjin	12	25	67	4	7		12	*	225	18	33		60	*
CHINA, Wenzhou	58	71	216	0	1	*	5	*	648	-1	1	*	12	*
CHINA, Xiamen	36	44	212	4	7		15		640	8	17		36	
CHINA, Yantai	115	119	33	0	1	*	7	*	118	5	11	*	28	*
CHINA, Zhanjiang	40	45	112	-4	-7	*	-12	*	435	-20	-39		-69	*
CHINA, HONG KONG SAR, Hong Kong	41	20	70	-1	-2		-5		247	-6	-13		-25	
COLOMBIA, Barranquilla	129	129	13	0	0	*	0	*	45	0	0	*	0	*
CÔTE D'IVOIRE, Abidjan	20	58	44	0	0	*	0	*	130	-1	-1	*	-1	*
CUBA, Havana	133	132	20	1	1	*	1	*	61	2	2	*	3	*
NORTH KOREA, Namp'o	87	121	167	3	5		12	*	548	9	18		37	
DENMARK, Copenhagen	82	53	27	8	15		9	*	67	21	36	*	29	*
DOMINICAN REPUBLIC, Santo Domingo	109	114	10	0	0		0	*	36	-1	-1	*	-1	*
ECUADOR, Guayaquil	26	41	152	3	5	*	7	*	428	10	17	*	23	*
EGYPT, Alexandria	9	26	11	0	1	*	1	*	34	1	2	*	4	
FINLAND, Helsinki	119	89	7	-1	0	*	2	*	19	1	5	*	6	*
FRANCE, Marseille-Aix-en-Provence	102	78	3	0	0		0	*	11	0	1		1	*
GERMANY, Hamburg	37	18	156	1	3	*	-1	*	425	4	10	*	7	*
GHANA, Accra	104	123	56	0	-1	*	-1	*	162	-1	-2		-3	*
GREECE, Athens	127	118	8	0	0	*	0	*	25	0	0	*	1	*
GUINEA, Conakry	70	113	156	-7	-13	*	-21	*	435	-20	-35	*	-57	*
HAITI, Port-au-Prince	135	136	17	0	0	*	0	*	59	0	0	*	0	*
INDIA, Madras	46	70	31	0	0	*	0	*	101	0	-1	*	-1	*
INDIA, Cochin	56	80	25	0	0	*	0	*	102	0	1		1	
INDIA, Calcutta	6	22	127	-3	-6		-12	*	373	-9	-17		-31	*
INDIA, Bombay	1	17	148	-2	-5		-8	*	489	-5	-10		-16	*
INDIA, Surat	24	46	228	2	4		9	*	759	7	15		32	
INDIA, Visakhapatnam	83	111	46	0	0	*	-1	*	148	0	-1	*	-1	*
INDONESIA, Jakarta	21	39	52	-1	-2	*	-4	*	163	-5	-11		-22	
INDONESIA, Palembang	48	73	76	6	10	*	18	*	192	13	24		43	*

COUNTRY, City/Agglomeration	Present Day Exposure Ranking		MHW (cm)						Max Range (cm)					
	Population	Asset	Control	+0.5UF	+1UF		+2UF		Control	+0.5UF	+1UF		+2UF	
INDONESIA, Surabaya	68	88	194	-7	-13		-25		651	-17	-33		-69	
INDONESIA, Ujung Pandang	118	126	38	0	0	*	1	*	144	1	1	*	3	
IRELAND, Dublin	95	62	129	3	6		12		363	8	17		34	
ISRAEL, Tel Aviv-Jaffa	136	135	16	0	1	*	2	*	48	1	3	*	6	*
ITALY, Naples	131	117	5	0	0	*	-1	*	19	0	-1	*	-2	
JAPAN, Fukuoka-Kitakyushu	33	16	79	0	0	*	-1		260	0	-1	*	-1	*
JAPAN, Hiroshima	44	24	175	-3	-5		-10	*	539	-8	-15		-28	*
JAPAN, Nagoya	19	8	67	0	-1		-1		230	-1	-3		-5	
JAPAN, Osaka-Kobe	8	4	102	-1	-2		-5	*	340	-3	-7		-16	*
JAPAN, Sapporo	121	100	10	0	0		0	*	39	0	1		2	*
JAPAN, Tokyo	11	5	43	0	0	*	0	*	162	0	0	*	0	*
KUWAIT, Kuwait City	101	84	99	2	5	*	9	*	384	10	22		36	*
LEBANON, Beirut	120	125	16	0	1	*	2	*	50	1	3	*	6	*
LIBYA, Banghazi	73	77	4	0	0	*	1	*	12	0	1	*	3	*
LIBYA, Tripoli	126	122	14	1	2		3		43	3	5		8	*
MALAYSIA, Kuala Lumpur	35	33	127	2	4		6	*	396	7	13		22	*
MOROCCO, Casablanca	75	97	120	0	-1		-1	*	347	-1	-2		-3	*
MOROCCO, Rabat	111	120	119	0	-1		-1	*	344	-1	-2		-3	*
MOZAMBIQUE, Maputo	66	112	101	-1	-2		-4		294	-3	-6		-11	
MYANMAR, Rangoon	22	60	158	8	16		33		471	23	46		92	
NETHERLANDS, Amsterdam	15	6	76	4	5	*	7	*	228	12	17	*	24	*
NETHERLANDS, Rotterdam	17	7	131	0	-3	*	-8	*	376	0	-7	*	-17	*
NEW ZEALAND, Auckland	116	92	112	0	0	*	0	*	305	1	0	*	0	*
NIGERIA, Lagos	30	76	58	-1	-1		-1	*	171	-1	-2	*	-4	*
PAKISTAN, Karachi	69	105	91	-1	-1	*	-2	*	313	-2	-4		-6	*
PANAMA, Panama City	99	109	237	-2	-4		-7		662	-4	-10		-19	
PERU, Lima	132	130	37	0	0	*	0	*	119	1	1	*	1	*
PHILIPPINES, Davao	130	131	60	0	0	*	0	*	214	0	1	*	1	
PHILIPPINES, Manila	53	66	55	0	-1	*	-2	*	219	-4	-10	*	-21	*
PORTUGAL, Lisbon	71	57	115	0	-1		-1	*	335	-1	-1		-2	*
PORTUGAL, Porto	103	82	119	0	-1		-1	*	345	-1	-1	*	-2	*

	Present Day Exposure Ranking		MHW (cm)						Max Range (cm)					
COUNTRY, City/Agglomeration	Population	Asset	Control	+0.5UF	+1UF		+2UF		Control	+0.5UF	+1UF		+2UF	
PUERTO RICO, San Juan	65	49	16	0	0	*	0	*	46	-1	-1	*	-2	*
SOUTH KOREA, Pusan	60	42	61	0	0	*	0	*	180	0	0		0	*
SOUTH KOREA, Ulsan	117	95	25	0	0		0	*	79	0	0	*	-1	*
SOUTH KOREA, Inchon	43	30	353	4	7		13		1045	11	21		37	*
RUSSIA, St. Petersburg	45	38	14	5	8	*	3	*	40	12	17	*	18	*
SAUDI ARABIA, Jiddah	97	85	7	0	0		1	*	27	1	2	*	3	*
SENEGAL, Dakar	90	124	48	0	0	*	0	*	146	0	1		2	*
SINGAPORE, Singapore	96	75	31	2	4		8	*	105	5	10		20	
SOMALIA, Mogadishu	114	133	66	0	0	*	1	*	232	0	1	*	1	*
SOUTH AFRICA, Cape Town	112	107	63	0	-1	*	-1	*	182	-1	-2		-3	*
SOUTH AFRICA, Durban	98	93	77	0	-1		-2	*	221	-1	-2	*	-4	*
SPAIN, Barcelona	108	81	2	0	0	*	0	*	8	0	1	*	1	*
SWEDEN, Stockholm	128	115	14	3	5	*	3	*	34	5	12		14	*
THAILAND, Bangkok	13	19	117	0	0	*	2	*	329	0	2	*	8	*
TOGO, Lomé	50	90	57	-1	-1	*	-1	*	168	-1	-2		-3	*
TURKEY, Istanbul	62	64	0	0	0	*	0	*	1	0	0	*	0	*
TURKEY, Izmir	79	87	32	0	0	*	2	*	91	1	3	*	7	*
UKRAINE, Odessa	61	67	10	-3	-3	*	-4	*	29	-7	-10	*	-12	*
UNITED ARAB EMIRATES, Dubai	38	23	52	1	2		3	*	189	7	14		13	*
UNITED KINGDOM, Glasgow	91	68	133	1	2		5	*	376	3	7		17	*
UNITED KINGDOM, London	28	14	273	2	5	*	0	*	752	3	10	*	3	*
TANZANIA, Dar-es-Salaam	74	127	99	0	1		1		324	1	1		3	
USA, Baltimore	52	29	32	1	1	*	3	*	85	0	0	*	4	*
USA, Boston	29	12	225	1	2	*	1	*	554	2	5	*	9	*
USA, Houston	67	36	65	1	-3	*	-15	*	213	6	-9	*	-31	*
USA, Los Angeles-Long Beach	59	32	72	0	0	*	0	*	267	0	0	*	0	*
USA, Miami	4	1	30	1	1	*	1	*	81	1	1	*	1	*
USA, New Orleans	10	3	16	3	7	*	14	*	46	8	21	*	41	*
USA, New York-Newark	7	2	55	0	0	*	0	*	147	-1	-2	*	-2	*
USA, Philadelphia	47	21	73	-1	-3		-5		190	-6	-10	*	-16	*
USA, Portland	106	69	104	0	0	*	1	*	395	0	0		1	*

COUNTRY, City/Agglomeration	Present Day Exposure Ranking		MHW (cm)						Max Range (cm)					
	Population	Asset	Control	+0.5UF	+1UF		+2UF		Control	+0.5UF	+1UF		+2UF	
USA, Providence	63	34	33	0	0	*	0	*	88	-1	-2	*	-2	*
USA, San Diego	125	94	72	0	0	*	0	*	266	0	0	*	-1	*
USA, San Francisco - Oakland	51	28	72	0	0	*	0	*	271	0	0	*	1	*
USA, San Jose	122	91	72	0	0	*	0	*	271	0	0	*	1	*
USA, Seattle	80	50	121	0	1		2	*	434	2	4		8	
USA, Tampa-St Petersburg	25	9	37	2	3	*	5	*	132	6	10		19	*
USA, Virginia Beach	27	10	35	0	-1	*	-2	*	94	-2	-3	*	-6	*
USA, Washington, D C	76	47	29	1	1		3	*	77	0	1	*	5	*
URUGUAY, Montevideo	94	96	20	3	6	*	11	*	58	12	25		48	
VENEZUELA, Maracaibo	85	101	42	2	4	*	2	*	118	6	7	*	2	*
VIETNAM, Hai Phòng	16	37	95	2	3		6		270	4	8		17	
VIETNAM, Ho Chi Minh City	5	27	128	-9	-15	*	-27	*	480	-26	-48		-95	*

Full version of Table 3.7

	Present Day Exposure Ranking		MHW (cm)													
COUNTRY, City/Agglomeration	Population	Asset	Control	+2UF		+2UR		+5UF		+5UR		+10UF		+10UR		
ALGERIA, Algiers	88	99	4	0	*	0	*	0	*	0	*	0	*	0	*	
ANGOLA, Luanda	134	134	54	-2	*	0	*	-4	*	-2	*	2	*	-3	*	
ARGENTINA, Buenos Aires	64	52	98	-15	*	-64	*	-5	*	-79	*	48	*	-68	*	
AUSTRALIA, Adelaide	123	103	86	0	*	17	*	28	*	19	*	54	*	26	*	
AUSTRALIA, Brisbane	86	61	64	-1	*	-3	*	-2	*	-3	*	-6		-5		
AUSTRALIA, Melbourne	100	74	74	7		10	*	19		22	*	37		22	*	
AUSTRALIA, Perth	77	51	25	0	*	-1	*	-1	*	0	*	-2	*	-1	*	
AUSTRALIA, Sydney	124	104	55	-1	*	-2	*	-2	*	-1	*	-6	*	-4		
BANGLADESH, Chittagong	39	72	147	16	*	-13	*	53	*	1	*	115	*	-1	*	
BANGLADESH, Dhaka	14	43	134	25		-1	*	70	*	-41	*	133		-47	*	
BANGLADESH, Khulna	23	54	87	-4	*	19	*	-8	*	9	*	-8	*	-8	*	
BRAZIL, Santos	89	98	74	-6	*	1	*	-17	*	-7	*	-31	*	-13	*	
BRAZIL, Belém	72	79	233	28	*	-131	*	51	*	-139	*	101	*	-150	*	
BRAZIL, Fortaleza	107	110	100	-2		1	*	-4	*	-3	*	-6	*	-9		
BRAZIL, Grande Vitória	31	35	65	-3	*	3	*	-9	*	-2	*	-18	*	-5	*	
BRAZIL, Maceió	105	106	86	-4		4	*	-9		0	*	-15	*	-5	*	
BRAZIL, Natal	93	102	86	-2		4	*	-4	*	0	*	-7	*	-4	*	
BRAZIL, Recife	81	86	86	-3		4	*	-7		0	*	-12	*	-4	*	
BRAZIL, Porto Alegre	78	83	14	7		18	*	6	*	21	*	17	*	40	*	
BRAZIL, Rio de Janeiro	54	56	54	-3	*	1	*	-10	*	-4	*	-20	*	-7	*	
BRAZIL, Salvador	113	116	81	-3		8	*	-8	*	6	*	-15		1	*	
CAMEROON, Douala	110	128	70	-3	*	-16	*	-4	*	5	*	7	*	17	*	
CANADA, Montréal	84	55	182	-8	*	66	*	-37	*	113	*	-49	*	21	*	
CANADA, Vancouver	32	15	170	3	*	-9	*	8	*	-20	*	18	*	-20	*	
CHINA, Dalian	55	63	67	12		-3	*	34	*	7	*	72	*	17	*	
CHINA, Fuzhou Fujian	42	48	234	22		6	*	62	*	20	*	113	*	38	*	
CHINA, Guangzhou Guangdong	2	11	121	-23	*	-19	*	-40	*	-30	*	-34	*	-61	*	
CHINA, Shenzen	18	31	100	-11	*	-8	*	-24	*	-17	*	-17	*	-40	*	
CHINA, Hangzhou	92	108	166	16		25	*	37	*	22	*	66	*	-75	*	
CHINA, Ningbo	34	40	68	28		20	*	62	*	34	*	110	*	21	*	
CHINA, Qingdao	57	65	93	9		0	*	29	*	10	*	81	*	38	*	

COUNTRY, City/Agglomeration	Present Day Exposure Ranking		MHW (cm)													
	Population	Asset	Control	+2UF		+2UR		+5UF		+5UR		+10UF		+10UR		
CHINA, Shanghai	3	13	205	-21	*	-22		-41	*	-29	*	-33	*	-79	*	
CHINA, Taipei	49	59	85	16		8	*	45	*	26	*	89	*	45	*	
CHINA, Tianjin	12	25	67	12	*	1	*	31	*	-21	*	38	*	-47	*	
CHINA, Wenzhou	58	71	216	5	*	15	*	30	*	15	*	52	*	28	*	
CHINA, Xiamen	36	44	212	15		2	*	45	*	31	*	86	*	26	*	
CHINA, Yantai	115	119	33	7	*	-5	*	37	*	4	*	68	*	6	*	
CHINA, Zhanjiang	40	45	112	-12	*	-7	*	-22	*	-20	*	-15	*	-35	*	
CHINA, HONG KONG SAR, Hong Kong	41	20	70	-5		-2	*	-10	*	-8	*	-1	*	-17	*	
COLOMBIA, Barranquilla	129	129	13	0	*	2	*	-2	*	1	*	-2	*	0	*	
CÔTE D'IVOIRE, Abidjan	20	58	44	0	*	1	*	1	*	2	*	8	*	4	*	
CUBA, Havana	133	132	20	1	*	-1	*	1	*	-1	*	1	*	-1	*	
NORTH KOREA, Namp'o	87	121	167	12	*	-6	*	37	*	8	*	87	*	9	*	
DENMARK, Copenhagen	82	53	27	9	*	15	*	-21	*	-8	*	-8	*	-17	*	
DOMINICAN REPUBLIC, Santo Domingo	109	114	10	0	*	1	*	-1	*	0	*	-1	*	-1	*	
ECUADOR, Guayaquil	26	41	152	7	*	-71	*	-1	*	-91	*	-20	*	-73	*	
EGYPT, Alexandria	9	26	11	1	*	1	*	0	*	0	*	0	*	-1	*	
FINLAND, Helsinki	119	89	7	2	*	0	*	1	*	-2	*	2	*	-1	*	
FRANCE, Marseille-Aix-en-Provence	102	78	3	0	*	0	*	0	*	0	*	1	*	0	*	
GERMANY, Hamburg	37	18	156	-1	*	-96	*	8	*	-143	*	32	*	-137	*	
GHANA, Accra	104	123	56	-1	*	0	*	0	*	0	*	8	*	2	*	
GREECE, Athens	127	118	8	0	*	0	*	0	*	-1	*	-1	*	-1	*	
GUINEA, Conakry	70	113	156	-21	*	-15	*	-34	*	-31	*	-49	*	-46	*	
HAITI, Port-au-Prince	135	136	17	0	*	0	*	-1	*	0	*	-1	*	-2	*	
INDIA, Madras	46	70	31	0	*	0	*	-1	*	0	*	-2	*	-1	*	
INDIA, Cochin	56	80	25	0	*	2	*	1	*	2	*	3	*	0	*	
INDIA, Calcutta	6	22	127	-12	*	-43	*	-23	*	-36	*	-37	*	-40	*	
INDIA, Bombay	1	17	148	-8	*	9	*	-10	*	20	*	-4	*	31	*	
INDIA, Surat	24	46	228	9	*	26	*	26	*	58	*	60	*	66	*	
INDIA, Visakhapatnam	83	111	46	-1	*	0	*	-1	*	-1	*	-4	*	-3	*	
INDONESIA, Jakarta	21	39	52	-4	*	0	*	-15	*	-5	*	-18	*	5	*	
INDONESIA, Palembang	48	73	76	18	*	-10	*	36	*	-9	*	61	*	6	*	

COUNTRY, City/Agglomeration	Present Day Exposure Ranking		MHW (cm)													
	Population	Asset	Control	+2UF		+2UR		+5UF		+5UR		+10UF		+10UR		
INDONESIA, Surabaya	68	88	194	-25		-50	*	-52	*	-57	*	-86	*	-98	*	
INDONESIA, Ujung Pandang	118	126	38	1	*	-1	*	3	*	2	*	1	*	3	*	
IRELAND, Dublin	95	62	129	12		-22	*	29		-29	*	54	*	-19	*	
ISRAEL, Tel Aviv-Jaffa	136	135	16	2	*	1	*	1	*	0	*	0	*	-2	*	
ITALY, Naples	131	117	5	-1	*	0	*	-1	*	0	*	-1	*	0	*	
JAPAN, Fukuoka-Kitakyushu	33	16	79	-1		-1		-3	*	-2	*	-7	*	3	*	
JAPAN, Hiroshima	44	24	175	-10	*	-58	*	-22	*	-45	*	-46	*	-15	*	
JAPAN, Nagoya	19	8	67	-1		-1	*	-3	*	1	*	-6	*	3	*	
JAPAN, Osaka-Kobe	8	4	102	-5	*	-1	*	-17	*	-6	*	-37	*	9	*	
JAPAN, Sapporo	121	100	10	0	*	0	*	1	*	1	*	1		1		
JAPAN, Tokyo	11	5	43	0	*	1	*	-1	*	2	*	-1	*	3	*	
KUWAIT, Kuwait City	101	84	99	9	*	-13	*	-5	*	-41	*	-22	*	-44	*	
LEBANON, Beirut	120	125	16	2	*	1	*	1	*	0	*	0	*	-2	*	
LIBYA, Banghazi	73	77	4	1	*	0	*	2		-1	*	3	*	-1	*	
LIBYA, Tripoli	126	122	14	3		1	*	3	*	-2	*	3	*	-3	*	
MALAYSIA, Kuala Lumpur	35	33	127	6	*	-15	*	9	*	-20	*	5	*	-16	*	
MOROCCO, Casablanca	75	97	120	-1	*	3	*	-3	*	2	*	-6	*	-3	*	
MOROCCO, Rabat	111	120	119	-1	*	4	*	-3	*	3	*	-6	*	-3	*	
MOZAMBIQUE, Maputo	66	112	101	-4		-2	*	-10	*	-5	*	-16	*	-7	*	
MYANMAR, Rangoon	22	60	158	33		-6	*	85		-21	*	168		-12	*	
NETHERLANDS, Amsterdam	15	6	76	7	*	-33	*	9	*	-22	*	23	*	-10	*	
NETHERLANDS, Rotterdam	17	7	131	-8	*	-69	*	-18	*	-72	*	-11	*	-65	*	
NEW ZEALAND, Auckland	116	92	112	0	*	0	*	-3	*	-1	*	-4	*	-1	*	
NIGERIA, Lagos	30	76	58	-1	*	0	*	-1	*	0	*	9	*	2	*	
PAKISTAN, Karachi	69	105	91	-2	*	10	*	-3	*	10	*	1	*	5	*	
PANAMA, Panama City	99	109	237	-7		2	*	-19	*	-9	*	-33		-28	*	
PERU, Lima	132	130	37	0	*	-2	*	-1	*	-2	*	-2	*	-3	*	
PHILIPPINES, Davao	130	131	60	0	*	-2	*	0	*	-1	*	-2	*	0	*	
PHILIPPINES, Manila	53	66	55	-2	*	-4	*	-6	*	-8	*	-5	*	-11	*	
PORTUGAL, Lisbon	71	57	115	-1	*	4	*	-3	*	2	*	-5	*	-4	*	
PORTUGAL, Porto	103	82	119	-1	*	3	*	-2	*	1	*	-4	*	-4		

COUNTRY, City/Agglomeration	Present Day Exposure Ranking		MHW (cm)													
	Population	Asset	Control	+2UF		+2UR		+5UF		+5UR		+10UF		+10UR		
PUERTO RICO, San Juan	65	49	16	0	*	-2	*	0	*	-4	*	0	*	-5	*	
SOUTH KOREA, Pusan	60	42	61	0	*	-1	*	-2	*	4	*	-4	*	2	*	
SOUTH KOREA, Ulsan	117	95	25	0	*	-1	*	-1	*	-2	*	-2	*	1	*	
SOUTH KOREA, Inchon	43	30	353	13		-10	*	26	*	4	*	0	*	-32	*	
RUSSIA, St. Petersburg	45	38	14	3	*	7	*	-3	*	-3	*	-1	*	-6	*	
SAUDI ARABIA, Jiddah	97	85	7	1	*	1	*	2	*	0	*	3	*	1	*	
SENEGAL, Dakar	90	124	48	0	*	-2	*	1	*	-3	*	0	*	-5	*	
SINGAPORE, Singapore	96	75	31	8	*	-12	*	27	*	-16	*	67	*	3	*	
SOMALIA, Mogadishu	114	133	66	1	*	3	*	2	*	3	*	4	*	3	*	
SOUTH AFRICA, Cape Town	112	107	63	-1	*	6	*	-3	*	6	*	-3	*	6	*	
SOUTH AFRICA, Durban	98	93	77	-2	*	0	*	-5	*	-1	*	-8		0	*	
SPAIN, Barcelona	108	81	2	0	*	0	*	0	*	0	*	0	*	0	*	
SWEDEN, Stockholm	128	115	14	3	*	3	*	-11	*	-6	*	-9	*	-10	*	
THAILAND, Bangkok	13	19	117	2	*	-7	*	5	*	-55	*	-1	*	-43	*	
TOGO, Lomé	50	90	57	-1	*	0	*	-1	*	0	*	8	*	2	*	
TURKEY, Istanbul	62	64	0	0	*	0	*	0	*	0	*	0	*	0	*	
TURKEY, Izmir	79	87	32	2	*	3	*	-1	*	-4	*	-6	*	-8	*	
UKRAINE, Odessa	61	67	10	-4	*	-4	*	-5	*	10	*	-6	*	-7	*	
UNITED ARAB EMIRATES, Dubai	38	23	52	3	*	-6	*	6	*	1	*	26	*	25		
UNITED KINGDOM, Glasgow	91	68	133	5	*	-29	*	14	*	-43	*	26	*	-33	*	
UNITED KINGDOM, London	28	14	273	0	*	-12	*	9	*	11	*	30		21	*	
TANZANIA, Dar-es-Salaam	74	127	99	1		5	*	3	*	4	*	6		3	*	
USA, Baltimore	52	29	32	3	*	-7	*	9	*	1	*	21	*	-6	*	
USA, Boston	29	12	225	1	*	-15	*	0	*	-23	*	-10	*	-29	*	
USA, Houston	67	36	65	-15	*	-30	*	-26	*	-32	*	-39	*	-45	*	
USA, Los Angeles-Long Beach	59	32	72	0	*	0		1	*	-1	*	4	*	1	*	
USA, Miami	4	1	30	1	*	-3	*	4	*	-6	*	5	*	-8	*	
USA, New Orleans	10	3	16	14	*	16	*	24		6	*	20	*	1	*	
USA, New York-Newark	7	2	55	0	*	-7	*	-1	*	-13	*	-1	*	-15	*	
USA, Philadelphia	47	21	73	-5		4	*	-10	*	-16		-14	*	-11	*	
USA, Portland	106	69	104	1	*	0	*	2	*	-1	*	5	*	-1	*	

COUNTRY, City/Agglomeration	Present Day Exposure Ranking		MHW (cm)													
	Population	Asset	Control	+2UF		+2UR		+5UF		+5UR		+10UF		+10UR		
USA, Providence	63	34	33	0	*	-4	*	1	*	-15	*	7	*	-14	*	
USA, San Diego	125	94	72	0	*	0	*	0	*	0	*	3	*	1	*	
USA, San Francisco - Oakland	51	28	72	0	*	0	*	1	*	0	*	5	*	4	*	
USA, San Jose	122	91	72	0	*	0	*	1	*	0	*	5	*	4	*	
USA, Seattle	80	50	121	2	*	-15	*	6	*	-17	*	12	*	-17	*	
USA, Tampa-St Petersburg	25	9	37	5	*	-10	*	1	*	15	*	-4	*	10	*	
USA, Virginia Beach	27	10	35	-2	*	-4	*	-4	*	2	*	-8	*	7	*	
USA, Washington, D C	76	47	29	3	*	-1	*	10	*	4	*	21	*	-4	*	
URUGUAY, Montevideo	94	96	20	11	*	3	*	30		-5	*	82	*	1	*	
VENEZUELA, Maracaibo	85	101	42	2	*	3	*	-12	*	-13	*	-22	*	-26	*	
VIETNAM, Hai Phòng	16	37	95	6		3	*	14	*	10	*	36	*	22	*	
VIETNAM, Ho Chi Minh City	5	27	128	-27	*	-46	*	-41	*	-70	*	6	*	-74	*	

Full version of Table 3.13

	Present Day Exposure Ranking		MHW (cm)						
COUNTRY, City/Agglomeration	Population	Asset	Control	+2UF	+2NUGF	+2NUWAF	+2NUBF	+2UR	+2NUBR
ALGERIA, Algiers	88	99	4	0	0	0	0	0	0
ANGOLA, Luanda	134	134	54	-2	-2	-2	-2	0	0
ARGENTINA, Buenos Aires	64	52	98	-15	-17	-13	-15	-64	-63
AUSTRALIA, Adelaide	123	103	86	0	2	3	2	17	4
AUSTRALIA, Brisbane	86	61	64	-1	-1	-2	-1	-3	-3
AUSTRALIA, Melbourne	100	74	74	7	8	7	7	10	10
AUSTRALIA, Perth	77	51	25	0	0	0	0	-1	-1
AUSTRALIA, Sydney	124	104	55	-1	0	-1	-1	-2	-2
BANGLADESH, Chittagong	39	72	147	16	18	16	17	-13	-17
BANGLADESH, Dhaka	14	43	134	25	28	26	27	-1	-40
BANGLADESH, Khulna	23	54	87	-4	-4	-4	-4	19	16
BRAZIL, Santos	89	98	74	-6	-6	-6	-5	1	0
BRAZIL, Belém	72	79	233	28	27	29	28	-131	-140
BRAZIL, Fortaleza	107	110	100	-2	-2	-2	-2	1	0
BRAZIL, Grande Vitória	31	35	65	-3	-3	-3	-3	3	1
BRAZIL, Maceió	105	106	86	-4	-3	-4	-3	4	2
BRAZIL, Natal	93	102	86	-2	-1	-2	-2	4	2
BRAZIL, Recife	81	86	86	-3	-2	-3	-3	4	2
BRAZIL, Porto Alegre	78	83	14	7	7	6	7	18	19
BRAZIL, Rio de Janeiro	54	56	54	-3	-3	-3	-3	1	0
BRAZIL, Salvador	113	116	81	-3	-2	-3	-3	8	7
CAMEROON, Douala	110	128	70	-3	-3	-2	-3	-16	-16
CANADA, Montréal	84	55	182	-8	8	-18	1	66	74
CANADA, Vancouver	32	15	170	3	2	3	3	-9	-9
CHINA, Dalian	55	63	67	12	14	12	13	-3	-5
CHINA, Fuzhou Fujian	42	48	234	22	26	22	24	6	-1
CHINA, Guangzhou Guangdong	2	11	121	-23	-26	-24	-25	-19	-18
CHINA, Shenzen	18	31	100	-11	-14	-12	-13	-8	-7
CHINA, Hangzhou	92	108	166	16	19	17	18	25	19

COUNTRY, City/Agglomeration	Present Day Exposure Ranking		MHW (cm)						
	Population	Asset	Control	+2UF	+2NUGF	+2NUWAF	+2NUBF	+2UR	+2NUBR
CHINA, Ningbo	34	40	68	28	32	29	31	20	17
CHINA, Qingdao	57	65	93	9	11	9	10	0	-4
CHINA, Shanghai	3	13	205	-21	-23	-22	-23	-22	-19
CHINA, Taipei	49	59	85	16	19	17	18	8	5
CHINA, Tianjin	12	25	67	12	13	12	13	1	-3
CHINA, Wenzhou	58	71	216	5	7	5	6	15	8
CHINA, Xiamen	36	44	212	15	19	16	17	2	19
CHINA, Yantai	115	119	33	7	9	7	8	-5	-6
CHINA, Zhanjiang	40	45	112	-12	-13	-12	-13	-7	-6
CHINA, HONG KONG SAR, Hong Kong	41	20	70	-5	-6	-6	-6	-2	-2
COLOMBIA, Barranquilla	129	129	13	0	0	-1	0	2	2
CÔTE D'IVOIRE, Abidjan	20	58	44	0	0	0	0	1	1
CUBA, Havana	133	132	20	1	1	1	1	-1	-1
NORTH KOREA, Namp'o	87	121	167	12	14	12	13	-6	-6
DENMARK, Copenhagen	82	53	27	9	4	8	17	15	-4
DOMINICAN REPUBLIC, Santo Domingo	109	114	10	0	0	0	0	1	1
ECUADOR, Guayaquil	26	41	152	7	7	7	7	-71	-70
EGYPT, Alexandria	9	26	11	1	1	1	1	1	1
FINLAND, Helsinki	119	89	7	2	-1	2	1	0	0
FRANCE, Marseille-Aix-en-Provence	102	78	3	0	0	0	0	0	0
GERMANY, Hamburg	37	18	156	-1	-1	0	3	-96	-99
GHANA, Accra	104	123	56	-1	-1	-1	-1	0	0
GREECE, Athens	127	118	8	0	0	0	0	0	0
GUINEA, Conakry	70	113	156	-21	-19	-23	-22	-15	-16
HAITI, Port-au-Prince	135	136	17	0	0	0	0	0	0
INDIA, Madras	46	70	31	0	0	0	0	0	0
INDIA, Cochin	56	80	25	0	1	0	0	2	1
INDIA, Calcutta	6	22	127	-12	-12	-11	-12	-43	-40
INDIA, Bombay	1	17	148	-8	-4	-10	-7	9	5

COUNTRY, City/Agglomeration	Present Day Exposure Ranking		MHW (cm)						
	Population	Asset	Control	+2UF	+2NUGF	+2NUWAF	+2NUBF	+2UR	+2NUBR
INDIA, Surat	24	46	228	9	14	7	11	26	22
INDIA, Visakhapatnam	83	111	46	-1	-1	0	0	0	0
INDONESIA, Jakarta	21	39	52	-4	-5	-6	-5	0	-2
INDONESIA, Palembang	48	73	76	18	19	20	19	-10	-21
INDONESIA, Surabaya	68	88	194	-25	-27	-29	-29	-50	-50
INDONESIA, Ujung Pandang	118	126	38	1	1	1	1	-1	-1
IRELAND, Dublin	95	62	129	12	-2	14	6	-22	-28
ISRAEL, Tel Aviv-Jaffa	136	135	16	2	1	2	1	1	1
ITALY, Naples	131	117	5	-1	0	-1	0	0	0
JAPAN, Fukuoka-Kitakyushu	33	16	79	-1	-1	-1	-1	-1	0
JAPAN, Hiroshima	44	24	175	-10	-11	-11	-11	-58	-68
JAPAN, Nagoya	19	8	67	-1	-2	-2	-2	-1	NaN
JAPAN, Osaka-Kobe	8	4	102	-5	-7	-6	-7	-1	-2
JAPAN, Sapporo	121	100	10	0	0	0	0	0	0
JAPAN, Tokyo	11	5	43	0	0	0	0	1	2
KUWAIT, Kuwait City	101	84	99	9	10	8	10	-13	-15
LEBANON, Beirut	120	125	16	2	1	2	1	1	1
LIBYA, Banghazi	73	77	4	1	1	1	1	0	0
LIBYA, Tripoli	126	122	14	3	2	3	2	1	0
MALAYSIA, Kuala Lumpur	35	33	127	6	7	7	7	-15	-20
MOROCCO, Casablanca	75	97	120	-1	0	-2	-1	3	-3
MOROCCO, Rabat	111	120	119	-1	0	-2	-1	4	-2
MOZAMBIQUE, Maputo	66	112	101	-4	-5	-4	-4	-2	-2
MYANMAR, Rangoon	22	60	158	33	36	34	35	-6	-2
NETHERLANDS, Amsterdam	15	6	76	7	4	7	6	-33	-41
NETHERLANDS, Rotterdam	17	7	131	-8	2	-9	-4	-69	-75
NEW ZEALAND, Auckland	116	92	112	0	-1	-1	-1	0	0
NIGERIA, Lagos	30	76	58	-1	-2	-1	-1	0	0
PAKISTAN, Karachi	69	105	91	-2	0	-3	-2	10	7

	Present Day Exposure Ranking		MHW (cm)						
COUNTRY, City/Agglomeration	Population	Asset	Control	+2UF	+2NUGF	+2NUWAF	+2NUBF	+2UR	+2NUBR
PANAMA, Panama City	99	109	237	-7	-7	-9	-8	2	1
PERU, Lima	132	130	37	0	0	0	0	-2	-2
PHILIPPINES, Davao	130	131	60	0	0	0	0	-2	-3
PHILIPPINES, Manila	53	66	55	-2	-3	-3	-3	-4	-4
PORTUGAL, Lisbon	71	57	115	-1	-1	-1	-1	4	-2
PORTUGAL, Porto	103	82	119	-1	-1	-1	-1	3	-2
PUERTO RICO, San Juan	65	49	16	0	0	0	0	-2	1
SOUTH KOREA, Pusan	60	42	61	0	0	0	0	-1	7
SOUTH KOREA, Ulsan	117	95	25	0	0	0	0	-1	-1
SOUTH KOREA, Inchon	43	30	353	13	15	13	14	-10	-6
RUSSIA, St. Petersburg	45	38	14	3	3	3	8	7	1
SAUDI ARABIA, Jiddah	97	85	7	1	1	1	1	1	1
SENEGAL, Dakar	90	124	48	0	0	1	0	-2	-1
SINGAPORE, Singapore	96	75	31	8	9	9	9	-12	-9
SOMALIA, Mogadishu	114	133	66	1	1	1	1	3	2
SOUTH AFRICA, Cape Town	112	107	63	-1	0	-2	-1	6	4
SOUTH AFRICA, Durban	98	93	77	-2	-1	-1	-1	0	0
SPAIN, Barcelona	108	81	2	0	0	0	0	0	0
SWEDEN, Stockholm	128	115	14	3	2	3	6	3	0
THAILAND, Bangkok	13	19	117	2	3	2	3	-7	-67
TOGO, Lomé	50	90	57	-1	-1	-1	-1	0	0
TURKEY, Istanbul	62	64	0	0	0	0	0	0	0
TURKEY, Izmir	79	87	32	2	1	2	1	3	3
UKRAINE, Odessa	61	67	10	-4	-4	-4	-4	-4	-4
UNITED ARAB EMIRATES, Dubai	38	23	52	3	4	3	4	-6	-6
UNITED KINGDOM, Glasgow	91	68	133	5	0	6	2	-29	-36
UNITED KINGDOM, London	28	14	273	0	-2	0	4	-12	-26
TANZANIA, Dar-es-Salaam	74	127	99	1	2	1	1	5	4
USA, Baltimore	52	29	32	3	1	4	2	-7	-4

	Present Day Exposure Ranking		MHW (cm)						
COUNTRY, City/Agglomeration	Population	Asset	Control	+2UF	+2NUGF	+2NUWAF	+2NUBF	+2UR	+2NUBR
USA, Boston	29	12	225	1	-2	2	0	-15	-4
USA, Houston	67	36	65	-15	-15	-13	-15	-30	-34
USA, Los Angeles-Long Beach	59	32	72	0	0	0	0	0	0
USA, Miami	4	1	30	1	0	1	0	-3	0
USA, New Orleans	10	3	16	14	11	16	14	16	17
USA, New York-Newark	7	2	55	0	-1	-1	-1	-7	1
USA, Philadelphia	47	21	73	-5	-5	-6	-6	4	18
USA, Portland	106	69	104	1	1	0	1	0	0
USA, Providence	63	34	33	0	-1	0	-1	-4	3
USA, San Diego	125	94	72	0	0	0	0	0	0
USA, San Francisco - Oakland	51	28	72	0	0	0	0	0	0
USA, San Jose	122	91	72	0	0	0	0	0	0
USA, Seattle	80	50	121	2	1	2	2	-15	-14
USA, Tampa-St Petersburg	25	9	37	5	4	8	5	-10	-13
USA, Virginia Beach	27	10	35	-2	-2	-2	-2	-4	1
USA, Washington, D C	76	47	29	3	1	4	2	-1	1
URUGUAY, Montevideo	94	96	20	11	13	9	11	3	4
VENEZUELA, Maracaibo	85	101	42	2	3	1	2	3	2
VIETNAM, Hai Phòng	16	37	95	6	7	6	7	3	8
VIETNAM, Ho Chi Minh City	5	27	128	-27	-30	-30	-30	-46	-57

Full version of Table 3.4

	Present Day Exposure Ranking		Local SLR (cm)			Local SLR (cm)				Local SLF (cm)
COUNTRY, City/Agglomeration	Population	Asset	+2UR	+5UR	+10UR	+2NUGF	+2NUWAF	+2NUBF	+2NUBR	-2UA
ALGERIA, Algiers	88	99	200	500	1000	114	209	162	162	-200
ANGOLA, Luanda	134	134	82	183	527	215	215	215	-3	-200
ARGENTINA, Buenos Aires	64	52	75	375	875	247	148	197	72	NaN
AUSTRALIA, Adelaide	123	103	126	249	470	194	214	204	19	-200
AUSTRALIA, Brisbane	86	61	174	428	910	203	220	211	175	-151
AUSTRALIA, Melbourne	100	74	161	377	787	195	208	201	123	-200
AUSTRALIA, Perth	77	51	88	328	758	201	232	217	46	-200
AUSTRALIA, Sydney	124	104	62	362	862	199	213	206	68	-200
BANGLADESH, Chittagong	39	72	129	298	714	213	197	205	100	-200
BANGLADESH, Dhaka	14	43	12	254	754	212	196	204	-42	-200
BANGLADESH, Khulna	23	54	-111	189	689	214	198	206	-105	-200
BRAZIL, Santos	89	98	139	418	918	240	184	212	129	-200
BRAZIL, Belém	72	79	59	359	859	204	213	208	68	NaN
BRAZIL, Fortaleza	107	110	57	276	698	216	218	217	10	-200
BRAZIL, Grande Vitória	31	35	-152	126	574	240	196	218	-135	-200
BRAZIL, Maceió	105	106	39	297	772	226	213	220	44	-147
BRAZIL, Natal	93	102	2	244	744	222	219	221	-16	-200
BRAZIL, Recife	81	86	-48	208	708	226	217	221	-72	-200
BRAZIL, Porto Alegre	78	83	109	397	887	245	166	205	102	-31
BRAZIL, Rio de Janeiro	54	56	-213	-15	424	241	189	215	-198	-200
BRAZIL, Salvador	113	116	66	327	776	228	206	217	70	-47
CAMEROON, Douala	110	128	138	438	938	195	209	202	140	-198
CANADA, Montréal	84	55	200	500	1000	21	238	130	130	-200
CANADA, Vancouver	32	15	-621	-419	-20	140	240	190	-630	-200
CHINA, Dalian	55	63	180	459	959	223	200	212	171	-200
CHINA, Fuzhou Fujian	42	48	200	489	989	232	209	220	209	-200
CHINA, Guangzhou Guangdong	2	11	186	486	942	227	205	216	202	NaN
CHINA, Shenzen	18	31	173	461	893	227	206	217	190	NaN
CHINA, Hangzhou	92	108	200	470	924	230	205	218	203	-200
CHINA, Ningbo	34	40	182	482	822	233	208	220	201	-200
CHINA, Qingdao	57	65	200	247	634	225	201	213	108	-200
CHINA, Shanghai	3	13	162	372	621	232	207	220	181	-200
CHINA, Taipei	49	59	-38	-158	143	236	212	224	-233	-200
CHINA, Tianjin	12	25	188	440	792	217	195	206	180	-190

	Present Day Exposure Ranking		Local SLR (cm)			Local SLR (cm)				Local SLF (cm)
COUNTRY, City/Agglomeration	Population	Asset	+2UR	+5UR	+10UR	+2NUGF	+2NUWAF	+2NUBF	+2NUBR	-2UA
CHINA, Wenzhou	58	71	200	488	988	233	208	221	220	-155
CHINA, Xiamen	36	44	165	452	870	232	209	220	172	-190
CHINA, Yantai	115	119	200	463	963	225	201	213	195	-200
CHINA, Zhanjiang	40	45	117	242	663	226	206	216	58	-200
CHINA, HONG KONG SAR, Hong Kong	41	20	162	462	857	229	208	218	180	-200
COLOMBIA, Barranquilla	129	129	49	253	690	191	230	211	15	-200
CÔTE D'IVOIRE, Abidjan	20	58	200	500	1000	198	217	208	208	-200
CUBA, Havana	133	132	200	500	-901	171	244	207	207	-200
NORTH KOREA, Namp'o	87	121	23	227	552	225	202	214	-25	-200
DENMARK, Copenhagen	82	53	118	279	696	29	206	117	35	-200
DOMINICAN REPUBLIC, Santo Domingo	109	114	200	-682	-1317	174	240	207	-974	-200
ECUADOR, Guayaquil	26	41	65	291	791	212	211	212	3	-200
EGYPT, Alexandria	9	26	183	379	716	159	194	176	160	-200
FINLAND, Helsinki	119	89	200	500	1000	32	199	116	116	-200
FRANCE, Marseille-Aix-en-Provence	102	78	200	393	782	89	208	149	149	-200
GERMANY, Hamburg	37	18	94	388	888	31	207	119	13	NaN
GHANA, Accra	104	123	200	500	1000	197	216	207	206	-200
GREECE, Athens	127	118	200	311	441	136	197	167	167	-200
GUINEA, Conakry	70	113	100	383	794	188	220	204	105	NaN
HAITI, Port-au-Prince	135	136	121	421	921	175	240	207	129	-200
INDIA, Madras	46	70	200	500	1000	219	212	215	215	-200
INDIA, Cochin	56	80	-31	177	677	218	215	217	-81	-200
INDIA, Calcutta	6	22	173	473	973	213	198	205	178	-81
INDIA, Bombay	1	17	119	363	836	209	202	205	101	NaN
INDIA, Surat	24	46	80	346	763	205	197	201	60	NaN
INDIA, Visakhapatnam	83	111	200	500	1000	216	205	210	210	-200
INDONESIA, Jakarta	21	39	148	342	770	220	234	227	124	-28
INDONESIA, Palembang	48	73	87	387	887	221	230	225	112	-95
INDONESIA, Surabaya	68	88	150	369	774	220	235	227	177	-200
INDONESIA, Ujung Pandang	118	126	134	394	787	220	232	226	149	-127
IRELAND, Dublin	95	62	68	354	782	-9	221	106	-27	-200
ISRAEL, Tel Aviv-Jaffa	136	135	129	360	786	160	191	176	105	-200
ITALY, Naples	131	117	-123	-134	-222	114	203	159	-164	-200
JAPAN, Fukuoka-Kitakyushu	33	16	87	281	781	237	213	225	6	-200

	Present Day Exposure Ranking		Local SLR (cm)			Local SLR (cm)				Local SLF (cm)
COUNTRY, City/Agglomeration	Population	Asset	+2UR	+5UR	+10UR	+2NUGF	+2NUWAF	+2NUBF	+2NUBR	-2UA
JAPAN, Hiroshima	44	24	136	303	662	237	213	225	161	-200
JAPAN, Nagoya	19	8	200	500	1000	240	217	228	NaN	-200
JAPAN, Osaka-Kobe	8	4	139	126	570	239	215	227	-39	-200
JAPAN, Sapporo	121	100	88	4	98	232	216	224	58	-200
JAPAN, Tokyo	11	5	200	241	741	241	219	230	230	-200
KUWAIT, Kuwait City	101	84	86	344	673	176	188	182	68	-200
LEBANON, Beirut	120	125	200	500	-1867	157	191	174	174	-200
LIBYA, Banghazi	73	77	63	234	496	148	199	173	37	-200
LIBYA, Tripoli	126	122	200	247	747	138	202	170	170	-200
MALAYSIA, Kuala Lumpur	35	33	112	406	906	221	223	222	128	-71
MOROCCO, Casablanca	75	97	-300	0	500	117	217	167	-333	-200
MOROCCO, Rabat	111	120	35	17	517	115	215	165	0	-200
MOZAMBIQUE, Maputo	66	112	193	483	969	228	225	226	219	-125
MYANMAR, Rangoon	22	60	38	313	778	220	207	213	35	NaN
NETHERLANDS, Amsterdam	15	6	200	500	1000	32	211	122	122	-98
NETHERLANDS, Rotterdam	17	7	200	500	1000	34	210	122	122	-200
NEW ZEALAND, Auckland	116	92	88	373	831	211	198	204	91	NaN
NIGERIA, Lagos	30	76	200	500	1000	193	212	203	203	-200
PAKISTAN, Karachi	69	105	112	336	709	199	194	196	108	-103
PANAMA, Panama City	99	109	144	401	765	198	230	214	139	-200
PERU, Lima	132	130	-328	-286	-33	225	198	211	-574	-200
PHILIPPINES, Davao	130	131	200	-1343	-1166	233	228	230	-565	-200
PHILIPPINES, Manila	53	66	190	490	990	235	220	227	217	-200
PORTUGAL, Lisbon	71	57	200	500	1000	93	221	157	157	-200
PORTUGAL, Porto	103	82	103	403	786	80	221	150	54	-200
PUERTO RICO, San Juan	65	49	-2021	-3218	-3827	174	242	208	-2300	-200
SOUTH KOREA, Pusan	60	42	57	144	550	235	211	223	-91	-200
SOUTH KOREA, Ulsan	117	95	88	-105	0	235	211	223	3	-200
SOUTH KOREA, Inchon	43	30	128	363	793	229	205	217	130	-200
RUSSIA, St. Petersburg	45	38	200	500	1000	44	196	120	120	-200
SAUDI ARABIA, Jiddah	97	85	-7120	-13603	-22754	180	194	187	-7132	-200
SENEGAL, Dakar	90	124	-527	-227	-1634	178	226	202	-525	-200
SINGAPORE, Singapore	96	75	167	467	967	224	228	226	192	-23
SOMALIA, Mogadishu	114	133	200	500	1000	209	216	213	212	-200

	Present Day Exposure Ranking		Local SLR (cm)			Local SLR (cm)				Local SLF (cm)
COUNTRY, City/Agglomeration	Population	Asset	+2UR	+5UR	+10UR	+2NUGF	+2NUWAF	+2NUBF	+2NUBR	-2UA
SOUTH AFRICA, Cape Town	112	107	200	248	748	243	217	230	102	-200
SOUTH AFRICA, Durban	98	93	200	500	1000	233	225	229	229	-200
SPAIN, Barcelona	108	81	200	350	-323	95	211	153	153	-200
SWEDEN, Stockholm	128	115	90	251	636	19	204	112	2	-200
THAILAND, Bangkok	13	19	200	500	1000	221	210	215	215	-177
TOGO, Lomé	50	90	120	301	801	195	214	204	85	-200
TURKEY, Istanbul	62	64	110	322	822	133	193	163	73	-200
TURKEY, Izmir	79	87	170	404	854	138	195	167	136	-200
UKRAINE, Odessa	61	67	200	500	1000	117	192	155	155	-200
UNITED ARAB EMIRATES, Dubai	38	23	148	394	800	190	192	191	139	-200
UNITED KINGDOM, Glasgow	91	68	-44	223	638	-31	220	94	94	-200
UNITED KINGDOM, London	28	14	-190	110	610	29	213	121	-269	-200
TANZANIA, Dar-es-Salaam	74	127	-1524	-1224	-724	212	219	216	-1509	-200
USA, Baltimore	52	29	146	446	946	104	242	173	119	-200
USA, Boston	29	12	98	398	868	72	244	158	56	-200
USA, Houston	67	36	100	393	893	160	239	199	99	NaN
USA, Los Angeles-Long Beach	59	32	200	500	1000	182	246	214	215	-200
USA, Miami	4	1	184	336	784	161	246	203	169	-200
USA, New Orleans	10	3	60	295	795	154	240	197	57	NaN
USA, New York-Newark	7	2	164	387	725	88	242	165	129	-200
USA, Philadelphia	47	21	200	500	1000	98	242	170	170	-200
USA, Portland	106	69	175	361	589	154	244	199	147	-200
USA, Providence	63	34	180	480	980	80	245	163	143	-200
USA, San Diego	125	94	140	402	713	182	245	214	154	-200
USA, San Francisco - Oakland	51	28	200	500	1000	179	248	213	214	-200
USA, San Jose	122	91	200	500	1000	179	248	213	214	-200
USA, Seattle	80	50	56	-43	200	144	241	192	49	-200
USA, Tampa-St Petersburg	25	9	168	468	968	156	244	200	168	NaN
USA, Virginia Beach	27	10	40	52	443	111	244	178	18	-200
USA, Washington, D C	76	47	-42	198	674	105	242	174	-69	-200
URUGUAY, Montevideo	94	96	128	428	928	248	149	199	127	-52
VENEZUELA, Maracaibo	85	101	98	398	898	187	227	207	105	NaN
VIETNAM, Hai Phòng	16	37	118	319	796	222	203	213	60	NaN
VIETNAM, Ho Chi Minh City	5	27	200	500	1000	226	218	222	221	-104

Full version of Table 3.12

	Present Day Exposure Ranking		MHW (cm)			
COUNTRY, City/Agglomeration	Population	Asset	Control	+2UF	+2UR	-2UA
ALGERIA, Algiers	88	99	4	0	0	0
ANGOLA, Luanda	134	134	54	-2	0	2
ARGENTINA, Buenos Aires	64	52	98	-15	-64	NaN
AUSTRALIA, Adelaide	123	103	86	0	17	-7
AUSTRALIA, Brisbane	86	61	64	-1	-3	6
AUSTRALIA, Melbourne	100	74	74	7	10	-4
AUSTRALIA, Perth	77	51	25	0	-1	0
AUSTRALIA, Sydney	124	104	55	-1	-2	-1
BANGLADESH, Chittagong	39	72	147	16	-13	-6
BANGLADESH, Dhaka	14	43	134	25	-1	-17
BANGLADESH, Khulna	23	54	87	-4	19	4
BRAZIL, Santos	89	98	74	-6	1	2
BRAZIL, Belém	72	79	233	28	-131	NaN
BRAZIL, Fortaleza	107	110	100	-2	1	3
BRAZIL, Grande Vitória	31	35	65	-3	3	1
BRAZIL, Maceió	105	106	86	-4	4	3
BRAZIL, Natal	93	102	86	-2	4	2
BRAZIL, Recife	81	86	86	-3	4	2
BRAZIL, Porto Alegre	78	83	14	7	18	1
BRAZIL, Rio de Janeiro	54	56	54	-3	1	0
BRAZIL, Salvador	113	116	81	-3	8	2
CAMEROON, Douala	110	128	70	-3	-16	3
CANADA, Montréal	84	55	182	-8	66	56
CANADA, Vancouver	32	15	170	3	-9	-3
CHINA, Dalian	55	63	67	12	-3	5
CHINA, Fuzhou Fujian	42	48	234	22	6	-16
CHINA, Guangzhou Guangdong	2	11	121	-23	-19	NaN

	Present Day Exposure Ranking		MHW (cm)			
COUNTRY, City/Agglomeration	Population	Asset	Control	+2UF	+2UR	-2UA
CHINA, Shenzen	18	31	100	-11	-8	NaN
CHINA, Hangzhou	92	108	166	16	25	-12
CHINA, Ningbo	34	40	68	28	20	-17
CHINA, Qingdao	57	65	93	9	0	-1
CHINA, Shanghai	3	13	205	-21	-22	8
CHINA, Taipei	49	59	85	16	8	-12
CHINA, Tianjin	12	25	67	12	1	-7
CHINA, Wenzhou	58	71	216	5	15	1
CHINA, Xiamen	36	44	212	15	2	-5
CHINA, Yantai	115	119	33	7	-5	8
CHINA, Zhanjiang	40	45	112	-12	-7	27
CHINA, HONG KONG SAR, Hong Kong	41	20	70	-5	-2	8
COLOMBIA, Barranquilla	129	129	13	0	2	1
CÔTE D'IVOIRE, Abidjan	20	58	44	0	1	0
CUBA, Havana	133	132	20	1	-1	0
NORTH KOREA, Namp'o	87	121	167	12	-6	9
DENMARK, Copenhagen	82	53	27	9	15	-17
DOMINICAN REPUBLIC, Santo Domingo	109	114	10	0	1	1
ECUADOR, Guayaquil	26	41	152	7	-71	-11
EGYPT, Alexandria	9	26	11	1	1	0
FINLAND, Helsinki	119	89	7	2	0	-2
FRANCE, Marseille-Aix-en-Provence	102	78	3	0	0	0
GERMANY, Hamburg	37	18	156	-1	-96	NaN
GHANA, Accra	104	123	56	-1	0	1
GREECE, Athens	127	118	8	0	0	-1
GUINEA, Conakry	70	113	156	-21	-15	NaN
HAITI, Port-au-Prince	135	136	17	0	0	0

COUNTRY, City/Agglomeration	Present Day Exposure Ranking		MHW (cm)			
	Population	Asset	Control	+2UF	+2UR	-2UA
INDIA, Madras	46	70	31	0	0	0
INDIA, Cochin	56	80	25	0	2	1
INDIA, Calcutta	6	22	127	-12	-43	10
INDIA, Bombay	1	17	148	-8	9	NaN
INDIA, Surat	24	46	228	9	26	NaN
INDIA, Visakhapatnam	83	111	46	-1	0	1
INDONESIA, Jakarta	21	39	52	-4	0	6
INDONESIA, Palembang	48	73	76	18	-10	-17
INDONESIA, Surabaya	68	88	194	-25	-50	23
INDONESIA, Ujung Pandang	118	126	38	1	-1	4
IRELAND, Dublin	95	62	129	12	-22	-12
ISRAEL, Tel Aviv-Jaffa	136	135	16	2	1	0
ITALY, Naples	131	117	5	-1	0	0
JAPAN, Fukuoka-Kitakyushu	33	16	79	-1	-1	3
JAPAN, Hiroshima	44	24	175	-10	-58	11
JAPAN, Nagoya	19	8	67	-1	-1	1
JAPAN, Osaka-Kobe	8	4	102	-5	-1	2
JAPAN, Sapporo	121	100	10	0	0	0
JAPAN, Tokyo	11	5	43	0	1	0
KUWAIT, Kuwait City	101	84	99	9	-13	-8
LEBANON, Beirut	120	125	16	2	1	0
LIBYA, Banghazi	73	77	4	1	0	-1
LIBYA, Tripoli	126	122	14	3	1	-3
MALAYSIA, Kuala Lumpur	35	33	127	6	-15	2
MOROCCO, Casablanca	75	97	120	-1	3	2
MOROCCO, Rabat	111	120	119	-1	4	2
MOZAMBIQUE, Maputo	66	112	101	-4	-2	4

	Present Day Exposure Ranking		MHW (cm)			
COUNTRY, City/Agglomeration	Population	Asset	Control	+2UF	+2UR	-2UA
MYANMAR, Rangoon	22	60	158	33	-6	NaN
NETHERLANDS, Amsterdam	15	6	76	7	-33	59
NETHERLANDS, Rotterdam	17	7	131	-8	-69	-21
NEW ZEALAND, Auckland	116	92	112	0	0	NaN
NIGERIA, Lagos	30	76	58	-1	0	1
PAKISTAN, Karachi	69	105	91	-2	10	1
PANAMA, Panama City	99	109	237	-7	2	-2
PERU, Lima	132	130	37	0	-2	0
PHILIPPINES, Davao	130	131	60	0	-2	0
PHILIPPINES, Manila	53	66	55	-2	-4	-6
PORTUGAL, Lisbon	71	57	115	-1	4	2
PORTUGAL, Porto	103	82	119	-1	3	2
PUERTO RICO, San Juan	65	49	16	0	-2	1
SOUTH KOREA, Pusan	60	42	61	0	-1	2
SOUTH KOREA, Ulsan	117	95	25	0	-1	1
SOUTH KOREA, Inchon	43	30	353	13	-10	16
RUSSIA, St. Petersburg	45	38	14	3	7	-4
SAUDI ARABIA, Jiddah	97	85	7	1	1	0
SENEGAL, Dakar	90	124	48	0	-2	1
SINGAPORE, Singapore	96	75	31	8	-12	-2
SOMALIA, Mogadishu	114	133	66	1	3	1
SOUTH AFRICA, Cape Town	112	107	63	-1	6	0
SOUTH AFRICA, Durban	98	93	77	-2	0	0
SPAIN, Barcelona	108	81	2	0	0	0
SWEDEN, Stockholm	128	115	14	3	3	-9
THAILAND, Bangkok	13	19	117	2	-7	-3
TOGO, Lomé	50	90	57	-1	0	1

	Present Day Exposure Ranking		MHW (cm)			
COUNTRY, City/Agglomeration	Population	Asset	Control	+2UF	+2UR	-2UA
TURKEY, Istanbul	62	64	0	0	0	0
TURKEY, Izmir	79	87	32	2	3	-1
UKRAINE, Odessa	61	67	10	-4	-4	16
UNITED ARAB EMIRATES, Dubai	38	23	52	3	-6	-11
UNITED KINGDOM, Glasgow	91	68	133	5	-29	-3
UNITED KINGDOM, London	28	14	273	0	-12	-4
TANZANIA, Dar-es-Salaam	74	127	99	1	5	1
USA, Baltimore	52	29	32	3	-7	0
USA, Boston	29	12	225	1	-15	-2
USA, Houston	67	36	65	-15	-30	NaN
USA, Los Angeles-Long Beach	59	32	72	0	0	0
USA, Miami	4	1	30	1	-3	0
USA, New Orleans	10	3	16	14	16	NaN
USA, New York-Newark	7	2	55	0	-7	6
USA, Philadelphia	47	21	73	-5	4	17
USA, Portland	106	69	104	1	0	-1
USA, Providence	63	34	33	0	-4	3
USA, San Diego	125	94	72	0	0	0
USA, San Francisco - Oakland	51	28	72	0	0	0
USA, San Jose	122	91	72	0	0	0
USA, Seattle	80	50	121	2	-15	-2
USA, Tampa-St Petersburg	25	9	37	5	-10	NaN
USA, Virginia Beach	27	10	35	-2	-4	5
USA, Washington, D C	76	47	29	3	-1	-1
URUGUAY, Montevideo	94	96	20	11	3	19
VENEZUELA, Maracaibo	85	101	42	2	3	NaN
VIETNAM, Hai Phòng	16	37	95	6	3	NaN
VIETNAM, Ho Chi Minh City	5	27	128	-27	-46	42

Appendix 3.2- Table of Locations used for Global Coastal Cities and representative Tide Gauges for ESLs

Table of the latitude, longitude position of the model grid points used to represent the cities and flags for city centres far from this grid point (e.g. up an estuary) and the UHSLC tide gauge stations used for the return periods analysis (Section 3.5.2).

	Representative Model Grid Point			
COUNTRY, City/Agglomeration	Latitude	Longitude	City Centre not near Model Coastline (*)	UHSLC Tide Gauge for Return Period Analysis
ALGERIA, Algiers	36.8125	3.0000		
ANGOLA, Luanda	-8.8125	13.2500		
ARGENTINA, Buenos Aires	-34.9375	-57.0000		
AUSTRALIA, Adelaide	-34.9375	138.5000		
AUSTRALIA, Brisbane	-27.4375	153.2500		
AUSTRALIA, Melbourne	-37.9375	145.0000		
AUSTRALIA, Perth	-31.9375	115.7500		
AUSTRALIA, Sydney	-33.8125	151.3750		
BANGLADESH, Chittagong	22.3125	91.7500		
BANGLADESH, Dhaka	22.5625	90.8750	*	Charchanga (h138a)
BANGLADESH, Khulna	21.8125	89.5000	*	
BRAZIL, Santos	-24.0625	-46.3750		
BRAZIL, Belém	-0.9375	-48.5000		
BRAZIL, Fortaleza	-3.6875	-38.5000		
BRAZIL, Grande Vitória	-20.3125	-40.2500		
BRAZIL, Maceió	-9.6875	-35.7500		
BRAZIL, Natal	-5.8125	-35.1250		
BRAZIL, Recife	-8.1875	-34.8750		
BRAZIL, Porto Alegre	-30.4375	-51.0000		
BRAZIL, Rio de Janeiro	-22.9375	-43.1250		
BRAZIL, Salvador	-12.9375	-38.5000		
CAMEROON, Douala	3.8125	9.5000		
CANADA, Montréal	48.1875	-69.3750	*	
CANADA, Vancouver	49.3125	-123.2500		
CHINA, Dalian	38.9375	121.7500		
CHINA, Fuzhou Fujian	26.0625	119.7500	*	
CHINA, Guangzhou Guangdong	22.5625	113.6250	*	
CHINA, Shenzen	22.4375	113.8750		
CHINA, Hangzhou	30.4375	121.0000		

COUNTRY, City/Agglomeration	Representative Model Grid Point Latitude	Longitude	City Centre not near Model Coastline (*)	UHSLC Tide Gauge for Return Period Analysis
CHINA, Ningbo	30.0625	121.6250		Kanmen (h632a)
CHINA, Qingdao	36.0625	120.5000		
CHINA, Shanghai	31.3125	121.7500		
CHINA, Taipei	25.1875	121.3750		
CHINA, Tianjin	38.9375	117.7500		
CHINA, Wenzhou	27.8125	120.8750		
CHINA, Xiamen	24.4375	118.2500		Xiamen (h376a)
CHINA, Yantai	37.5625	121.5000		
CHINA, Zhanjiang	21.1875	110.6250		
CHINA, HONG KONG SAR, Hong Kong	22.1875	114.1250		
COLOMBIA, Barranquilla	11.0625	-74.8750		
CÔTE D'IVOIRE, Abidjan	5.1875	-4.0000		
CUBA, Havana	23.1875	-82.3750		
NORTH KOREA, Namp'o	38.6875	125.2500		
DENMARK, Copenhagen	55.6875	12.6250		
DOMINICAN REPUBLIC, Santo Domingo	18.4375	-69.8750		
ECUADOR, Guayaquil	-2.9375	-79.8750	*	
EGYPT, Alexandria	31.0625	29.8750		
FINLAND, Helsinki	60.0625	25.0000		
FRANCE, Marseille-Aix-en-Provence	43.3125	5.2500		
GERMANY, Hamburg	53.9375	8.8750		
GHANA, Accra	5.4375	-0.2500		
GREECE, Athens	37.9375	23.6250		
GUINEA, Conakry	9.6875	-13.6250		
HAITI, Port-au-Prince	18.6875	-72.5000		
INDIA, Madras	13.0625	80.3750		
INDIA, Cochin	9.9375	76.2500		
INDIA, Calcutta	21.6875	88.0000		
INDIA, Bombay	18.9375	72.8750		

COUNTRY, City/Agglomeration	Representative Model Grid Point Latitude	Representative Model Grid Point Longitude	City Centre not near Model Coastline (*)	UHSLC Tide Gauge for Return Period Analysis
INDIA, Surat	21.0625	72.7500		
INDIA, Visakhapatnam	17.6875	83.3750		
INDONESIA, Jakarta	-6.0625	106.7500		
INDONESIA, Palembang	-2.3125	105.0000	*	
INDONESIA, Surabaya	-7.1875	112.8750		
INDONESIA, Ujung Pandang	-5.1875	119.3750		
IRELAND, Dublin	53.3125	-6.1250		
ISRAEL, Tel Aviv-Jaffa	32.0625	34.7500		
ITALY, Naples	40.8125	14.2500		
JAPAN, Fukuoka-Kitakyushu	33.6875	130.2500	*	
JAPAN, Hiroshima	34.1875	132.3750		
JAPAN, Nagoya	34.9375	136.7500		
JAPAN, Osaka-Kobe	34.6875	135.3750		
JAPAN, Sapporo	43.1875	141.2500		
JAPAN, Tokyo	35.1875	139.7500		
KUWAIT, Kuwait City	29.3125	48.1250		
LEBANON, Beirut	33.9375	35.5000		
LIBYA, Banghazi	32.0625	20.0000		
LIBYA, Tripoli	32.9375	13.1250		
MALAYSIA, Kuala Lumpur	3.0625	101.2500		
MOROCCO, Casablanca	33.6875	-7.6250		
MOROCCO, Rabat	34.0625	-6.8750		
MOZAMBIQUE, Maputo	-25.9375	32.7500		
MYANMAR, Rangoon	16.4375	96.3750		
NETHERLANDS, Amsterdam	52.3125	4.8750		
NETHERLANDS, Rotterdam	51.9375	4.5000		
NEW ZEALAND, Auckland	-36.8125	174.8750		
NIGERIA, Lagos	6.3125	3.3750		
PAKISTAN, Karachi	24.8125	67.0000		

COUNTRY, City/Agglomeration	Representative Model Grid Point Latitude	Representative Model Grid Point Longitude	City Centre not near Model Coastline (*)	UHSLC Tide Gauge for Return Period Analysis
PANAMA, Panama City	8.9375	-79.5000		
PERU, Lima	-12.0625	-77.1250		
PHILIPPINES, Davao	7.0625	125.6250		
PHILIPPINES, Manila	14.5625	120.8750		
PORTUGAL, Lisbon	38.5625	-9.2500		
PORTUGAL, Porto	41.1875	-8.7500		
PUERTO RICO, San Juan	18.4375	-66.0000		
SOUTH KOREA, Pusan	35.0625	129.0000		
SOUTH KOREA, Ulsan	35.4375	129.3750		
SOUTH KOREA, Inchon	37.4375	126.6250		
RUSSIA, St. Petersburg	60.0625	29.0000		
SAUDI ARABIA, Jiddah	21.5625	39.1250		
SENEGAL, Dakar	14.8125	-17.3750		
SINGAPORE, Singapore	1.1875	103.8750		
SOMALIA, Mogadishu	1.9375	45.3750		
SOUTH AFRICA, Cape Town	-33.9375	18.3750		
SOUTH AFRICA, Durban	-29.8125	31.1250		
SPAIN, Barcelona	41.3125	2.1250		
SWEDEN, Stockholm	59.1875	18.5000		
THAILAND, Bangkok	13.4375	100.5000		
TOGO, Lomé	6.0625	1.2500		
TURKEY, Istanbul	40.9375	29.0000		
TURKEY, Izmir	38.4375	26.8750		
UKRAINE, Odessa	46.4375	30.8750		
UNITED ARAB EMIRATES, Dubai	25.3125	55.2500		
UNITED KINGDOM, Glasgow	55.6875	-4.8750		
UNITED KINGDOM, London	51.4375	0.8750		
TANZANIA, Dar-es-Salaam	-6.8125	39.3750		
USA, Baltimore	38.1875	-76.2500	*	

COUNTRY, City/Agglomeration	Representative Model Grid Point		City Centre not near Model Coastline (*)	UHSLC Tide Gauge for Return Period Analysis
	Latitude	Longitude		
USA, Boston	42.3125	-70.7500		
USA, Houston	29.5625	-94.8750		
USA, Los Angeles-Long Beach	33.6875	-118.2500		
USA, Miami	25.8125	-80.1250		
USA, New Orleans	30.0625	-90.0000		Grand Isle (h765a)
USA, New York-Newark	40.5625	-74.0000		
USA, Philadelphia	39.1875	-75.2500		
USA, Portland	46.1875	-123.8750		
USA, Providence	41.3125	-71.3750		
USA, San Diego	32.6875	-117.1250		
USA, San Francisco - Oakland	37.8125	-122.5000		
USA, San Jose	37.8125	-122.5000		
USA, Seattle	48.1875	-122.7500		
USA, Tampa-St Petersburg	27.6875	-82.7500		
USA, Virginia Beach	36.9375	-76.0000		
USA, Washington, D C	38.0625	-76.3750		
URUGUAY, Montevideo	-34.9375	-56.1250		
VENEZUELA, Maracaibo	10.9375	-71.6250		
VIETNAM, Hai Phòng	20.8125	106.8750		
VIETNAM, Ho Chi Minh City	10.3125	106.8750		

Appendix 3.3- Cumulative Frequency Distributions for MHW Changes at all Global Coastal Cities

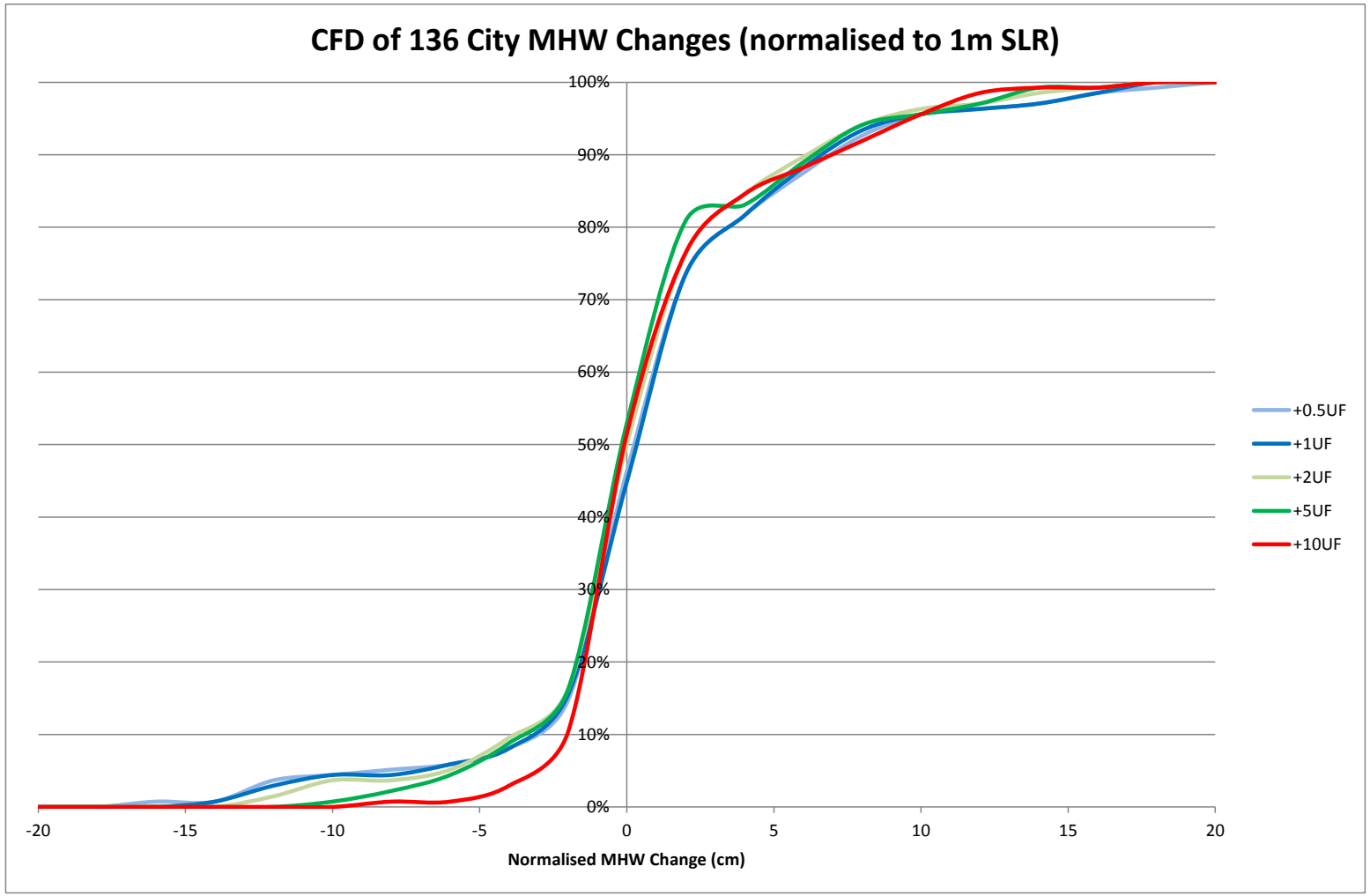

CFDs of MHW changes at all 136 cities comparing all UF scenarios (changes normalised to 1m SLR).

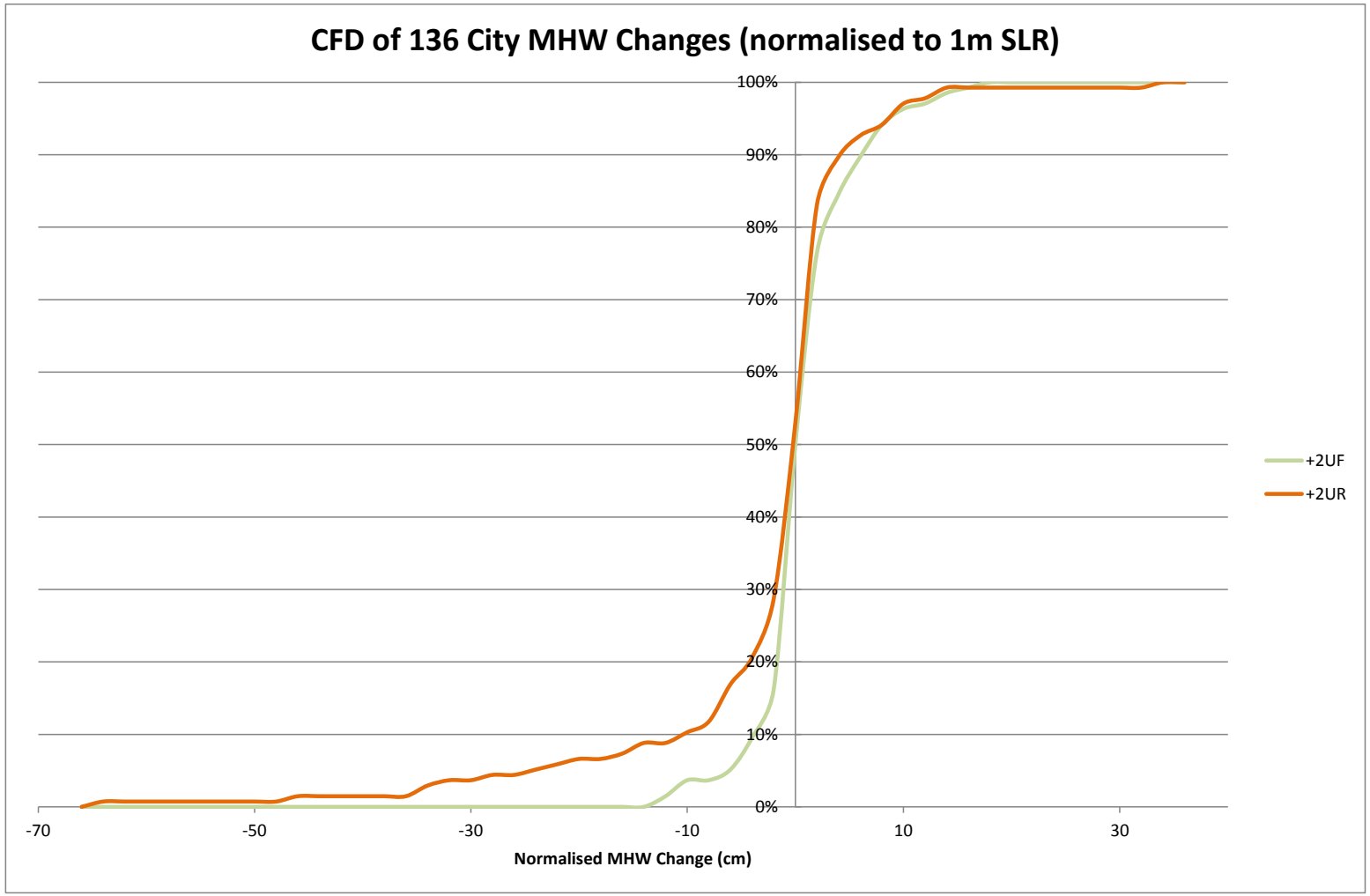

CFDs of MHW changes at all 136 cities for +2UF and +2UR scenarios (changes normalised to 1m SLR).

Appendix 3.4- Regional enlargements of Global MHW Changes under 2m SLR including coastal recession (+2UR)

Regional enlargements of Figure 3.10- MHW change for +2UR- for comparison with Figure 3.11-3.16

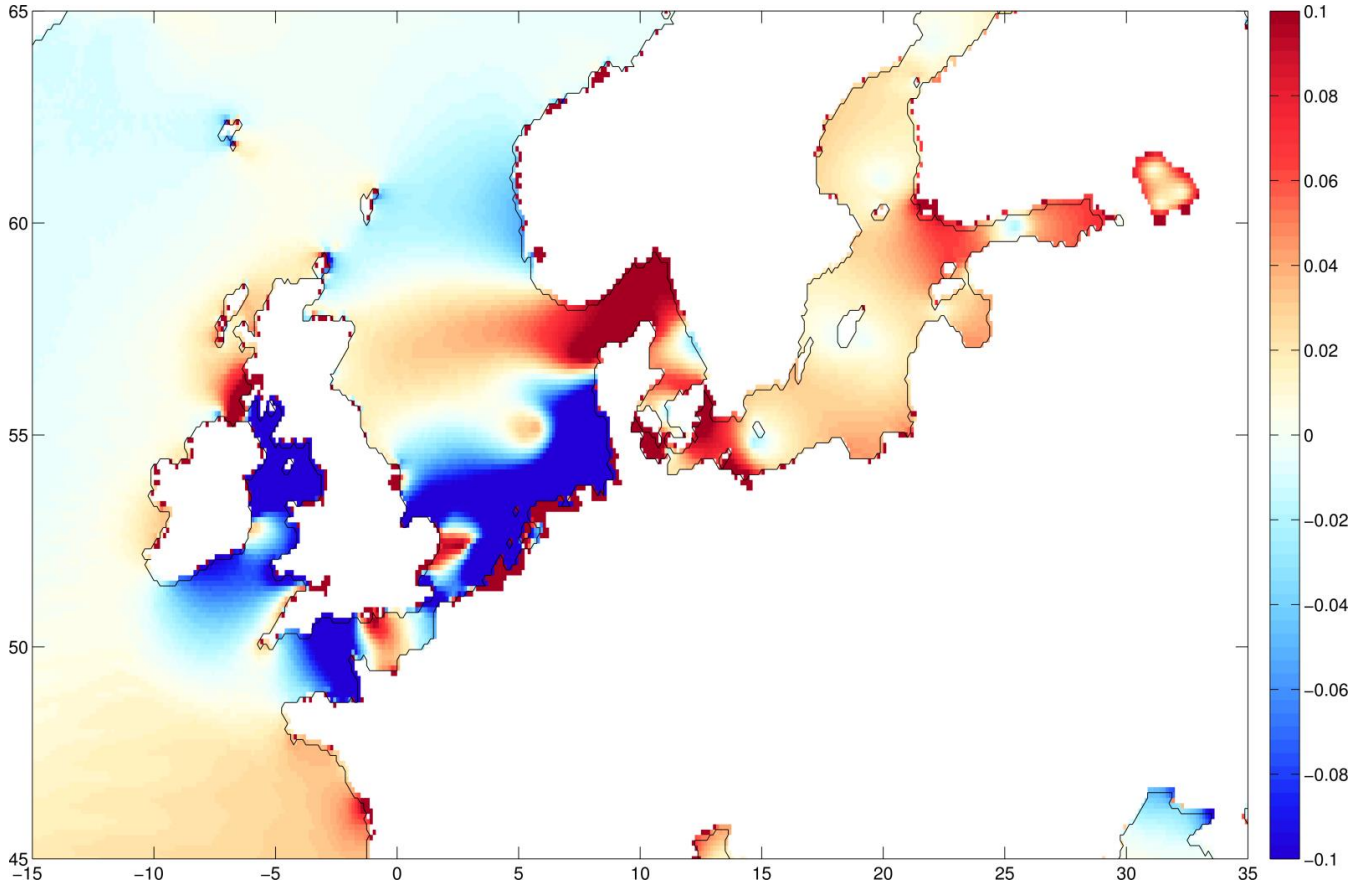

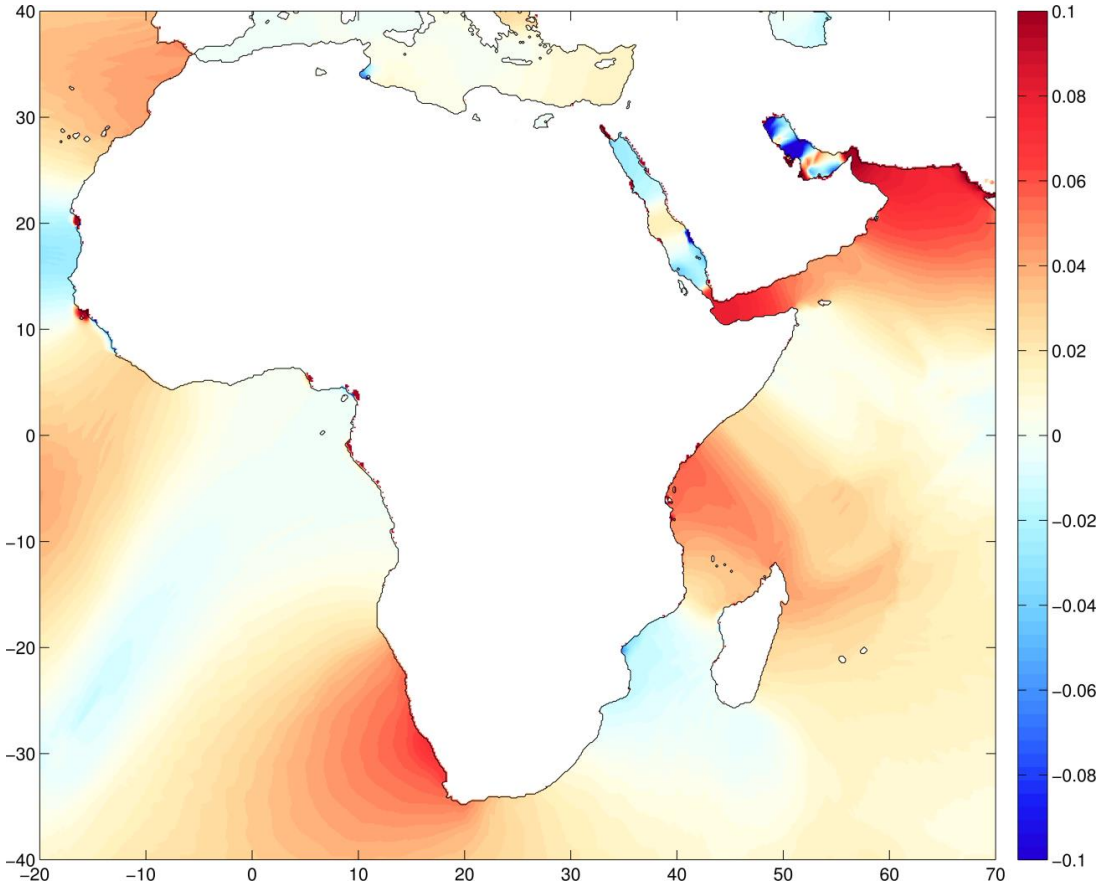
40
30
20
10
0
−10
−20
−30
−40
−20
−10
0
10
20
30
40
50
60
70
0.1
0.08
0.06
0.04
0.02
0
−0.02
−0.04
−0.06
−0.08
−0.1

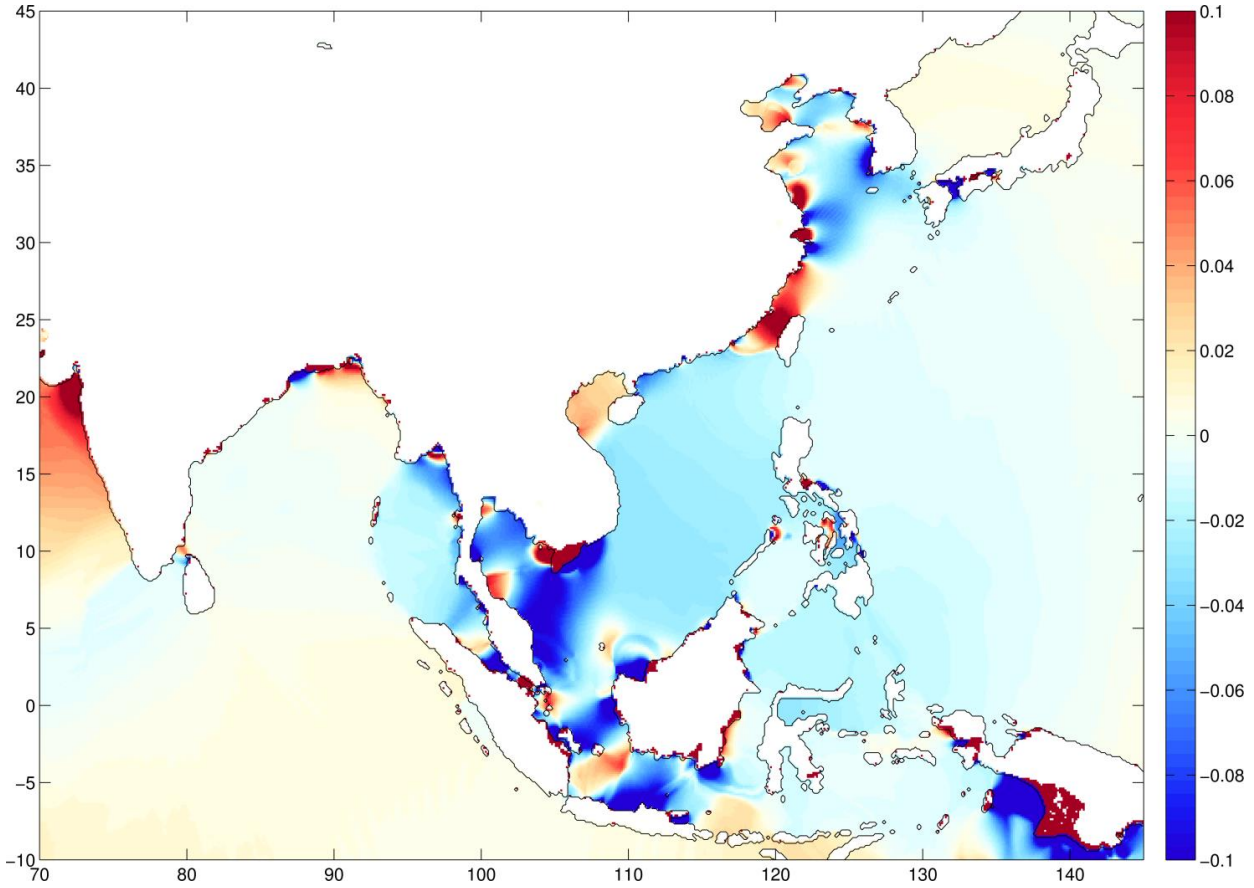
45
40
35
30
25
20
15
10
5
0
−5
−10
70
80
90
100
110
120
130
140
0.1
0.08
0.06
0.04
0.02
0
−0.02
−0.04
−0.06
−0.08
−0.1

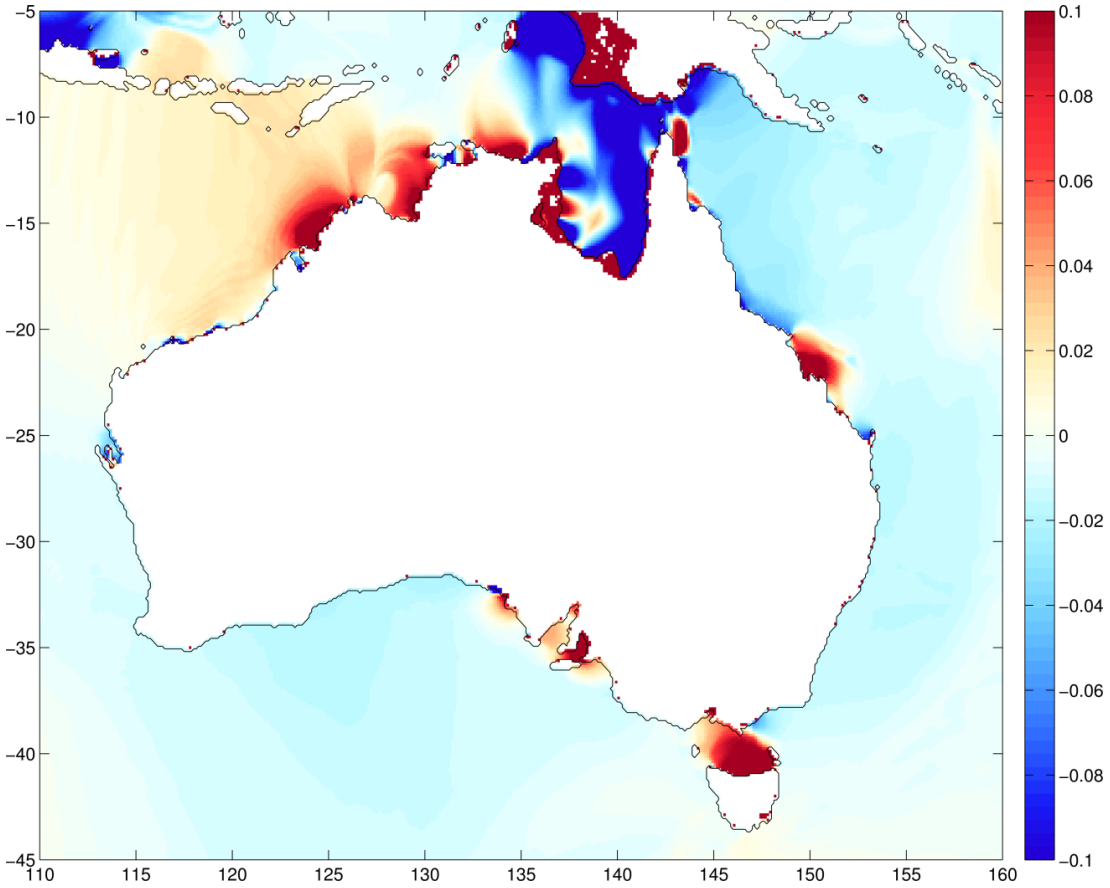
−5
−10
−15
−20
−25
−30
−35
−40
−45
110
115
120
125
130
135
140
145
150
155
160
0.1
0.08
0.06
0.04
0.02
0
−0.02
−0.04
−0.06
−0.08
−0.1

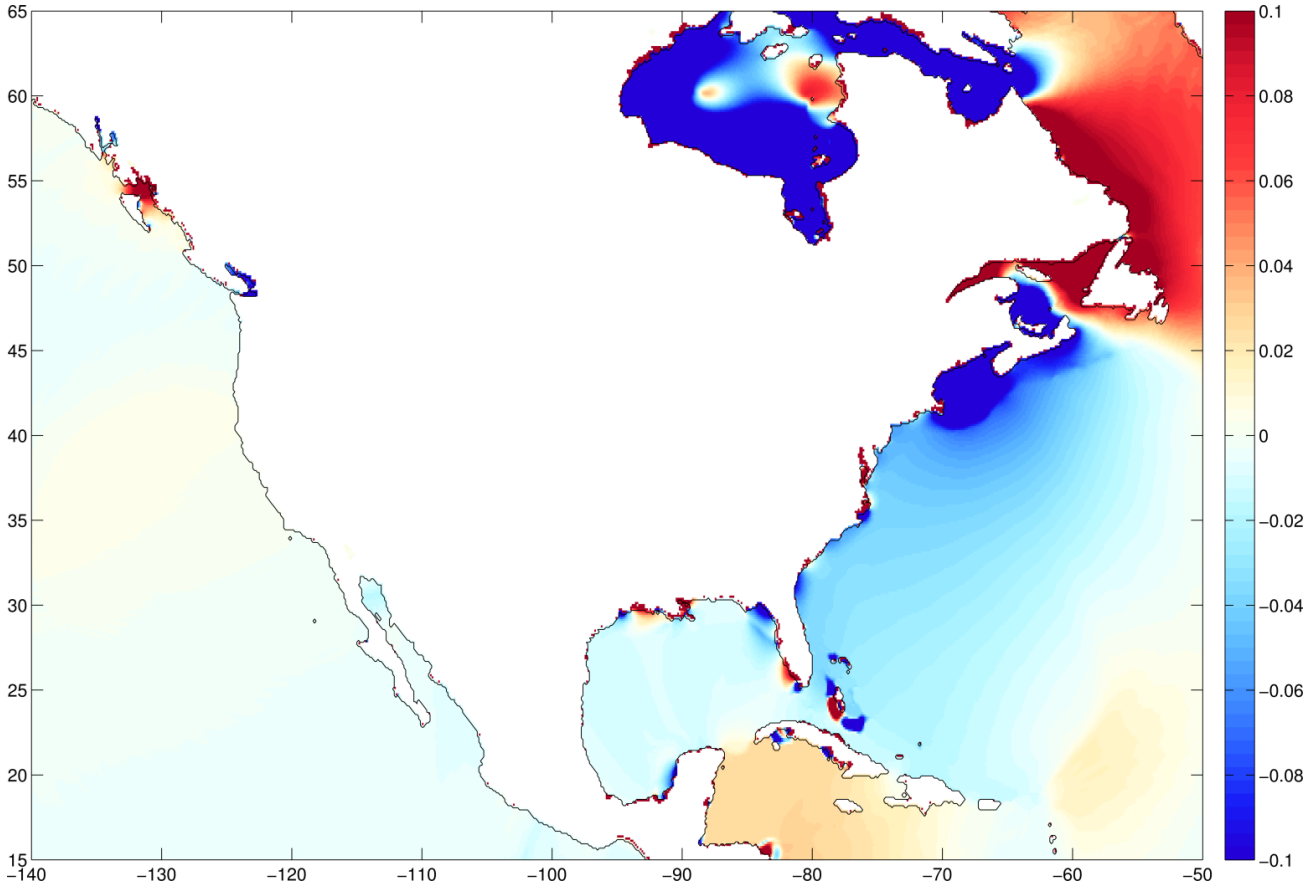
65
60
55
50
45
40
35
30
25
20
15
−140
−130
−120
−110
−100
−90
−80
−70
−60
−50
0.1
0.08
0.06
0.04
0.02
0
−0.02
−0.04
−0.06
−0.08
−0.1

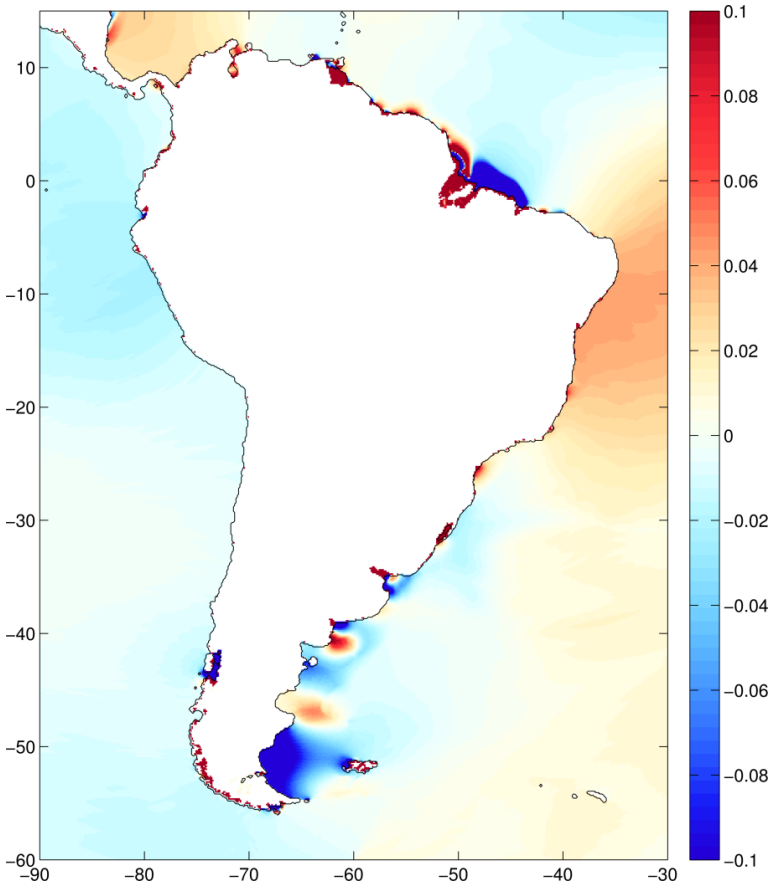
10
0
−10
−20
−30
−40
−50
−60
−90
−80
−70
−60
−50
−40
−30
0.1
0.08
0.06
0.04
0.02
0
−0.02
−0.04
−0.06
−0.08
−0.1

Appendix 3.5- Global Results plotted regionally for comparison with previous studies

OTISmpi M_2 amplitude change with (a) 2m and (b) 10m SLR assuming a fixed coastline. To compare with Chapter 2 Figure 2.4 and 2.5.

a)

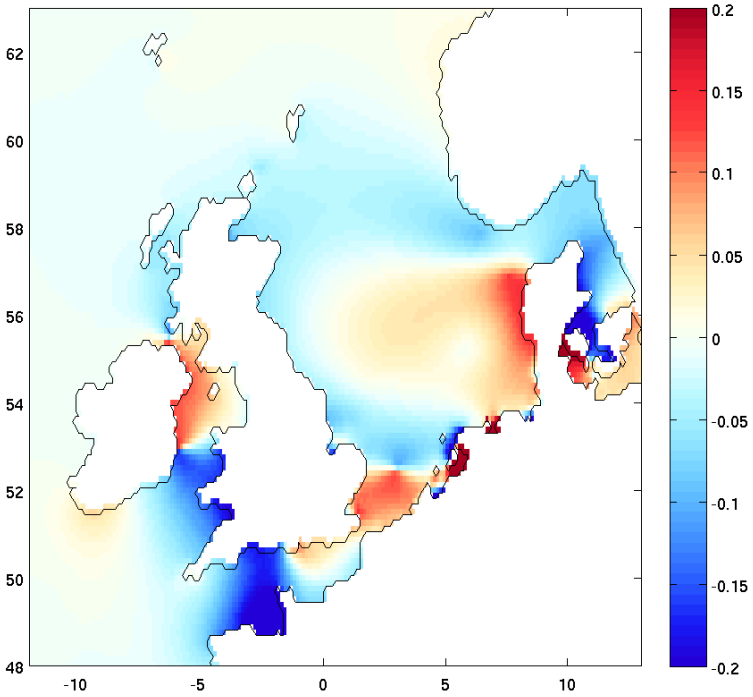

b)

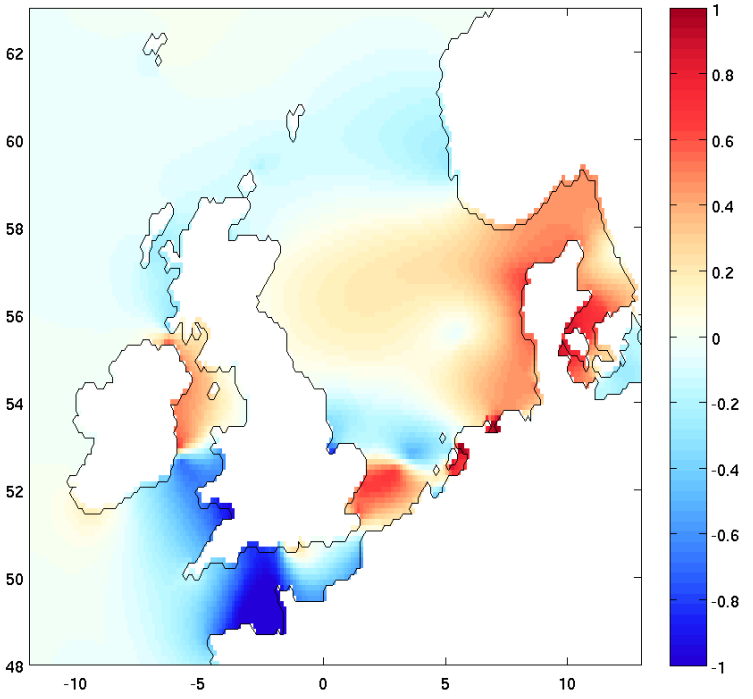

OTISmpi M_2 amplitude change with 2m SLR assuming (a) coastal recession and (b) a fixed coastline. To compare with Pelling et al. (2013b) Figs. 1c and 1d.

a)

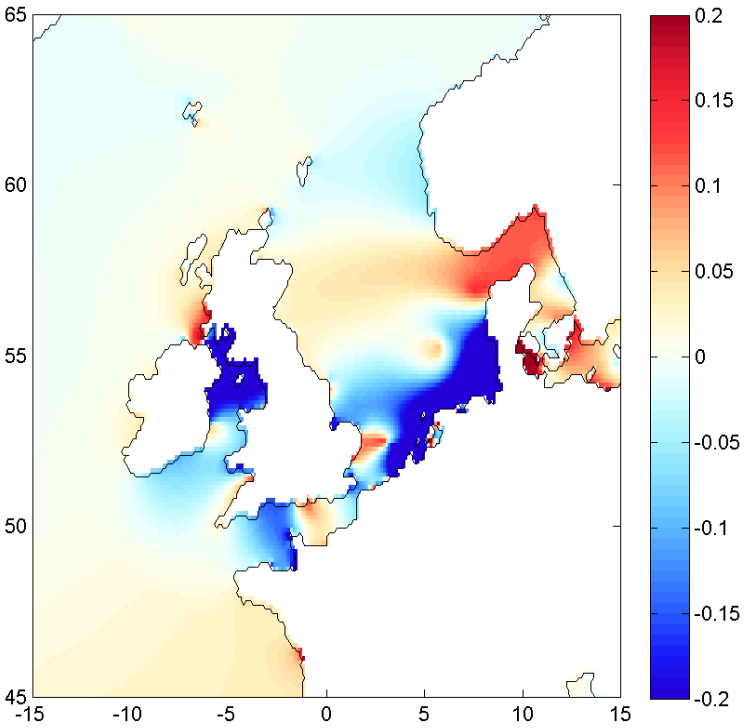

b)

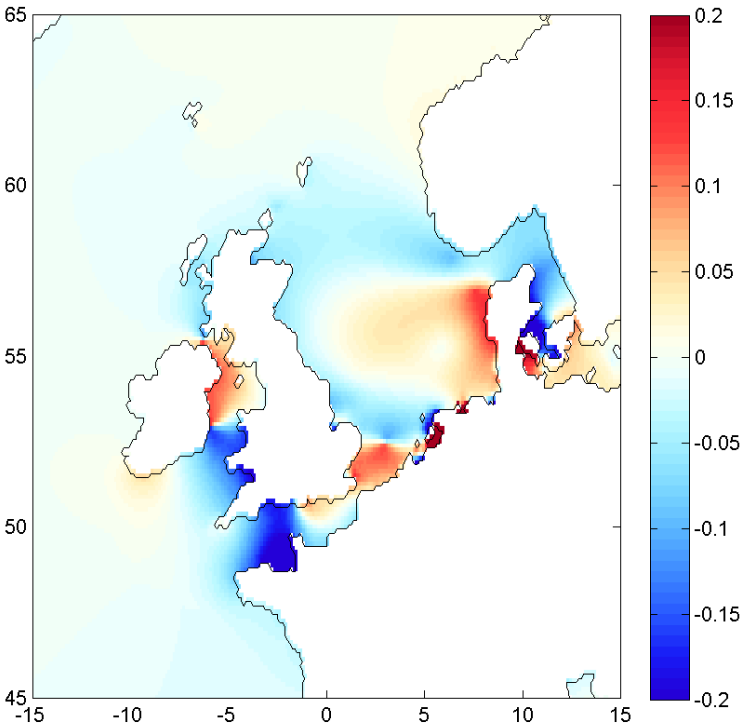

OTISmpi M_2 amplitude change with (a) 2m and (b) 5m SLR assuming coastal recession. To compare with Ward et al. (2012) Figs. 3a and 3c.

a)

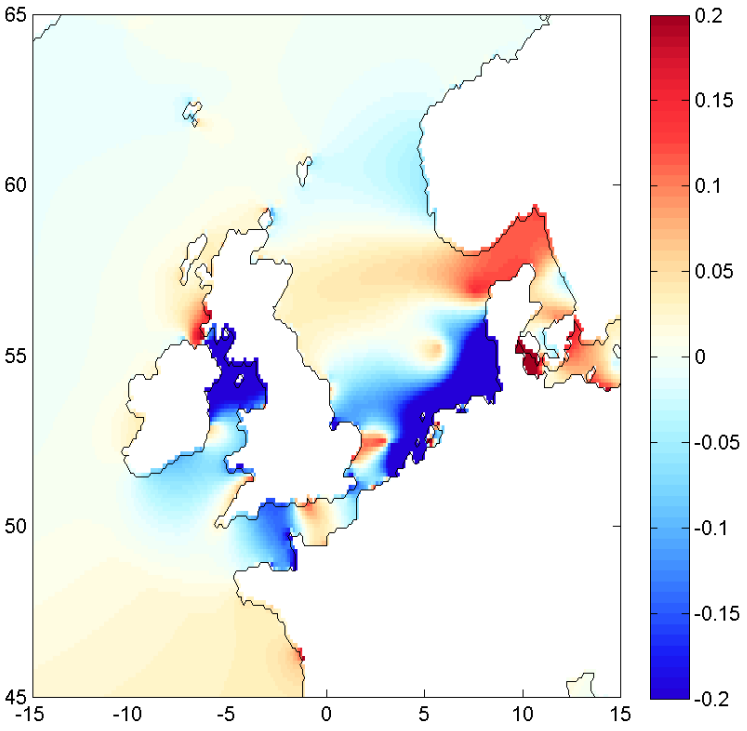

b)

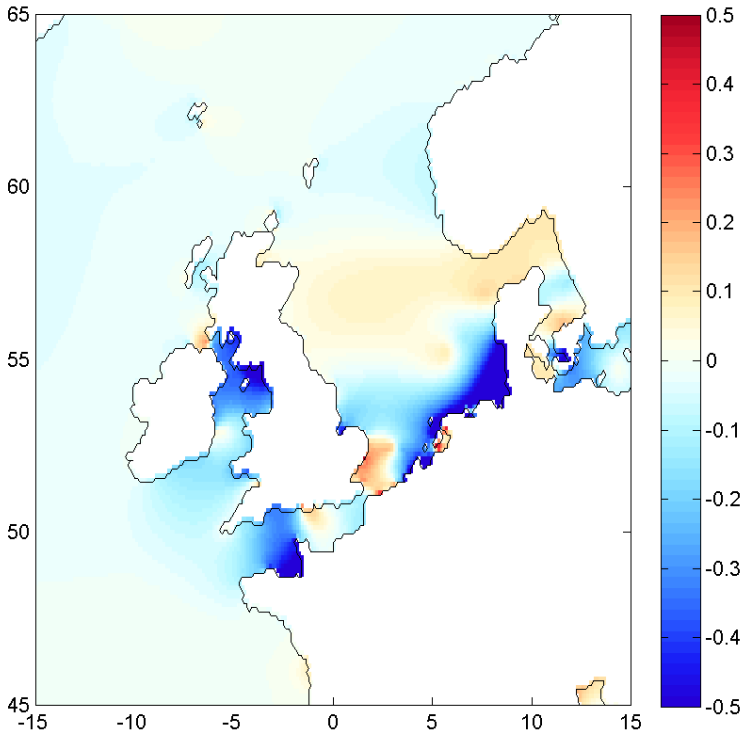

OTISmpi MHW change with 0.5m SLR assuming a fixed coastline. To compare with Flather et al. (2001) Fig. 7.

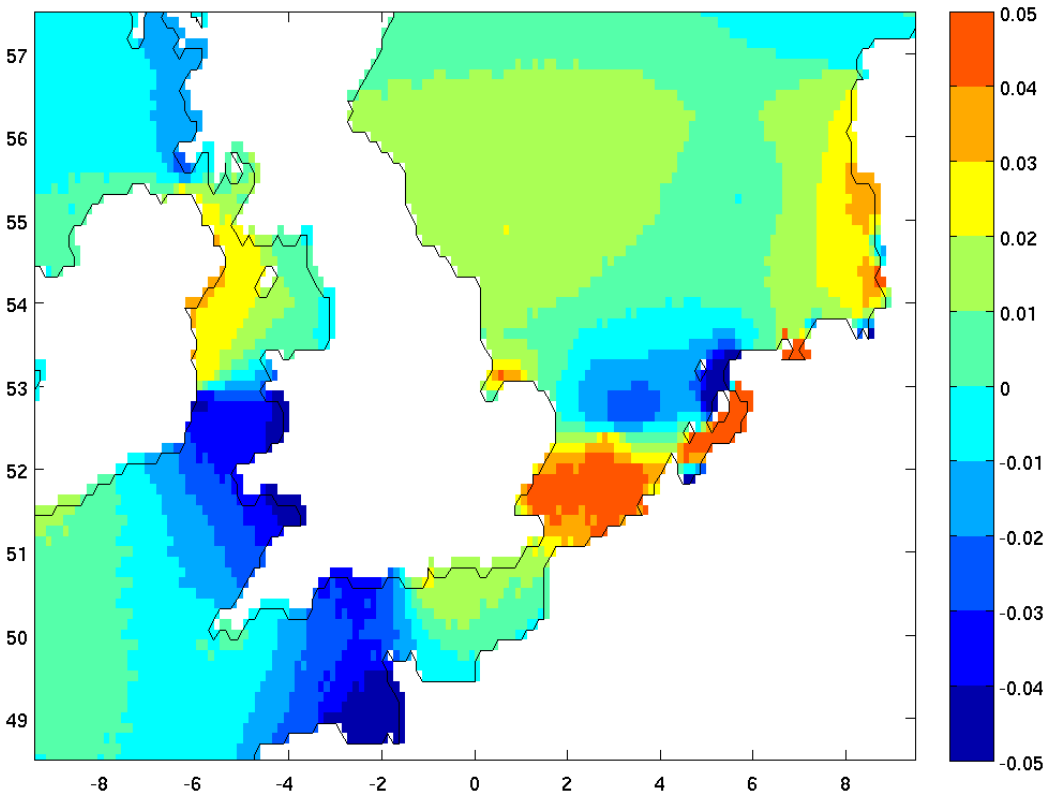

OTISmpi M_2 amplitude change with 2m SLR assuming (a) coastal recession and (b) a fixed coastline. To compare with Pelling et al. (2013a) Figs. 6a and 6b.

a)

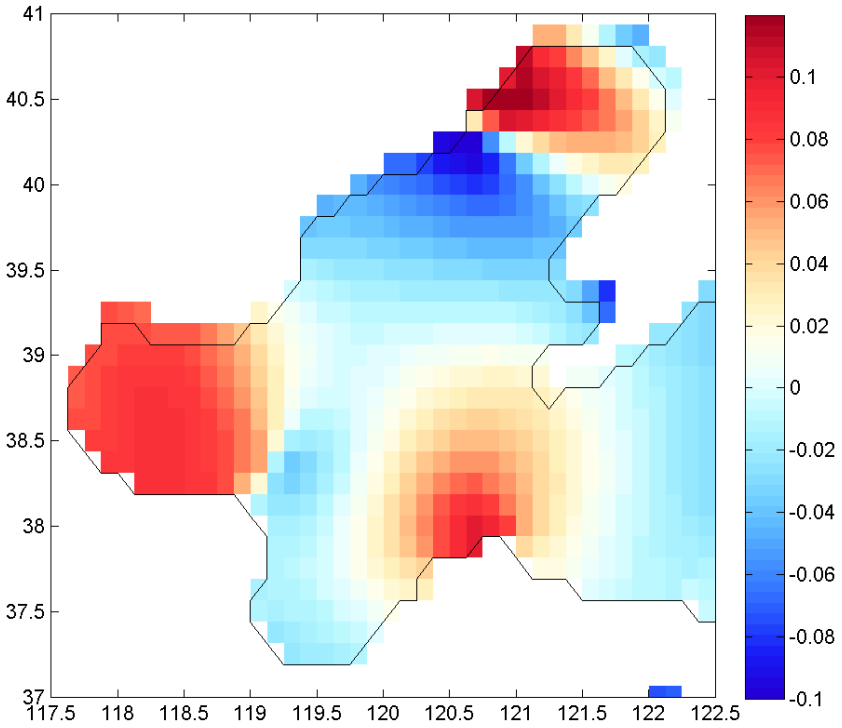

b)

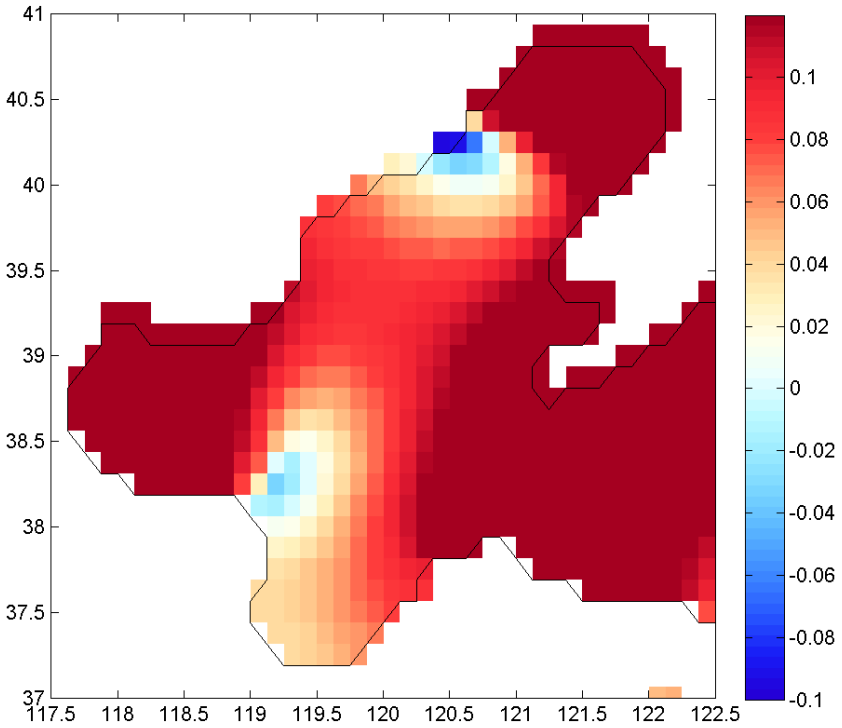

OTISmpi ‘astronomic tidal range’ (sum of M_2, S_2, K_1, O_1 amplitudes) change with 1m SLR assuming (a) coastal recession and (b) a fixed coastline, with 2m SLR assuming (c) coastal recession and (d) a fixed coastline and with 5m SLR assuming (e) coastal recession and (f) a fixed coastline. To compare with Pelling and Green (2013) Figs. 6a-f (n.b. Pelling and Green (2013) ‘astronomic tidal range’ also includes N2).

a)

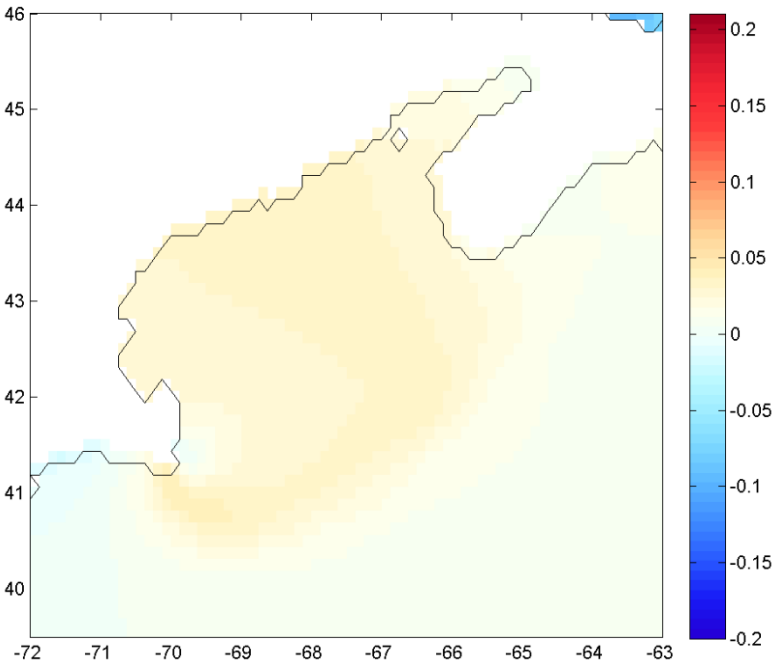

b)

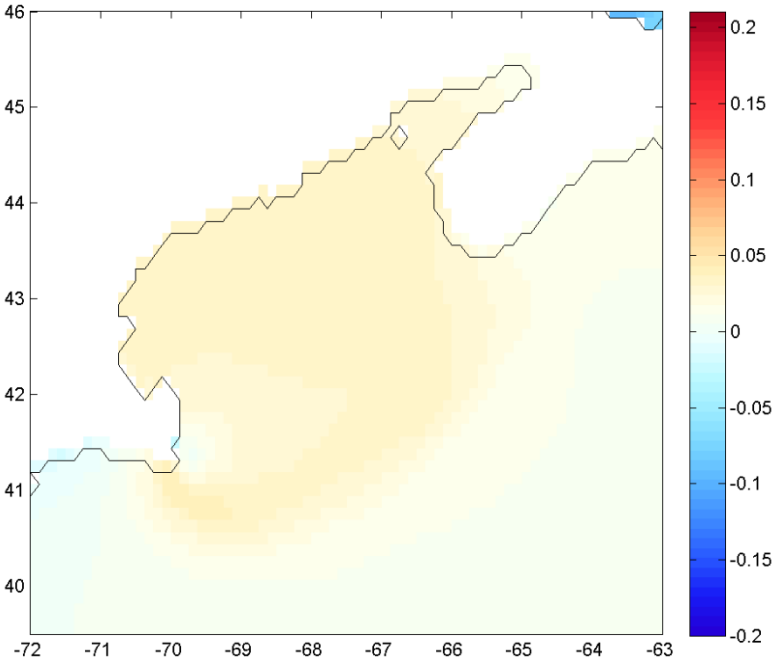

c)

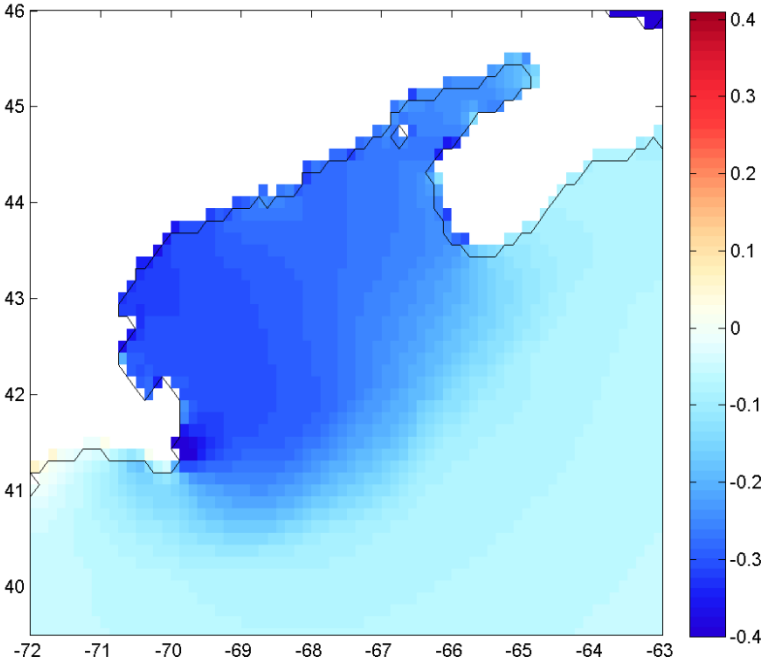
46
45
44
43
42
41
40
-72
-71
-70
-69
-68
-67
-66
-65
-64
-63
0.4
0.3
0.2
0.1
0
-0.1
-0.2
-0.3
-0.4

d)

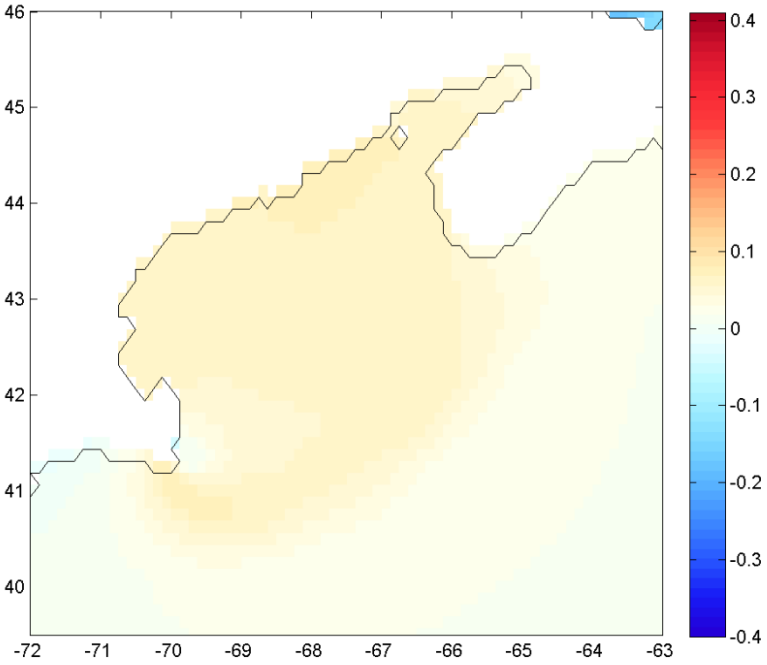
46
45
44
43
42
41
40
-72
-71
-70
-69
-68
-67
-66
-65
-64
-63
0.4
0.3
0.2
0.1
0
-0.1
-0.2
-0.3
-0.4

e)

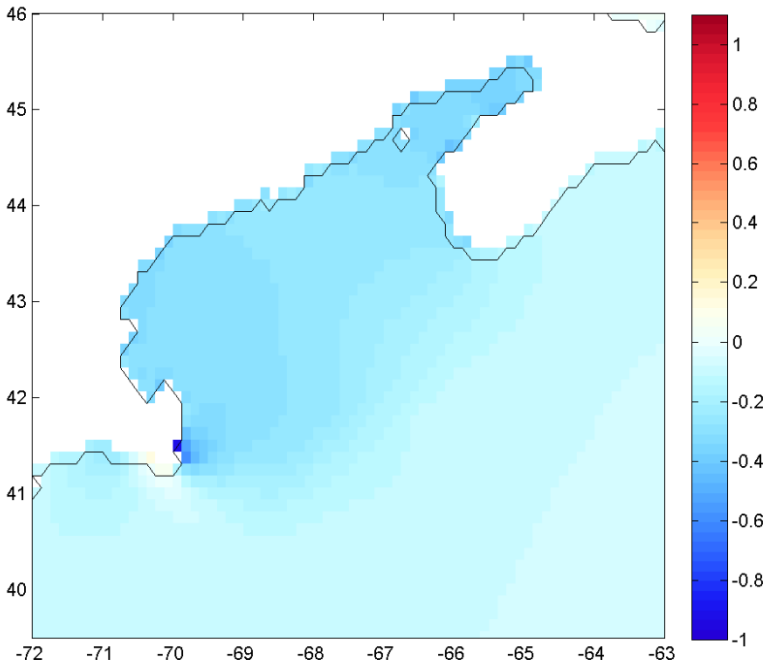
46
45
44
43
42
41
40
-72
-71
-70
-69
-68
-67
-66
-65
-64
-63
1
0.8
0.6
0.4
0.2
0
-0.2
-0.4
-0.6
-0.8
-1

f)

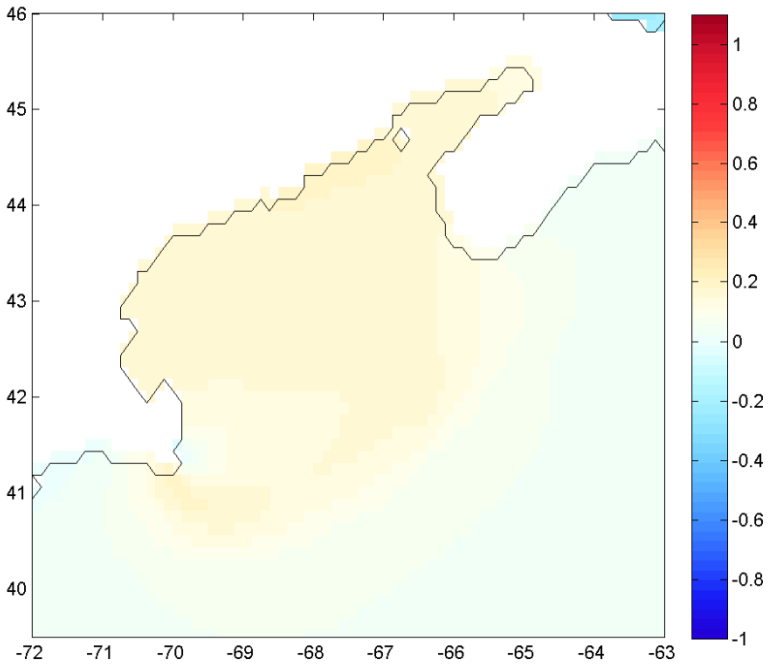
46
45
44
43
42
41
40
-72
-71
-70
-69
-68
-67
-66
-65
-64
-63
1
0.8
0.6
0.4
0.2
0
-0.2
-0.4
-0.6
-0.8
-1

List of References

ABP Marine Environmental Research Ltd, The Met Office, Garrad Hassan, and Proudman Oceanographic Laboratory, 2004. Atlas of UK marine renewable energy resources. Technical Report R, 1106.

Allen, J.R.L., 1990. Salt-marsh growth and stratification: a numerical model with special reference to the Severn Estuary, southwest Britain. Marine Geology 95, 77–96.

Araújo, I.B., Dias, J.M., Pugh, D.T., 2008. Model simulations of tidal changes in a coastal lagoon, the Ria de Aveiro (Portugal). Continental Shelf Research, 28, 1010-1025.

Araújo, I.B., Pugh, D.T., 2008. Sea levels at Newlyn 1915–2005: analysis of trends for future flooding risks. Journal of Coastal Research, 203–212.

Arbic, B.K., Garner, S.T., Hallberg, R.W., Simmons, H.L., 2004. The accuracy of surface elevations in forward global barotropic and baroclinic tide models. Deep-Sea Research Part II: Topical Studies in Oceanography 51, 3069–3101.

Arbic, B.K., Garrett, C., 2010. A coupled oscillator model of shelf and ocean tides. Continental Shelf Research 30, 564–574.

Arbic, B.K., Karsten, R.H., Garrett, C., 2009. On Tidal Resonance in the Global Ocean and the Back-Effect of Coastal Tides upon Open-Ocean Tides. Atmosphere-Ocean, 47, 239-266.

Arizaga, J., Andueza, M., Tamayo, I., 2013. Spatial behaviour and habitat use of first-year Bluethroats Luscinia svecica stopping over at coastal marshes during the autumn migration period. Acta Ornithologica, 48, 17-25.

Austin, R.M., 1991. Modelling Holocene tides on the NW European continental shelf. Terra Nova, 3, 276-288.

Balke, T., 2013. Establishment of biogeomorphic ecosystems a study on mangrove and salt marsh pioneer vegetation. PhD Thesis. Radboud University Nijmegen, Netherlands. 177 p

Balke, T., Bouma, T.J., Horstman, E.M., Webb, E.L., Erftemeijer, P.L., Herman, P.M., 2011. Windows of opportunity: thresholds to mangrove seedling establishment on tidal flats. Marine Ecology Progress Series, 440.

Batstone, C., Lawless, M., Tawn, J., Horsburgh, K., Blackman, D., McMillan, A., Worth, D., Laeger, S., Hunt, T., 2013. A UK best-practice approach for extreme sea-level analysis along complex topographic coastlines. Ocean Engineering, 71, 28-39.

Bertin, X., Bruneau, N., Breilh, J.-F., Fortunato, A.B., Karpytchev, M., 2012. Importance of wave age and resonance in storm surges: The case Xynthia, Bay of Biscay. Ocean Modelling, 42, 16-30.

Bertness, M.D., 2007. Atlantic shorelines: natural history and ecology. Princeton University Press, Princeton, 431 pp

Blunden, L., Bahaj, A., 2007. Tidal energy resource assessment for tidal stream generators. Proceedings of the Institution of Mechanical Engineers, Part A: Journal of Power and Energy, 221, 137-146.

Blunden, L.S., Bahaj, A.S., 2006. Initial evaluation of tidal stream energy resources at Portland Bill, UK. Renewable Energy, 31, 121-132.

Bolle, A., Wang, Z.B., Amos, C., De Ronde, J., 2010. The influence of changes in tidal asymmetry on residual sediment transport in the Western Scheldt. Continental Shelf Research 30, 871–882.

Bos, A.R., Bouma, T.J., de Kort, G.L., van Katwijk, M.M., 2007. Ecosystem engineering by annual intertidal seagrass beds: sediment accretion and modification. Estuarine, Coastal and Shelf Science, 74, 344-348.

Bouma, T., Olenin, S., Reise, K., Ysebaert, T., 2009. Ecosystem engineering and biodiversity in coastal sediments: posing hypotheses. Helgoland Marine Research, 63, 95-106.

Bretschneider, C.L., 1964. The Ash Wednesday east coast storm, March 5-8, 1962 A hindcast of events, causes and effects. Coastal Engineering Proceedings, 1.

Buxton, H.T., Andersen, M.E., Focazio, M.J., Haines, J.W., Hainly, R.A., Hippe, D.J., and Sugarbaker, L.J., 2013, Meeting the science needs of the Nation in the

wake of Hurricane Sandy—A U.S. Geological Survey science plan for support of restoration and recovery: U.S. Geological Survey Circular 1390, 26 p., <http://pubs.usgs.gov/circ/1390/>.

Caires, S., Diermanse, F., Dillingh, D., de Graaff, R., 2007. Extreme still water levels. Proc. of the 10th int. workshop on wave hindcasting and forecasting and Coastal Hazard Symposium, WMO/TD-No. 1442, Hawaii, U.S.A, 11-16 November 2007.

Cartwright, D.E., 1972. Secular changes in the oceanic tides at Brest, 1711–1936. Geophysical Journal of the Royal Astronomical Society 30, 433–449.

Cazenave, A., Nerem, R.S., 2004. Present-day sea level change: Observations and causes. Reviews of Geophysics 42, RG3001.

Chen, J.L., Wilson, C.R., Tapley, B.D., 2006. Satellite gravity measurements confirm accelerated melting of Greenland ice sheet. Science 313, 1958–1960.

Church, J., White, N., 2011. Sea-Level Rise from the Late 19th to the Early 21st Century. Surveys in Geophysics, 32, 585-602.

Church, J.A., Clark, P.U., Cazenave, A., Gregory, J.M., Jevrejeva, S., Levermann, A., Merrifield, M.A., Milne, G.A., Nerem, R.S., Nunn, P.D., Payne, A.J., Pfeffer, W.T., Stammer, D., Unnikrishnan, A.S., 2014 Sea Level Change. In: Climate Change 2013: The Physical Science Basis. Working Group I Contribution to the Fifth Assessment Report of the Intergovernmental Panel on Climate Change [Stocker, T.F., Qin, D., Plattner, G.-K., Tignor, M., Allen, S. K., Boschung, J., Nauels, A., Xia, Y., Bex, V. and Midgley, P.M. (eds.)] Cambridge University Press, Cambridge, United Kingdom and New York, NY, USA

Church, J.A., White, N.J., 2006. A 20th century acceleration in global sea-level rise. Geophysical Research Letters 33, L01602.

Church, J.A., White, N.J., Aarup, T., Wilson, W.S., Woodworth, P.L., Domingues, C.M., Hunter, J.R., Lambeck, K., 2008. Understanding global sea levels: past, present and future. Sustainability Science, 3, 9-22.

Church, J.A., Woodworth, P.L., Aarup, T., Wilson, W.S., 2010. Understanding sea-level rise and variability. Wiley-Blackwell, London.

Colosi, J.A., Munk, W., 2006. Tales of the venerable Honolulu tide gauge. Journal of Physical Oceanography 36, 967–996.

Convey, P., Bindschadler, R., di Prisco, G., Fahrbach, E., Gutt, J., Hodgson, D.A., Mayewski, P.A., Summerhayes, C.P., Turner, J., 2009. Antarctic climate change and the environment. Antarctic Science 21, 541–563.

de Ronde, J.G., 1983. Changes of relative mean sea-level and of mean tidal amplitude along the Dutch coast. In: Ritsema, A.R., Gurpinar, A., (Eds.), Seismicity and Seismic Risk in the Offshore North Sea Area, Dordrecht, pp. 131–141.

de Ronde, J.G., 1986. Bepaling knoopfactoren harmonische analyse met het Continental Shelf Model, Notitie GWAO-86.309. Dienst Getijdewateren, Rijkswaterstaat.

de Ronde, J.G., 1989. Past and Future sea level rise in the Netherlands in Workshop on Sea Level Rise and Coastal Processes, Palm Beach, Florida, 9–11 March 1988, US Department of Energy Report DOE/NBB-0086, Washington, DC, pp. 253–280.

de Ronde, J.G., 1993. What will happen to The Netherlands if sea level rise accelerates? In R.A. Warrick, E.M. Barrow, T.M.L. Wigley (Eds.), Climate and sea level change: observations, projections and implications (p. 424). Cambridge: Cambridge University Press.

Deltares, 2009a. Delft3D FLOW simulation of multi-dimensional hydrodynamic flows and transport phenomena, including sediments, v. 3.14.7864, Delft, Deltares.

Deltares, 2009b. Delft3D-TRIANA User Manual Tidal Analysis of FLOW time series and comparison with observed constants, v.3.00.7258, Delft, Deltares.

Di Silvio, 1989. Modelling of the morphologic evolution of tidal lagoons and their equilibrium configurations. In: Final Proceedings of the IAHR, XXIII Congress, Ottawa, Canada, pp. C169–C175.

Dillingh, D., 2006. Waterstanden Nederlandse kust en estuaria- Statistieken t.b.v. de hydraulische randvoorwaarden, rapport RIKZ/2006.012, Den Haag, June 2006, Rijkswaterstaat RIKZ.

Dolan, R., 1987. The Ash Wednesday storm of 1962: 25 years later. Journal of Coastal Research, 3.

Dyer, K.R., 1997. Estuaries - a physical introduction. 2nd edition. 195p. Chichester: John Wiley & Sons.

Egbert, G.D., Ray, R.D., 2000. Significant dissipation of tidal energy in the deep ocean inferred from satellite altimeter data. Nature, 405, 775-778.

Egbert, G.D., Ray, R.D., 2001. Estimates of M-2 tidal energy dissipation from TOPEX/Poseidon altimeter data. Journal of Geophysical Research-Oceans 106, 22475–22502.

Egbert, G.D., Ray, R.D., Bills, B.G., 2004. Numerical modeling of the global semidiurnal tide in the present day and in the last glacial maximum. Journal of Geophysical Research-Oceans, 109.

Embling, C.B., Illian, J., Armstrong, E., van der Kooij, J., Sharples, J., Camphuysen, K.C.J., Scott, B.E., 2012. Investigating fine-scale spatio-temporal predator–prey patterns in dynamic marine ecosystems: a functional data analysis approach. Journal of Applied Ecology, 49, 481-492.

Environment Agency, 2013. Communities urged to prepare for worst east coast tidal surge in 30 years. <http://www.environment-agency.gov.uk/news/151065.aspx>. Last Accessed 17/03/14.

European Commission, 1996. The exploitation of tidal and marine currents: wave energy—project results. Technical Report EUR 16683 EN, Commission of the European Communities. Directorate-General for Science Research and Development.

European Nuclear Society, 2014. <http://www.euronuclear.org/info/encyclopedia/n/nuclear-power-plant-europe.htm>. Last Accessed: 12/02/14.

Feng, X., Tsimplis, M.N., 2014. Sea level extremes at the coasts of China. Journal of Geophysical Research: Oceans, 119, 1593-1608.

Feng, X. and Tsimplis, M.N. in preparation for Journal of Geophysical Research: Oceans. Long-term changes in observed tides at the coasts of China.

Flather, R.A., 1984. A numerical model investigation of the storm surge of 31 January and 1 February 1953 in the North Sea. Quarterly Journal of the Royal Meteorological Society, 110, 591-612.

Flather, R.A., Baker, T., Woodworth, P., Vassie, I., Blackman, D., 2001. Integrated effects of climate change on coastal extreme sea levels. Proudman Oceanographic Laboratory Internal Document No. 140. 20 pp.

Flather, R.A., Khandker, H., 1993. The storm surge problem and possible effects of sea level changes on coastal flooding in the Bay of Bengal. In R.A. Warrick, E.M. Barrow, T.M.L. Wigley (Eds.), Climate and sea level change: observations, projections and implications (pp. 229-245). Cambridge: Cambridge University Press.

Flather, R.A., Williams, J.A., 2000. Climate change effects on storm surges: methodologies and results. In: Beersma, J., et al. (Eds.), Climate Scenarios for Water Related and Climate Impacts, ECLAT-2 Workshop Report No. 3, KNMI, the Netherlands, 10–12 May 2000, CRU, Norwich, 2000, pp. 66–78.

Flick, R.E., Murray, J.F., Ewing, L.C., 2003. Trends in United States tidal datum statistics and tide range. Journal of Waterway Port Coastal and Ocean Engineering- ASCE 129, 155–164.

Führböter, A., Dette, H. and Töppe, A., 1990. Recent changes in sea level rise. In: Proceedings of the Skagen Symposium, 1990 2–5 September, Skagen, Denmark, Journal of Coastal Research Special Issue No. 9, pp.146–159.

Führböter, A., Jensen, J., 1985. Longterm changes of tidal regime in the German Bight (North Sea). In: Magoon, O.T. (Ed.), Fourth Symposium on Coastal and Ocean Management, Baltimore.

Ge, J., Much, D., Kappenberg, J., Nino, O., Ding, P., Chen, Z., 2013. Simulating storm flooding maps over HafenCity under present and sea level rise scenarios. Journal of Flood Risk Management.

Gebraad, A.W., Philippart, M.E., 1998. The Dutch Continental Shelf Model DCSM98: calibration using altimeter data, Werkdocument, RIKZ/OS-98.121x.

Gerritsen, H., 2005. What happened in 1953? The Big Flood in the Netherlands in retrospect. Philosophical Transactions of the Royal Society A: Mathematical, Physical and Engineering Sciences, 363, 1271-1291.

Gerritsen, H., Berentsen, C.W., 1998. A modelling study of tidally induced equilibrium sand balances in the North Sea during the Holocene. Continental Shelf Research, 18, 151-200.

Gerritsen, H., de Fries, H., Philippart, M., 1995. The Dutch Continental Shelf Model. Coastal and Estuarine Studies 47, 425-467.

Green, J., 2010. Ocean tides and resonance. Ocean Dynamics 60, 1243–1253.

Greenberg, D.A., Blanchard, W., Smith, B., Barrow, E., 2012. Climate Change, Mean Sea Level and High Tides in the Bay of Fundy. Atmosphere-Ocean, 1-16.

Gregory, J.M., Church, J.A., Boer, G.J., Dixon, K.W., Flato, G.M., Jackett, D.R., Lowe, J.A., O'Farrell, S.P., Roeckner, E., Russell, G.L., Stouffer, R.J., Winton, M., 2001. Comparison of results from several AOGCMs for global and regional sea-level change 1900–2100. Climate Dynamics 18, 225–240.

Gregory, J.M., Lowe, J.A., 2000. Predictions of global and regional sea-level rise using AOGCMs with and without flux adjustment. Geophysics Research Letters 27, 3069–3072.

Griffiths, S.D., Peltier, W.R., 2009. Modeling of Polar Ocean Tides at the Last Glacial Maximum: Amplification, Sensitivity, and Climatological Implications. Journal of Climate, 22, 2905-2924.

Grinsted, A., Moore, J.C., Jevrejeva, S., 2010. Reconstructing sea level from paleo and projected temperatures 200 to 2100 ad. Climate Dynamics, 34, 461-472.

Grossmann, I., Woth, K., von Storch, H., 2007. Localization of global climate change: storm surge scenarios for Hamburg in 2030 and 2085. Die Küste 71:169–182

Gudmundsson, G.H., 2006. Fortnightly variations in the flow velocity of Rutford Ice Stream, West Antarctica. Nature, 444, 1063-1064.

Haecon, 2006. Actualisatie van de zandbalans van de Zee-en Westerschelde. Report 1249760008/lvp.

Haigh, I., Mawdsley, R.J., Pickering, M.D., Wadey, M.P., In preparation for Limnology and Oceanography: Methods. Mean high water, other datums and the global tides.

Haigh, I., Nicholls, R., Wells, N., 2010a. Assessing changes in extreme sea levels: Application to the English Channel, 1900–2006. Continental Shelf Research, 30, 1042-1055.

Haigh, I.D., Nicholls, R., Wells, N., 2010b. A comparison of the main methods for estimating probabilities of extreme still water levels. Coastal Engineering, 57, 838-849.

Haigh, I., Nicholls, R., Wells, N., 2011. Rising sea levels in the English Channel 1900 to 2100. Proceedings of the ICE - Maritime Engineering, Vol. 164 (pp. 81-92).

Hallegatte, S., Green, C., Nicholls, R.J., Corfee-Morlot, J., 2013. Future flood losses in major coastal cities. Nature Clim. Change, 3, 802-806.

Hanson, S., Nicholls, R., Ranger, N., Hallegatte, S., Corfee-Morlot, J., Herweijer, C., Chateau, J., 2011. A global ranking of port cities with high exposure to climate extremes. Climatic Change, 104, 89-111.

Hardisty, J., 2009. Principles of Tidal Power Devices. The Analysis of Tidal Stream Power (pp. 55-88): John Wiley & Sons, Ltd.

Heaps, N., 1978. Linearized vertically-integrated equations for residual circulation in coastal seas. Ocean Dynamics 31, 147–169.

Hill, A., Brown, J., Fernand, L., 1996. The western Irish Sea gyre: a retention system for Norway lobster (Nephrops norvegicus)? Oceanologica Acta, 19, 357-368.

Holgate, S.J., 2007. On the decadal rates of sea level change during the twentieth century. Geophysics Research Letters 34, 4.

Hollebrandse, F.A.P., 2005. Temporal development of the tidal range in the southern North Sea. Master Thesis, Faculty of Civil Engineering and

Geosciences, Delft University of Technology. <http://www.citg.tudelft.nl/live/binaries/ 4de0d195-5207-4e67-84bb-455c5403ae47/doc/2005Hollebrandse.pdfS.>

Holleman, R., and M. Stacey, 2014: Coupling of Sea Level Rise, Tidal Amplification and Inundation. J. Phys. Oceanogr. doi:10.1175/JPO-D-13-0214.1, in press.

Horsburgh, K.J., Hill, A.E., 2003. A Three-Dimensional Model of Density-Driven Circulation in the Irish Sea. Journal of Physical Oceanography, 33, 343-365.

Horsburgh, K.J., Wilson, C., 2007. Tide-surge interaction and its role in the distribution of surge residuals in the North Sea. Journal of Geophysical Research -Oceans 112.

Howard, T., Lowe, J., Horsburgh, K., 2010. Interpreting century-scale changes in southern North Sea storm surge climate derived from coupled model simulations. Journal of Climate 23, 6234–6247.

Howarth, M.J., 1990. Atlas of tidal elevations and currents around the British Isles. Department of Energy, Offshore Technology Report, OTH 89 293, appendix & charts, 16 pp.

Howarth, M.J., Pugh, D.T., 1983. Observations of tides over the continental shelf of northwest Europe. In: Johns, B. (Ed.), Physical Oceanography of Coastal and Shelf Seas. , Elsevier, Amsterdam.

Hughes, C.W., Williams, S.D.P., 2010. The color of sea level: Importance of spatial variations in spectral shape for assessing the significance of trends. Journal of Geophysical Research: Oceans, 115, C10048.

Huybrechts, P., Gregory, J., Janssens, I., Wild, M., 2004. Modelling Antarctic and Greenland volume changes during the 20th and 21st centuries forced by GCM time slice integrations. Global and Planetary Change 42, 83–105.

Jay, D.A., 2009. Evolution of tidal amplitudes in the eastern Pacific Ocean. Geophysical Research Letters 36, L04603.

Jensen, J. and Mudersbach, C.H., 2005. Recent Sea Level Variations at the North Sea and Baltic Sea Coastlines. Book of Abstracts ICEST 2005, New Orleans, USA.

Jensen, J., Mügge, H.-E., Visscher, G., 1988. Untersuchungen zur Wasserstandentwicklung in der Deutschen Buch. Die K¨ uste 47, 135–161.

Jevrejeva, S., Moore, J.C., Grinsted, A., 2012. Sea level projections to AD2500 with a new generation of climate change scenarios. Global and Planetary Change, 80–81, 14-20.

Kabat, P., Fresco, L.O., Stive, M.J.F., Veerman, C.P., van Alphen, J.S.L.J., Parmet, B.W.A.H., Hazeleger, W., Katsman, C.A., 2009. Dutch coasts in transition. Nature Geosci, 2, 450-452.

Katsman, C., Sterl, A., Beersma, J.J., Brink, H.W., Church, J.A., Hazeleger, W., Kopp, R.E., Kroon, D., Kwadijk, J., Lammersen, R., Lowe, J., Oppenheimer, M., Plag, H.P., Ridley, J., Storch, H., Vaughan, D.G., Vellinga, P., Vermeersen, L.L.A., Wal, R.S.W., Weisse, R., 2011. Exploring high-end scenarios for local sea level rise to develop flood protection strategies for a low-lying delta—the Netherlands as an example. Climatic Change, 109, 617-645.

Kauker, F., 1998. Regionalization of climate model results for the North Sea. Ph.D. Thesis, University of Hamburg, GKSS Report 99/E/6, p. 109.

Kauker, F., Langenberg, H., 2000. Two models for the climate change related development of sea levels in the North Sea—a comparison. Climate Research 15, 61–67.

Lane, A., 2004. Bathymetric evolution of the Mersey Estuary, UK, 1906–1997: causes and effects. Estuarine, Coastal and Shelf Science, 59, 249-263.

Lowe, J.A., Gregory, J.M., 2005. The effects of climate change on storm surges around the United Kingdom. Philosophical Transactions of the Royal Society of London. Series A. Mathematical, Physical and Engineering 363, 1313–1328.

Lowe, J.A., Gregory, J.M., Flather, R.A., 2001. Changes in the occurrence of storm surges around the United Kingdom under a future climate scenario using a dynamic storm surge model driven by the Hadley Centre climate models. Climate Dynamics 18, 179–188.

Lowe, J.A., Howard, T.P., Pardaens, A., Tinker, J., Holt, J., Wakelin, S., Milne, G., Leake, J., Wolf, J., Horsburgh, K., Reeder, T., Jenkins, G., Ridley, J., Dye, S., Bradley, S., 2009. UK Climate Projections science report: Marine and coastal

projections. Met Office Hadley Centre, Exeter, UK. <http://ukclimateprojections.defra.gov.uk/images/stories/marine_pdfs/UKP09_Marine_report.pdf>.

Lyard, F., Lefevre, F., Letellier, T., Francis, O., 2006. Modelling the global ocean tides: modern insights from FES2004. Ocean Dynamics, 56, 394-415.

MacKay, D.J.C., 2008. Sustainable Energy – without the hot air. UIT Cambridge, 2008. ISBN 978-0-9544529-3-3. <www.withouthotair.com>.

Manning R., 1891. On the flow of water in open channels and pipes. Transactions of the Institution of Civil Engineers of Ireland, 20, 161-207

Masselink, G., Russell, P., 2013. Impacts of climate change on coastal erosion. Marine Climate Change Impacts Partnership <http://www.mccip.org.uk/media/13234/2013arc_backingpapers_9_ce.pdf>.

Meehl, G.A., Stocker, T.F., Collins, W.D., Friedlingstein, P., Gaye, A.T., Gregory, J.M., Kitoh, A., Knutti, R., Murphy, J.M., Noda, A., Raper, S.C.B., Watterson, I.G., Weaver, A.J., Zhao, Z.-C., 2007. Global climate projections. In: Solomon, S., Qin, D., Manning, M., Chen, Z., Marquis, M., Averyt, K.B., Tignor, M., Miller, H.L., (Eds.), Climate Change 2007: The Physical Science Basis. Contribution of Working Group I to the Fourth Assessment Report of the Intergovernmental Panel on Climate Change, 2007. Cambridge University Press, Cambridge, United Kingdom and New York, NY, USA.

Merian, J.R., 1828. Ueber die Bewegung tropfbarer Flüssigkeiten in Gefässen [On the motion of drippable liquids in containers] (thesis) (in German). Basel: Schweighauser.

Mesinger, F., Arakawa, A., 1976. Numerical methods used in atmospheric models. GARP Publication Series. No. 17, p. 67, World Meteorological Organization. [Available from World. Meteor. Org., Case Postale No. 65, CH-1211, Geneva 1220, Switzerland].

Milne, G.A., Gehrels, W.R., Hughes, C.W., Tamisiea, M.E., 2009. Identifying the causes of sea-level change. Nature Geosci, 2, 471-478.

Mitrovica, J.X., Gomez, N., Morrow, E., Hay, C., Latychev, K., Tamisiea, M.E., 2011. On the robustness of predictions of sea level fingerprints. Geophysical Journal International, 187, 729-742.

Mitrovica, J.X., Tamisiea, M.E., Davis, J.L., Milne, G.A., 2001. Recent mass balance of polar ice sheets inferred from patterns of global sea-level change. Nature, 409, 1026-1029.

Morris, R.K.A., Mitchell, S.B., 2013. Has Loss of Accommodation Space in the Humber Estuary Led to Elevated Suspended Sediment Concentrations? Journal of Frontiers in Construction Engineering (FCE), 2, 9.

Mueller, R.D., Padman, L., Dinniman, M.S., Erofeeva, S.Y., Fricker, H.A., King, M.A., 2012. Impact of tide-topography interactions on basal melting of Larsen C Ice Shelf, Antarctica. Journal of Geophysical Research: Oceans, 117, C05005.

Müller, M., 2011. Rapid change in semi-diurnal tides in the North Atlantic since 1980. Geophysical Research Letters 38, L11602.

Müller, M., 2012. The influence of changing stratification conditions on barotropic tidal transport and its implications for seasonal and secular changes of tides. Continental Shelf Research, 47, 107-118.

Müller, M., Arbic, B.K., Mitrovica, J.X., 2011. Secular trends in ocean tides: Observations and model results. Journal of Geophysical Research: Oceans, 116, C05013.

Müller-Navarra, S., Bork, I., 2011. Development of an operational Elbe tidal estuary model. Coastal Engineering Proceedings, 1.

Myers, L., Bahaj, A.S., 2005. Simulated electrical power potential harnessed by marine current turbine arrays in the Alderney Race. Renewable Energy, 30, 1713-1731.

Nerem, R.S., Chambers, D.P., Choe, C., Mitchum, G.T., 2010. Estimating Mean Sea Level Change from the TOPEX and Jason Altimeter Missions. Marine Geodesy, 33, 435-446.

Nicholls, R., Wilson, T., 2001. Integrated impacts on coastal areas and river flooding. Regional Climate Change Impact and Response Studies in East Anglia

and North West England (RegIS). Oxford, UK: UK Climate Impacts Programme (UKCIP), 54-103.

Nicholls, R.J., Hanson, S., Herweijer, C., Patmore, N., Hallegatte, S., Corfee-Morlot, J., Château, J., Muir-Wood, R., 2008. Ranking port cities with high exposure and vulnerability to climate extremes: exposure estimates. Paris, France, Organisation for Economic and Co-operative development (OECD), 62pp. (Environment Directorate Working Papers, (ENV/WKP(2007)1)).

Nicholls, R.J., Hanson, S.E., Lowe, J.A., Warrick, R.A., Lu, X., Long, A.J., 2014. Sea-level scenarios for evaluating coastal impacts. Wiley Interdisciplinary Reviews: Climate Change, 5, 129-150.

Nicholls, R.J., Marinova, N., Lowe, J.A., Brown, S., Vellinga, P., De Gusmao, D., Hinkel, J., Tol, R.S.J., 2011. Sea-level rise and its possible impacts given a 'beyond 4 degrees C world' in the twenty-first century. Philosophical Transactions of the Royal Society of London. Series A. Mathematical, Physical and Engineering 369, 161–181.

Nicholls, R.J., Townend, I.H., Bradbury, A.P., Ramsbottom, D., Day, S.A., 2013. Planning for long-term coastal change: Experiences from England and Wales. Ocean Engineering, 71, 3-16.

NOAA (National Oceanic and Atmospheric Administration), 2008. The Physical Oceanographic Real-Time System (PORTS). <http://tidesandcurrents.noaa.gov/ports.html>

Orton, P., Georgas, N., Blumberg, A., Pullen, J., 2012. Detailed modeling of recent severe storm tides in estuaries of the New York City region. Journal of Geophysical Research: Oceans (1978–2012), 117.

Pachauri, R.K., Reisinger, A., (Eds.), 2007. Climate change 2007: Synthesis Report: Contribution of Working Groups I, II and III to the Fourth assessment report of the Intergovernmental Panel on Climate Change, Geneva, 104 pp.

Pelling, H.E., Mattias Green, J.A., 2013. Sea level rise and tidal power plants in the Gulf of Maine. Journal of Geophysical Research: Oceans, 118, 2863-2873.

Pelling, H.E., Mattias Green, J.A., Ward, S.L., 2013b. Modelling tides and sea-level rise: To flood or not to flood. Ocean Modelling, 63, 21-29.

Pelling, H.E., Uehara, K., Green, J.A.M., 2013a. The impact of rapid coastline changes and sea level rise on the tides in the Bohai Sea, China. Journal of Geophysical Research: Oceans, 118, 3462-3472.

Peltier, W.R., 2004. Global glacial isostasy and the surface of the ice-age earth: the ice-5G (VM2) model and grace. Annual Review of Earth and Planetary Sciences 32, 111–149.

Pfeffer, W.T., Harper, J.T., O'Neel, S., 2008. Kinematic constraints on glacier contributions to 21st-century sea-level rise. Science 321, 1340–1343.

Philippart, M.E., Gebraad, A.W., Scharroo, R., Roest, M.R.T., Vollebregt, E.A.H., Jacobs, A., van den Boogaard, H.F.P., Peters, H.C., 1998. Datum 2 Data assimilation with Altimetry Techniques used in a tidal Model, 2nd Program.

Pickering, M., 2009. An Investigation into how North Sea Tides and Storm Surges vary with Sea Level Rise using the Dutch Continental Shelf Model in Delft3D. Bachelors Thesis, School of Ocean and Earth Science, p. 132, University of Southampton, Southampton.

Pickering, M.D. 2010. Development and validation of a new barotropic tidal model in order to investigate the effect of future sea-level rise on the global tides. Masters Thesis, School of Ocean and Earth Science, p. 34. University of Southampton, Southampton.

Pickering, M.D., Wells, N.C., Horsburgh, K.J., Green, J.A.M., 2012. The impact of future sea-level rise on the European Shelf tides. Continental Shelf Research, 35, 1-15.

Piersma, T., Rogers, D. I., González, P. M., Zwarts, L., Niles, L. J., De Lima Serrano do Nascimento, I., Minton, C. D. T. and Baker, A. J., 2005. Fuel storage rates before northward flights in red knots worldwide: facing the severest ecological constraint in tropical intertidal environments?. – In: Greenberg, R. and Marra, P. P. (eds), Birds of two worlds: ecology and evolution of migration. Johns Hopkins University Press, Baltimore, pp. 262–273.

Platzman, G.W., Curtis, G.A., Hansen, K.S., Slater, R.D., 1981. Normal Modes of the World Ocean. Part II: Description of Modes in the Period Range 8 to 80 Hours. Journal of Physical Oceanography, 11, 579-603.

Plüß, A., 2004. Das Nordseemodell der BAW zur Simulation der Tide in der Deutschen Bucht. Die K¨ uste 67, 83–127.

Pond, S., Pickard, G.L., 1983. Introductory Dynamical Oceanography, 2nd ed. Pergamon Press Ltd, Oxford.

Pouvreau, N., Martin Miguez, B., Simon, B., Wöppelmann, G., 2006. Évolution de l'onde semi-diurne M2 de la marée à Brest de 1846 à 2005. Comptes Rendus Geosciences, 338, 802-808.

Prandle, D., Wolf, J., 1978. The interaction of surge and tide in the North Sea and River Thames. Institute of Oceanographic Sciences.

Provost, C.L., 2001. Ocean Tides. In L.-L. Fu, A. Cazenave (Eds.), Satellite Altimetry and Earth Sciences, Vol. 69. London: Academic Press.

Pugh, D. T., Vassie, J. M. 1980 Applications of the joint probability method for extreme sea level computations. Proc. Inst. Civil Eng. Part 2 69, 959-975.

Pugh, D., 1987. Tides, surges and mean sea-level Chichester: John Wiley & Sons Ltd.

Pugh, D.T., 1982. Estimating extreme currents by combining tidal and surge probabilities. Ocean Engineering 9, 361–372.

Pugh, D.T., 2004. Changing sea levels. Effects of tides, weather and climate. Cambridge University Press.

Rabaut, M., Audfroid Calderón, M., Van de Moortel, L., Van Dalfsen, J., Vincx, M., Degraer, S., Desroy, N., 2013. The role of structuring benthos for juvenile flatfish. Journal of Sea Research, 84, 70-76.

Rabaut, M., Guilini, K., Van Hoey, G., Vincx, M., Degraer, S., 2007. A bio-engineered soft-bottom environment: The impact of Lanice conchilega on the benthic species-specific densities and community structure. Estuarine, Coastal and Shelf Science, 75, 525-536.

Rahmstorf, S., 2007. A semi-empirical approach to projecting future sea-level rise. Science 315, 368–370.

Rakhorst, D., 2005. Tijverschillen langs de Nederlandse kust; De invloed van menselijke ingrepen, Haarlem, Rijkswaterstaat RIKZ.

Ranger, N., Reeder, T., Lowe, J., 2013. Addressing 'deep' uncertainty over long-term climate in major infrastructure projects: four innovations of the Thames Estuary 2100 Project. EURO Journal on Decision Processes, 1, 233-262.

Ray, R.D., 2006. Secular changes of the M-2 tide in the Gulf of Maine. Continental Shelf Research 26, 422–427.

Ray, R.D., 2009. Secular changes in the solar semidiurnal tide of the western North Atlantic Ocean. Geophysical Research Letters, 36.

Rignot, E., Velicogna, I., van den Broeke, M.R., Monaghan, A., Lenaerts, J.T.M., 2011. Acceleration of the contribution of the Greenland and Antarctic ice sheets to sea level rise. Geophysical Research Letters, 38, L05503.

Roberts, W., Dearnaley, M.P., Baugh, J.V., Spearman, J.R., Allen, R.S., 1998. The sediment regime of the Stour and Orwell estuaries. In Dronkers, J., Scheffers, M.B.A.M., (Eds.), Physics of Estuaries and Coastal Seas, Balkema, Rotterdam, pp. 93–102

Rohling, E.J., Grant, K., Bolshaw, M., Roberts, A.P., Siddall, M., Hemleben, C., Kucera, M., 2009. Antarctic temperature and global sea level closely coupled over the past five glacial cycles. Nature Geoscience 2, 500–504.

Rohling, E.J., Grant, K., Hemleben, C., Siddall, M., Hoogakker, B.A.A., Bolshaw, M., Kucera, M., 2008. High rates of sea-level rise during the last interglacial period. Nature Geoscience 1, 39–42.

Sayag, R., Worster, M.G., 2013. Elastic dynamics and tidal migration of grounding lines modify subglacial lubrication and melting. Geophysical Research Letters, 40, 5877-5881.

Schwiderski, E.W., 1980. On charting global ocean tides. Reviews of Geophysics, 18, 243-268.

Scott, B., Sharples, J., Ross, O., Wang, J., Pierce, G., Camphuysen, C., 2010. Sub-surface hotspots in shallow seas: fine-scale limited locations of top predator foraging habitat indicated by tidal mixing and sub-surface chlorophyll. Marine Ecology Progress Series, 408, 207-226.

Scott, B., Webb, A., Palmer, M., Embling, C., Sharples, J., 2013. Fine scale bio-physical oceanographic characteristics predict the foraging occurrence of

contrasting seabird species; Gannet (Morus bassanus) and storm petrel (Hydrobates pelagicus). Progress in Oceanography, 117, 118-129.

Scottish Government, 2012. Consultation seeking views on new controls in the Scottish creel fisheries and on increasing the minimum landing size for West of Scotland. <http://www.scotland.gov.uk/Publications/2012/08/7352/3>. ISBN 978 1 78045 988 2 (Web publication only). Last Accessed 23/03/14.

Seafish, 2007. http://www.seafish.org/media/Publications/PilotPotFishery.pdf. Last accessed 23/03/14.

Sharples, J., 2008. Potential impacts of the spring-neap tidal cycle on shelf sea primary production. Journal of Plankton Research, 30, 183-197.

Shaw, J., Amos, C.L., Greenberg, D.A., O'Reilly, C.T., Parrott, D.R., Patton, E., 2010. Catastrophic tidal expansion in the Bay of Fundy, Canada. Canadian Journal of Earth Sciences 47, 1079–1091.

Shennan, I., Lambeck, K., Flather, R., Horton, B., McArthur, J., Innes, J., Lloyd, J., Rutherford, M., Wingfield, R., 2000. Modelling western North Sea palaeogeographies and tidal changes during the Holocene, 166. Geological Society, London Special Publications, 299–319.

Shennan, I., Milne, G., Bradley, S.L., 2009. Late Holocene relative land- and sealevel changes : providing information for stakeholders. GSA Today 19, 52–53.

Shennan, I., Woodworth, P.L., 1992. A comparison of late Holocene and twentiethcentury sea-level trends from the UK and North Sea region. Geophysical Journal International 109, 96–105.

Shepherd, A., Ivins, E.R., A, G., Barletta, V.R., Bentley, M.J., Bettadpur, S., Briggs, K.H., Bromwich, D.H., Forsberg, R., Galin, N., Horwath, M., Jacobs, S., Joughin, I., King, M.A., Lenaerts, J.T.M., Li, J., Ligtenberg, S.R.M., Luckman, A., Luthcke, S.B., McMillan, M., Meister, R., Milne, G., Mouginot, J., Muir, A., Nicolas, J.P., Paden, J., Payne, A.J., Pritchard, H., Rignot, E., Rott, H., Sørensen, L.S., Scambos, T.A., Scheuchl, B., Schrama, E.J.O., Smith, B., Sundal, A.V., van Angelen, J.H., van de Berg, W.J., van den Broeke, M.R., Vaughan, D.G., Velicogna, I., Wahr, J., Whitehouse, P.L., Wingham, D.J., Yi, D., Young, D.,

Zwally, H.J., 2012. A Reconciled Estimate of Ice-Sheet Mass Balance. Science, 338, 1183-1189.

Simon, B., 1982. Prédiction de la marée à Brest. Annales Hydrographiques Series 5 (10), 33–50.

Simpson, J., Hunter, J., 1974. Fronts in the Irish sea. Nature, 250, 404-406.

Simpson, J.H., 1998. Tidal Processes in Shelf Seas, The SEA, vol 10, 113-150 The Celtic Seas, The SEA vol 11, 659-698 The Global Coastal Ocean (Editors K.Brink and A.Robinson), 113-150. John Wiley. .

Slangen, A.B.A., Carson, M., Katsman, C.A., van de Wal, R.S.W., Kohl, A., Vermeersen, L.L.A., Stammer, D., Submitted to Climatic Change. Projecting twenty-first century regional sea-level changes.

Song, D., Wang, X.H., Zhu, X., Bao, X., 2013. Modeling studies of the far-field effects of tidal flat reclamation on tidal dynamics in the East China Seas. Estuarine, Coastal and Shelf Science, 133, 147-160.

Souza, A.J., 2013. On the use of the Stokes number to explain frictional tidal dynamics and water column structure in shelf seas. Ocean Sci., 9, 391-398.

Sriver, R., Urban, N., Olson, R., Keller, K., 2012. Toward a physically plausible upper bound of sea-level rise projections. Climatic Change, 115, 893-902.

Stelling, G.S., 1984. On the construction of computational methods of shallow water flow problems. Rijkswaterstaat Communication, 35.

Sterl, A., van den Brink, H., de Vries, H., Haarsma, R., van Meijgaard, E., 2009. An ensemble study of extreme storm surge related water levels in the North Sea in a changing climate. Ocean Science 5, 369–378.

Stikvoort E. (ed.), Berrevoets, C., Kuijper M., Lefèvre F., Liek G.-J., Lievaart M., van Maldegem D., Meininger P., Peters B., Pouwer A., Schippers H. and Wijsman J., 2003. Monitoring van de effecten van de verruiming 48'-43', MOVE-rapport 7: MOVE hypothesen-document 2003, Onderliggende rapportage bij MOVE-rapport 8 (deel A en B) Evaluatierapport 2003. Rapport RIKZ/2003.009, Middelburg, the Netherlands.

Swinkels, C., van der Zwan, S., Bijlsma, A., Pothof, I., 2010. Technical feasibility of energy conversion from salinity gradients along the Dutch coast; a case study at IJmuiden. Proceedings from the 1st IAHR European Congress, Edinburgh, UK, 4-6 May 2010. Heriot-Watt University. <http://repository.tudelft.nl/view/ir/uuid%3A8f2ff2f3-9642-4399-9b1a-5b37918c93b1/>

The Common Wadden Sea Secretariat, 2010. Wadden Sea Wildlife. <http://www.waddensea-worldheritage.org/wadden-sea-world-heritage/wadden-sea-wildlife>. Last Accessed 28/04/2011.

Thomas, H., Bozec, Y., Elkalay, K., de Baar, H.J.W., 2004. Enhanced Open Ocean Storage of CO2 from Shelf Sea Pumping. Science, 304, 1005-1008.

Tomasin, A., 1974. Recent changes in the tidal regime in Venice. Rivista Italiana di Geofisica 23, 275–278.

Tonnon, P., Van Rijn, L., Walstra, D., 2007. The morphodynamic modelling of tidal sand waves on the shoreface. Coastal Engineering, 54, 279-296.

Townend, I., Whitehead, P., 2003. A preliminary net sediment budget for the Humber Estuary. Science of the total environment, 314, 755-767.

Uehara, K., Scourse, J.D., Horsburgh, K.J., Lambeck, K., Purcell, A.P., 2006. Tidal evolution of the northwest European shelf seas from the Last Glacial Maximum to the present. Journal of Geophysical Research: Oceans, 111, C09025.

Vafeidis, A.T., Nicholls, R.J., McFadden, L., Tol, R.S.J., Hinkel, J., Spencer, T., Grashoff, P.S., Boot, G., Klein, R.J.T., 2008. A New Global Coastal Database for Impact and Vulnerability Analysis to Sea-Level Rise. Journal of Coastal Research, 917-924.

Van Goor, M., Zitman, T., Wang, Z., Stive, M., 2003. Impact of sea-level rise on the morphological equilibrium state of tidal inlets. Marine Geology, 202, 211-227.

Vellinga, P., Katsman, C.A., Sterl, A., Beersma, J.J., Church, J.A., Hazeleger, W., Kopp, R.E., Kroon, D., Kwadijk, J., Lammersen, R., Lowe, J., Marinova, N., Oppenheimer, M., Plag, H.P., Rahmstorf, S., Ridley, J., von Storch, H., Vaughan,

D.G., van der Wal, R.S.W., Weisse, R., 2009. Exploring high-end climate change scenarios for flood protection of the Netherlands. International Scientific Assessment carried out at request of the Delta Committee. KNMI Scientific Report WR-2009-05, KNMI/Alterra, the Netherlands.

Verboom, G.K., Deronde, J.G., Vandijk, R.P., 1992. A fine grid tidal flow and stormsurge model of the North-Sea. Continental Shelf Research 12, 213–233.

Verlaan, M., Zijderveld, A., de Vries, H., Kroos, J., 2005. Operational storm surge forecasting in the Netherlands: developments in the last decade. Philosophical Transactions of the Royal Society A: Mathematical, Physical and Engineering Sciences 363, 1441–1453.

von Storch, H., Woth, K., 2008. Storm surges: perspectives and options. Sustainability Science 3, 33–43.

Voogt, L., 1984. A North Sea tidal model based on the JONSDAP-1976 measurements. Rijkswaterstaat, Report WWKZ-849.006 (in Dutch).

Walker, M.G., Jones, F.R.H., Arnold, G.P., 1978. The movements of plaice (Pleuronectes platessa L.) tracked in the open sea. Journal du Conseil, 38, 58-86.

Ward, S., Green, J.A.M., Pelling, H., 2012. Tides, sea-level rise and tidal power extraction on the European shelf. Ocean Dynamics, 62, 1153-1167.

Weilbeer, H., Klöpper, M., Bundesanstalt für Wasserbau, 2011. Model Validation and System Studies for Hydrodynamics, Salt and Sediment Transport in the Elbe Estuary-Basic Information for the River Engineering and Sediment Management. Draft Report A, 895604405.

Weisse, R., Bellafiore, D., Menéndez, M., Méndez, F., Nicholls, R.J., Umgiesser, G., Willems, P., 2013. Changing extreme sea levels along European coasts. Coastal Engineering.

Winterwerp, J., 2013. On the response of tidal rivers to deepening and narrowing. Deltares.

Winterwerp, J.C., 2011. Fine sediment transport by tidal asymmetry in the high-concentrated Ems River: indications for a regime shift in response to channel deepening. Ocean Dynamics, 61, 203-215.

Woodworth, P.L., 2010. A survey of recent changes in the main components of the ocean tide. Continental Shelf Research 30, 1680–1691.

Woodworth, P.L., Shaw, S.M., Blackman, D.L., 1991. Secular trends in mean tidal range around the British Isles and along the adjacent European coastline. Geophysical Journal International 104, 593–609.

Woodworth, P.L., Teferle, F.N., Bingley, R.M., Shennan, I., Williams, S.D.P., 2009. Trends in UK mean sea level revisited. Geophysical Journal International 176, 19–30.

Xu, S., Huang, W., 2011. Estimating extreme water levels with long-term data by GEV distribution at Wusong station near Shanghai city in Yangtze Estuary. Ocean Engineering, 38, 468-478.

Zaron, E.D., Egbert, G.D., 2006. Estimating Open-Ocean Barotropic Tidal Dissipation: The Hawaiian Ridge. Journal of Physical Oceanography, 36, 1019-1035.

Zhang, X., Church, J.A., 2012. Sea level trends, interannual and decadal variability in the Pacific Ocean. Geophysical Research Letters, 39, L21701.